Polymers in Aqueous Media

ADVANCES IN CHEMISTRY SERIES 223

Polymers in Aqueous Media

Performance Through Association

J. Edward Glass, Editor
North Dakota State University

Developed from a symposium sponsored
by the Division of Polymeric Materials:
Science and Engineering
at the 194th National Meeting
of the American Chemical Society,
New Orleans, Louisiana,
August 30–September 4, 1987

American Chemical Society, Washington, DC 1989

Advances in Chemistry Series

M. Joan Comstock, *Series Editor*

1989 ACS Books Advisory Board

FOREWORD

The ADVANCES IN CHEMISTRY SERIES was founded in 1949 by
the American Chemical Society as an outlet for symposia and
collections of data in special areas of topical interest that could
not be accommodated in the Society's journals. It provides a
medium for symposia that would otherwise be fragmented
because their papers would be distributed among several
journals or not published at all. Papers are reviewed critically
according to ACS editorial standards and receive the careful
attention and processing characteristic of ACS publications.
Volumes in the ADVANCES IN CHEMISTRY SERIES maintain the
integrity of the symposia on which they are based; however,
verbatim reproductions of previously published papers are not
accepted. Papers may include reports of research as well as
reviews, because symposia may embrace both types of
presentation.

ABOUT THE EDITOR
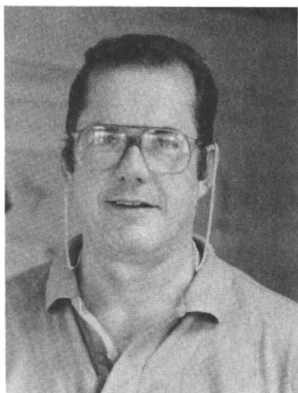
J. EDWARD GLASS is a professor of polymers and coatings at North Dakota State University. He received a bachelor of science degree in chemistry from Louisiana State University in 1959 and a Ph.D. degree from Purdue University in 1964. From 1963 to 1980, he worked for the Union Carbide Corporation at its South Charleston Research and Development Center.

His research interests have included almost all aspects of water-soluble polymers: kinetics and synthesis by free-radical processes, controlled substituent placement in the derivatization of carbohydrate polymers, solution and interfacial adsorption and viscosity behavior of both polymer types, and meaningful extrapolation of such fundamental data to the performance of water-soluble polymers in application formulations. He has published more than 70 technical papers and received several patents in these areas of study.

PREFACE

THIS BOOK IS INTENDED to complement and expand on the material covered in Advances in Chemistry 213, *Water-Soluble Polymers*. Some of the areas not covered in *Water-Soluble Polymers* are included in the first section (Chapters 1–7) of this book. Chapters present discussions ranging from chemical cross-linking among synthetic and carbohydrate polymers to gels via nonchemical bonding based on tacticity in synthetic and helical aggregates in carbohydrate polymers. The structures of these diverse gels are addressed through complex rheological analysis, light scattering, and novel NMR approaches.

The use of polyelectrolytes in a variety of applications was discussed in *Water-Soluble Polymers*, but not problems associated with their synthesis. The synthesis of polyelectrolytes is discussed in the second section of this book. In Chapter 8, which serves as an overview of the rest of the book, parallels in the synthesis of polyelectrolytes with the synthesis of surfactant-modified, water-soluble polymers are discussed. The importance of elongational viscosities in polymer applications has been an on-going, albeit low-profile effort of many researchers over the past decades. Its importance as a fundamental tool, through birefringence measurement, is highlighted in the first of two chapters on this subject (Chapters 11 and 12). Chapter 12 highlights areas where dynamic uniaxial extensional viscosity has and has not proven to be commercially significant and is reviewed in the context of its importance as a primary driving force for the development and commercial use of surfactant-modified, water-soluble polymers.

The chapters on elongational viscosities are followed in the next section by chapters on very eloquent spectroscopic studies that detail the usefulness of fluorescence and Fourier transform infrared methods in elucidating the associations among water-soluble polymers, particularly those that are surfactant modified.

The subject of surfactant-modified, water-soluble polymers, briefly discussed in *Water-Soluble Polymers*, is addressed in the last three sections (Chapters 16–28) of this book. These associative thickeners are covered in detail, ranging from the maleic acid copolymers of variable compositions introduced in various commercial markets in the early 1960s to the most recent entries (that is, in the open literature), hydrophobe-modified poly(acrylamide). Chapter 23 is complementary to the spectroscopic studies in Chapters 13–15; it explores new approaches to understanding associations in aqueous media. The three hydrophobe-modified polymers that have gained commercial acceptance in the 1980s, (hydroxyethyl)cellulose, ethoxylate urethanes, and alkali-swellable emulsions, are discussed in detail. In particular, hydrophobe-modified (hydroxyethyl)cellulose, which is

discussed in Chapters 18 and 19 as a model associative thickener, has achieved commercial success and is discussed from a commercial viewpoint in Chapter 27.

The understanding reflected in the flow of this text and investigations not currently described in the open literature provide the foundation for a strong symposium in 1992.

Acknowledgments

Perhaps Thomas Wolfe was wrong: It is possible to go home again and feel good about it, when you have distinctive contributors to facilitate the experience.

J. EDWARD GLASS
North Dakota State University
Fargo, ND 58105

April 25, 1989

Gelled Aqueous Systems

A. Silberberg

Department of Polymer Research, Weizmann Institute of Science, Rehovot 76100, Israel

Gels are swollen networks possessing both the cohesive properties of solids and the diffusive transport properties of liquids. Elastically, they tend to be soft, and osmotically they are highly reactive. Gels based on water incorporate water's unique properties, in particular, the facility for ionization that an aqueous environment conveys. All biological systems are water-based, and most are ionized aqueous gels. If some of the bonds holding the gel network together can "make-and-break", the gel is called reversible. If the bonds do not dissociate, the gel is called permanent. A permanent gel tends to carry the history of its formation in its structure; it is best described as a cross-linked system of clusters. The clusters of a particular gel show the same basic organization and size, which can vary extensively from system to system. Clusters range from small, starlike molecules to large heavily cross-linked, fairly concentrated microgel cores. Reversible gels are also formed between clusters. The clusters, however, must be copolymers. One type of monomer in the copolymeric cluster renders it soluble, the other confers sufficiently long-lived cross-links.

What Is a Gel?

Gels are porous solids. They involve, as their "solid" element, a continuous matrix, a skeletal network, that endows the system with the required mechanical stability and coherence. If the network is a permanent structure, it will possess a remembered, unstressed reference configuration to which it returns when all the external forces that deform it are removed. When network structure is labile, however, the length of time for which an unstressed starting conformation is remembered will be limited by the lifetime of the molecular connections in the network.

The space in the gel not filled by the network is occupied by a low molecular weight liquid, like water. The thinner the structural elements of the network, the easier it is to deform, and the lower is its elastic modulus. In most gels, indeed, the network is molecularly thin, and the strands are long-chain macromolecules. In permanent gels, these long-chain macromolecules are suitably cross-linked. A network of such thin strands will, in general, not be self-supporting, and, upon removal of the liquid from the network, the resulting xerogel will tend to collapse upon itself.

The stresses induced in collapsing the network out of its reference configuration are compensated by short-range, cohesive attractions between the individual macromolecular network strands. The presence of a liquid, a solvent for the macromolecules that constitute the network, is thus a necessity in order to maintain porosity. Only in the presence of a solvent will it be thermodynamically preferable for the network strands to be surrounded by the solvent rather than to self-associate into a precipitate. So strong, indeed, is the tendency to be mixed, that, in contact with excess solvent, a *permanent gel* (i.e., a covalently cross-linked network) will swell well beyond the unstressed reference configuration.

Only if the links that hold the network together involve covalent (i.e., permanent) chemical bonds can a gel system remain coherent in the presence of unlimited solvent. Any possibility of molecular make-and-break at the cross-links, or at any other points in the network, has to be separately considered and creates a different kind of system called a reversible gel.

Permanent gels prepared in the laboratory are most commonly covalently linked, macroscopically large networks of polymeric chains in a solvent environment. Such gels may appear to be homogeneous at the supermacromolecular, supercolloidal level but are inevitably disparate (i.e., microheterogeneous) at some microscopic scale. The structure of a permanent (irreversibly cross-linked) gel is strongly dependent upon its history. Each sample carries within it the permanent imprint of its mode of preparation and of the molecular size and concentration of the building materials from which it was made. A gel can, in general, be divided into an array of contiguous, solvent-filled macromolecular clusters of subcolloidal size that are statistically similar in makeup and are connected to each other by a limited number (f) of covalent, cluster-to-neighbor-cluster bridges.

A reversible gel based upon dissociable cross-links is characterized by the finite size of the network that is chemically linked into a unit at any instant. In a reversible gel, some of the network connections will always open, close, and interchange. A reversible gel, too, can thus be divided into structural subentities, but the bonds that link these substructures into a macroscopic whole do not possess infinite lifetimes. The coherence of the system depends upon it being contained in a chemically closed, semipermanent, mechanically rigid confinement. A reversible gel cannot, for example, be brought into true (open) swelling equilibrium with an excess of

the solvent medium. Permanent and reversible gels bear a structural resemblance to each other, but they respond similarly to certain external challenges only over a limited period of time. Both swelling behavior and structure will alter significantly when reversible gels are taken beyond this limit.

The special properties of water and the importance of gels in biology easily justify making a separate category of *aqueous gels*. Ionized aqueous gels, in particular, are different from gels in any other solvent medium. The naturally occurring biological gels are perhaps the most widespread water-based gels. All cellular interiors are gels, and the organizational context in which the cells function, the connective tissue, is a gel. There is, moreover, an interesting specialization that characterizes the components of the biological gel matrix. Whereas with synthetic systems, a single gel matrix component acts both mechanically and osmotically to establish the balance between expansion and dissolution, natural systems do not necessarily behave this way. In connective tissue, for example, the mechanical element is the collagen fiber network, whereas the interstitial proteoglycans and structural glycoproteins associated with the collagen fiber matrix are the soluble, osmotically active (solvent-imbibing) components (*1*).

Permanent Gel Microheterogeneity

Certain aspects of permanent gels are comparable if they are analyzed on the basis of the cluster structure of the system. A *cluster* is a particularly constructed, inhomogeneously linked, multichain macromolecule of a size generally similar to that of most macromolecules studied isolated in dilute solution. As a rule, the cluster is internally very heterogeneous in structure and composition, but, overall, the cluster is the statistically similar repeating unit that builds up the gel. In swelling equilibrium, all parts of a cluster, but its periphery in particular, are in equilibrium with an excess of pure solvent medium.

One of the most characteristic structural features of a cluster is the very large number, P, of interatomic bonds, about which rotation into two or more (Z) energetically roughly equivalent states is possible. The cluster can thus exist in some $\gamma(P,P_c)Z^P$ configurations of essentially equivalent energy and rather similar size and shape. The parameter $\gamma(P,P_c)$ is a constraining factor that makes allowance for the P_c permanent internal chemical correlations that constrict the average cluster dimensions. For polymeric chainlike structures, the randomly adopted cluster shapes ideally conform to a set of random walks with a mean-square end-to-end distance proportional to the number of bonds (in the main chain) about which rotational freedom exists. If a force is applied to the free ends of such a cluster, the distribution of chain conformations (the mean cluster shape) will change. The deformation, so induced, is opposed by the tendency of an altered distribution of con-

formations to return to the most probable one. At mechanical equilibrium, the forces applied and the stresses induced are in balance. An expansion by a factor, α, in all three directions, for example, will be resisted by an isotropic stress in the cluster that tends to reduce α, uniformly, to 1.

An important feature controlling the configuration of a real macromolecular chain is the energetic interaction between two parts of the chain that come close to each other in some configuration. An interaction between two chain segments can be repulsive or attractive, short-range or long-range. In the gel or in solution, the interaction occurs through the medium of the solvent (i.e., between different segments of the solvated macromolecule) and may or may not involve the displacement of the solvent molecules from their sites of close contact on the macromolecular surface. The medium in which the clusters are suspended and in which they change configuration, thus, plays a decisive role. Water, in particular, undergoes very strong and specific interactions. Hence, only in the simplest instances is the macromolecular chain so chemically uniform that all chain–chain contacts are the same. This uniformity is certainly not present when the chain is a copolymer, and, in such instances, additional local interactions may further constrain the cluster structure.

The interaction and mixing of the gel-substance with the solvent medium in the cluster affects solvent chemical potential and thus creates osmotic effects. Even at high degrees of swelling, the innermost core of a macromolecular cluster is a region of relatively high polymer segment concentration. Solvent (in this case, water) activity, a_W, in these regions of the cluster is, therefore, considerably less than 1. To raise the solvent's chemical potential to the level of the pure medium outside, the pressure, p, must locally be increased by (2, 3)

$$\Delta p = \pi = -(k_B T / V_W) \ln a_W \tag{1}$$

where V_W is the solvent molecular volume, T is the absolute temperature, k_B is the Boltzmann constant, and π is the osmotic pressure, which is defined in terms of a_W, by equation 1. Whereas Δp is a real pressure, the osmotic "pressure" π is merely a way to represent the effective concentration a_W in terms of pressure units (2). Only in swelling equilibrium will π (numerically and dimensionally) also express the pressure difference, Δp, between the solvent domains of the cluster and the pure solvent phase (3). Neither Δp nor π is uniformly the same in all volume elements of the gel, even in swelling equilibrium.

The required increases in pressure are mechanically induced by local coil expansion and give rise to stresses, tensions, in the macromolecular chains of the cluster. The tensor characterizing the stresses present locally in the gel matrix must have nonzero components that generate (i.e., compensate) the pressure increase both in the liquid and solid parts of the cluster.

If the expansion coefficient, α, is locally uniform, the tension σ in the gel matrix substance will add itself isotropically to the pressure Δp in the gel matrix (2). This gives

$$-(1 - \phi)\Delta p + \phi(-\Delta p + \sigma) = 0 \qquad (2a)$$

which can be rearranged to yield

$$-\Delta p + \phi\sigma = 0 \qquad (2b)$$

where ϕ is the volume fraction of the macromolecular matrix, the network component. Pressure, by convention, acts *upon* the system and thus appears with a negative sign. In the present case, equation 2b is a scalar expression. The proper tensorial character appears when we multiply equation 2b by the unit tensor.

An equation for α is obtained by eliminating Δp between equations 1 and 2b. In mean-field approximation the following expression for a cluster that consists of a single, isolated, long-chain macromolecule in swelling equilibrium was derived by Flory (4):

$$\alpha^5 - \alpha^3 \approx (\tfrac{1}{2} - \chi)P^{\frac{1}{2}} \qquad (3)$$

where χ is the Flory–Huggins segment–solvent interaction parameter, and P is the size, the number of interatomic bonds, in the cluster (i.e., the chain). When $\chi = \tfrac{1}{2}$ the situation corresponds to the undistorted tensionless case with $\alpha = 1$. The effective excluded volume (taking solute–solvent interactions into account) is

$$u = (\tfrac{1}{2} - \chi)a^3 \qquad (4)$$

where a, in contrast to $u^{1/3}$, is the real size of the chain segment. When $\chi = \tfrac{1}{2}$, the excluded volume is zero. When $\chi < \tfrac{1}{2}$, u is positive, polymer segments repel each other, and the cluster is expanded (swollen). When $\chi > \tfrac{1}{2}$, the excluded volume is negative, there is attraction between polymer segments, and the macromolecule collapses upon itself. The case studied by Flory (4) was that of a single chain of P bonds connected in linear sequence. Flory treated this polymer as a gel particle, a single cluster of essentially independent segments, with a Gaussian concentration distribution of characteristic (undeformed) dimension, $R_{F_o} \sim P^{\frac{1}{2}}a$, and real extent, αR_{F_o}. The factor $P^{\frac{1}{2}}$ is used because the right side of equation 3 is scaled by the R_{F_o} of the cluster. When $\alpha \gg 1$, equation 3 yields $\alpha \sim P^{1/10}$ and $R_F = \alpha R_{F_o} \sim P^{3/5}$, a famous result.

If the cluster is not in dilute solution, but represents the situation in the gel in swelling equilibrium, two features about its periphery will change.

The f free ends of the connecting chains will be coupled to f such free ends on neighboring clusters, and the concentration between adjoining clusters will never reach zero. As a function of distance, however, the gel-substance volume fraction, ϕ, in passing from cluster to cluster, will cross a point of symmetry. In other words, the segment concentration passes through a minimum at which its gradient is zero. The infinitesimally thin zone symmetrically separating the clusters from each other is, thus, the ideal region to use as reference for a comparison with pure solvent in swelling equilibrium. Because the segment concentration is nonzero in this zone, neither Δp nor σ will be zero. The tension, σ, in fact, will be determined by the effective tension in the bridges that link the neighboring clusters and in the loops that emanate from a cluster and cross into its neighbors.

DeGennes (5) hinted at the usefulness of subdivision into clusters. He, however, considered only ideal gels and suggested that the cluster is constituted by the chain that links two cross-links, rather than by the region centered upon the cross-link. We believe it to be more significant to have, as the dividing surface between clusters, the surface of symmetry that corresponds to the region of zero concentration gradient. For example, the cluster in the case of polyelectrolytes in which the gel matrix bears ionizable groups is an electroneutral entity. It may not be possible to deduce the interior structure of the cluster, swollen or unswollen, but a reasonable assessment can be made, in terms of equations 1 and 2b, of the isotropic equilibrium expansion, α^*, in the cluster periphery and thus, the isotropic tension σ^* in those gel matrix sections that build up the concentration, ϕ^*, in the concentration-gradient-free peripheral zone in swelling equilibrium.

Water as Solvent

Water is a rather exceptional solvent. It is strongly polar and interacts very extensively with itself and with many other chemical groups by way of hydrogen bonds. The most outstanding effect of an aqueous environment derives from water's extremely high dielectric constant and the possibility thus created that certain groups on a polymer network can ionize. Ionic dissociation produces two kinds of charged groups: charged groups on particles (ions free to diffuse through the water space) and charged groups on the gel matrix (which stay immobilized). The constraints of electroneutrality still apply, and fluctuations in space charge are kept small. However, if the only ions in solution within the cluster are the counterions to the fixed charges, their concentrations are, in general, too low for them to shield the fixed charges on the network from each other effectively. A long-range repulsion is experienced, and in permanent gels swelling increases markedly and the effective excluded volume is enlarged (6). Reversible gels under these circumstances tend to form solutions called sols.

The ions, freed into the solvent, have a profound effect on the osmotic

pressure in the permanent gel. If we consider univalent–univalent charge pairs only, and there are ν groups per unit volume of gel matrix substance that can ionize, the major contribution of the released counterions to the osmotic pressure in the cluster will be the creation of a large first-order term, $\nu\phi$, in the virial expansion for π. At high charge densities (and no added neutral salt), π, (i.e., Δp), σ, and, therefore, α will be largely increased.

This effect is essentially squashed as neutral salts are added (7). Ionic concentration will increase both in the cluster and in the equilibrium solvent phase outside. When the amount of added salt in the outside solvent phase corresponds to about $\nu\phi$, the effect of the counterion concentration $\nu\phi$ inside the gel will be reduced to less than half.

When the added salt concentration is larger still, the effect on equilibrium swelling is largely suppressed (7). In reversible systems, the gel state tends to form again. The increasing neutral salt concentration causes increased shielding of the fixed charges, and charge–charge repulsion eventually becomes confined to the interaction between a fixed charge and a close-in ion atmosphere of opposite sign. Residual effects remain, but they are far less significant. To the extent that the behavior of a particular gel is dominated by the ionization of fixed groups on its matrix, such effects tend to disappear when adequate amounts of totally ionized neutral salts are added to the system.

Poly(acrylamide) Gels

The differences in local organization that give rise to the cluster structure of permanent gels depend upon and are related to the mode of gel preparation. An important illustration is provided by the poly(acrylamide) gels that are generally made by the copolymerization of a monofunctional acrylamide monomer and a bifunctional bisacrylamide monomer by radical polymerization in an aqueous environment. Poly(acrylamide) gels made by this procedure, or some variant of it, are very extensively used in the laboratory for biopolymer and other aqueous-phase chromatographic separations. The structure of poly(acrylamide) gels and our ability to control it is, thus, of fundamental interest for these applications.

The radicals produced by the initiator molecules each activate a monomer molecule and form a reaction center. These reaction centers quickly grow in size and structural complexity as they incorporate both the monofunctional and the bifunctional monomers that reach them by diffusion. Their own rate of diffusion rapidly decreases as their size increases. Then, as the free monomer concentration drops, more and more of the reaction of the activated growing chain-end will involve loop formation with one of the unused second functionalities on the growing center itself. Each initiator molecule, thus, starts a process that first produces a fairly concentrated,

internally highly cross-linked particle, the cluster core, and then creates a very dilute gel that holds the system together. In other words, the macroscopic gel produced is based on clusters of a very high core-gel concentration and a very dilute peripheral connecting gel (8). The number of clusters corresponds, roughly, to the number of initiator molecules.

We have shown (8) that the permeability of such gels is determined mainly by the dilute peripheral gel. Their viscoelasticity, their elastic storage modulus in particular, is determined by the number of clusters (i.e., the number of initiator molecules, per unit volume) (9). A two-gel cluster model of this kind has proved most successful (8).

Reversibly Cross-Linked Gels

Reversible gels, (i.e., the class of gels in which some links in the network have finite lifetimes) differ from permanent gels mainly in two respects:

1. The structure of the reversible gel is determined by chemical equilibrium between the cross-linking entities; it is not the fossil record of the conditions under which the gel was formed.

2. There are no infinite mechanical relaxation times for reversible gels. If the macroscopic coherent network present at any instant is deformed rapidly by some applied strain, the stress stored in this deformation can relax through the chemical reaction, even if the mechanical relaxation time of the network (had the cross-links been permanent) would have been infinite.

A simple formula gives the effective relaxation time, τ_i', of a mechanism, i, of inherent mechanical relaxation time τ_i, when the rate at which mechanisms i are transformed chemically into other structures is k_i (10, 11).

$$1/\tau_i' = 1/\tau_i + k_i \tag{5}$$

If k_i is zero, the gel is permanent and the measured relaxation time and the observed relaxation behavior correspond to τ_i. In that case, if τ_i is infinite, so is τ_i'. On the other hand, if k_i is finite, then τ_i' will be finite, even if τ_i is infinite. In other words, even if, over any period of time, the reversible and permanent gel have indistinguishable structures and, inherently, possess the same spectrum of mechanical relaxation times, τ_i, the reversible gel will be characterized by a truncated spectrum. Relaxation times longer than $1/k_i$ will be bypassed by relaxation through the chemical reaction. A reversible gel is thus liquidlike and cannot support itself against mechanical stresses over times in excess of $1/k_i$. Moreover, if the volume of solvent

accessible to the reversibly cross-linked macromolecular building blocks is not confined, the system will dilute itself to the maximum extent possible.

Under what conditions will a solution of macromolecular building blocks form a reversible gel? The conditions must be such that strong, sufficiently long-lived interactions between segments of the polymer (i.e., cross-links) can arise. The concentration of the building blocks, therefore, should be in the range where the coils will interpenetrate and overlap on the average. If the interactions are strong enough, effective polymer–polymer associations can occur even in dilute systems, and would lead to a cross-link-induced phase separation in which the concentrated, the gel, phase would again be in coil overlap. We know, indeed, that if the polymer segment–segment interaction is favored energetically, a phase separation will occur whether or not a gel is formed. The energy change, $\Delta\epsilon$, per contact when we replace two segment–solvent contacts and form a segment–segment and a solvent–solvent contact, is

$$\Delta\epsilon = \epsilon_{pp} + \epsilon_{oo} - 2\epsilon_{po} \qquad (6)$$

Phase separations can occur when

$$\chi \geq \tfrac{1}{2}[1/(1 + P^{1/2})] \qquad (7)$$

In terms of $\Delta\epsilon$, the Flory–Huggins parameter, χ, referred to in connection with equation 3, is given by

$$\chi = \text{constant } (-\Delta\epsilon/k_B T) \qquad (8)$$

where k_B is the Boltzmann constant and T is absolute temperature. In the case of most polymer–solvent pairs $\Delta\epsilon < 0$ and for solubility $\chi < \tfrac{1}{2}$.

The strong polymer–polymer contacts that are needed to make long-lived cross-links require negative ϵ_{pp} values that are much greater in absolute terms. These values lead to a very large χ, much in excess of $\tfrac{1}{2}$. There are, thus, conflicting requirements to be fulfilled. To render the system soluble, χ must be less than $\tfrac{1}{2}$. Only very short lifetimes can result from polymer–polymer contacts in such a case, even if allowance is made for the fact that it is not the difference in equilibrium energy levels that determines the reaction rate, but the level of the activated state. On the other hand, to make the system gel (i.e., to render the cross-link sufficiently stable), the interaction has to be strong. Thus, only a copolymer can give rise to reversible gels. A minority segment that interacts very strongly with itself must be present in the structure. This situation then permits the remainder of the chain to be in stable solution.

The lifetime of the cross-link, however, can be increased if a number

of adjoining minority segments in the chain, simultaneously present at one site, interact with a number of adjoining segments of this kind at another site. In such a case, the difference in the strength of the overall bonding interaction can be made to depend less and less on the contribution of the individual contact. A difference in steric matching between interacting segments of similar chemistry is then enough to give a bond of sufficient strength. Hence even a "stereo copolymer", an atactic chain on which syndiotactic and isotactic sequences alternate, can give rise to long-lived bonds. An example is poly(methacrylic acid) (12). In this case, two syndiotactic sequences of sufficient length, when matched to each other, give rise to a very effective bond. In all cases of reversible gelation, therefore, the majority of segments in the chain do not form long-lived interactions, but behave as though they were "in good solution", whereas some other segments, present in minority, form the long-lived correlations.

Reversibly Cross-Linked Aqueous Gels

Most interactions in water involve hydrogen bonds that either promote the hydrogen bonding of two solute particles to each other or promote the hydrogen bonding of water to itself because of the inability (hydrophobic character) of a group on a particle to interact in a hydrogen bond. The energy level of most interactions in water is thus scaled by the relatively low energy level of the hydrogen bond. It follows that individual contacts carry little permanence with them as is obvious from the fact that water is a low-viscosity, Newtonian fluid.

Many important structures, mainly in the biological world, exist as aqueous systems and enjoy lifetimes that are markedly longer than that of a water–water association. This difference in lifetimes can be explained by the prevalence of cooperative bonding in such systems. Whole sections of macromolecular chains are associated in parallel arrangements that permit a very effective locking-in of reaction partners in a zipperlike fashion. Although any tendency to add one more bond to the zipper is highly reversible, the probability that the whole zipper will open is cumulatively small. The bonds, although by no means permanent, have acquired a very long lifetime. The so-called α-helix or β-sheet arrangement that characterizes the structure and folding of many proteins is based mainly on sets of cooperatively joined hydrogen bonds. The same is true for the strand pairing of nucleic acids and the structures adopted by many other fiber-producing biopolymers. These principles are very well illustrated by a very simple synthetic polymer, poly(methacrylic acid).

Poly(methacrylic acid) can ionize in an aqueous environment, can form hydrogen bonds with its carboxyl groups, and can create hydrophobic interactions with its methyl groups. It is, moreover, an inherently stiff chain. Every second main-chain carbon atom carries two substituent side chains

upon it. This structure severely hinders rotation. The carbon atoms so involved are asymmetric, and both isotactic and syndiotactic placements of the monomers are a possibility. Two syndiotactic sequences of poly(methacrylic acid) associate very well with each other, and the strength of the bond increases with the length of the matched stereospecific sequence. The purely syndiotactic chain is so heavily agglomerated that it is essentially insoluble in water. Only if the chains are charged by neutralization will the purely syndiotactic chain go into solution.

Atactic poly(methacrylic acid), on the other hand, is soluble, but at some concentration beyond macromolecular coil overlap, it forms totally transparent, very stiff gels (*13*). At these concentrations, the pH of the system is low, and most carboxyl groups are un-ionized. Hydrogen bonds and hydrophobic interactions between syndiotactic sequences some 10 or more monomers long produce the cross-links that characterize the gel. Because strong bonding is confined to adequately long, matching stereo sequences, the number of strong chain–chain associations is limited and a total collapse of the system is prevented. The hydrophobic character of these bonds is evident because gel strength increases with temperature, there is a lower critical temperature for phase separation, and there is a gel–sol transition upon cooling (*14*). The finite lifetime of the cross-link is shown by the fact that the "gel" flows, given adequate periods of time.

Poly(methacrylic acid) is, indeed, a most remarkable polymer (*12*). Studies of its behavior in aqueous systems can be made to illustrate almost everything that characterizes water as a solvent for polymeric systems (*15*).

Conclusions

Water-based permanent gels are not structurally different from other permanent gel systems. They acquire special character mainly when they are ionized and the ionic strength of the medium is sufficiently low. Suitable copolymers in aqueous solution can form a vast variety of reversible gel systems because of the moderately strong, primary interactions possible within the aqueous environment. Structural organization (mainly cooperative effects) are then used, to a limited extent, to create sufficiently long-lived bonds that form gels of adequately long relaxation and cross-link turnover times.

References

1. Meyer, F. A.; Gelman, R. A.; Silberberg, A. In *Hydrogels for Medical and Related Applications*; Andrade, Joseph D., Ed.; ACS Symposium Series 31; American Chemical Society: Washington, DC, 1976; pp 52–59.
2. Silberberg, A. *Macromolecules* **1980**, *13*, 742.
3. Silberberg, A. In *Tissue Fluid Pressure and Composition*; Hargens, A. R., Ed.; Waverly: Baltimore, 1981; p 71.

4. Flory, P. J. *J. Chem. Phys.* **1949**, *17*, 303.
5. DeGennes, P.-G. *Scaling Concepts in Polymer Physics*; Cornell University Press: Ithaca, NY, 1979; p 152.
6. Hill, T. L. *An Introduction to Statistical Thermodynamics*; Addison–Wesley: Reading, PA, 1960; p 414.
7. Katchalsky, A.; Michaeli, I. *J. Polym. Sci.* **1955**, *15*, 69.
8. Weiss, N.; van Vliet, T.; Silberberg, A. *J. Polym. Sci., Polym. Phys. Ed.* **1979**, *17*, 2229.
9. Weiss, N.; Silberberg, A. *Br. Polym. J.* **1977**, *June*, 144.
10. Silberberg, A.; Hennenberg, M. *Nature* **1984**, *312*, 746.
11. Hill, T. L. *An Introduction to Statistical Thermodynamics*; Addison–Wesley: Reading, PA, 1960; p 409.
12. Eliassaf, A.; Silberberg, A.; Katchalsky, A. *Nature* **1955**, *176*, 1119.
13. Silberberg, A.; Mijnlieff, P. F. *J. Polym. Sci., Part A-2* **1970**, *8*, 1089.
14. Eliassaf, J.; Silberberg, A. *Polymer* **1962**, *3*, 555.
15. Priel, Z.; Silberberg, A. *J. Polym. Sci., Part A-2* **1970**, *8*, 689.

Structure and Swelling of Some Synthetic, Semisynthetic, and Biopolymer Hydrogels

W.-M. Kulicke and H. Nottelmann

Institut für Technische und Makromolekulare Chemie, Universität Hamburg, Bundesstrasse 45, 2000 Hamburg 13, Federal Republic of Germany

The water absorption capacity of some synthetic, semisynthetic, and biopolymer hydrogels was studied in distilled water. The swelling behavior in both water and salt solutions (M^+, M^{2+}, ...) was studied for various hydrogels. Comparable networks were synthesized by starting with a nonionic polyacrylamide gel and then by introducing ionic groups via polymer-analogous reactions. Rheological investigations of a few gels were performed, and the cross-linking efficiency was between 5% and 36% of the value calculated by using purely stoichiometric methods. The discrepancy in cross-linking efficiencies is probably caused by the lack of homogeneity of the networks.

H YDROGELS ARE WATER-SWELLABLE, THREE-DIMENSIONAL polymeric networks. Interest in hydrogels has increased in the past several years as new applications have been discovered (1). The capacity of the hydrogels to absorb water is enormous and can be as much as 1000 times the weight of the polymer. For this reason, hydrogels are used in many fields. Some of the applications of hydrogels are

- Hydrogels are used as thickening agents (e.g., starch and gelatin) in foods.
- Hydrogels are used in pharmaceutical preparations (2) as solubility enhancers or as time-release preparations. The hydro-
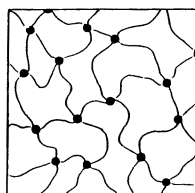
gels are needed because orally administered treatments must
either diffuse very quickly or be released in gradual doses over
a long period of time.

- The continuous release of moisture to plants can be regulated
  by the addition of hydrogels (3).

- The addition of hydrogel-forming agents to incontinence prod-
  ucts increases the fluid uptake and ensures improved retention
  capacity (4, 5).

- Technical and electronic instruments can be protected from
  corrosion and short-circuit by enclosure of, or sheathing with,
  highly absorbent hydrogel-forming agents (6).

- In electrophoresis and chromatography, the separation and dif-
  fusion characteristics of the gel structure are exploited. Hy-
  drogels, thus applied, operate within only a very limited range
  of swelling (7).

- Hydrogels are used in photographic technology because they
  are light-permeable and can also store light-sensitive sub-
  stances.

- Hydrogels are used in the manufacture of soft contact lenses
  because they ensure gas and moisture exchange with the eye
  (8).

The gel system must be adapted to meet the specific requirements.
As shown in Figure 1, gels can be differentiated by cross-linking into
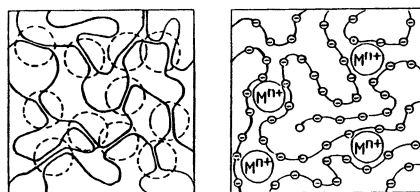
physical   ionotropic
secondary valence network bondings

Figure 1. Schematic representation of   covalent
hydrogel structures.   primary valence network bondings

secondary and primary valence-linked polymeric networks. In physically valence-linked gels, the network structure is formed by either physical interactions from van der Waals forces or by hydrogen bonds (e. g., as in native starch) or by ionic interactions (predominantly with multivalent metal cations). The latter are called *ionotropic gels*. This study focuses on covalent cross-linked polymeric ionic and nonionic networks. Figure 2 shows that this type of network may be prepared either by using bifunctional monomers and multifunctional cross-linking agents or by using the reactive side or end groups of linear polymers. End groups are used especially in the preparation of biopolymer networks.

The sources of the varying water-bonding capacities and the underlying molecular structures that govern the stability of the hydrogels are largely unexplained. A gel always consists of a three-dimensional polymeric network and a fluid. If the interactions of the components are strong enough, the polymer network immobilizes the fluid, which, in turn, prevents collapse of the network structure. The gel state lies between solid and liquid, and it can be easily influenced by temperature, pressure, and solvent quality. The influence of solvent quality is very strong with polyelectrolytic hydrogels
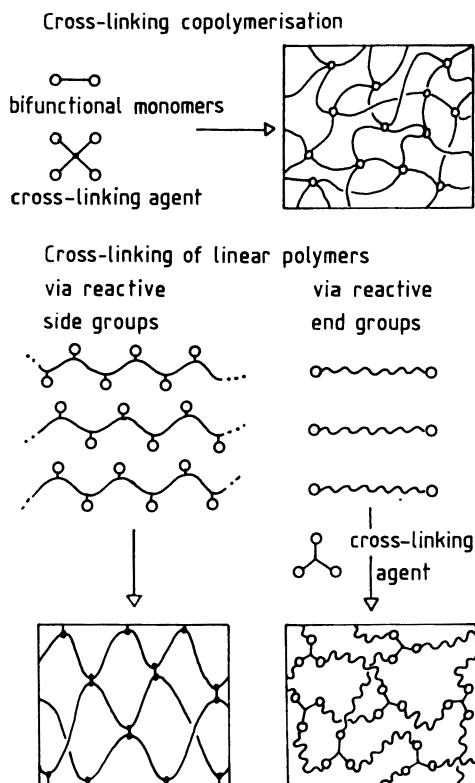
Cross-linking copolymerisation

bifunctional monomers

cross-linking agent

Cross-linking of linear polymers
via reactive   via reactive
side groups   end groups

cross-linking agent

Figure 2. Typical cross-linking reactions that form covalent network structures.

(8–10). The addition of a low molecular weight electrolyte can result in a reduction of absorption capacity by several orders of magnitude. Furthermore, synthetic polymers are limited in their range of application by food regulations. To better evaluate the advantages and disadvantages of hydrogels, it is necessary to carry out basic investigations into their swelling capacities in relation to the following parameters: type of network (physical, covalent, or ionic); chemical nature; mesh width (molecular weight between two entanglement coupling points $[M_e]$); and entanglement density, to name but a few. The macrostructure of such systems may be characterized, with the aid of rheology, by correlation of plateau modulus G_p' with mesh width M_e by using the theory of rubber elasticity (11).

Experimental Details

Synthetic Gels. The synthetic hydrogels were produced (with total gel masses of 10 g) by radical copolymerization in aqueous solution with a redox initiator system of ammonium peroxodisulfate $((NH_4)_2S_2O_8)$ and N,N,N',N'-tetramethylethylenediamine (TEMED) (12, 13).

Nonionic Gels. Poly(acrylamide-co-bis(acrylamide)) (PAAm–BisAAm) gels were prepared from acrylamide (AAm) and the tetrafunctional cross-linking agent N,N'-methylenebis(acrylamide) (BisAAm), with total monomer contents of 5 and 10 wt %, respectively. The level of cross-linking agent varied between 1 and 10 wt % relative to the total initial weight of monomer. A 40-mg quantity of $(NH_4)_2S_2O_8$ and 100 μL of TEMED were added as redox initiators.

Anionic Gels. Poly(acrylamide-co-bis(acrylamide)-co-acrylate) (PAAm–AAc–BisAAm) gels were synthesized by polymer-analogous saponification with 2 M NaOH solution from PAAm–BisAAm gels of varying degrees of saponification. The acrylate content could only be raised above 67 mol % by acid hydrolysis. In this case, 0.2 M hydrochloric acid was used. Poly(2-acrylamido-2-methylpropanesulfonic acid-co-triallylamine) gels (PAMPS–TriAA) (14) were synthesized from 2-acrylamido-2-methylpropanesulfonic acid (AMPS) and the hexafunctional cross-linking agent triallylamine (TriAA). Total monomer contents were between 10 and 25 wt %. The cross-linking agent content was varied between 15 and 25 mol % relative to the total initial monomer concentration. Sodium hydroxide solution (3 M) was added to the original reaction mixture as a neutralizing agent. A 60-mg quantity of $(NH_4)_2S_2O_8$ and 100 μL of TEMED were added as redox initiators.

Cationic Gels. Poly(dimethylaminoethyl acrylate) gels (PDAEA–TriAA) were synthesized from N,N-dimethylaminoethyl acrylate (DAEA) and the hexafunctional cross-linking agent triallylamine (TriAA), with total monomer contents of 10 to 25 wt %. The cross-linking agent content was varied between 15 and 30 mol % relative to the total initial concentration of monomers. Hydrochloric acid (6 M) was added to the original reaction mixture as a neutralizing agent. Immediately after addition of the second redox component (TEMED), the reaction mixtures (still liquid) were transferred to cylindrically shaped vessels of a specific geometry that depended on the intended application. For swelling measurements, vessels with heights of 1.45 cm and diameters of 1.5 cm were used. For rheological oscillation measurements, discs of gel with diameters of 5 cm and thicknesses of 0.2 to 0.5 cm were prepared.

Semisynthetic and Biopolymer Gels. *Nonionic Gels.* Starch–phosphoryl chloride (starch–POCl₃) gels were prepared by dissolving 5 g of starch in 25 mL of 1 M NaOH solution and then cooling to 0 °C. A mixture of 0.5 g of ice-cold phosphoryl chloride and 10 g of ice water was added to the solution. For swelling measurements, the reaction mixture was transferred to vessels of defined geometry and cooled to 0 °C for a further 3 h. For rheological oscillation measurements, part of the reaction mixture was transferred directly into the apparatus. Starch-*graft*-poly(acrylamide-*co*-bis(acrylamide)) (starch-*g*-PAAm–BisAAm) gels were synthesized by dissolving 10 g of starch in 60 mL of twice-distilled water, to which 10 g of acrylamide and 0.5 g of *N,N'*-methylenebis(acrylamide) were added. An initiating solution of 2 g of ammonium cerium(IV) nitrate dissolved in 17.5 mL of twice-distilled water was added to the original reaction mixture. The resultant gel was subjected to dialysis with twice-distilled water and then was freeze-dried.

Anionic Gels. Starch-*graft*-poly(acrylamide-*co*-bis(acrylamide)-*co*-acrylate) (starch-*g*-PAAm–AAc–BisAAm) gels were prepared by polymer-analogous saponification of starch–AAm–BisAAm gels with saponification degrees of 11 and 60 mol % acrylate. Saponification was effected in 0.1 and 2.0 M NaOH solution for 7.5 and 120 h, respectively. The gels were subjected to dialysis with twice-distilled water and then freeze-dried.

(Carboxymethyl)cellulose–phosphoryl chloride gels (CMC–POCl₃) were synthesized by dissolving 4 g of CMC in twice-distilled water, to which 4 mL of a 10 M NaOH solution was added. The solution was cooled to 0 °C. Ice-cold POCl₃ (0.6 mL) was then stirred into the reaction mixture, which, after completion of gel formation, was subjected to dialysis with twice-distilled water and then was freeze-dried.

Swelling Investigations. A determination of the degree of swelling (V/V_0) was carried out for gels that had been synthesized in cylindrical vessels. V_0 represents the initial volume of the gel shape and V represents the volume in the swelled, equilibrium condition. The gels were swelled for at least a week (to ensure equilibrium conditions for all samples) in salt solutions (NaCl, MgCl₂, CaCl₂, Al(NO₃)₃) of differing concentrations. The weight and volume changes of the samples were then measured. Gel shapes that broke during the swelling process because of insufficient firmness had their volumes determined by differential weighing with an appropriate salt solution of known density. For freeze-dried gels, only the determination of the water absorption capacity (grams of H₂O per gram of polymer) was carried out.

Rheological Investigations. The oscillation measurements were carried out by using a mechanical spectrometer (Rheometrics, System Four). As can be seen from the schematic representation of the measuring system in Figure 3, a sinusoidal oscillation with a fixed deformation (γ) was transferred to a gel body that was located between the plates in a plate–plate arrangement. The deformation chosen had to guarantee that the measurement took place in the linear viscoelastic range at every instance (i.e., the complex shear modulus G^* was independent of the imposed deformation.) Between the complex shear modulus G^*, the deformation γ, and the torque M_{pp} in the plate–plate system, the following relationships applied:

$$G^* = \frac{\sigma_0}{\gamma_0} - e^{i\delta} = \frac{M_{pp}2h}{\pi R^4} \tag{1}$$

where σ_0 is the maximum shear stress; γ_0 is the maximum deformation amplitude;
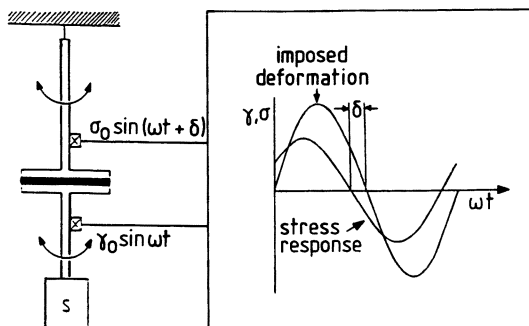
Figure 3. Schematic diagram of a mechanical oscillation measurement in the plate–plate system of a rheometer.

i is $-1^{1/2}$; δ is the phase shift; M_{pp} is the torque in the plate–plate system; h is the distance between the two plates (< 5 mm); and R is radius of the plates (25 mm).

The complex shear modulus (G^*) can be calculated from the resulting torque, and by application of complex oscillation equations, can be resolved into a real component (G') and an imaginary component, G'' according to the following equation (*15–17*).

$$G^* = G' + iG'' \qquad (2)$$

The real component, G', called the storage modulus, is a measure of the reversibly elastic storable deformation energy. The imaginary component, G'', called the loss modulus, represents a measure of the irreversible energy dissipated during flow. A hydrogel consisting of a three-dimensional polymer network and the solvent immobilized within this network represent an elastic solid. As the network structure cannot dissipate energy through flow, the resultant G'' comes from a viscous flow (η_s) of the solvent molecules within the gel, and the following equation applies:

$$G'' - \eta_s \cdot \omega \approx 0 \qquad (3)$$

The measured values of G'' are on the order of 0.1% to 5% of the value of G', so G'' can be neglected in calculations.

Figure 4 represents the basic plot of G' against ω; it can be subdivided into four phase ranges. In range (I), curve *a* is obtained for liquidlike polymer solutions
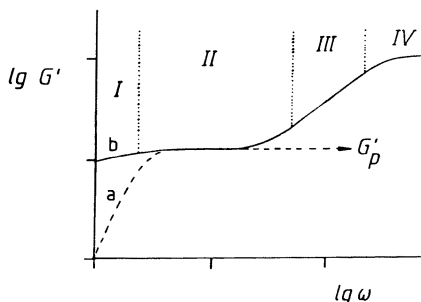

Figure 4. Basic plot of the storage modulus G' vs. frequency ω in elastic bodies.

and melts (linear or branched). For three-dimensionally cross-linked hydrogels, curve *b* and consequently the plateau range (II) is obtained; the accompanying modulus is called the plateau modulus $G_p{}'$, and it provides information about the network structure (*see* **Results and Discussion**). The subsequent regions represent the transition (III) and glass (IV) zones. In these regions, the mobilities of the chain segments can no longer maintain the applied oscillation. The oscillation energy can only be stored by deformation of the bonding angles.

NMR Investigations. ¹H and ¹³C NMR spectroscopic investigations (*18*) were carried out to determine the copolymer composition of the saponified PAAm–BisAAm gels. Bruker MSL 300 and Bruker AM 360 spectrometers were used. The gels were synthesized in 9-mm-i.d. tubes, saponified in 2 M NaOH solution, irrigated, and dried in a drying cabinet at 40 °C. The completely dried gel was then placed in an NMR tube with D_2O and swelled.

Results and Discussion

Synthetic Hydrogels. Qualitative swelling investigations on the nonionic poly(acrylamide-*co*-bis(acrylamide)) gels showed that the degree of swelling in aqueous solutions ($V/V_0 \sim 2$) does not exceed the value in the state immediately after preparation ($V/V_0 = 1$) to any significant extent. The pressure that determines the swelling is essentially influenced by three components, namely (*11, 19, 20*)

1. π_{net}, the changes in the gel volume that give rise to an elastic network pressure.

2. π_{dil}, the pressure due to dilution that occurs because of absorption of the solvent. This dilution produces a pressure that arises from the gain in entropy.

3. π_{ion}, the osmotic pressure that originates from the ions present in the gel.

When the gel is in equilibrium, these pressures must balance each other out, thus it follows that

$$\pi_{net} + \pi_{dil} + \pi_{ion} = 0 \tag{4}$$

The ionic pressure π_{ion} is a decisive factor in the swelling behavior of ionic hydrogels. It should, therefore, be possible to achieve a stronger swelling effect by the introduction of ionic groups. To this end, one of two different synthetic pathways can be followed: copolymerization and polymer-analogous reaction (*21*). In this study, the latter path was taken (i.e., a nonionic gel was synthesized from AAm and BisAAm and then partially saponified). This method had the advantage that the network structure of the nonionic gel was consistent with that of the synthesized ionic gels, which had varying

degrees of saponification. The method of synthesis is represented schematically in Scheme I.

The experimental results obtained from linear poly(acrylamide-*co*-acrylate) are of interest in this respect (*21–23*). Figure 5 compares the change in relative viscosity (η_{rel}) as a function of the comonomer composition for polymer mixtures of PAAm with PAAcNa with that of PAAm-*co*-AAcNa, which was obtained by a polymer-analogous reaction (i.e., by alkaline and acid hydrolysis). Figure 5 shows that for alkaline hydrolysis the viscosity increases strongly as a function of the degree of polymerization and salt concentration and reaches a maximum at approximately 33 mol % of the acrylate portion. Samples with lower acrylamide contents can only be achieved by further acid hydrolysis. The reason for this behavior can be described statistically. At the maximum viscosity during alkaline hydrolysis,
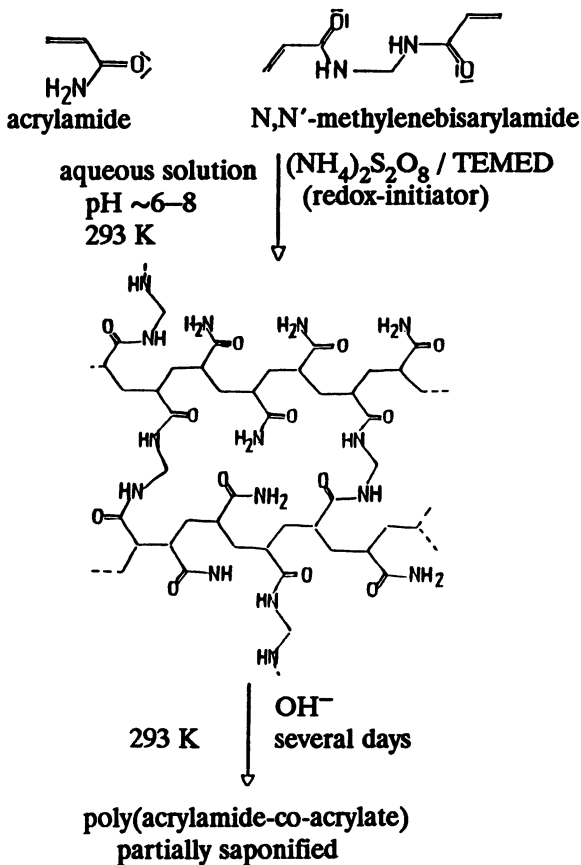
Scheme I. *Schematic pathway for the synthesis of PAAm–BisAAm gels with subsequent saponification to PAAM–BisAAm gels.*

two acrylate groups lie adjacent to an acrylamide group in the medium, and thus present a screen against attack by like-charged hydroxyl ions. Table I, as calculated from ^{13}C NMR investigations, shows that this finding is at least approximately correct. The interpretation of the polymer signals (peaks and triads) are from ref. 24.

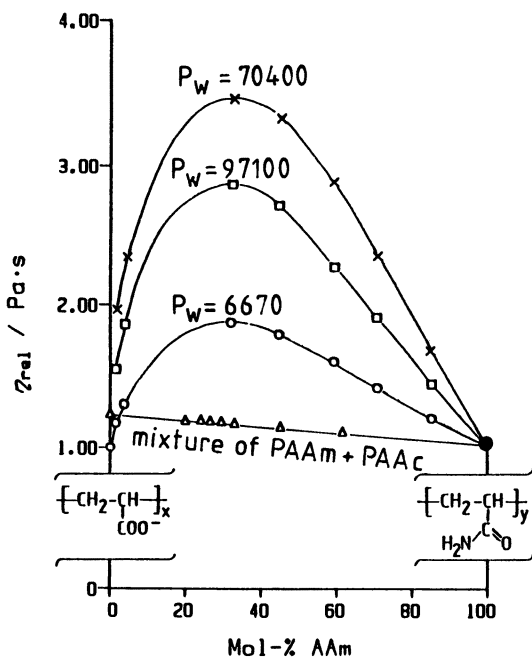At 60 mol % of the acrylate component, the two permitted triad ar-

Figure 5. Comparison of the dependence of the relative viscosity (η_{rel}) of saponified, linear poly(acrylamide-co-acrylate). P_w is the degree of polymerization.

Table I. Triad Distribution in 60 mol % Hydrolyzed Poly(AAm–PAAm–BisAAm) Gel from ^{13}C NMR Investigations

Monomer Triad	^{13}C NMR Signal Position (ppm)	Acrylate (%)
AAc–AAc–AAc	185.1	8
AAc–AAc–AAm	184.6	35
AAm–AAc–AAm	183.9	17
AAc–AAm–AAc	181.6	37
AAm–AAm–AAc	181.2	3
AAm–AAm–AAm	—	—

rangements AAc–AAc–AAm and AAc–AAm–AAc total 72%. The triads, which relative to the ideal state are not allowed, such as AAm–AAc–AAm and AAm–AAm–AAc account for 17% and 3%, respectively. It must be possible that similar proportions would be found during the alkaline hydrolysis of hydrogels. This condition would also have to result in a greater increase in swelling. Figure 6 shows the dependence of the degree of swelling of polymerlike saponified PAAm–BisAAm gels on the $CaCl_2$ concentration. The values on the abscissa represent the degrees of swelling determined in distilled water.

Theoretically, the degree of swelling of PAAm–AAc–BisAAm gels rises with increasing acrylate content. When 0.01 M NaOH solution is used for the polymer-analogous saponification of PAAm–BisAAm, a maximum saponification degree of only approximately 25 mol % acrylate is obtained (19). However if the saponification is carried out in 2 M NaOH solution or at higher concentrations, a saponification degree of approximately 64 mol % acrylate portion can be obtained, which is similar to the already established findings for linear poly(acrylamide-co-acrylates).

Figure 6 shows that the gel saponified to a degree of 64 mol % acrylate exhibits the maximum degree of swelling. This result is seen by comparison to a gel with 78 mol % acrylate produced by further acid hydrolysis, which shows a decrease in the degree of swelling after passing through a maximum. Although nonionic, unsaponified PAAm–BisAAm gel shows no recognizable dependence on concentration, the anionic saponified PAAm–AAc–BisAAm
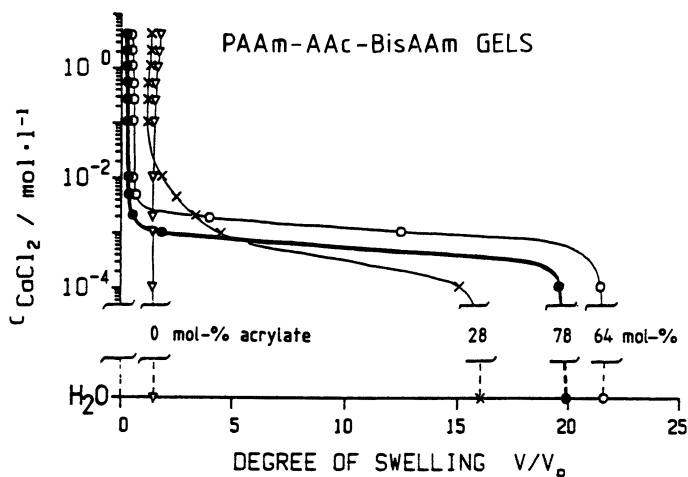

Figure 6. Influence of the degree of hydrolysis (mol % AAc) of PAAM–AAc–BisAAm gels on the degree of swelling, relative to the $CaCl_2$ concentration.

gels exhibit distinct sol–gel phase transitions in the concentration range between 5×10^{-3} and 1×10^{-3} mol L^{-1} $CaCl_2$ (25).

Figure 7 illustrates the influence of the total monomer concentration in preparation on the degree of swelling in $CaCl_2$ solutions of different concentrations. The results shown are for two PAAm–AAc–BisAAm gels saponified to a degree of 64 mol %. In both cases, the content of cross-linking agent amounted to 3 wt %. In the ideal case, both gels should exhibit the same average molecular weight between two entanglement points, and accordingly the gel with the higher total initial weight of monomer should have the higher degree of swelling in a thermodynamically good solvent. In contrast to this theoretical prediction, however, the 5-wt % gel, with V/V_0 = 42 in distilled water, attained a degree of swelling twice that of the gel synthesized with an initial monomer content of 10 wt % (V/V_0 = 21). The number of effective entanglement points in the 5-wt % gel must, therefore, be considerably lower. An explanation for this behavior is offered by the occurrence of inhomogeneities within the network during synthesis. This phenomenon is frequently mentioned in the literature. (*See* **Hydrogel Comparison.**)
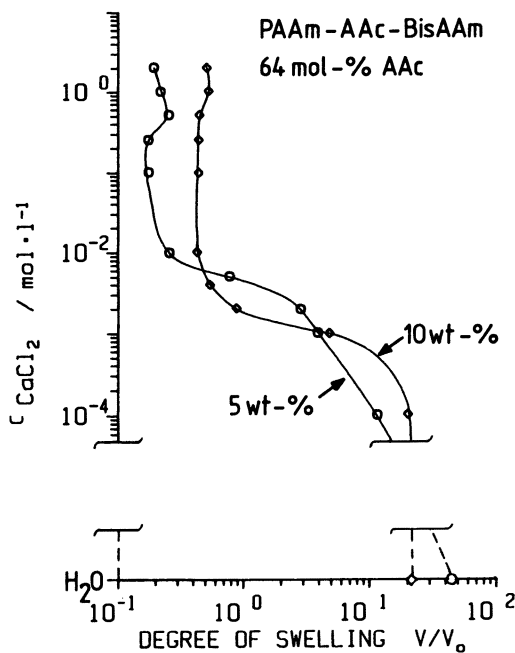

Figure 7. Influence of the total monomer concentration on the degree of swelling of 60 mol % saponified PAAM–AAc–BisAAm gels relative to the $CaCl_2$ concentration.

Figure 7 shows that the PAAm–AAc–BisAAm gel synthesized with a lower total polymer concentration shrinks more markedly at higher salt concentrations ($> 10^{-2}$ mol L^{-1} $CaCl_2$). This behavior corresponds to that predicted by Hild et al. (26), who applied the scaling concept developed by DeGennes (27). According to this concept, the osmotic pressure in semi-concentrated solutions is a function of the total polymer concentration. In solutions with lower salt concentrations, the polyelectrolytic character of the PAAm–AAc–BisAAm gels becomes noticeable. Because of electrostatic repulsion, an expansion of the polymeric network takes place, and the classical scaling concept does not lead to satisfactory predictions. If, as is represented in Figure 8, only the content of cross-linking agent is varied, then it can be established that the degree of swelling in distilled water increases in almost inverse proportion to the content of cross-linking agent. This effect can be attributed to the higher swelling capacity of networks with larger mesh widths (28, 29).

Unlike the situation when the total monomer content is varied, no dependence on cross-linking agent content is observed above 5×10^{-3} mol L^{-1} $CaCl_2$. The swelling behavior in solutions of higher salt concentrations
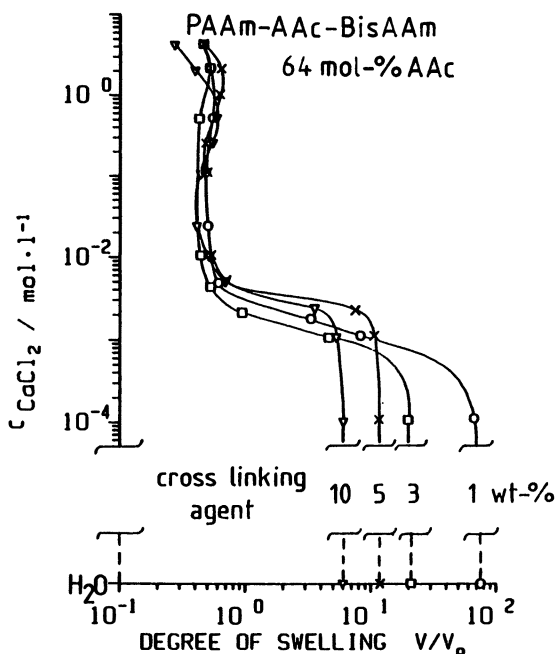

Figure 8. Influence of the cross-linking agent content on the degree of swelling relative to the $CaCl_2$ concentration for 64 mol % saponified PAAm–AAc–BisAAm gels.

is, thus, essentially dependent on the total initial monomer content rather than on the content of cross-linking agent.

The hydrogels' stability to salts and associated swelling capacities play a special role in technical applications. For PAAm–AAc–BisAAm gels, polymers with a polyelectrolytic character are involved that would have to react particularly strongly to a change in salt concentration. It is, therefore, especially important to investigate the influence of differently charged electrolyte solutions on the degree of swelling. Although the swelling behavior of anionic gels is largely independent of the concentration of the electrolytic anions, it is not independent of the concentration of the cations (*30*). Figure 9 shows the dependence of the degree of swelling on the concentrations of various M^{n+} salt solutions with a PAAm–AAc–BisAAm gel saponified to 64 mol % (*31*). The gel will remain stable up to an Na^+ concentration of approximately 5×10^{-3} mol L^{-1}; however, the influence of Mg^{2+} ions at concentrations above 1×10^{-4} mol L^{-1} leads to gel shrinkage. Al^{3+} ions have the same effect and cause gels to shrink drastically at lower concentrations. Although influenced by a 2 M NaCl solution, the degree of swelling has a value of approximately 2, which lies above the value in the preparation state ($V/V_0 = 1$). The degree of swelling falls just below that of the prep-
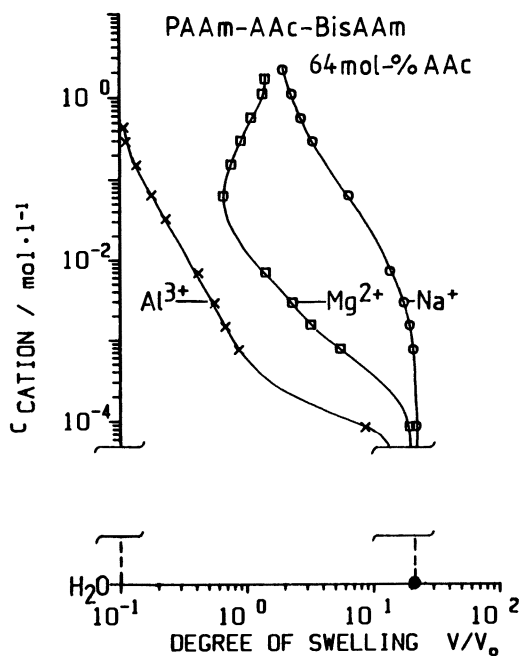

Figure 9. *Influence of the M^{n+} concentration (Na^+, Mg^{2+}, Al^{3+}) on the degree of swelling for 64 mol % saponified PAAM–AAc–BisAAm gels.*

aration state and increases again above 0.6 mol L^{-1} under the influence of 0.01 mol L^{-1} magnesium salt solution. The influence of the Al^{3+} ions is very drastic, and the degree of swelling falls below 1 even at 5×10^{-4} mol L^{-1} and leads subsequently to a continual collapse of the gel.

The increase of the degree of swelling at high magnesium salt concentrations can be attributed to a reverse in the polarity of the polyelectrolyte network. The network now bears positive charges (RCOO$^-$Mg$^+$) that cause a rise in the osmotic pressure and hence an increase in the degree of swelling (31). No such reverse in polarity occurs and thus no increase in the degree of swelling is observed for Ca^{2+} ions (Figure 7). In contrast to Mg^{2+} ions, Ca^{2+} ions have a considerably stronger tendency to form insoluble alkaline earth carboxylates that may account for the divergent behavior. Furthermore, a chelating effect cannot be excluded, which, in the case of the Al^{3+} ions, presumably represents the decisive factor in the collapse of the gel.

Mechanical oscillation measurements could only be carried out on nonionic PAAm–BisAAm gels. Because of their high degree of swelling, the saponified swelled gels could not be cut into suitable samples without their being destroyed. Via the theory of rubber elasticity developed by Flory (32), the value of the plateau modulus (G_p') obtained by mechanical oscillation measurements is directly related to the number of elastically effective chains per unit volume (ν_e).

$$G_p' = (1 - 2/f)\nu_e RT \frac{<r^2>}{<r_0^2>} \tag{5}$$

where G_p' is in Pa, ν_e is in mol m^{-3}, f is the functionality of the cross-linking agent, R is the universal gas constant (8.314 J mol^{-1}K^{-1}), T is the absolute temperature, $<r^2>$ represents the average square end-to-end distance in the swelled state, and $<r_0^2>$ is this distance in the preparation state. The gels prepared in this work were measured only in the unswelled state (i.e., $<r^2> = <r_0^2>$), and the quotient in equation 5 was 1 and can was ignored. The number of elastically effective chains per unit volume (ν_e) is linked to the number of elastically effective, covalent entanglement points (n_e) via the functionality of the cross-linking agent (f). The following applies:

$$\nu_e = (f/2)n_e \tag{6}$$

where ν_e is in mol m^{-3}.

On the other hand, as the following relationship applies between the mesh width M_e (molecular weight between two entanglement points) and the number of elastically effective covalent entanglement points (n_e)

$$n_e = C/M_e \tag{7}$$

n_e is in mol m^{-3}; C is the total monomer concentration in kg m^{-3}; and M_e is in kg mol^{-1}. The following correlation between the various parameters and the plateau modulus G_p' applies:

$$G_p' = \left(1 - \frac{2}{f}\right)\nu_e RT = \frac{f-2}{2}\, n_e RT = \frac{(f-2)C}{2M_e}\, RT \qquad (8)$$

The comparison of the theoretical values with those determined from G_p' supplies information about the effectiveness of the cross-linking agent and the homogeneity of the gel solid. The mechanical oscillation measurements were carried out on PAAm–BisAAm gels for which both the total monomer and cross-linking agent contents were varied.

Figure 10 shows the typical course of the storage modulus G' plotted against the oscillation frequency ω, for 5 wt % PAAm–BisAAm with a cross-linking agent content of 3 wt % relative to the total initial monomer weight. The accompanying value of the plateau modulus is approximately 2150 Pa. As can be seen from Figure 10, the plateau modulus does not change over a range of at least 3 decades of ω.

Figure 11 shows the dependence of the plateau modulus on the content of cross-linking agent for PAAm–BisAAm gels with 5 and 10 wt % total initial weight of monomer. The number of elastically effective chains, which is proportional to G_p', decreases after passing through a maximum.

Table II contains the values for the number of elastically effective entanglement points both as calculated from G_p' ($n_e(\exp)$) and as calculated theoretically for an ideal network ($n_e(\text{theo})$). The ratio $n_e(\exp)/n_e(\text{theo})$ re-
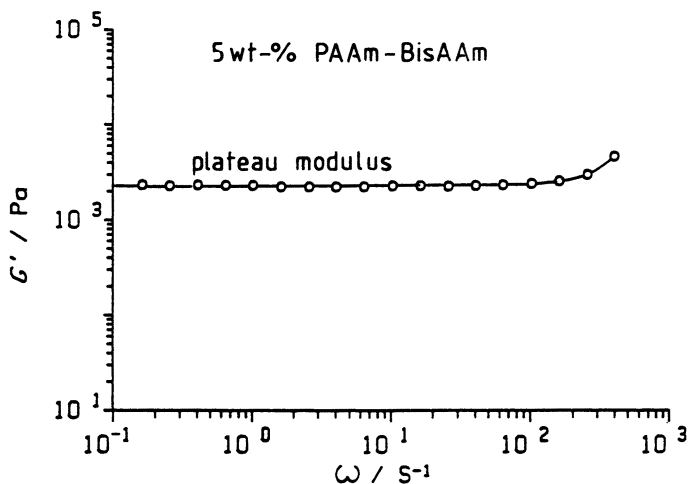

Figure 10. Plateau region of the material function G' against ω for a 5 wt % nonionic PAAM–BisAAm gel.

flects the effectiveness of cross-linking. As can be gathered from the table, the effectiveness of the cross-linking agent lies between approximately 5 and 36% and increases with decreasing proportion of cross-linking agent. These data emerge from the comparison of PAAm–BisAAm gels with the same proportion of cross-linking agent and differing total initial monomer weights (5 and 10 wt %). The effectiveness of cross-linking is approximately 1.5 to 2 times greater for the sample with the higher initial weight of monomer. Both the maximum behavior and the concentration-related effectiveness of the cross-linking agent can be attributed to the occurrence of inhomogeneities within the network, as has already emerged from the swelling measurements (cf. **Hydrogel Comparison**).

In addition to the anionic PAAm–AAc–BisAAm gels, additional anionic (PAMPS–TriAA) and cationic (PDAEA–TriAA) gels were also synthesized. The schematic reaction path is displayed in Scheme II for both types of gels and shows that all the reaction conditions are comparable, with the exception of the monomers and neutralizing agents.

Instead of N,N'-methylenebis(acrylamide), triallylamine was chosen as the cross-linking agent. Because of its higher functionality, triallylamine use should have been more efficient, although steric hindrance probably led to only a small percentage being converted to a hexafunctional cross-linking agent. Additionally, triallylamine, as opposed to bis(acrylamide), guarantees that the resulting product may be used in applications subject to food regulations (being a tertiary amine, it cannot form nitrosamine). The use of PAMPS as opposed to poly(acrylamide-co-acrylates) should ensure a greater stability to salts (33).
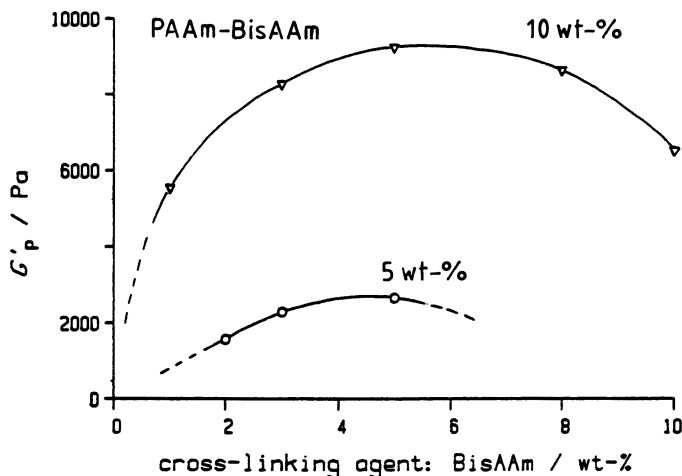

Figure 11. Dependence of the plateau modulus G_p' on the cross-linking agent content (wt %).

Table II. Elastically Effective Entanglement Points as Calculated from G_p' and
for an Ideal Network

BisAAm (*wt %*)	G_p' (*Pa*)	n_e (*exp*) (*mol m^{-3}*)	n_e (*theo*) (*mol m^{-3}*)	n_e (*exp*)/n_e (*theo*)
Total amount of monomer: 5 wt %				
2	1,540	0.62	6.49	0.10
3	2,150	0.87	9.73	0.09
5	2,250	0.91	16.22	0.06
Total amount of monomer: 10 wt %				
1	5,830	2.35	6.49	0.36
3	9,900	3.99	19.46	0.21
5	11,030	4.45	32.43	0.13
10	7,780	3.14	64.86	0.05
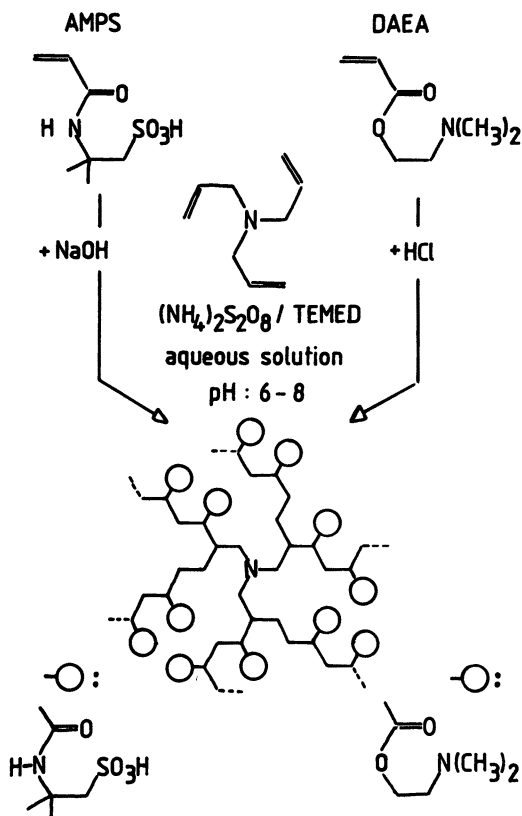
Scheme II. *Synthetic pathway for the production of PAMPS and PDAEA gels with triallylamine as the cross-linking agent.*

Figure 12 illustrates the dependence of the degree of swelling on $Al(NO_3)_3$ concentration. The cross-linking agent contents of a 15 wt % PAMPS–TriAA gel is plotted against the $Al(NO_3)_3$ concentration. The gel with the lower concentration of cross-linking agent (15 mol %) obtained a degree of swelling (V/V_0) of 71 in distilled water. This value is approximately double the degree of swelling (34) obtained for the gel with the higher concentration of cross-linking agent (25 mol %). In both cases, shrinkage of the gel body occurs at $Al(NO_3)_3$ concentrations of approximately 5×10^{-4} mol L^{-1}. For all higher salt concentrations, the degree of swelling follows a more or less identical course, and has values in the range approximately 1.8 to 3. Here too, as in the examples of saponified PAAm–AAc–BisAAm gels, the degree of swelling is independent of the cross-linking agent content at higher salt concentrations. In highly dilute salt solutions, the gel with the lower content of cross-linking agent exhibits a high degree of swelling because of the large mesh width.

Figure 13 shows the influence of multivalent cations on the degree of swelling for PAMPS–TriAA gels. In sodium salt solutions above a concentration of 5×10^{-3} mol L^{-1} only a small decrease in the degree of swelling is observed $(V/V_0 = 5$ at 0.5 mol L^{-1}.) The influence of magnesium and
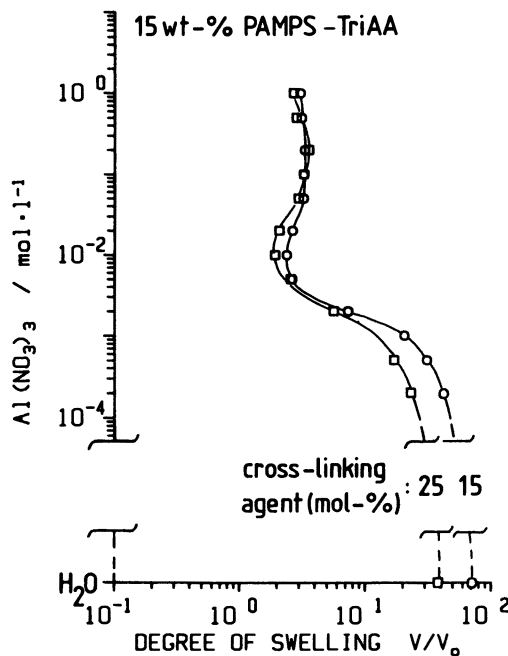

Figure 12. Influence of the cross-linking agent content of 15 wt % PAMPS–TriAA gels relative to the $Al(NO_3)_3$ concentration.

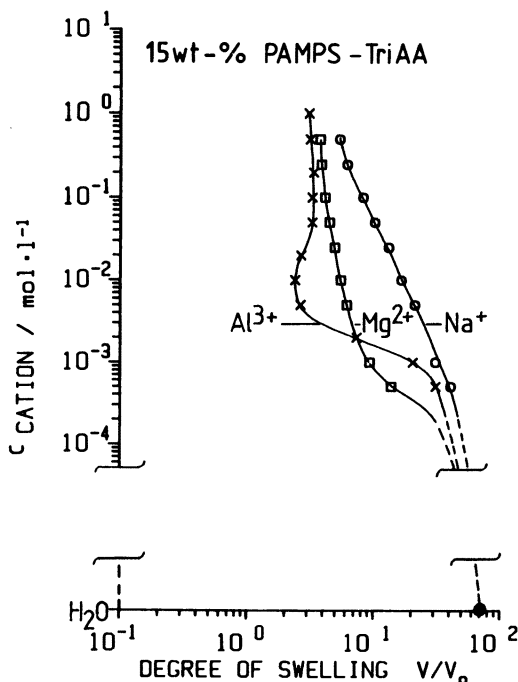*Figure 13. Influence of the M^+ concentration (Na^+, Mg^{2+}, Al^{3+}) on the degree of swelling for 15 wt % PAMPS–TriAA gels.*

aluminum ions, however, shows a significant phase transition. For increasing salt concentration, the magnesium ions at first display a greater influence on the degree of swelling than the aluminum ions, and, with increasing concentration, a steady reduction in the degree of swelling can similarly be observed. At a magnesium ion concentration of 0.5 mol L^{-1}, the degree of swelling has a value of 3.7. The shrinkage that occurs at an aluminum ion concentration of approximately 5×10^{-3} mol L^{-1} is very drastic. It does not, however, lead to a collapse of the gel, but instead, after passing through a minimum at 10^{-2} mol L^{-1} with $V/V_0 = 2.4$, shows a slight increase up to 3.2.

The PAMPS–TriAA gels, accordingly, exhibit a higher salt stability than the PAAm–AAc–BisAAm gels. Because the molecular weight of AMPS is approximately 3 times that of acrylamide, higher weights of this monomer must be used to obtain the same concentration and elasticity in the gel. Rheological investigations have only been carried out in a random manner, and no conclusive statements have yet been made on this subject.

A similar method to that for the PAMPS–TriAA gel was used to synthesize the cationic PDAEA–TriAA gel, for which the degree of swelling

was determined relative to the NaCl concentration (Figure 14). The molecular weight of N,N-dimethylaminoethyl acrylate (DAEA) is only two-thirds that of AMPS; thus, gels of comparable stability should result from correspondingly lower initial monomer weights. In comparison to the strongly acidic AMPS however, DAEA is a fundamentally weaker basic monomer. As a result, less osmotic pressure is created, which means that PDAEA–TriAA gels must be synthesized from considerably higher total initial monomer weights to produce comparable degrees of swelling. Gels with initial monomer weights below 20 wt % were not manageable in the swelled state and resulted in excessively high deviations during weight and volume determinations.

For gels synthesized with a total initial monomer content of 30 wt % and a cross-linking agent proportion of 25 mol %, the degree of swelling in distilled water is 21 (Figure 14). The degree of swelling in NaCl solutions remained practically unaltered for concentrations up to approximately 5 × 10^{-3} mol L^{-1} and slowly decreased with further rise in concentration. Nevertheless, in 1 M NaCl solution, $V/V_0 = 5$. PDAEA–TriAA gels, thus, exhibit a relatively high salt stability. Rheological investigations have not been carried out.
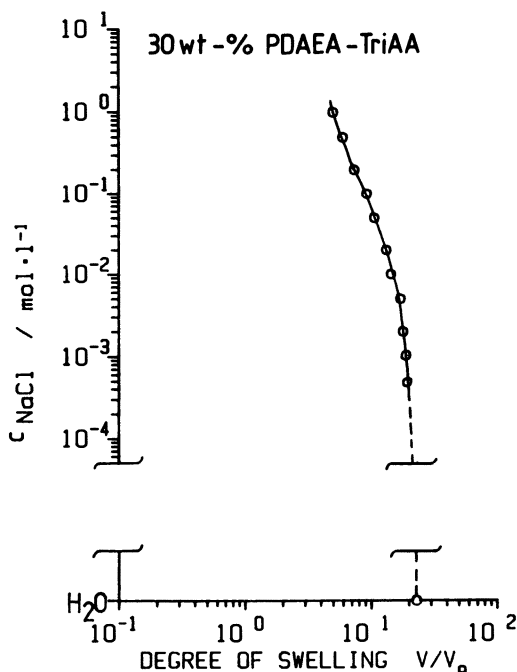

Figure 14. Influence of the NaCl concentration on the degree of swelling of 30 wt % PDAEA–TriAA gels with 25 mol % TriAA.

Biopolymer Hydrogels. The aim of this study is to present some biopolymer hydrogels based on starch and CMC derivatives. A great deal of interest has centered on these gels in recent years because starch is a naturally occurring, extremely inexpensive, and nontoxic raw material. These qualities make it particularly interesting for applications in the fields of foodstuffs, hygiene, and moisture control in agriculture (35–39).

Homogeneous cross-linking is very difficult because of insolubility in organic solvents, the high degree of crystallinity of the polymeric substrate, and the incompatibility of the substrate with many of the cross-linking agents. Biopolymers are rendered more soluble by the preparation of derivatives or dissolution in highly concentrated sodium hydroxide solutions. Numerous methods of cross-linking starch have been developed commercially. Some multifunctional cross-linking agents are epichlorohydrin, trimetaphosphate, N,N-methylenebis(acrylamide), formaldehyde, and phosphoryl chloride.

A diagram of the proposed reaction pathway for the cross-linking of starch with phosphoryl chloride is given in Scheme III; however, it remains difficult to determine the degree of cross-linking because of the heterogeneity of the samples and the low level to which cross-linking occurs. Little has been published concerning the rheological properties of hydrogels and the influence of the network structure upon them. A starch gel was prepared by cross-linking with phosphoryl chloride.

Figure 15 indicates the dependence of V/V_0 on the concentration of sodium chloride and magnesium chloride for some of the gels prepared as in Scheme III. The gels exhibit stability up to a salt concentration of 1×10^{-4} mol L^{-1}. Further increase of the Na^+ concentration leads to a decrease in V/V_0 to 1 at 1 M NaCl.

For $MgCl_2$, an increase of concentration is more effective than it is for NaCl on the reduction in the degree of swelling, and V/V_0 reaches a minimum of 0.8. Above a Mg^{2+} concentration of 0.1 mol L^{-1}, increases in V/V_0 can be attributed to a reversal in the polarity of the polyelectrolyte network. The network now bears positive charges (starch–O–Mg^+) that lead to a rise in the osmotic pressure and, hence, an increase in the degree of swelling.

The plateau modulus (G_p') for starch–$POCl_3$ gel was determined by mechanical oscillation measurements. Figure 16 represents the values of the storage moduli in the plateau region as a function of the reaction rate of starch–$POCl_3$ gel. Gel formation takes several hours to reach completion; this time requirement points to a very slow condensation during phosphate formation.

Semisynthetic Hydrogels. Starch-g-PAAm–AAc–BisAAm gels with acrylate contents of 11 and 80 mol % were produced by polymerlike saponification of starch-g-PAAm–BisAAm gels. The latter had been synthesized
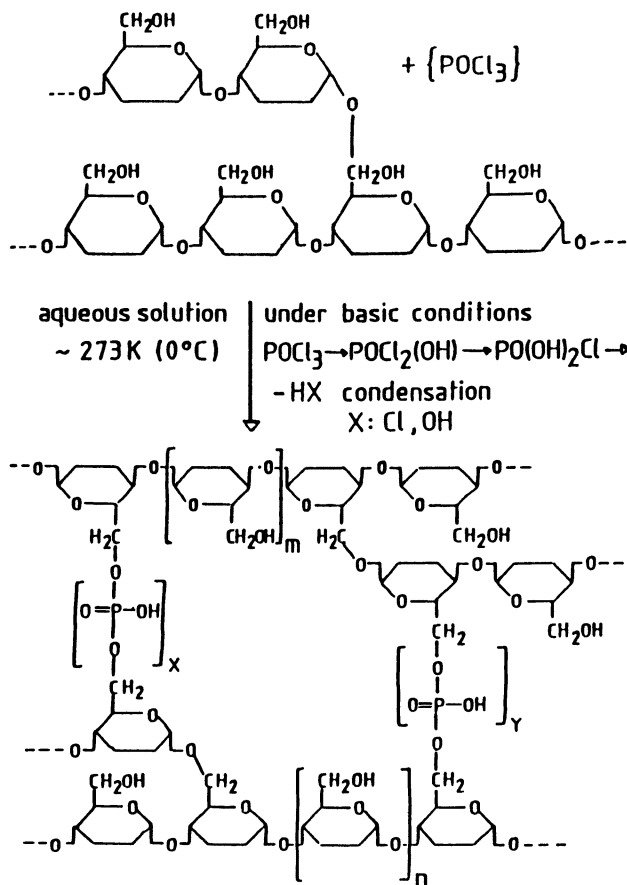
Scheme III. Synthetic pathway for the production of starch–POCl₃ gels.

by graft copolymerization of starch with acrylamide and bis(acrylamide). In Figure 17, the relationship between the degree of swelling and the Na$^+$ and Mg^{2+} concentrations is shown for an unsaponified starch-g-PAAm–BisAAm gel and the starch-g-PAAm–AAc–BisAAm gel saponified to 60 mol % acrylate. Unsaponified gel (0 mol % AAc) showed the same relationship for both Na$^+$ and Mg^{2+} concentration. Compared to the preparation state, neither swelling nor shrinking can be observed for either pure water or very high salt concentrations. Consequently, unsaponified gel possesses the same swelling behavior as nonionic PAAm–BisAAm gel. This behavior is unusual because with a starch proportion of 10 wt %, a course similar to the starch–POCl₃ would have to occur. The starch-g-PAAm–AAc–BisAAm gel, saponified to 60 mol % acrylate, has a degree of swelling of 50 in pure water.

The proportion of synthetic components in the final gel relative to the
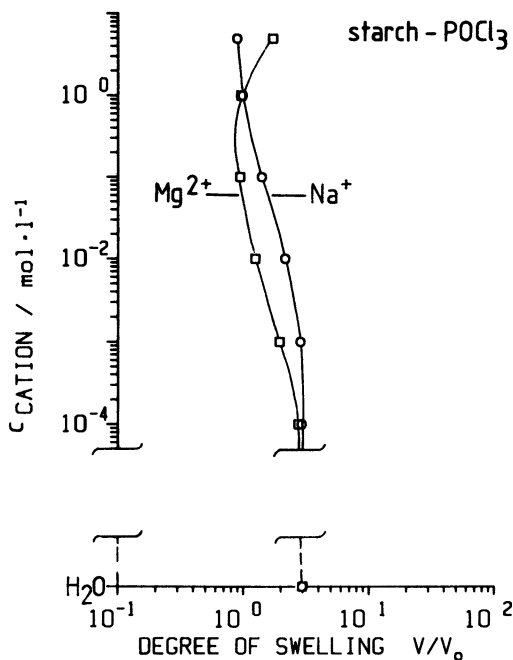
Figure 15. Influence of the Na^+ and Mg^{2+} concentration on the degree of swelling for starch–$POCl_3$ gels.

preparation condition in starch-g-PAAm–AAc–BisAAm gel was 10 wt %. The relationship of the swelling behavior to the Na^+ and Mg^{2+} concentration corresponds to that of the synthetic PAAm–AAc–BisAAm gel (Figure 9).

The degree of swelling of the synthetic gel in distilled water was 21; the degree of swelling in the saponified graft-copolymerization state with starch was 50.

The starch-g-PAAm–AAc–BisAAm gel behaves qualitatively like a corresponding PAAM–AAc–BisAAm gel. However, due to the bond with starch, it possesses a larger mesh width and thus exhibits a correspondingly higher degree of swelling. Visibly more significant inhomogeneities occur during the synthesis of the starch-g-PAAM–AAc–BisAAm gels than of the starch–$POCl_3$ gels. The swelling measurements were, therefore, carried out on crushed freeze-dried samples. Because it was not possible to synthesize uniform gel bodies, rheological investigations were not performed.

Hydrogel Comparison.   Figure 18 is a survey of the water absorption capacity for some of the synthetic, semisynthetic, and biopolymer gels. The values given refer to 1 g of dry material. For comparison, some types of gel are included in Figure 18 that were not mentioned in the previous discussion.
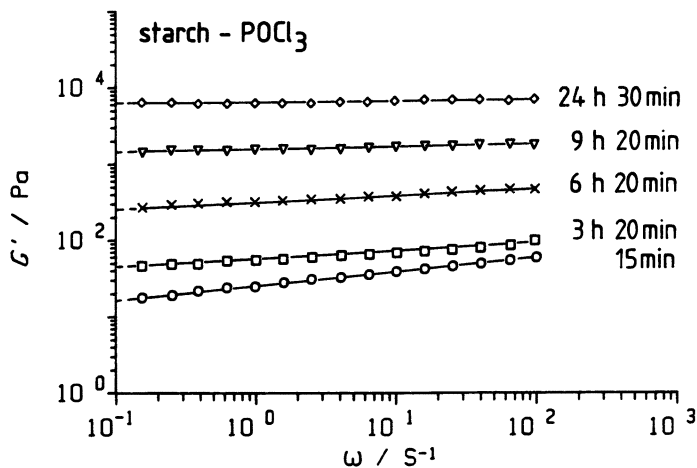
Figure 16. Time dependence of the material function G' against ω for starch–$POCl_3$ gels in the plateau region.
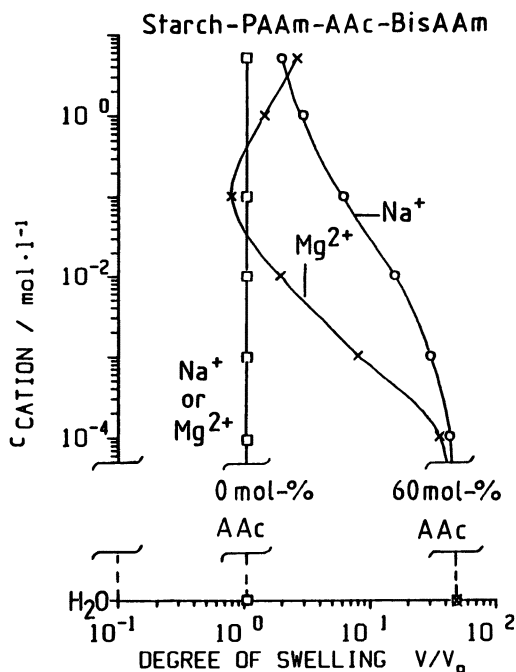

Figure 17. Influence of the Na^+ and Mg^{2+} concentration on the degree of swelling for unsaponified (0 mol % AAc) and highly saponified (60 mol % AAc) starch-g-PAAm–AAc–BisAAm gels.
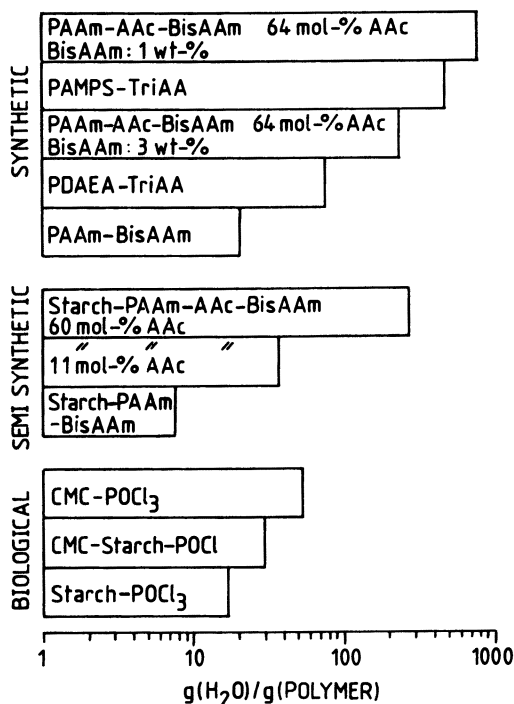
Figure 18. Comparison of the water absorption capacity (grams of H₂O per gram of polymer) for various synthetic and semisynthetic biopolymer gels.

No additional salt-dependent swelling measurements or rheological investigations were carried out on these gels. The following trends can be inferred:

1. Water absorption capacity rises with increasing proportion of ionic groups in the gel.

2. Compared to equivalent semisynthetic gels, the degree of swelling for synthetic hydrogels is approximately about 2 to 3 times greater, and to biopolymer gels, 13 to 40 times greater.

The survey does, however, only show the gels' absorption capacity in distilled water, and incorrect conclusions might be drawn with respect to salt-containing solutions. The salt concentration vs. degree of swelling for the polymers is shown in Figures 19 and 20. For the sake of the survey, the saponified semisynthetic starch-g-PAAM–AAc–BisAAm gels were omitted, because their course largely corresponded to that of the PAAM–AAc–BisAAm gels. As Figure 19 shows, in KCl solutions, the
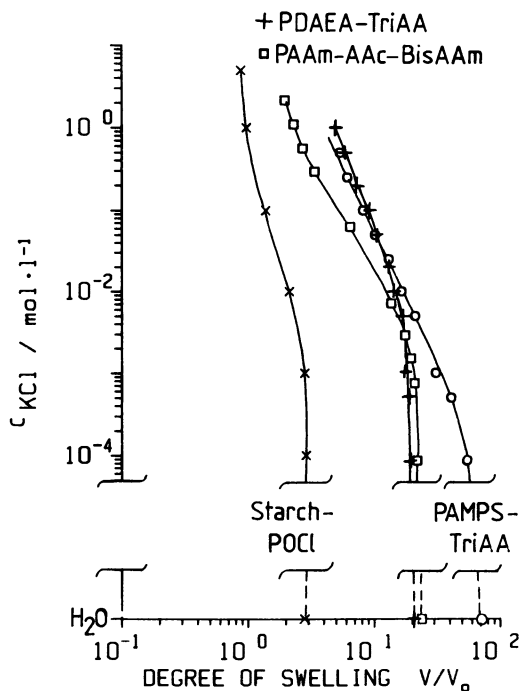
Figure 19. Comparison of the graphs of concentration against degree of swelling in KCl solutions for the gels.

synthetic hydrogels possess a greater stability to salts than the starch–POCl$_3$ gels.

If, however, the synthetic gels are compared with one another, the relationships relative to salt stability are reversed as the KCl concentration increases. The gels with triallylamine as a cross-linking agent exhibit a significantly higher salt stability than the PAAM–AAc–BisAAm gel. Salt solutions with concentrations between approximately 0.001 and 0.1 mol L^{-1} occur in technical product applications and particularly in nature. These solutions contain high percentages of multivalent cations such as Ca^{2+}, Mg^{2+}, and Al^{3+} and are therefore of particular interest concerning salt stability.

Figure 20 shows the dependence of the degree of swelling on the Mg^{2+} concentration for the different hydrogels. Worthy of particular note is the very good salt stability and high V/V_0 of the PAMPS–TriAA gels. Furthermore, for PAAm–AAc–BisAAm gels in this concentration range, the degree of swelling falls below that for the starch–POCl$_3$ gels. The starch–POCl$_3$ gels exhibit a higher salt stability despite their lower absorption capacity of distilled water. Starch–POCl$_3$ gels also offer the advantages of being legally permissible in foodstuffs and being biologically degradable.
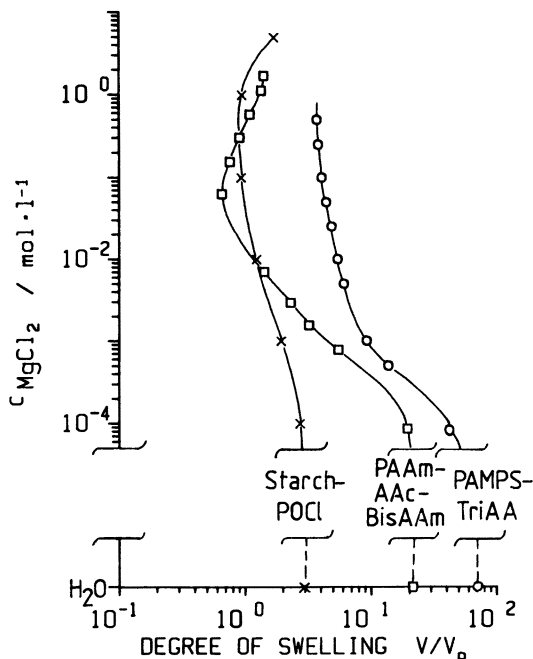
Figure 20. Comparison of the graphs of concentration against degree of swelling in MgCl$_2$ solutions for the gels.

The determination of network parameters (density of entanglement, average molecular weight between two entanglement points, etc.) from swelling measurements for highly cross-linked polymers is subject to a relatively high degree of error and requires a prior knowledge of the Flory–Huggins interaction parameter (χ). In contrast, mechanical oscillatory shear experiments are considerably easier to carry out and correlate with the network parameters. Figure 21 shows the rate of gel formation as a function of the storage modulus for starch–POCl$_3$ gel and synthetic PAAm–BisAAm gel. During the radical-initiated copolymerization of synthetic gels, gel formation terminates within a very short time. In contrast, the biopolymer gels need considerably longer reaction times for the network formation to reach completion. In the present example, the gel formation does not reach completion for approximately 20–24 h. This lengthy interval can presumably be attributed to the very slow condensation during esterification across the phosphate bridges. Uniform, homogeneous gel bodies are needed to determine the network parameters by rheological parameters. Comparable rheological measurements on gel suspensions are not, therefore, possible. This problem is especially true of biopolymer gels, which, because
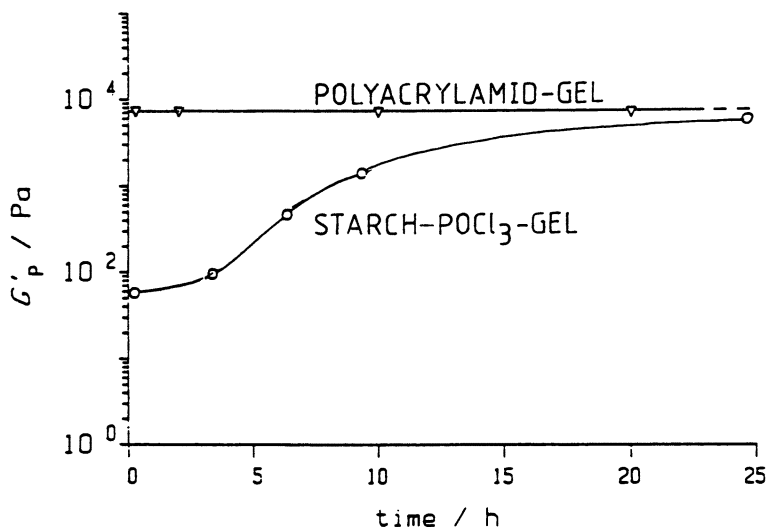
Figure 21. Comparison of the time-dependent gel formation of PAAm–BisAAm and starch–POCl₃ gels as a material function of G_p' against time.

of their varied preparation methods, can frequently only be investigated in the form of gel suspensions.

Network Inhomogeneities

If the molar ratios of bifunctional monomer and polyfunctional cross-linking agent are given, then a theoretical value for the number of elastically effective entanglement points can be determined for any gel. The length between entanglements for a real network will, however, always have a more-or-less broad distribution. In Figure 22, examples of the occurrence of network inhomogeneities are shown. The number of free chain ends, which do not contribute to the elasticity of the network, for rates of radical-initiated co-polymerization is dependent upon the concentration of the radical initiator, among other factors. The compatibility and solubility of the components during synthesis represents a further item to consider in the occurrence of network inhomogeneities.

The cross-linking agents bis(acrylamide) and triallylamine are only slightly soluble in aqueous media and therefore tend toward phase separation. At very high concentrations of cross-linking agent, aggregation occurs, and the network reacts in total like a single elastically effective entanglement point. This effect is responsible for the occurrence of the maximum behavior relative to the plateau modulus for the PAAm–BisAAm gels (Figure 11). The

free chain ends

aggregation of the
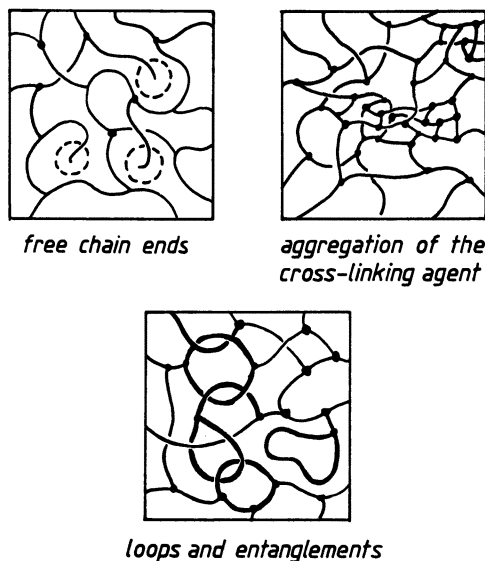cross-linking agent

loops and entanglements

Figure 22. Network defects and inhomogeneities.

probability of ring and loop formation rises with decreasing total monomer concentration if the cross-linking agent concentration is still relatively large. This effect occurs in PAAm–BisAAm gels as well as their polymerlike saponified PAAM–AAc–BisAAm gels, as follows from both swelling and vibration measurements (cf. Figure 7 and Table II). The PAAM–AAc–BisAAm gel synthesized from a total monomer concentration of 5% shows a higher degree of swelling compared to the gel from a monomer concentration of 10%, although the proportion of cross-linking agent is the same in both cases. Correspondingly, a considerably lower entanglement density can be observed with decreasing total concentration from the rheological measurements, and this result can be attributed to the formation of rings and loops with decreasing total monomer concentration.

References

1. Nagy, M. *Colloid Polym. Sci.* **1985**, *263*, 245–265.
2. Hasirci, U. N. *J. Appl. Polym. Sci.* **1982**, *27*, 33–41.
3. Werner, G. *avr-Allgemeiner Vliesstoff-Report* **1984**, *4*, 178–182.
4. Stuckenbrock, K.-H.; Werner, G. *Melliand Textilber.* **1985**, *65*, 173–175.
5. Brandt, K. A.; Goldman, S. A.; Inglin, T. A. U.S. Patent 4 654 039, 1987.
6. Masuda, F. *CEER, Chem. Econ. Eng. Rev.* **1983**, *15*, 19–22.
7. Boyde, T. R. C. *J. Chromatogr.* **1978**, *124*, 219–230.
8. Kossmehl, G.; Klaus, N.; Schäfer, H. *Angew. Makromol. Chem.* **1984**, *123/124*, 241–259.

9. Katayama, S.; Ohata, A. *Macromolecules* **1985**, *18*, 2781–2782.
10. Hirokawa, Y.; Tanaka, T.; Sato, E. *Macromolecules* **1985**, *18*, 2782–2784.
11. Flory, P. J. *Principles of Polymer Chemistry*; Cornell University Press: Ithaca, London, 1953; p 577.
12. Nossal, R. *Macromolecules* **1985**, *18*, 49–54.
13. Weiss, N.; van Vliet, T.; Silberberg, A. *J. Polym. Sci., Polym. Phys. Ed.* **1981**, *19*, 1505–1512.
14. Chmelir, M.; Dahmen, K.; Türk, W. German Patent DE 3124008, 1983.
15. Oppermann, W.; Rose, S.; Rehage, G. *Br. Polym. J.* **1985**, *17*, 175–180.
16. Ferry, J. D. *Viscoelastic Properties of Polymers*, 3rd ed.; Wiley: New York, 1980.
17. Gerth, C. *Ullmann's Enzyklopädie der technischen Chemie*, Bd. 5; Verlag Chemie: Weinheim, 1980.
18. Mochel, V. D. *J. Macromol. Sci., Rev. Macromol. Chem.* **1972**, *C8*(2), 289–347.
19. Tanaka, T. *Spek. Wissenschaft (Ger. ed. Sci. Am.)* **1981**, *3*, 79–93.
20. Tanaka, T. *Phys. Rev. Lett.* **1978**, *40/12*, 820–823.
21. Kulicke, W.-M.; Hörl, H.-H. *Colloid Polym. Sci.* **1985**, *263*, 530–540.
22. Klein, J.; Heitzmann, R. *Makromol. Chem.* **1978**, *179*, 1895–1904.
23. Klein, J.; Conrad, K.-D. *Makromol. Chem.* **1978**, *179*, 1635–1638.
24. Halverson, F.; Lancaster, J. E.; O'Connor, M. N. *Macromolecules* **1985**, *18*, 1139–1144.
25. Erman, B.; Flory, P. J. *Macromolecules* **1986**, *19*, 2342–2353.
26. Hild, G.; Okasha, R.; Macret, M.; Gnanou, Y. *Makromol. Chem.* **1986**, *187*, 2271–2288.
27. DeGennes, P.-G. *Scaling Concepts in Polymer Physics*; Cornell University Press: Ithaca, London, 1979; pp 128–162.
28. Bansil, R.; Gupta, M. K. *Ferroelectrics* **1980**, *30*, 63–71.
29. Ilavsky, M.; Hrouz, J. *Polym. Bull. (Berlin)* **1982**, *8*, 387–394.
30. Ohmine, I.; Tanaka, T. *J. Chem. Phys.* **1982**, *77*, 5725–5729.
31. Muller, G.; Laine, J. P.; Fenyo, J. C. *J. Polym. Sci., Polym. Chem. Ed.* **1979**, *17*, 659–672.
32. Dusek, K.; Prins, W. *Adv. Polym. Sci.* **1969**, *6*, 1–102.
33. Neidlinger, H.-H.; McCormick, C.-L. *J. Am. Chem. Soc.* **1986**, *56*, 1584.
34. Ferry, J. D. *Viscoelastic Properties of Polymers*; Wiley: New York, 1980.
35. Labana, S. S. *Encyclopedia of Polymer Science and Engineering*; Wiley: New York, 1986; Vol 4, pp 350–395.
36. Hallinger, C. H.; Whistler, R.; Paschall, E. F. In *Starch: Chemistry and Technology*; Academic: New York, 1984.
37. Roy, L.; Whistler, J.; Bemiller, N.; Paschall, E. F. *Starch: Chemistry and Technology*; Academic: New York, 1984.
38. Doublier, J. L. *Starch/Staerke* **1981**, *33*, 415–420.
39. Hollinger, G.; Kuniak, L.; Marchessault, R. H. *Biopolymers* **1974**, *13*, 879–890.

3

Cooperative Diffusion
in Water-Swellable Polymeric Networks

A. Peters[1], F. Schosseler[2], and S. J. Candau[1]

[1]Laboratoire de Spectrométrie et d'Imagerie Ultrasonores, Unité Associée
au Centre National de la Recherche Scientifique, Université Louis Pasteur, 4,
rue Blaise Pascal, 67070 Strasbourg Cedex, France
[2]Institut Charles Sadron (CRM–EAHP), 6, rue Boussingault, 67083 Strasbourg
Cedex, France

*Current theories for the dynamic fluctuations and kinetics of poly-
meric gel swelling are reviewed. The cooperative diffusion constant
can be determined either from quasi-elastic light scattering experi-
ments or from the swelling kinetics of spherical or cylindrical gels.
The influence of the structure and ionization degree of the network
on the cooperative diffusion constant is discussed.*

WATER-SWELLABLE POLYMERIC NETWORKS have received considerable
attention from both academic and applied research laboratories. The dis-
covery of volume–phase transitions upon changes of external conditions,
such as temperature, solvent composition, or osmotic pressure (*1–7*), has
initiated research on new technological applications of gels as switches, ac-
tuators, memories, and display units. The capacity of highly ionized gels to
retain large amounts of water makes the gels useful as reservoirs (*8*) and for
other new industrial applications. To put new applications into practice, an
understanding of the dynamic properties of water-swellable networks is of
fundamental importance.

It has been shown both theoretically and experimentally that the kinetics
of volume change and the dynamics of concentration fluctuations of a gel
are controlled by a diffusive process in which many chains of the network
move cooperatively (*9–13*). The first part of this chapter describes how the

techniques of quasi-elastic light scattering (QELS) and kinetics of swelling can be used in a complementary way to determine the diffusion constant associated with swelling. The second part of this chapter discusses the relation between the cooperative diffusion constant and the microscopic structure of the networks.

Experimental Details

The polyacrylamide gels were prepared by a standard redox reaction with ammonium persulfate and tetramethylethylenediamine (TEMED). Recrystallized acrylamide monomer (5 g), N,N'-methylenebis(acrylamide) (0.133 g), ammonium persulfate (40 mg), and TEMED (400 μL) were dissolved in water to make a total volume of 100 mL. After thorough mixing, the preparation was poured through a small aperture into cylindrical or spherical glass molds. Upon gelation, the molds were broken and the gel samples were transferred into a cell containing an excess of water. This time was taken to be zero ($t = 0$) for the kinetics experiments.

Ionized gels were acrylic acid–sodium acrylate copolymers. The samples were provided by Norsolor Company. The gels were obtained through an inverse suspension process. In this technique, the aqueous phase, containing an hydrophilic monomer, was dispersed in an organic phase, such as an alicyclic or aliphatic hydrocarbon.

The first step of the synthesis was the neutralization of acrylic acid by an aqueous sodium hydroxide solution. The degree of neutralization determined the ionization degree. A cross-linking agent and an initiator were then dissolved in the aqueous phase.

The inverse suspension was obtained by mixing the organic solution of a nonionic surfactant with the aqueous solution of partially neutralized acrylic acid salt. The temperature was then raised, and the polymerization reaction was carried out for several hours. The samples were then dried and ready for swelling kinetics experiments. They were transferred into an excess of solvent, and the time at which they looked homogeneous was $t = 0$ for the kinetics experiments.

Determination of the Cooperative Diffusion Coefficient

Equation of Motion. A gel consists of a cross-linked network immersed in a fluid, so coupled equations should be used to describe the motion of the solvent molecules and of the polymer network. However, the motion of solvent molecules is about 10^6 times faster than that of the polymer network. Thus, on the time scale of the thermal fluctuations of the network, solvent effects are always averaged. An equation of motion for a gel network was proposed by Tanaka et al. (9). In the derivation of the equation of motion, solvent effects are taken into account only through a viscosity term.

As a further approximation, a gel can be treated as a continuous medium with uniform density ρ. This approximation is valid for collective modes that have wavelengths much larger than the average distance between two neighboring cross-links. The time and space dependences of the structure of the

network can then be described by the displacement vector $u(r, t)$, which represents the displacement at time t of a point r on the polymer network from its equilibrium location. In the case of a small deformation of a unit cube of gel, the equation for $u(r, t)$ is given by Newton's second law:

$$\rho \frac{\partial^2 u(r, t)}{\partial t^2} = \nabla \cdot \sigma - f \frac{\partial u(r, t)}{\partial t} \tag{1}$$

The two terms on the right represent the forces exerted on the unit cube. The stress tensor (σ) has a component σ_{ik}, the force along the k-axis on a unit plane perpendicular to the i-axis. This component is related to the displacement vector through

$$\sigma_{ik} = K_{os} \nabla \cdot u \delta_{ik} + 2\mu(u_{ik} - \frac{1}{3} \nabla \cdot u \delta_{ik}) \tag{2}$$

where

$$u_{ik} = \frac{1}{2} \left(\frac{\partial u_k}{\partial x_i} + \frac{\partial u_i}{\partial x_k} \right) \tag{3}$$

and K_{os} and μ are the osmotic compressional modulus and the shear modulus of the gel, respectively. Thus, the first term on the right side of equation 1 represents the elastic force acting on the unit cube. The second term is a friction force that includes solvent effects through the friction coefficient f.

Substituting equations 2 and 3 into equation 1 yields

$$\rho \frac{\partial^2 u}{\partial t^2} = \mu \Delta u + \left(K_{os} + \frac{1}{3} \mu \right) \nabla(\nabla \cdot u) - f \frac{\partial u}{\partial t} \tag{4}$$

Generally, the inertial term is much smaller than the other terms of equation 4, and the equation of motion becomes:

$$\frac{\partial u}{\partial t} = \frac{K_{os} + \mu/3}{f} \nabla(\nabla \cdot u) + \frac{\mu}{f} \Delta u \tag{5}$$

Equation 5 describes the fluctuations of the network structure and the kinetics of swelling of the gel.

Kinetics of Swelling of Spherical and Cylindrical Gels.
Spherical and elongated cylindrical (ratio of height/radius $\gg$ 1) gel samples were

studied. A cross-linked polymeric network was prepared in the presence of a given amount of diluent. When the gelation reaction was complete, the gel sample was transferred to a cell containing an excess of solvent. The cell was placed onto the stage of a profile projector. As the gel swelled to its equilibrium concentration, its size was recorded photographically. This method allowed an accurate measurement of the time evolution of the gel size during the swelling process.

The kinetics of swelling are described by equation 5, in which $u(r, t)$ represents the displacement of a point in the network from its final equilibrium location after the gel is fully swollen. This deformation is radial with respect to the center of the sphere or the axis of the cylinder. In an actual experiment, the radius $a(t)$ of the sphere or of the cylinder is measured as a function of time. The deformation at the surface of the gel can be described by

$$u(a, t) = a(\infty) - a(t) \tag{6}$$

By using the following initial and boundary conditions, equation 5 has been solved to describe the kinetics of swelling of a sphere (10–11) and cylinder (13). The initial condition for $u(r, t)$ is obtained by assuming that before the gel is transferred into the fluid ($t \leq 0$), that the network is uniformly compressed so that:

$$\frac{u(r, 0)}{u(a, 0)} = \frac{r}{a} \tag{7}$$

The boundary condition on the surface of the gel is obtained by canceling the stress normal to the surface.

By solving equation 5 with the boundary conditions described, it was found that the relationship between the evolution of the radius of the sphere or the cylinder to its equilibrium value can be described by an infinite sum of exponential decays. Modes with the smallest relaxation times vanish rapidly, and the final stage of the swelling process is described by a single exponential relaxation.

$$-\ln \frac{u(a, t)}{u(a, 0)} = -\ln \frac{a(\infty) - a(t)}{a(\infty) - a(0)} = e^{-t/\tau} + B \tag{8}$$

where B depends on the ratio μ/K_{os} and the shape of the gel sample. The relaxation time τ_1 is given by:

$$\text{sphere: } \tau_1 = \frac{a^2}{DX_1^2} \tag{9}$$

$$\text{cylinder (infinite height): } \tau_1 = \frac{a^2}{DX'_1{}^2(1 + \mu/M_{os})}$$

where the cooperative diffusion coefficient $(D = M_{os}/f)$, the osmotic longitudinal modulus $(M_{os} = K_{os} + 4\mu/3)$, and X_1 (for a sphere) or X'_1 (for a cylinder), respectively, are the first roots of equations 10 and 11.

$$\tan X_n = \frac{(4\mu/M_{os})X_n}{(4\mu/M_{os}) - X_n{}^2} \tag{10}$$

and

$$X_n{}' J_0(X_n{}') - 2(\mu/M_{os})J_1(X_n{}') = 0 \tag{11}$$

$J_0(X)$ and $J_1(X)$ are the Bessel functions of zeroth and first order, respectively.

Equation 9 shows that the relaxation time is proportional to the square of the distance between the gel surface and its center, that the kinetic process is diffusive, and that all chains of the network diffuse cooperatively through the water to relaxation equilibrium.

Figure 1 shows the theoretical swelling curves calculated for the two limits, $\mu/M_{os} = 0$ and $\mu/M_{os} = 0.5$. The extrapolations to 0 time of the asymptotic straight lines depend on μ/M_{os}. On the same plot, the experimental data obtained for three polyacrylamide gels are given. A least-squares fit of the data led to an intercept corresponding to $\mu/M_{os} = 0.3 \pm 0.1$. The
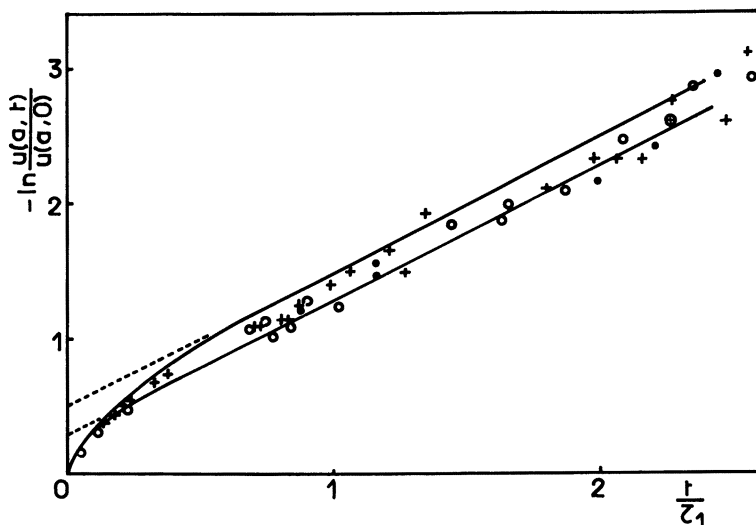
Figure 1. Experimental swelling curves for three spherical polyacrylamide gels at the equilibrium swelling concentration 3.3×10^{-2} g cm^{-3}. Radii were 4.43 mm (●), 6.17 mm (○), and 11.15 mm (+). The temperature was 22 °C. The two lines are the theoretical swelling curves for the two limiting values $\mu/M_{os} = 0$ (top curve) and $\mu/M_{os} = 0.5$ (bottom curve). The mean square fit to the data led to $\mu/M_{os} = 0.3 \pm 0.1$.

relationship between τ_1 and D depends on μ/M_{os} directly or through the roots X_1 or X_1'. It is convenient to introduce the apparent diffusion coefficient D', which is obtained by assuming $\mu = 0$.

$$\text{sphere } D' = \frac{a^2}{\tau_1 \pi^2} \quad \frac{D'}{D} = \left(\frac{X_1'}{\pi}\right)^2$$

$$\text{cylinder (infinite height) } D' = \frac{a^2}{\tau_1 \lambda_1^2} \quad \frac{D'}{D} = \left(\frac{X_1'}{\lambda_1}\right)^2 (1 + \mu/M_{os})$$

(12)

where λ_1 is the first root of $J_0(X)$.

The variations of D'/D as a function of μ/M_{os} for an elongated cylinder and a sphere are shown in Figure 2. D'/D does not deviate significantly from 1 for elongated cylinders; whereas, D'/D decreases considerably for spheres with increasing μ/M_{os}. Therefore, if the ratio μ/M_{os} is not known, it is preferable to study the kinetics of swelling of an elongated cylinder. The latter quantity can be evaluated by comparing the D' values of a sphere and an elongated cylinder of the same gel. Figure 3 represents the theoretical variation of $D'_{cylinder}/D'_{sphere}$ as a function of μ/M_{os}. On the same plot the experimental values of $D'_{cylinder}/D'_{sphere}$ obtained for sample gels of polydimethylsiloxane in toluene (14) and polyacrylamide in water are reported. The value $\mu/M_{os} = 0.28 \pm 0.04$ obtained for the polyacrylamide gels is in good agreement with that obtained from the extrapolation to $t = 0$ for the asymptotic straight line of Figure 1.

Theory of the Quasi-Elastic Light Scattering from Gels.

The equation of motion (equation 5) has three solutions that correspond to one longitudinal and two transverse diffusive modes. These modes give rise to polarized and depolarized light scattering, respectively (11–13, 15). The depolarized light scattering from gels is generally very small, and so far, no experiments have reported unexpected data. This chapter discusses only the polarized scattering that arises from the longitudinal diffusive modes.

In a QELS experiment, the autocorrelation function of the polarized scattered field $<E(K, t)*E(K, 0)>$ is measured with K as the scattering vector. The scattered field is proportional to the amplitude of the fluctuations of the local polymer concentration in the gel. These concentration fluctuations are related to the local deformation in the gel.

The introduction of the Fourier transform $u(K, t)$ of the displacement vector in equation 5 leads to the following result for longitudinal displacement modes:

$$u(K, t) \propto e^{-K^2 D t}$$

(13)

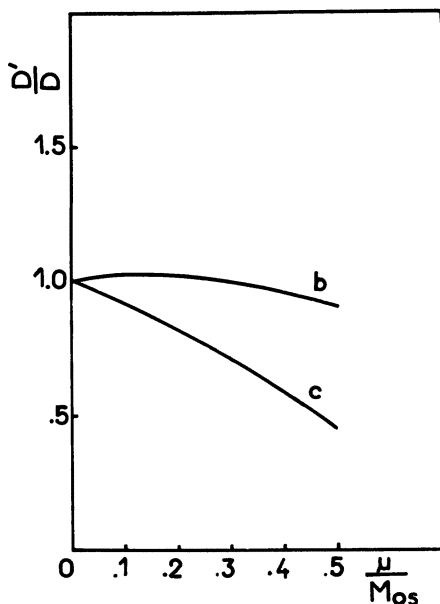Equation 13 shows that displacement modes diffuse in the gel with a diffusion

Figure 2. Variation of D'/D as a function of μ/M_{os} for spherical (c) and cylindrical (b) gels. D' is the apparent diffusion coefficient obtained by assuming $\mu = 0$. D is the actual diffusion coefficient that can be calculated only if μ/M_{os} is known. Neglecting the shear modulus introduces only a small error for cylindrical samples.

coefficient D. As a consequence, the autocorrelation function of the scattered field obeys

$$<E(K, t)*E(K, 0)> = C \left(\phi \frac{\partial n}{\partial \phi} \right)^2 \frac{k_B T}{K_{os} + 4\mu/3} e^{-K^2 Dt} \qquad (14)$$

where ϕ is the volume fraction of polymer in the gel, n is the index of refraction of the sample, and C is a constant that depends on the scattering geometry.

In an actual QELS experiment performed by using the homodyne regime, the time correlation function of the intensity of the scattered light $<I_s(K, t) I_s(K, 0)>$ is measured. Because of the Gaussian nature of the electric field, the time correlation function is given by the square of the correlation function of the electric field (*see* equation 14). The equation is

$$<I_s(K, t) I_s(K, 0)> \propto e^{-2K^2 Dt} \qquad (15)$$

In the heterodyne regime, (i.e., when the scattered signal is mixed with an external oscillator of much larger intensity) the experimental autocorre-
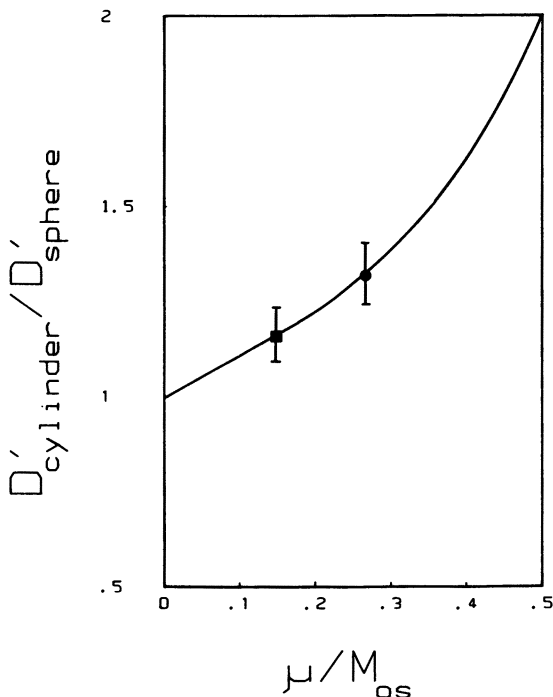
Figure 3. The ratio μ/M_{os} can be obtained from the ratio of the apparent diffusion coefficients measured on cylindrical and spherical gels. The theoretical curve is obtained from equation 12. The two experimental points correspond to a polyacrylamide gel in water (circle) and a polydimethylsiloxane gel in toluene (box). The temperature was 22 °C.

lation function is given by equation 14. Static inhomogeneities inside the gel samples usually play the role of oscillator, and are always heterodyned to some extent to the dynamic component of the scattered signal.

Quasi-Elastic Light Scattering from Gels: General Features. An exponential form for the correlation function of scattered light and K^2 dependence of the decay rate are expected from equations 14 and 15. These expectations were experimentally verified on several covalently cross-linked networks (9, 12, 16, 17). The autocorrelation function was described either by a single exponential decay or by a narrow distribution of exponential decays. Cumulants analysis (18) leads to variances less than 0.1, if one ignores gels with very low degrees of cross-linking, for which significant deviations from exponentiality were observed (16). An important contribution to the scattered signal arises from the long-range stationary spatial fluctuations in polymer segment density associated with nonrandom cross-linking of the

polymeric chains (*19–22*). This quasi-static scattering acts as a local oscillator that partially heterodynes the dynamic signal.

At small scattering vectors, the autocorrelation function is often fully heterodyned, and the dynamic part of the scattered intensity is only a few percent of the total intensity. At large scattering vectors, the signal is partially heterodyned and the measured decay constant, Γ, has a value between the heterodyne value DK^2 and the homodyne value $2DK^2$. As a result, the K^2 dependence of Γ no longer seems to be satisfied (Figure 4). This artifact can be eliminated by using a heterodyne geometry to obtain a meaningful value for the diffusion coefficient.

Another type of behavior is obtained with thermoreversible gels like agarose. Electron microscopy has shown that the network structure of these gels consists of fibers made from many polymer chains. In such gels, elasticity doesn't come from the entropy of the chains, as in the case of covalently cross-linked polymers, but from the mechanical bending elasticity of the fibers. The elastic moduli are about 10 times larger than those of entropic
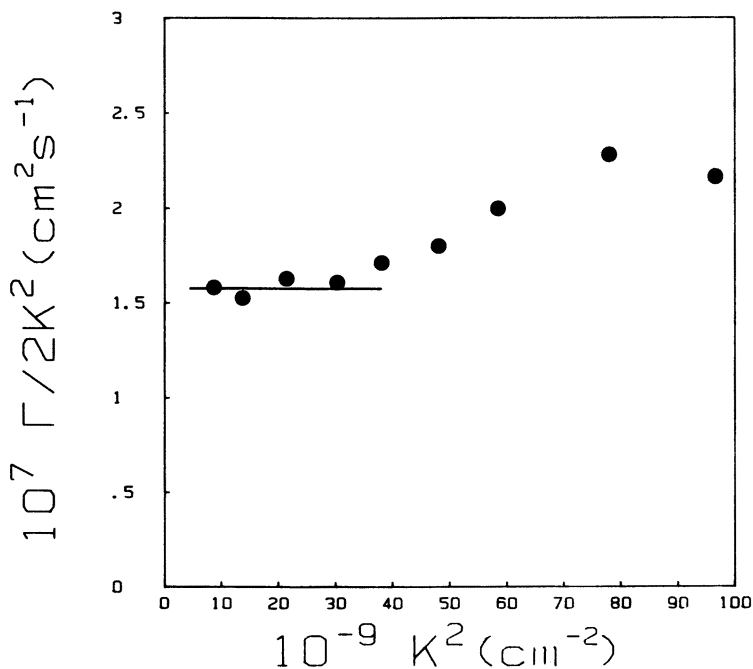
Figure 4. Variation of $\Gamma/2K^2$ as a function of K^2 for a typical polyacrylamide gel sample at the swelling equilibrium concentration 2.5×10^{-2} g cm^{-3}. The temperature was 22 °C. Static concentration fluctuations did not heterodyne completely the dynamic intensity at large values of the scattering vector. As a result $\Gamma/2K^2$ varied with K^2.

gels with same concentration. As a consequence, the dynamic part of the scattered intensity, which is inversely proportional to $(K_{os} + 4\mu/3)$, becomes very small (*see* equation 14).

QELS experiments have been performed in agarose and calcium alginate gels (23–25). The static scattering from both types of gels is about 2 orders of magnitude greater than that from a polyacrylamide gel. The intensity of the dynamic component is less than 1% of the total signal. The correlation functions are strongly nonexponential. Forced exponential fitting gives decay times of the order of tens of milliseconds that do not vary as a function of K^2. It is not, therefore, appropriate to describe the fluctuations in terms of diffusive process, and QELS experiments do not provide useful information on the structure of the network. On the other hand, QELS is well-suited to the study of tracer diffusion to gain insight into the structure of rigid fibrous gels (e.g., globular proteins) (23–25).

Comparison Between Light Scattering and Kinetics of Swelling. The cooperative diffusion process governs both the kinetics of swelling and the concentration fluctuations of gels. Figure 5 reports the values of D obtained from quasi-elastic light scattering and kinetics of swelling of cylindrical and spherical gel samples. The agreement between the two sets of results is very good.

The two techniques, QELS and kinetics of swelling, are complementary. In general, the QELS experiments are easier to perform and more accurate. However, highly ionized gels, characterized by large diffusion constants and high degrees of swelling, scatter very little light, and therefore macroscopic measurements are more appropriate. Macroscopic measurements are also more appropriate when the refractive index increment of the polymer with respect to the diluent is very small. On the other hand, kinetic experiments provide measurement of D only for gels close to the swelling equilibrium. QELS experiments allow determination of D at any stage of swelling.

Cooperative Diffusion Constant and Microstructure of the Network

The cooperative diffusion constant is related to the network properties through

$$D = (K_{os} + 4\mu/3)/f \qquad (16)$$

Covalently cross-linked networks built from highly hydrosoluble polymeric chains will now be considered. Neutral and ionized gels are discussed separately.

Neutral Gels. The link between the elastic moduli K_{os} and μ, the friction factor f, and the local structure of the gel can be established by using
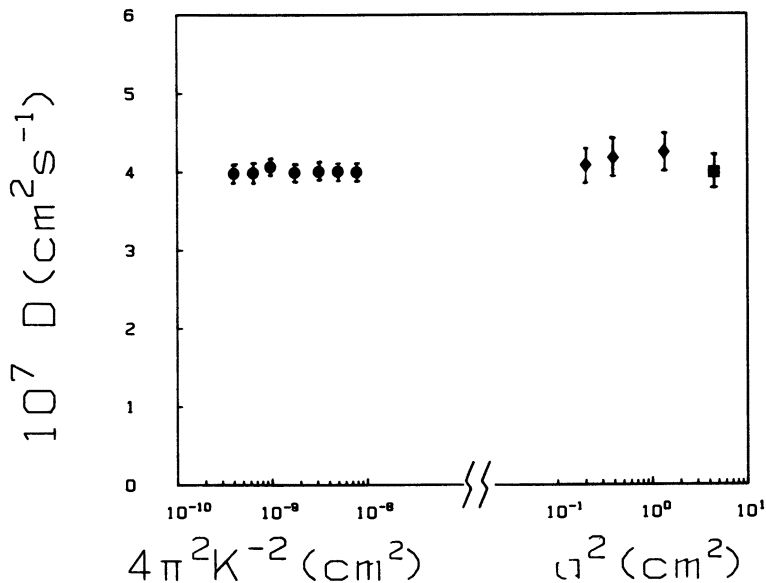
Figure 5. Comparison of D values obtained by QELS and swelling kinetics experiments on a polyacrylamide gel in water. The concentration was 3.3 × 10^{-2} g cm^{-3}. The temperature was 22 °C. The diffusive nature of the polymer network motion was apparent because the measured D was independent of K^{-2} in QELS experiments (●) and of a^2 in swelling kinetics experiments performed on spheres (◆) and on a cylinder (■).

an analogy between a gel swollen at equilibrium and a semidilute solution of large macromolecules at the same concentration (*12, 26*). The scaling concepts, which were developed for semidilute solutions (*26*), can be applied to the swollen networks. The scaling concepts allow expression of the complicated dependence of the elastic moduli on the cross-link density, polymer concentration, and solvent–polymer interactions in terms of a single parameter: ξ, the average distance between two neighboring cross-links. For a series of networks of a given polymer with different cross-link densities, ξ is related to the swelling equilibrium volume fraction, Φ_e, through

$$\xi \propto \Phi_e^{-\nu/(3\nu-1)} \qquad (17)$$

where ν is the excluded volume exponent relating the end-to-end distance R to the polymerization index N:

$$R \propto N^\nu \qquad (18)$$

It can be shown that the elastic moduli increase in proportion to the

density of elastic strands of size ξ (12, 26), and this condition leads to

$$K_{os}, \; \mu \propto k_B T \xi^{-3} \propto k_B T \Phi_e{}^{9/4} \tag{19}$$

The linear dependence of the moduli on temperature results from the entropic origin of the elasticity.

The effective friction coefficient, f, is related to the static spatial correlation function $g(r)$ through:

$$f^{-1} \propto \int dr \, \frac{1}{\eta_s r} \, g(r) \tag{20}$$

where η_s is the viscosity of the solvent. Equation 20 takes the sum of the hydrodynamic interactions between monomers by using the spatial correlation function as a weighting factor. This correlation function involves a correlation length that describes the screening of the long-range hydrodynamic interactions and that is imposed by ξ alone. Thus, $g(r)$ is a scaling function, and $g(r) \propto h(r/\xi)$ so that equation 20 becomes:

$$f \propto \eta_s \xi^{-2} \tag{21}$$

Combining equations 16, 19, and 21 leads to:

$$D \propto \frac{k_B T}{\eta_s \xi} \propto \Phi_e{}^{-3/4} \tag{22}$$

Thus, D increases in inverse proportion to the correlation length, and by analogy, in the case of solutions, a hydrodynamic correlation length ξ_H can be defined by:

$$D = \frac{k_B T}{6\pi \eta_s \xi_H} \tag{23}$$

The scaling law (equation 22) suggests that the ratio ξ_H/ξ is a universal number (independent of the chemical nature of the polymer and the solvent). There is not, at the moment, theoretical calculation of ξ_H/ξ. An experiment combining neutron scattering and QELS measurements on polystyrene gels swollen by benzene allowed measurement of both the radius of gyration of a strand of the network and the hydrodynamic correlation length (27). The latter was found to be about one-half the static length. The same result, R_G/R_H, was found for dilute solutions of macromolecules in good solvent

(excluded volume regime); therefore, the measurement of D in swollen networks provides a good estimate of the mesh-size of the network.

The scaling behavior of D with the equilibrium polymer concentration was observed for several gels. The experimental values of the exponent ranged from 0.66 to 0.77 (*12, 16, 17, 28*). The nonuniversal value of the exponent can be explained, as in the case of semidilute solutions, by crossover effects (*28*). Figure 6 shows the log–log plot of the cooperative diffusion versus the swelling equilibrium concentration for polyacrylamide gels at the swelling equilibrium. The value obtained for the exponent is very close to the theoretical prediction.

Remarks

1. If the gel contains a large number of dangling chains connected at one end to the network, ξ represents the average size of
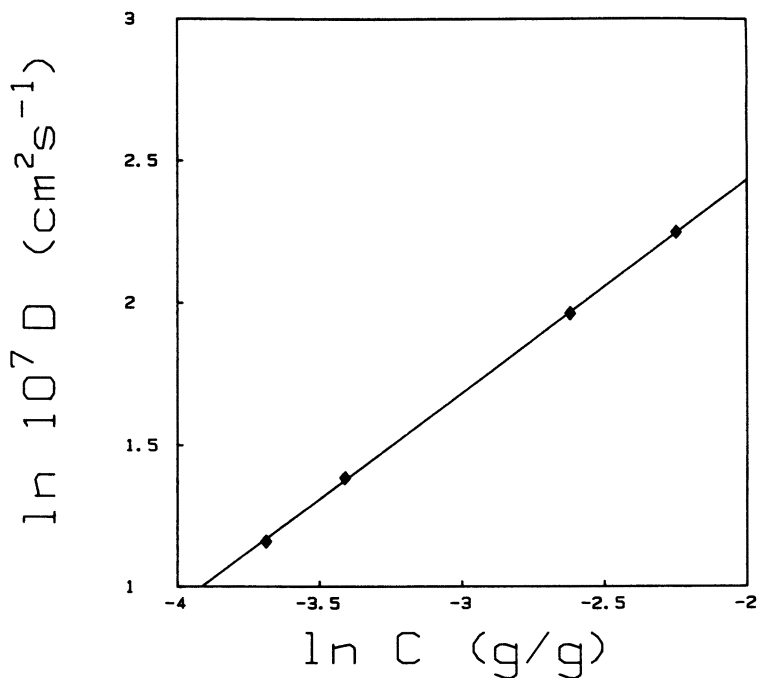
Figure 6. Variation of the diffusion coefficient of polyacrylamide gels on a double logarithmic scale as a function of their concentration at swelling equilibrium. The temperature was 22 °C. The slope was 0.74 and agreed with the exponent predicted by equation 21.

the branched chain connecting two neighboring elastically ef-
fective cross-links, and the scaling relation (equation 22) is no
longer valid (*29*).

2. The dynamics of gels in poor solvent, (i.e., when the poly-
mer–polymer affinity becomes equal to or less than the poly-
mer–solvent affinity), are also characterized by a diffusive
process. A hydrodynamic correlation length can still be de-
fined through equation 23, but this length represents the dis-
tance over which the network motions are correlated and
involves many cross-linking units. By lowering the tempera-
ture, a spinodal line is approached and the correlation length
increases and diverges (*15, 20–32*).

Ionized Gels.   Ionized water-swellable polymeric networks are used
in an increasingly large number of applications because of their very high
water retention capacity (up to about 1000 times the volume of the dry
polymer in pure water) and their very fast kinetics of volume change. These
features, which have been recently investigated in hydrolyzed polyacryl-
amide (*3–7, 33*) and acrylic acid–sodium acrylate copolymer gels (*8*), are due
to the ionic pressure. This contribution to the osmotic pressure arises from
the ionization of the polymer network that releases positively charged hy-
drogen or sodium ions within the gel. These ions move freely without es-
caping the gel and produce pressure that causes expansion of the gel in an
excess of water and increases the rate of swelling (*3–5*). In the limiting case
of small degrees of ionization, the contribution of the ion pressure to the
cooperative diffusion constant can be taken into account by adding a term
proportional to the ionization degree to the longitudinal modulus. As a result,
the cooperative diffusion is a linear function of the ionization degree. This
hypothesis was verified on a series of polyacrylamide gels with different
degrees of hydrolysis (*31*).

For gels with high degrees of ionization, no theory is available to describe
the kinetics of swelling and the dynamics of fluctuations. A study (*8*) carried
out on small beads of cross-linked acrylic acid–sodium acrylate copolymers
has shown that the kinetics of swelling are still governed by a diffusive
process. The cooperative diffusion coefficient, as well as the equilibrium
swelling degree, are controlled mainly by the effective ionization of the
network. This parameter can be varied either by changing the charge density
on the network or the salt concentration of the swelling agent. Figure 7
shows the variation of the cooperative diffusion coefficient and swelling ratio
at the equilibrium for gels with an ionization degree of 80% as a function of
the salt content in the diluent. Very large changes in the extent and kinetics
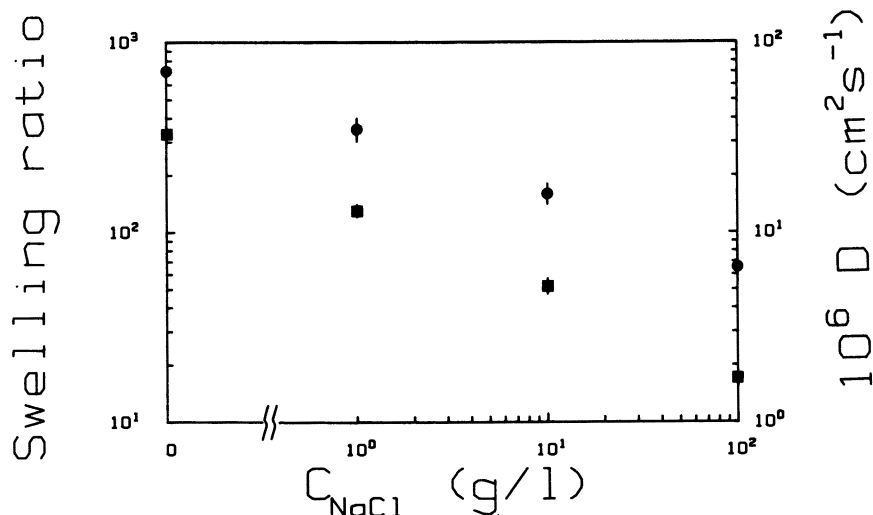of swelling can be induced by varying the screening of electrical interactions.

Figure 7. Variation of the swelling ratio (■) and the diffusion coefficient (●) of acrylic acid–sodium acrylate copolymer gel beads in water as a function of the concentration of added salt. The neutralization degree of the gel was 80% and the temperature was 22 °C. Results were obtained through swelling kinetics experiments.

Conclusion

The study of the cooperative diffusion in gels provides important information on the structure of the networks and is also relevant for technological applications involving large volume changes of the gels. The cooperative diffusion constant can be determined either from QELS experiments or from the kinetics of swelling of spherical or cylindrical gels. The scaling behavior of the cooperative diffusion coefficient as a function of the equilibrium swelling concentration of neutral gels in good solvents is well-established. The theoretical description of the swelling process and of the fluctuations in ionized gels is yet to be made.

References

1. Tanaka, T. *Phys. Rev. Lett.* **1978**, *40*, 820.
2. Tanaka, T.; Fillmore, D. J.; Sun, S. T.; Nishio, I.; Swislov, G.; Shah, A. *Phys. Rev. Lett.* **1980**, *45*, 1636.
3. Tanaka, T.; Nishio, J.; Sun, S. T.; Ueno-Nishio, S. *Science (Washington, D.C.)* **1982**, *218*, 467.
4. Ilavsky, M. *Macromolecules* **1982**, *15*, 782.
5. Hirokawa, T.; Tanaka, T.; Sato, E. *Macromolecules* **1985**, *18*, 2782.
6. Ricka, J.; Tanaka, T. *Macromolecules* **1985**, *18*, 83.

7. Ricka, J.; Tanaka, T. *Macromolecules* **1984**, *17*, 2916.
8. Schosseler, F.; Mallo, P.; Crétenot, C.; Candau, S. J. *J. Dispersion Sci. Technol.* **1987**, *8*, 321.
9. Tanaka, T.; Hocker, L.; Benedek, G. B. *J. Chem. Phys.* **1973**, *59*, 5151.
10. Tanaka, T.; Fillmore, D. J. *J. Chem. Phys.* **1979**, *70*, 1214.
11. Peters, A.; Candau, S. J. *Macromolecules* **1986**, *19*, 1952.
12. Candau, S. J.; Bastide, J.; Delsanti, M. *Adv. Polym. Sci.* **1982**, *44*, 27.
13. Peters, A.; Candau, S. J. *Macromolecules* **1988**, *21*, 2278.
14. PDMS networks have kindly been provided by J. Herz. They have been prepared by end-linking of preexisting chains as described in ref. 16.
15. Tanaka, T. In *Dynamic Light Scattering*; Pecora, R., Ed.; Plenum: New York, 1985; p 347.
16. Munch, J. P.; Candau, S. J.; Hild, G.; Herz, J. *J. Phys. (Les Ulis, Fr.)* **1977**, *38*, 1499.
17. Geissler, E.; Hecht, A. M. *Macromolecules* **1980**, *13*, 1276.
18. Koppel, D. E. *J. Chem. Phys.* **1972**, *57*, 4814.
19. Pines, E.; Prins, W. *Macromolecules* **1973**, *6*, 888.
20. Wun, K. L.; Prins, W. *J. Polym. Sci., Polym. Phys. Ed.* **1974**, *12*, 533.
21. Geissler, E.; Hecht, A. M. *J. Chem. Phys.* **1976**, *65*, 103.
22. Candau, S. J.; Young, C. Y.; Tanaka, T.; Lemarechal, P.; Bastide, J. *J. Chem. Phys.* **1979**, *70*, 4694.
23. Key, P. Y.; Sellen, D. B. *J. Polym. Sci., Polym. Phys. Ed.* **1982**, *20*, 659.
24. Mackie, W.; Sellen, D. R.; Sutcliffe, J. *Polymer* **1978**, *19*, 9.
25. Sellen, D. B. *Polymer* **1978**, *19*, 1110.
26. De Gennes, P. G. In *Scaling Concepts in Polymer Physics*; Cornell: Ithaca, N.Y., 1985.
27. Bastide, J.; Duplessix, R.; Picot, C.; Candau, S. J. *Macromolecules* **1984**, *17*, 83.
28. Schaeffer, D. W.; Han, C. C. In *Dynamic Light Scattering*; Pecora, R., Ed.; Plenum: New York, 1985; p 181.
29. Bastide, J.; Picot, C.; Candau, S. J. *J. Polym. Sci., Polym. Phys. Ed.* **1979**, *17*, 1441.
30. Tanaka, T. *Phys. Rev.* **1978**, *A17*, 763.
31. Hochberg, A.; Tanaka, T.; Nicoli, D. *Phys. Rev. Lett.* **1974**, *43*, 217.
32. Candau, S. J.; Munch, J. P.; Hild, G. *J. Phys. (Les Ulis, Fr.)* **1980**, *41*, 1031.
33. Mallo, P.; Cohen, C.; Candau, S. J. *Polym. Commun.* **1985**, *26*, 232.

Semicrystalline Poly(vinyl alcohol) Hydrogels

Ronald F. Ofstead[1] and Claudia I. Poser[2]

3M Company, Life Sciences Sector Research Laboratory, 201–2W–17
3M Center, Saint Paul, MN 55144

Un-cross-linked semicrystalline poly(vinyl alcohol) hydrogels were prepared by solvolysis of the corresponding vinyl trifluoroacetate polymers and copolymers. The relationships between polymer crystallinity, hydrogel structure, and mechanical properties in the subject hydrogels were examined. Evidence was presented that comonomers acted to disrupt crystal structure and increase water content. The effects of copolymer structure on surface characteristics important to biomedical applications were examined, and the importance of hydrogel nonionic character was demonstrated through protein binding studies.

SYNTHETIC HYDROGEL POLYMERS, first introduced in the early 1960s, made a major impact, initially in the soft contact lens field, and more recently in other biomedical or specialty applications. The first synthetic poly(2-hydroxyethyl methacrylate) [poly(HEMA)] hydrogel developed by Wichterle (1) remains very important, as do its copolymers with monomers such as N-vinyl-2-pyrrolidinone, acrylic and methacrylic acids, glycerol methacrylate, various acrylamides, and alkoxyalkyl methacrylates.

In addition, many of the known hydrophilic monomers have been used to prepare synthetic hydrogel polymers and copolymers of a wide range of compositions, mostly for contact lens uses. In such materials, water insol-

[1]Current address: 3M Company, Health Care Specialties Division, 260–3A–04 3M Center, Saint Paul, MN 55144
[2]Current address: 3M Company, Medical/Surgical Products Division, 270–2N–05 3M Center, Saint Paul, MN 55144

ubility and dimensional stability are normally provided by covalent cross-links that involve an additional multifunctional monomer component. In some cases, reinforcement is provided by other comonomers (often methyl methacrylate) that may function by providing very small scale phase separation and producing physical cross-links. Such synthetic polymer hydrogels are typically of low tensile strength (tensile strengths for low-water-content hydrogels fall below 1 MPa), low initial modulus, very low tear strength, and show an undesirable lack of durability in use. For example, high-water-content soft contact lenses are very susceptible to damage during the routine cleaning required to maintain clarity and good hygiene.

Stoy and co-workers (2) reported an approach that used alternative materials and involved the partial hydrolysis of poly(acrylonitrile) to form a complex structure that was presumed to involve sequences of unhydrolyzed poly(acrylonitrile) interspersed with acrylamide and acrylic acid sequences that resulted from hydrolyzed nitrile groups. Crystallites of unhydrolyzed poly(acrylonitrile) provided the physical cross-link domains within a matrix of the water-swellable portions of the structure. The tensile properties for such materials were considerably enhanced in comparison to the conventional covalently cross-linked hydrogels, and the absence of cross-links allowed processing under certain conditions.

In addition, conventional hydrogels consisting of water-swollen three-dimensional networks have been made from poly(vinyl alcohol) (PVA) and exhibit properties typical of such systems (3). Peppas and Merrill (4) recognized that the mechanical properties of these materials could be improved by annealing to deliberately introduce reinforcing crystallites into the network. The researchers were able to obtain tensile moduli in the range of 1.4–6.8 MPa for hydrogels with water contents ranging from 50 to 80% (wt % water). Although the properties attained in these experiments were useful, the drying and annealing procedures were slow and not easily adapted to commercial processing. Further work has been carried out in this area on PVA gels cross-linked with borate salts (5).

Work done by Haas et al. (6) in the mid-1950s demonstrated that PVA made from poly(vinyl trifluoroacetate) (PVTFA) generally has a greater tendency to crystallize than commercial PVA made from poly(vinyl acetate) because of the high degree of syndiotacticity achievable in these materials. Hydrogels made from PVTFA-derived PVA (syndiotactic PVA or sPVA) have been studied by Ogasawara et al. (7–11). In that work, the PVTFA was converted to sPVA with diethylenetriamine, which is a solvent for PVA. The sPVA was then recovered from solution and dissolved in boiling water at various concentrations. Hydrogels were obtained by cooling the solutions and annealing at a temperature below the gelation point. Water contents of the gels studied were between 80 and 90 wt %, and the authors reported three-point bending moduli of less than 0.2 MPa in all cases. (If Poisson's ratio is assumed to be 0.5, the tensile modulus in this case would lie below

0.07 MPa). Although the authors did not give a reason for not examining higher starting concentrations, they were very likely limited to the lower concentration region by the limited solubility of sPVA in boiling water.

The aim of the current studies was to investigate an approach to the preparation of very high strength water-swellable polymers that would provide processability and control of the extent of water swell. The approach centered upon

a. the use of syndiotactic order and structural regularity to achieve very highly crystalline and high-strength un-cross-linked vinyl alcohol polymers,

b. control of water swell through the ability to regulate polymer crystallinity via copolymerization, and

c. direct conversion of a precursor polymer into a xerogel without dissolution.

The rationale for this approach further involved the hypothesis that swelling in water occurs by virtue of water uptake in the amorphous regions of the polymers with network structure provided by relatively water-insensitive crystallites in the polymers. In this approach, vinyl trifluoroacetate was polymerized or copolymerized to provide highly syndiotactic thermoplastic polymeric intermediates that were converted to the corresponding syndiotactic PVA homopolymers or copolymers by solvolysis with mild nucleophilic reagents in media that were not solvents for both starting and end-product polymers.

Experimental Details

Materials. Vinyl trifluoroacetate monomer was prepared by the reaction of acetylene with trifluoroacetic acid in the presence of HgO catalyst and small amounts of trifluoroacetic anhydride as a water scavenger. An adaptation of the procedure of Howk (12) was used to obtain very high purity monomer. Vinyl acetate (Aldrich Chemical Company) was distilled before use; maleic anhydride (Aldrich Chemical Company) was used as received.

Polymerization Procedures. Bulk polymerizations were conducted by charging monomer(s) and initiator to heavy-walled glass ampoules, freezing with liquid nitrogen, degassing under vacuum, and sealing. These steps were followed by heat or UV treatment to effect polymerization. Solution polymerizations were conducted by thoroughly purging the reaction vessel with inert gas; charging dry solvent, monomer(s), and initiator; and stirring with heat or UV treatment to polymerize. Polymer products were then isolated by precipitation into nonsolvent. In some cases, (e.g., when 1,1,2-trichloro-2,2,1-trifluoroethane was used as the solvent) the polymers were insoluble in the reaction medium and were isolated directly by filtration.

Sample Preparation. Films were made from the polymers that were isolated after synthesis by solvent-casting from acetone solution and drying at room temperature under slow nitrogen flow. Solvolysis of PVTFA to PVA was carried out by a 2-h immersion of the film in a 10-wt % solution of reagent grade ammonium hydroxide in methanol. The films were then immersed in water for hydration and washing.

Analysis and Characterization. Gas chromatography was performed with a Hewlett-Packard model 5880A equipped with capillary columns and a flame-ionization detector. Gel permeation chromatography was performed with a Hewlett-Packard HPLC model 1090A with a refractive index detector. Tacticity determinations were conducted with an F-19 nuclear magnetic resonance (NMR) spectrophotometer (Varian XL-100) at 94.12 MHz for triad analyses (13). Inherent viscosity measurements were performed in 2-butanone at 25.0 °C.

Protein adsorption studies were done by immersing polymer discs for 24 h in room-temperature solutions of radiolabeled gamma-globulin, albumin, and lysozyme. Standard scintillation counting methods were used to quantify the amount of protein bound to the polymer surfaces after a thorough rinse with physiological saline solution (0.9% aqueous NaCl).

Tensile testing was done by using a table-top tensile tester (MTS) and American Society for Testing and Materials (ASTM) D412-83 methods for cut ring samples tested in the fully immersed state at room temperature.

Differential scanning calorimetry (DSC) was performed by using a Mettler DSC 30 at a rate of 10 K/min with a nitrogen purge, the flow rate of which was adjusted to 50 mL/min. For wet samples, large-volume stainless steel pans that sealed with an o-ring (Perkin-Elmer) were used to prevent evaporation.

Small-angle X-ray scattering (SAXS) was performed on wet gel samples that were inserted into quartz capillary tubes. These experiments were carried out by using copper radiation and a Kratky set-up.

After 1 week of hydration, water contents were obtained by weighing samples on a Mettler M3 microbalance. Surface water was removed before weighing by patting samples dry with paper tissues. Dry weights were obtained by letting samples air-dry overnight, followed by overnight drying in a vacuum desiccator. This method resulted in a 3–4% underestimate of the actual water content, because a small but reproducible amount of water was retained. Complete removal of water could have been accomplished by overnight drying in a vacuum oven at 90 °C, but this treatment results in a change in morphology as evidenced by a lowered water uptake on rehydration.

Infrared spectra were obtained by using a Fourier transform infrared spectrometer (FTIR) (Nicollet model 7199). The degree of crystallinity of the dry PVA was calculated by using the procedure in ref. 4.

Results and Discussion

Vinyl trifluoroacetate (VTFA) monomer was readily prepared by the vinylation of trifluoroacetic acid. Purification was difficult because of the very similar boiling points of the monomer (39 °C) and trifluoroacetic anhydride (38–39 °C). An effective procedure involved the "titration" of the anhydride with water to form the more readily separable carboxylic acid (b.p. is 72 °C). By using this approach, VTFA monomer of very high purity (>99.8%) has been routinely prepared. Monomer stability was excellent if cold, dark, dry conditions were maintained.

Free-radical polymerizations were conducted under a wide range of conditions that included photochemical, thermochemical, and low-temperature alkylborane–oxygen initiation methods. Both bulk and solution methods were used with somewhat unexpected results. Temperature appeared to have relatively little effect on the tactic order (percent syndiotacticity) of VTFA polymers. Polymerization temperatures ranged from –80 to 150 °C and gave syndiotacticities between 50 and 55% by triad analysis. Polar solvents affected tacticity more. For example, polymerization in 1,2-dichloroethane resulted in a syndiotacticity of 43%. Presumably, such effects were related to a disruption of the association of VTFA monomer with the growing chain end.

Polymer molecular weight investigations and control received significant attention because of the large loss of molecular mass that occurred upon conversion from PVTFA to PVA (approximately 2/3 mass loss) and the need to have adequate molecular weight in the PVA hydrogels for good mechanical properties. Molecular weight studies involved gel permeation chromatography (GPC) molecular weight determinations vs. polystyrene standards and the development of GPC molecular weight–inherent viscosity relationships (Table I). Molecular weight control was achieved by control of initiator level, temperature, monomer concentration in solution polymerizations, and monomer purity. A key monomer contaminant was acetaldehyde that resulted from inadvertent monomer hydrolysis and led to pronounced chain-transfer activity (Table II).

Table I. Molecular Weight and Inherent Viscosity for PVTFA Homopolymers

Inherent Viscosity	Average M_w ($\times 10^5$)
0.19	0.98
0.45	3.50
0.54	4.05
0.62	6.03
0.98	8.67
1.35	18.20
1.90	23.30
2.00	40.30

Table II. Acetaldehyde Content of VTFA Monomer and Number-Average Molecular Weight (M_n) of Resulting PVTFA

Acetaldehyde (wt %)	Average M_n ($\times 10^5$)
0.031	4.03
0.144	4.13
0.334	2.93
0.735	2.05

Thin film samples of poly(VTFA) homopolymer were prepared by solvent casting (e.g., from ketone solvents) or hot pressing. DSC showed a glass transition temperature (T_g) of approximately 75 °C and a broad melt transition with completion of melting at approximately 180 °C. Films of poly(VTFA) were solvolyzed with a wide range of nucleophilic reagents. A convenient reagent was a 90/10 mixture of methanol and concentrated aqueous ammonium hydroxide. Solvolyses occurred rapidly, and when conducted in diluents that were not good solvents for either the starting poly(VTFA) or the product PVA, the resulting xerogels absorbed water readily to form strong transparent hydrogels. The properties of these PVA hydrogels were compared to the properties of conventional covalently cross-linked hydrogels of a wide variety (Table III). Commercially available hydrogel contact lenses were used as sources of test materials. Tensile testing was done in water on ring samples cut directly from contact lenses. The striking differences in mechanical properties were easily evident.

Increases in the levels of water swell of the PVA hydrogels were initially presumed to be possible according to the mechanism commonly followed by covalently cross-linked hydrogels, namely, the incorporation of monomer components with exceptional affinities for water (typically, charged species such as carboxylic acid functional monomers). Thus, copolymers of VTFA and maleic anhydride were prepared, which when solvolyzed in methanolic ammonium hydroxide, would be expected to give poly[(vinyl alcohol)-co-(maleic acid)] products. Film samples of such copolymer hydrogels were prepared, and surprising sensitivity of water swell to acidic comonomer content was observed (Table IV).

This sensitivity of water swell to composition led to the hypothesis that the presence of a comonomer might itself be more important than the ionic nature of the comonomer, and that the water swell effects were due to the amorphous polymer volume fraction rather than to the ionic character of the

Table III. Comparison of the Properties of Commercial Hydrogels and the sPVA Hydrogel

Material	Water (wt %)	Tensile Strength (MPa)
Poly-HEMA[a]	39	0.69
Softcon[b]	55	0.16
Permalens[c]	71	0.08
Sauflon[d]	79	0.08
PVA[e]	51	17.7

[a]Poly(2-hydroxyethyl methacrylate).
[b]Copolymer of HEMA, N-vinyl-2-pyrrolidinone, methacrylic acid, and cross-linker.
[c]As in footnote b with different ratios.
[d]Copolymer of N-vinyl-2-pyrrolidinone, methyl methacrylate, and cross-linker.
[e]Homopolymer of PVA derived from poly(VTFA).

Table IV. Effect of Maleic Anhydride Content on Water
Swell of PVA Hydrogels

Maleic Anhydride (wt %)	Water (wt %)
0.00	51
0.25	54
0.50	65
1.00	72

polymer. Thus, numerous other copolymers were prepared; the behavior of the poly[(vinyl alcohol)-*co*-(vinyl acetate)] copolymers served to illustrate this effect (Table V). This approach to the incorporation of precisely controlled levels of vinyl acetate was possible because of the very great difference in solvolytic susceptibility of trifluoroacetate vs. acetate (the rate constants differed by about 6 orders of magnitude).

An important practical advantage of uncharged monomers in controlling water swell is found in certain biomedical applications, (e.g., contact lenses) in which charged monomers can lead to undesirably high levels of protein adsorption, lens surface contamination, and deposit problems. Table VI shows the difference between the uncharged PVA homopolymer, and PVA/vinyl acetate copolymer hydrogels and the charged PVA/maleic acid hydrogel.

To confirm that the hydrogels obtained by direct solvolysis of PVTFA were indeed insolubilized only by crystallites, we conducted the following experiments: wet DSC, SAXS of the hydrogel, and dissolution of the hydrogels in boiling water. The sPVA was fully soluble in water, and wet DSC scans showed an endotherm that began around 60 °C. These results were in good agreement with the melting behavior observed in hydrated annealed samples in the work of Peppas and Merrill (4). SAXS results indicated that the gel is a two-phase system. For the homopolymer an interdomain spacing of 10.4 nm and a radius of gyration estimate (assuming spherical scattering centers) of 5.8 nm were obtained. The hydrogels were thus modeled as a two-phase system with a crystalline phase acting as pseudo-cross-links and an amorphous phase providing water swell. Table VII shows the modifications observed in hydrogel properties upon incorporation of a few percent of vinyl acetate (VOAc) comonomer into PVTFA.

To elucidate the mechanism by which the addition of hydrophobic comonomer increases water content and lowers strength, the change in percent crystallinity in sPVA copolymer films obtained by drying the gels was examined. Figure 1 shows the water content as well as the percent crystallinity determined by FTIR in the dried samples plotted against the amount of VOAc incorporated into the PVTFA. The percent crystallinity decreased strongly with the increasing amount of VOAc. By assuming that there was a direct relationship between the dried sample morphology and the direct

Table V. Effect of Vinyl Acetate Content on Water Swell
of PVA Hydrogels

Vinyl Acetate (wt % in PVTFA-co-VOAc)	Water (wt %)
0.0	51
1.0	71
2.0	81
3.0	87
4.0	92
5.0	94

Table VI. Protein Absorption ($\mu g/cm^2$) of Hydrogel Polymers

Hydrogel Polymer	Albumin	γ-Globulin	Lysozyme
PVA homopolymer	0.5	0.10	1.20
PVA-co-maleic acid	1.8	0.40	65.0
PVA-co-vinyl acetate	0.5	0.25	2.40

hydrogel morphology, the increased water uptake and decreased tensile properties observed with an increasing amount of VOAc can be explained. Incorporation of the VOAc appears to have interfered with crystallization, and thus reduced the effective "cross-link density" of the semicrystalline network. This effect was plausible because commercial PVA exhibited analogous behavior. PVA made by hydrolysis of poly(vinyl acetate) (PVOAc) dissolved more easily in water when the hydrolysis was less complete. This effect was also caused by the higher degree of crystallinity in samples with fewer residual VOAc groups.

Polymer Morphology During Processing

For the purpose of this work, "processing" includes three steps: PVTFA sample preparation, solvolysis, and hydration. PVTFA is a semicrystalline polymer that has not been studied extensively because of its poorly defined crystallinity. Wide-angle X-ray diffraction of unoriented polymer tends to give very diffuse scattering maxima. The polymer exhibited a distinct melting endotherm with a small ΔH of around 13 cal/g. In the most detailed structural study published, Bohn et al. (14) suggested that the X-ray data indicated a large-pitch helical structure for the chain. PVA, on the other hand, is believed to crystallize in a planar zig-zag conformation (15) with a much more typical ΔH of fusion of 30 cal/g (16).

Because the conversion of PVTFA used in this work occurred essentially in the solid state, one question that immediately arose was whether the

Table VII. Hydrogel Properties on Incorporation of VOAc Comonomer into PVA Hydrogels

VOAc[a] (wt %)	Water (wt %)	Tensile Modulus (MPa)	Tensile Strength (MPa)
0	51	6.8 ± 0.3	17.7 ± 2.4
1	71	0.82 ± 0.07	6.5 ± 1.0
2	81	0.27 ± 0.03	4.1 ± 1.4
3	87	0.10 ± 0.01	3.4 ± 0.7
4	92	0.01 ± 0.003	0.3 ± 0.1
5	94	<0.01	<0.3

[a]Polymer composition is expressed as weight % of the vinyl acetate in the PVTFA/VOAc copolymer used to prepare the PVA (copolymer) hydrogels.
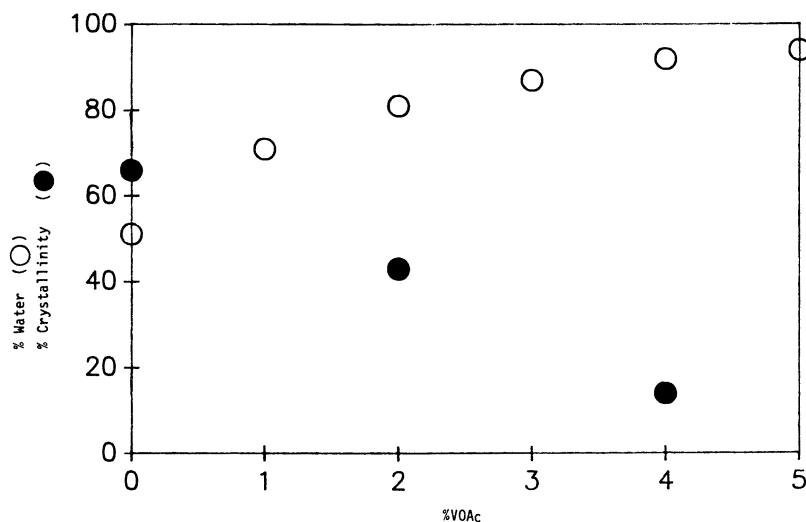
Figure 1. Water content and percent crystallinity in PVA hydrogels determined by FTIR in the dried samples vs. the amount of VOAc incorporated into the PVTFA.

morphology induced in the PVTFA film formation affected the morphology of the final PVA. To investigate this question, we prepared samples of PVTFA film in two ways: the solvent casting procedure already described and melt pressing in a hot press at 200 °C between aluminum platens. The significant differences that arose as a result of these procedures are illustrated by the melting endotherms in Figure 2. When both of these films were converted to PVA hydrogels, they exhibited the same water uptakes. In addition, DSC scans of the two dried films were identical, so it appears that morphological features present in the initial PVTFA samples were not retained throughout the conversion process.

1.5% VOAc Copolymer

Solvent-Cast PVTFA/VOAc   Melt-Pressed PVTFA/VOAc

Solvolysis

PVA/VOAc
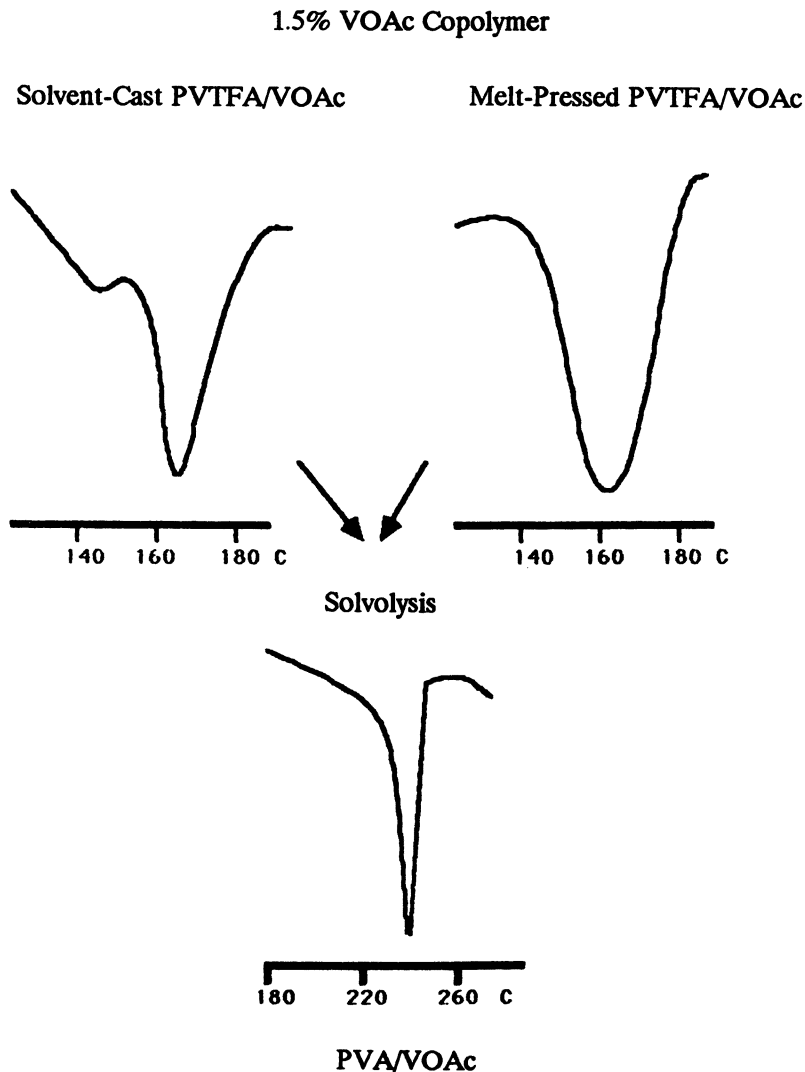
Figure 2. Endotherms for PVTFAs from the solvent casting procedure and melt pressing procedure and endotherm for PVA formed from PVTFA.

Effect of Hydration on Hydrogel Morphology

Samples were converted to sPVA and extensively washed with methanol to remove reaction byproducts. The solvolysis conditions remained constant. A portion of the samples were dried; the rest were first hydrated then dried.

Before hydration, the degree of crystallinity was measured as 56% and 53% by DSC and FTIR, respectively. After hydration, the degree of crys-
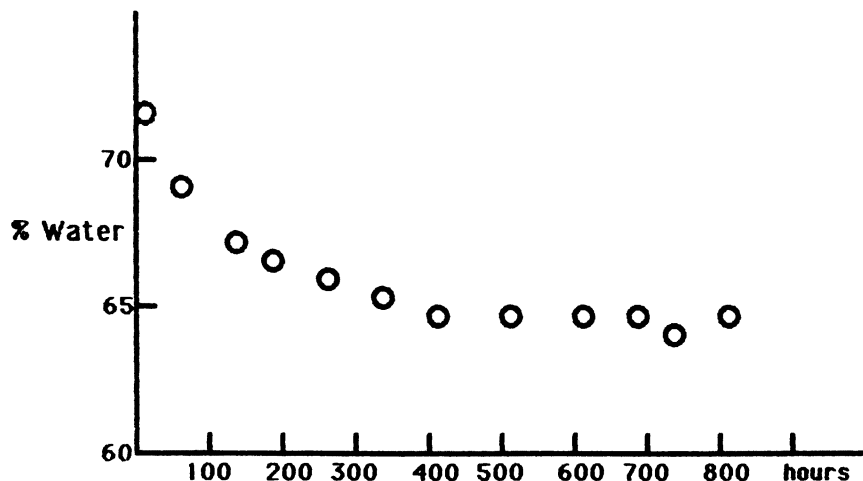
Figure 3. Water content of PVA hydrogel vs. time of hydration.

tallinity was measured as 64% and 66% by DSC and FTIR, respectively. There was a significant increase in the degree of crystallinity calculated by both techniques. The diffusion of water into the sPVA film should have introduced mobility into the system that could certainly have led to significant rearrangement. We cannot determine from these data alone whether the increased ΔH is caused by additional crystals forming or if it represents a rearrangement leading to more perfect crystallites. Additional information can be obtained by following the kinetics of water uptake in detail. When we collected such data, we found that there was substantial initial overshoot in water content followed by a gradual decline and equilibration (Figure 3). Such an overshoot suggests that rearrangement occurred.

Acknowledgments

References

1. Wichterle, O. U.S. Patent 2 976 576, 1960.
2. Stoy, V.; Stoy, A.; Zima, J.; Kala, J. U.S. Patent 4 173 606, 1979.
3. Peppas, N. A.; Mikos, A. G. In *Hydrogels in Medicine and Pharmacy*; Peppas, N. A., Ed.; CRC Press: Cleveland, OH, 1986; Vol. 1, pp 1–25.
4. Peppas, N. A.; Merrill, E. W. *J. Polym. Sci., Polym. Chem. Ed.* 1976, *14*, 441.

5. Lee, P. I. U.S. Patent 4 559 186, 1985.
6. Haas, H. C.; Emerson, E. S.; Schuler, N. W. *J. Polym. Sci.* **1956**, *22*, 291.
7. Ogasawara, K.; Nakajima, T.; Yamaura, K.; Matsuzawa, S. *Prog. Colloid Polym. Sci.* **1975**, *58*, 145.
8. Ogasawara, K.; Nakajima, T.; Yamaura, K.; Matsuzawa, S. *Colloid Polym. Sci.* **1976**, *254*, 456.
9. Ogasawara, K.; Nakajima, T.; Yamaura, K.; Matsuzawa, S. *Colloid Polym. Sci.* **1976**, *254*, 553.
10. Ogasawara, K.; Nakajima, T.; Yamaura, K.; Matsuzawa, S. *Colloid Polym. Sci.* **1976**, *254*, 982.
11. Matsuzawa, S.; Yamaura, K.; Maeda, R.; Ogasawara, K. *Makromol. Chem.* **1979**, *180*, 229.
12. Howk, B. U.S. Patent 2 436 144, 1948.
13. Vollmer, R.; Pritchard, J.; Lawrence, W.; Black, W. *J. Polym. Sci., Part A-1* **1966**, *4*, 707.
14. Bohn, C. R.; Schaefgen, J. R.; Statton, W. O. *J. Polym. Sci.* **1961**, *55*, 531.
15. Tadokoro, H. *Structure of Crystalline Polymers*; John Wiley & Sons: New York, 1979; p 153.
16. *Polymer Handbook*, 2nd ed.; Brandrup, J.; Immergut, E. H., Eds.; John Wiley & Sons: New York, 1975; pp 111–113.

Curdlan and Scleroglucan

NMR Characterization of Solution and Gel Properties

Arthur J. Stipanovic and Paul J. Giammatteo

Texaco Research Center, P.O. Box 509, Beacon, NY 12508

Cross polarization/magic angle spinning (CP/MAS) ^{13}C NMR and two-dimensional NMR methods were used to elucidate the molecular conformation, self-association mechanism, and gel domain structure of curdlan and scleroglucan in aqueous media. These polymers share a common molecular backbone [(1→3)-β-D-glucan], and both prefer to adopt a triple-helical (triplex) molecular conformation in the solid and solution states. Two-dimensional nuclear Overhauser enhancement (2D NOE) experiments on curdlan in aqueous NaOD confirm that a triplex to random-coil transformation occurs as NaOD concentration increases to near 0.25 M. CP/MAS ^{13}C NMR spectra of heat-annealed curdlan gels reveal the existence of anhydrous microcrystalline domains that strengthen the gel network. For scleroglucan gels, the domain morphology studied by CP/MAS differs from the solid state, particularly for the C-6 OH group. This observation suggests that these domains are not crystalline, a finding that is consistent with the thermally reversible character of scleroglucan gels.

W ATER-SOLUBLE MICROBIAL POLYSACCHARIDES represent an important class of compounds that are used to control the rheology of aqueous fluids and gels in applications ranging from foods to enhanced oil recovery (1–5). From a molecular perspective, the unique solution properties of many polysaccharides reflect a helical architecture that provides high viscosity and may encourage self-association in aqueous solution. Intermolecular association can be energetically driven by unfavorable polymer–solvent interactions and

hydrogen bonding. Aggregated or microcrystalline domains can then act as cross-links to establish viscoelastic solutions at low concentrations (0.025–0.25% w/v) and rigid gels at higher levels of polysaccharide (0.25–2.0% w/v) (6, 7).

We have used several NMR methods including ^{13}C NMR, cross polarization/magic angle spinning (CP/MAS) ^{13}C NMR, and two-dimensional (2D) NMR techniques to elucidate the molecular conformation, self-association mechanism, and cross-link domain structure of curdlan and scleroglucan in aqueous media. These extracellular microbial polysaccharides are produced by the bacterium *Alcaligenes faecalis* var *myxogenes* for curdlan and the fungus *Sclerotium rolfsii* for scleroglucan. Curdlan is a linear (1→3)-β-D-glucan; scleroglucan is branched on every third glucose residue (*see* structure). For both polysaccharides, a triple-helical molecular conformation (triplex) has been demonstrated to exist in the solid and solution states (8–17).
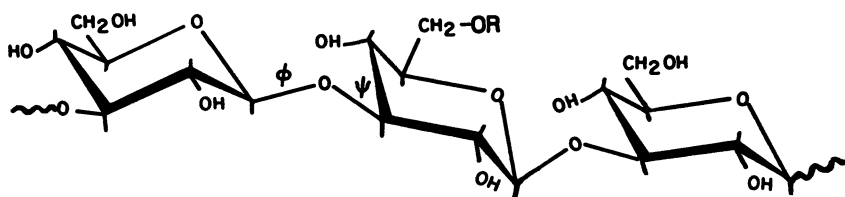
(1→3)-β-D-glucan: curdlan, R = H; scleroglucan, R = β-D-glucose

Experimental Details

Curdlan was obtained as a dry powder from Wako Pure Chemical Industries. The molecular weight distribution of similarly prepared samples typically ranges from 0.66 to 6.83 × 10^5 (13). A partially hydrolyzed curdlan sample was obtained by treating a 1.0% slurry of curdlan with β-(1→3)-hydrolase enzyme (Zymolase, Miles Scientific) at 40 °C for 2 h at pH 6.5. Crystalline polymorphic forms of curdlan were obtained and characterized as described previously (7). Scleroglucan was synthesized by the organism *Sclerotium rolfsii* in an aqueous fermentation medium containing glucose and nutrients. A molecular weight near 1.5 × 10^6 has been reported for this molecule (8, 18).

Curdlan gels were prepared by dispersing dry powder in D_2O followed by annealing in a sealed ampule at 60–120 °C. Scleroglucan gels were obtained by an ultrafiltration procedure that resulted in a concentration polarization of scleroglucan at the membrane surface. An Amicon stirred cell with an XM300 membrane was used. Gels were also prepared by cooling solutions of scleroglucans to below 10 °C. Rheological measurements were made at 25 °C with a Haake rotational viscometer with a Mooney–Ewart Couette sensor system.

One- and two-dimensional NMR spectra were recorded on a Varian VXR-300 instrument operating at 300 MHz for ¹H and 75 MHz for ¹³C. Homonuclear ¹H–¹H chemical shift correlation spectra (COSY) and two-dimensional nuclear Overhauser enhancement (2D NOE) experiments were performed as described in refs. 19 and 20. The heteronuclear proton–carbon correlation pulse sequence used was that of Garbow et al. (*21*) as modified by Wilde and Bolton (*22*). For the 2D NOE experiments, a 100-ms mixing time optimized observation of interresidue, conformation-dependent NOEs (Giammatteo, P.J., Texaco Research Center, unpublished data; *see* ref. 23). CP/MAS ¹³C NMR spectra were recorded by using bullet-type Kel-F rotors on a JEOL FX-60QS spectrometer, which was retrofit with a Chemagnetics M-100S magnet and solids accessory, at 25 MHz for ¹³C. For solid samples, a 1-ms contact time was used with a ¹H decoupling frequency of 44.1 KHz. CP/MAS spectra on gels were obtained by using a sealed glass rotor insert (described in ref. 24). Spectra were referenced to external hexamethylbenzene.

Results and Discussion

Solution Properties of Curdlan and Scleroglucan.   Although curdlan is insoluble in water at room temperature, it is readily dissolved in aqueous NaOH above 0.05 M (*10–12*). Further addition of NaOH results in a transformation from a triple-helix to random-coil conformation near 0.25 M NaOH. This denaturation process has been observed by optical rotation (*10*), flow birefringence (*11*), and ¹³C NMR (*13*). As shown in Figure 1, we followed this transformation by using steady shear viscosity measurements at a shear rate of 7.5 s⁻¹. A significant viscosity increase was observed in the range of 0.05–0.1 M NaOH corresponding to the solvation of intact rodlike triple helices followed by a viscosity reduction above 0.2 M NaOH as the triplex molecules are disassociated into single chains of lower molecular weight and aspect ratio. ¹³C NMR experiments support this conclusion on the basis of peak width narrowing that occurs upon denaturation of the rigid curdlan helix.

Solution viscosity and network strength data are given as a function of temperature in Figure 2 for scleroglucan in water. Network strength, or thixotropy, was determined by computing the area between shear stress vs. shear rate rheograms taken at increasing and decreasing rates of shear (0–15 and 15–0 s⁻¹). Thixotropy reflects the magnitude of self-association experienced by scleroglucan. Because this parameter is sensitive to many rheometer variables, it should be used only for comparison of samples recorded under similar conditions. As shown in Figure 2, scleroglucan displays a pronounced increase in network strength below 10 °C that is measurable to very low concentrations (125 ppm). A thermally driven transition to a gel state was reported previously (*8*, *14*) for significantly higher concentrations of scleroglucan. An increase in solution viscosity from 75 to 133 cP (7.5 s⁻¹) accompanied the increase in network strength for scleroglucan at 1000 ppm.

Viscosity – Centipoise (7.5s–1, 25C)

Homogeneous Solution of Triple Helices

13C–NMR Chemical Shifts = "Swollen" 7/1 Triplex

Random Coil – Single Chains
Narrow 13C–NMR Peakwidths

Curdlan Slurry

NaOH Concentration (Molar)
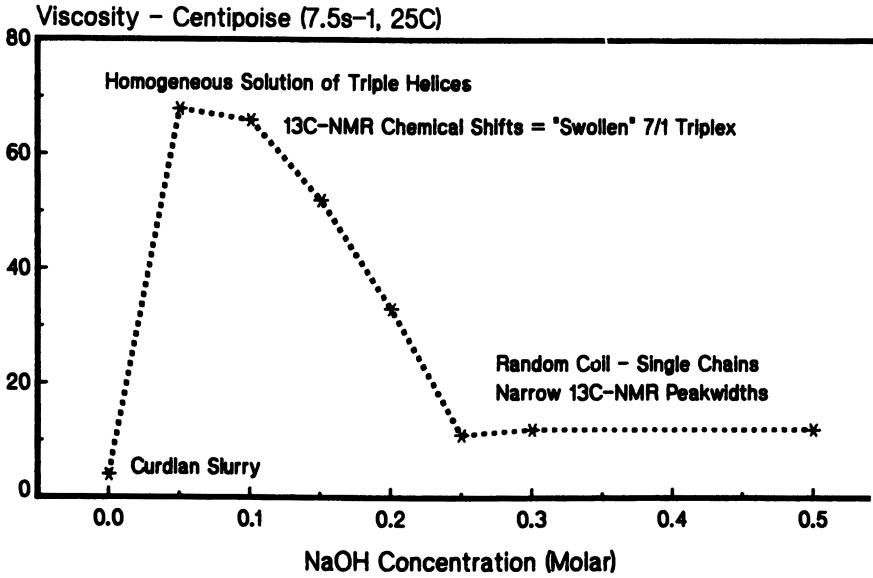
Figure 1. Viscosity of 1.0% curdlan in aqueous NaOH.

1000ppm   500ppm   250ppm   125ppm
────────   ·········   ×   ■

Network Strength (Joule x 10⁻3)

Viscosity (cps) =   133   74   75   75   75
1000 ppm

Temperature – °C
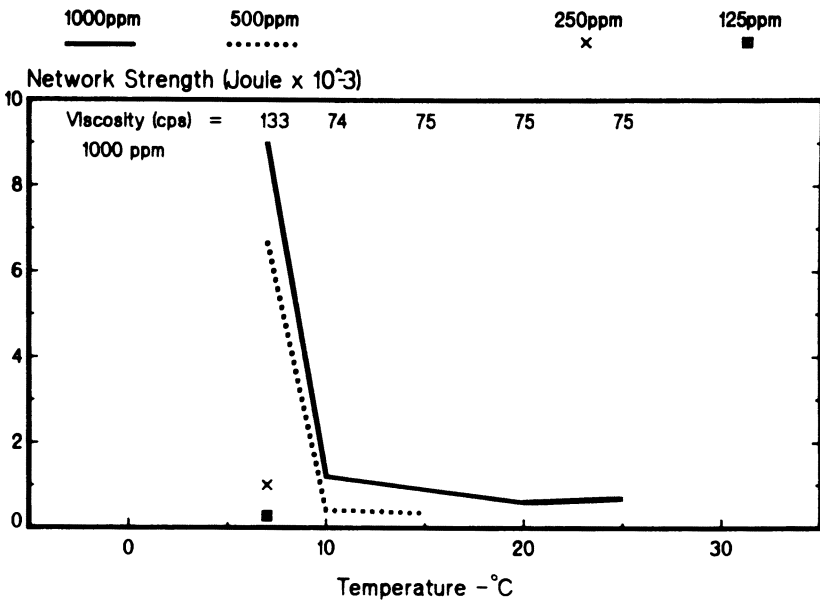
Figure 2. Network strength (thixotropy) of scleroglucan in H_2O.

Solution NMR Experiments with Curdlan.   In an effort to correlate the solution properties of curdlan with features of molecular conformation, the influence of NaOD concentration was studied by ^{13}C NMR as shown in Figure 3. In 0.1 M NaOD, curdlan displayed relatively broad resonance peaks corresponding to the restricted molecular motion of the triplex. The spectrum recorded at 0.5 M NaOD, above the critical denaturation concentration of 0.2 M, showed considerably improved resolution typical of a random-coil molecular conformation. Similar results were reported by Saito and Kasai (*11, 13*).

To probe further the coil conformation of curdlan in 0.5 M NaOD, 2D NMR methods were applied. The 2D ^{1}H–^{13}C heteronuclear correlation experiment (HETCOR) was useful in assigning proton chemical shifts to specific carbon atoms in the glucose residue (*19, 20*). For the spectrum given in Figure 4, the vertical axis (F2) represents carbon atom chemical shift, and the horizontal axis (F1) provides proton chemical shift information. A one-dimensional ^{13}C or ^{1}H spectrum can be obtained by projecting the contour plots onto the vertical or horizontal axis, respectively. Figure 4
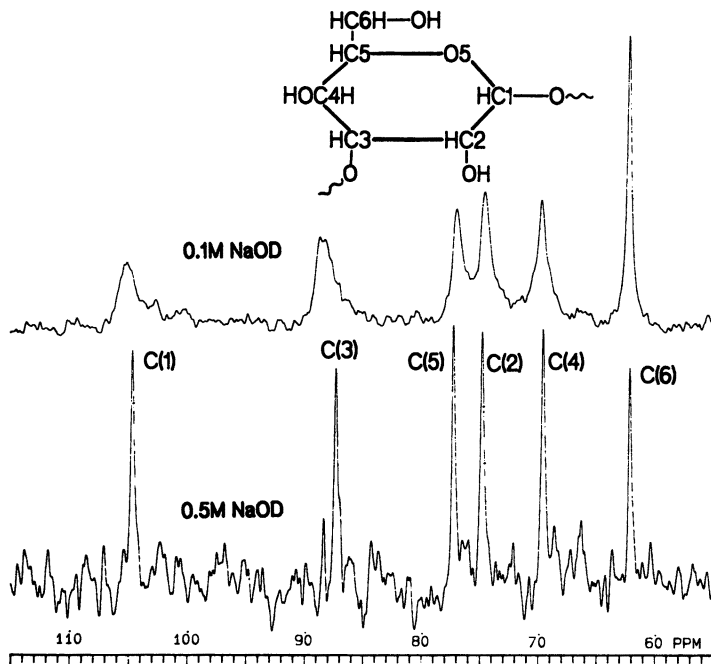
Figure 3. *^{13}C NMR of 1.0% curdlan in aqueous NaOD. Carbon atom assignments from ref. 11.*

contains seven contour peaks corresponding to the C–H atom pairs on C-1–C-5 and the H-6A–H-6B protons on C-6. On the basis of the curdlan carbon atom chemical shift assignments made by Saito (11) (Figure 3), 2D HETCOR data indicate that the chemical shifts for H-1, H-6A, and H-3 were near 4.6, 3.8, and 3.6 ppm, respectively. ¹H chemical shifts for the remaining protons were not easily assigned because they were all near 3.4 ppm.

The ¹H–¹H homonuclear correlation spectrum (COSY) in Figure 5 helps to confirm the proton assignments made by HETCOR for curdlan in 0.5 M NaOD. In this experiment, the diagonal axis represents a normal ¹H NMR spectrum, and off-diagonal contours result from proton–proton coupling interactions. From this information, connectivities between atoms in the ring system can be elucidated (19, 20). The dashed lines in Figure 5 illustrate that H-1 is coupled to the peaks at 3.35 ppm and confirm that H-2 is located in this group. The off-diagonal peaks coupled to H-2 help to confirm the assignment of H-3 at 3.55 ppm. Because the H-6A atom displays an off-
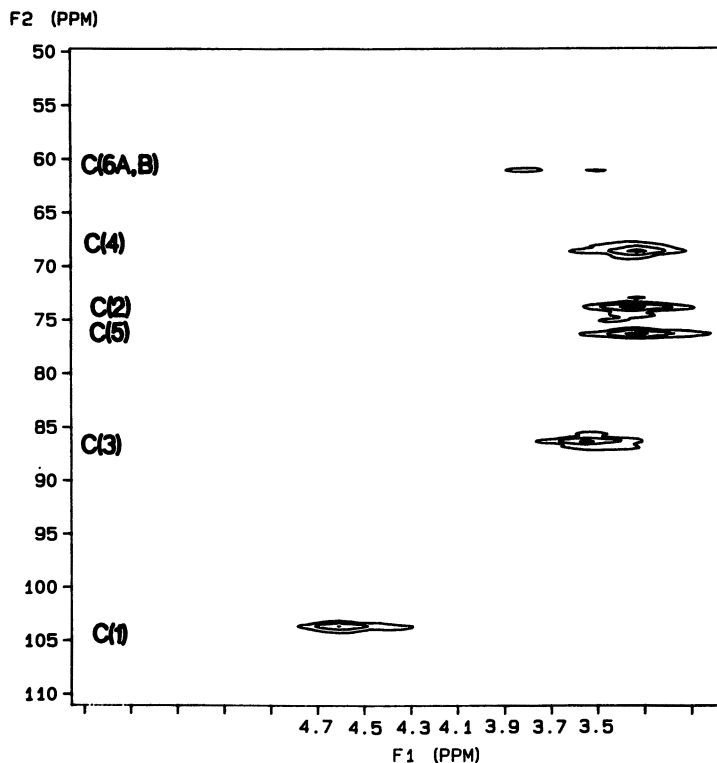
Figure 4. ¹³C–¹H heteronuclear correlation 2D NMR spectrum of 1.0% curdlan in 0.5 M NaOD.

F2 (PPM)
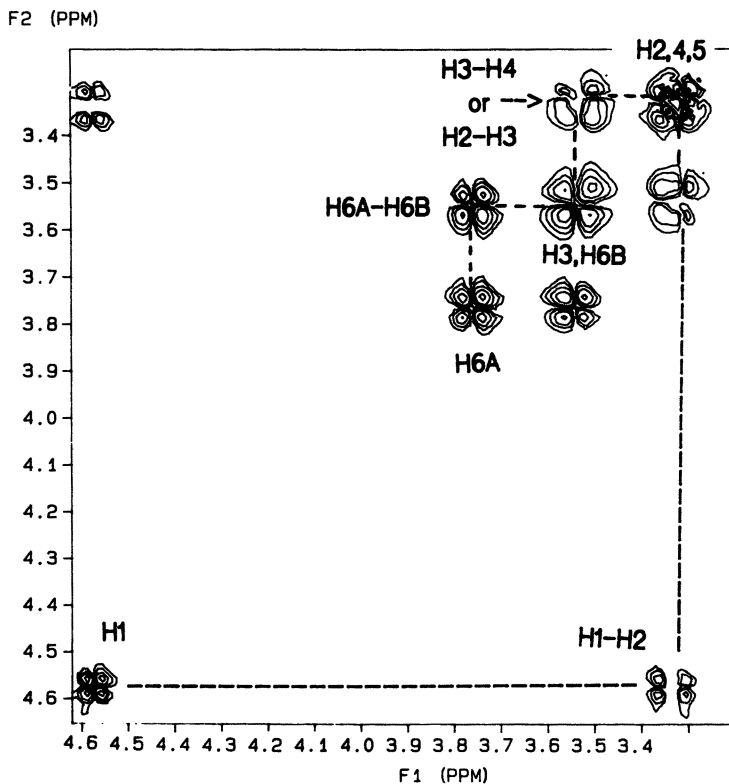
Figure 5. ¹H–¹H homonuclear correlation 2D NMR spectrum of 1.0% curdlan in 0.5 M NaOD. ¹H NMR spectrum lies along the diagonal.

diagonal interaction with the peak at 3.55 ppm, it may also be concluded that H-6B is found at this chemical shift.

With these proton assignments and the 2D NOE experiment, we monitored the molecular conformation of curdlan in 0.5 M NaOD. This method approximates interproton distances between nonbonded protons over the range of 1 to 5 Å. For the 2D NOE spectrum shown in Figure 6, both axes represent proton chemical shifts, and the diagonal is a normal ¹H NMR spectrum. Off-diagonal contours, in this case, indicate the through-space interactions of nearby protons (<5 Å). Interactions shown by the dashed lines in Figure 6 occur between H-1 and H-3; H-1 and H-2, 4, 5 unresolved proton cluster at 3.35 ppm; H-6A and H-6B; and H-3 and the H-2, 4, 5. Because these interacting protons are separated by less than 4.0 Å in the glucose monomer unit, the NOE data suggest that interresidue interactions are not present in 0.5 M NaOD. This result is most consistent with a random-

F2 (PPM)
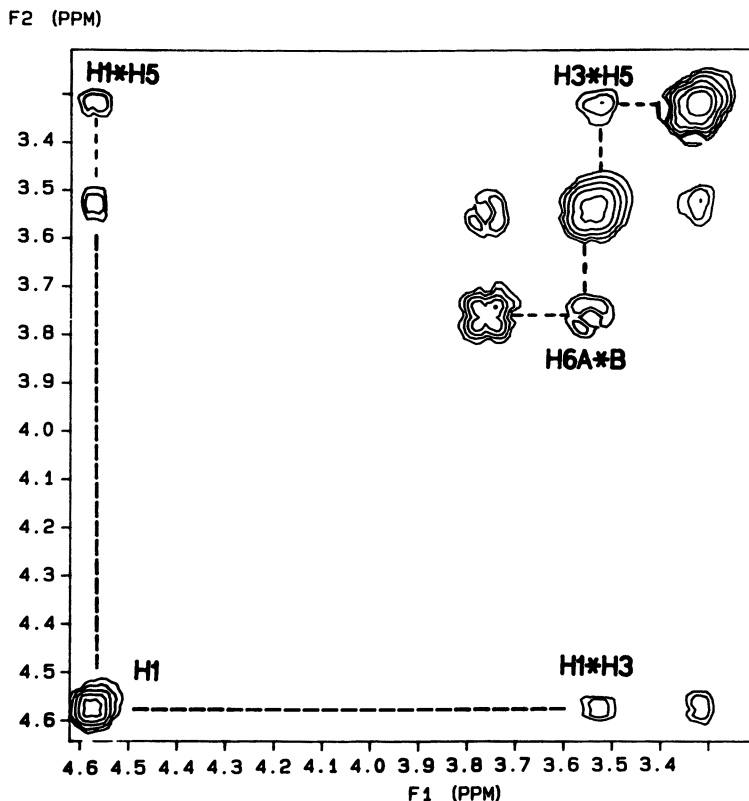
Figure 6. 2D NOE spectrum of 1.0% curdlan in 0.5 M NaOD. * denotes a through space interaction. ¹H NMR spectrum lies along the diagonal.

coil conformation for curdlan in aqueous NaOD. For other gel-forming water-soluble polysaccharides such as pustulan and gellan, NOE experiments revealed intermonomer proton interactions that arise from conformational ordering and helix formation (Giammatteo, P.J.; Stipanovic, A.J., Texaco Research Center, unpublished data).

A 2D NOE experiment was not attempted for as-received curdlan in 0.1 M NaOD because of signal broadening created by the restricted motion of the triplex conformation. However, a lower molecular weight (MW) enzyme-hydrolyzed sample provided improved resolution. This sample was prepared under heterogeneous-phase reaction conditions to preserve the native triplex. Saito (11) showed that triple helix formation for (1→3)-β-linked glucans requires a single chain degree of polymerization in excess of 49 (or a minimum triple helix MW ≥ 24,000). Single-chain molecular weights resulting from triplex denaturation in 0.5 M NaOD would be one-third that of native curdlan (0.22 to 2.3 × 10⁵). Therefore, assuming enzyme hydrolysis

reduces the effective MW of curdlan by cleaving intact triple helices, the effective MW of the enzyme-treated (0.1 M NaOD) and base-denatured (0.5 M NaOD) samples would be roughly comparable (10^4–10^5), but the 2D NOE results were vastly different.

Figure 7 contains a comparison of 2D NOE spectra for the random-coil (0.5 M NaOD) and the reduced-MW triplex structure (0.1 M NaOD) of curdlan. Figure 7a was obtained with data from the same experiment that produced Figure 6, but the 2D NOE data were rescaled to correspond to the contour magnitudes shown in Figure 7b (i.e., the H-1 on the diagonal had a similar signal-to-noise ratio in Figures 7a and 7b). For all NOE cross peaks, a significant increase in intensity was evident for the 0.1 M NaOD triplex solution, especially for the H-1–H-3; H-1–H-2, 4, 5; and H-6A–H-2, 4, 5 interactions. In the triplex conformation, opportunities exist for both intraresidue and interresidue NOE interactions across the glycosidic (1→3)-β-linkage of curdlan. With the sixfold triplex proposed for solid curdlan hydrate as a model (*16*), a strong H-1–H-3' interresidue NOE was expected because these atoms were separated by less than 2.0 Å. If rotation about the (1→3)-linkage is energetically allowed in 0.5 M NaOD, the average H-1–H-3' distance increased to 3–4 Å for the random-coil and would result in a reduced NOE cross peak as is observed in Figure 6. The H-1–H-2, 4, 5 cross peak shown in Figure 7b may also contain a contribution from interresidue NOEs because H-1–H-2', H-1–H-4', and H-1–H-5' are separated by 3.8, 4.4, and 3.8 Å, respectively, in the triplex structure.

It is more difficult to envision that the H-6A–H-2, 4, 5 cross peak displayed in Figure 7b resulted from an interresidue interaction. Calculations show that both C-6 protons are 5–8 Å removed from H-2', H-4', and H-5' of the successive residue. However, an O-4–O-6 intertriplex hydrogen bond that exists in the solid state of curdlan (*15*, *16*) may also persist in 0.1 M NaOD and yield an NOE cross peak resulting from a H-6–H-4 interaction between helices in an aggregated network structure.

CP/MAS ^{13}C NMR of Curdlan Gels.

The physical properties and morphology of aqueous curdlan gels were studied extensively by Harada and co-workers (*10*, *13*). Gels are typically prepared by heating a slurry of curdlan in water (1–3% w/v) to 60 °C where a low strength network is established. Upon further annealing of curdlan gels to 80–90 °C, a significant increase in strength is observed yielding a high-set gel (*10*, *12*). Harada (*10*) attributed this increase in strength to the development of additional cross-links via hydrophobic bonding. In this study, CP/MAS ^{13}C NMR was used to characterize the differences in molecular conformation and supramolecular morphology between the low- and high-strength forms of curdlan gel.

To establish a CP/MAS ^{13}C NMR data base for curdlan, partially crystalline solid samples were first analyzed. As shown in Table I, curdlan exists
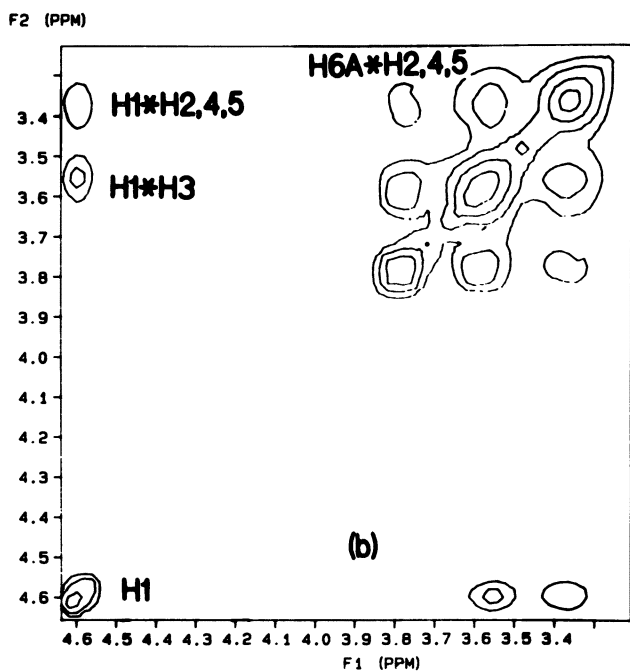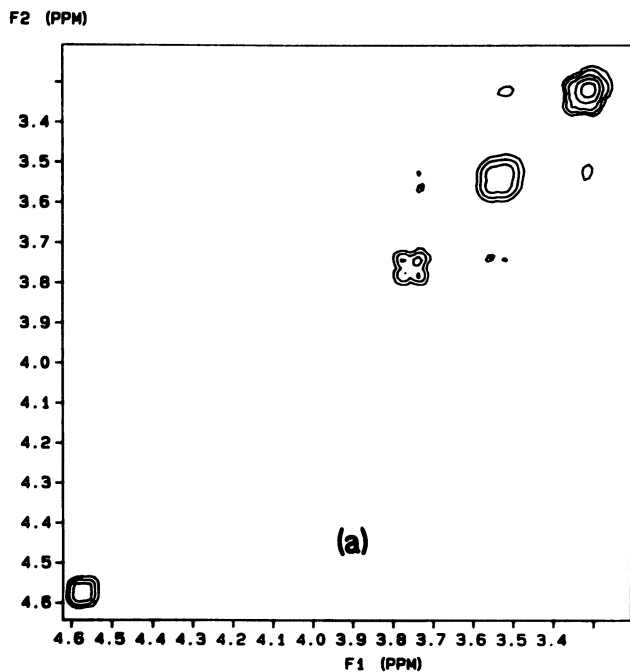
Figure 7. 2D NOE of 1.0% curdlan. a, 0.5 M NaOD, and b, 0.1 M NaOD, enzyme-hydrolyzed sample.

Table I. Crystal Polymorphism of Curdlan

Polymorphic Form	Molecular Conformation	Helix Repeat (Å)	Rise/Glucose (Å)
Anhydrous (20)	6/1 triplex	17.6	2.93
Hydrate (21)	6/1 triplex	18.8	3.13
Swollen (12, 22)	7/1 triplex (?)	22.7	3.24

in at least three polymorphic crystalline forms differing in the degree of lattice hydration and chain extension. The anhydrous and hydrate forms adopt a sixfold triple-helical conformation, whereas the swollen polymorph is a sevenfold helix that may also be a triplex (12, 17). CP/MAS ^{13}C NMR data recorded for the three crystalline polymorphs of curdlan are summarized in Table II. Carbon atom assignments were made on the basis of solution experiments for C-1, C-3, and C-6 because extrapolation to the solid state could be made with confidence. Resonances due to C-2, C-4, and C-5 were not assigned. Table II reveals that the C-1 linkage atom is near 104–105 ppm for all polymorphs, whereas the C-3 resonance of anhydrous curdlan is shifted 3–4 ppm downfield to 91 ppm compared to the other forms. Chemical shift differences are also apparent at 79 ppm, where only the hydrate spectrum shows a resonance, and near 74 ppm where the swollen and anhydrous polymorphs provide a peak.

Using these chemical shift differences as probes of crystalline polymorphy, we applied CP/MAS ^{13}C NMR to the low- and high-strength gels of curdlan in water (20% w/v in D_2O). As shown in Figure 8a, the gel prepared at 60 °C yielded a spectrum similar to the swollen sevenfold helical form of solid curdlan in that probe resonances are seen at 88, 74, and 69 ppm. Because the extensively hydrated, swollen sevenfold polymorphic form of curdlan is likely to be present in the aqueous curdlan slurry used to form the low-set gel, the initial gelation process at 60 °C does not introduce a major conformational transformation of the sevenfold model. As this gel is further annealed at 95 °C, the CP/MAS spectrum develops a multiplicity in the C-3 resonance, a result suggesting a partial transformation from the swollen sevenfold form to the anhydrous sixfold triplex, which is characterized by a C-3 signal near 91 ppm (compare Figures 8a and 8b). These domains apparently provided an additional degree of cross-linking that accounts for the enhanced strength of the high-set gel. With more extensive annealing at 120 °C, the CP/MAS gel spectrum becomes dominated by the hydrate

Table II. CP/MAS ^{13}C NMR of Solid Curdlan

Polymorphic Form	Chemical Shift (ppm)							
	C-1	C-3	79	76	74	71	69	C-6
Anhydrous	105	91	−	+	+	+	−	63
Hydrate	104	87	+	+	−	−	+	62
Swollen	105	88	−	+	+	−	+	62

NOTE: +, peak observed; −, no resonance.
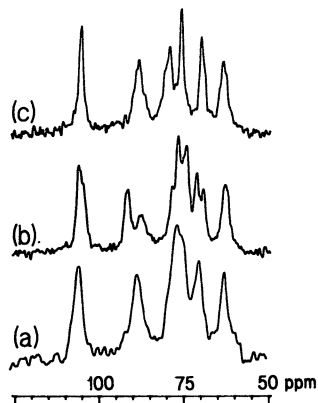
Figure 8. CP/MAS ^{13}C NMR spectra of curdlan gels (20% w/v in D_2O). a, 60 °C, 2 min; b, 95 °C, 2 h; and c, 120 °C, 72 h.

crystalline polymorph, which is also a sixfold molecular conformation containing water between helical cylinders of curdlan (16).

Gels of curdlan can also be prepared by neutralizing an aqueous NaOH solution of this polysaccharide. For the system we have studied, a 0.5 M NaOH solution containing 5% curdlan was subjected to dialysis against water to yield a gel. Under these conditions curdlan would be present as random-coil rather than triplex structure before gelation. A CP/MAS ^{13}C NMR spectrum of this gel is compared in Figure 9 to the heat-treated low-set gel that contains the sevenfold conformation of the swollen polymorphic form. The regenerated gel displays a more complex peak profile with the 79-ppm resonance typical of the sixfold hydrate polymorph. Possibly, hydrogen bonding patterns between curdlan and water are similar in the regenerated gel and the solid hydrate; this possibility accounts for the 79-ppm resonance.

CP/MAS ^{13}C NMR of Scleroglucan.

Solid, crystalline scleroglucan exists as a single anhydrous polymorph in contrast to the several crystalline forms of curdlan (8). Bluhm (8) proposed that the molecular conformation of scleroglucan is a triplex structure with a repeat distance along the chain
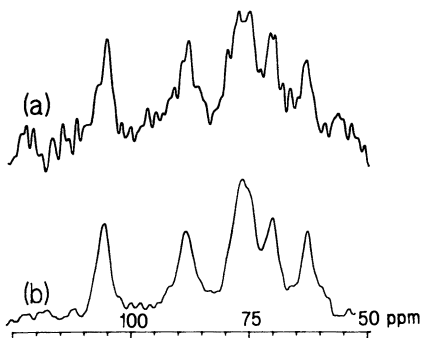
Figure 9. CP/MAS of curdlan gels. a, 5% w/v regenerated from 0.5 M NaOH; and b, 60 °C low-set gel.

axis of 18 Å (*see* Table I for a comparison to curdlan). Yanaki (*9*) determined that this triplex also exists in neutral, aqueous solution. A CP/MAS ^{13}C NMR spectrum of solid scleroglucan is shown in Figure 10. The relatively poor signal resolution is consistent with the low degree of crystallinity determined by X-ray diffraction (*8*) and is an obvious manifestation of the branched structure of scleroglucan.

The C-6 resonance of scleroglucan occurs near 70 ppm where it is unresolvable from the C-4 resonance. A relationship between C-6 chemical shift and O-6 rotation about the C-5–C-6 bond has been described by Horii for (1→4)-β-D-glucose model compounds (*25*). If this correlation holds for (1→3)-linked glucans as well, the C-6 chemical shift of scleroglucan suggests an O-6 orientation of *tg* (*trans* to C-5–O-5 and *gauche* to C-4–C-5). Although an X-ray crystal structure analysis has not been performed on scleroglucan, results for anhydrous curdlan have shown that *tg* is the favored position for O-6 in the triplex. CP/MAS ^{13}C NMR data could not reveal the O-6 orientation of the branch linkage because the incorporation of C-6 into a glycosidic bond has the effect of shifting its resonance to 70 ppm where it overlaps with other resonances (*6*).

The CP/MAS ^{13}C NMR spectrum of scleroglucan gel is also given in Figure 10. This spectrum differs from the solid material in that the C-6 resonance is shifted upfield to 62 ppm. The Horii correlation predicts that the O-6 atom is rotated away from the favored *tg* position in the solid to a *gg* orientation in the gel. Such a rotation may encourage intermolecular hydrogen bonding and thereby drive the self-association of triplex molecules. Testing this hypothesis is not easy because relatively poor signal resolution
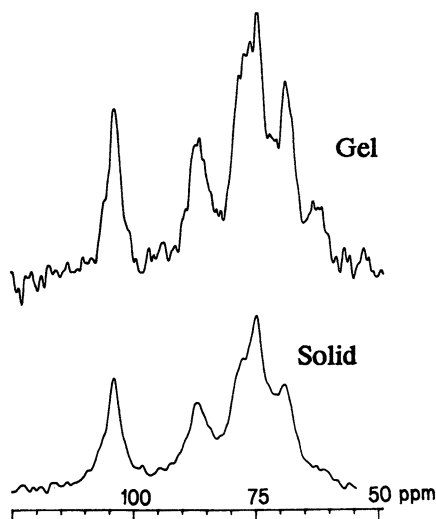
Figure 10. CP/MAS ^{13}C NMR of scleroglucan (approximately 10% w/v in D$_2$O).

is observed for the solid and gel scleroglucan samples. It is, therefore, difficult to quantify the contribution of each O-6 rotamer (*tg*, *gg*) to the total C-6 signal observed. However, for scleroglucan, it appears that crystalline domains are not formed in the gel, and this finding may account for the thermally reversible character of these materials.

Summary

The solution conformation and gel domain structure of curdlan and scleroglucan were evaluated by CP/MAS and 2D NMR methods. Results were in agreement with previous conclusions indicating that these polysaccharides adopt a rodlike triplex conformation in aqueous media and readily self-associate to form networks and gels. For curdlan, gel domains were crystalline; scleroglucan gels did not display a direct correlation to the crystalline polymorphic form of this molecule. The branched structure of scleroglucan apparently perturbs the crystallization of associated domains in water, although more transient, temperature-dependent interactions are evident from rheological measurements.

Acknowledgment

References

1. *Extracellular Microbial Polysaccharides*; Sandford, P. A.; Laskin, A., Eds.; ACS Symposium Series 45; American Chemical Society: Washington, DC, 1977.
2. *Solution Properties of Polysaccharides*; Brant, D. A., Ed.; ACS Symposium Series 150; American Chemical Society: Washington, DC, 1981.
3. Crescenzi, V.; Dea, I. C. M.; Stivala, S. S. *New Developments in Industrial Polysaccharides*; Gordon and Breach: New York, 1985.
4. Stivala, S. S.; Crescenzi, V.; Dea, I. C. M. *Industrial Polysaccharides: The Impact of Biotechnology and Advanced Methodologies*; Gordon and Breach: New York, 1987.
5. Davidson, R. L. *Handbook of Water-Soluble Gums and Resins*; McGraw-Hill: New York, 1980.
6. Stipanovic, A. J.; Giammatteo, P. J.; Robie, S. B. *Biopolymers* **1985**, *24*, 2333–2343.
7. Stipanovic, A. J.; Giammatteo, P. J. *Ind. Polysac.: Genet. Eng. Struct. Prop. Relat. Appl.* **1987**, *3*, 281–292.
8. Bluhm, T. L.; Deslandes, Y.; Marchessault, R. H.; Perez, S.; Rinaudo, M.; *Carbohydr. Res.* **1982**, *100*, 117–130.
9. Yanaki, T.; Kojima, T.; Norisuye, T. *Polym. J. (Tokyo)* **1981**, *13*(12), 1135–1143.
10. Harada, T. In *Extracellular Microbial Polysaccharides*; Sandford, P. A.; Laskin, A., Eds.; ACS Symposium Series 45, American Chemical Society: Washington, DC, 1977; pp 265–283.

11. Saito, H. In *Solution Properties of Polysaccharides*; Brant, D. A., Ed.; ACS Symposium Series 150; American Chemical Society: Washington, DC, 1981; pp 125–147.
12. Fulton, W. S.; Atkins, E. D. T. In *Fiber Diffraction Methods*; French, A. D.; Gardner, K. H., Eds.; ACS Symposium Series 141; American Chemical Society: Washington, DC, 1980; pp 385–410.
13. Kasai, N.; Harada, T. In *Fiber Diffraction Methods*; French, A. D.; Gardner, K. H., Eds.; ACS Symposium Series 141; American Chemical Society: Washington, DC, 1980; pp 363–383.
14. Biver, C.; Lesel, J.; Allain, C.; Salome, L.; Lecourtier, J. *Polym. Commun.* **1986**, *27*, 351–353.
15. Deslandes, Y.; Marchessault, R. H.; Sarko, A. *Macromolecules* **1980**, *13*, 1466–1471.
16. Chuah, C. T.; Sarko, A.; Deslandes, Y.; Marchessault, R. H. *Macromolecules* **1983**, *16*, 1375–1382.
17. Takeda, H.; Yasuoka, N.; Kasai, N.; Harada, T. *Polym. J. (Tokyo)* **1978**, *10*(3), 365–368.
18. *Actigum CS11*; technical bulletin; CECA SA: Velizy—Villacoublay Cedex, France, 1982.
19. Kessler, H.; Oschkinat, H.; Loosli, H. R. In *Two-Dimensional NMR Spectroscopy: Applications for Chemists and Biochemists*; Croasmum, W. F.; Carlson, R. M. K., Eds.; VCH Publishers: New York, 1987; pp 259–295.
20. Dabrowski, J. In *Two-Dimensional NMR Spectroscopy: Applications for Chemists and Biochemists*; Croasmum, W. R.; Carlson, R. M. K., Eds.; VCH Publishers: New York, 1987; pp 349–386.
21. Garbow, J. R.; Weitekamp, D. P.; Pines, A. *Chem. Phys. Lett.* **1982**, *93*, 504–509.
22. Wilde, J. A.; Bolton, P. H. *J. Magn. Reson.* **1984**, *59*, 343–346.
23. Homans, S. W.; Dwek, R. A.; Rademacher, T. W. *Biochemistry* **1987**, *26*, 6571–6578.
24. Giammatteo, P. J.; Hellmuth, W. W.; Ticehurst, F. G. *J. Magn. Reson.* **1987**, *71*, 147–150.
25. Horii, F.; Hirai, A.; Kitamaru, R. *Bull. Magn. Reson.* **1983**, *5*, 190.

The Effects of Shear History on the Rheology of Hydroxypropyl Guar Gels

Robert K. Prud'homme[1], Vernon Constien[2], and Susan Knoll[3]

[1]Department of Chemical Engineering, Princeton University,
 Princeton, NJ 08544
[2]Dowell Schlumberger, P.O. Box 2710, Tulsa, OK 74101
[3]Aqualon Corporation, Houston, TX 77084

We present both a review and new data on the rheology of gels formed by cross-linking water-soluble polymers with metal ions. These gels are used in the oil and gas industries to transport solid particulates (proppants) in hydraulic fracturing operations in which hydraulic pressure is used to fracture subterranean oil formations to increase the rate of oil production. The rheology of the gels is determined by complex interactions between the polymer and metal-ion chemistries, the temperature history, and the shear history experienced by the gel during cross-linking. We review the chemistry of the polysaccharide polymers (substituted guar gums) most widely used in these processes and the reactions occurring with titanate, zirconate, and borate cross-linkers. The effects of mixing on gel structure and rheology are demonstrated, and techniques for reproducible micromixing are described. Exposure to high shear rates during cross-linking are shown to decrease the viscosity of the gels. Delayed cross-linker systems that achieve cross-linking after the high-shear period has passed are shown to produce higher viscosity gels. Finally, it is demonstrated that with proper control of mixing, temperature, and shear rate, it is possible to obtain similar viscosity values from measurements with different Couette and capillary viscometers.

WATER-SWELLABLE GELS AND GELATION have recently become the objects of considerable interest. Gels can be formed by a number of mecha-

nisms: physical association (*1, 2*), copolymerization with multifunctional monomers (*3, 4*), or metal-ion cross-linking (*5–9*). One of the major industrial applications of water-soluble polymer gels occurs in the oil and gas industries where polymer molecules are cross-linked with metal ions to form viscous fluids used to transport solid particles into fractures in subterranean oil formations in a process called hydraulic fracturing. The most common polymers used in fracturing processes are guar gums and guar gum derivatives. Cross-linking is achieved by any one of a number of metal ions (*9*); titanates, zirconates, and borates are among the most widely used. In this chapter, our goal is to present a review of the current understanding of the rheology and properties of cross-linked gels used in hydraulic fracturing. Of particular interest is the effect of shear history on the viscosity of fracturing fluid gels. The fundamental principles that govern the cross-linking of fracturing fluids apply broadly to other systems in which polymer molecules in semidilute solution are cross-linked.

The chapter is organized in the following manner. First, a description of the hydraulic fracturing process is presented to highlight those chemical and process variables that are most important in understanding gel rheology. The chemistry of the guar polymers and metal-ion cross-linkers are presented in the section entitled Gel Structure: Chemical Effects. In the section entitled Viscosity Measurements, the effect of flow history on the gelation process is discussed. The interaction of cross-linking chemical kinetics and mixing is shown to have a dominant effect on the morphology and rheology of the gels. These interactions dictate conditions required to make meaningful and reproducible measurements of the viscosity of fracturing fluid gels. Finally, methods to uncouple chemical kinetics from mixing by using delayed cross-linking systems are described.

Hydraulic fracturing is a method of stimulating production of oil or gas from reservoir formations. Fracturing fluids are pumped into a well bore at sufficient pressure and rate to create a fracture in the rock formation. Solid particles in the size range of 0.1–2.0 mm in diameter ("proppants") are transported down the well bore and out into the fracture by the viscous fracturing fluid. The propping agents are sand or sintered bauxite, which, when consolidated, have a higher permeability than the surrounding oil-bearing rock. When pumping is stopped, and the hydraulic pressure decreases, the fracture closes except for those portions that have been held open by the propping agents. The proppant-filled fracture provides a highly permeable channel for flow to the well bore, and thus increases the rate of oil or gas production.

A hydraulic fracturing operation might involve pumping several million gallons of gelled polymer solution and several million pounds of proppant. Because of the expense and effort required to drill, complete, and stimulate oil and gas wells, considerable effort is made designing the fracturing treatment to produce the optimum results. Reliable data on the rheology of the fracturing fluid is critical to estimate the fracture dimensions that will be

created, the placement of the propping agent in the fracture, and the friction pressure that will result from pumping the fluid at high rates through tubing or casing in the well bore. A major problem in fracture design has been the lack of representative and reproducible fluid rheology data for cross-linked gels.

Un-cross-linked hydroxypropyl guar (HPG) solutions are frequently used as fracturing fluids in low-temperature applications where only moderate fluid viscosities are required. For higher temperature treatments or designs requiring high viscosities at low polymer concentrations, cross-linking agents are used to produce viscoelastic gels. Cross-linking agents most frequently used are borate salts and chelated forms of Ti(IV) or Zr(IV). The cross-linking agents are metered into the fluid during the fracturing treatment as the polymer and proppant are injected into the well bore. Cross-linking either occurs immediately or can be delayed chemically or thermally until the fluid is deeper into the formation. Additional details on the formulation of commercial fracturing fluids can be found in a recent review (*10*).

The rheology of the more complex cross-linked HPG gels is determined by the structure of the gel network, which in turn is controlled by cross-linker reaction kinetics and flow conditions during cross-linking. Fracturing fluids experience wide variations in shear and temperature during injection. The highest shear rates experienced by the fluid occur immediately after addition of cross-linking agents as the fluid is being pumped through the well bore tubing and through the perforations in the well bore casing. Shear rates in the well bore range from several hundred to over 1000 s^{-1}, but the exposure time is relatively short—on the order of tens of minutes. Once the fluid enters the fracture, the shear on the fluid is substantially reduced because the cross-sectional area for flow is greatly enlarged. The time for fluid to flow to the tip of the fracture might range from 30 min to 8 h. In the fracture, the fluid temperature increases until it reaches formation temperature, which varies from 25 °C in shallow wells to over 150 °C in very deep formations.

The strong dependence of gel properties on chemistry, thermal history, and shear history during cross-linking has made the task of making reproducible laboratory rheological measurements and relating these results to actual field performance an especially difficult problem. Resolving the problem has required the development of improved instruments and techniques for preparing and testing fracturing fluids under controlled shear and temperature conditions. Also, a better fundamental understanding of the cross-linker and gel structure was required.

Gel Structure: Chemical Effects

Guar Polymer Chemistry. Guar is a high molecular weight polysaccharide composed of a linear chain of D-mannose residues with randomly pendant D-galactosyl units (*see* structure). The ratio of anhydromannose to
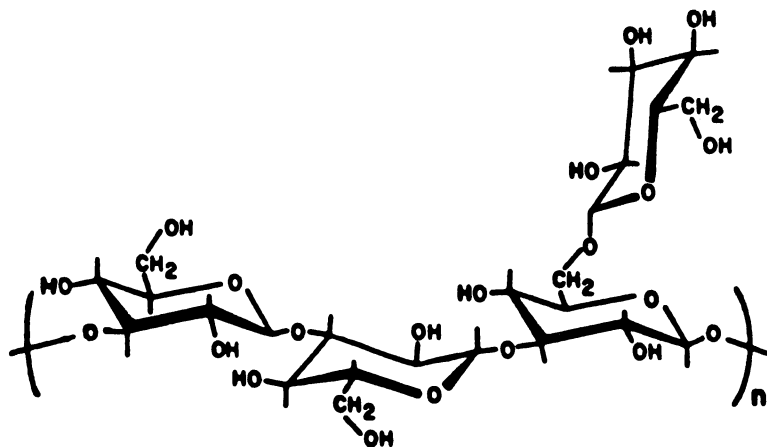
Molecular structure of guar gum showing the mannose backbone structure and the random galactose side-chain structure.

anhydrogalactose units is reportedly in the range of 1.7 to 1 (*11*). The role of the polysaccharide molecular structure on its solubility and reactivity has been discussed by Glass (*12*) and others (*1, 2, 13*). The guar polymer has many hydroxyl groups that will react with propylene oxide under basic conditions to form HPG. The final amount of propylene oxide attached to the polymer can be expressed in terms of *molar substitution*, frequently abbreviated as MS, which is defined as the moles of propylene oxide per mole of pyranose groups. The placement of the propylene oxide groups on the guar was investigated by Albersheim (*13*) using NMR. Typically, less than 40% of the sugar residues are substituted with at least one hydroxy-propyl group.

Hydroxypropylation of the guar polymer was initially instituted to aid in the removal of protein from the raw guar polymer to produce polymer solutions that did not plug the pore spaces in reservoir formations. However, the amount of hydroxypropyl substitution on the polymer also affects the gel structure that is formed when the polymer is cross-linked in two ways. First, the hydroxypropyl group may be added at a hydroxyl that is in a cis config-uration, for example at the C-2 or C-3 position of a mannose residue or the C-3 or C-4 position of a galactose residue. This geometry plays a role in the formation of cross-links, although the details of the reaction mechanism are still poorly defined (*14, 15*). When hydroxypropyl groups are substituted at these cis positions, the number of cross-link sites on the polymer is reduced, and a weaker gel structure results. Second, the addition of propyl groups sterically prevents polymer chain interactions. Mannose-rich regions in the polymer chain tend to associate via hydrogen bonding to form supramolecular aggregates (*1, 2*) that increase solution viscosity and increase the kinetics of HPG gelation because the reaction is no longer controlled by the polymer

chain diffusion. Decreasing association by increasing propylene oxide substitution alters the gelation process by both mechanisms just described (*16*).

Metal-Ion Cross-Linker Chemistry.

The most commonly used metal-ion cross-linkers are titanates, zirconates, and borates. Titanate and zirconate gels display significantly different properties than borate gels, and these differences indicate the different nature of the cross-linking for the two types of ions. For example, gels produced by transition metal ions are more thermally stable than borate gels and do not recover viscosity after exposure to shear.

These differences are shown in the following examples where measurements of the dynamic moduli, G' and G'' are used to monitor the structure of gel networks. Measurements are performed by imposing an oscillatory shear field on the material and measuring the oscillatory stress response. The stress is decomposed into a component in phase with the displacement (which defines the storage modulus G') and a component 90° out of phase (which defines the loss modulus G''). The value of G' indicates the elastic and network structure in the system (*15*, *17*, *18*) and can be interpreted by using polymer kinetic theories.

Figure 1 shows the dynamic moduli as a function of frequency for an HPG–borate gel (0.48 wt % HPG, 3 wt % sodium tetraborate, 2 wt % KCl) at ambient temperature. The moduli show solidlike behavior: the storage modulus is independent of frequency and higher than the loss modulus. At 65 °C, in Figure 2, the moduli show fluidlike behavior, and both moduli decrease at low frequency. This thermal "melting" is characteristic of borate gels and limits their application in high-temperature environments.
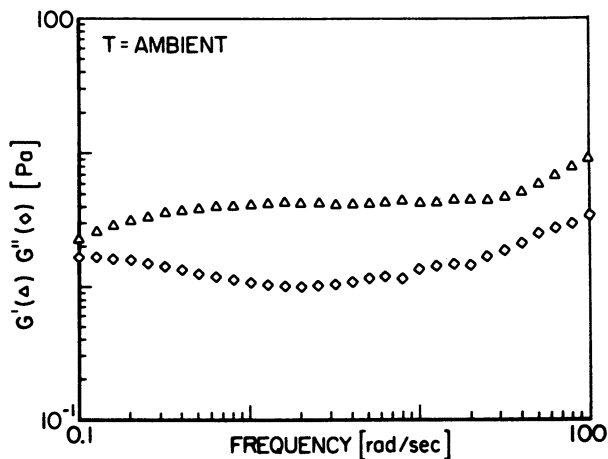
Figure 1. Storage modulus, G', vs. frequency for an HPG–borate gel at ambient temperature. 0.48 wt % HPG, 2 wt % KCl, 3 wt % sodium tetraborate at pH 9. (Reproduced with permission from ref. 6. Copyright 1988 Steinkopff.)
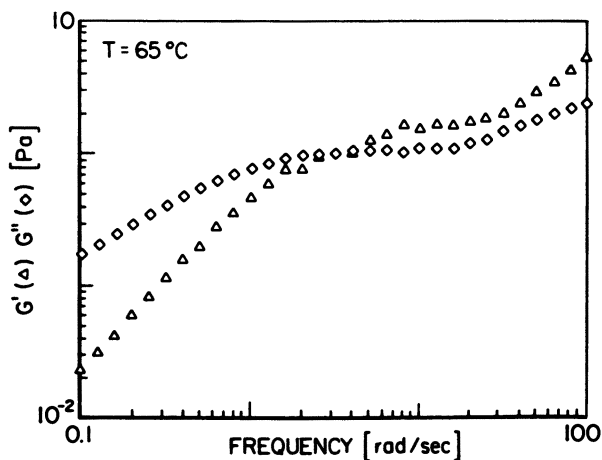
Figure 2. Storage modulus, G', vs. frequency for an HPG–borate gel at 65 °C. 0.48 wt % HPG, 2 wt % KCl, 3 wt % sodium tetraborate at pH 9. (Reproduced with permission from ref. 6. Copyright 1988 Steinkopff.)

In contrast, titanate gels show no appreciable degradation in structure until temperatures are raised high enough to degrade the guar mannose backbone. The moduli of HPG titanate gels formed quiescently are shown in Figure 3. If the gel is sheared for 15 min at 1350 s^{-1} and the moduli are measured after shearing, the values are decreased as shown in Figure 4. The level of the storage modulus, G', has dropped below the level of the loss modulus G'', a result indicating a disruption of the network structure by shear. The original level of structure can never be recovered with HPG–titanate gels; however, for HPG–borate gels, shear has no effect on the moduli.

The borate–HPG cross-links are labile and lead to the gels healing rapidly after shear. A number of studies (16, 19, 20) have used NMR to investigate boron–hydroxyl interactions. ^{11}B NMR measurements (16) on model galactopyranose and mannopyrannose sugars showed that the lifetime of a borate–polymer interaction is on the order of 1 ms. Some evidence indicates that the borate–polymer interaction occurs through cis hydroxyls on the sugar residues (19), which is the reason that other polysaccharides with equal numbers of hydroxyls but without cis hydroxyls cannot be cross-linked.

The chemistry of the titanate or zirconate–polymer interactions is more complex. Both titanates and zirconates are highly reactive with water and undergo hydrolysis reactions that lead to inorganic oxides. The desired cross-linking reaction between the sugar hydroxyls and the transition metal ions is analogous to esterification reactions involving the production of polyester in which titanates are used as catalysts (21). However, the organic esterification reactions are always conducted under anhydrous conditions to prevent
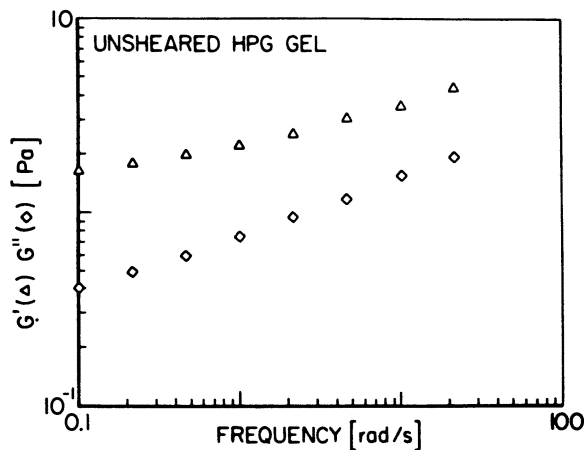
Figure 3. Storage modulus, G', vs. frequency for unsheared HPG–titanate gel. 0.48 wt % HPG, 2 wt % KCl, cross-linked with 0.4 vol % solution of 9 parts by volume isopropyl alcohol to 1 part Tyzor AA (titanium acetylaceto-nate). Data taken at 100% strain. (Reproduced with permission from ref. 6. Copyright 1988 Steinkopff.)
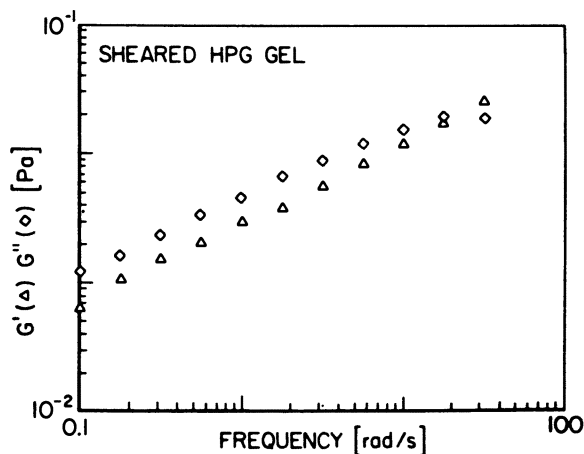
Figure 4. Storage modulus, G', vs. frequency for sheared HPG–titanate gel. Conditions: same as in Figure 3. (Reproduced with permission from ref. 6. Copyright 1988 Steinkopff.)

the unwanted hydrolysis reactions of the metal ion. The literature on tran-sition metal-ion–hydroxyl interactions is, therefore, limited to nonaqueous systems.

Understanding the cross-linking of polysaccharides with transition metal ions requires understanding the competition between hydrolysis and cross-

linking reactions. We recently demonstrated (6, 22) that the hydrolysis reactions for titanate lead to the formation of colloidal titanium dioxide (TiO_2) particles in solution. The hydrolysis reactions for titanate are similar to reactions for silicates by which colloidal silica particles are made (23). The sequence of reactions is shown in Scheme I, beginning with hydrolysis, followed by condensation polymerization, and finally network formation. The TiO_2 particles attain a final equilibrium size because of electrostatic interactions between the particle surfaces that arise from the ionization of surface TiOH groups.

The presence of TiO_2 particles was demonstrated by dynamic light scattering measurements on solutions of titanium triethanolamine (Tyzor TE, Du Pont) mixed with water (6). These water–titanate solutions were used as cross-linkers for HPG solutions (24). Figure 5 shows the growth of approximately 20-Å particles over a period of 4 h. The particle size was stable over this period and only slowly grew to 40 Å over 24 h. This small particle size led to solutions that were water-clear. To show that the particles are stabilized by electrostatic forces, we added KCl to the solution after aging

Hydrolysis

$$Ti(OR)_4 + H_2O \leftrightarrows (RO)_3TiOH + HOR$$

$$(RO)_3TiOH + H_2O \leftrightarrows (RO)_2Ti(OH)_2 + HOR$$

etc.

Polymerization

$$(RO)_3TiOH + HOTi(OR)_3 \rightarrow (RO)_3TiOTi(OR)_3 + H_2O$$

Cross-Linking

$$\begin{array}{ccc} & & TiO \\ & & | \\ OH & & O \\ | & & | \\ -O-Ti-O & + & HO-Ti-O \rightarrow O-Ti-O- \\ | & & | \\ OH & & OH \end{array}$$
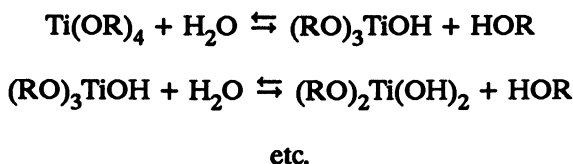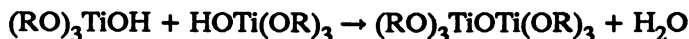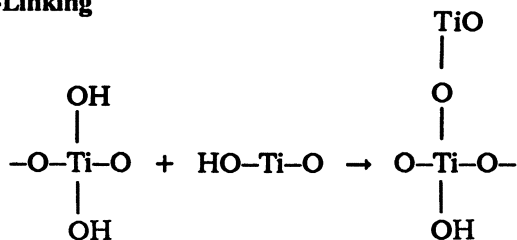
Scheme I. Reaction pathways for hydrolysis and cross-linking of titanates.
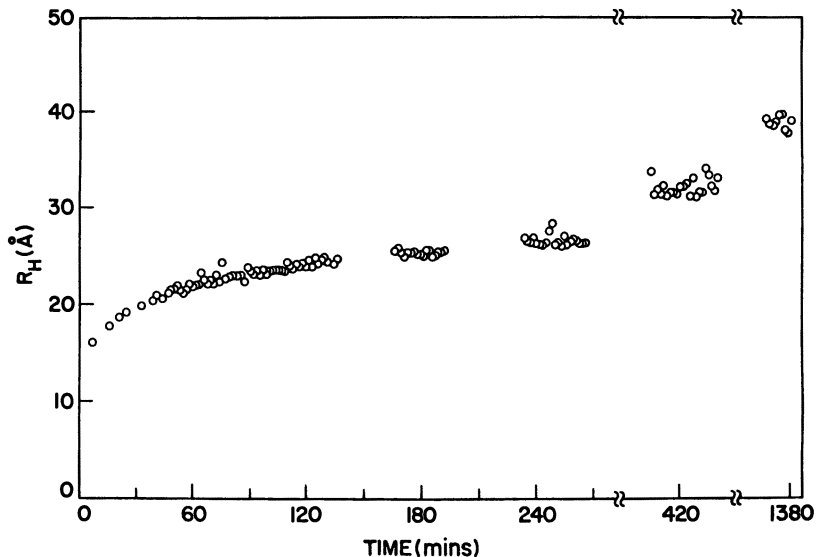
Figure 5. Growth of TiO₂ particles. Hydrodynamic radius of particles formed by mixing 9:1 by volume water and Tyzor TE (titanium triethanolamine). (Reproduced with permission from ref. 6. Copyright 1988 Steinkopff.)

for 24 h. KCl is normally added to fracturing fluids to prevent swelling of clays in the formation. The particle size rapidly grew to several hundred angstroms (Figure 6) as the salt screened the electrostatic forces and destabilized the colloidal dispersion.

A similar growth is seen if the pH is decreased from 9.0 to 7.0. As shown in Figure 7, the particles again grow because at this lower pH, fewer of the surface TiOH groups are ionized, and the electrostatic repulsion is lower. A second set of experiments were performed on titanium acetylacetonate cross-linker (Tyzor AA). The acetylacetone ligand is much more weakly bound to the Ti than the triethanolamine (*21*); therefore, if the Tyzor AA is added directly to water, a white precipitate immediately forms. The hydrolysis reactions can be limited by mixing the Tyzor AA with mixtures of isopropyl alcohol and water. The added isopropyl alcohol drives the reaction

$$Ti-(OR)_4 + H_2O \leftrightharpoons (RO)_3-Ti-OH + HOR$$
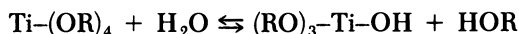
in the reverse direction and limits hydrolysis. Figure 8 shows a series of experiments with increasing ratios of water to isopropyl alcohol. The colloidal TiO₂ particle size increases with increasing amounts of water.

On the basis of these results, it appears that cross-linking of polysaccharides with titanates occurs through the surfaces of the colloidal particles as shown in Figure 9. Studies demonstrating the existence of colloidal par-
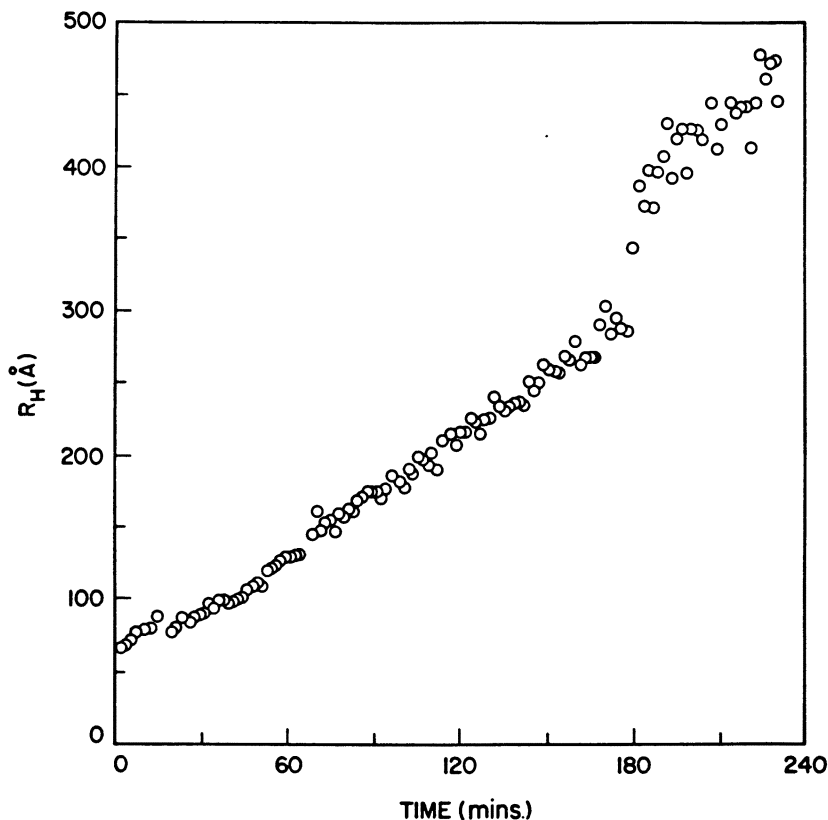
Figure 6. Growth of TiO₂ particles with added KCl. Stable TiO₂ particles after 24 h of aging (i.e., those in Figure 5) are destabilized by the addition of KCl. The final KCl concentration is 0.1 M. Time t = 0 corresponds to the time when KCl is added to the solution. Growth occurs due to screening of electrostatic charge by the added electrolyte.

ticles for zirconate cross-linkers have not been done to date, but qualitatively similar results would be expected. Different ligands and metal ions have different stability constants that control oxide particle formation and the availability of cross-linking sites. Because the surface area available for cross-linking depends on the size of the colloidal particles, which is sensitive to pH, temperature, ionic strength, and solution composition, these cross-linking reactions are relatively difficult to control. The need for better control of reaction conditions led to the development of delayed cross-linkers: systems where the release of the metal-ion ligands could be controlled.

Delayed Cross-Linkers.   Chelated forms of the metals are much less reactive than the alkyl forms and, therefore, provide a method of delaying
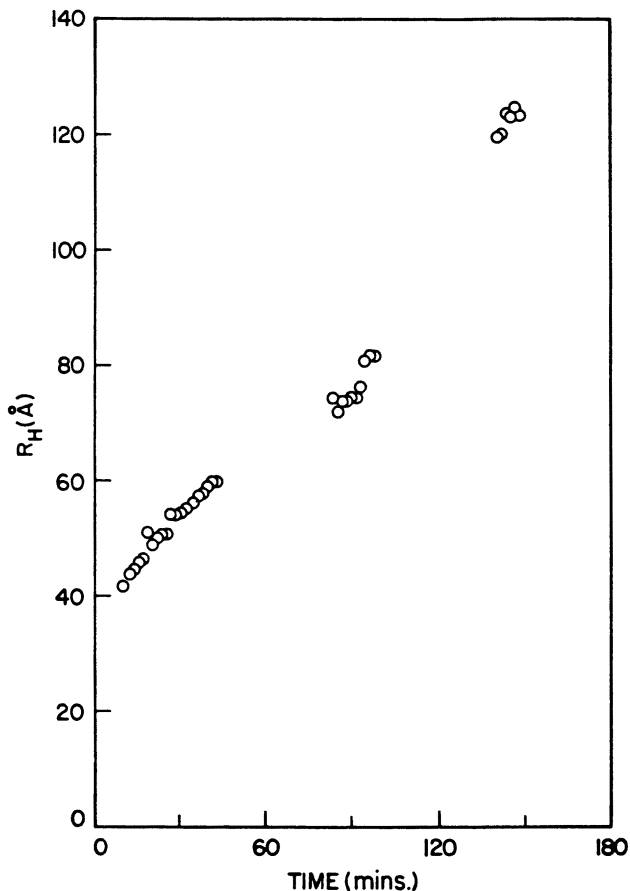
Figure 7. Growth of TiO₂ particles with lowered pH. Stable TiO₂ particles in Figure 5 after 24 h of aging are destabilized by the addition of acetic acid, which shifts the pH from 9 to 7. Growth occurs because of the decreased charge on the particle surfaces.

the cross-linking reaction (25). Some typical ligands used in transition metal cross-linkers are triethanolamine, acetylacetone (2,4-pentanedione), and ammonium lactate. By careful selection of metal, chelant, and pH, reaction rates can be adjusted so that cross-linking occurs after exposure to high shear rates, so that high-viscosity gels can be produced that are relatively insensitive to the lower shear history encountered in the formation.

Another approach to controlling reaction rate has been to add competitive ligands to fluids cross-linked with fast-reacting cross-linkers. Small amounts of materials such as 2,4-pentanedione can be added to fluids cross-linked with titanium acetylacetonate, triethanolamine titanate, or zirconium(IV) acetylacetonate to delay the reaction rate.
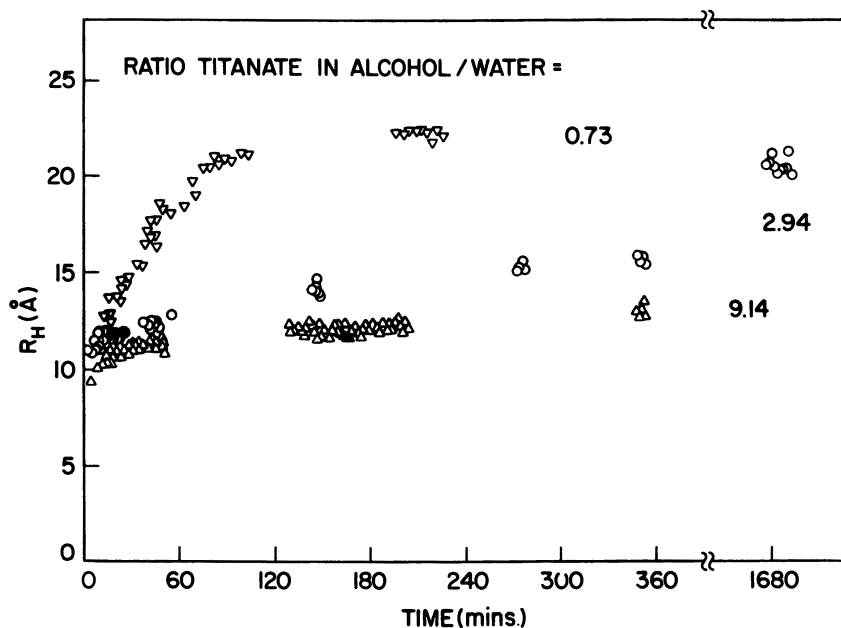
Figure 8. Growth of TiO₂ particles from isopropyl alcohol–water solutions. Titanium acetylacetonate is added to mixtures of isopropyl alcohol–water. Particle size grows with increasing water concentration, a result that shows the regulation of hydrolysis by added alcohol.
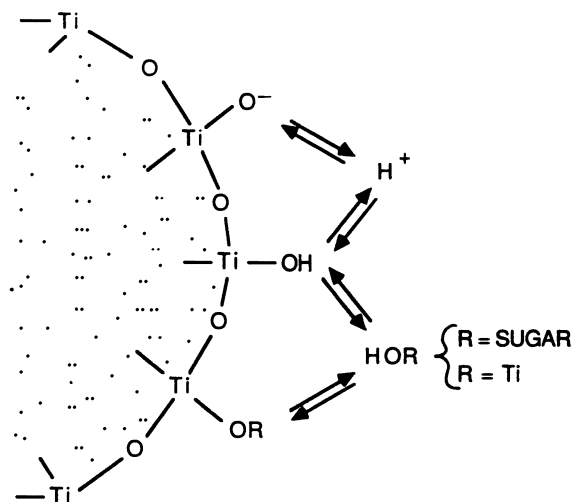
Figure 9. Schematic of TiO₂ surface. The various surface groups are shown along with their ionization states.

Viscosity Measurements

The most important data required for field application of fracturing fluid gels is viscosity because these data are used in numerical simulations to determine fracture geometry, pumping rates, and proppant-settling characteristics. In this section, procedures required for reproducible rheological measurements are defined and examples are given in the section describing the procedure. Data taken on Couette and capillary viscometers demonstrate that reliable viscosity values can be obtained independently of the measuring device. The effect of shear history on cross-linking and the advantages of delayed cross-linkers are shown in the sections on fast and delayed cross-linking systems.

Procedure. *Mixing.* The initial studies of fracturing fluid rheology (26–29) showed that homogeneous mixing is crucial in the formation of HPG gels. If the mixing time is longer than the reaction time, as is the case with fast-reacting titanate cross-linkers, an inhomogeneous gel structure is produced. Freeze-fracture electron microscopic studies (30) showed the non-uniform lamella and striations that are produced by inadequate mixing (see Figure 10). Gels with very heterogeneous structure display erratic, unstable, and generally high viscosity values. Figure 11 shows the stress vs. time profiles for two titanate gels: one produced in an impingement mixer that provides intimate micromixing and the other produced by batch mixing in a blender (which was the mixing protocol previously recommended for these fluids and which leads to inhomogeneous structures).

The other source of poor repeatability for the batch-mixed gel is the quiescent period during gelation when the gel is transferred from the blender to the viscometer. The impingement-mixed gel flows under continuous shear into the Couette geometry as it rotates. The viscosity values of the dynamically mixed gel are lower than that of the batch-mixed gel. Whereas the batched-mixed gel is not reproducible, the viscosity of the impingement-mixed gel is reproducible. Also, in the field application of these gels, the metal-ion cross-linker is added to the continuously flowing gel; therefore, the impingement-mixed, continuously sheared gel is more representative of actual field conditions.

The excellent reproducibility of HPG–titanate gel viscosities is shown in Figure 12 in which data from two experiments are superimposed (29). The stress vs. time data are nearly indistinguishable. These data were taken in a narrow-gap Couette geometry (the ratio of the cup radius to bob radius was 1.1) that was loaded as it was rotating by using the impingement-mixing device (27).

Three different impingement or dynamic mixers were built to achieve homogeneous mixing. The devices are similar in concept, and the results to be presented show that the viscosities of the gels are not especially sensitive

1 μm

HPG Gel without KCl, Sheared
(Magnification 25,000 X)
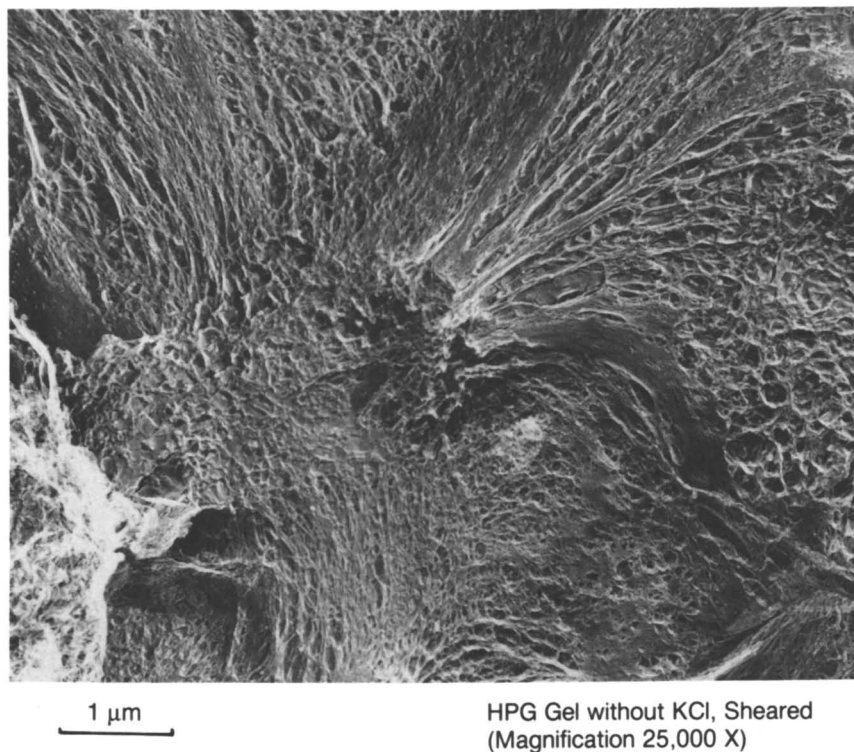
Figure 10. Freeze-fracture electron micrograph of inhomogeneous gel structure produced by inadequate mixing. (Reproduced with permission from ref. 25. Copyright 1985 American Petroleum Institute.)

to the details of the impingement mixer. These mixers were built in our three laboratories to feed four different viscometers. For small volumes of fluid that were tested on a Rheometrics Inc. System IV (RSIV) rheometer with a fluids transducer, an impingement-mixing device (described in detail in ref. 27) was constructed on the basis of ideas from the reaction injection molding industry. The device, shown schematically in Figure 13, consists of two syringes that are pneumatically driven, one for the HPG solution and one for titanate. The stoichiometry of the polymer solution and metal-ion cross-linker are established by the cross sections of the two syringes. The HPG solution and titanate cross-linker streams flow into a mixing tee, through a packed bed of sand in a stainless steel tube, and through Teflon [poly(tetrafluoroethylene)] tubing into the gap between the cup and bob in a Couette geometry.

For tests using a Rheometrics pressure rheometer (RPR), the HPG solution is pumped with a chromatography pump, and the cross-linker is injected into the flowing polymer solution with a syringe pump. The two
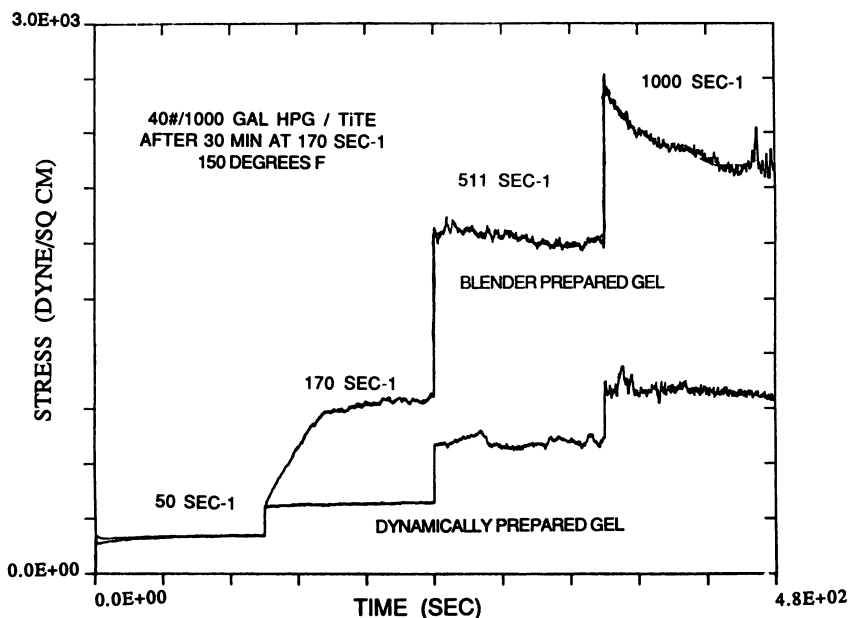
Figure 11. Effect of mixing conditions on the rheology of HPG–titanate gels.
The stress vs. time data for two gels made with differing mixing techniques is
shown. Shear rates of 50, 170, 511, and 1000 s⁻¹ were imposed for 100 s each.
The gel with the higher stress was prepared in a blender, and the data are
not reproducible from run to run. Data prepared in an impingement mixer
are reproducible but lower in value. Data were taken in an RPR rheometer
with a Couette geometry at 150 °F. (Reproduced with permission from ref. 24.
Copyright 1985 Society of Petroleum Engineers.)

streams are mixed by passing through a static mixer (Chemineer Kenics
type) immediately after the two streams meet. The flow rate in the 1/8-in.
i.d. tubing running to the rheometer cell is adjusted to produce a shear rate
at the tubing wall of 675 or 1350 s⁻¹. The schematic of the apparatus is shown
in Figure 14.

The third mixing arrangement involved a larger scale mixing and shear
history simulator described previously (29). The system consists of a large
chromatography pump for the polymer solution and a syringe pump (Isco)
for the cross-linker. The two streams are mixed by impingement in a "zero-
dead-volume" tee in the 1/8-in. i.d. stainless steel tubing. The reacting gel
is pumped at flow rates corresponding to wall shear rates of 675 or 1350 s⁻¹
through lengths of coiled 1/8-in. i.d. tubing to give residence times under
shear between 0 (i.e., no additional tubing) and 6.33 min. The HPG gel is
loaded through a rotating union at the bottom of the Couette cup on a
viscometer (Fann model 50) while it is rotating. The rotation rate produces
a shear rate of 170 s⁻¹.
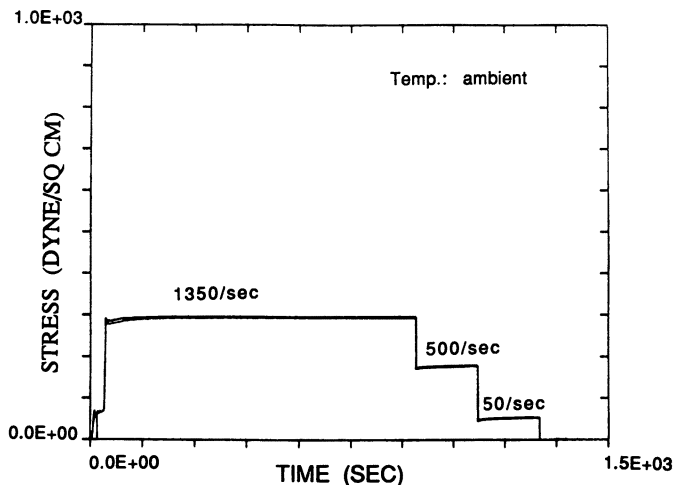
Figure 12. Reproducibility of viscosity data. Two sets of data are superimposed and show excellent reproducibility. Data were taken at ambient temperature in an RSIV rheometer with a Couette geometry and by using impingement mixing. (Reproduced with permission from ref. 27. Copyright 1987 American Petroleum Institute.)

These mixing apparatuses were built to ensure pulse-free flow to obtain a uniform cross-linker concentration throughout the gel. In addition, the mixing devices were connected directly to the viscosity measuring device, so that the gel is continuously sheared from the time of cross-linker injection. Finally, it is recommended that metal content of gels be analytically verified to ensure that the proper amount of cross-linker has been delivered. We have analyzed for titanium with X-ray fluorescence and atomic adsorption spectroscopy.

Elevated Temperature Testing. The tests in the RSIV were conducted only at ambient temperature. Elevated-temperature tests were conducted by using a Fann viscometer, a Rheometrics pressure rheometer (RPR), and a reciprocating capillary viscometer. The basic test procedure used for testing at 80 °C with the Fann viscometer and reciprocating capillary viscometer is as follows.

The HPG solution, at 25 °C, is pumped through 1/8-in. i.d. tubing at a flow rate that produces a wall shear rate of 675 or 1350 s^{-1}. The cross-linking reagent is injected into the flowing polymer solution at the appropriate rate to give a final titanium concentration in the gel of 30 ppm. The flow is allowed to equilibrate for 5 to 10 min before the gel is directed into the viscometer. When the HPG–titanium gel is loaded into the Fann viscometer at ambient temperature (25 °C), the rheometer cup is rotating at a rate to give a wall shear rate of 170 s^{-1}. When the gel is loaded into the
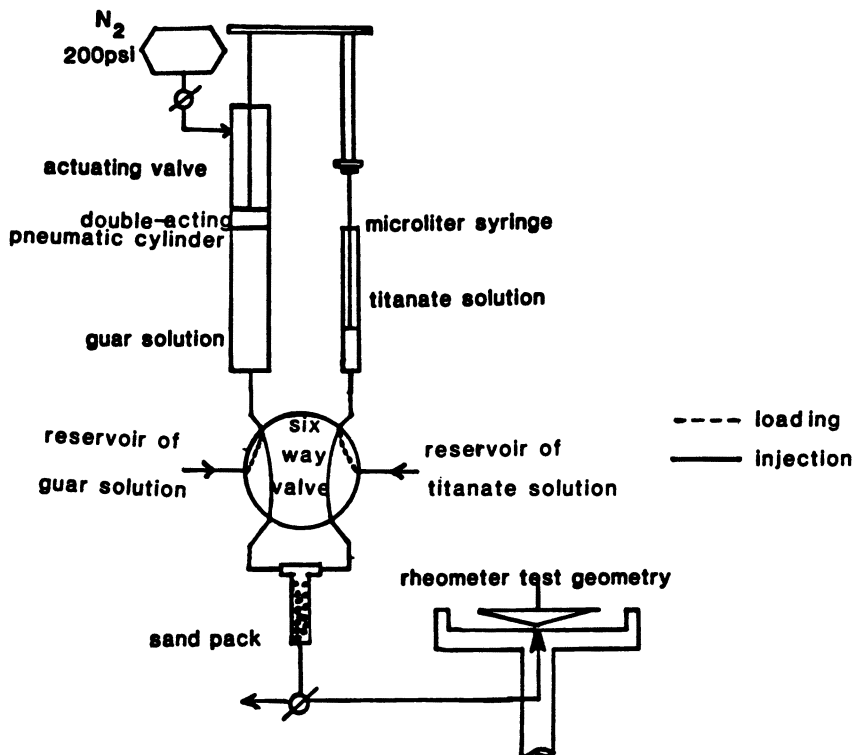
Figure 13. Schematic of impingement-mixing device. Two syringes are mechanically coupled and driven with nitrogen gas. The smaller microliter syringe contains the metal-ion solution and the larger stainless steel syringe contains the polymer solution.

reciprocating capillary viscometer, it flows directly into the capillary and is kept under shear as the capillary fills (29).

The viscosity is then measured at ambient temperature at increasing shear rates of 85, 170, 255, 340, and 425 s^{-1}. The shear rate scans are produced in the rotational viscometer by increasing the rotation rate, and the scans are produced in the reciprocating capillary by changing the flow rate in discrete steps. After the initial shear scan, the sample is heated at about 2.7 °C/min while being sheared at a constant rate of 170 s^{-1}. The sample temperature is about 80 °C in 25 min; time zero is at the start of the ambient temperature scan. Shear scans are taken at 25, 40, 55, and 70 min with the shear rate maintained at 170 s^{-1} between scans. Power-law parameters n' and K' are calculated from the shear stress measurements obtained from the scans. The viscosity at 170 s^{-1} is calculated from these power-law parameters and reported.

For the RPR, the shear history was produced not in an external capillary
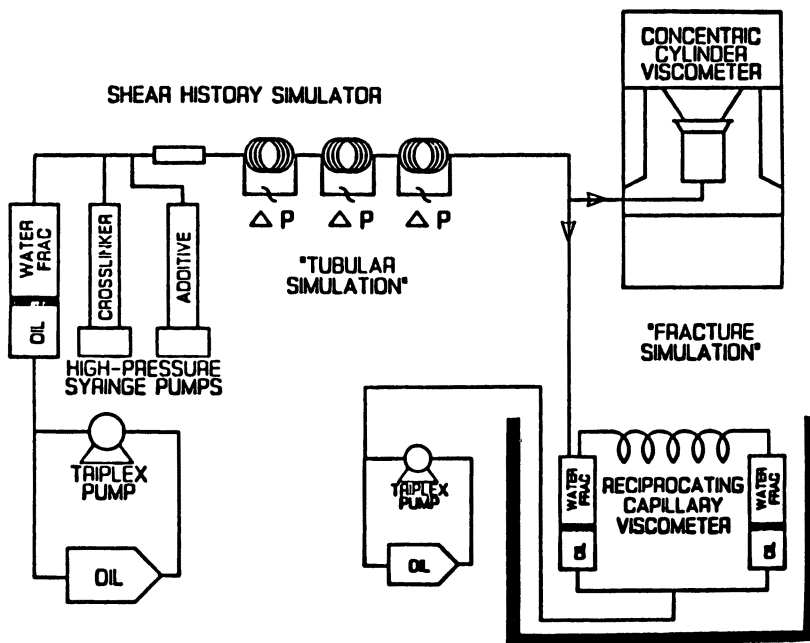
Figure 14. Schematic of mixing device for loading an RPR rheometer.

tubing system, but by shearing the sample at high rates in the closed Couette cell. Because the reactions are very temperature-sensitive, a key variable was the heat-up rate among the devices. The temperature bath in the RPR was programmed to match the heat-up rate in the Fann and capillary viscometers.

Fast Cross-Linking Systems.   By *fast cross-linking systems* we mean those systems for which the cross-linking reaction is rapid enough that the gel structure is established during the mixing process or during the exposure to high shear rates (corresponding to the time during which the fluid is pumped down the well bore). We show here the effects of shear history on the ultimate gel viscosity for fast cross-linking systems. We then show that with careful attention to the shear and temperature histories during the formation of the gel, it is possible to get similar viscosity values from different viscometers. Although for simple fluids the measurement of fluid viscosity is easily accomplished in any viscometer, for these complex reacting fluids previous researchers had not been able to produce viscosity results that were independent of the measuring geometry.

Effect of Shear During Cross-Linking.   The magnitude and duration of shear during cross-linking can profoundly affect the formation of the gel

network structure. Figure 15 illustrates the effect that shear during cross-linking has on HPG cross-linked with titanium acetylacetonate. These data were generated with a viscometer (Fann 50C) using the external tubing shear history simulation device shown in Figure 15. The same fluid composition (i.e., 0.48 wt % HPG and 2 wt % KCl solution cross-linked with 0.04 % (w/v) TAA cross-linker) was prepared with four different shear histories that correspond to representative oil field conditions. Increasing the time that the fluid was at high shear in the tubing decreased the final viscosity of the cross-linked fluid; also, increasing the magnitude of shear to 1350 s^{-1} significantly reduced the final viscosity. Similar results for this fluid composition were found by Gardner who tested it in a circulating pipe viscometer (*30*).

This experiment illustrates the problems encountered when trying to design fracturing treatments by using fast nonequilibrium cross-linked fluids. Every different configuration of tubing geometry and pumping rate produces
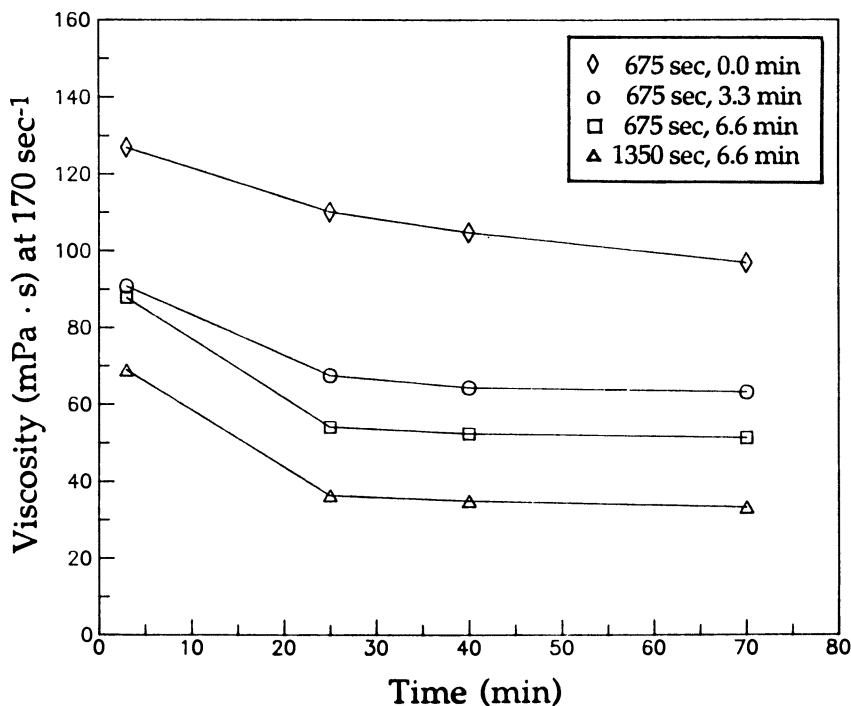
Figure 15. Effect of shear during cross-linking of fast-reacting titanate cross-linker. Viscosity values measured at 170 s^{-1} are shown for gels exposed to various shear histories. It takes approximately 20 min to reach the final temperature of 80 °C. Increasing time at high shear rates (675 s^{-1}) decreases the viscosity, and increasing the shear rate (1350 s^{-1} vs. 675 s^{-1}) decreases the viscosity.

different gel networks and different fluid rheology; furthermore, the information helps explain the difficulties in generating reproducible rheology data in the laboratory. The same gel chemistry has different viscosities depending upon the magnitude and duration of shear. Reproducible viscosity measurements can be obtained once these variables are controlled.

Reproducibility of Gel Viscosity Measurements in Different Apparatuses. Having demonstrated that well-defined mixing and shear conditioning were required to generate reproducible viscosity measurements with one apparatus, it was necessary to establish that reproducible measurements could be obtained by using similar devices in different laboratories by controlling these variables. In one laboratory, viscosity measurements were taken by a rotational viscometer (Fann model 50C) and a reciprocating capillary viscometer (28) on gels prepared with the mixing–shear history device described earlier. In the second laboratory, the RPR rheometer was loaded as described. Both rotational viscometers were fitted with narrow-gap Couette geometries with similar ratios of bob-to-cup radii (0.868 for the Fann 50 and 0.944 for the RPR).

With the basic test procedure established, it was first necessary to determine the accuracy with which the viscosity of a simple fluid (i.e., not time- and shear-dependent) could be measured between laboratories and instruments. A hydroxypropyl guar solution at 0.48% (w/v) was measured under the test conditions described, and the results are shown in Figure 16. The tests were conducted at 80 °C, a temperature representative of field conditions and high enough to produce polymer degradation from breakage of the acetal linkage between sugar residues. The calculated viscosity at 170 s^{-1} showed reasonable agreement between instruments at 80 °C. It appears that the solution viscosity decreased more rapidly in the Fann 50 viscometer, probably because of the polymer degradation initiated by metal-ion contaminants from the Couette tools of the instrument.

The effects of gel preparation and shear history could then be compared. The HPG–titanium gels were cross-linked at a shear rate of 675 s^{-1} in the two mixing devices. The viscosity measurements for samples with no additional shear conditioning are presented in Table I. Data are shown for the two rotational viscometers and two different reciprocating capillary viscometers. The viscosity values compare favorably between the instruments with a range from 89 to 109 mP · s at 70 min. These data demonstrate that reproducible viscosity measurements (i.e., the same viscosity measured for the same gel composition) can be made, provided that the gel structure is formed under similar conditions. (For these experiments, the magnitude and time at shear, heat-up rate, etc., were matched as closely as possible.)

Delayed Cross-Linking Systems. As illustrated in Figure 16, high magnitudes and long periods of shear reduce the viscosity of HPG–titanium
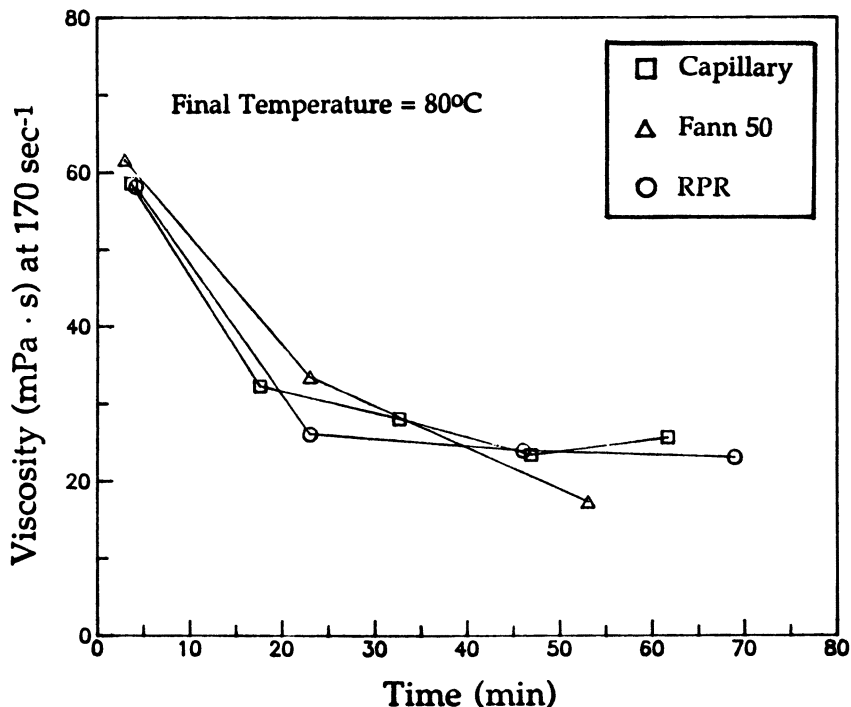
Figure 16. Reproducibility of viscosity data taken on Fann 50, RPR, and capillary viscometers.

Table I. Viscosity Measurements for Samples with No
Additional Shear Conditioning

Time (min)	Fann	Cap1	Cap2	RPR
4	127	118	131	97
25	97	100	105	122
40	104	94	110	128
55	99	92	108	125
70	97	89	109	106

NOTE: All results are in centipoises at 170 s^{-1} and 80 °C.

gels. For this particular chemistry, the gel structure forms quickly and then degrades upon exposure to shear. Delaying gel formation until only low levels of shear will be experienced by the fluid (i.e., after the fluid travels through the well bore), allows a more highly structured gel to form, and thereby results in higher viscosity.

The rate at which the gel is chemically formed can be controlled by the addition of chelates that slow the reaction between the HPG molecules and the transition metal ion. An HPG gel was prepared with a zirconium cross-

linker of this type and tested under the same conditions as the fast cross-linking HPG–titanium gel. The HPG–zirconium gel began to form at ambient temperature; however, the reaction was extremely slow and rapidly accelerated only when the temperature reached 47 °C. The viscosity data for the slow cross-linking HPG–zirconium gel and the HPG–titanium gel are plotted as a function of time in Figure 17. The viscosity of the delayed system was nearly 2.5 times greater than that of the fast cross-linking gel and maintained higher viscosity at elevated temperature. These results demonstrate that higher gel viscosity can be obtained for a given chemistry if gel formation occurs after exposure to high shear rates.

Also plotted in Figure 17 are data for delayed- and fast-cross-linking HPG gels that have been shear conditioned immediately after cross-linking for 6.6 min at 675 s^{-1}. Although the cross-linking reaction has been substantially retarded at ambient temperature, some gel structure has formed, as evidenced by the higher initial viscosity of the shear-conditioned sample.
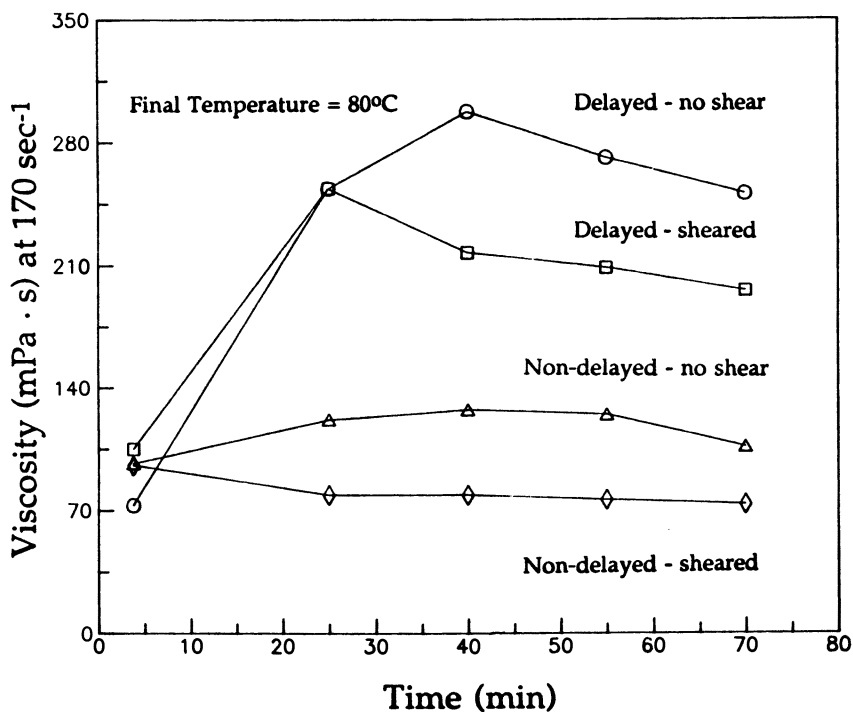
Figure 17. Enhanced viscosities with delayed cross-linker. Delayed zirconate cross-linkers produce gels with higher viscosity levels because the network does not develop during the high shear part of the history simulation. In this system cross-linking is initiated as the temperature rises from ambient to 60 °C over the first 20 min of the test.

A reduction in viscosity occurs for the shear conditioned sample at 80 °C because of degradation of the gel formed during the shear period.

Summary

The viscosity of metal-ion cross-linked gels depends on the chemistry, shear history, and temperature history that the gels experience. In a hydraulic fracturing application, fast-reacting titanate and zirconate gels form during the time of highest shear rate as the gel is pumped down the well bore. Exposure to high shear during cross-linking decreases the viscosity of the gel when measured later at lower shear rates. This sensitivity to shear history has made it difficult to obtain reproducible laboratory measurements of gel viscosity.

We have shown, for the first time, that with proper control of conditions, it is possible to reproduce viscosity measurements in different geometries and devices. The key variables to control are dynamic or impingement mixing, continuous shear during the gelation process, time of exposure to high shear rates, temperature history, and concentration of metal ions in the final gel. Data presented were taken on a Fann 50C rotational viscometer and a Rheometrics pressure rheometer with Couette geometries. With the Couette geometry it was found that narrow gaps are required to obtain reliable data. Data were also obtained by using a capillary viscometer. The viscosities from all three viscometers agreed if the shear rates at the wall of the capillary were matched to the average shear rate in the narrow-gap Couette.

The titanate and zirconate gels involve irreversible cross-linking and are therefore sensitive to the shear history during cross-linking. The sensitivity of the gel viscosity to shear history can be reduced by delaying the cross-linking reaction until after the period of high shear rate has passed. This strategy is used extensively in commercial fracturing fluid formulations in which cross-linking is delayed until the fluid is out of the well bore and into the formation. Data on a representative delayed zirconate system show that delayed cross-linkers result in higher viscosity and more stable fluids.

References

1. Dea, I. C. M.; Morris, E. R.; Rees, D. A.; Walsh, E. J.; Barnes, H. A.; Price, J. *Carbohydr. Res.* 1977, 57, 249.
2. Morris, E. R. *Br. Polym. J.* 1986, 18, 14.
3. Tanakam, T.; Sun, S-T.; Hirokawa, Y.; Katayama, S.; Kucera, J.; Hirose, Y.; Amiya, T. *Nature (London)* 1987, 325, 796.
4. Nossal, R. *Macromolecules* 1985, 18, 49.
5. Prud'homme, R. K.; Uhl, J. T.; Poinsatte, J. P.; Halverson, F. *SPEJ, Soc. Pet. Eng. J.* 1983, 23, 804.
6. Kramer, J.; Prud'homme, R. K.; Wiltzius, P.; Knoll, S. *Colloid Polym. Sci.* 1988, 266, 1.

7. Terry, R. E.; Huang, C.; Green, D. W.; Michnik, M. J.; Wilhite, G. P. *SPEJ, Soc. Pet. Eng. J.* **1981**, *21*, 229.
8. Chatterji, J.; Borchardt, J. K. *JPT, J. Pet. Technol.* **1981**, *33*, 2042.
9. Conway, M. W.; Almond, S. W.; Briscoe, J. E.; Harris, L. E. Presented at the 55th Annual Fall Technical Conference of the Society of Petroleum Engineers, Dallas, TX, Sept. 21–24, 1980; paper no. 9335.
10. Economides, M. J.; Nolte, K. G. *Reservoir Stimulation*; Schlumberger Educational Services: Houston, TX, 1987.
11. Grasdalen, H.; Painter, T. J. *Carbohydr. Res.* **1980**, *81*, 59.
12. Glass, J. E. In *Water-Soluble Polymers: Beauty with Performance*; Glass, J. E., Ed.; Advances in Chemistry 213; American Chemical Society: Washington, DC, 1986; p 16.
13. Albersheim, A. *Carbohydr. Res.* **1984**, *131*, 139.
14. *Guar and Derivatives: Oilfield Applications*; Henkel Corporation: Houston, TX, 1986.
15. Menjivar, J. A. In *Water-Soluble Polymers: Beauty with Performance*; Glass, J. E., Ed.; Advances in Chemistry 213; American Chemical Society: Washington, DC, 1986; pp 209–226.
16. Kramer, J. Ph.D. Thesis, Princeton University, 1987.
17. Sinton, S.; Maerker, J. *J. Rheol.* (N.Y.) **1986**, *30*, 77.
18. Gorin, P.; Mazurek, M. *Carbohydr. Res.* **1973**, *27*, 325.
19. Rondesvedt, C. In *Titanium Compounds (Organic)*; Kirk-Othmer Encyclopedia of Chemical Technology, 3rd ed.; Wiley: New York, 1976; Vol. 23.
20. Kramer, J.; Prud'homme, R. K.; Wiltzius, P. *J. Colloid Interface Sci.* **1987**, *118*, 294.
21. Stober, W.; Fink, A.; Bohn, E. J. *J. Colloid Interface Sci.* **1968**, *26*, 62–69.
22. Conway, M. U.S. Patent 4 462 917, Haliburton Services Co., 1984.
23. Rummo, C. J. *Oil Gas J.* **1982**, *80*, 84.
24. Knoll, S. Presented at the Society of Petroleum Engineers–Department of Energy Symposium on Low-Permeability Reservoirs, Denver, CO, 1985; paper no. 13904.
25. Prud'homme, R. K. final report API PRAC project 84–45, American Petroleum Institute, Dallas, TX, 1985.
26. Prud'homme, R. K. final report API PRAC project 85–45, American Petroleum Institute, Dallas, TX, 1986.
27. Prud'homme, R. K. final report API PRAC project 86–45, American Petroleum Institute, Dallas, TX, 1987.
28. Zasadzinski, J.; Chu, A.; Prud'homme, R. K. *Macromolecules* **1986**, *19*, 2960.
29. Constien, V. G.; Fellin, E. L.; King, M. T.; Graves, G. G. In *Computer Applications in the Polymer Laboratory*; Provder, Theodore, Ed.; ACS Symposium Series 313; American Chemical Society: Washington, DC, 1986.
30. Gardner, D. C.; Eikerts, J. V. Society of Petroleum Engineers; paper no. 12025, Dallas, TX, 1983.

7

Poly(acrylic acid) Thickeners

The Importance of Gel Microrheology and Evaluation of Hydrophobically Modified Derivatives as Emulsifiers

Robert Y. Lochhead, John A. Davidson, and G. M. Thomas

BFGoodrich Company, Avon Lake Technical Center, Avon Lake, OH 44012

The gel microstructure of poly(acrylic acid) thickeners is a key variable that defines the rheology conferred to and end-use applications of these products. The microstructure can be probed by using a quasi-elastic light-scattering technique to measure the Stokes–Einstein microdiffusion coefficient of colloidal gold sol particles immersed within the thickened system. The microstructures of two such thickeners have been determined. The structure of swollen microgels packed in intimate contact is postulated for an efficient thickener that confers pseudoplastic rheology. A less efficient thickener that confers viscoelastic rheology on aqueous systems is shown to be a true solution of polymer molecules. The structure of this compound is important in end-use applications such as the prevention of wicking in the printing of textiles. This chapter also discusses hydrophobic modification of poly(acrylic acid) thickeners to yield products that are useful as primary emulsifiers for oil-in-water systems. These emulsions are stable for years, but they break and coalesce almost instantly when electrolyte is introduced into the aqueous phase.

HIGH-MOLECULAR-WEIGHT POLY(ACRYLIC ACID) THICKENERS have been used successfully in many aqueous systems for more than a quarter of a century. The general structure of these thickeners is shown in structure 1. When dissolved in water in their native form, these polymer molecules adopt
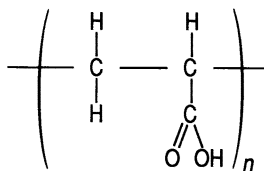
Structure 1. Poly(acrylic acid).

the relatively relaxed configuration shown in Figure 1. Upon neutralization with a suitable base, the carboxylate groups ionize, and mutual ionic repulsion between these groups causes the molecule to adopt a greatly expanded configuration (Figure 2) (1, 2).

In principle, however, mutual electrostatic repulsion between neighboring carboxylate groups only partially explains the swelling of the polyelectrolyte molecule, because this repulsion is screened by other ions in the system, including hydrated protons and hydroxyl ions from dissociated water and the polyelectrolyte's own counterions. Each polyelectrolyte molecule can be regarded as a microscopic ionic network (3). The counterions are exchanged between the swollen ionic network and its surrounding external solution. Diffusion of the mobile counterions away from the immediate vicinity of the polyelectrolyte molecule leads to a net negative charge within the polymer molecule, which increases the electrical potential within the molecule relative to its surroundings. Such conditions favor a higher concentration of counterions within the domain of the polymer molecule than in the external solution.

In reality, a state of equilibrium is reached where the ionic attraction of the counterions by the polyanion is just balanced by diffusion into the external solution, which is driven by the chemical potential gradient, which in turn arises from the difference in counterion concentrations between the two domains. The overall effect closely resembles Donnan membrane equilibria (4) (Figure 3). As a consequence of the difference in counterion concentrations, the osmotic pressure inside the polymer domain exceeds that of the external solution, and the expansion of the polyelectrolyte can be equated to the difference in osmotic pressures of the intramolecular and intermolecular solutions.

The quantitative treatment of the force of expansion can be carried out by assuming either pure ionic repulsion or that osmotic pressure is entirely responsible for the expansion. These two models yield identical results (3) because they are mutually related. No net charge would develop if the counterions were immobile, and no excess of mobile ions would be present to generate an osmotic pressure difference if they did not carry a charge of opposite sign to that of the polyion.

Addition of a microion salt, such as sodium chloride, to the solution causes a decrease in the extent of polymer swelling. This effect can be
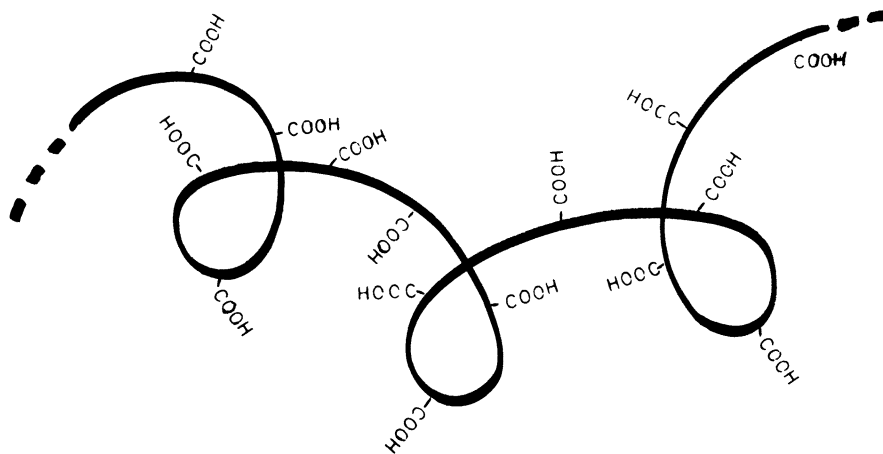
Figure 1. Schematic diagram of poly(acrylic acid) in relaxed configuration.

explained as arising from a reduction in the osmotic force due to a lessening of the difference in counterion concentration between the domains (3). Alternatively, collapse of the polymer could be ascribed to collapse of its ionic double layer upon addition of excess salt (5).

Typical thickening curves for poly(acrylic acid) thickeners are shown in Figure 4. Neutralization to pH 5 causes polyion expansion. Measured viscosity reaches a plateau between pH 5 and 10. Above pH 10 the effective increase in counterion concentration causes a successive reduction in the swelling of the polyelectrolyte molecules.

Figure 4 shows four different types of commercial poly(acrylic acid) thickeners. These products differ in molecular weight, but there are also subtle differences in molecular architecture that lead to very different rheological characteristics and end-use application behavior. These polymers differ not only in bulk rheology, but also in microrheology. The microrheology is important in many applications and is a manifestation of the microstructure of gels thickened by these polymers.

Previous work has shown that gels formed from cross-linked polyacrylamide (6), alginate (6), hydrolyzed starch–polyacrylonitrile (7), and a cross-linked poly(acrylic acid) (8), consist of discontinuous structures with micro-regions of extremely low viscosity. Such microscopic heterogeneity has been attributed to permanent or diffusing fluctuations within the gel (1) or to a structure of closely packed, swollen microgels in a continuous water phase (2, 3).

This study was aimed at probing the microstructure of two poly(acrylic acid) thickeners, which will be called type A and type B polymers. Polymer type A has a reported number-average molecular weight of 4 million, and polymer type B has a reported number-average molecular weight of 500,000
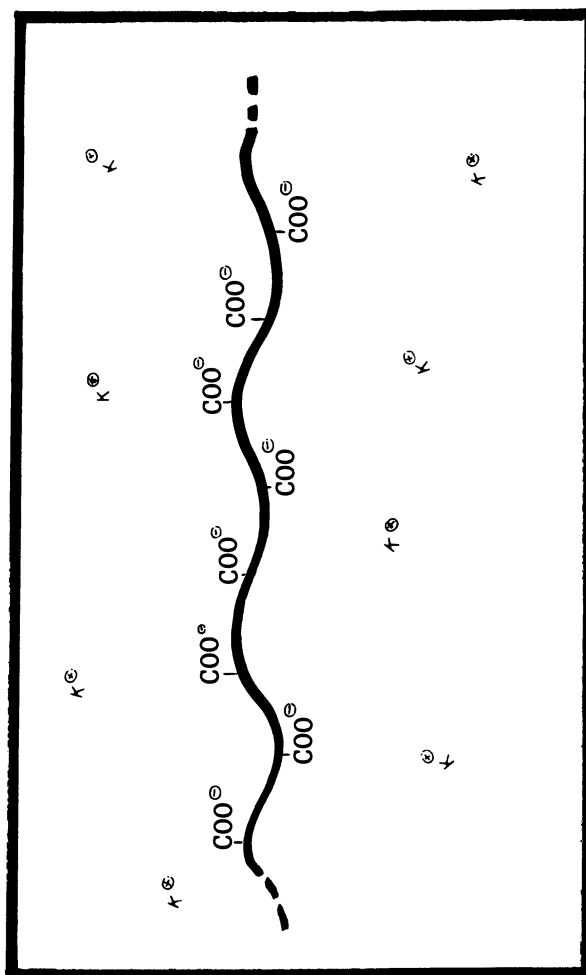
Figure 2. Schematic representation of stretched configuration of potassium salt of poly(acrylic acid) dissolved in water.
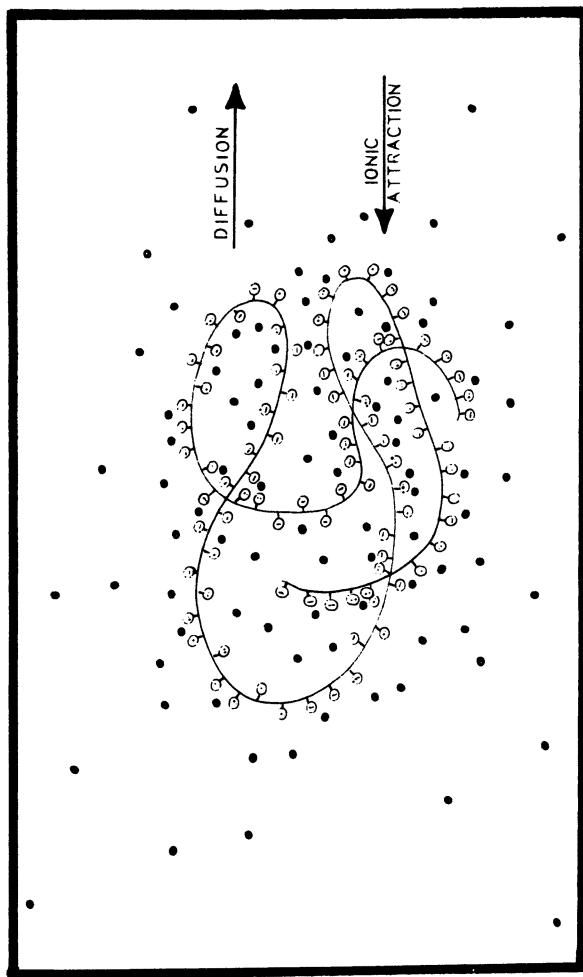
Figure 3. Donnan-type equilibrium of a swollen anionic polyelectrolyte.
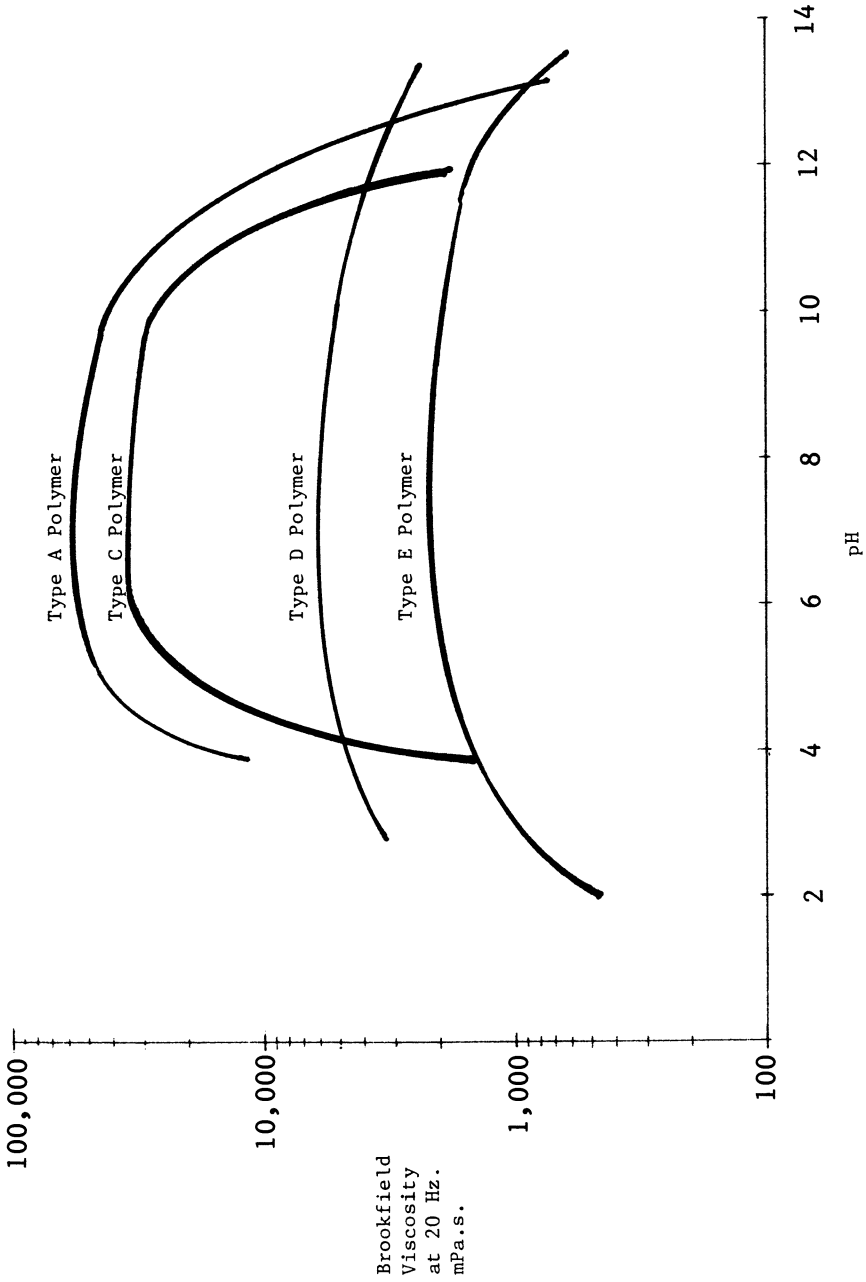
Figure 4. Variation of Brookfield viscosity with pH for various poly(acrylic acid) thickeners.

(1). These polymers display different bulk rheology. Type A shows viscoelastic characteristics, and type B displays plastic rheology.

Microstructures were probed by measuring the microdiffusion coefficients of bimodal gold sols within the polyelectrolyte gel structure by using quasi-elastic light scattering. Gold sols were ideal for this purpose because of their high refractive index, and because any flocculation of the sol caused by interaction with the polymer would be signaled by a change in the color of the sol. The colloidal stability of gold sol–gel systems was first noted by Faraday (9). Faraday prepared soluble "ruby jellies" 130 years ago by the reduction of gold chloride solution with elemental phosphorus dissolved in carbon disulfide in the presence of gelatin. Such gels did not change color with time, even in the presence of relatively high salt concentrations. The bimodality of the gold sols used in this study allowed examination of two size regions of the microstructure centered around 10 nm in one case and 100 nm in the other.

Experimental Details

Sols were prepared by the Zsigmondy technique. "Colloid-free" water (quartz-distilled, 120 mL), 15 mg of $AuHCl_4 \cdot 3H_2O$, and 37 mg of K_2CO_3 were heated to boiling, and a few drops of formaldehyde were added. The sol was run through a mixed-bed ion-exchange column to remove any unreacted reagents. The sol used in these experiments was bimodal with distributions centered around 10 and 100 nm.

Mucilages of poly(acrylic acid) in the gold sols were prepared by dispersing polymer powder in the rapidly agitated sol. Each mucilage was neutralized directly in the light-scattering cuvette by addition of the appropriate amount of sodium hydroxide solution. The mucilages were neutralized to a pH within the range 7.2 to 7.6. In all cases, the color of the gold sol was unchanged upon the addition of poly(acrylic acid) and subsequent neutralization.

Quasi-elastic light scattering (QELS) experiments were conducted on both neutralized and unneutralized sols, in a Brookhaven model BI-90 particle sizer. This instrument measured the autocorrelation function, $C(t)$, and fit this function to

$$C(t) = Ae^{(-2\Gamma t + B)} \tag{1}$$

where A is an optical constant, and t is the time between sampling intervals for the fluctuating light signal. As t increases, correlation is lost, and the function approaches a constant background term, B. For short t times, the correlation is high. In equation 1, Γ is related to the relaxation of fluctuations by

$$\Gamma = Dq^2 \tag{2}$$

where D is the translational diffusion coefficient and q is calculated from

$$q = \left(\frac{4\pi n}{\lambda_0}\right) \sin\left(\frac{\theta}{2}\right) \tag{3}$$

For the Brookhaven instrument, the scattering angle, θ, is constant at 90°; the wavelength of the laser light, λ_0, is 0.6328 μm; and n is the refractive index of the solution.

A diffusion coefficient, D, is used to calculate particle size (assuming spherical geometry) from the Stokes–Einstein equation

$$D = \frac{k_B T}{3\pi\eta d} \tag{4}$$

where k_B is the Boltzmann constant (1.38054×10^{-16} ergs/K); T is absolute temperature; η is the viscosity of liquid in which the particle is moving; and d is the particle diameter. Alternatively, if the particle diameter of the scattering particles is known, the microviscosity encountered by these particles in Brownian motion can be measured. The microviscosity measurements are described in this chapter.

The Brookhaven instrument did not measure the angular dependence of scattering. However, it has been shown (6) for diffusion of bovine plasma albumin in polyacrylamide gels, that the calculated value of D was independent of scattering angle. Gold sols dispersed within poly(acrylic acid) mucilages would be expected to show similar constancy of the measured diffusion coefficient with scattering angle.

Results of Viscosity Measurements

The shear dependence of Brookfield viscosity is shown in Figures 5 through 8 for unneutralized (type A) and neutralized (type B) poly(acrylic acid)s. Type B showed little change in viscosity with rate of shear, whereas the highly efficient thickener displayed shear-thinning behavior. The concentration dependence of microviscosities measured from the Brownian motion of 10- and 100-nm gold particles was compared with Brookfield viscosities of the poly(acrylic acid) mucilages in Figures 9 and 10 for type A polymer and in Figures 11 and 12 for type B polymer.

Discussion

Type A Polymer. Type A polymer is an efficient gelling and suspending agent for cosmetic and pharmaceutical gels. For these end uses, plastic rheology is desired, and the gel must display a yield value that is sufficiently high to allow permanent suspension of the particles that are formulated into the gel. Shear-thinning behavior is desirable for ease of spread of the gel in its end-use. Type A polymer confers these desirable rheological characteristics (Figures 5 and 6).

The concentration dependence of the Brookfield viscosity (Figures 9 and 10) indicates a rapid drop in viscosity upon dilution below a critical concentration. Bagley (7) attributed such rheological behavior to a structure of swollen, deformable gel particles closely packed in intimate contact. Davidson (8) later attributed the thickening efficiency of a cross-linked poly(acrylic acid) to the dispersed rather than the continuous phase. In general, pseudoplastic and viscoplastic rheology is characteristic of dispersions with low
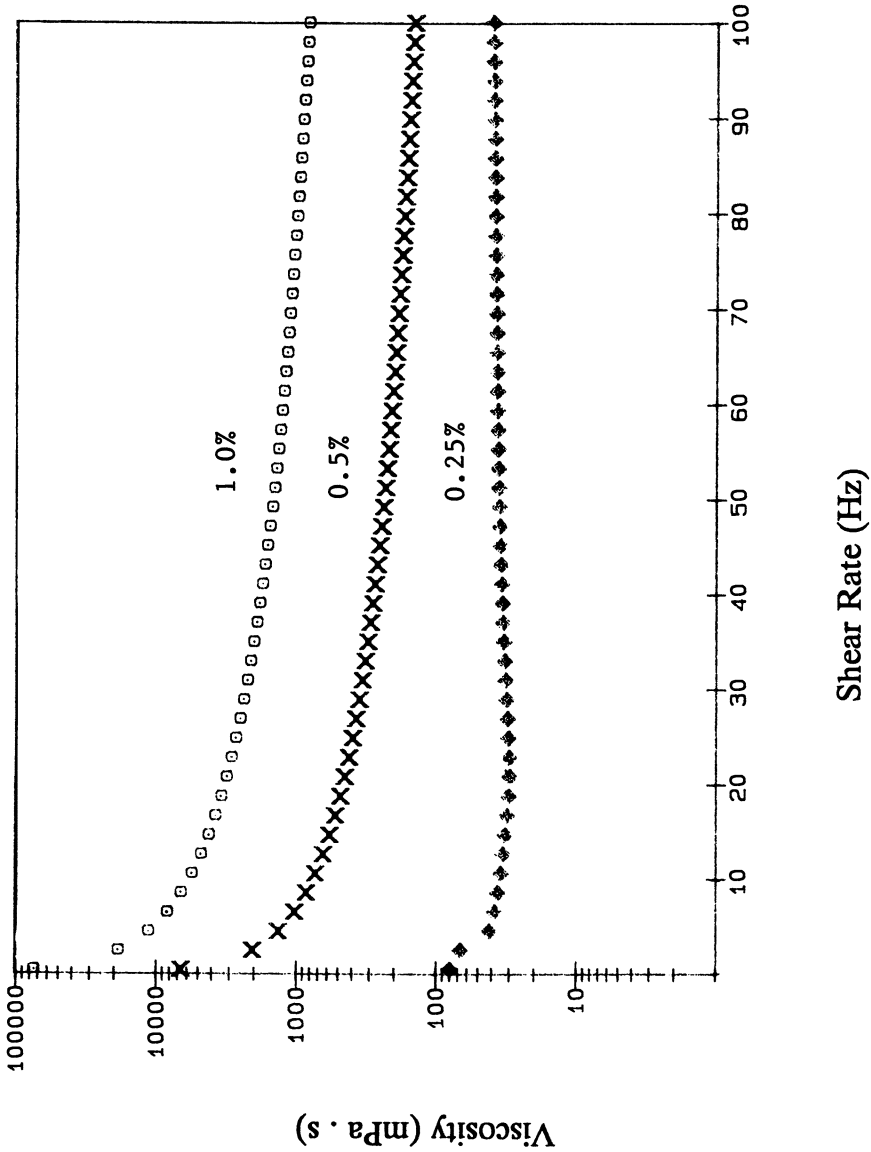
Figure 5. Shear dependence of unneutralized type A polymer mucilages.
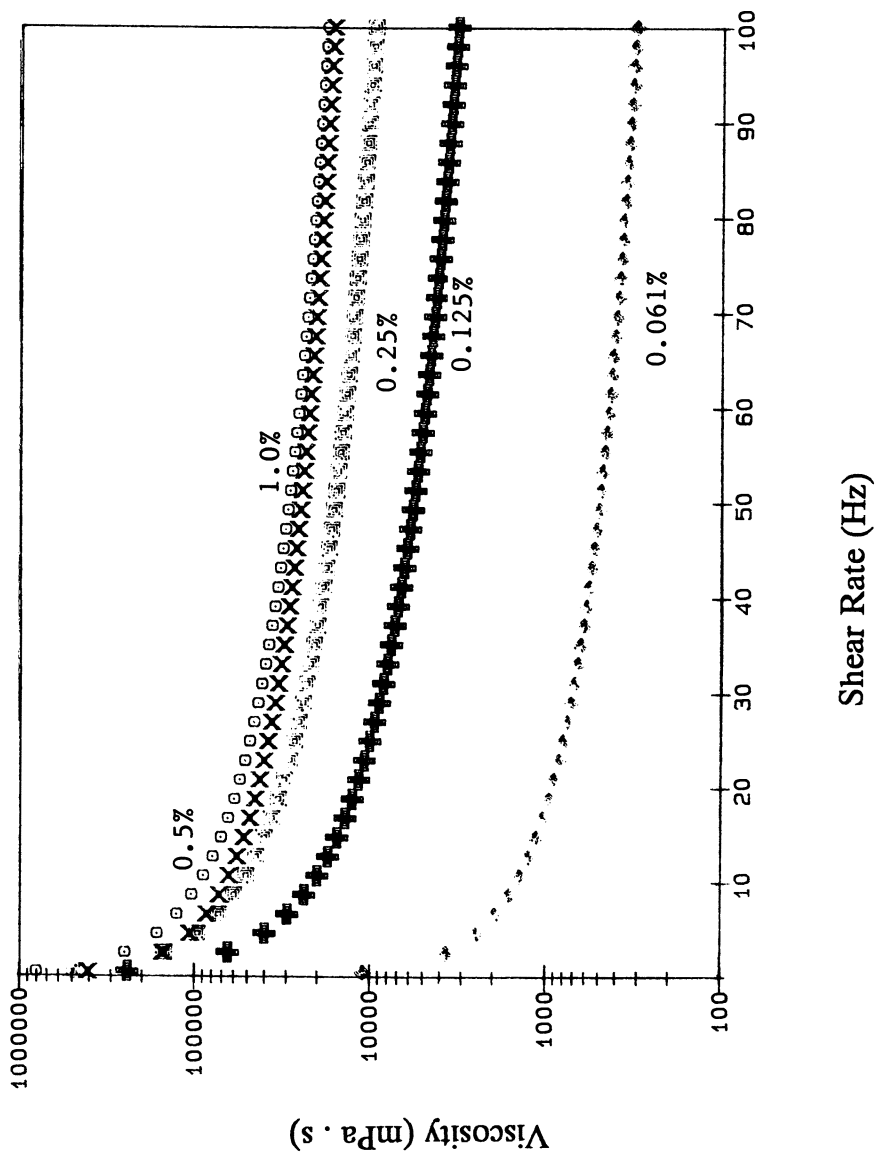
Figure 6. Shear dependence of neutralized type A polymer resin mucilages.
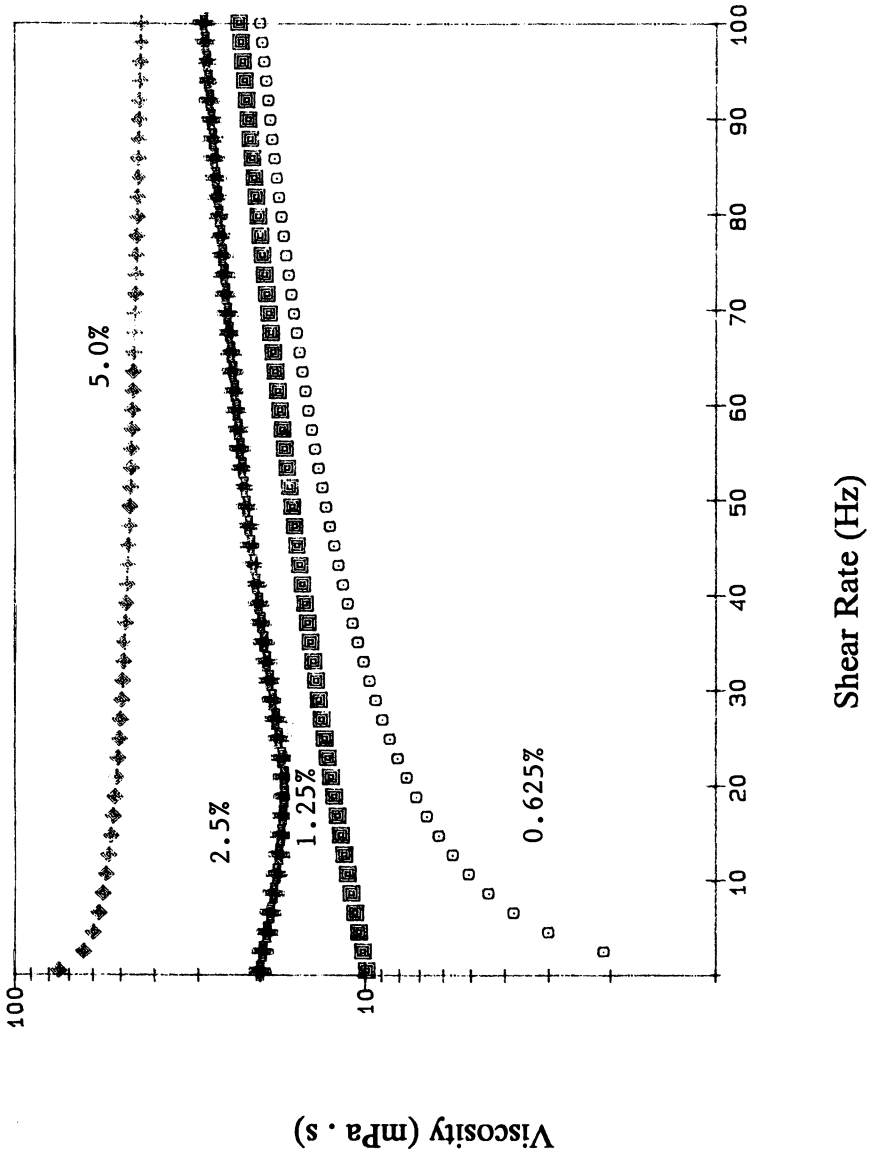
Figure 7. Shear dependence of unneutralized type B polymer mucilages.
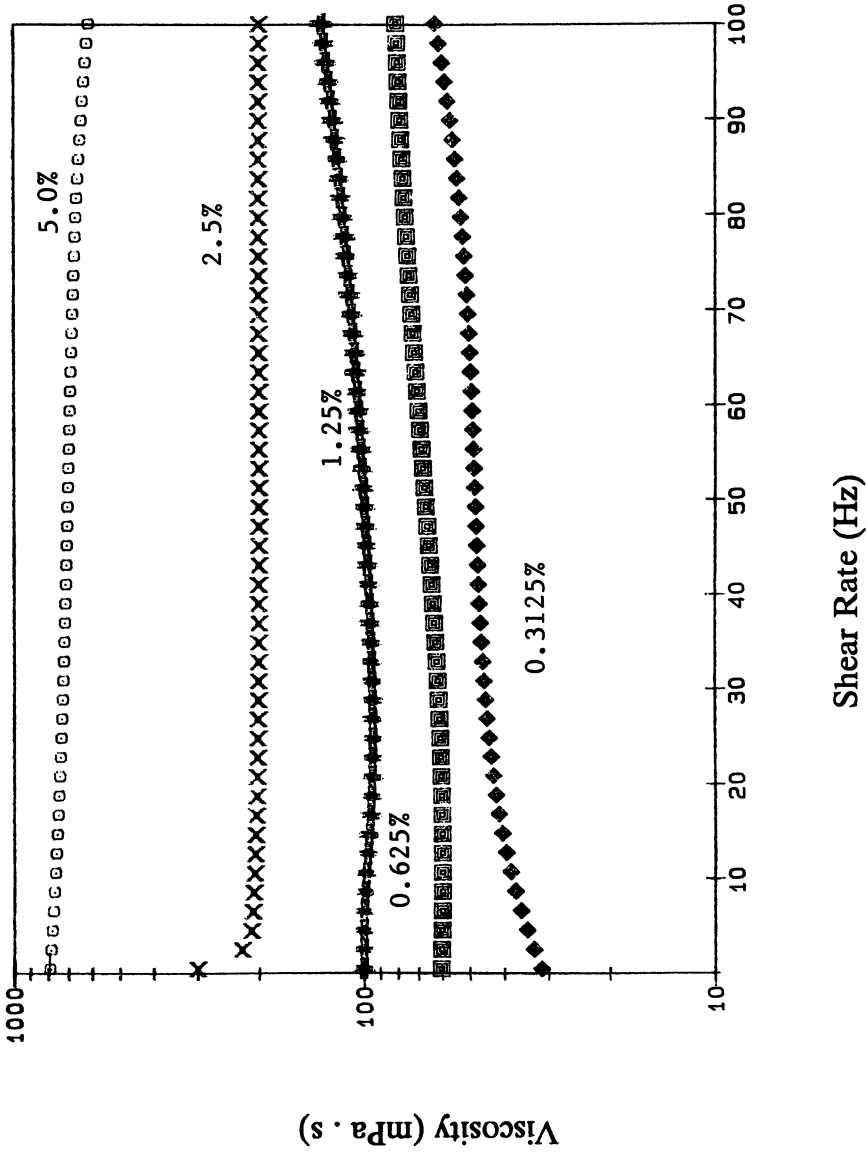
Figure 8. Shear dependence of neutralized type B polymer mucilages.
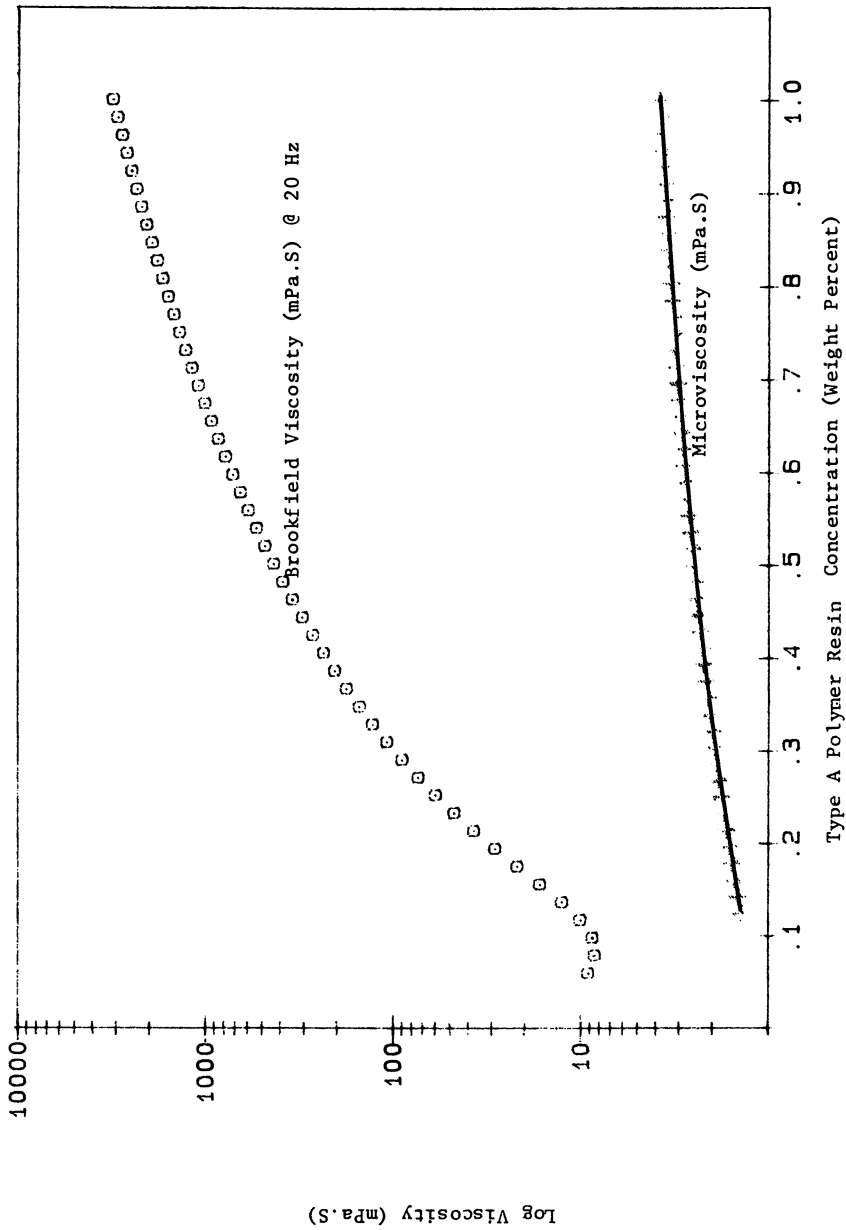
Figure 9. Concentration dependence of microviscosities and Brookfield viscosities of unneutralized type A polymer mucilages.
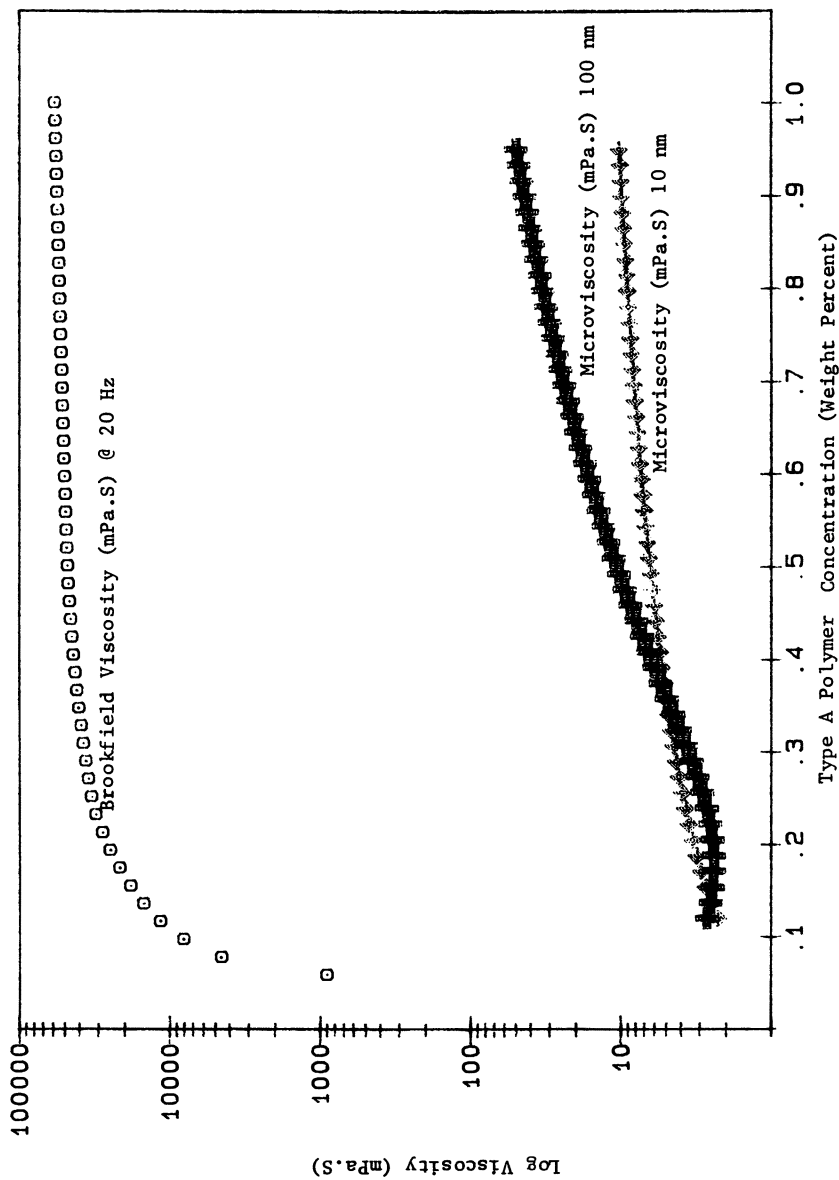
Figure 10. Concentration dependence of microviscosities and Brookfield viscosities of neutralized type A polymer mucilages.
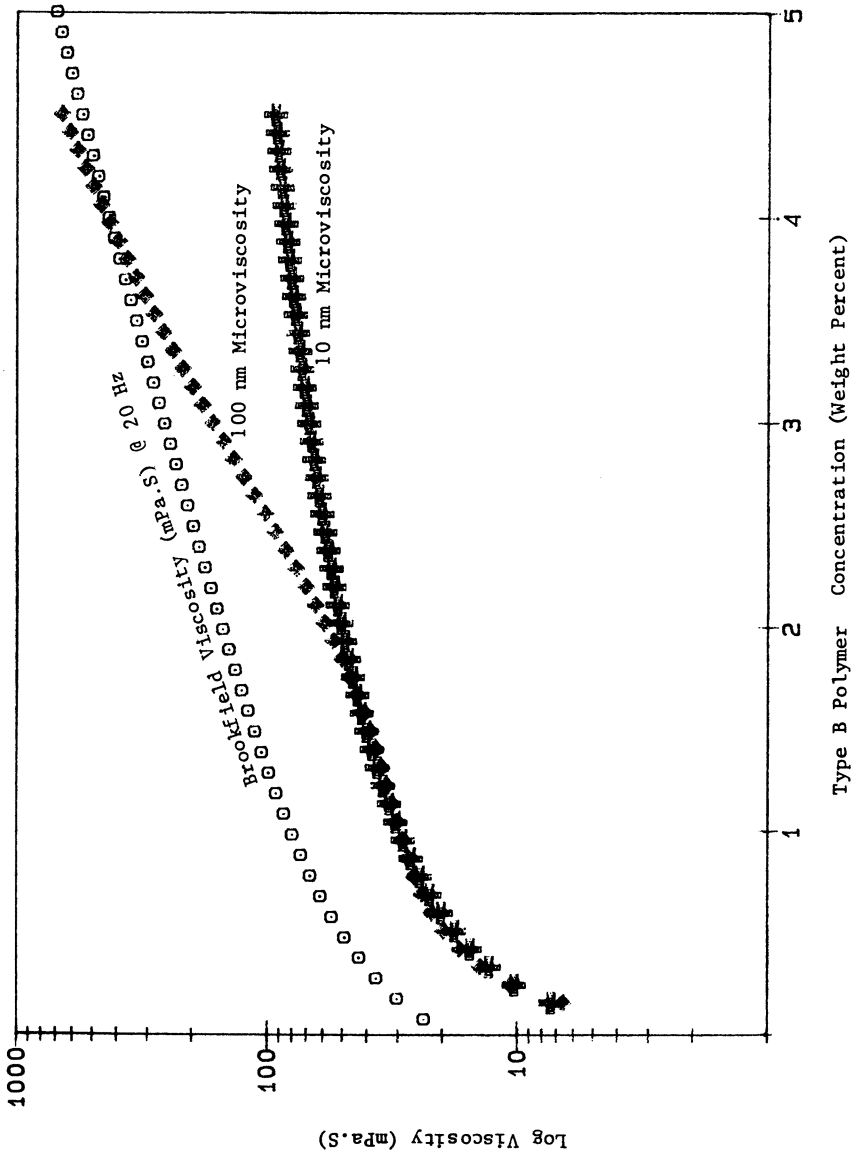
Figure 11. Concentration dependence of microviscosity and Brookfield viscosities of neutralized type B polymer mucilages.
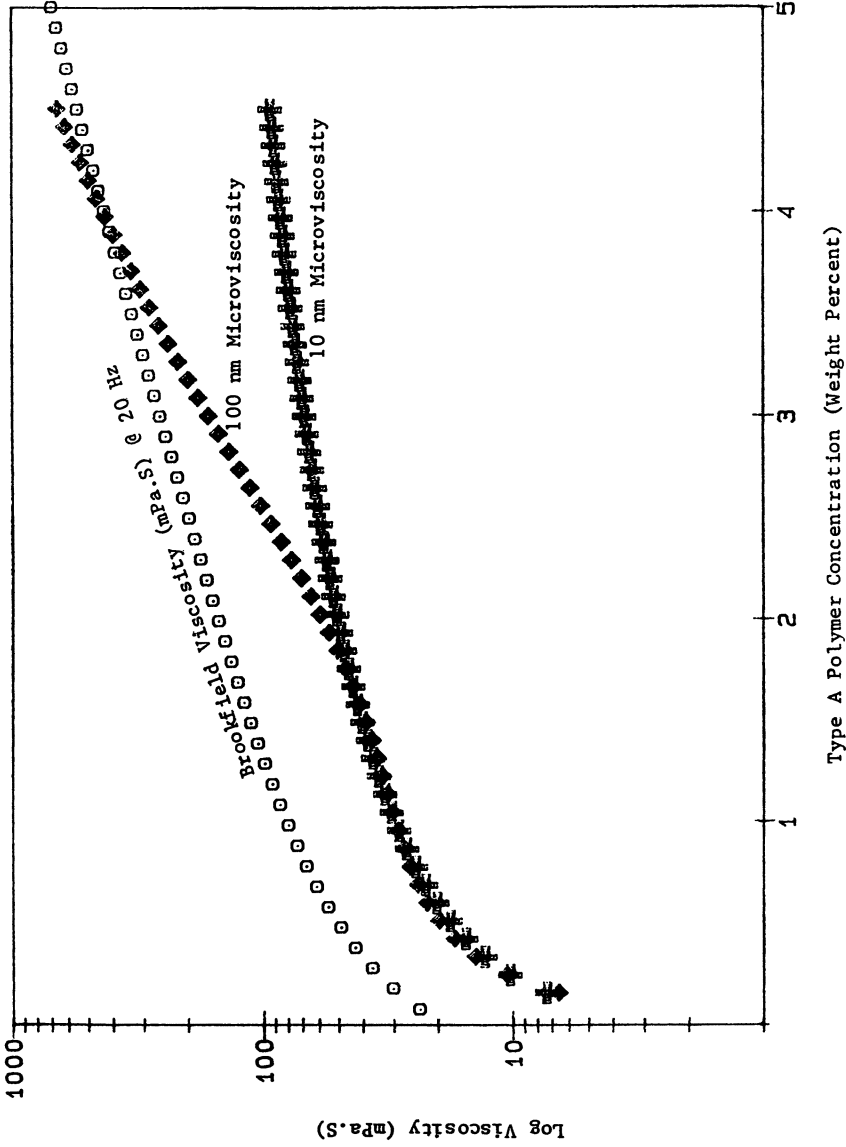
Figure 12. Concentration dependence of microviscosity and Brookfield viscosities of neutralized type A polymer mucilages.

to medium interparticle interaction and medium interparticle hydrodynamic interaction (*10*).

The results presented in Figures 9 and 10 show that, despite the high Brookfield viscosities, the gold sol experienced viscosities close to that of water. It can, therefore, be inferred that the gold sol particles occupied low-viscosity regions in the gel, which, from Bagley's hypothesis, could be viewed as the interstices between the swollen microgel particles.

Above a concentration of about 0.5%, the microviscosity measured by using the 100-nm particles began to deviate positively from that measured by the 10-nm particles. Such a deviation could be explained by a relative decrease in the mean displacement due to diffusion of the larger particles. Thus, the disparity in viscosity between the 10- and 100-nm particles may yield an approximate measure of the size of the interstitial spacing within the swollen gel network.

Type B Polymer. Type B polymer is used as an antiwicking agent for textile printing. During printing, transverse wicking of dyes from a pattern results in poor print definition (Figure 13) (*11*). Two-dimensional circular capillary spreading of a liquid on a porous substrate is described by the Gillespie equation (*12*)

$$R^2(R^4 - R_0^4) = \frac{3\beta}{2}\left(\frac{3V}{2\pi h}\right)^2 t \qquad (5)$$

where R denotes the radius of the stain at time t, R_0 is the radius of the stain at time zero, V is the volume of the liquid, h is the thickness of the substrate, t is the spreading time, and β is given by equation 6:

$$\beta = \frac{bq_s \cos\theta}{C_s^3\eta} \qquad (6)$$
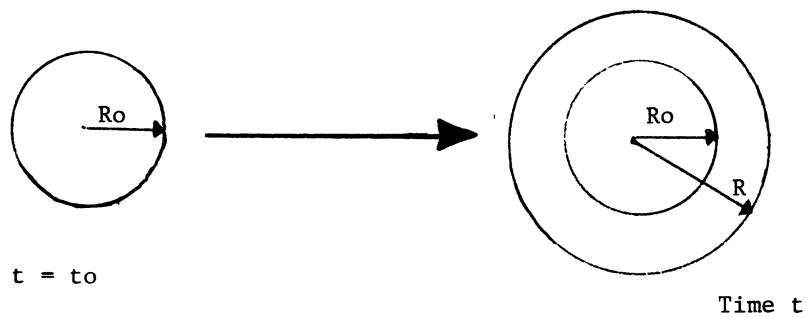
Figure 13. Schematic depiction of wicking.

where b is a constant that describes the substrate, q_s is the substrate permeability, γ is the surface tension, θ is the advancing contact angle, C_s is the saturation concentration of the liquid in the substrate, and η is the viscosity of the liquid.

The Brookfield viscosities of print pastes containing different types of thickeners do not correlate with their effectiveness in preventing wicking. Only thickeners that tenaciously bind the solvent, in this case water, can function as antiwicking agents (11). Binding of water is reflected in the microviscosities of thickened systems rather than their bulk rheology. It is not surprising, therefore, to discover that type B polymer displays microviscosities close to the bulk viscosity of the thickened system. The high microviscosities of type B polymer, in comparison to type A polymer, are a manifestation of the tenacity with which water is bound by type B resin.

No attempt has been made in this chapter to measure wicking and to correlate it directly with microviscosities, because the kinetics of sorption may be complicated by diffusion of liquid *into* the fibers rather than capillary movement *between* fibers (13). In a real printing operation, the fixation conditions and rate of drying of the print, the type of fabric used and its thickness, the twist of the yarns, and the type of fibers used have a strong influence on wicking behavior (11).

Hydrophobically Modified Poly(acrylic acid) (HMPAA) as an Emulsifier

Emulsion Stability. An *emulsion* is defined as a macroscopic dispersion of two liquids, one of which forms the continuous phase of the system and the other forms the discrete phase. An emulsion of two liquids without a stabilizer will quickly break into two liquid layers. Emulsions destabilize by three distinct processes: breaking, creaming, and flocculation (Figure 14). When emulsions break, the initial small droplets of the emulsion spontaneously join to form larger droplets. This process is termed "coalescence", and it ultimately leads to two separate liquid layers.

Creaming is the separation of dispersed droplets from the continuous phase under the action of gravity. The droplets do not coalesce when they touch. If the dispersed medium is less dense than the continuous phase, the emulsion will cream upwards. Conversely, for a more dense dispersed phase, the emulsion will cream downwards or sediment. Creaming will inevitably occur in any dilute emulsion in accordance with Stokes's law if the phases are not exactly equal in density. Creaming is, therefore, a trivial form of instability that can be avoided by addition of thickeners that confer plastic rheology, and, therefore, yield value to the aqueous phase.

Flocculation is the mutual adhesion of droplets to form a three-dimensional network without coalescence. To prepare a stable emulsion of oil and water, it is essential to add a third component as emulsifier. There are several classes of emulsifying agents.
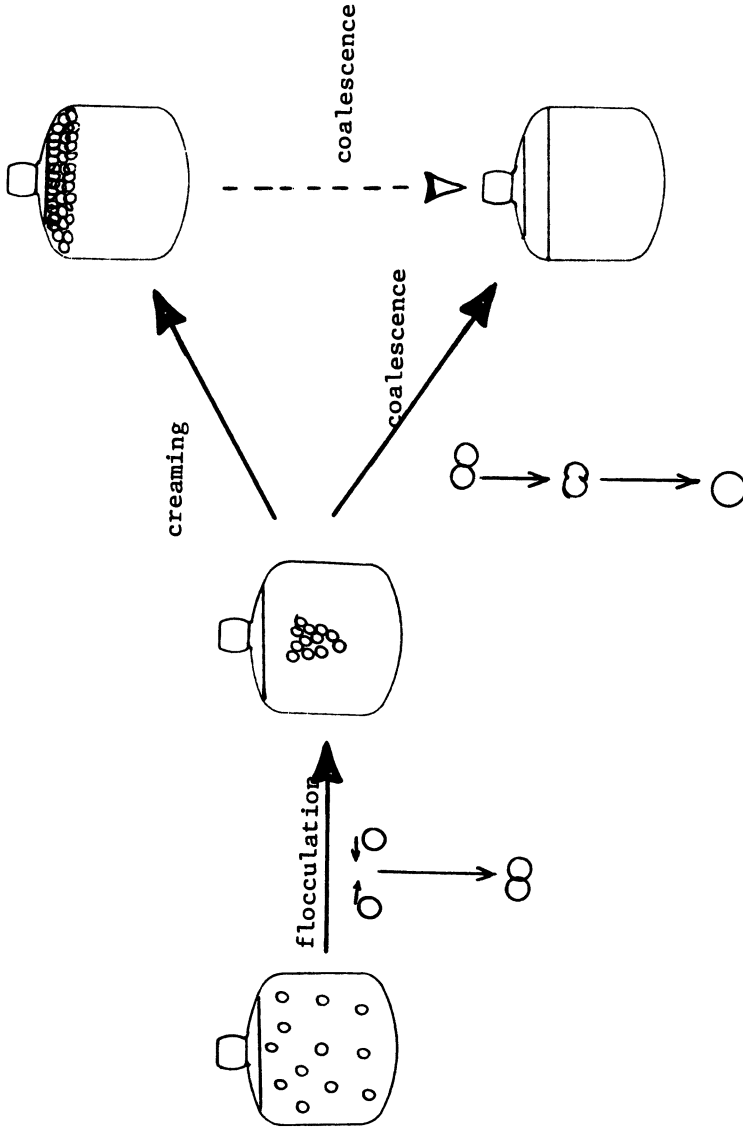
Figure 14. Emulsion instability.

Stabilization by Soaps and Detergents.   The amphipathic molecules of soaps and detergents are strongly adsorbed at the oil–water interface and cause a significant reduction in interfacial tension. This reduction in interfacial tension cannot, by itself, account for emulsion stability; however, because the surface free energy will always be positive, the drive to equilibrium will inevitably result, sooner or later, in coalescence. Reduction of the surface energy is not of any great importance in reducing the energy required for emulsification because about 90% of the energy used for emulsification is dissipated to counter viscosity (*14*). Factors that are important in stabilizing emulsions are electrical double-layer repulsion, the lateral chain–chain interaction of the detergent, and the structure of water surrounding the emulsion droplet (*15*).

The Electrical Double Layer.   Ionized surfactants stabilize oil-in-water emulsions by means of an electrical double-layer in the aqueous phase. For an oil–water interface in the absence of surfactants, most of the double-layer potential difference will be in the oil layer. Addition of an ionic surfactant causes a potential jump due to the presence of dipoles and, for ionic surfactants, a localization of a large double-layer potential difference in the aqueous phase (Figure 15) (*16*).

The stabilizing potential can be evaluated from electrophoresis measurements of the zeta potential and substitution into

$$V = \zeta B^2 \tag{7}$$

where V is the double-layer potential, ζ is the zeta potential, and $B = 0.24$. If electrical double-layer forces are the main stabilizing force, a surface potential of about 20 mV is necessary to prevent flocculation and coalescence.

Double-layer potential effects, however, cannot be responsible for the stabilization conferred by nonionic surfactants, nor can they explain the stability of water-in-oil emulsions where the double layer would be exceedingly extensive and the potential drop would be gradual. These emulsions are stabilized by a stable, thick, liquid-crystalline film at the interface or by steric stabilization.

Liquid Crystal Stabilization.   Davies (*15*) first proposed the formation of a viscous layer around emulsion droplets when he calculated that the electrical forces, interfacial tension, and solvation were not sufficient to explain the stability observed experimentally in many emulsions. Furthermore, he could not explain why many emulsions containing aromatic hydrocarbons formed flocculated clusters that resisted coalescence, whereas the same systems, in which aliphatic hydrocarbons were substituted for the aromatic hydrocarbons, displayed no such stability against coalescence. Davies reasoned that his postulated thick, viscous layers arose from interaction between the liquid molecules and the emulsifier.
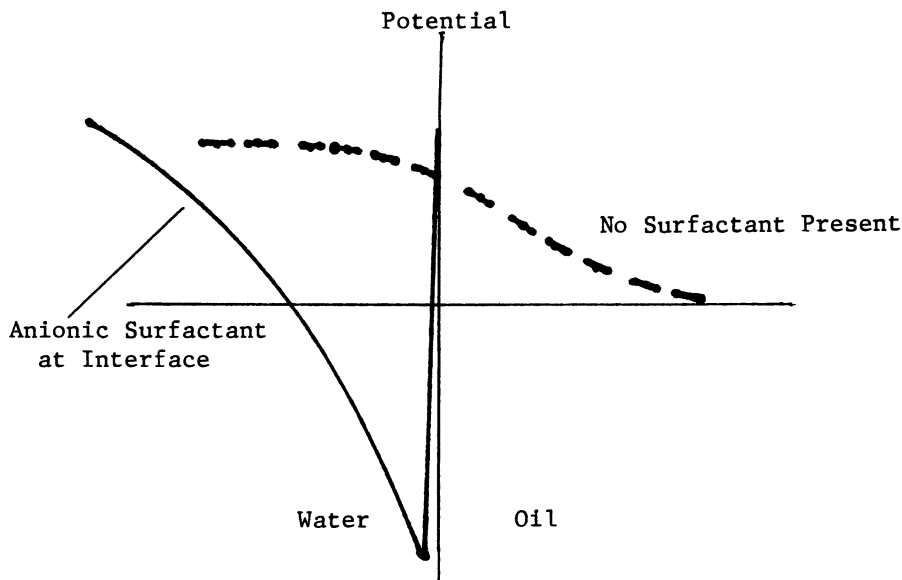
Figure 15. Change in the localization of the electrical double layer due to adsorption of an anionic surfactant.

Friberg et al. (*17*) demonstrated that a sudden increase in emulsion stability arose in the concentration range where a liquid-crystalline phase could be separated from the emulsion. They postulated, with good reason, that this liquid-crystalline phase was the viscous layer around the emulsion droplets that Davies had been seeking. Further, the liquid-crystal stabilization hypothesis explained the difference in stability between emulsions of aromatic and aliphatic hydrocarbons, because aromatic hydrocarbons, because of their large polarizability, are more prone to form lyotropic liquid-crystal structures than aliphatic hydrocarbons.

The presence of liquid-crystalline material at the emulsion interface has been shown by electron microscopy using the freeze-etching technique (*18*). Typical liquid-crystalline structures are shown in Figure 16. These liquid-crystalline compositions are viscous, and the lamellar phase displays pseudo-plastic rheology. The lamellar phase is the most important of all liquid-crystalline phases for emulsion stability. The presence of a liquid-crystalline phase causes a reduction of the available London–van der Waals forces for coalescence (*16*). As a consequence of the reduction of the influence of these dispersion forces and the high viscosity of the liquid-crystal layer, the time for coalescence is increased dramatically.

The formation of liquid-crystal structures also reduces the need for dispersant, because much of the liquid crystal consists of water and oil phases. A typical emulsifier concentration of about 7% is sufficient to give 40% liquid-crystalline phase in one-to-one emulsion (*16*).

Hexagonal Phase

Water

Lamellar Phase

Water
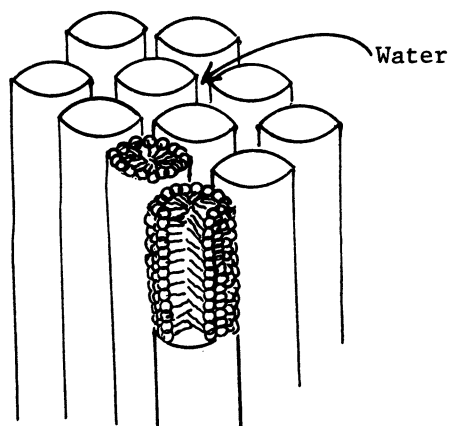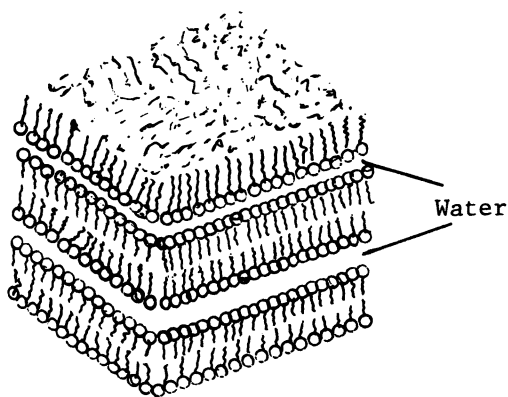
In the above diagrams, each surfactant molecule is represented by

Hydrophilic head group ——————— ⌒⌒⌒⌒⌒⌒ ——————— Hydrophobic tail group

Figure 16. Typical lyotropic liquid-crystal structures.

Steric Stabilization.   A third stabilization mechanism that is normally achieved by amphipathic polymers or by nonionic surfactants is steric stabilization. To be a candidate for steric stabilization, the polymers must consist of long segments, which are soluble in the liquid medium, interspersed by short segments, usually called "anchors" which are strongly adsorbed at the oil–water interface (Figure 17).

When two sterically stabilized particles with adsorbed polymer layers approach one another sufficiently closely for the adsorbed layers to interact, two extreme cases can occur (*19*).

1. The soluble segments of the polymer chains may mix.

2. The soluble segments of the polymer chains do not mix but are compressed as the droplets approach each other.

These cases are depicted schematically in Figure 18. In case 1, mixing of the chains causes an increase in polymer concentration between the droplets, which is resisted by an osmotically driven inflow of solvent between the droplets, which drives the droplets apart. In case 2, loss of configurational freedom of the polymer chains results in a decrease in their configurational
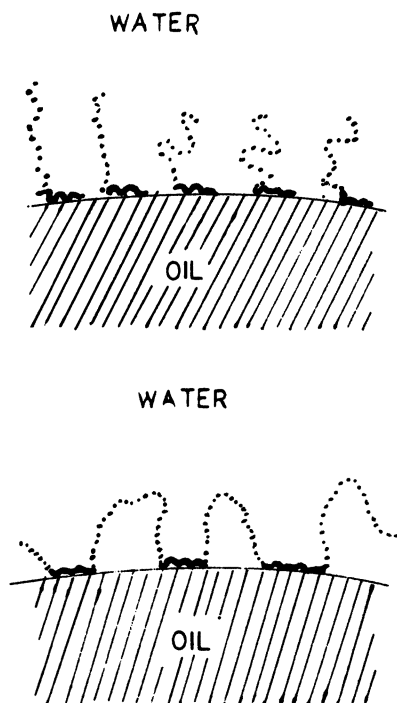
Figure 17. Adsorption of steric stabilizing polymer at an oil–water interface.
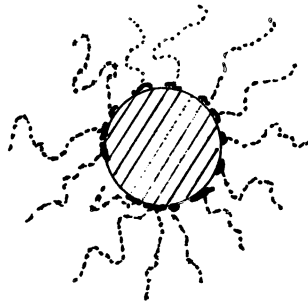
Sterically Stabilized Particle
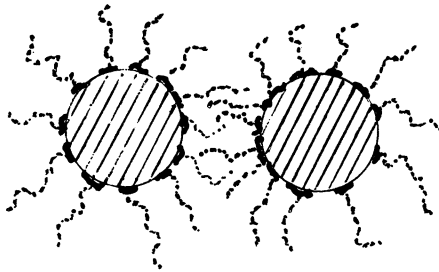
Overlap of Polymer Segments Between Two Particles
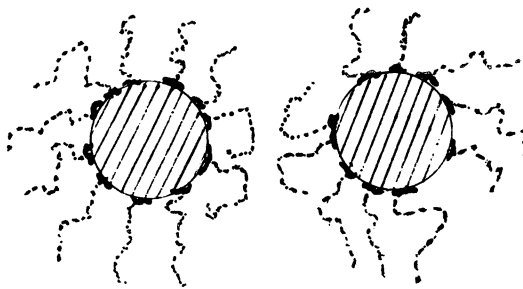
Compression of the Polymer Layers upon Mutual
Approach of Two Particles

Figure 18. Steric stabilization.

entropy. This loss of entropy is resisted by expansion of the chains that, once more, forces the droplets apart. High surface coverage of the droplet is essential. If the polymer concentration is too low, the same polymer molecule can become attached to two or more particles, and bridging flocculation may occur (Figure 19). The same phenomenon is observed when the polymers are linear and molecular weight is excessively high.

Conditions that cause the extended polymer segments to become insoluble in the medium will also, in general, give rise to flocculation and even coalescence of the emulsion. Flory (3) defined *theta conditions* as conditions of temperature and solvent composition under which the free energy of interaction between polymer segments equals the free energy of polymer–solvent interaction. Under theta conditions, the soluble segments of a steric stabilizer would collapse, the repulsion between droplets would diminish, and flocculation of the system would be expected to ensue. This prediction has been demonstrated experimentally (*20, 21*).

Alkyl ethylene oxide condensates and nonionic polymers such as poly(vinyl alcohol) or poly(propylene oxide)–poly(ethylene oxide) block copolymers become insoluble in water above a certain temperature, usually designated as the *cloud point*. The polymer chains collapse at this temperature, and, consequently, flocculation of aqueous dispersions or emulsions stabilized by these surfactants occurs when the system is heated above the cloud point.

The factors that are important in steric stabilization are

1. thickness of the adsorbed layer,
2. configuration of the polymer chain,
3. fraction of segments adsorbed, and
4. segment density distribution (both perpendicular and parallel to the surface).

When the stabilizing entity is a polyelectrolyte, the droplets are stabilized by electrosteric stabilization, which is a combination of electrostatic and steric stabilization (*22*).

Stabilizing Effect of Solid Particles. Emulsion droplets can be stabilized against coalescence by adsorption of solid particles at the oil–water interface. Some common emulsifiers function by this mechanism by crystallizing during their use and adsorbing as solids at the interface. The way to achieve emulsion stability in this case is to choose solids that have a contact angle of 90° with the disperse phase, which will cause immersion of part of the particle in the disperse phase, but will prevent spreading wetting to occur over the rest of the particle (Figure 20).
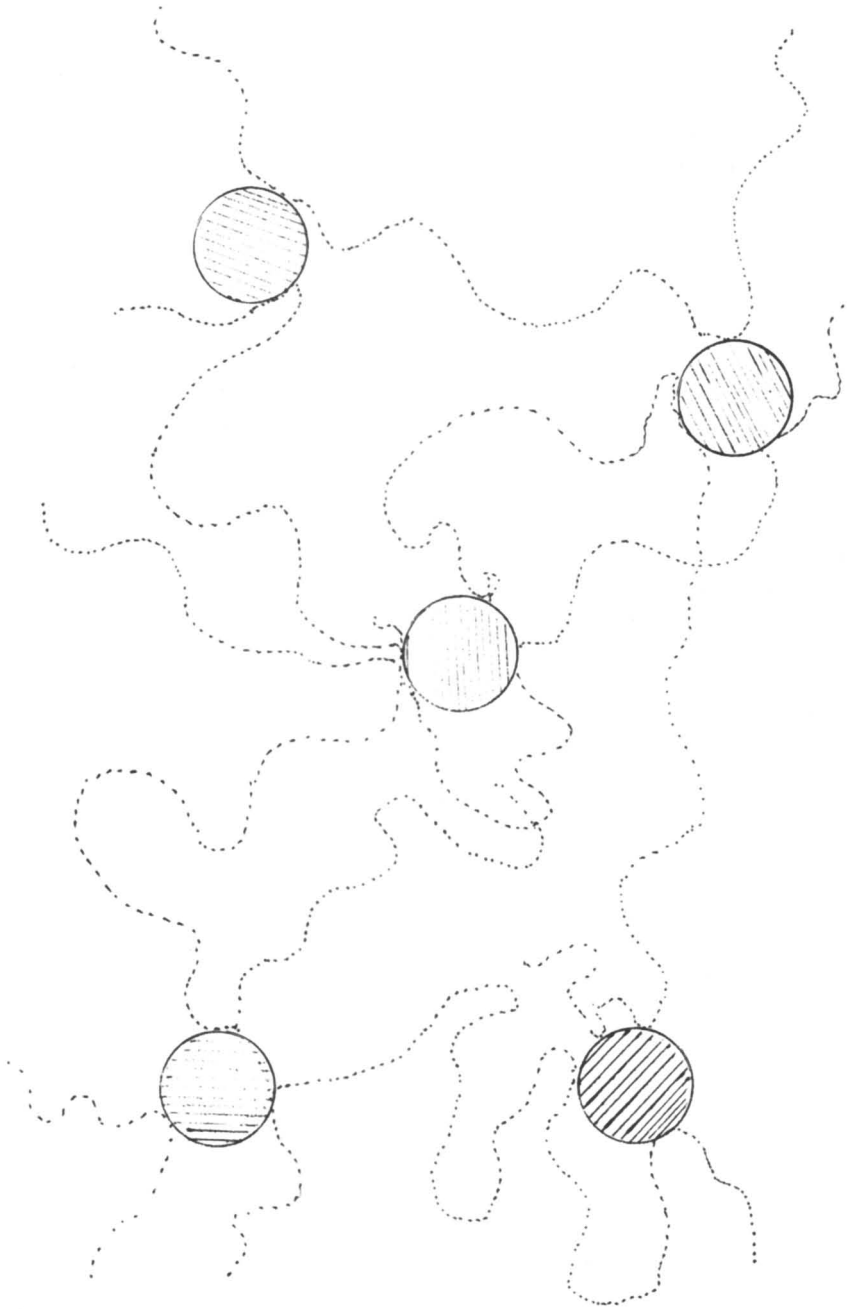
Figure 19. Schematic illustration of bridging flocculation.
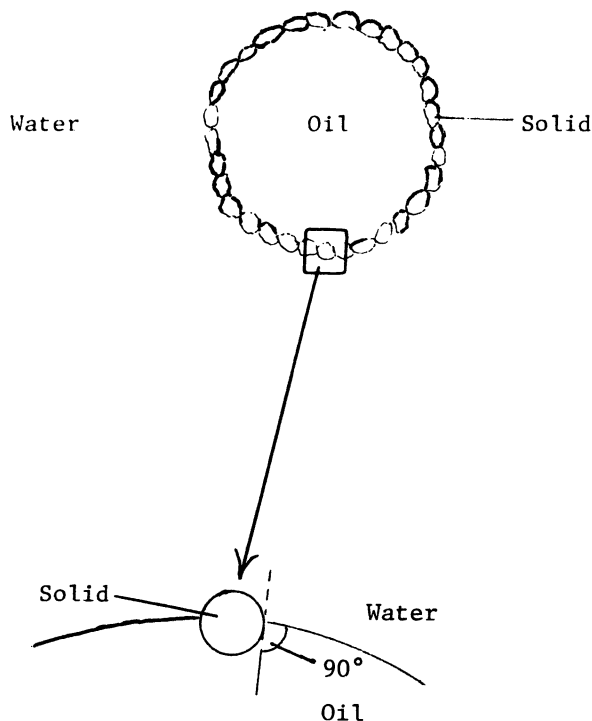
Figure 20. Emulsion stabilization by solid particles.

The Function of Poly(acrylic acid) Thickeners in Emulsion Compositions. Poly(acrylic acid) thickeners are used in many commercial emulsion formulations. In general, the poly(acrylic acid) thickeners are not adsorbed at the oil–water interface and, therefore, cannot, by themselves, prevent coalescence of the emulsion droplets. Primary emulsifiers are required for emulsification and stabilization of the emulsion droplets against coalescence. Poly(acrylic acid) thickeners are now used principally to modify the rheology of the continuous water phase and to confer viscosity and yield value on that phase. As a consequence, emulsion droplets are effectively suspended, and creaming of the emulsion is prevented.

Hydrophobically modified poly(acrylic acid) (HMPAA) thickeners, however, contain a certain proportion of long-chain alkyl groups (usually within C_8 to C_{22} chain lengths). These alkyl groups set the hydrophobically modified polymers apart from their unmodified counterparts because they provide sites that allow anchoring of the polymer at an oil–water interface by hydrophobic interaction. The modified polymers, therefore, should behave as

primary emulsifiers. The work in this section was conducted to assess the efficacy of one such hydrophobically modified poly(acrylic acid) as a primary emulsifier.

Experimental Details

In the initial phase of this work, attempts were made to prepare emulsions of 5% mineral oil in water by using only poly(acrylic acid) thickeners. The mineral oil was a pure clear, white grade with a viscosity of 100 mPa · s at room temperature. Polymers A and B from the studies reported in the first half of this chapter were screened for their ability to emulsify the oil. In addition, two other grades of poly(acrylic acid) thickener (types C and D, with number-average molecular-weights of 1.25 million and 3 million, respectively) (1), and a hydrophobically modified poly(acrylic acid) were studied.

The poly(acrylic acid) was dispersed in vigorously agitated water at ambient temperature, and stirring was continued for 20 min. The solution was then stored, without agitation, for 1 h in a water bath at 25 °C to ensure hydration of the polymer. Agitation was resumed and the oil phase was added to the polymer solution. Agitation was continued for a further 30 min, then the solution was neutralized to the desired pH by addition of appropriate amounts of triethanolamine. Polymer concentrations of 0.1 to 1.0 wt % over a pH range of 3 to 9 were studied.

Results

In all cases, stabilization with unmodified polymer types A, B, C, and D yielded emulsions that broke within hours of preparation to give complete coalescence of the oil phase. Emulsions prepared with the hydrophobically modified polymer, however, were, in many cases, quite stable. The results for this hydrophobically modified polymer are summarized in Figures 21 and 22. Stable emulsions were achieved at all pH values studied at a concentration of 0.4% of the hydrophobically modified polymer. These emulsions exhibit stability for years at ambient temperature. For 0.2 and 0.6% polymer, however, emulsions were stable only below pH 8.

The effect of oil loading on emulsion stability for systems containing 0.4% polymer are shown in Figure 22. Stable emulsions over the entire pH range could be obtained when the oil content was less than 20% by weight. At higher oil loadings, the emulsions were unstable above pH 4 to 4.5.

Discussion

Dependence of Emulsion Stability on Polymer Concentration. The optimum concentration of this particular hydrophobically modified poly(acrylic acid) for emulsion stability appears to be 0.4%. This level gives emulsion stability over the pH range 3 to 9 at oil loadings up to 20% by weight. At 0.2 and 0.6% of the polymer, however, instability of the emulsion occurs at pH values higher than 8 (Figure 20).
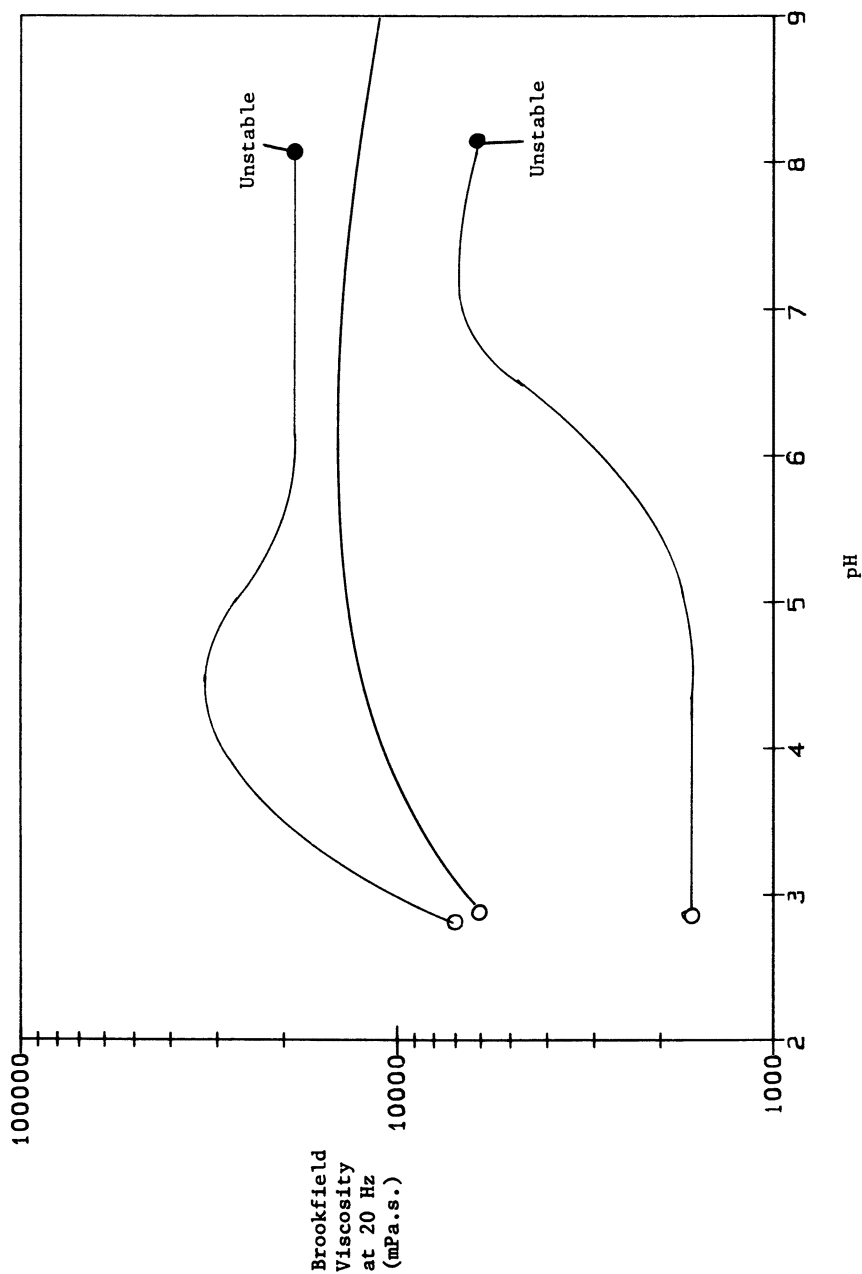
Figure 21. Emulsion viscosity and stability at various HMPAA concentrations.
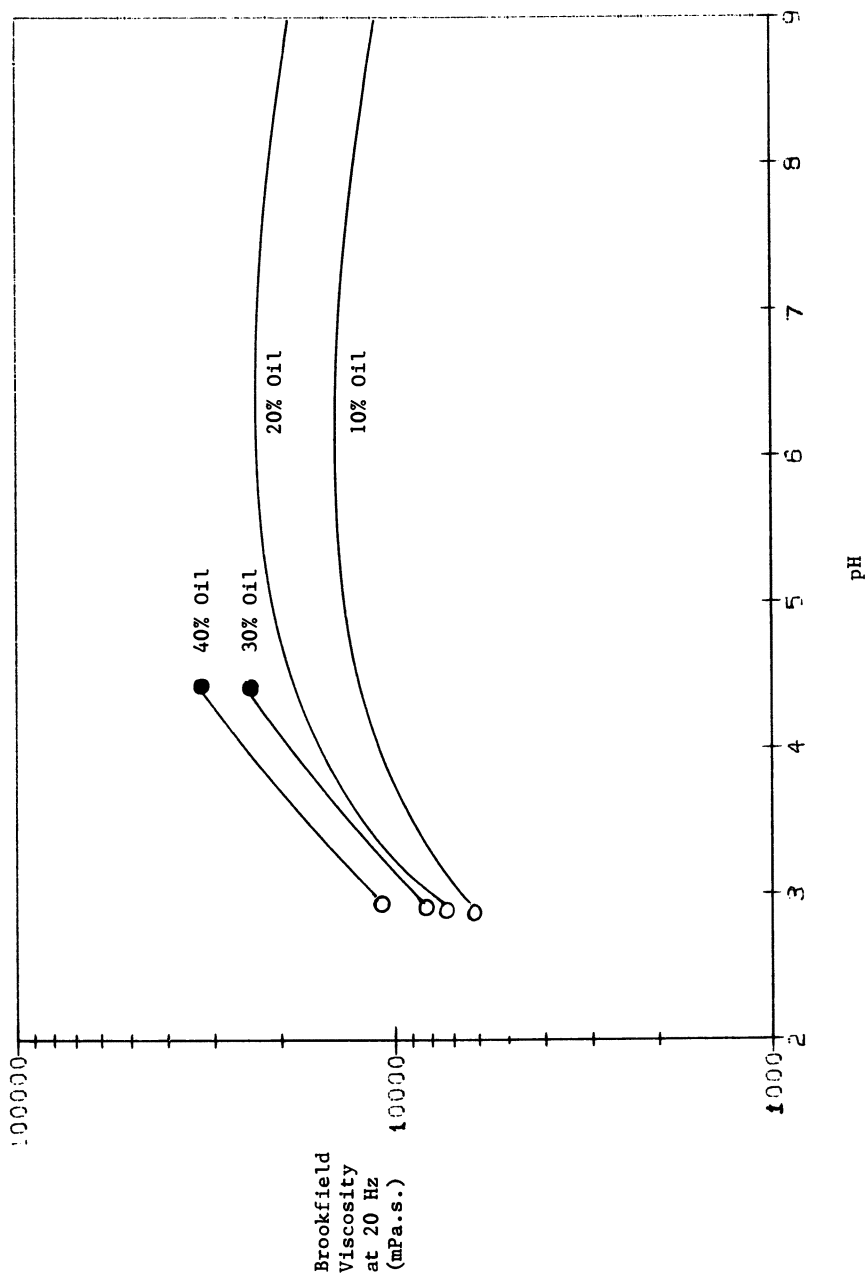
Figure 22. Emulsion viscosity and stability at different oil loadings. HMPAA (0.4 wt %) neutralized with triethanolamine.

The neutralized polymer is more hydrophilic than its unneutralized counterpart, and the resulting enhanced compatibility with water would be expected to diminish the driving force for adsorption at the oil–water interface. The emulsion instability at higher pH values for systems containing 0.2% polymer can probably be explained by depletion of hydrophobe at the interface due to the enhanced hydrophilicity of the polymer at these pH values.

At the highest polymer concentration studies (0.6%), however, this mechanism cannot apply because stable emulsion can be reproducibly prepared at higher pH values with 0.4% polymer. A possible explanation for the instability at the highest concentrations may be that these concentrations lie in the semidilute region, where the polymer coils just touch (23). Vincent (24) has shown that in this concentration range, dimensional collapse of the polymer chains occurs, and stabilization is lost.

Effect of Electrolyte. Emulsions stabilized with hydrophobically modified poly(acrylic acid) are sensitive to electrolytes. Upon contact with a brine solution, emulsion stability is immediately lost, and rapid coalescence of the oil droplets ensues (Figure 23). This instability can be understood by consideration of the Donnan equilibrium of counterions in polyelectrolytes (discussed earlier in this chapter). Addition of salt causes collapses of the polyelectrolyte microgels that are adsorbed at the oil–water interface. Shrinkage of the microgels could conceivably lead to immediate loss of stability, as depicted schematically in Figure 24.
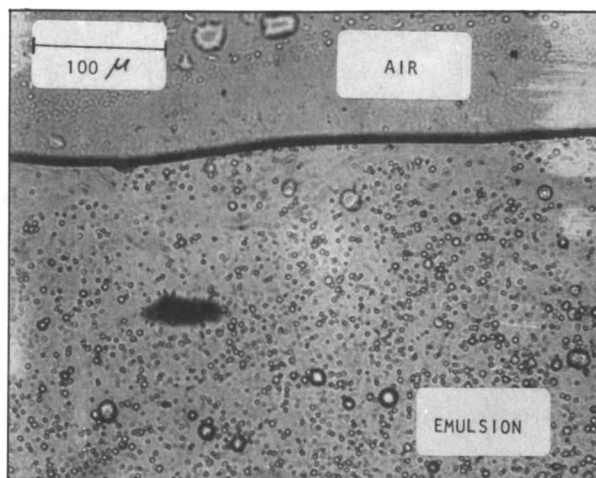
Figure 23. The effect of electrolyte on emulsions stabilized with HMPAA. Continued on next page.
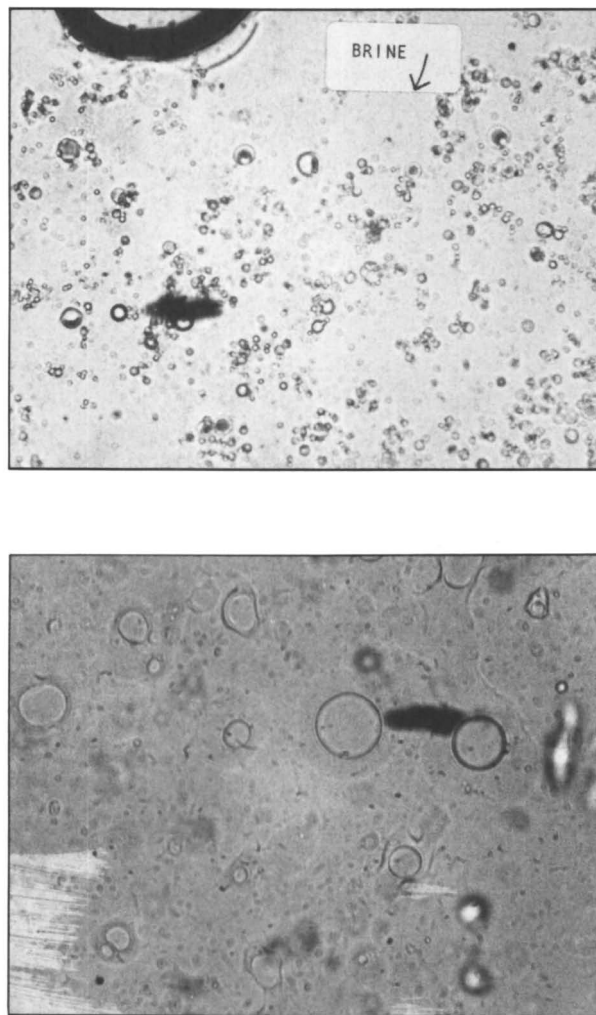
Figure 23.—Continued.
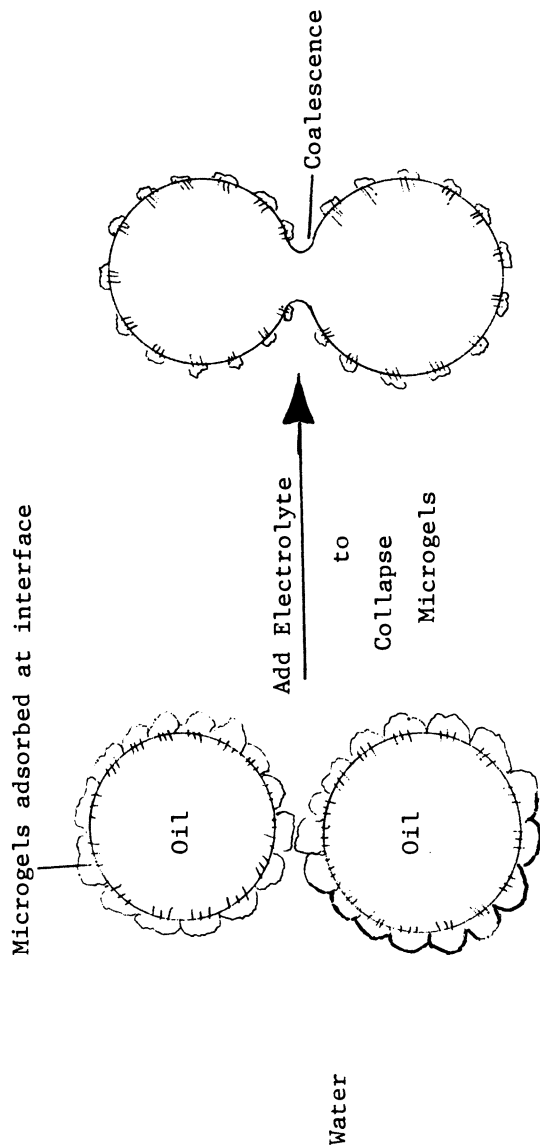
Figure 24. Schematic illustration of destabilization of HMPAA emulsion by addition of salt.

Summary

Measurement of the Stokes–Einstein microdiffusion coefficient by quasi-elastic light scattering of aqueous gels of two high molecular weight poly(acrylic acid) thickeners has shown vast differences in their microrheology. Type A polymer displays extremely high bulk viscosities, but the microviscosities of its gels approach the viscosity of water. A structure of swollen gels packed in intimate contact is postulated. Such a structure would explain the pseudoplastic rheology of these gels. This rheology is more often associated with dispersions than with true polymer solutions. For systems thickened with type B polymer, the microviscosities closely approach the measured bulk viscosities. These systems, therefore, are true polymer solutions, and the tenacity with which these polymer molecules hold water (down to the 10 nm level measured in this study) lends a plausible explanation to the use of this resin as an antiwicking agent in textile printing applications.

Hydrophobically modified poly(acrylic acid) thickeners do show efficacy as primary emulsifiers. These emulsions, although stable for long periods will break and coalesce almost instantly when electrolyte is introduced into the aqueous phase.

References

1. *Carbopol Water Soluble Resins*, technical bulletin GC-67, BFGoodrich Company, Cleveland, Ohio.
2. Rice, S. A.; Nagasawa, M. *Polyelectrolyte Solutions*; Academic: New York, 1961.
3. Flory, P. J. *Principles of Polymer Chemistry*; Cornell University Press: Ithaca, NY, 1953.
4. Hermans, J. J.; Pals, D. T. F. *J. Polym. Sci.* **1950**, *5*, 733.
5. Verwey, J.; Overbeek, J. Th. *Theory of the Stability of Lyophobic Colloids*; Elsevier: Amsterdam, 1948.
6. Sellen, D. B. *J. Polym. Sci., Polym. Lett. Ed.* **1987**, *25*, 699.
7. Taylor, N. W.; Bagley, E. G. *J. Appl. Polym. Sci.* **1974**, *18*, 2747.
8. Davidson, J. A.; Collins, E. A. *J. Colloid Interface Sci.* **1975**, *55*, 163.
9. Faraday, M. *Philos. Trans. R. Soc. London* **1857**, *145*, 23.
10. Cheng, D. C.-H. *Chem. Ind. (London)* **1980**, *10*, 311.
11. Huang, C.; Nieding, D. C. *Book Pap., Natl. Tech. Conf.—AATCC* (American Association of Textile and Color Chemists), **1982**, 137.
12. Gillespie, T. *J. Colloid Sci.* **1958**, *13*, 32.
13. Kissa, E. *J. Colloid Interface Sci.* **1981**, *83*, 265.
14. *Emulsion Science*; Danielli, J. F.; Pankhurst, K. G. A.; Riddiford, A. C., Eds.; Academic Press: New York, 1968.
15. Davies, J. T. *Rec. Prog. Surf. Sci.* **1964**, *2*, 129.
16. Friberg, S. *Food Emulsifiers*; Marcel Dekker: New York, 1976.
17. Friberg, S.; Mandell, L.; Larsson, K. *J. Colloid Interface Sci.* **1969**, *29*, 155.
18. Friberg, S.; Larsson, K. *Adv. Liq. Cryst.* **1976**, *2*, 173.
19. Osmond, D. W. J.; Waite, F. A. *Dispersion Polymerization in Organic Media*; Barret, K. E. J., Ed.; John Wiley and Sons: New York, 1975; Chapter 2, p 24.
20. Napper, D. H. *Trans. Faraday Soc.* **1968**, *64*, 1701.
21. Napper, D. H. *J. Colloid Interface Sci.* **1969**, *29*, 168.

22. Napper, D. H. *Polymeric Stabilization of Colloidal Dispersions*; Academic Press: New York, 1983.
23. Tadros, Th. F. *The Effect of Polymers on Dispersion Properties*; Academic Press: New York, 1982.
24. Vincent, B.; Whittington, S. *Colloid and Surface Science*; Matijevic, E., Ed.; Plenum Press: New York, 1982.

Influence of Polarity in Water-Soluble Polymer Synthesis

Thomas W. Beihoffer[1], David J. Lundberg, and J. Edward Glass

Polymers and Coatings Department, North Dakota State University, Fargo, ND 58105

A historical perspective on the development of hydrophobe-modified, water-soluble polymers is presented. The various synthetic procedures used to obtain different associative thickeners are discussed in terms of the complexities in ionogenic monomer polymerizations. This discussion serves two purposes. The first is to present the peculiarities in anionic and cationic polymer synthesis in contiguity with previous work on water-soluble polymers that related only to their use. The second purpose is to draw parallels between the discontinuities in the classical chain-growth polymerization of nonionic with ionogenic monomers and those that should be expected to occur with hydrophobe-modified monomers, but for which there are insufficient data in associative thickener technology to define properly.

Historical Development of Hydrophobe-Modified, Water-Soluble Polymers

The concept of hydrophobe modification of water-soluble polymers may have arisen from the hydrophobic half-esters of maleic anhydride–methyl vinyl ether copolymers, which were commercially available products in the 1960s (*1*). Replacement of the methyl vinyl ether with styrene produced more stable copolymers in general (*2*), but hydrophobes attached through the ester

[1]Current address: Amoco Production Company, Research and Development Center, Tulsa, OK 74102

linkage were easily hydrolyzed in alkaline media. Most applied formulations are alkaline. Alternative approaches to the hydrophobe-modified maleic acid polymers can be achieved by the copolymerization of maleic anhydride with α-olefins (3). Some of the unique features of hydrophobe-modified maleic acid copolymers are discussed in Chapters 16 and 17.

The synthesis of styrene–maleic acid terpolymers (SMAT) was a more serious test of associative thickener technology. The termonomer was an adduct of the reaction of a nonylphenol ethoxylate anion with vinylbenzyl chloride. The key to its limited success was the separation of the surfactant hydrophobe from the main chain by 40 or more ethoxylate units. The thrust for the development of such a terpolymer (4) was the need for improved coatings rheology (5). There were a number of production and application problems with SMAT. For example, the ethoxylation of any hydrophobe results in a hydrophobe with variable ethoxylate chain lengths and the production of free poly(oxyethylene glycol) with two active hydrogens. In the reaction of the ethoxylate anion with vinylbenzyl chloride, the glycol ether byproduct reacts to form a difunctional monomer (Scheme I). In the ter-polymerization of the SMAT monomers, the difunctional monomer can lead to cross-linked product and insoluble material. This result and the rapid interaction in heat aging tests of the maleic acid units with pigments and fillers in a coating formulation limited the marketability of SMAT.

During these developments, hydrophobically modified ethoxylated ure-thane (HEUR) thickeners were synthesized and patented (6, 7). Their application in coatings was discussed, but the emphasis was on improved barrier properties (8), not on rheological influences. The HEUR polymers of the
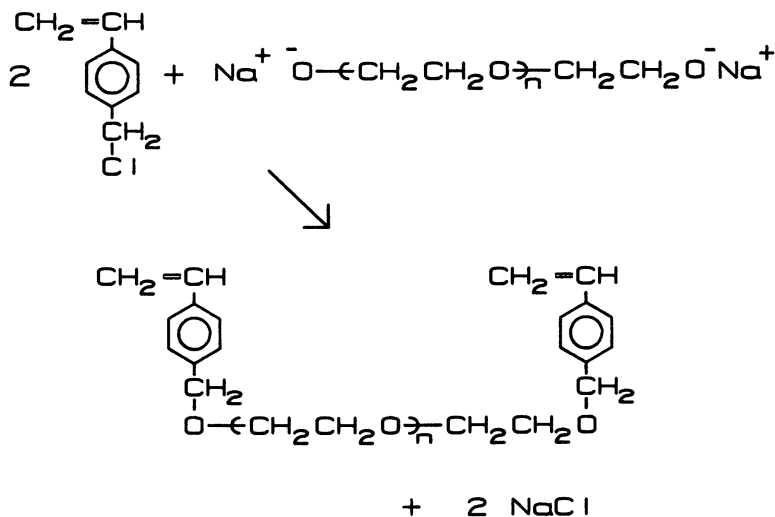
Scheme I

1960s and 1970s appear to have had their greatest success in the hydraulic fluids area. In this respect, it is interesting that a recent patent (9) claims the hydrophobe modification of acrylamide as an effective hydraulic fluid additive.

The HEUR thickeners of the early patents were, in general, not complementary to water-borne latex systems popular in the United States. Patents related to thickeners effective with a wider variety of latex types were introduced in the United States in the early 1980s (10–12). With market acceptance of HEUR thickeners, which were more expensive than the cellulose ethers replaced, formulators made numerous efforts to maintain constant formulation costs. The blending of thickeners achieved this goal. Blending also permitted the separation of the $75\text{-}s^{-1}$ formulation viscosity (5) from the viscosity at high shear rates (10^4 s^{-1}) and thereby allowed formulation of HEUR thickeners that were ineffective viscosifiers at formulation shear rates (75 s^{-1}) but effective viscosifiers at high (10^4 s^{-1}) shear-rate viscosities (HSV). These HEUR products (Chapter 27) probably bear a close structural resemblance to the HEUR products of the early 1960s. The introduction of hydrophobe-modified (hydroxyethyl)cellulose (HMHEC) eventually resulted in the definition of a linear relationship for HSVs in blends of HMHEC with "ineffective" HEURs (Chapter 27).

Petroleum recovery applications represent such large market potentials that even coatings companies organized subsidiaries to capture a share of the sales potential. Acrylamide, for reasons to be discussed, has been the synthetic monomer of choice. It is used as a copolymer, either by partial hydrolysis or by direct copolymerization with acrylic acid (hydrolyzed poly(acrylamide), HPAM). The neutralized acid enhances performance both by increasing the hydrodynamic volume (and viscosity) because of electrostatic repulsions and by decreasing the polymer's adsorption (Table I) on subterranean substrates. Such high molecular weight polymers have two inherent problems: poor mechanical stability (related to elongational behavior, discussed in Chapters 11 and 12), and divalent ion sensitivity. The chelating characteristics of carboxylate groups promote precipitation in brines high in divalent ion. This behavior has prompted the use of sulfonate-containing monomers.

Table I. Static Adsorption of Polyacrylamide
on Silica Powder

Polyacrylamide	Static Absorption (μg/g)
Unhydrolyzed	75
15% HPAM	65
25% HPAM	50
15% HPAM	<10

SOURCE: Martin, D.; Sherwood, S. Society of Petroleum Engineers Publication No. 5339, 1975.
NOTE: 600 mg/L of polymer in 2% NaCl; 24-h cycle.

The poor mechanical stability of high molecular weight HPAM is a problem encountered in basically all stages of use. To bypass the mechanical instability of acrylamide on dissolution, an inverse emulsion (i.e., an acrylamide–water dispersion in oil) process was designed (13). Such dispersions are stabilized by steric factors (electrostatic forces are insufficient in a continuous hydrocarbon media), and coagulation of such emulsions are common. Greater amounts of surfactant with a branched structure (14) and cosurfactant (alcohol or glycol ether) (15) are effective in producing 5- to 10-nm microemulsions that are thermodynamically stable. Unlike the conventional free-radical process discussed later, high rates of polymerization can be realized without compromising molecular weight. In microemulsion studies using sodium bis(2-ethylhexyl)sulfosuccinate (16), a few polymeric chains per particle with collapsed structures, but high in molecular weight, are observed.

In the initial stages of hydrophobe modification of acrylamide, the acrylic acid moiety in HPAM was replaced (17, 18) with a hydrophobe-modified ethoxylated acrylate ester. Both the hydrophobe and the oxyethylene units aggregate with increasing temperature and salinity (2). Increased solution viscosities were realized by hydrophobe associations of the acrylate derivative, but high chain transfer of the oxyethylene units, in large part, negates the inherent efficiency of the acrylamide monomer. Many formulations (e.g., exterior coatings) are alkaline, and viscosity losses due to hydrolysis of the hydrophobe-modified acrylic esters were probably observed. The incorporation of ethoxylate units between the hydrophobe and the main chain (19) is necessary in small particle coatings (Chapter 26) but is not necessary for effective viscosification of aqueous solutions of the type used in petroleum applications. The emphasis shifted to copolymerization of acrylamide with hydrophobe-modified acrylamide (RAM) free of ethoxylate units.

Regardless of the application, the placement (i.e., terminal or internal, isolated or in block sequences) of the hydrophobe-modified monomer in the macromolecular chain is important to the performance of the polymer. The difficulties encountered in determining the sequence structure of hydrophobe-modified acrylamide (water-insoluble) monomers in acrylamide copolymers are discussed in Chapter 20. In this respect, the bicontinuous nature of microemulsions may prove an advantageous method of synthesis. The surfactants used in such a process, however, are significantly more interfacially active than the surfactants used in most application formulations and may detract from the performance of RAM copolymers. The most recent patent (20) in the RAM area discusses the synthesis of RAM copolymers by a microemulsion process, but complexities due to surfactant differences in formulations are not addressed.

The data on the chain-growth polymerization of hydrophobe-modified monomers are insufficient to provide a quantitative analysis of the influence of hydrophobe sequence lengths and placement in copolymers on solution properties. The concentration of the hydrophobe-modified monomer in the

copolymer must be low to ensure intermolecular associations for increased viscosity, and not intramolecular associations that would collapse the chain. In the previous ACS symposium on water-soluble polymers (5), the use of polyelectrolytes in many applications was discussed but not the complexities in their synthesis. For these reasons, and because the copolymerization of ionogenic monomers with nonionic comonomers exhibits departures similar (albeit opposite in direction) to what should be expected in the copolymerization of hydrophobe-modified monomers with nonionic monomers, the deviations in ionogenic monomers are discussed in the next section. A description of inverse suspension or emulsion processes in the polymerization of ionogenic monomers is given in Chapter 10.

Chain-Growth Polymerization

Homopolymerization. *Nonionic Monomers.* The chain-growth polymerization of vinyl monomers occurs via a three-part mechanism: initiation, propagation, and termination. Under steady-state conditions, the rate of polymerization (R_p) is defined (21–24) by equation 1:

$$R_p = (R_i)^{0.5}(k_p/k_t^{0.5})[M] \tag{1}$$

The number-average degree of polymerization (X_n) is given in equation 2:

$$X_n = \frac{k_p^2[M]^2}{k_t R_p} + \frac{1}{C_m} + \frac{1}{C_s}\frac{[M]}{[S]} \tag{2}$$

where k_p and k_t are the propagation and termination rate constants, respectively; $[M]$ and $[S]$ are the concentration of monomer and solvent, respectively; and R_i is the rate of initiation. If the monomer concentration and initiation rate are held constant, the rate of polymerization is dependent on the ratio $k_p/k_t^{0.5}$. The molecular weight of the polymer also is dependent on the ratio of these rate constants. Monomers possessing large k_p and small k_t values provide faster rates of polymerization and higher molecular weights. Often, molecular weights that are obtained are lower than predicted by these rate constants, because of premature termination of the propagating radical by transfer to the monomer $(C_m = k_{tr,M}/k_p)$ and solvent $(C_s = k_{tr,S}/k_p)$. The transfer constants (k_{tr}) (25) for several monomers are given in Table II. The very high k_p and low k_t and C_m for acrylamide reflect its ability to polymerize to very high molecular weights at efficient rates of polymerization. In comparison, high molecular weight poly(vinyl alcohol), a widely used water-soluble polymer obtained from the partial hydrolysis of poly(vinyl acetate), is not obtained. The molecular weight of vinyl acetate, with a large chain transfer to monomer caused in part by the reactivity of the propagating species (26), is lower than expected from its k_p and k_t values.

Table II. Polymerization and Chain-Transfer Constants for Various Monomers

Monomer	k_p	$k_t \times 10^{-6}$	$k_p/k_t^{0.5}$	$C_m \times 10^4$
Acrylamide	17,200	16.3	4.26	0.2
Vinyl acetate	1,100	80	0.234	1.45
2-Vinylpyridine	186	33	0.0323	0
4-Vinylpyridine	12	3	0.00693	6.7
Styrene	44	47.5	0.00638	0.28
Methyl methacrylate	21	12.3	0.00599	0.26

NOTE: k_p is the propagation rate constant, k_t is the termination rate constant, and C_m is the chain-transfer constant. All values are at 25 °C, reference.

Ionogenic Monomers. Polyelectrolytes (cationic or anionic) can be synthesized via the free-radical-initiated chain growth of ionogenic monomers, but departures from the behavior of nonionic monomers are observed. For example, in the polymerization of acrylic and methacrylic acid, a decrease in the rate of polymerization (27) (Figure 1) is observed as the pH is increased from 1 to 6. The decrease is related to coulombic repulsions between the monomer and growing macroradical with increasing pH. In the 6–7 pH range, the macroradical and monomer are fully ionized, and coulombic repulsions result in a polymerization rate minimum. With continued increase in the pH (7–11), the polymerization rate increases. The increase in ionic strength, resulting from NaOH addition (pH adjustment), minimizes repulsions, and the formation of macroradical–monomer ion pairs is suggested to facilitate the rate increase. Such an association (structure 1) results from the strong ion-binding behavior of carboxylate groups (28). Rate increases are also observed with NaCl addition (Figure 2). With additional increases in solution pH (>11), a decrease in polymerization rate is observed and is attributed to replacement of monomer anions with hydroxide units. The termination rate constant does not change (Table III, determined by rotating sector measurements) at high pH and at low and high ionic strength levels; the increase in the rate of polymerization results from an increasing propagation rate constant. This result is in contrast to the chain growth polymerization of nonionic monomers, in which both the rate and molecular weight increase at high conversions because of a decrease in the termination rate constant resulting from restricted diffusion of the chain and segmental motions in an increasingly viscous medium.

The salts of strong acids are desirable in many applications because of their lower ion-binding capabilities and their ionization over a greater pH range. Homopolymerization of such monomers (structures 2–5) has been reported. The consensus of the literature (29–32) is that repulsions in the polymerization of ionogenic monomers hinder the attainment of high molecular weights and high conversions, and this condition is a particular problem on a commercial scale with the salts of strong acids (31). In other respects, the polymerizations are similar to that observed with carboxylate monomers. Thus, routes to higher molecular weight polyelectrolytes have been ap-
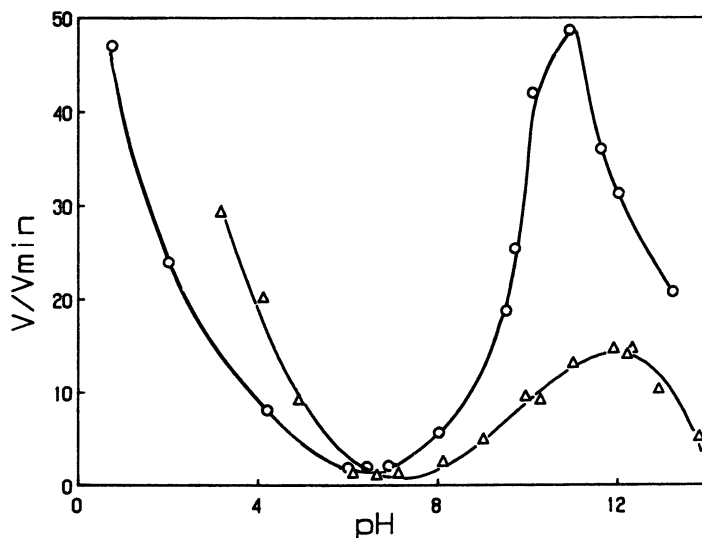
Figure 1. Relative rate of polymerization of methacrylic acid (V/V$_{min}$) *as a function of system pH. The pH was adjusted by adding NaOH. (Reproduced from ref. 2. Copyright 1987 American Chemical Society.)*
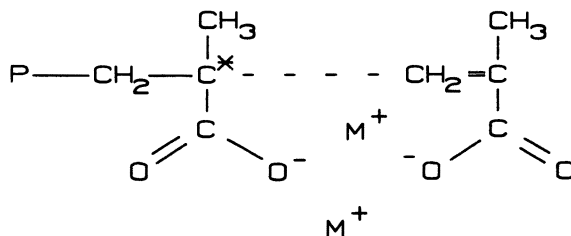
1 Ion-pair formation in the polymerization of methacrylic acid (salt form)

proached through copolymerization with nonionic monomers (this approach also lowers the cost in the production of such polyelectrolytes) or through the postmodification of nonionic polymers. The homopolymerization of hydrophobically modified monomers is of a different magnitude and would result in water-insoluble polymers. Interest in this area would be restricted to Langmuir–Blodgett films.

Copolymerization. Monomer reactivity ratio parameters (r_1 and r_2) have been defined as the ratio of the rate constant for a reactive species adding to its own type of monomer to the rate constant for its addition to the other monomer. The parameters have been very useful in predicting sequence distributions among different monomers in multicomponent polymerizations and in delineating compositional variations with conversion.
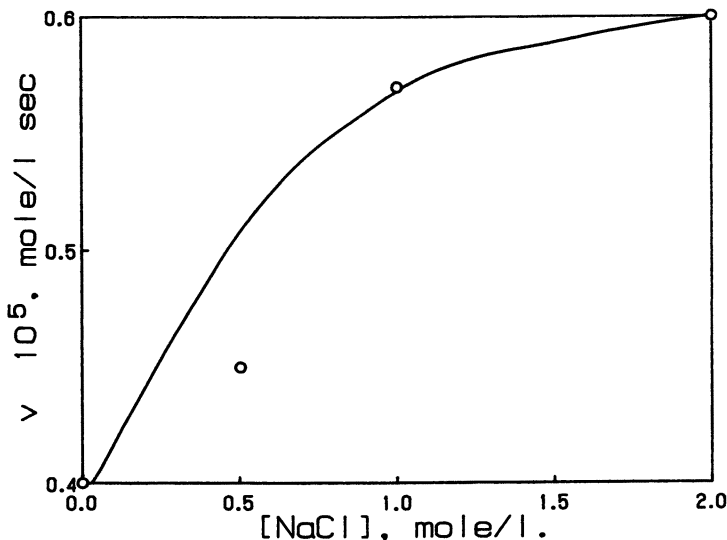
Figure 2. Effect of sodium chloride concentration (ionic strength) on initial polymerization rate of methacrylic acid. The pH was 10.5, adjusted with NaOH. (Reproduced with permission from ref. 35. Copyright 1977 Huethig & Wepf.)

Table III. Elementary Rate Constants for Polymerization of Acrylate and Methacrylate Anions

pH	$R_p \times 10^5$	k_p	$k_t \times 10^{-8}$
Acrylate			
7.9	0.51	650	2.6
7.9, 1.5 N NaCl	2.5	3150	2.6
11	5.0	6600	2.7
13.6	2.1	2500	2.8
Methacrylate			
8.6	0.42	670	2.1
13.6	1.2	1950	2.25

NOTE: All values are given in moles per second. Conditions for acrylate were as follows: [AA] = 1.2 M, [AIBN] = 8.3×10^{-4} M, 365 nm, 23 °C aqueous solution of NaOH. Conditions for methacrylate were as follows: [MAA] = 0.92 M, [AIBN] = 2.5×10^{-4} M, 365 nm, 23 °C aqueous solution of NaOH.

These parameters also have been useful through the Alfrey–Price Q–e scheme (33) for assessing the merit of new monomers in multicomponent macromolecular compositions. From the data just cited for ionogenic monomers and from the strength of associations that affect significant viscosity increases cited in Chapters 18 and 21–27 for hydrophobic monomers, it

$$H_2C=CH$$

2 sodium styrenesulfonate

structure with SO_3Na

$$H_2C=C$$ with CH_3, $C=O$, O, $CH_2CH_2-SO_3Na$
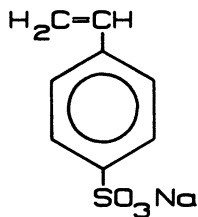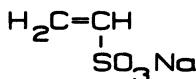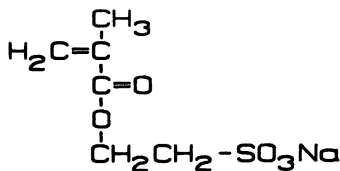
3 sodium 2-sulfoethyl methacrylate

$$H_2C=CH$$ with SO_3Na

4 vinyl sulfonate

$$H_2C=CH$$ with $C=O$, $H-N$, $H_3C-C-CH_3$, CH_2-SO_3Na
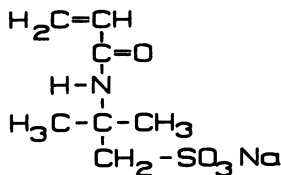
5 sodium 2-acrylamido-2-methylpropanesulfonate

should be expected that Q–e and reactivity ratios would be of limited value in the copolymerization of ionogenic or hydrophobe-modified monomers.

This conclusion has been reached in the copolymerization of acrylic acid (AA) and methacrylic acid (MAA) with *N*-vinylpyrrolidone (*34, 35*) (a monomer noted for its thermal stability (*36*) and discussed in Chapter 9) and with acrylamide (*37*). The incorporation of the acid monomer in the copolymer decreases with increasing solution pH. The *r* values with MAA are particularly low at pH <5 because of hydrophobic associations of the methyl groups. Laser–Raman studies (*38*) have also indicated intramolecular association among the methyl groups of syndiotactic poly(methacrylic acid) (PMAA) in aqueous solution. The addition of NaCl, at a moderate pH, increases the amount of neutralized, weak acid monomer incorporated (Table III). A more gradual change is observed with pH in the MAA–AM combination than in the AA–AM pair because of the hydrophobic interactions cited. The relationships are nearly quantitative with the ionization of the acids as reflected by the pK_a of the monomer and polymer acid sequences.

The reactivity of the neutralized, strong-acid monomers [e.g., sodium styrenesulfonate (*32*) and 2-sulfoethyl methacrylate (*30*)] with nonionic monomers also is dependent on the changes in polarity of the system (i.e., dielectric constant, solvation, and hydration) and with solution pH (Table IV for the sodium styrenesulfonate studies). The effect also is evident (*39*) in the copolymerization of two ionogenic monomers, acrylic acid and 2-acrylamido-2-methylpropanesulfonic acid, with different pK_a values. For acrylic acid, the reactivity ratio is 0.740 ± 0.13 at pH 7 and 1.58 ± 0.15 at pH 2–4. For 2-acrylamido-2-methylpropanesulfonic acid, the reactivity ratio was 0.187 ± 0.09 at pH 7 and 0.111 ± 0.03 at pH 2–4. These studies (*39*)

Table IV. Polymerization Parameters for Sodium Styrenesulfonate in Water–
DMSO Mixtures at 70 °C

Polymerization Medium	Dielectric Constant	$[M]_o$ $(mol/L\ s)$	M_v (10^{-4})	$k_p/k_t^{0.5}$ $(L/mol\ s)^{0.5}$
Water–DMSO (3:1)	67.8	0.969	13.51	0.62
		0.485	8.87	
		0.340	7.64	
		0.243	6.81	
Water–DMSO (1:3)	58.5	0.969	12.60	0.47
		0.485	8.00	
		0.340	6.85	
		0.243	6.46	
DMSO	48.9	0.969	12.00	0.37
		0.485	7.68	
		0.340	6.40	
		0.243	6.19	

NOTE: $[I]_o = [AIBN]_o = 6.09 \times 10^{-4}$ mol/L; $[I]_o = [K_2S_2O_8]_o = 0.93 \times 10^{-4}$ mol/L.
SOURCE: Reprinted with permission from ref. 37. Copyright 1979 Wiley.

have also delineated the importance of group placement in water-soluble polymer performance. The reactivity of each was controlled by solution pH. Less of the weak acid was incorporated at higher pH values, but a more even distribution of carboxylate units was obtained in neutral solutions. The latter polymers provided greater uniformity in cross-linking with chromium ion gels when analyzed via storage modulus measurements.

The copolymerization of hydrophobically modified monomers should exhibit similar behavior, but opposite in direction to ionogenic monomers. Increasing hydrophobe size and solubility differences with the nonionic monomer should make it difficult to obtain significant spacings between hydrophobic monomers in chain-growth copolymerizations. In view of what has been delineated in surfactant–micelle (40) and ionogenic monomer behaviors, a multitude of unique structural possibilities could be obtained in hydrophobically modified copolymers synthesized by free-radical chain-growth processes.

Post- and Premodification

An alternative to the problems in the synthesis of polyelectrolyte- and surfactant-modified water-soluble polymers is pre- and postmodification. Unless the ion-binding character of the carboxylate group is desired for a specific application, the salts of strong acids are the most desirable hydrophilic units (for reasons cited in the ionogenic discussion). The introduction of hydrophilic sulfonate functionality to unsaturated polymers has been a common procedure for over 30 years. Most of these studies relate to the synthesis of strong acid, insoluble ion-exchange resins (41, 42), or to the synthesis of ionomers (43). The sulfonation of polymers to achieve water solubility is a more recent development (41, 44). The most common sulfonating agents are

complexes and hydrates of sulfur trioxide. Because these reactions are not very similar to the post-hydrophobe-modification of water-soluble polymers, their discussion will be omitted.

The postintroduction of hydrophobes could offer an effective alternative to the mutual solubility problems (Chapter 20) encountered in chain-growth copolymerizations. The introduction of difunctional monomers that contain both unsaturation and isocyanate units (e.g., isocyanatoethyl methacrylate or *m*-isopropenyl α,α-dimethylbenzylisocyanate) with lower cost non-isocyanate-containing monomers (45) provides two routes for postmodification. One route could be the copolymerization with methyl acrylate, followed by the reaction of the isocyanate function with an ethoxylated surfactant, then hydrolysis of the methyl acrylate units.

A second route could be the copolymerization of the unsaturated urethane obtained from the reaction of the isocyanate unit with an ethoxylated hydrophobe. Only marginal changes in solubility would be noted with water-soluble monomers. Routes of this nature promise new categories of water-soluble ionogenic polymers with the salts of strong acid, that have not been available. The development of these areas will depend upon finding unique properties specific to a given application area.

Step-Growth Polymerization

No ionogenic polymers of commercial interest are synthesized in a manner similar to associative thickeners prepared by a step-growth type polymerization. Polymers prepared by classical step-growth processes are not high in molecular weight. This low molecular weight would be a disadvantage if thickening were totally dependent on the hydrodynamic or "pseudohydrodynamic" (i.e., via hydrophobic associations) volume. Surfactant-modified water-soluble polymers bypass this limitation through hydrophobic bonding and other associations in disperse systems of the polymer. Coating formulations in which commercial hydrophobically modified ethoxylated urethane (HEUR) thickeners are used contain dispersed phases (latex, pigment, and exterior pigments) that contribute to the formulation's viscosity. The dispersed phases, along with excess surfactant that promotes viscosity through induced network formation and other interactions (Chapter 26), determine the dispersion's viscosity.

Specific routes for HEUR synthesis are given in Chapter 26. The way the market has segregated the numerous commercial HEUR thickeners currently available is interesting. The thickener exhibiting a highly elastic network (Figure 7, Chapter 26) is used primarily with large-particle vinyl acrylic latices that are stabilized by grafted (hydroxyethyl)cellulose fragments (ref. 5, Chapter 18). There is little opportunity for a strong interaction of the thickener with this type of latex, and the elastic network structure is a major contributor to the dispersion's viscosity. The HEUR thickener exhibiting a predominantly viscous response (Figure 8, Chapter 26) in latex dis-

persions is lower in molecular weight and is used primarily with intermediate and small acrylic latices usually stabilized by oligomeric acid segments. In these systems, interactions of the associative thickener with the dispersed phases is a major contributor to the dispersion's viscosity.

Other Hydrophobe-Modified Polymers

The two associative thickeners examined in the remainder of this text whose synthesis has not been discussed are hydrophobe-modified alkali-swellable emulsions (HASE) discussed in Chapters 25, 27, and 28, and hydrophobe-modified (hydroxyethyl)cellulose (HMHEC, discussed in Chapters 17, 18, and 27). HASE thickeners, by far the lowest cost hydrophobe-modified thickeners produced, should have achieved the largest market share on the basis of cost of production, but this situation does not appear to be the case (discussed in Chapter 28) in large part because of the poor properties observed with the lowest cost latex, vinyl acetate, used to form the continuous film. The applied-film properties (46) of vinyl acetate can be substantially improved through the use of HEUR polymers. HMHEC, synthesized by a matured (30-year-old) commercial slurry process (47) has achieved commercial acceptance, in large part because of linear high shear rate viscosities achieved in blends with HEUR thickeners (Chapter 27).

Conclusions

The historical development of associative thickeners has followed the usual phases of polymer development. The products available in the early 1960s were probably prepared with little thought of the concepts presented in the related chapters of this text. Somewhere, these products sparked the concept of induced micelle participation of polymeric hydrophobes and of a synergistic influence on viscosity. The "somewhere" was probably two places, Midland, MI, and Rutgers, NJ. These contributions were taken with others from continental Europe and focused on the coatings industry and, with time, on other industries.

The industrial problems limiting earlier industrial thickeners in the coatings area were overcome with HEUR thickeners. With increasing sales, production limitations were addressed and the batch processes were replaced with semicontinuous techniques. Hydrophobe modification of industry standards (hydroxyethylcellulose and alkali-swellable emulsions) produced by proven industrial processes entered the market and broadened the technology.

Will a significant market development occur with the RAM thickeners or hydrophobe-modified, water-soluble polymers not discussed in this text (e.g., in petroleum recovery processes)? Adsorption and divalent ion sensitivity are key parameters in this area, and the properties are not properly

addressed in this text. HEUR thickeners are more expensive than the cel-
lulose ether thickeners that they have replaced or the other hydrophobe-
modified thickeners available. HEUR thickeners are successful because of
improved film properties and the lower total costs that can be achieved with
their use. As the HEUR market developed, lower cost commercial processes
were developed. If such niches are achieved in specific applications areas
for RAM polymers, the commercial limitations to reasonable-cost production
routes will be resolved.

Acknowledgment

References

1. "Thickener L and LN" commercial brochure, GAF Corporation, 1966.
2. Evani, S. R.; Rose, G. D. *Proceedings of the ACS Division of Polymeric Ma-
    terials: Science and Engineering*, ACS Meeting, New Orleans, LA; American
    Chemical Society: Washington, DC, 1987; p 477.
3. "Polyanhydride Resins" commercial brochure, Gulf Oil Chemicals Company,
    Houston, 1976.
4. *Water-Soluble Polymers: Beauty with Performance*; Glass, J. E., Ed.; Advances
    in Chemistry 213; American Chemical Society: Washington, DC, 1986.
5. Evani, S. R.; Lalk, R. H.; Fiero, T. H. *Proceedings of the ACS Division of
    Organic Coatings and Plastics Chemistry*, ACS Meeting, Atlantic City, NJ;
    American Chemical Society: Washington, DC, 1974; p 142.
6. Winddemuth, E.; Berlenbach, W. U. K. Patent 1 069 735, issued to BASF,
    1964.
7. Gassmann, H. U.S. Patent 2 946 767, issued to Ciba, 1960.
8. BASF Corporation *Paint Colour J.* 1983, *170*, 378.
9. Rose, G. D. U. S. Patent 4 534 875, issued to Dow Chemical, 1985.
10. Emmons, W. D.; Stevens, T. S. U.S. Patent 4 079 028, issued to Rohm and
    Haas, 1978.
11. Schimmel, K. F.; Seiner, J. A.; Rostyslaw, D.; Christenson, R. M. U.S. Patent
    4 298 511, issued to PPG, 1981.
12. Hoy, R. C.; Hoy, K. L. U.S. Patent 4 426 485, issued to Union Carbide, 1984.
13. Vanderhoff, J. W.; Bradford, E. B.; Tarkowski, H. L.; Shaffer, J. B.; Wiley, R.
    M. *Polymerization and Polycondensation Processes*; Platzer, N. A. J., Ed.; Ad-
    vances in Chemistry 34; American Chemical Society: Washington, DC, 1962;
    pp 32–51.
14. Wade, W. H.; Morgan, J. C.; Schechter, R. S.; Jacobsen, J. K.; Salager, J. L.
    Soc. Pet. Eng. J. 1978, *18*(4), 242.
15. Strey, R. *J. Phys. Chem.* 1986, *90*, 671.
16. Candau, F.; Leong, Y. S.; Fitch, R. M. *J. Polym. Sci., Polym. Chem. Ed.* 1985,
    23, 193.
17. Evani, S. R., U.S. Patent 4 432 881, issued to Dow Chemical, 1984.
18. Schulz, D. N. U.S. Patents 4 463 151 and 4 463 152, issued to Exxon Corporation,
    1984.

19. Glass, J. E. *Advances in Organic Coatings Science and Technology Series*, Vol. II; Parfitt, G. D.; Patsis, A. V., Eds.; Technomics: Westport, CT, 1980; Chapter 7.
20. Pancansky, T. J. European Patent Application 8 730 925, 1987.
21. Odian, G. *Principles of Polymerization*; Wiley: New York, 1981; Chapter 6.
22. Billmeyer, F. W., Jr. *Textbook of Polymer Science*; Wiley: New York, 1971.
23. Elias, H. G. *Macromolecules*, Vol. 2; Plenum: New York, 1977.
24. Bowden, M. J. In *Macromolecules: An Introduction to Polymer Science*; Bovey, F. A.; Winslow, F. H., Eds.; Academic: New York, 1979; Chapter 2.
25. *Polymer Handbook*, 2nd ed.; Brandrup, J.; Immergut, E. H., Eds.; Wiley–Interscience: New York, 1975.
26. Litt, M.; Patsiga, R.; Stannett, V. *J. Polym. Sci.* **1970**, *8*, 3607.
27. Kabanov, A.; Topchiev, D. A.; Karaputadze, T. M. *J. Polym. Sci., Polym. Symp.* **1973**, *42*, 173.
28. Breuer, M. M. In *Polymer Science*; Jenkins, A. D., Ed.; North Holland: New York, 1972; Chapter 16.
29. Breslow, D. S.; Kutner, A. *J. Polym. Sci.* **1958**, 27, 295.
30. Kangas, D. A.; Pelletier, R. R. *J. Polym. Sci., Polym. Chem. Ed.* **1970**, *8*, 3543.
31. "Sodium Styrene Sulfonate" commercial brochure, E. I. du Pont Company, Wilmington, DE, 1986.
32. Kurenkov, V. F.; Orlova, G. P.; Myagchenkov, V. A. *Eur. Polym. J.* **1978**, *14*, 657.
33. Alfrey, T.; Price, C. C. *J. Polym. Sci.* **1947**, 101.
34. Cabaness, W. R.; Lin, T. Y. C.; Parkanyi, C. *J. Polym. Sci., Polym. Chem. Ed.* **1971**, *9*, 2155.
35. Ponratnam, S.; Kapur, S. L. *Makromol. Chem.* **1977**, *178*, 1029.
36. Stahl, G. A.; Moradi-Araghi, A.; Doe, P. H. *Water-Soluble Polymers for Petroleum Recovery*; Stahl, G. A.; Schulz, D. N., Eds.; Plenum: New York, 1988; p 121.
37. Kurenkov, V. F.; Myagchenkov, V. A. *Eur. Polym. J.* **1979**, *15*, 849.
38. Koenig, J. L.; Angood, A. C.; Semen, J.; Lando, J. B. *J. Am. Chem. Soc.* **1969**, *91*, 7250.
39. Ryles, R. G.; Neff, R. E. *Water-Soluble Polymers for Petroleum Recovery*; Stahl, G. A.; Schulz, D. N., Eds.; Plenum: New York, 1988; p 139.
40. *Phenomena in Mixed Surfactant Systems*; Scamehorn, J. F., Ed.; ACS Symposium Series 311, American Chemical Society: Washington, DC, 1986.
41. Wheaton, R. M.; Harrington, D. F. *Ind. Eng. Chem.* **1952**, *44*, 1796.
42. Gilbert, E. E. *Sulfonation and Related Reactions*; Robert E. Krieger Publishing: Huntington, NY, 1977.
43. *Ions in Polymers*; Eisenberg, A., Ed.; Advances in Chemistry 187; American Chemical Society: Washington, DC, 1980.
44. Turbak, A. F. *Polym. Prepr. (Am. Chem. Soc., Div. Polym. Chem.)* **1961**, *2*(1), 140.
45. Brown, R. G. Ph.D. Thesis, North Dakota State University, in preparation.
46. Murakami, T.; Fernando, R. H.; Glass, J. E. *J. Oil Colour Chem. Assoc.* **1988**, *71*(10), 315.
47. Glass, J. E.; Buettner, A. M.; Lowther, R. G.; Young, C. S.; Cosby, L. A. *Carbohydr. Res.* **1980**, *84*, 245.

Copolymers of *N*-Vinylpyrrolidone and Sulfonate Monomers

Synthesis and Solution Properties

D. N. Schulz[1], K. Kitano[2], J. A. Danik[1], and J. J. Kaladas

Exxon Research and Engineering Company, Corporate Research Science Laboratories, Route 22 East, Annandale, NJ 08801

This chapter describes the synthesis, kinetics, and solution properties for copolymers of N-vinylpyrrolidone (NVP) with sulfonate ionic and zwitterionic monomers. Examples of the sulfonate ionic monomers are sodium styrenesulfonate (NaSS) and sodium acrylamido-2-methylpropanesulfonate (NaAMPS); an example of the zwitterionic sulfonate monomer is (2-hydroxyethyl)dimethyl(3-sulfopropyl)-ammonium inner salt, methacrylate (SPE). The NVP–NaAMPS monomer pair was exceptional, showing evidence for donor–acceptor character and an alternating tendency in copolymerization. The NVP copolymers containing simple sulfonate ionic monomers (e.g., NaAMPS) showed polyelectrolyte solution properties. On the other hand, the NVP copolymers with zwitterionic sulfonate monomers showed "antipolyelectrolyte" solution behavior.

N EW SULFONATE MONOMERS, both the simple ionic [e.g., sodium styrenesulfonate (NaSS) and sodium acrylamido-2-methylpropanesulfonate (NaAMPS) (*1*)], and zwitterionic [e.g., (2-hydroxyethyl)dimethyl(3-sulfopropyl)ammonium, inner salt, methacrylate (SPE) (*2*)] types, have recently become available. Homopolymers of such simple sulfonate monomers are characterized by good thermal and hydrolytic stability; however, their so-

---

[1]Current address: Exxon Chemical Company, P.O. Box 45, Linden, NJ 07036
[2]Current address: Tonen Petrochemical Ltd., Tokyo 104, Japan

lutions lose viscosity in the presence of added salts because of their poly-electrolytic character. In contrast, poly(sulfo zwitterions) exhibit "anti-polyelectrolytic" solution behavior (3–6).

Poly(N-vinylpyrrolidone), P(NVP), is a nonionic, water-soluble polymer with high thermal and hydrolytic stability (7–9). Copolymers of N-vinylpyr-rolidone (NVP) with various carboxylate and carboxylate–precursor mono-mers (e.g., acrylic acid, sodium acrylate, crotonic acid, itaconic acid, and maleic anhydride) are also well-known (10). In addition, the homo- and copolymerization kinetics of these monomers are well-established. On the other hand, reports of copolymerizations of NVP with sulfonate monomers are sparse (11, 12). This chapter describes the synthesis, kinetics, and reac-tivity ratios for the copolymerization of NVP and some of the newer sulfonate monomers. A comparison of some of the solution properties for such co-polymers is also included.

Experimental Details

Materials.   NVP was received from Aldrich Chemical Company and purified by vacuum distillation (bp 88 °C at 5 mmHg; literature value, bp 96 °C at 14 mmHg). Sodium styrenesulfonate (NaSS) was obtained from Airco; sodium acrylamido-2-meth-ylpropanesulfonate (NaAMPS) was obtained from Lubrizol; SPE, (3-methacrylami-dopropyl)dimethyl(3-sulfopropyl)ammonium, inner salt (SPP), and 1-(3-sulfopropyl)-2-vinylpyridinium, inner salt (SPV) were obtained from Raschig (Germany) via its American distributor, Howard Hall International (Cos Cob, CT). SPE, SPP, and SPV were rectified by recrystallization.

Copolymer Characterization.   Copolymer compositions were determined by elemental analysis and thermal gravimetric analysis. A Perkin-Elmer TGS-2 ther-mogravimetric analyzer, programmed from ambient to 800 °C in N_2 and air, was used. Spectroscopic analysis of the copolymers was not as useful as elemental analysis and thermal gravimetric analysis measurements for analyzing these copolymers. Vis-cometric measurements were made in a solution of water and NaCl with a Contraves low-shear viscometer.

Molecular weight and second virial coefficient (A_2) measurements were made on a KMX-6 fixed low-angle light-scattering (LALLS) spectrometer at 25 °C. The refractive index increments (dn/dc) in 2% NaCl were 0.163 for NVP/NaAMPS (50/50), 0.136 for NVP/SPE (50/50), 0.159 for NVP/SPE (80/20), and 0.139 for NVP/SPE (10/90), as measured on a KMX-16 differential refractometer at 25 °C. Quasi-elastic light scattering measurements were made on a Brookhaven apparatus.

Copolymerization Procedures.   The copolymerization kinetics runs were made using azobis(isobutyronitrile) (AIBN) as the initiator, at $[M][I]^{-1/2} = 15$, a total mon-omer concentration of 14 wt % in water, at 60 °C under N_2. Polymers were isolated by precipitation in acetone. The initial rate of polymerization (R_p) was determined by measuring the initial slope of time vs. conversion plots. Analysis of reactivity ratio data was performed by using the Kelen–Tüdös method (13, 14).

Results and Discussion

In this chapter, we describe the synthesis, kinetics, and solution properties of poly(N-vinylpyrrolidone-*co*-sodium styrenesulfonate) [poly(NVP-*co*-NaSS)], poly(N-vinylpyrrolidone-*co*-sodium acrylamido-2-methylpropane-sulfonate [poly(NVP-*co*-NaAMPS)], poly(N-vinylpyrrolidone-*co*-N,N-di-methyl-N-methacroyloxyethylammoniopropanesulfonate [poly(NVP-*co*-SPE)], poly(N-vinylpyrrolidone-*co*-N,N-dimethyl-N-methacroylamidopropylam-moniopropanesulfonate [poly(NVP-*co*-SPP)], and poly(N-vinylpyrrolidone-*co*-2-vinylpyridiniopropanesulfonate [poly(NVP-*co*-SPV)]. Radical copoly-merizations were carried out in water solutions with AIBN initiator at ele-vated temperature (e.g., 60 °C), (*see* reactions 1–5).

The rates of polymerization (R_p) for the copolymerization of NVP and the various sulfonate monomers (simple ionic and zwitterionic) as a function of sulfonate content are shown in Figure 1. The R_p for the copolymerization of NVP with the sulfonate monomers is

$$NaAMPS \gg SPP \sim SPE \sim NaS \gg SPV$$

The R_p of the copolymerization of NVP with NaAMPS is not only several

(1)

poly(NVP-*co*-NaSS)

(2)

poly(NVP-*co*-NaAMPS)

NVP   SPE

poly(NVP-*co*-SPE)   (3)

NVP   SPP

poly(NVP-*co*-SPP)   (4)

NVP   SPV

poly(NVP-*co*-SPV)   (5)
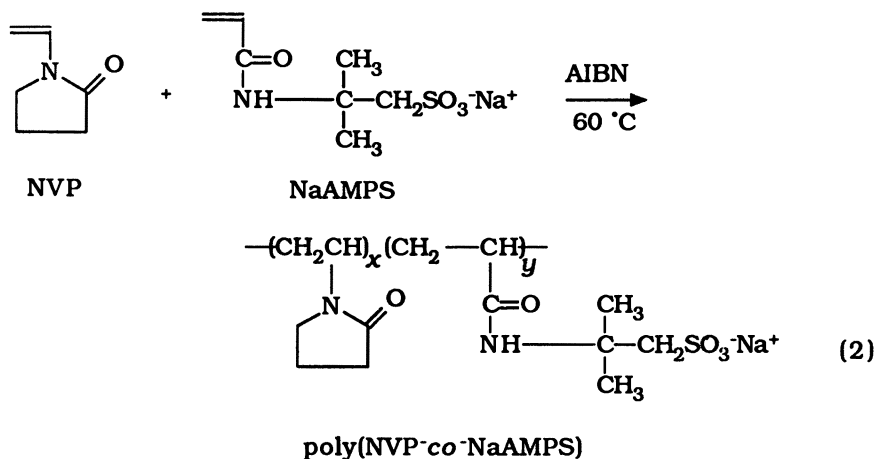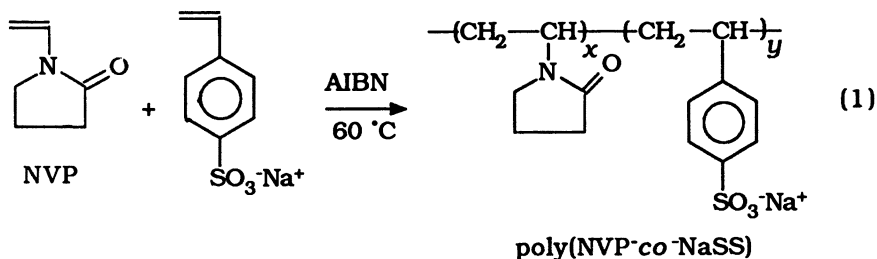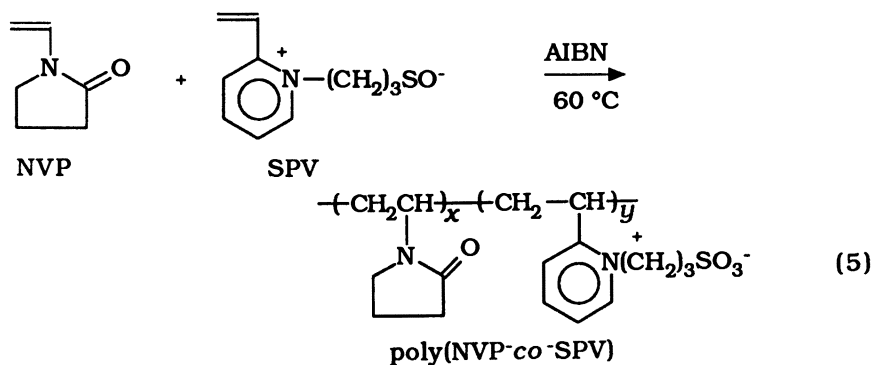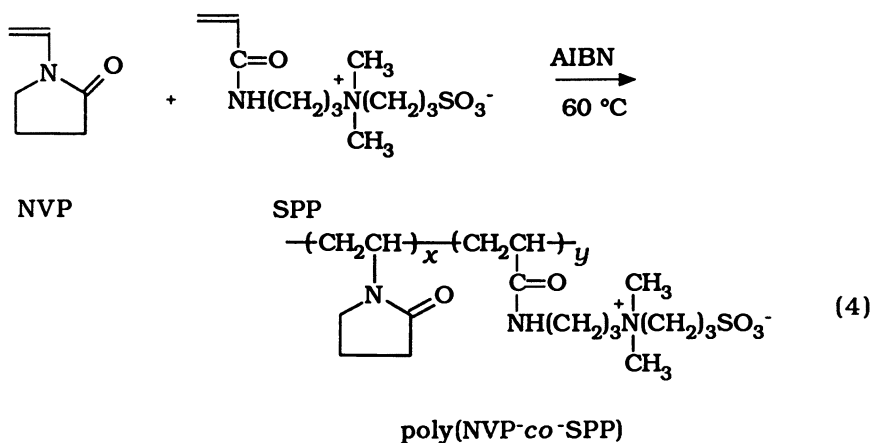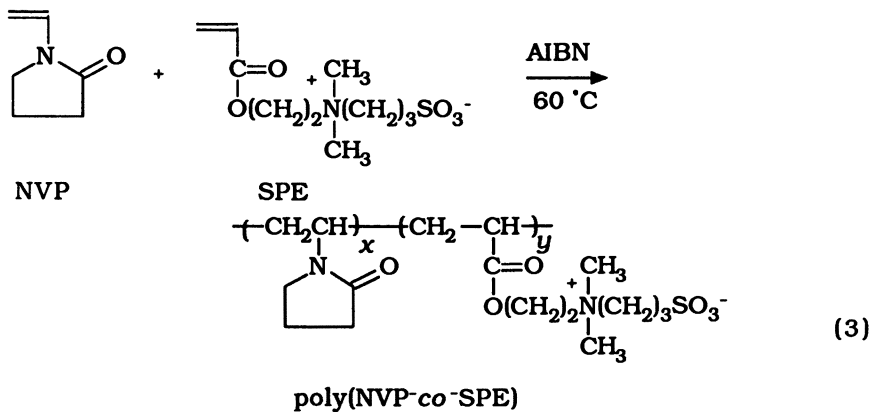
orders of magnitude faster than that of SPP, SPE, and NaSS, but it also shows a maximum in the R_p vs. sulfonate curve near the 1:1 NVP–sulfonate charge ratio. This result suggests some donor–acceptor (D–A) character for this monomer pair (*15*). Also, consistent with the involvement of donor–acceptor complexes (*16*), the NVP–NaAMPS monomer pair polymerizes in
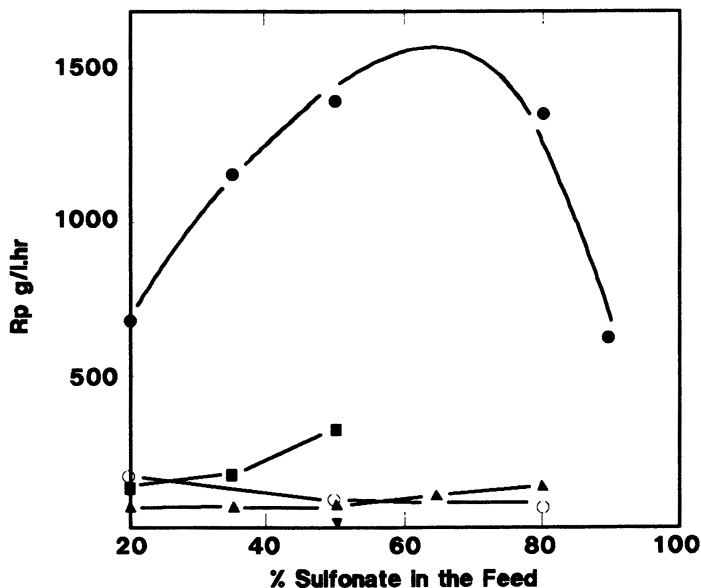
Figure 1. Rates of copolymerization of NVP with sulfonate monomers.
Key: ●, *NVP/NaAMPS;* ▲, *NVP/NaSS;* ○, *NVP/SPE;* ■, *NVP/SPP;*
▼, *NVP/SPV.*

the absence of initiator at room temperature in water or salt solution, whereas NaAMPS itself does not. The NVP–zwitterion monomers SPE and SPP can also autopolymerize, but for a different reason (*17*). In contrast, NVP and SPV do not copolymerize under either the catalyzed or uncatalyzed conditions used in this study. Presumably, the reactivity of the 1-(3-sulfopropyl)-2-vinylpyridinium inner salt is depressed for steric reasons.

NVP is a mildly electron-donating monomer, and the various sulfonates are mildly electron-accepting monomers. Reactivity ratios were determined for the copolymerization of NVP with the simple and zwitterionic sulfonate monomers and are presented in Table I. Such data indicate that NVP and NaAMPS have a tendency to alternate (i.e., r_{NVP} = 0.13, r_{NaAMPS} = 0.66, and $r_{NVP}r_{NaAMPS}$ = 0.086). The level of alternating tendency is similar to that exhibited by NVP–methyl methacrylate and NVP–acrylamide but less than that for NVP–acrylonitrile. The NVP–NaAMPS comonomer pair also has an azeotropic composition at 70 mol % sulfonate (Figure 2). Such data are also consistent with some donor–acceptor involvement for this monomer pair (*16*). As expected, there is little drift in the copolymer composition with conversion near the azeotropic composition (Figure 3).

In contrast, the other simple ionic sulfonate monomer, NaSS, copolymerizes with NVP with preferential incorporation of NaSS (r_{NVP} = 0.084, r_{NaSS} = 7.19) (Table I and Figure 2). Furthermore, there is significant drift in copolymer composition with conversion for this polymer (Figure 4).

The zwitterionic sulfonates (sulfobetaine monomers) also show a higher

Table I. Reactivity Ratios for Copolymerization of NVP
with Sulfonate Monomers

Sulfonate Monomer	R_1	R_2	R_1R_2	$1/R_1$
Simple ionic				
NaAMPS	0.13	0.66	0.086	7.7
NaSS	0.84	7.2	0.60	12
Zwitterionic (sulfobetaines)				
SPP	0.11	2.60	0.29	9.0
SPE	0.066	6.50	0.43	15
Footnote a				
AN	0.06	0.18	0.010	17
MMA	0.020	5.0	0.10	50
MA	0.041	0.27	0.11	24
AM	0.17	0.66	0.11	5.8
ST	0.45	15	0.76	22

NOTE: All copolymerizations were with NVP. Ratios were deter-
mined by the Kelen–Tüdős method (13–14) at average conversions
of 15–18% for NaSS, NaAMPS, and SPE copolymers and 28% for
the SPP copolymer. No data were obtained for the copolymerization
of NVP and SPV.
a"V-Pyrol, N-Vinyl-2-pyrrolidone", technical bulletin, GAF Cor-
poration, New York.
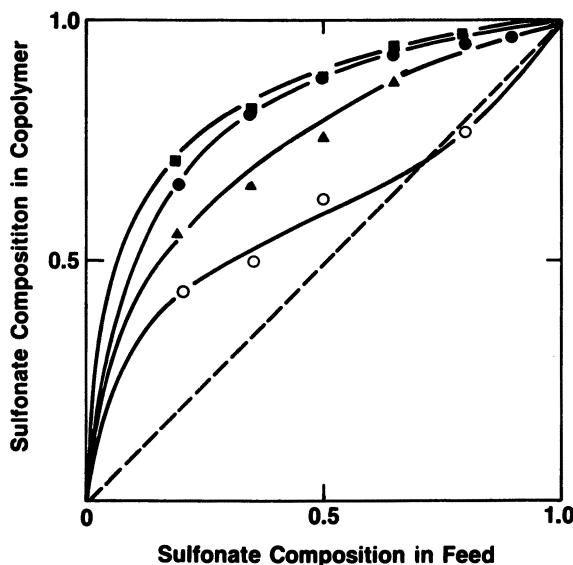
Figure 2. NVP/sulfonate monomer copolymerization curves. Key: ■,
NVP/SPE; ●, NVP/NaSS; ▲, NVP/SPP; ○, NVP/NaAMPS.

relative reactivity of sulfonate monomer compared to NVP (Figure 2). On
the basis of r_{NVP}^{-1} values, the order of sulfonate monomer reactivities toward
the the NVP radical is

SPE > NaSS > SPP > NaAMPS >> SPV
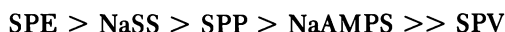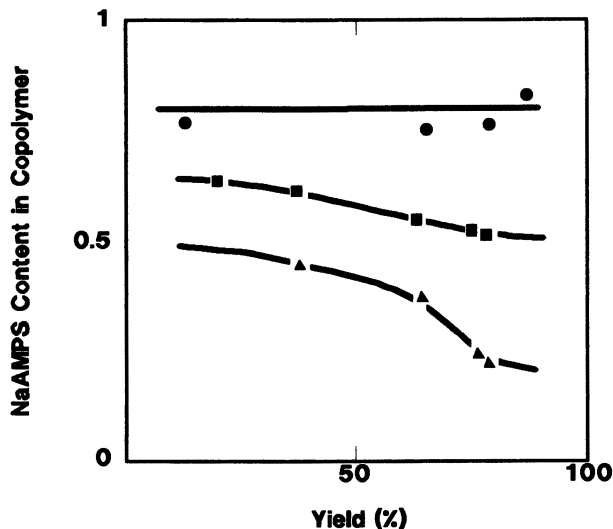
Figure 3. NVP/NaAMPS: yield vs. copolymer composition curves. Key: ●, 20/80 NVP/NaAMPS; ■, 50/50 NVP/NaAMPS; ▲, 80/20 NVP/NaAMPS.
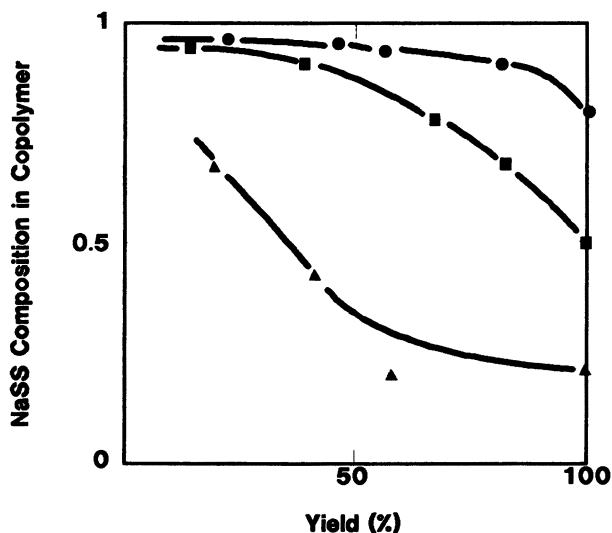
Figure 4. NVP/NaSS: yield vs. copolymer composition curves. Key: ●, 20/80 NVP/NaSS; ■, 50/50 NVP/NaSS; ▲, 80/20 NVP/NaSS.

NVP–simple ionic sulfonate polymers (e.g., NVP–NaAMPS) are typical polyelectrolytes in solution. Thus, such polymers show enhanced viscosities in H_2O (0% NaCl) but exhibit lower viscosities at higher salt concentrations. In contrast, NVP–zwitterion sulfonate copolymers (e.g., NVP–SPE) actually show a slight increase in viscosity with increasing salt concentration (Figure 5).
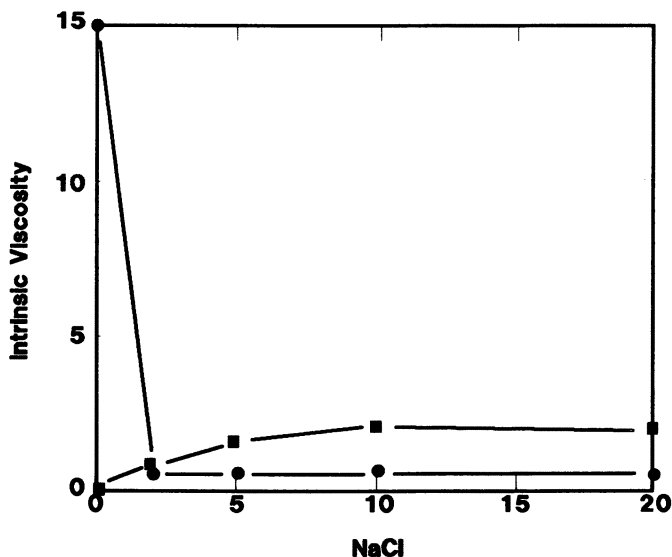
Figure 5. Salt effect on intrinsic viscosity at 25 °C. Key: ●, *NVP/NaAMPS (50/50);* ■, *NVP/SPE (50/50).*

These macroscopic viscosity measurements have been confirmed at the molecular level. For example, dynamic light-scattering methods show an average hydrodynamic diameter (D_w) of about 370 Å for a 50/50 copolymer of NVP/SPE in low salt (<2%) and a D_w of about 390 Å in high-salt (20% NaCl) concentrations (*18*). Moreover, in solutions of water or low concentrations of salt, solvent quality (as measured by second virial coefficient, A_2) decreases with increasing levels of SPE. LALLS measurements for NVP/SPE 80/20 and 10/90 copolymers in 2% NaCl solution yielded molecular weights of 1.1×10^{-6} and 1.4×10^{-6} g mol^{-1}, respectively. The same compositions yielded second virial coefficients of 9.0×10^{-4} and 0.6×10^{-4}, respectively. In this case, a higher virial coefficient means better solution quality.

Thus, macroscopic (e.g., viscosity) and molecular-level (e.g., D_w and A_2) measurements are consistent with a model for NVP/SPE copolymers that is intramolecularly associated in water or low-salt solutions. These intramolecular aggregates are both of the intragroup and intrachain type. Such intramolecular aggregates are broken up by external electrolytes (e.g. NaCl), with a consequent modest expansion of the polymer coil (Figure 6). Thus, the solution properties for sulfo zwitterion copolymers with NVP confirm earlier trends reported for sulfo zwitterion homopolymers (*3–6*).
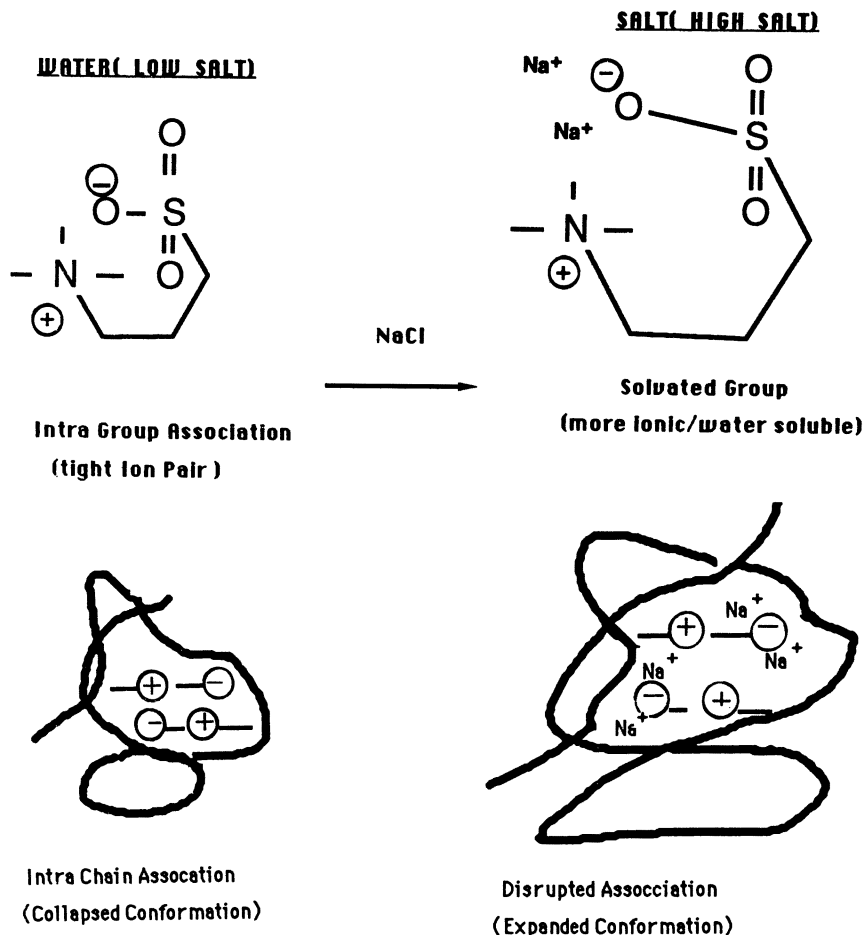
Figure 6. Schematic model for zwitterion (betaine) polymer in water (low-salt) and high-salt solutions.

References

1. AMPS Monomer 2-Acrylamido-2-methylpropanesulfonic acid, technical bulletin 780–360–43, Lubrizol Company, Cleveland, OH, 1981.
2. Chemikalien, Chemicals, Products Chimiques, technical bulletin VCH–11/82–50–19/ME, Raschig GMBH, 1982.
3. Hart, R.; Timmerman, D. *J. Polym. Sci.* 1958, 28, 118.
4. Salamone, J. C.; Voksen, J. C.; Olson, P.; Israel, S. C. *Polymer* 1978, 19, 1157.
5. Monroy Soto, V. M.; Galin, J. C. *Polymer* 1984, 25, 121, 254.
6. Schulz, D. N.; Peiffer, D. G.; Agarwal, P. K.; Larabee, J.; Kaladas, J. J.; Soni, L.; Handwerker, B.; Garner, R. T. *Polymer* 1986, 27, 1734.

7. NVP Polyvinylpyrrolidone, technical bulletin 9642–070, GAF Corporation, New York.
8. Frank, H. P. *J. Polym. Sci.* **1954**, *12*, 565.
9. Conix, A. *J. Polym. Sci.* **1955**, *15*, 221.
10. Sandler, S. R.; Karo, W. *Polymer Synthesis*; Academic Press: New York, 1977; Chapter 8.
11. Kutner, A.; Breslow, D. S. *J. Polym. Sci.* **1959**, *38*(133), 274.
12. Stahl, G. A. Eur. Patent Application 84100918.6, 1984.
13. Kelen, K.; Tuo, F. *J. Macromol. Sci. Chem.* **1975**, *A9*(1), 1.
14. Kennedy, J. P.; Kelen, T.; Tuo, F. *J. Polym. Sci. Polym. Chem. Ed.* **1975**, *13*, 2277.
15. Olson, K. G.; Butler, G. B. *Macromolecules* **1984**, *17*, 2486.
16. Odian, G. *Principles of Polymerization*; Wiley: New York, 1984; p 463.
17. Onchi, T.; Nomoto, K.; Hosaka, Y.; Imoto, M. *J. Macromol. Sci. Chem.* **1984**, *A21*(6,7), 859.
18. Hager, B. L. Exxon Research and Engineering, Annandale, NJ, 1984, unpublished results.

The Polymerization of Quaternary Ammonium Cationic Monomers with Acrylamide

D. Hunkeler, A. E. Hamielec, and W. Baade[1]

Institute for Polymer Production Technology, Department of Chemical Engineering, McMaster University, Hamilton, Ontario L8S 4L7, Canada

The free-radical copolymerization of acrylamide with three common cationic comonomers: diallyldimethylammonium chloride, dimethylaminoethyl methacrylate, and dimethylaminoethyl acrylate, has been investigated. Polymerizations were carried out in solution and inverse microsuspension with azocyanovaleric acid, potassium persulfate, and azobisisobutyronitrile over the temperature range 45 to 60 °C. The copolymer reactivity ratios were determined with the error-in-variables method by using residual monomer concentrations measured by high-performance liquid chromatography. This combination of estimation procedure and analytical technique has been found to be superior to any methods previously used for the estimation of reactivity ratios for cationic acrylamide copolymers. A preliminary kinetic investigation of inverse microsuspension copolymerization at high monomer concentrations is also discussed.

$\mathbf{T}$HE PRODUCTION OF CATIONIC WATER-SOLUBLE HOMOPOLYMERS and copolymers with acrylamide has grown rapidly in recent years (*1*) because of their diverse commercial applications. These polymers are used for fines retention in paper making, as flocculants and biocides in waste water treatment, as stabilizers for emulsion polymerization, in cosmetics and phar-

[1]Current address: Bayer AG, Division KAF, D-4047 Dormagen, Federal Republic of Germany

maceuticals, and, in general, wherever aqueous solid–liquid separations are required.

Cationic polymers can be grouped in three categories: ammonium (primary, secondary, tertiary, and quaternary); sulfonium; and phosphonium compounds. Of these, the ammonium-based polymers have been the most popular, because phosphonium compounds have not been synthesized to high molecular weights (2–8), and sulfonium monomers are generally unstable and less readily available than quaternary ammonium monomers (9–12).

Quaternary ammonium polymers were first discovered by Butler and Bunch (13) in 1949. In that investigation, tri- and tetraallyl quaternary ammonium salts were polymerized to form highly cross-linked water-insoluble polymers. In 1951, Butler and Ingley (14) reacted diallyl quaternary bromide salt to produce a polymer that was water-soluble and did not form a gel. Later, Butler (15) showed that the chloride ion form of diallylammonium monomers gave more useful polymers because of their higher molecular weights.

To explain the reactivity of diallyldimethylammonium chloride, Butler (16) proposed a ring-closing mechanism. This type of polymerization has been called intra-intermolecular, transannular, and cyclopolymerization (the latter is the most common). Initial research in the area of cyclopolymerization indicated that six-member rings were produced (16–20); however, Brace (21, 22) showed in the mid-1960s that five-member ring formation was actually more common. Recent ^{13}C NMR studies (23–25) confirm these findings.

Poly(diallyldimethylammonium chloride) was the first quaternary ammonium polymer approved for potable water clarification by the United States Public Health Service, and has historically been the most widely produced cationic polyelectrolyte. There have been several studies on the kinetics (26–37) and uses of diallyldimethylammonium chloride (DADMAC) (38–45); however, there have been no investigations in inverse microsuspension, the most common industrial method of polymerization. Furthermore, there is considerable disagreement between published reactivity ratios, probably because no satisfactory analytical methods have been described in the literature for residual monomer concentration or copolymer composition. For other commercially important quaternary ammonium polymers, such as dimethylaminoethyl methacrylate and dimethylaminoethyl acrylate, few kinetic data are available (46–51); only Tanaka (37) measured the reactivity ratios.

In the present work, the copolymerization of acrylamide (AAM) with three cationic comonomers: DADMAC, dimethylaminoethyl methacrylate (DMAEM), and dimethylaminoethyl acrylate (DMAEA) (the latter two quaternized with methyl chloride) was investigated. The reactivity ratios were determined by using continuous solution polymerization with the error-invariables method, a technique that provides estimates of the joint confidence

regions. In the final part of this chapter, the kinetics of the inverse micro-suspension copolymerization of AAM–DMAEM will be discussed.

Experimental Details

Polymerizations. Polymerizations were performed in solution with a 0.5-L continuous stirred tank reactor; this apparatus provided polymers of constant composition. After steady-state operation was obtained (approximately three residence times, *see* Figure 1), 10-mL samples were periodically taken from the effluent, added to 200 μL of a hydroquinone solution, and stored at 10 °C. These samples were subsequently analyzed by HPLC to estimate the mean and variance of the residual monomer concentration and copolymer composition. The polymerization temperatures were 45 and 60 °C for the dimethylamines and 50 °C for DADMAC. The initial monomer concentration was 0.5 mol L^{-1}, and the monomer feed ratio was varied between 0.3 and 0.7. Azocyanovaleric acid (ACV, Wako Chemical Co.) and potassium persulfate (KPS, BDH Chemicals) were used to initiate the reaction. The solution was agitated at 300 ± 1 rpm for the duration of the polymerization.

Acrylamide (Cyanamid C.V.) was recrystallized once from chloroform (Caledon, reagent grade), washed with benzene (BDH, reagent grade), dried in vacuo, and stored over silica gel in a desiccator. For the kinetic studies, DMAEM was purified
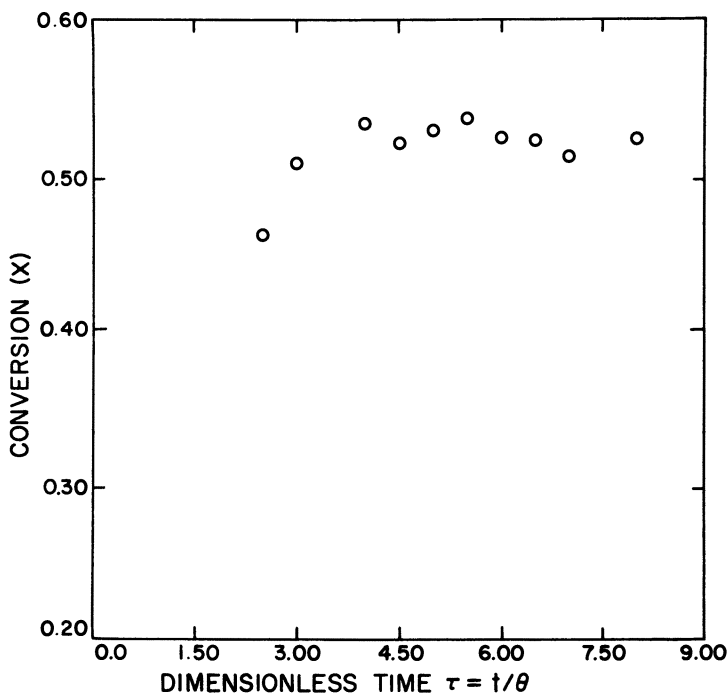
Figure 1. Dependence of conversion on dimensionless time (τ) for AAM–DMAEA. The monomer feed ratio was 1.7:1, and the residence time (θ) was 30 min.

by precipitation in acetone. This procedure reduced the concentration of inhibitor (hydroquinone monomethyl ether) from 600 ppm to below 0.5 ppm. The monomer was then stored as a solid in a desiccator until required.

Aqueous monomer solutions were prepared with distilled deionized water. Mild heating was required to overcome the negative heat of mixing. During this procedure, the temperature was maintained below 15 °C to avoid prepolymerization. Monomer solutions were subsequently purged with rarefied nitrogen until the dissolved oxygen concentration was below 1.5 ppm.

For inverse microsuspension* experiments, sorbitan monooleate (Alkaril Chemicals) was used as a stabilizer. The continuous phase was a narrow cut of isoparaffinic solvent (Isopar K, Esso Chemicals). The emulsifier dissolved rapidly in the dispersive medium, and the mixture was purged with nitrogen for 15–20 min. The initiator solution was prepared by dissolving azobisisobutyronitrile (AIBN, Kodak), once recrystallized from methanol (BDH, reagent grade) in 15 g of acetone (BDH, reagent grade). Polymerizations were carried out in a 1-gal (4.54-L) stainless steel batch reactor agitated at 323 ± 1 rpm. Equal masses of aqueous and organic phases (1000 g) were used, corresponding to a phase ratio of 0.74:1. The emulsifier and monomer concentrations were 10 wt % of the organic phase and 50 wt % of the aqueous phase, respectively. The initial mole fraction of quaternary ammonium monomer was 0.125. Polymerizations were performed isothermally at temperatures between 40 and 60 °C.

Analytical Methods.   Historically, the copolymer composition of cationic acrylic polymers has been measured by conductiometric (28), silver nitrate (29), or colloid titration (52, 53). Chromatographic methods have been reported for acrylamide monomer (54–56); however, no such methods have been employed for quaternary ammonium monomers. In this chapter, a new HPLC method (Nalco) is described for the simultaneous determination of both comonomers. Colloid titration is described in the next paragraph and was used only for comparison purposes.

Potassium poly(vinyl alcohol) sulfate (PVSK) was standardized against 2.5 × 10^{-3} N cetylpyridinium chloride monohydrate. A 1-mL aliquot of a 200–600-ppm copolymer solution was combined with 1 drop of toluidine blue indicator and agitated with a magnetic stirrer. PVSK was added dropwise until the endpoint was reached. Each titration was repeated a minimum of four times.

HPLC measurements were performed on a Waters radial-compression system with a CN column (particle size: 5 μm, cartridge: 8-mm i.d.). The HPLC apparatus consisted of an ERC-3110 degasser (Erma Optical Works), a Waters U6K injection system, a filter and a precolumn (CN), and a Beckman 160 UV detector with a zinc lamp at a wavelength of 214 nm. The liquid phase was a mixture of 50 vol % acetonitrile and 50 vol % water that contained 0.005 M dibutylamine phosphate. The flow rate was 2.0 mL min^{-1}.

Each sample (100 μL) was injected into the HPLC apparatus, and four replications were performed. Residual monomer concentrations were determined from a regressed calibration curve that was obtained from standard samples prepared with recrystallized and dried monomer over the range 0–100 ppm. All samples from a given experiment were analyzed within 10 h.

For the HPLC measurements, samples were diluted in double-distilled deionized water to provide residual monomer concentrations between 10 and 100 ppm.

* Inverse microsuspension is a commercial process for the production of high molecular weight, water-soluble polymers. Monomers are dispersed in a continuous organic phase, usually paraffinic, and sterically stabilized. Polymerization can be initiated with an oil- or water-soluble initiator.

The pH was adjusted to 3.0. The polymer in the sample was separated by high-speed centrifugation (20 min at 11,000 g with a Sorvall RC5B Superspeed centrifuge). Remaining polymer was kept back by a guard column that was changed every 100 injections. The injection volume was 100 μL. Every sample was measured three to five times. Figure 2 is an example of a typical chromatogram of AAM and DMAEM. There was good separation, and the signal areas could be quantitatively measured within 1% error limits.

^{13}C NMR spectra were recorded for an 8.06 wt % D$_2$O solution at 62.89 MHz and ambient temperature on a Bruker WM 250 spectrometer operating at 5.87 T in the pulsed Fourier transform mode with inverse-gated decoupling. The ^{13}C pulse width and acquisition time were 30.5 ms and 0.442 s, respectively. Each spectrum contained 16,000 data points over a frequency of 18,518 Hz with about 2000 acquisitions.
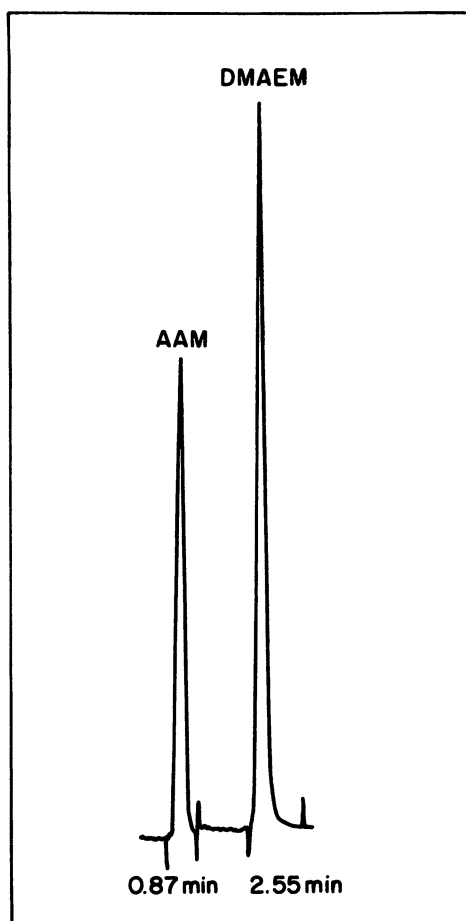
Figure 2. Example of HPLC chromatogram for AAM–DMAEM. The peaks correspond to a concentration of 47.5 ppm of AAM and 90.1 ppm of DMAEM, respectively.

Results and Discussion

The error-in-variables method was used to estimate the reactivity ratios. This method was developed by Reilly et al. (57, 58), and it was first applied for the determination of reactivity ratios by O'Driscoll, Reilly, and co-workers (59, 60). In this work, a modified version by MacGregor and Sutton (61) adapted by Gloor (62) for a continuous stirred tank reactor was used. The error-in-variables method shows two important advantages compared to the other common methods for the determination of copolymer reactivity ratios, which are statistically incorrect, as for example, Fineman–Ross (63) or Kelen–Tüdös (64). First, it accounts for the errors in both dependent and independent variables; the other estimation methods assume the measured values of monomer concentration and copolymer composition have no variance. Second, it computes the joint confidence region for the reactivity ratios, the area of which is proportional to the total estimation error.

The use of a continuous stirred tank reactor permits one to apply the instantaneous copolymer equation for reactivity ratios estimation.

$$F_1 = \frac{r_1 f_1^2 + f_1(1 - f_1)}{(r_1 + r_2 - 2)f_1^2 + 2(1 - r_2)f_1 + r_2} \tag{1a}$$

where

$$f_1 = \frac{[M_1]}{[M_1] + [M_2]} \tag{1b}$$

and

$$F_1 = \frac{m_1}{m_1 + m_2} \tag{1c}$$

where r_1 and r_2 are the reactivity ratios, M_1 and M_2 are the monomer concentrations at the outlet of the reactor, and m_1 and m_2 are the monomer bound in the copolymer. In this chapter, the index 1 refers always to the AAM and the index 2 to the cationic monomer. Equation 1 may be written as

$$\text{residual } (R) = \frac{r_1 f_1^2 + f_1(1 - f_1)}{(r_1 + r_2 - 2)f_1^2 + 2(1 - r_2)f_1 + r_2} - F_1 \tag{2}$$

and the residual for each observation of a series can be determined. Afterwards, r_1 and r_2 are estimated in a nonlinear regression, in which the sum of the squared residuals weighted in relation to the variance is minimized by using Marquardt's procedure. The variance of the residuals can be de-

termined by summing the products of the partial differential of the residuals for each variable and the variances of the variables.

$$V_R = \left(\frac{\partial R}{\partial [M_1]}\right)^2 V_{M_1} + \left(\frac{\partial R}{\partial [M_2]}\right)^2 V_{M_2} + \left(\frac{\partial R}{\partial [F_1]}\right)^2 V_{F_1} \tag{3}$$

V represents the variance, and R represents the residual of equation 2. The confidence region can be determined by plotting the sum-of-squares contour for several r_1 and r_2 values that satisfy the instantaneous copolymer equation for the variables given.

Reactivity Ratios in Solution Polymerization

Table I lists the monomer concentrations and their variances experimentally determined by HPLC as well as the mole fractions of AAM in the copolymer and its variances for the copolymerization of AAM with DMAEM at 60 °C using ACV and KPS as initiators. The reactivity ratios and their confidence regions were calculated from these data. The same calculations were performed for the copolymerization of DMAEA and DADMAC. The results are listed in Table II. Figures 3–5 show the 95% confidence regions of these reactivity ratios. The 95% confidence regions for the copolymerization of AAM and DMAEM with ACV and KPS overlap extensively, and the reactivity ratios determined with the two initiators are not significantly different. A slight difference can be explained in that KPS is charged, and, therefore, interactions with the cationic monomer are possible. The temperature variation causes only slight changes in the reactivity ratios, as expected. Figures 6–8 show plots of the instantaneous copolymer composition equation for the reactivity ratios determined for these three systems. An azeotropic point is only observed for the system AAM–DMAEA.

The results for AAM–DADMAC were in good agreement with those of Wandrey and Jaeger (Table III). According to the results obtained by these authors for various monomer concentrations and those obtained for a monomer concentration of 0.5 mol L^{-1} in this work, the reactivity ratios of both monomers decrease slightly with decreasing monomer concentration.

The accuracy of the reactivity ratios determined by HPLC and colloid titration are compared in Figure 9. The errors involved in colloid titration are several orders of magnitude larger than for HPLC. Furthermore, the individual 95% confidence intervals from colloid titration surround the origin, which implies that inferences based on such data are arbitrary and insignificant. Therefore, reactivity ratios that have been estimated from colloid titration must be regarded with extreme skepticism. We recommend using the reactivity ratios determined by the error-in-variables high-performance liquid chromatographic (EVM HPLC) method.

Table I. Residual Monomer Concentrations and Mole Fraction of AAM
in the Polymer for the Copolymerization of AAM and DMAEM with KPS
and ACV at 60 °C in Solution at Various Feed Ratios

Initiator[a]	Sample Number	[M₁] (AAM) (mol/L)	V_{M_1}	[M₂] (DMAEM) (mol/L)	V_{M_2}	F_1	V_{F_1}
KPS	II-mono	0.384	0.0010	0.116	0.00010	—	—
	II-7	0.286	0.0006	0.070	0.00001	0.680	0.0012
	II-8	0.291	0.0008	0.071	0.00001	0.675	0.0016
	II-10	0.270	0.0005	0.065	0.00002	0.691	0.0010
	II-11	0.286	0.0005	0.069	0.00002	0.676	0.0010
KPS	III-mono	0.272	0.0008	0.228	0.00004	—	—
	III-8	0.211	0.0005	0.141	0.00002	0.412	0.0016
	III-9	0.191	0.0006	0.124	0.00002	0.438	0.0016
	III-11	0.204	0.0006	0.132	0.00002	0.415	0.0016
	III-12	0.191	0.0005	0.125	0.00002	0.440	0.0016
KPS	IV-mono	0.166	0.0005	0.334	0.00003	—	—
	IV-7	0.108	0.0005	0.147	0.00002	0.238	0.0010
	IV-9	0.106	0.0006	0.146	0.00001	0.242	0.0012
	IV-11	0.106	0.0005	0.146	0.00002	0.242	0.0010
	IV-12	0.107	0.0004	0.149	0.00002	0.243	0.0010
ACV	I-mono	0.384	0.0010	0.116	0.00001	—	—
	I-7	0.236	0.0005	0.054	0.00002	0.703	0.0010
	I-9	0.240	0.0006	0.055	0.00001	0.702	0.0012
	II-10	0.246	0.0006	0.057	0.00001	0.701	0.0012
	II-11	0.249	0.0006	0.056	0.00001	0.693	0.0012
ACV	V-mono	0.268	0.0005	0.232	0.00005	—	—
	V-9	0.177	0.0007	0.107	0.00002	0.420	0.0014
	V-11	0.202	0.0005	0.123	0.00001	0.376	0.0010
	V-12	0.193	0.0005	0.115	0.00002	0.392	0.0010
	V-13	0.173	0.0004	0.105	0.00003	0.429	0.0010
ACV	VI-mono	0.182	0.0007	0.318	0.00002	—	—
	VI-7	0.127	0.0004	0.164	0.00001	0.262	0.0014
	VI-8	0.122	0.0003	0.159	0.00002	0.275	0.0014
	VI-10	0.130	0.0003	0.172	0.00001	0.262	0.0014
	VI-11	0.135	0.0003	0.178	0.00001	0.250	0.0014

[a]ACV, azocyanovaleric acid; KPS, potassium persulfate.

Table II. Reactivity Ratios of the Polymerization of Acrylamide with Different
Cationic Monomers at Various Conditions

Monomer System	r_1 (AAM)	r_2 (cationic)	Initiator[a]	Temp. (°C)
AAM/DMAEM[b]	0.49 ± 0.15	2.46 ± 0.40	ACV	60
AAM/DMAEM	0.61 ± 0.07	2.52 ± 0.19	KPS	60
AAM/DMAEM[b]	0.43 ± 0.18	2.39 ± 0.38	ACV	45
AAM/DMAEA[c]	0.29 ± 0.07	0.34 ± 0.09	ACV	60
AAM/DMAEA[c]	0.33 ± 0.09	0.40 ± 0.11	ACV	45
AAM/DADMAC	6.4 ± 0.4	0.06 ± 0.03	ACV	50

[a]ACV, azocyanovaleric acid; KPS, potassium persulfate.
[b]$r_1 = 7.823 \exp(-923/T)$, $r_2 = 4.538 \exp(-204/T)$.
[c]$r_1 = 1.871 \times 10^{-2} \exp(913/T)$, $r_2 = 1.083 \times 10^{-2} \exp(1148/T)$.
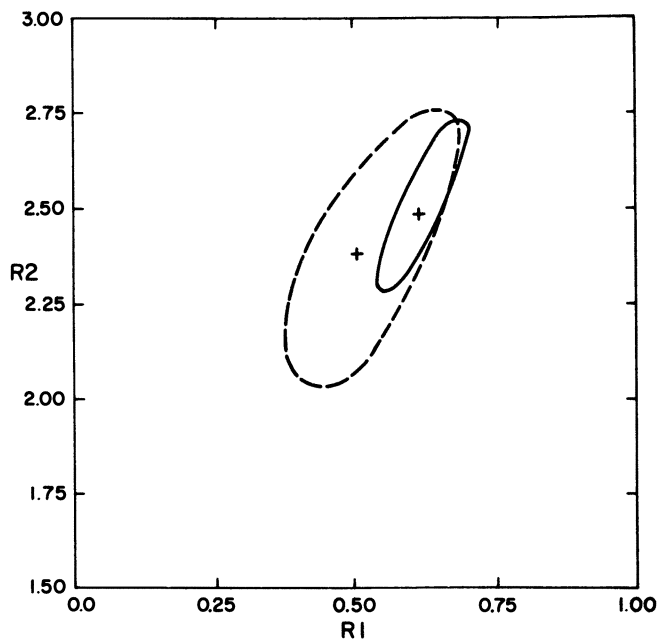
Figure 3. Joint confidence regions for the reactivity ratios in AAM–DMAEM at 60 °C. Key: —, KPS initiator; - - -, ACV initiator.
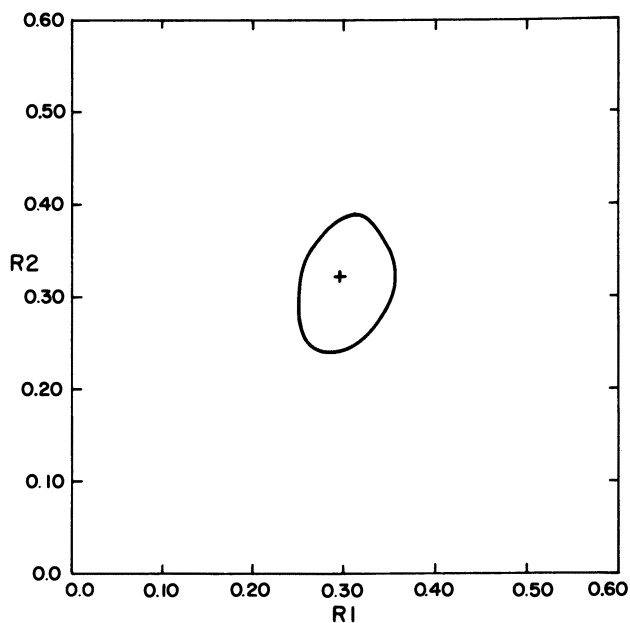
Figure 4. Joint confidence region for the reactivity ratios in AAM–DMAEA at 60 °C with ACV as the initiator.
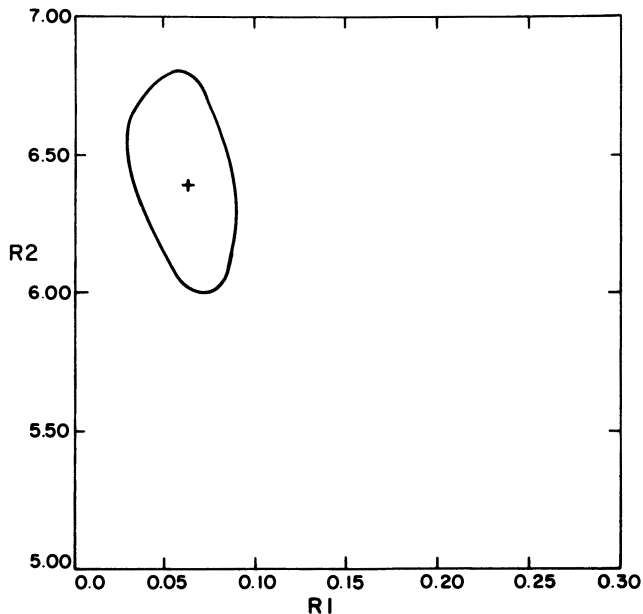
Figure 5. Joint confidence region for the reactivity ratios in AAM–DADMAC at 50 °C with ACV as the initiator.
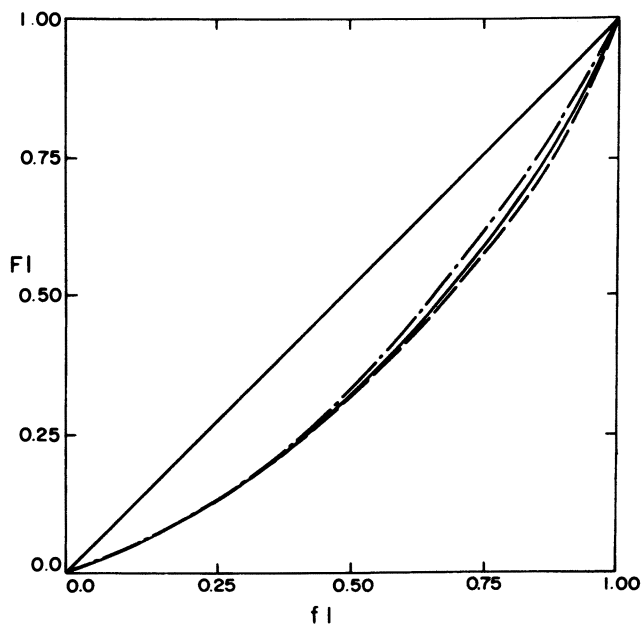
Figure 6. Copolymer composition diagram for AAM–DMAEM. Key: —, 60 °C with ACV; - · - · , 60 °C with KPS; - - -, 45 °C with ACV.
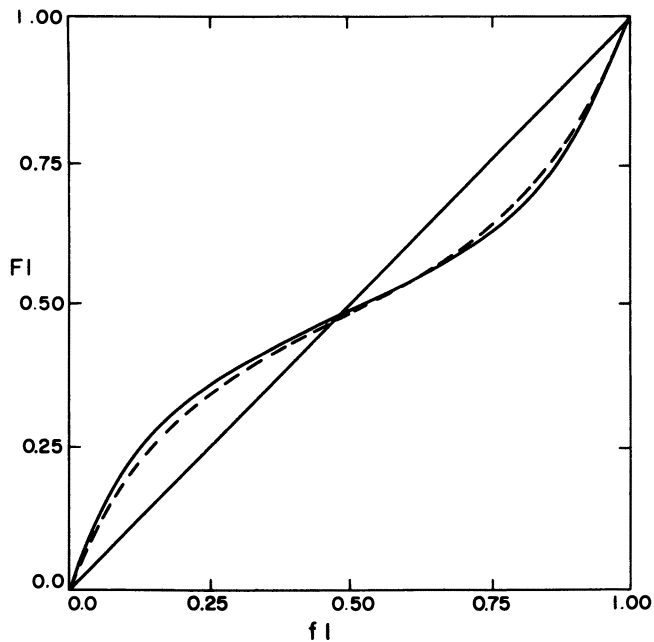
*Figure 7. Copolymer composition diagram for AAM–DMAEA. Key: —, 60 °C;
- - -, 45 °C.*
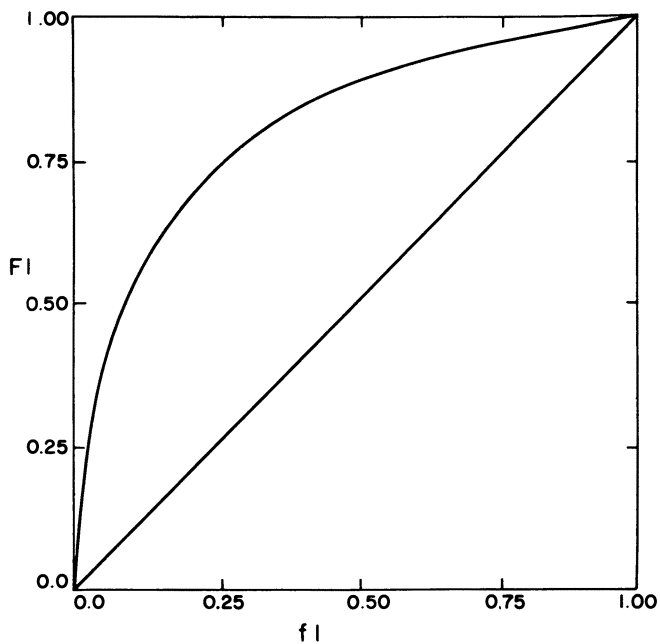
Figure 8. Copolymer composition diagram for AAM–DADMAC at 50 °C.

Table III. Comparison of the Reactivity Ratios Determined by Different Authors for the Copolymerization of Acrylamide with Diallyldimethylammonium Chloride

r_1	r_2	Monomer Concentration (mol/L)	Temp. (°C)	Range of Feed Ratios (f_1)	Author
6.4 ± 0.4	0.06 ± 0.03	0.5	50	0.3 → 0.7	this work
6.7	0.58	1.5	20	0.1 → 0.9	Tanaka (37)
6.62[a]	0.074[a]	3.0	35	0.11 → 0.89	Wandrey and Jaeger (28)
7.14[a]	0.22[a]	4.0	35	0.2 → 0.72	Wandrey and Jaeger (28)
7.54[b]	0.049[b]	5.75	47	0.2 → 0.8	Huang et al. (33)

[a]These are average values; r_1 and r_2 were observed to depend on the feed ratio.
[b]Determined in inverse emulsion polymerization.
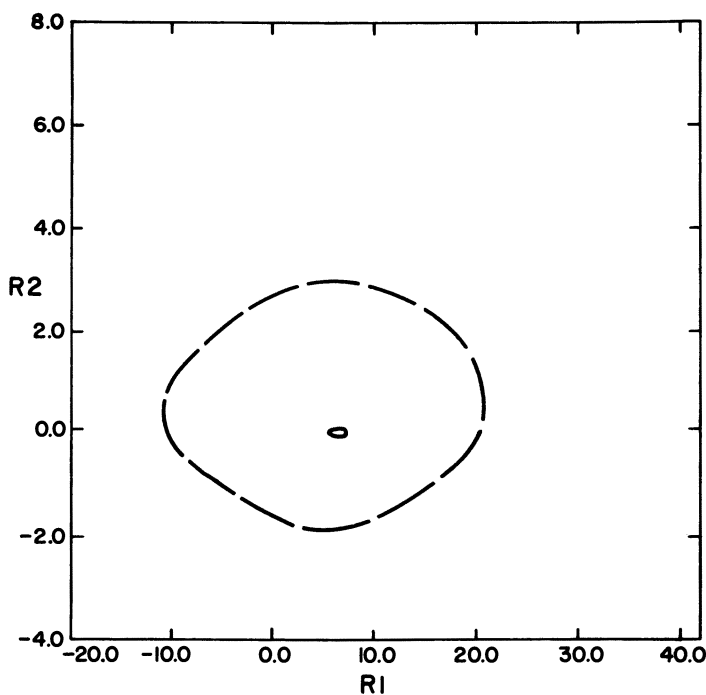
Figure 9. Comparison of the joint confidence regions obtained by HPLC (—) and colloid titration (- - -) for AAM–DADMAC at 50 °C.

^{13}C NMR measurements confirmed that five-member rings were formed in the copolymerization of DADMAC and AAM. A typical NMR spectrum is shown in Figure 10. The assignments agree with those made by Lancaster for DADMAC homopolymers (24). Also, the compositions obtained by HPLC and NMR agreed reasonably well. However, the time required for an NMR analysis is about 20 h, so it is obviously not suitable for routine measurement of a series of samples. One HPLC measurement takes, by
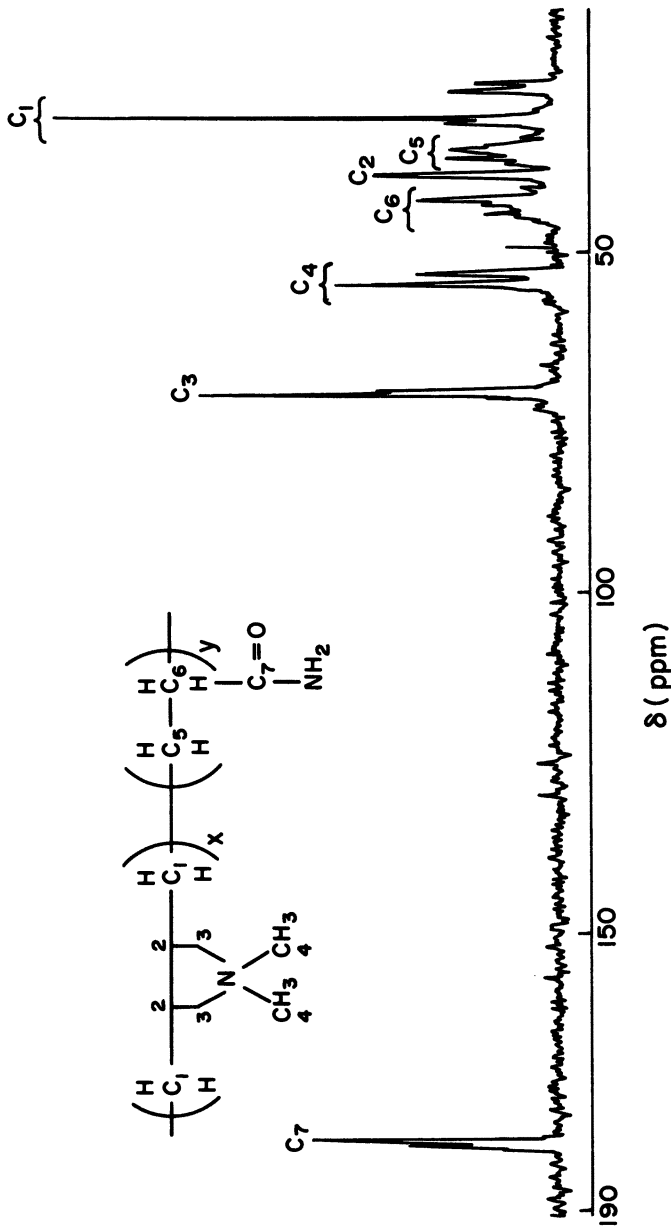
Figure 10. ^{13}C NMR spectrum of an AAM–DADMAC copolymer with peak assignments. $F_1 = 0.680$ by HPLC and 0.639 by NMR.

comparison, only about 3 or 4 min. The determination of the sequence length distribution may be possible by ^{13}C NMR, as has already been described for other systems in the literature (65). Further investigations are necessary to confirm this for these cationic copolymers.

Polymerization in Inverse Microsuspension

Figures 11 and 12 show experimental data for copolymerizations of acrylamide with DMAEM at 60 and 50 °C. The solid line is the kinetic model for inverse microsuspension polymerization in isoparaffinic solvents stabilized with fatty acid esters of sorbitan. This model was derived for acrylamide homopolymers (66) and has been extended to include copolymerizations with cationic monomers. Good agreement with the data can be observed. The details of the mechanism will be discussed in a subsequent publication (67).

Figure 13 shows the compositional drift for a polymerization of acrylamide with DMAEM at 50 °C. The quaternary ammonium monomer is consumed much faster than the acrylamide. Included in the figure is the predicted copolymer composition based on the reactivity ratios described in the second part of this chapter. With one exception, all the data are contained within the 95% confidence limits. We can, therefore, conclude
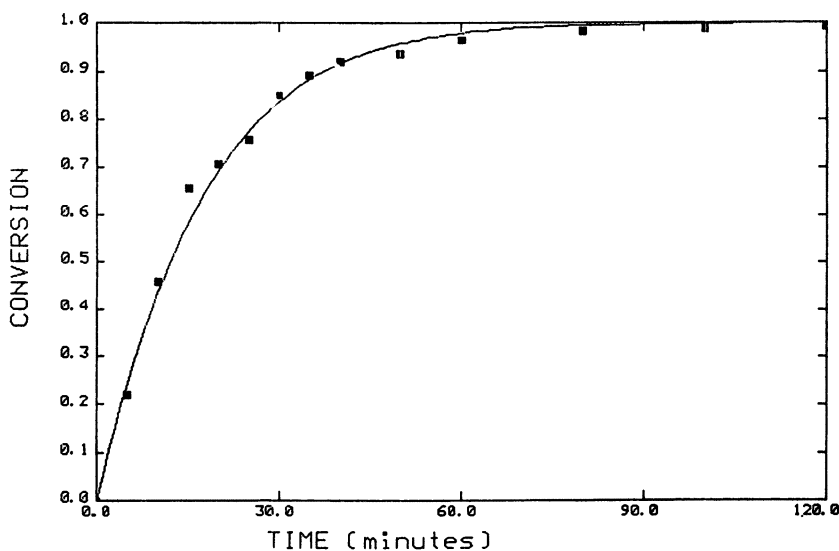
Figure 11. Conversion vs. time data of an inverse microsuspension polymerization of acrylamide and DMAEM at 60 °C and 50 wt % total monomer concentration ($f_{10} = 0.875$). The phase ratio of water to oil was 0.74:1, with 10 wt % sorbitan monooleate (based on the organic phase). Polymerization was initiated with 3.329×10^{-3} mol L^{-1} AIBN. The solid line is the model prediction.
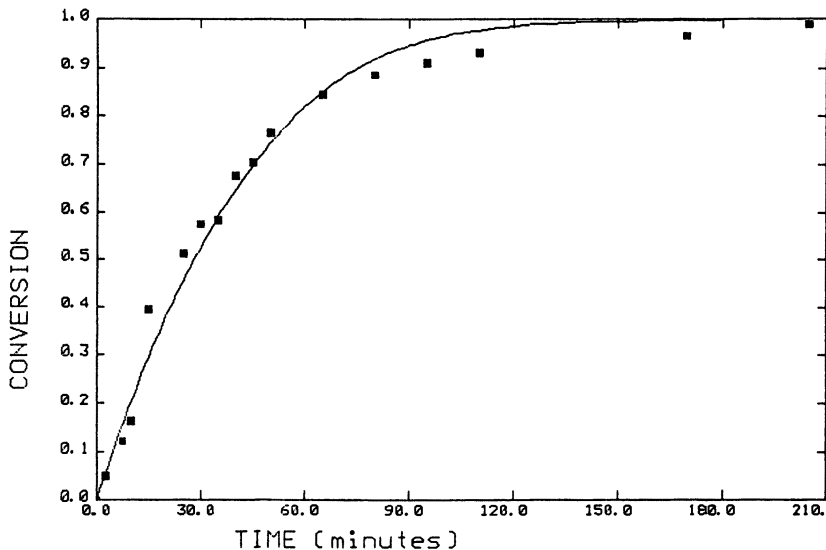
Figure 12. Conversion vs. time data of an inverse microsuspension polymerization of acrylamide and DMAEM at 50 °C and 50 wt % total monomer concentration (f_{10} = 0.875). The phase ratio of water to oil was 0.74:1, with 10 wt % sorbitan monooleate (based on the organic phase). Polymerization was initiated with 7.373 × 10^{-3} mol L^{-1} AIBN. The solid line is the model prediction.
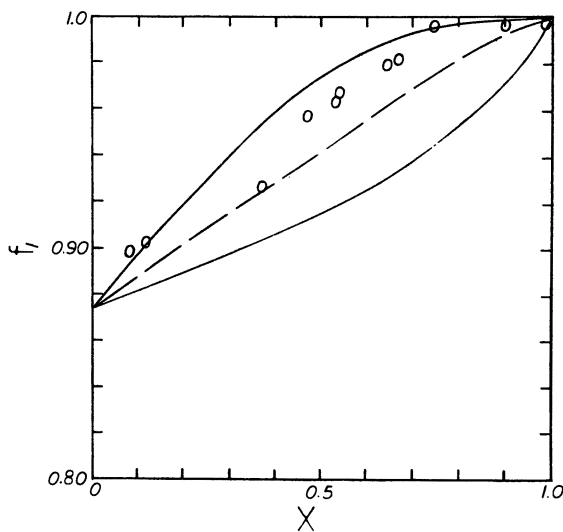
Figure 13. Experimental monomer composition (○) for an AAM–DMAEM inverse microsuspension copolymerization at 50 °C. The reaction conditions are the same as in Figure 12. The dashed line is the predicted compositional drift based on the reactivity ratios measured in solution polymerization. The solid lines are the 95% confidence limits.

that the reactivity ratios in solution and inverse microsuspension do not differ significantly.

The severity of the compositional inhomogeneity, even at very low conversions, renders molecular weight measurement methods invalid on these samples. Additional experiments will be required at the azeotropic composition (for DMAEA) or in a continuous reactor.

Acknowledgments

References

1. *Chemical Economics Handbook*; Stanford Research Institute: Menlo Park, CA, 1983; pp 581–1011I, 581–5022L, 581–1012D.
2. Anderson, R.; Bell, G. R. U.S. Patent 3 235 495, 1966.
3. Bailey, F. E., Jr.; LaCombe, E. M. U.S. Patent 3 214 370, 1965.
4. Bell, G. R. U.S. Patent 3 227 650, 1966.
5. Eldred, N. R.; Buttrick, G. W.; Spicer, J. C. U.S. Patent 3 207 656, 1965.
6. LaCombe, E. M. U.S. Patent 3 238 276, 1966.
7. Smith, K. L. U.S. Patent 3 332 835, 1967.
8. Sopoci, J. U.S. Patent 3 247 106, 1966.
9. Hoffmann, A. W. *Liebigs Ann. Chem.* 1861, *145* (Suppl. 1), 275.
10. Pellon, J. J.; Valan, K. *J. Chem. Ind. (London)* 1963, *32*, 2358.
11. Rabinowitz, R.; Marcis, R.; Pellon, J. *J. Polym. Sci. Part A* 1964, *2*, 1233.
12. Tsetlin, B. L.; Medved, T. Ya.; Chiksev, Yu. G.; Polikarpov, Ya. M.; Rafikov, S. P.; Kabachnik, M. I. *Vysokomol. Soedin.* 1961, *3*, 1117.
13. Butler, G. B.; Bunch, R. *J. Am. Chem. Soc.* 1949, *71*, 320.
14. Butler, G. B.; Ingley, F. L. *J. Am. Chem. Soc.* 1951, *73*, 895.
15. Butler, G. B. U.S. Patent 3 288 770, 1966.
16. Butler, G. B.; Angelo, R. J. *J. Am. Chem. Soc.* 1957, *79*, 3128.
17. Berlin, D.; Butler, G. B. *J. Am. Chem. Soc.* 1960, *82*, 2712.
18. Butler, G. B.; Crawshaw, A.; Miller, W. L. *J. Am. Chem. Soc.* 1958, *80*, 3615.
19. Crawshaw, A.; Jones, A. G. *J. Macromol. Sci., Chem.* 1972, *A6*, 65.
20. Simpson, W.; Holt, T.; Zetie, J. *J. Polym. Sci.* 1953, *10*, 489.
21. Brace, N. O. *J. Org. Chem.* 1966, *31*, 2879.
22. Brace, N. O. *J. Am. Chem. Soc.* 1964, *86*, 523.
23. Johns, S. R.; Willing, R. I.; Middleton, S.; Ong, A. K. *J. Macromol. Sci., Chem.* 1976, *A10*, 875.
24. Lancaster, J.; Baccei, L.; Panzer, H. *J. Polym. Sci., Polym. Lett. Ed.* 1976, *14*, 549.

25. Ottenbrite, R. M.; Shillady, D. D. In *Polymeric Amines and Ammonium Salts*; Goethals, E. J., Ed.; Pergamon: Oxford, England, 1980; p 143.
26. Easterly, J. P. European Patent 0 107 226, 1984.
27. Boothe, J. E.; Hoover, M. F.; Flock, H. G. *J. Macromol. Sci., Chem.* **1970,** *A4,* 1419.
28. Wandrey, Ch.; Jaeger, W. *Acta Polym.* **1985,** *36,* 100.
29. Jaeger, W.; Hahn, M.; Reinisch, G.; Seehaus, F. *J. Macromol. Sci., Chem.* **1984,** *A21,* 593.
30. Martynenko, A. I.; Wandrey, Ch.; Jaeger, W.; Hahn, M.; Topchiev, D. A.; Reinisch, G.; Kabanov, V. A. *Acta Polym.* **1985,** *36,* 547.
31. Klenina, O. V.; Fomina, V. A.; Klenin, V. I.; Avetisyan, P. K.; Medvedev, G. P.; Klenin, S. I.; Bylova, Ye. N.; Milovskaya, Ye. B. *Polym. Sci. USSR (Engl. Transl.)* **1984,** *26,* 296.
32. Ottenbrite, R. M.; Ryan, W. S., Jr. *Ind. Eng. Chem. Prod. Res. Dev.* **1980,** *19,* 528.
33. Huang, P. C.; Singh, P.; Reichert, K.-H. In *Polymer Reactor Engineering*; Rechert, K.-H.; Gressler, W., Eds.; Hüthig and Wepf Verlag: New York, 1986; p 125.
34. Schuller, W. H.; Price, J. A.; Moore, S. T.; Thomas, W. M. *J. Chem. Eng. Data* **1959,** *4,* 273.
35. Singh, P. DFG Report 223/13-1, Institut für Technische Chemie der Technischen Universität Berlin.
36. Singh, U. C.; Manickam, S. P.; Venkatarao, K. *Makromol. Chem.* **1979,** *180,* 589.
37. Tanaka, H. *J. Polym. Sci., Polym. Chem. Ed.* **1986,** *25,* 29.
38. Black, A. P.; Birkner, F. B.; Morgan, J. J. *J. Am. Water Works Assoc.* **1965,** *57,* 1547.
39. Black, A. P.; Birkner, F. B.; Morgan, J. J. *J. Colloid Interface Sci.* **1966,** *21,* 626.
40. Dajani, M. T. U.S. Patent 3 409 547, 1968.
41. Dajani, M. T.; Cocks, T. G. U.S. Patent 3 408 292, 1968.
42. Jones, R. H. Ph.D. Thesis, Univerity of Florida, 1966.
43. Kleber, J. P. *Water Wastes Eng.* **1969,** *6,* 42.
44. Pressman, M. *J. Am. Water Works Assoc.* **1967,** *59,* 169.
45. Posselt, H. S.; Reidies, A. H.; Weber, W. H., Jr. *J. Am. Water Works Assoc.* **1968,** *60,* 48.
46. Fordyce, D. B.; Glavis, F. J.; Malamed, S. U.S. Patent 3 023 162, 1962.
47. Grey, R. H.; Webers, V. J. U.S. Patent 2 892 822, 1959.
48. Grey, R. H.; Webers, V. J. U.S. Patent 2 839 401, 1959.
49. Gruntfest, I. J.; Fordyce, D. B. U.S. Patent 2 838 397, 1958.
50. Pradny, M.; Sevcik, S. *Makromol. Chem.* **1987,** *188,* 227.
51. Nagai, K.; Ohishi, Y. *J. Polym. Sci., Polym. Chem. Ed.* **1987,** *25,* 1.
52. Ueno, K.; Kina, K. *J. Chem. Ed.* **1985,** *62,* 627.
53. Schempp, W.; Tran, H. T. *Wochenbl. Papierfabr.* **1981,** *109,* 726.
54. Husser, E. R.; Stehl, R. H.; Price, D. R.; DeLap, R. A. *Anal. Chem.* **1977,** *49,* 155.
55. Ludwig, F. J., Sr.; Besand, M. F. *Anal. Chem.* **1978,** *50,* 185.
56. Onuoha, N. J.; Chaplain, R. P.; Wainwright, M. S. *Chromatographia* **1979,** *12,* 709.
57. Reilly, P. M.; Blau, G. E. *Can. J. Chem. Eng.* **1974,** *52,* 289.
58. Reilly, P. M.; Patino-Leal, H. *Technometrics* **1981,** *23,* 221.
59. Laurier, G. C.; O'Driscoll, K. F.; Reilly, P. M. *J. Polym. Sci., Polym. Symp.* **1985,** *72,* 17.

60. Patino-Leal, H.; Reilly, P. M.; O'Driscoll, K. F. *J. Polym. Sci., Polym. Lett. Ed.* **1980**, *18*, 219.
61. Sutton, T. L.; MacGregor, J. F. *Can. J. Chem. Eng.* **1977**, *55*, 602 and 609.
62. Gloor, P. Estimation of Reactivity Ratios Using the Error-in-Variables Method and Data Collected from a Continuous Stirred Tank Reactor, MIPPT-Report, McMaster University, Hamilton, Ontario, Canada, 1987.
63. Fineman, M.; Ross, S. D. *J. Polym. Sci.* **1950**, *5*, 259.
64. Kelen, T.; Tüdös, F. *J. Macromol. Sci., Chem.* **1975**, *A9*, 1.
65. Brar, A. S.; Saini, A. K. *J. Appl. Polym. Sci.* **1986**, *32*, 4607.
66. Hunkeler, D.; Hamielec, A. E.; Baade, W. *Polymer* **1989**, *30*, 127.
67. Hunkeler, D.; Hamielec, A. E., submitted for publication in *Polymer*.

Extensional Flow Behavior of Macromolecules in Solution

J. A. Odell, A. Keller, and A. J. Müller

H. H. Wills Physics Laboratory, University of Bristol, Bristol BS8 1TL, England

Studies of macromolecular solutions in idealized flow fields provide fundamental information concerning the rheological behavior of solutions in real flow situations. The most fundamental behavior in stagnation point flows of dilute solutions is the coil–stretch transition, and this transition is clearly associated with significant increases in the elongational viscosity, as anticipated by a number of theories. At higher concentrations, the important role of macromolecular interactions becomes clear. Such interactions occur at far lower concentrations in flow than is generally realized. We propose the interpretation of the semidilute solution behavior in terms of transient networks. We show that such networks are responsible for the extreme dilatant behavior of solutions in idealized extensional flow fields. Further, we suggest that many anomalous non-Newtonian effects reported previously in pore flow are analogous to this phenomenon and are best explained in terms of transient networks. In monodisperse solutions we investigate the extensional viscosity as a function of concentration and molecular weight; we identify the overlap concentrations and its molecular weight dependence. Such transient network behavior is always associated with molecular degradation. We investigate the dependence of degradation rate upon concentration and polydispersity.

Extending Isolated Molecules

Principle. The behavior of an isolated molecule is best approached by dilute solutions (*1–5*). The molecule itself will generally be considered

as highly flexible and non-free draining. This approach is readily extendable to more rigid and permeable chains.

To extend a molecule by flow, the flow field has to be of extensional character, which means that the fluid must be persistently extending. The molecule contained by the fluid will follow this extension to the degree determined by its frictional interaction with the fluid. However, it will be able to do so only when the elongational strain rate $\dot{\epsilon}$ characterizing the flow exceeds a critical value $\dot{\epsilon}_c$ of the order of the reciprocal of the conformational relaxation time τ (where $\tau = f/K$, f and K being the friction coefficient and the entropic restoring force, respectively) of the coil. In this case the extensional influence of the flow, as transmitted by the friction, will overcome the entropic resistance of the coil, tending to retain its random conformation. Once this stage is reached and coil extension starts, the coil will become increasingly more permeable to the fluid; hence the frictional interaction and the extensional forces will increase. In consequence, the extension becomes a run-away process until it is halted by the increasing restoring forces. Halting will occur only very close to full chain extension; hence, for all practical considerations, virtually full chain extension should be achievable (6). It follows, as indeed predicted by preceding theory (7, 8), that chain extension is critical in strain rate ($\dot{\epsilon}$); below $\dot{\epsilon}_c$ the coil remains virtually unextended, but above it, the coil extends practically fully. This critical coil–stretch transition is defined by

$$\dot{\epsilon}_c\tau \approx 1 \tag{1}$$

In view of the fact that, for a usual long flexible polymer τ is on the order of milliseconds, the required $\dot{\epsilon}$ needs to exceed 10^3 s^{-1} for most systems used in practice.

However, the attainment of $\dot{\epsilon} \geq \dot{\epsilon}_c$ is a necessity, yet not sufficient for full chain extension, because a further criterion, that of sufficient strain ($\dot{\epsilon}$), also needs to be satisfied. This criterion is rather demanding in view of the fact that, for a long molecule, the coil–stretch transition may require strains of $500\times$ or more. In experimental terms this requirement means that the molecule must have a long enough residence time within a flow field of $\dot{\epsilon} \geq \dot{\epsilon}_c$ for the required strains to be attained.

Method.   We succeeded in realizing this dual condition for full chain extension, namely sufficient strain rate and its maintenance for long enough time for a given fluid element to attain the required strain. In the process we also tested and verified the predictions inherent in eq 1. This verification was achieved experimentally by generating controlled elongational flow fields either through double suck jets creating uniaxial stretching flows, through a cross-slot device, or alternatively through a four-roll mill producing simple shear flows. The double jet case, most widely used, will be briefly described.

Figure 1a illustrates the principle involved, and Figure 4, the method of realization (to be discussed later). With suction applied, extensional flow between the jets is generated. Figure 1b shows the experimental flow field as visualized by light scattered at 90° from tracer particles. The chain extension, when it sets in, is then apparent through birefringence, which for dilute solutions is seen as a bright line against a dark background between
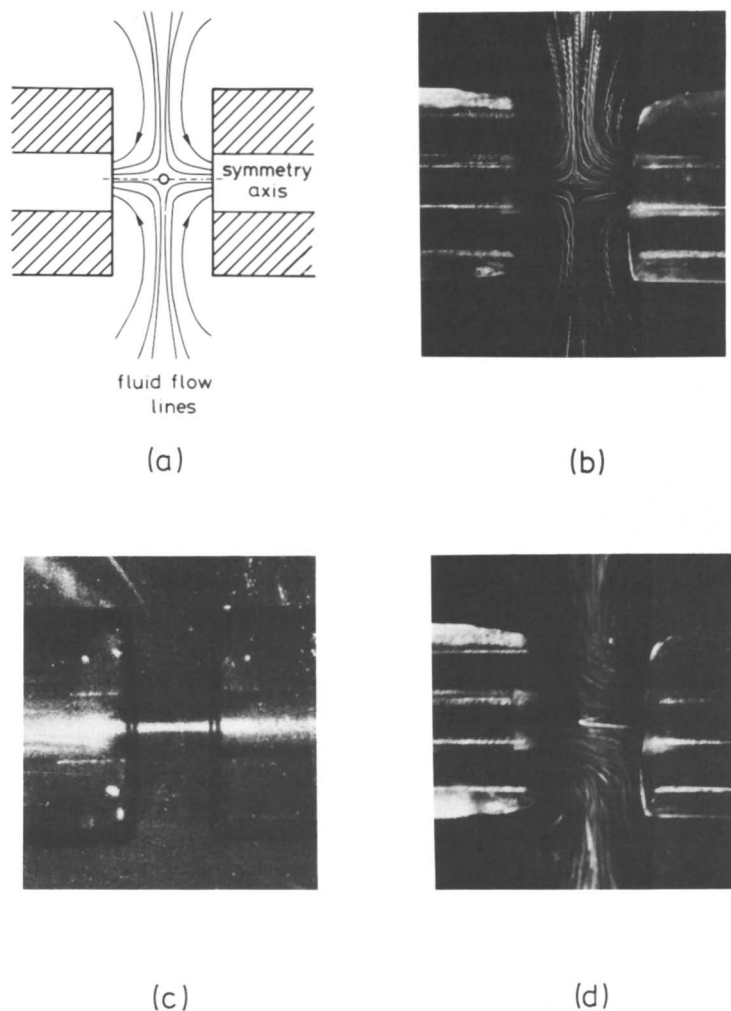
Figure 1. a, The opposed jets. The polymer solution is sucked into the jets along the symmetry axis. ○ represents the stagnation point in the center of the flow field. b, The flow field visualized by light scattered at 90° from tracer particles. c, A birefringent line between the jets for a 0.1% solution of atactic polystyrene (a-PS). d, The perturbed flow field during flare formation in a semidilute polyethylene oxide solution.

crossed polars (Figure 1c). The birefringence can be measured, or as is most usually done for continuous monitoring, the intensity (I) of transmitted light is recorded as a function of $\dot{\epsilon}$ (for low values the retardation is proportional to $I^{0.5}$).

The two requirements are readily achieved: the high strain rates through appropriate dimensions of the orifices and their separation, coupled with appropriate suction speeds, with due attention to staying within the laminar flow limits. The high strains themselves are automatically achieved because of the intrinsic nature of the flow field. Namely, the flow field contains a stagnation point (○ in Figure 1a), which means that fluid elements along streamlines passing through it will have, in principle at least, infinite residence time, hence will become correspondingly extended. This effect has the further important consequence that chain extension will be confined to those streamlines that pass through or close to the stagnation point. The result of this confinement is a high degree of localization of chain extension within the flow field, even when the strain rate itself would be sufficient for chain extension to occur over the whole volume between the jets. It follows that the localization defines the regions of adequate strain. The narrow birefringent line in Figure 1c (as compared to the full jet orifice) corresponds to this localization. The appreciation of this localization is paramount for what is to follow, where departures from the sharply defined localization will acquire special significance.

Establishment of Criticality. By using the methodology just outlined, the criticality inherent in eq 1, as predicted by theory, could be verified, as far as we know, for the first time. In view of the molecular weight dependence of τ (discussed later) this verification required ideally monodisperse material, which amongst readily available polymers is best approximated by anionically polymerized polystyrene, a material used in much that is to follow.

The birefringent line in Figure 1c indeed appeared suddenly as $\dot{\epsilon}$ was increased, and so did the birefringence in a corresponding trace (Figure 2). This finding verifies the criticality of chain extension and also provides a value for $\dot{\epsilon}_c$ and, through eq 1, for τ. This parameter proved to be most valuable for characterizing the isolated macromolecule. A few instances will be listed; further information can be found in ref. 5.

Relaxation Time as a Means of Molecular Characterization

Draining Characteristics of the Random Coil: Hysteresis. τ, determined as just described, was found to be close to expectations for the non-free-draining Zimm model, within any uncertainty arising from choice of input parameters. τ is a well-defined function of molecular weight M (discussed later), and for a given M of the viscosity η. In the dilute solutions
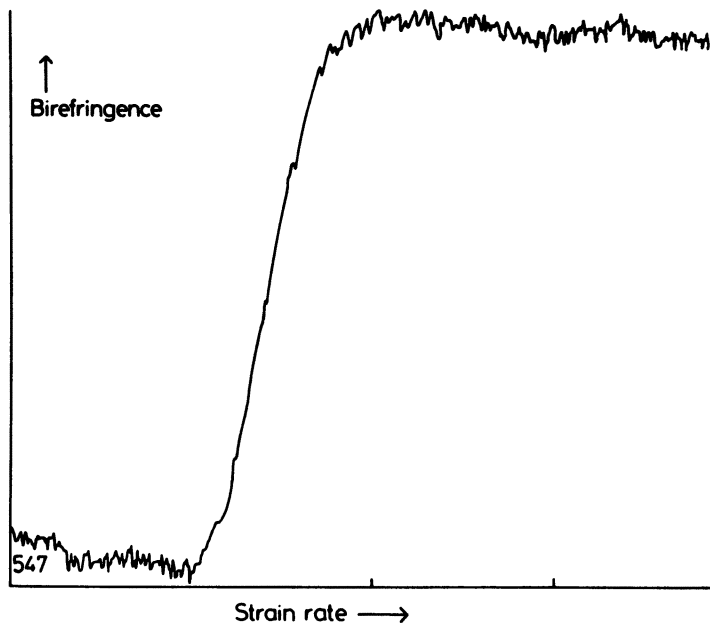
Figure 2. Experimentally determined flow-induced birefringence vs. strain rate for atactic polystyrene. The maximum value of birefringence is 1.15 × 10⁻⁵, which corresponds to an optical retardation of 27 nm for a cell depth of 1.8 mm (0.1% solution, $\overline{M}_w$ 5.5 × 10⁶ in decahydronaphthalene).

considered here η is that viscosity pertaining to the solvent in line with expectations from solution theory. This τ characterizes the response of the chain in its initial undeformed state, and is different from the relaxation time(s) corresponding to the extension process itself, and is significantly different from the relaxation time associated with the retraction from the extended state. Preliminary experiments indicate that the latter is very much longer, by 1–2 magnitudes. Such a hysteresis between extension and re-traction was predicted by de Gennes (8). In physical terms this longer time scale of the contraction is due to the increased frictional contact of the chain with the solvent when in its fully extended form, in which case it will approach that in a free-draining situation.

Molecular Weight Dependence and a Method for Molecular Weight Determination.   It is anticipated, even by qualitative consider-ations, that the longer molecules will be increasingly readily extendable, and more quantitatively, that (5)

$$\tau \propto \frac{\eta_s M^\alpha}{kT} \tag{2}$$

where η_s is the solvent viscosity, and α is a constant in the range of 1.5–2.0. The value of 1.5 is expected for the non-free-draining chain in the θ (or pseudo-ideal) state, and the larger values correspond to increasingly expanded and increasingly nonhydrodynamically screened, or more free-draining situations (5). In the rather limited number of cases where narrow molecular weight samples of sufficiently high molecular weight were available (discussed later) this molecular weight dependence could be tested.

The validity of the power law, eq 2, was established in all cases. For atactic polystyrene (a-PS) and polyethylene oxide (PEO) α was found to be 1.5, and rather remarkably, irrespective of solvent quality, in the few instances when the solvent was varied. A value of 1.7 for α has just been reported (9) for the good solvent bromobenzene (not used by us) from a different source. For the bacterial polysaccharide pullulan, which happened to be obtainable in comparatively sharp fractions, α was 1.8 in what is believed to be good solvent (10).

The actual α values, as obtained in this way, lead to many weighty questions relevant to solution theories, and findings with different solvents and materials and arising from different sources clearly require coordination. Given that a single α value exists for a polymer–solvent system, this value can be used for determining molecular weights, not only an average value, but the actual distribution. The situation for a single molecular weight is approximated by Figure 2. In case of a broad molecular weight spectrum, the I vs. $\dot{\epsilon}$ curve will be a superposition of a continuous spectrum of such curves, appropriately weighted and displaced along the $\dot{\epsilon}$ axis. Such a full curve, when expressed in terms of eq 2 with the appropriate α, in fact provides the cumulative molecular weight distribution itself, from which the actual differential molecular weight can be readily constructed.

We expect some instrumental broadening. The birefringent line broadens during the transition, thereby extending into regions further from the stagnation point, and with lower total fluid strain. Nevertheless, the derived molecular weight distribution curve is quite consistent for samples of known polydispersity, a condition suggesting, empirically, that broadening is not significant (11). If a curve, comparable to a GPC curve, is to be generated, then the log (mol wt) is generated from $2/3 \log \dot{\epsilon} + C$, where C is a constant derived by calibration against a known molecular weight. Mass per decade can be calculated from

$$\frac{dI}{d\dot{\epsilon}} \cdot \frac{d\dot{\epsilon}}{d(\log M)}$$

The inverse relation between $\dot{\epsilon}_c$ and M (from eqs 1 and 2) has two important consequences. First, this method of molecular weight determination will be most readily applicable to the longest molecules, that is, to those least accessible by conventional methods. Second, a cutoff for chain extension at

a low molecular weight limit will be determined by the maximum $\dot{\epsilon}$ that can be realized in a given experiment. Agreement between results of this technique and gel permeation chromatography (GPC) or light scattering is good (*11*).

Flow-Induced Chain Scission.

If the chains are overstretched, that is, $\dot{\epsilon}$ increases along the plateau in Figure 2, they will eventually break (*12*, *13*). The molecular weight of the fracture products can then be determined by the method just outlined. Thus, through our technique we can both break chains in a controlled manner and analyze the resulting fracture products within the same apparatus, this double capacity enabling a systematic study of the flow-induced chain fracture. The principal results, to be of consequence later, are as follows:

1. The chains break into two closely equal halves, hence accurately at their centers.

2. The critical fracture strain rate ($\dot{\epsilon}_f$) obeys the relation

$$\dot{\epsilon}_f \propto \frac{1}{M^2} \tag{3}$$

3. It follows from a combination of eqs 1 and 3 that there is a limiting upper M beyond which the chains cannot be stretched out, unavoidably breaking in the process. This conclusion has been confirmed experimentally (*13*).

These results can be simply interpreted by applying Stokes' law to a stretched-out string of beads; in fact the applicability of Stokes' law in this way is possibly the clearest evidence that the chains are indeed close to their stretched-out state. (Other evidence is given in refs. 5, 12, and 13.) The fracture stress itself can be calculated, and it was found to correspond to that of the breaking strength of a C–C backbone bond, within an order of magnitude. The fact that chain breakage is practically exactly (and not only statistically) central can be accounted for by considering the fracture as an activated process, where the exponential nature of the transition probability from the intact to the fractured state confines the probable fracture sites close to the stretched-out chain (*11*, *13*, *14*).

Recently there has been considerable controversy concerning the possibility of scission in the partially stretched state (*15*, *16*). One suggestion, on the basis of Ryskin's yo-yo model (*17*), is that scission could occur in transient flows. A theoretical treatment has predicted a different molecular weight dependence and a much higher absolute value for critical fracture strain rate; and it has predicted central scission less precisely. We have

recently unsuccessfully attempted to observe such scission in the opposed jets (11), and are left with the conclusion that scission occurs only for chains that are highly stretched.

Chain Stiffness—Polyelectrolytes. The extensibility of the chains is greatly affected by their stiffness: the stiffer the chain, the more readily it is extended. In the limit of a fully rigid rod there is no extension, only orientation. More explicitly, for stiffer chains both the strain rate and the strain required for full chain extension are lower. In terms of our experiment, this lower strain rate requirement means that $\dot{\epsilon}_c$ will be reduced as far as the extension remains critical in $\dot{\epsilon}$. However, with increasing chain stiffness, the criticality in $\dot{\epsilon}$, which is associated with entropic retraction within the chain itself, becomes less pronounced, until for a closely rigid rod system the chain (rod) alignment itself becomes a smooth function of strain rate determined by the orientability (the rotational diffusion coefficient D_r) of the rigid entity. The requirement of lower total strain has the additional consequence that there will be a lower degree of localization; that is, the birefringent line will become broader with increasing stiffness, because for a given $\dot{\epsilon}$, chain extension can be achieved for shorter residence times, hence along more peripherally situated streamlines. Therefore, our elongational-flow-based approach provides a new method for assessing chain stiffness or flexibility.

On the basis of these principles we have studied extensively the orientability of a rigid rod system (PBT, poly-*p*-phenylenebenzobisthiazole) in terms of rotational diffusion coefficients and the mutual interference ("entanglement") of the rods as the concentration is increased (18, 19). Similar studies are being conducted here also on biomolecules forming rigid or wormlike systems such as collagen (where denaturation can be followed) and xanthan gum.

Closer to the present subject of flexible molecules are our studies on the polyelectrolyte polystyrenesulfonate (PSS), where the flexibility (or rigidity) of the chains can be sensitively influenced by the ionic environment (20). For the stoichiometric PSS salt the chain is in a highly expanded conformation due to mutual repulsion of incompletely screened charged groups along the chain. Such an expanded chain collapses into what would characterize a flexible neutral molecule on addition of excess ions in the form of salts as a consequence of the more complete charge screening that results. In a previous work (20) these changes in flexibility–rigidity were followed in terms of eq 1, in the flexibility regime where criticality in $\dot{\epsilon}$ still pertains. Here, τ values, which were larger by 2–3 magnitudes than in the corresponding collapsed chain, could be observed in the most expanded salt-free system. The simultaneously occurring substantial delocalization (broadening of the line) has been analyzed in terms of the chain stiffness (6). Such environmentally influenced chain expansions are particularly relevant to the

issue of the onset of entanglements as will be referred to in the section on non-Newtonian behavior of polyacrylamide.

Extensional Viscosity

Polymer melts and solutions show pronounced non-Newtonian flow behavior. In rotational flows, polymer solutions typically show a shear-thinning behavior (*21, 22*) where the apparent viscosity reduces as the shear rate is increased. In extensional, or stretching flows, however, polymer solutions often show a marked increase in viscosity as the shear rate is increased, termed *dilatancy* (*23–26*). Stretching flows are of considerable importance and generally occur in flows through orifices, filters, porous media, constrictions in pipes, and in any flow possessing turbulence or vorticity, in fact as a component of most real flow systems.

The theoretical treatment of such non-Newtonian behavior has been through the development of constitutive equations to replace the Newtonian relationship between stress and strain rate, and to be used in continuum mechanical treatments of real flows. The constitutive equation has often been largely empirical in origin (like, for example, power law fluids), but increasingly has been derived from molecular theories, where macromolecules are modeled as bead-spring, bead-rod, or finitely extendable dumbbells.

The origin of extreme dilatancy in extensional flows has been accounted for by a gross change occurring in molecular conformation. This change is the so-called coil–stretch transition, where, as we have seen, beyond a certain critical strain rate ($\dot{\epsilon}_c$) in flows of a predominantly stretching character, the random coil molecule will rapidly unravel to become highly extended (*7, 8, 27, 28*). Little deformation of the coil is expected until the critical strain rate exceeds the reciprocal of the coils' longest relaxation time. Beyond this point the coil begins to extend; this extension may increase the draining (moving solvent penetration) of the coil, and thus produce an increase in its relaxation time. This increase induces even faster extension, which becomes a runaway or critical process, eventually limited by the increasing entropic elastic stiffness of coil as its conformation becomes strongly non-Gaussian.

It is easy to see intuitively that a solution of highly extended molecules subjected to further extension will show an increased flow-resistance as the molecules' deformation in the flow is limited.

This process has been examined theoretically by a number of authors (*29–31*), who derived constitutive equations based upon finitely extendable nonlinear elastic (FENE) dumbbell models (*29*), bead-rod models (*30*), and bead-spring models (*31*). There is general agreement that a large increase in elongational viscosity should be expected.

That such increases have been observed in apparently dilute solutions, particularly in capillary entrance and pore-flow experiments (*23–26*) (Figure

3) has led many to suggest that the coil–stretch transition of isolated molecules is the origin of such effects.

Recently we reported (32, 33) the development of techniques that enable the simultaneous assessment of macroscopic flow resistance and visual observation of molecular strain in idealized flow fields.

Apparatus. Figure 4 shows a schematic diagram of the apparatus used to control and measure strain rate, observe birefringence, and monitor the pressure drop across the jets.

A vacuum pump is used to suck the fluid through the jets in a controlled fashion. The flow rate is obtained from the pressure drop that is due to air flowing into the solution reservoir through a capillary (ΔP_1). With this flow rate (Q) and the dimensions of the jets, the strain rate can be approximately calculated by (34):

$$\dot{\epsilon} = \frac{Q}{Ad} \qquad (4)$$

where A is the area of the jets' entrance, and d is the separation of the jets; $d = 1.2$ mm, and the radius of both jets is 0.45 mm. The suction applied to the jets (ΔP_3) is monitored by a microcomputer, which drives a solenoid valve in order to uniformly increase the strain rate. While $\dot{\epsilon}$ is being uniformly increased, the pressure drop across the jets (ΔP_2) is also recorded by the microcomputer.

The ΔP_2 vs. $\dot{\epsilon}$ traces thus obtained showed a curvature even with pure
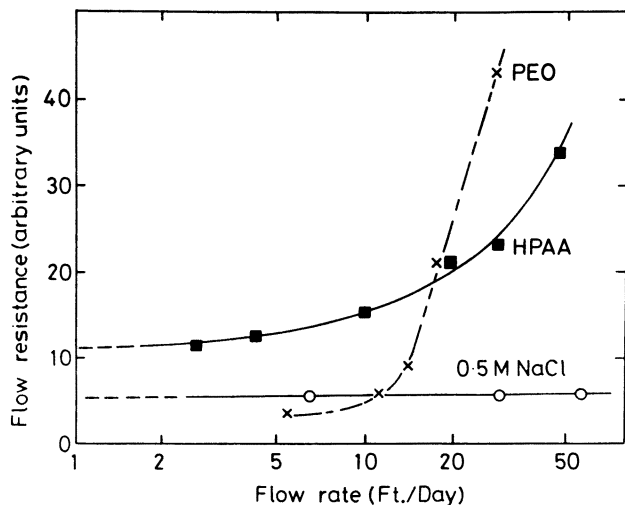
Figure 3. Flow resistance as a function of flow rate for 0.05% polymer solutions in 0.5 M NaCl in sandstone. (After ref. 44.)
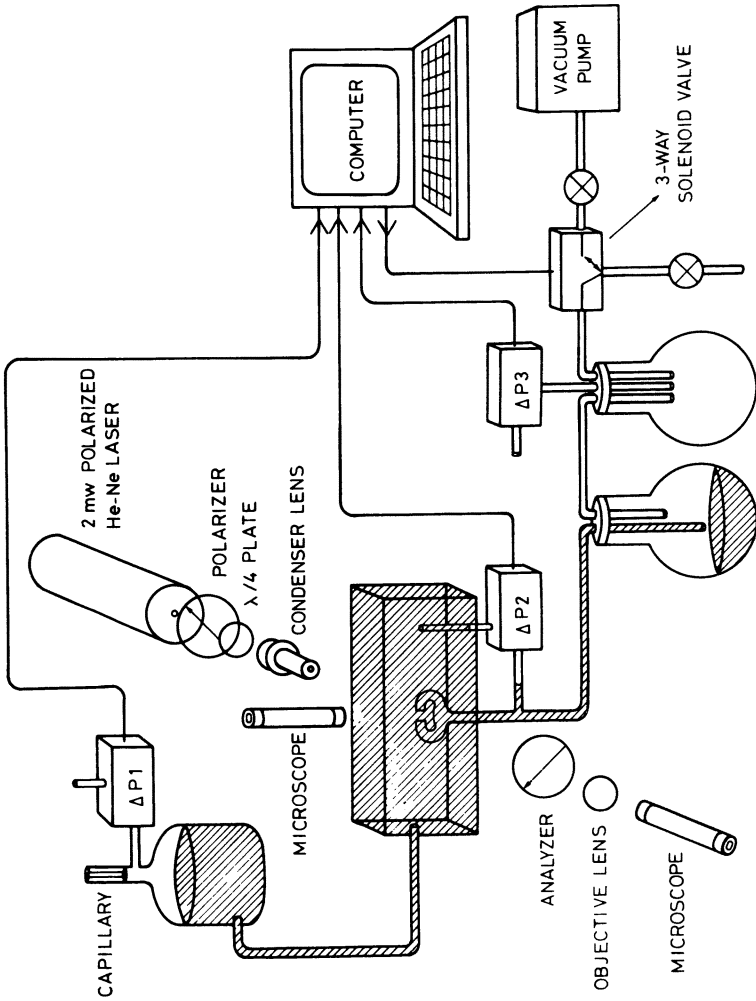
Figure 4. A schematic diagram of the apparatus used for measurement of extensional birefringence and flow resistance.

solvent (Figure 24, discussed later), which originated from the Bernoulli effect because of convergent flow, an effect that can be corrected for analytically (discussed later). The slope of the corrected ΔP_2 vs. $\dot{\epsilon}$ curve $d(\Delta P_2)/d\dot{\epsilon}$ then provides a quantity proportional to an elongational viscosity; this quantity we have defined as the effective elongational viscosity η_e'. This measure of extensional viscosity is a well-defined function of macroscopic strain rate, but, because of the presence of a flow singularity, it must correspond to a combination of a wide range of fluid strains. Because of the way ΔP_2 is measured, there will also be a contribution to η_e' from Poiseuille flow inside the jets. Thus, because of the spatial variation of strain and strain rate, η_e' must not be regarded as a true elongational viscosity.

The optical system used to assess flow-induced birefringence consisted of a 2-mW polarized He–Ne laser focused by a condenser lens on the center of the flow field. The birefringence patterns are observed between crossed polars by using a quarter wave ($\lambda/4$) retardation plate as a Senarmont compensator. The polarized laser has an extinction ratio of 100:1; the polarizer and analyzer are Carl Zeiss components with extinction ratios of approximately 10^4.

Observations of light scattered at 90° from tracer particles were made on-line through a microscope, as shown in Figure 4. However, best results and maximum scattered intensity were obtained by removing the polarizer and $\lambda/4$ plate and substituting the condenser lens with a long working distance cylindrical lens. In this way the flow field is illuminated by a sheet of laser light approximately 20 mm thick.

Dilute Solutions.   In dilute solutions the behavior of the birefringence is as shown in Figure 2. The birefringence occurs at a critical strain rate $\dot{\epsilon}_c$ (corresponding to the order of the reciprocal of the longest conformational relaxation time τ). The birefringence is closely localized around the stagnation point because of the requirement for large strains to completely stretch the isolated molecule; thus only a small fraction of the molecules passing through the jets are extended.

As we have seen, there exist a number of treatments of the increase in extensional viscosity of the solution corresponding to the coil–stretch transition. In particular, the Warner FENE dumbbell model (29) and the Kramers bead-rod model (30) predict increases in normalized extensional viscosity of the order of N, the number of statistical segment units in the flexible chain. The normalized extensional viscosity (η_e^+) compares the increase in extensional viscosity due to the polymer to three times (the Trouton ratio) the corresponding increase in the simple shear viscosity and is given by

$$\eta_e^+ = \frac{\eta_e - 3\eta_0}{3(\eta_0 - \eta_s)} \text{ for } C \to 0 \tag{5}$$

where η_e is the extensional viscosity, η_0 is the zero-shear viscosity, and η_s is the solvent viscosity. It is thus close to the ratio of the intrinsic extensional viscosity to the intrinsic shear viscosity. For a typical a-PS (5) examined here N is of the order of 1000, so large increases in η_e^+ of similar magnitude should be anticipated.

Figure 5 shows results from our experiments on dilute solutions of
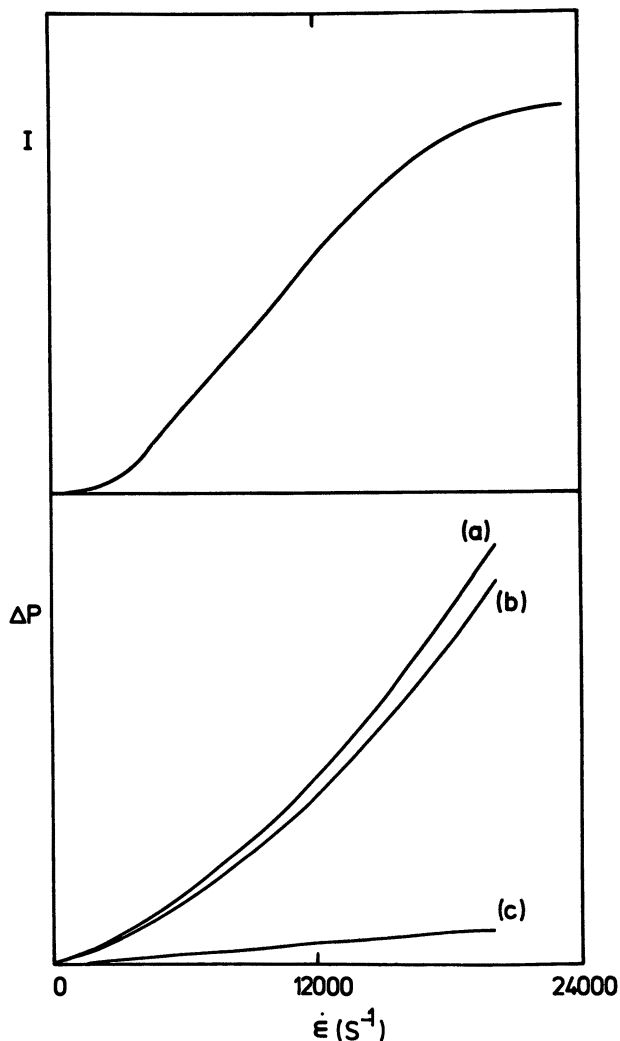
Figure 5. Top: Intensity (arbitrary units) vs. strain rate curve for a 0.025% solution of a-PS in decahydronaphthalene. $\overline{M}_w$ 4.4 × 10⁶. Bottom: Pressure drop (arbitrary units) across the jets vs. strain rate curves of a, 0.025% solution of $\overline{M}_w$ 4.4 × 10⁶ a-PS–decahydronaphthalene; b, decahydronaphthalene; and c, the result from subtraction of curve b from curve a.

$4.4 \times 10^6 \ \overline{M}_w$ a-PS. Figure 5 top shows the increase in birefringence associated with the onset of the line. This increase is gradual rather than critical because of the high degree of broadening of the line during increasing strain rate. This broadening is a function of the precise jet geometry; it can be corrected for by dividing the signal by the width of the line. This increased breadth of line is advantageous in the present experiments, because it increases the proportion of the material flowing through the jets, which is highly stretched.

Figure 5 bottom shows the measured pressure drop associated with the solution (curve a) and the solvent (curve b). A small but distinct increase in pressure drop is associated with the coil–stretch transition. To separate the polymer contribution, curve c shows curve a minus curve b: now the polymer contribution can be seen to increase gradually as the coil–stretch transition proceeds.

An effective intrinsic extensional viscosity for our data can be calculated from

$$[\eta_e'] = \frac{\Delta P_s - \Delta P_0}{C \Delta P_0} \text{ for } C \to 0 \tag{6}$$

where ΔP_s and ΔP_0 are the pressure drops across the jets for the solution and solvent, respectively. We must of course allow for the relatively small fraction of the molecules passing through the jets that are extended. In the present case the terminal line width was 100 μm across jets of 600-μm internal diameter; therefore, approximately 1/36 of the molecules are presumed to have undergone the coil–stretch transition. After this correction the value of η_e' was 1240 mL/g. Taking accepted values for the constants k and a in the Mark–Houwink equation

$$[\eta_0] = kM^a = 161 \tag{7}$$

where $[\eta_0]$ is the intrinsic viscosity, and the constant is expressed in units of milliliters per gram. The normalized extensional viscosity $\eta_e'/3\eta_0$ yields a value of 92. This magnitude is appreciable, but it is considerably lower than the factor exceeding 1000, which might be anticipated from various theories.

Possibly, we are overestimating the numbers of stretched chains, and among those that are birefringent, only those closest to the stagnation point are fully stretched. The theories are, however, also subject to considerable uncertainties, and are not based upon realistic assumptions of polymer behavior on short time scales.

Nevertheless, as we shall show, we do see much larger dilatant effects are associated with the pore flow and capillary entrance results (23–26, 33) as we increase polymer concentration (though still below conventional C^*, the concentration at which contact between spheres is established).

Identifying Entanglements

Disentanglement and Network Formation. As the concentration is increased, and as the chains begin to overlap, hence interact, the extension behavior, as diagnosed by our method, will be affected. This behavior change should provide a sensitive tool to identify the stage where the initially isolated entities will begin to stretch out cooperatively.

With solution concentration increasing, the first effect observed remained, as before, the onset of a narrow birefringent line along the jet axis setting in at a critical strain rate $\dot{\epsilon}_c$ (Figure 6a). At this stage no discontinuity has so far been observed regarding this effect with increasing concentration (C): the only influence of concentration is a steady linear increase in τ ($\dot{\epsilon}_c^{-1}$), proportional to the solution viscosity η_s (which itself increases, in first approximation, linearly with concentration) (Figure 7). This result, together with the persistence of extremely high localization (Figure 6a) means that even for concentrations where chain overlap would otherwise be expected, the chains continue to extend as they have done in the most dilute solutions where their isolated state can be regarded as assured. In fact, the observed
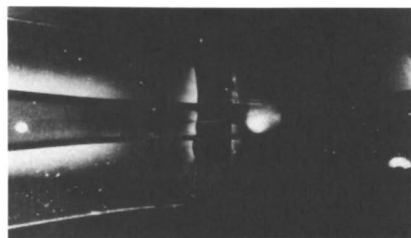
a
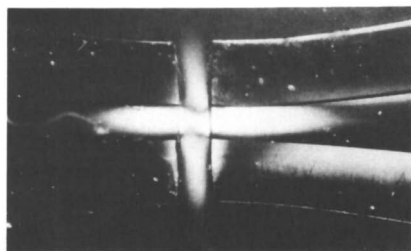
b

Figure 6. a, The narrow birefringent line observed between observed jets in a semidilute solution with $\dot{\epsilon}_c \leq \dot{\epsilon} \leq \dot{\epsilon}_p$ (0.1%, $\overline{M}_w$ 7.2 × 10⁶ a-PS). b, Flaring of birefringence in the same solution with $\dot{\epsilon} \leq \dot{\epsilon}_n$. Photographs, crossed Polaroid.
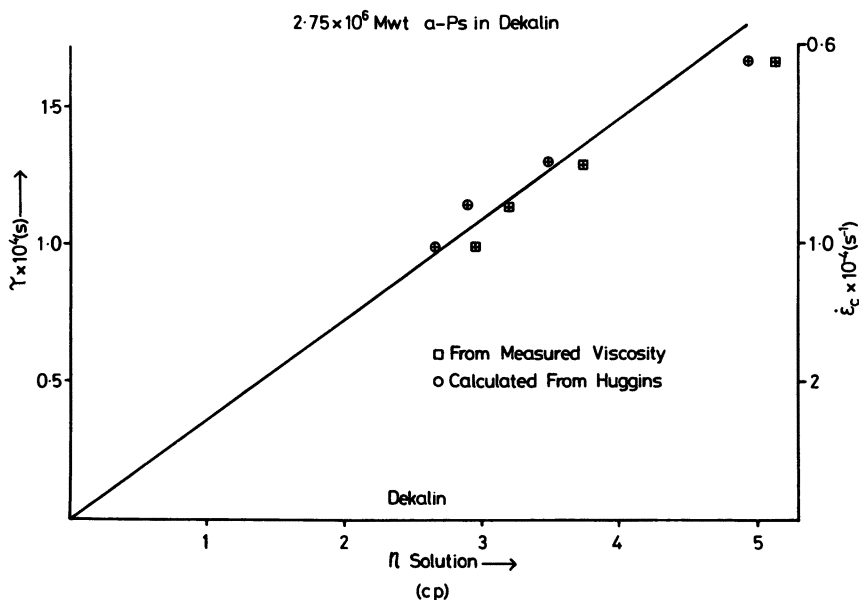
Figure 7. The coil–stretch relaxation time (τ) as a function of solution viscosity.

concentration, hence viscosity dependence, is consistent with the same trend that was found for dilute solutions when the solvent was varied, for a constant concentration (1). Therefore, apparently τ is proportional to the viscosity of the medium in which the molecule extends irrespective of how far the medium is constituted by molecules of the same or of different species. In other words, on the time scale of $1/\dot{\epsilon}_c$, a given chain continues to extend as if in isolation irrespective of coil overlap, and is seeing other molecules of its own kind only as a source of viscous energy dissipation and not as physical entanglements.

Nevertheless, when $\dot{\epsilon}$ is increased beyond $\dot{\epsilon}_c$, new effects set in beyond a sharply defined concentration C^+. At $C \geq C^+$, a series of happenings are observable for $\dot{\epsilon} \geq \dot{\epsilon}_c$ even by visual inspection, of which the final and most dramatic is illustrated by Figure 6b. We shall present and discuss this dominant effect first, then individual stages leading up to it.

Figure 6b is one particular variant of a whole range of appearances, which we collectively term "flare". Their common features are

- delocalized birefringence, which here can occupy the whole volume between the jets, and

- instability; the bright area, like a flame, is seen in continual motion.

The flare effect sets in suddenly at a critical $\dot{\epsilon}$, to be termed $\dot{\epsilon}_n$ (n stands for

network). $\dot{\epsilon}_n$ is a decreasing function of concentration; this decrease is very rapid shortly beyond C^+, gradually leveling out for higher concentrations (discussed in the section on the evolution of network).

We interpret the flare effect as a cooperative extension of molecules over the volume seen as birefringent. This cooperative extension would arise if the chains were behaving as if connected, that is, like a transient network. The fact that this connectedness arises only beyond a given concentration signifies that a cooperative effect is involved, implicit in the network model just described. The fact that it appears only at a critical strain rate, $\dot{\epsilon}_n$, however, introduces a new important factor: the time dependence of the connectedness. Namely, the connectedness can exist only over a very short time (τ_n) defined by

$$\tau_n = \frac{1}{\dot{\epsilon}_n} \tag{8}$$

Thus for times of τ_n or shorter, and only for these times, an assembly of mutually overlapping chains can act as a mechanically connected network.

At this point an essential interjection needs to be made. For the given experimental circumstances, the passage time of the molecule within the gap between the jets is very short compared with the change in strain rate. Thus, the coil–stretch and flare effects (as in fact the whole range of effects inbetween the two, to be described in the section to follow) are *not* consecutive responses of the same molecule to the increasing strain rate, as a given chain will have long left the system before the strain rate could have increased substantially enough to evoke a noticeably different effect. Each consecutive event therefore pertains to a *different* group of molecules as they successively enter the flow field.

The overall message of these experiments is now obvious. For a given molecular weight, the chains will stretch out virtually completely once a critical strain rate $\dot{\epsilon}_c$, corresponding to the coil–stretch transition, is attained. This behavior remains true irrespective of the existence or degree of chain overlap, and is affected only by the *mean* viscosity of the medium in which the chains are located (i.e., the solution viscosity). The fact that chains extend even in a molecularly overlapping environment means that on the time scale of $\tau = 1/\dot{\epsilon}_c$ they can still disentangle. This ability of the chains to disentangle will persist up to the shorter time scale of τ_n, when the overlapping chains will begin to "grip each other", so to speak, and thus give rise to the network effect.

It follows that two criticalities are involved in the creation of the transient network: a critical minimum concentration (C^+), and for each concentration of $C \geq C^+$ a critical minimum time (τ_n). The time effect will be considered first.

Criticality in Time Scale. The quantity τ_n, readily determinable through the flare effect, represents the shortest time during which a given molecule can disengage itself from its neighbors in the course of the chain extension, and will be termed as the "disentanglement time" accordingly. Its dependence on concentration for a particular a-PS sample is given by Figure 8. As seen, it is an increasing function of concentration. The actual times are of the order of 10^{-5} s, a plausible time scale in terms of molecular dynamics for chains in that length range (*1, 35*).

We may examine this time scale more specifically in terms of other available information. Possibly the most relevant is the translational diffusion coefficient D measured exhaustively in nonflowing systems by Leger et al. (*36*). Their data points can be interpolated to obtain D for our molecular weights and concentrations. With the knowledge of D the distance x through which a molecule would diffuse during a given time (t) can be calculated readily from the relation $x = Dt^{1/2}$. For the times represented by τ_n in Figure 8 the values range from 7 to 38 nm for a-PS in decahydronaphthalene (dekalin) ($\overline{M}_w$ 2.75 $\times$ 10^6). These values can be usefully compared with the radius of gyration of the same molecule under θ conditions, known with some confidence to be 70 nm.

Thus our τ_n values correspond to times during which, within a stationary system, our molecule would diffuse over a fraction (0.1 to 0.5) of a coil radius, as expressed by radius of gyration. This result is at least consistent with the
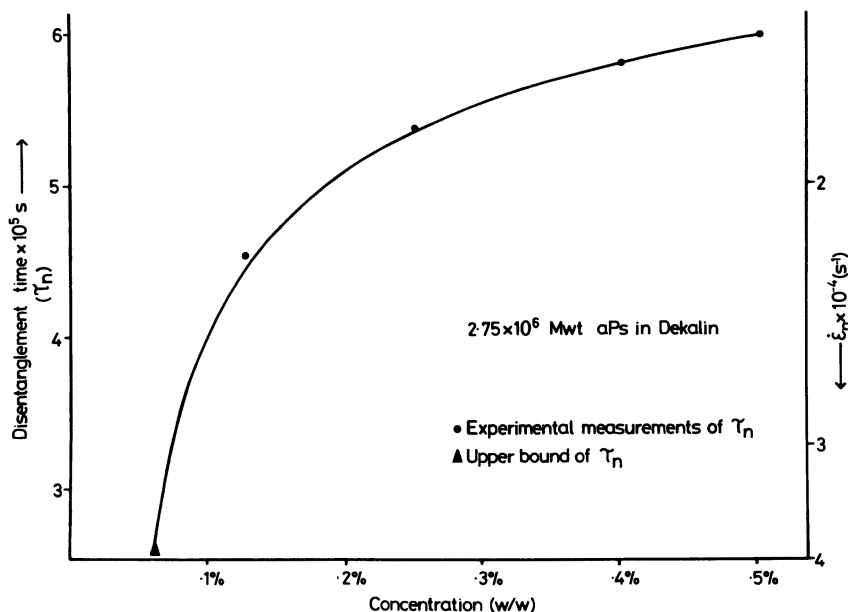
Figure 8. Disentanglement time (τ_n) as a function of solution concentration.

picture that the coils overlap through a fraction of their diameter and will behave as isolated chains on extension if they are given the time to diffuse out of each other's environment, a time that we may identify as the disentanglement time. Admittedly, the invoking of values for D that pertain to a nonflowing system may well be questionable. Even so, the mere fact that the values thus arrived at seem reasonable is noteworthy and, if taken at face value, could even suggest that the flow itself may have little effect on the disentanglement as such, at least at strain rates not exceeding $\dot{\epsilon}_n$.

Criticality in Concentration. The sharp downturn of the disentanglement time vs. concentration curve for the flare effect (Figure 8) indicates that the flare sets in within a narrow concentration range as C is increased. This is the critical concentration already identified as C^+. The postulation of the existence of a critical lower concentration is consistent with the concept of a network, because for a network to arise there needs to be a pathway of contact across the whole macroscopic system, the establishment of which, as common with all such percolation problems, is a critical phenomenon. In our case the minimum contact criterion is clearly the existence of coil overlap.

The criterion of coil overlap is familiar in solution theory, where it represents the transition from dilute to semidilute solutions, the corresponding concentration being denoted as C^*. C^* is calculated on the basis that the chains can be represented as spheres of dimensions defined by the radius of gyration (R_g), and corresponds to the concentration at which contact between spheres is established. This criterion for C^* is calculated in slightly different ways by the different authors. Depending on the criterion used, for our system of a-PS with M_w 2.75 × 10^6, C^* is in the range of 1–5%. The experimental determination using neutron scattering yields a C^* of 5% for the same system (37).

As seen from Figure 8, C^+, the lower limit for the flare effect, is somewhat below 0.1%; that is, it is at a concentration lower by a factor of 10–50 than the calculated C^*. Without any further assumption this lower C^* means that the elongational flow-induced extension registers a much lower degree of chain overlap than implied by the conventional C^* criterion for semidilute solutions. Or looking at it in another way, our methodology provides a considerably more sensitive test for chain overlap, hence entanglements, than the traditional criterion for semidilute solutions.

The reason for this result is likely to reside in the fact that a single parameter, such as R_g, is inadequate for defining conditions for interchain contact; the segment density in the overlap region as a function of center-to-center distance, which in turn is a function of concentration, needs considering instead. The approach to this possibility is as follows.

The distribution of the segments of flexible coils in the θ state (in the

absence of excluded volume effects) is well described by a normal distribution ($\sigma(r)$) (38)

$$\sigma(r) \propto \frac{M}{R_{g_3}} \exp \frac{-3r^2}{2R_{g_2}} \tag{9}$$

Two such coils can presumably interpenetrate freely. Figure 9 shows coils overlapping; interactions can occur with separations much greater than $2R_g$, and thus at concentrations considerably below conventional C^*.

Considering two coils (1 and 2) ρ apart, the probability of coil 1 interacting with coil 2 (p_{12}) is the integral of the product of the segment densities of the two coils (σ_1 and σ_2) over all volume V ($\sigma_1\sigma_2 dV$), which leads to

$$p_{12} \propto \frac{M^2}{R_{g_3}} \exp \frac{-3\rho^2}{4R_{g_2}} \tag{10}$$

This proportion yields a number that characterizes the degree to which two coils in the θ state "see" each other. The effect is overlayed by any specific interactions between coils. In the simplest case it describes the opportunity for topological entanglements. Thus, entanglement effects that show up on a macroscopic time scale are characterized by a particular degree of interaction p_{12} (e.g., neutron scattering (37) and viscometry). At short times the
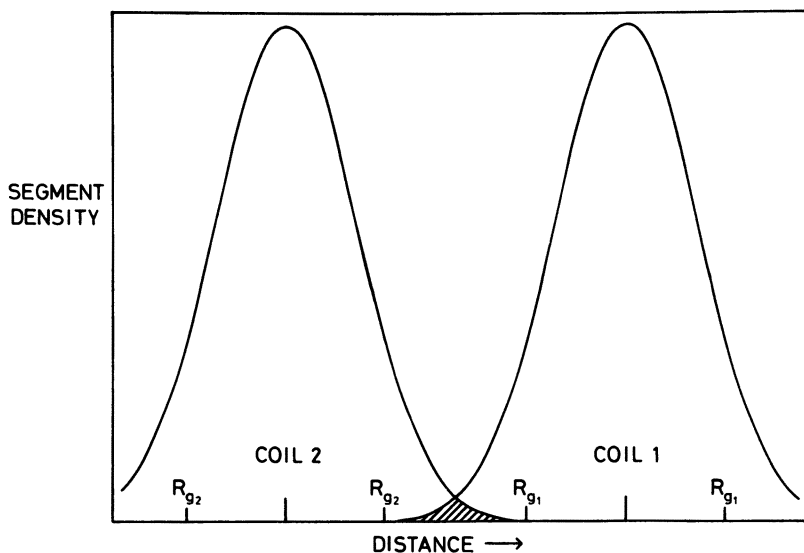
Figure 9. A schematic representation of the overlap of two normal distributions of segment density. R_{g_1} and R_{g_2} define the respective radii of gyration. The overlap area is shaded.

degree of interaction p_{12} required for connectivity is much reduced because even tenuous entanglements on the periphery of the coils cannot disentangle quickly enough.

Setting p_{12} to a constant to describe a given degree of interaction, or the onset of connectivity, or even gelation, gives different values of C^*, which depend upon the nature of the interaction concerned and particularly the time scale of observation. Indeed from eq 10, neglecting logarithmic terms and using $M \propto R_{g_2}$ in the θ state:

$$C^* \propto M^{-0.66} \tag{11}$$

in contrast to the -0.5 exponent generally assumed. Indeed, based upon gelation criteria, some evidence favors the higher exponent (*39, 40*).

Evolution of the Network

In the preceding experimentation the flare was observed to set in suddenly at $\dot{\epsilon}_n$. However, on more detailed scrutiny it could be seen to develop through a well-defined sequence of stages as $\dot{\epsilon}_n$ was being closely approached. The existence of these stages does not detract from the decisive role of the flare, and of issues based upon it, which remain central to our argument; yet the individual steps leading up to the flare have much further and rather subtle information to convey. In particular, this information relates to the gradual development of the "infinite" connected network, both in terms of spatial spread and in terms of the time scale of connectedness. In the course of this development, the two criticalities, that in strain rate (time scale) and localization (space), became apparent in a rather instructive way.

Two different systems will be referred to: closely monodisperse a-PS ($\overline{M}_w$ 2.75×10^6) and polydisperse high molecular weight PEO ($\overline{M}_w$ 6×10^5, 4×10^6, and 5×10^6). The a-PS permitted quantitative deductions about relaxation times and overlap concentrations, as already discussed. The polydisperse PEO, although less suitable for quantitative assessment, proved convenient to display qualitatively the sequence of events involved. The convenience arises because here, for each $\dot{\epsilon}$, a given species within the broad molecular weight spread available becomes extended, and this extension leads to a ready display of the full sequence within an accessible range of $\dot{\epsilon}$ for one and the same material.

Here we shall proceed to show that in the time scale between τ and τ_n a number of complex phenomena occur, and they reflect the systematic development of molecular connectedness.

Figure 10a–10h illustrates a typical sequence of observations as the strain rate is increased. With increasing $\dot{\epsilon}$, a sharply localized line appears (Figure 10a), which progressively broadens (Figure 10b). Next a dark central line appears at $\dot{\epsilon}_p$ (the first appearance of the pipe, Figure 10c), which itself
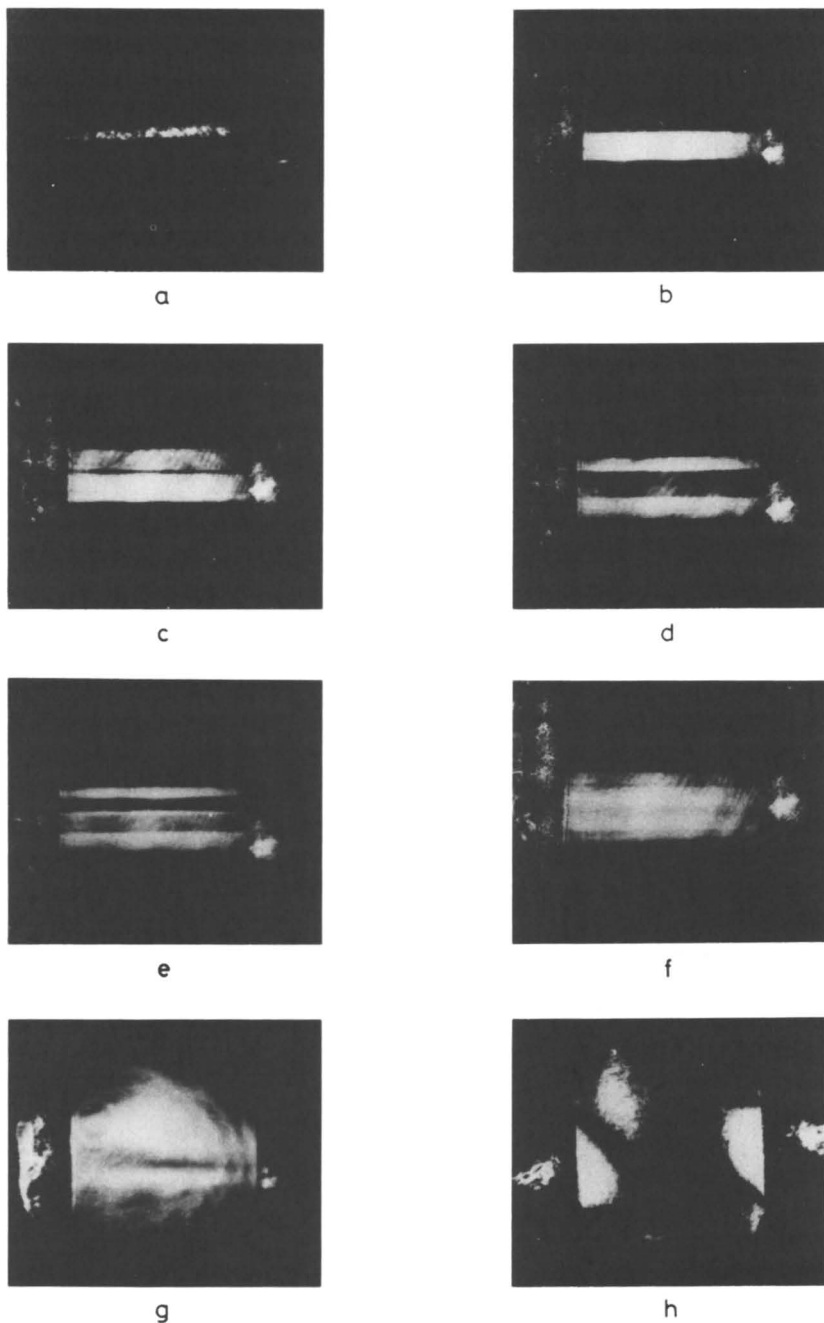
Figure 10. Stages of development of connectivity as the strain rate is increased. The corresponding strain rates (s^{-1}) for a 0.2% solution of PEO ($\overline{M}_w \geq 5 \times 10^6$) in water are a, 150; b, 200; c, 450; d, 500; e, 575; f, 650; g, 700; and h, 800.

broadens progressively (Figure 10d). For further increase in $\dot{\epsilon}$ a central narrow bright line reappears within the dark central zone (Figure 10e). Occasionally the new central line has been seen to split and produce the appearance of four parallel bright lines (Figure 10f). These birefringent structures can develop up to the complete width of the capillary cross section. Following this development the whole system becomes unstable and oscillates (Figure 10g) until the fully developed flare appears (Figure 10h).

Extensive observations revealed that the appearance of a dark central line corresponds to the onset of the formation of a birefringent "pipe" with a "hollow" (i.e., nonbirefringent) interior. This pipe formation is deduced from the fact that the maximum retardation in our experiments is always much below one wavelength (λ). Consequently, the dark bands cannot be ascribed to retardation of multiples of λ, which is substantiated by their visibility in white light, as for Figure 15 in ref. 5 without observation of interference colors. Relative darkening, therefore, corresponds to lowered retardation, hence, for a given birefringence to a shorter path length, which will be the situation pertaining to the central axial regions when viewing a birefringent pipe. Further, recent observations of light scattered at 90° from the stretched molecules have also revealed a pipelike structure beyond $\dot{\epsilon}_p$ (discussed in the section on non-Newtonian behavior of polyacrylamide). This phenomenon was previously ascribed in a-PS (*12*) to a change of sign of the birefringence with stretching due to free rotation of phenyl rings, an explanation no longer viable, because the same phenomenon is now seen to occur in PEO and polyacrylamide (*41*).

Figure 11 provides a "phase diagram" for the appearance of the visually observed phenomena as a function of concentration and strain rate for PEO (5×10^6 $\overline{M}_w$). The following features are indicated: $\dot{\epsilon}_c$, $\dot{\epsilon}_p$ (first appearance of the pipe), and $\dot{\epsilon}_n$ (the flare) with $\dot{\epsilon}_c < \dot{\epsilon}_p < \dot{\epsilon}_n$.

The low concentration cutoff signifies that both $\dot{\epsilon}_p$ and $\dot{\epsilon}_n$ are manifestations of the onset of molecular interactions. We will return to their interpretation later.

The whole sequence shifts both to lower C and to lower $\dot{\epsilon}$ with increasing molecular weight. This result follows from the established molecular weight dependence of $\dot{\epsilon}_c$ (5) and from the expectation that longer chains will overlap at lower concentrations and that lower $\dot{\epsilon}$ are required to extend a more overlapping system. For a broad molecular weight distribution, as in the present PEO, the high molecular weight end dominates the effects displayed; at any particular strain rate, only those molecules with sufficiently long relaxation times or that satisfy the overlap criterion will participate.

One can be more quantitative from the analogous experiments on the closely monodisperse a-PS. Figure 12 shows a "phase diagram" analogous to that of Figure 11, but for a-PS of $\overline{M}_w$ 2.75×10^6 ($\overline{M}_w/\overline{M}_n \sim 1.05$). The overall behavior follows the same sequence with increasing strain rate and concentration as for PEO. The critical network overlap concentration (C^+_n) is of the order of 0.1%, and that for incipient entanglement formation (C^+_p)
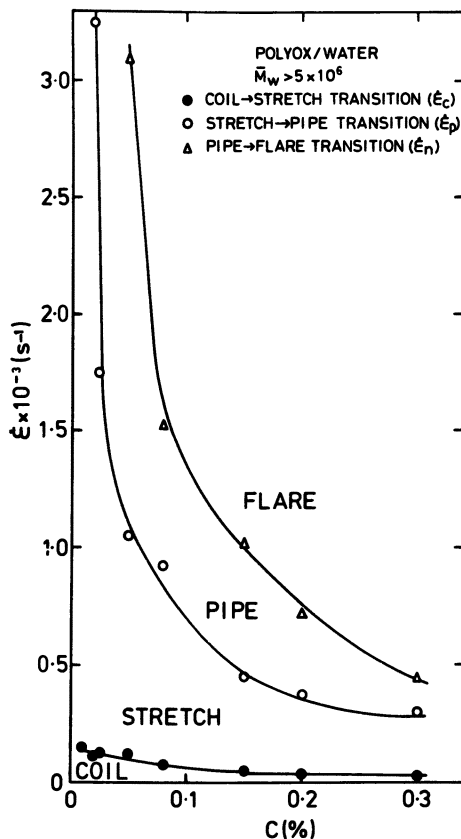
Figure 11. A "phase diagram" of the development of connectivity as a function of strain rate and concentration (PEO–water, $\overline{M}_w \geq 5 \times 10^6$).

could even be lower (*see* Figures 11 and 12). This finding means, as stated in the section on identifying entanglements, that our elongational flow effects are sensitive to lower degrees of chain overlap, or to network effects that are on a very short time scale, compared with the conventional C^* calculations (1–5%) and corresponding static experiments, respectively (*1*).

The "phase diagrams" of Figures 11 and 12 have a further notable feature. Although the curves for $\dot{\epsilon}_c$, $\dot{\epsilon}_p$, and $\dot{\epsilon}_n$ at first seem to converge with C, they do not cross, up to the highest concentrations examined. This finding means that chains remain fully extendable as individuals provided they are being stretched on a long enough time scale to allow them to disentangle from the increasingly overlapping environment. Clearly, the issue of what the upper limiting concentration may be, or whether there is one at all, is of great potential interest for attempts to stretch out chains in the condensed phase.
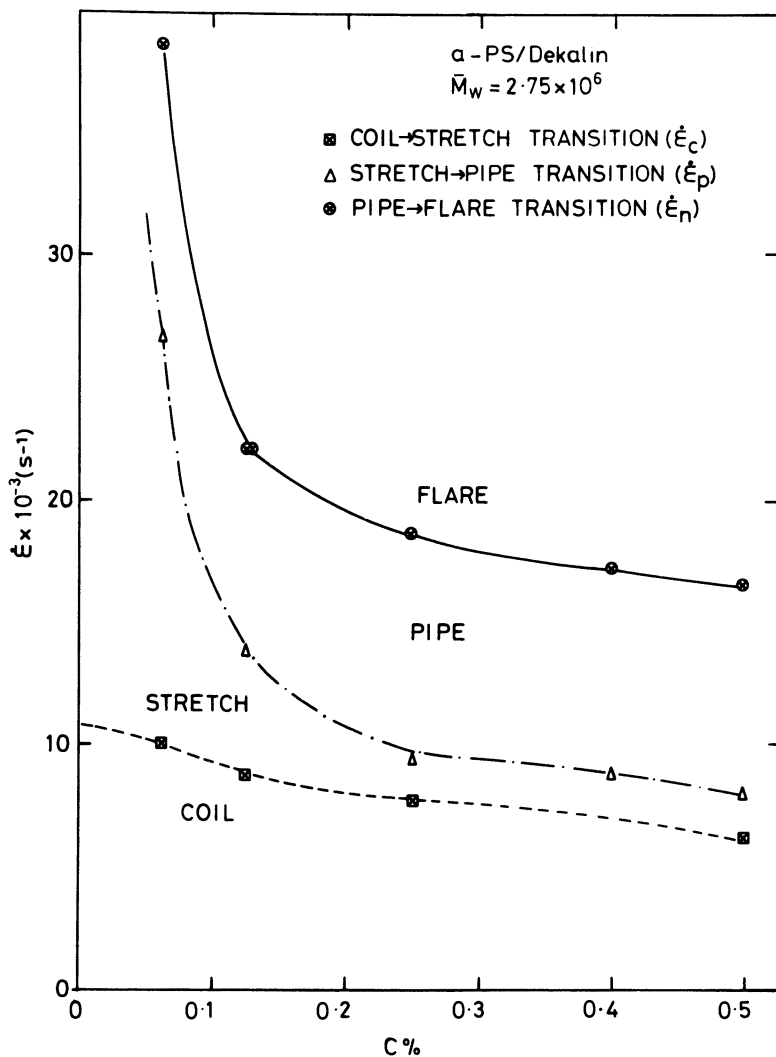
Figure 12. A "phase diagram" for a-PS, $\overline{M}_w$ 2.75 × 10⁶ in decahydro-naphthalene.

Origin of the Pipe and Local Flow Velocities.   For an understanding of the origin of the pipe effect, the influence of the chain extension on the local flow field, which initially created the chain extension, needs invoking. Local flow modification arises through a combination of two factors: (1) the energy requirement for chain extension, and (2) the localized nature of the chain extension. It follows from factors 1 and 2 that the flow velocity is expected to become modified at strain rates when the chains start to

extend, that is, at $\dot{\epsilon}_c$ and beyond, but only within the localized region of the chain extension. Establishment of this feature calls for local flow velocimetry.

The real fringe photon-correlator velocimetric system presently used (42) is capable of precise measurements of local velocity within a volume of about 10 μm^3. Figure 13a shows the velocity profile scanning across a bi-refringent line of 30-μm width (i.e., above $\dot{\epsilon}_c$) in a dilute (0.03%) solution of a-PS ($\overline{M}_w$ 4 × 10^6) in decahydronaphthalene. The velocity distribution is not significantly different from that of pure solvent, corroborating that in sufficient dilution the extended molecules do not significantly perturb the flow field. Indeed, even in semidilute solutions the flow field is not signif-icantly perturbed for $\dot{\epsilon} < \dot{\epsilon}_p$ below the appearance of the pipe. This result is shown in a qualitative sense by the flow field illustrated in Figure 1b, which corresponds to a 0.2% solution of 5 × 10^6 $\overline{M}_w$ PEO above the coil–stretch transition but below the pipe (corresponding to the birefringent line of Figure 10a. This flow field is indistinguishable from that of pure water.

Figure 13b shows a similar scan but across a line of 100-μm width, displaying a pipe birefringence obtained for a more concentrated solution (0.2%). The pipe birefringence displays a clear "dip" in the velocity along the axis of the jet system where the dark line is seen in the image. Such effects were previously observed by Lyazid et al (43). This solution corre-sponds closely to the pipe region of the "phase diagram" shown in Figure 12. Visually the appearance is similar to Figure 10d for PEO.

This result is quite general. The appearance of the pipe is associated with a corresponding local reduction in flow velocity, and conversely, the extending chains produce observable flow modification only beyond the concentration (C^+_p) and strain rate ($\dot{\epsilon}_p$) where the pipe effect appears.

Interpretation of Flow Patterns. Consider for simplicity a mono-disperse system (the same should apply for a polydisperse one, but with reference to the range of molecular weights). At $\dot{\epsilon}_c$ the chains stretch out individually, yet the extension remains confined to those streamlines that pass close to the stagnation point and thus ensures sufficient residence time, hence molecular strain. The molecular strain can be much lower than the strain of a corresponding fluid element but increases toward this value at high strain rate (6). As the strain rate is increased beyond $\dot{\epsilon}_c$, progressively higher molecular strains are attained also along outer streamlines corre-sponding to decreasing residence times, and the birefringent line broadens accordingly. The extending chains are expected to extract energy from the flow in the localized regions where the extension occurs, with a concomitant reduction in local flow velocity. Furthermore, such energy extraction will affect the flow increasingly toward the interior of the cylindrical extended-chain region, where molecular strains are highest. As the cylinder broadens, the flow velocity should be progressively reduced along the central axis, the
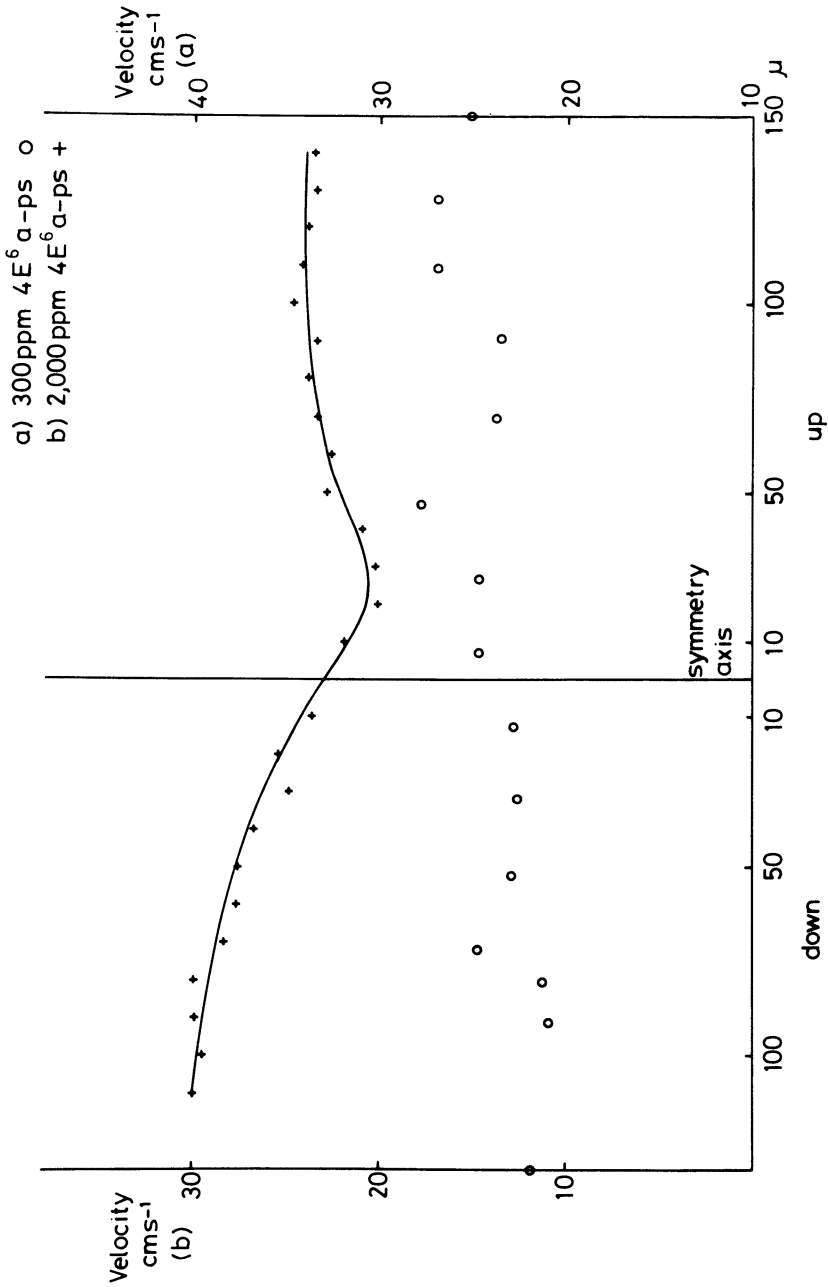
Figure 13. Velocimetric scans. Velocity as a function of position across the birefringent line. a, ○, dilute (0.03%); and b, +, semidilute (0.2%) solution (a-PS, $\overline{M}_w$ 4×10^6 in decahydronaphthalene).

result given by our flow velocimetry. Once it falls below that corresponding to the critical strain rate $\dot{\epsilon}$, the chains will cease to become extended there, from which the central dark line; hence, the hollow pipe effect follows.

Any flow-modifying effect will be larger for higher concentration, where there are more molecules to extend per unit volume even without considering molecular interaction. As already stated, the fluid strain diminishes when passing from central axis to periphery; this diminished fluid strain will limit the chain extension, and hence the birefringent line width, that can be attained. However, for the transient network that arises beyond C^+, much less is required for full orientation than for isolated molecules. Network chain extension will spread out to more peripheral streamlines than encompassed by the original birefringent line. This spreading out, coupled with the higher concentration, leads to a correspondingly increased screening of the flow along the central axis and sets off the sequence of effects under consideration.

The broadening of the pipe would clearly follow from the preceding considerations. Indeed, on the basis of a semiempirical model of the opposed jet flow field (6), the outermost pipe diameter (~ 300 μm) corresponds to a fluid strain of the order of only $10\times$. Such low strains would not produce appreciable birefringence for isolated molecules; only deformation of a network would give significant molecular orientation. However, as the screening of the pipe interior is not expected to be complete, the velocity will also rise there on further increase of the mean $\dot{\epsilon}$. The central strain rate could reattain the value $\dot{\epsilon}_c$ when a new localized central birefringent line should arise, as in fact observed (Figure 10e).

During the process of pipe development, the network behavior itself remains highly localized; this localization enables the fluid as a whole to conform with the convergent flow field. At higher strain rates, corresponding to τ_n, the whole region becomes a transient network (because of the very short time scale of deformation). Affine deformation of such a network is inconsistent with an extensional flow field incorporating a stagnation point (and hence infinite strains). Consequently, the cylindrically symmetric nature of the flow field breaks down completely (discussed in the section on non-Newtonian behavior of polyacrylamide), the result being the generalized birefringence and marked flow instability observed. The flow lines in flare are shown in Figure 12 as revealed by light scattered at 90° from tracer particles. Although the streamlines observed clearly show a flow instability, it is not associated with intertial turbulence, because the Reynolds number is approximately 1000, calculated on the basis of Poiseuille flow in the jets, and turbulence can be identified in pure solvent at 2888 s^{-1} (i.e., Reynolds number 3087). The supposition that no turbulence occurs is strongly supported by subsequent viscometric data (Figure 14).

Strictly speaking, all of the preceding discussion relates to one particular type of flow field. Special, and perhaps artificial as it may appear, it is possibly
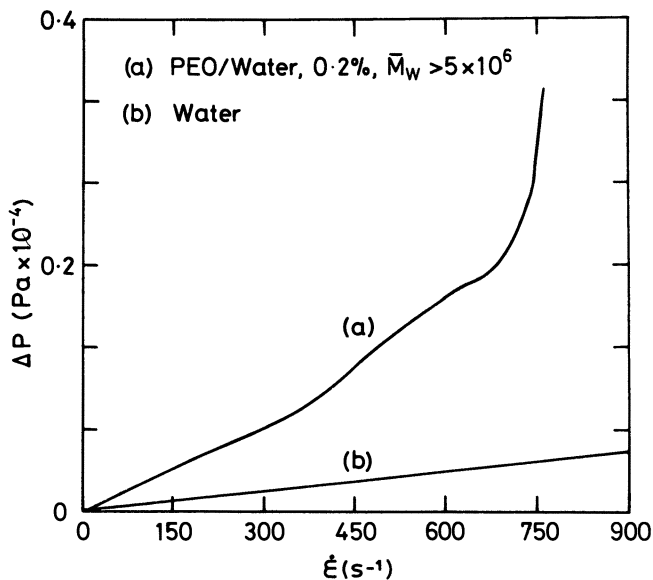
Figure 14. Pressure drop across the jets vs. ἐ (Bernoulli corrected curves) for a, semidilute PEO and b, water.

the simplest realization of an elongational, hence necessarily spatially inhomogeneous, laminar flow field. While recognizing this fact, we maintain that the conclusions reached on this system should be pertinent to more complex inhomogeneous flow fields with predominantly extensional components, such as may arise in practical applications.

The jet system is not quite uniquely defined, even for the present purposes. Thus, the thickness of the jet walls (in addition to the orifice diameter and separation) has an effect on the stability–instability criterion. For all these reasons, exact quantifications of the analysis of the events here presented, beyond giving order of magnitudes, would be of no general significance, except as pertinent to the particular experiment involved. Of wider significance is the newly recognized general trend of progressive network formation, its particular manifestations through criticalities, both timewise and spatial, and the introduction of a new methodology for the study of either entanglements or of flow phenomena produced by polymeric additives.

Elongational Viscosity of Entangled Systems

The dramatic effects associated with the formation of transient networks will also have a correspondingly pronounced influence on the macroscopic flow behavior, and the visually observed events are reflected by changes in the flow resistance presented by the jet system as a whole. For this reason we

have applied the extensional viscometric techniques previously described to assess the extensional viscosity of a semidilute solution of PEO as a function of strain rate.

Figure 15 shows η_e' as a function of $\dot{\epsilon}$. The initial constant value corresponds to a pseudo-Newtonian viscosity. At the point at which the pipe is formed there is a pronounced peak, in the present case at $\dot{\epsilon} = 465$ s^{-1}. At still higher $\dot{\epsilon}$, when the birefringence flares, the flow becomes irregular and the extensional viscosity enormously increased (only the initial portion of the rise is shown). The reality of all these effects is borne out by comparison with the totally invariant η_e' value for the pure solvent (water) recorded under otherwise identical circumstances. Closer inspection of Figure 15 reveals further details. Thus, a shoulder on the high end of the peak is associated with the pipe effect. Other traces may in fact show a double (Figure 16) or even a triple peak (some traces in Figure 17) within the pipe effect region. By all indications these periodicities in the η_e' vs. $\dot{\epsilon}$ curves correspond to the periodic sequences in the visual image of pipe development described previously.

In summary, we thus have a correspondence between the visually registered development of transient entanglement formation and the macroscopic flow characteristics. Accordingly, entanglement formation is associated with an increase in flow resistance and in η_e' derived therefrom, leading up to a massive increase when the network becomes infinite as signaled by the flare. The overall direction of the effect, that is, an increase
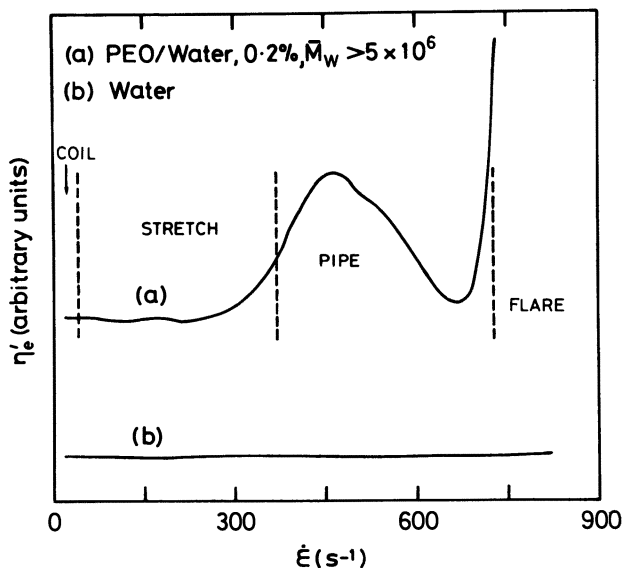
Figure 15. η_e' vs. $\dot{\epsilon}$ curves derived from Figure 14 for a, semidilute PEO indicating the characteristic flow behavior as in Figure 10; and b, water.
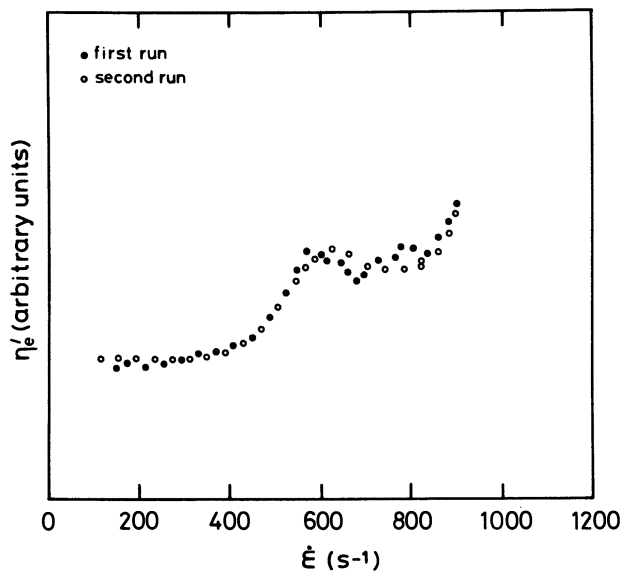
Figure 16. η_e' *vs.* $\dot{\epsilon}$ *for two successive runs of a 0.2% PEO–water solution* $(\overline{M}_w \geq 5 \times 10^6)$ *where the experiment was stopped below* $\dot{\epsilon}_n$.
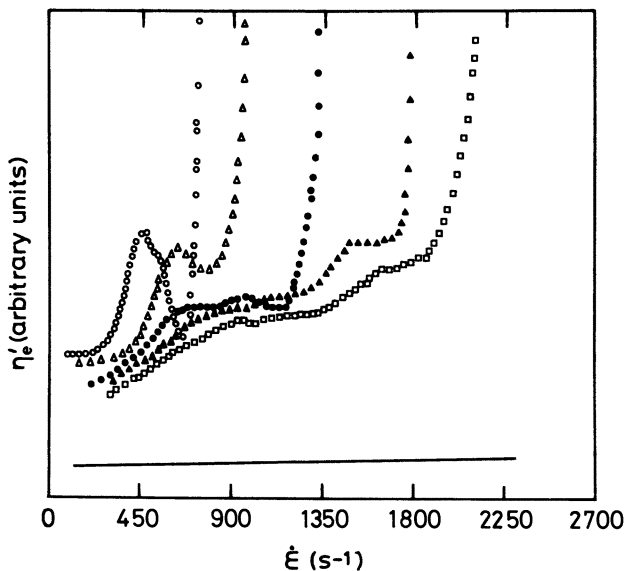
Figure 17. η_e' *vs.* $\dot{\epsilon}$ *for successive runs of a 0.2% PEO–water solution* $(\overline{M}_w \geq 5 \times 10^6)$ *where each run extends beyond* $\dot{\epsilon}_n$: ○, *first run;* △, *second run;* ●, *third run;* ▲, *fourth run;* □, *fifth run; and* —, *pure water.*

in η_e' with $\dot{\epsilon}$, might have been anticipated. However, the minima in η_e', with increasing $\dot{\epsilon}$, are unexpected. Nevertheless, even these effects seem to fall into a consistent scheme in the light of the sequence of visual images observed. The fall in η_e' corresponds closely to the transition from a broadened line to a pipe of initially similar diameter. The pipe, therefore, corresponds to fewer birefringent (i.e., stretched) molecules in the flow field, presenting a lower net resistance to the extensional flow.

These findings have wider implications for the study of inhomogeneous but still laminar flows. Namely, any macroscopically measured flow parameter can only be an aggregate expression of the wide spatial variations within the flow field, resulting from inhomogeneities in molecular strain. Conversely, molecular behavior cannot be extracted from macroscopic flow measurements alone, without local probing of the "morphology" of both strain and flow fields.

A further important aspect emerges from the reversibility characteristics of the curves such as in Figures 16 and 17. The ΔP_2 (and the derived η_e' vs. $\dot{\epsilon}$) plots are almost perfectly reproducible for reruns up to the onset of flare, including the pipe effect (Figure 16). However, once the flare stage has been reached, the same plots for subsequent consecutive reruns show a reduction in the initial value of η_e', and the flare and associated effects are shifted to higher strain rates corresponding to a progressive reduction in molecular weight, as chains are broken by stretching beyond $\dot{\epsilon}_n$. Such chain scission is confirmed by gel permeation chromatographic molecular weight measurements that show a progressive destruction of the high molecular weight tail. Clearly, as discussed in the section on the evolution of network, deformation of such a network is inconsistent with an extensional flow field incorporating a stagnation point: the consequences are molecular scission and flow modification (annihilation of the stagnation point).

Thus, in addition to its intrinsic significance, the rheological behavior provides strong additional support for our picture of network formation, in particular the interpretation of the flare effect. Further, and rather unexpectedly, it conveys information on flow-induced chain scission. We have now identified two kinds of flow-induced degradation. First, the isolated chain, when stretched out, breaks virtually exactly in the center, yielding two closely equal chain halves as the elongational flow rate is increased far enough beyond the coil–stretch transition (12, 13). The second mode of scission applies to overlapping chains that break during the flare stage. Although not yet fully confirmed, here fracture is not expected to be closely central to the molecule. Although both fracture modes can occur, the second, involving entanglements, takes place at lower strain rates.

Applications

Soluble high molecular weight polymeric additives can influence macroscopic flow behavior with diverse practical applications (21, 44). Understand-

ing of the behavior of the often minute amount of polymeric additive is essential for the design and control of the flow system. There is growing awareness that elongational flow-induced chain extension must be ultimately responsible for the flow-modifying action of many polymeric additives; however, in real applications and even in engineering modeling, the situation is far too complex for identification of the basic phenomena involved. Our type of flow experimentation has much to offer in this applied scheme, and conversely, interpretation of practical flow effects from our new point of view can further basic understanding. The latter holds in particular for entanglements, the reason for inclusion of this section.

The extension of chains must extract energy from the flow. For practically relevant situations, this requirement can have two diametrically opposed consequences.

The first is the intriguing Thoms effect, also known as "drag reduction". In macroscopic terms this effect consists of turbulence suppression and consequent energy saving in fluid transport, through the addition of even minute amounts of very high molecular weight polymer. Through presently shaping views (45) this effect is likely to be due to chain extension within the localized elongational flow field arising between incipient vortices. Here the energy expended on localized chain extension suppresses further vortex development and consequent much larger energy dissipation. In view of the extreme dilutions involved, these effects are attributable to the extension of truly isolated molecules (45, 46).

In the second family of applications, the energy dissipation associated with chain stretching is used directly in the form of enhanced viscosity, in cases where enhanced viscosity is desirable. However, this application is not the trivial matter of increasing fluid viscosity all round, as this approach would lead to uneconomically high expenditure of energy when driving a viscous fluid along its full path. Rather, it is often desirable to create high flow resistance within an otherwise low viscosity fluid at a particular locality or state of flow. Such a localized or transient viscosity enhancement will arise in elongational flow when favorable circumstances for chain stretching are created.

Here, two examples will be quoted. In enhanced oil recovery, fluid is pumped into porous rock to expel the oil. For this purpose the viscosity has to be sufficiently high to displace the oil and not to bypass it. The flow through a complex, open pore system will be repeatedly and consecutively convergent and divergent, hence locally of elongational character, with stagnation points behind the obstacles and at bifurcations. Clearly, conditions for chain stretching and corresponding viscosity enhancement, here confined to within the pore bed, will be met. The fluid being used in engineering practice is water with polyacrylamide as the most frequent additive. Much research (25, 26) on the subject is centered on flow through model pore systems (e.g., beds of beads). One common result is the registering of a sudden rise in flow resistance at a particular macroscopic flow velocity (most

commonly expressed by the Reynolds number). This rise may or may not level off, and can occur even at very high dilutions (0.01%) (25). The effect is interpreted, by some sources at least (25, 26), as arising through the stretching of individual chains in the elongationally effective portions of the flow field.

Non-Newtonian Behavior of Polyacrylamide

Ouibrahim and Fruman (47) in 1980 found dilational flow in three distinct flow situations, which each involve an extensional component: capillary tube flow, orifice flow, and pitot tube flow. They examined extensively hydrolyzed polyacrylamide (HPAA) and found that the dilatant effect was greatly reduced in the presence of excess salt. This finding was attributed to the effect of the salt ions in screening the charges on the polyelectrolytic HPAA and thus causing the contraction of the highly expanded molecule.

Chauveteau and co-workers (24, 48) examined the flow of PEO and HPAA through the extensional flow produced in severe constrictions. They concluded that a coil–stretch transition was responsible for the dilatant behavior observed, and that the critical shear rate required was of the order of 10 times the reciprocal of the Rouse relaxation time. Perhaps the most extensive studies have been those of Haas and co-workers (25, 26, 49). They have explored the critical dilatant behavior on flow through porous media and pursued the hypothesis that the phenomenon is primarily due to a coil–stretch transition beyond a critical deformation rate. They attempted a semiquantitative description based upon the dependence of the lowest order relaxation time of the random coil upon polymer type, molecular weight, solvent quality, and ionic environment.

Figure 18 illustrates the pronounced effect of the presence of counterions in HPAA. In pure water as a solvent, the flow resistance enhancement occurs at a very low flow rate. As the ionic strength is increased, the strain rate at which the dramatic enhancement in flow resistance occurs is markedly increased until beyond about 0.5 M, where no further effect occurs. The magnitude of the effect, however, remains approximately constant. The shear viscosity is greatly reduced by the increase in ionic strength. This effect is attributed to a progressive collapse of the HPAA coils because of counterion screening and results in a reduction in the conformational relaxation time and a consequent increase in the strain rate required to produce a coil–stretch transition.

As their solutions approach the θ state, Haas and co-workers (25, 26, 49) observe a more sharply critical transition with a shorter apparent relaxation time, which they ascribe to the Zimm relaxation time in the limit of hydrodynamic screening. Figure 19 shows the flow resistance as a function of Reynolds number for a range of concentrations. They identify the condition
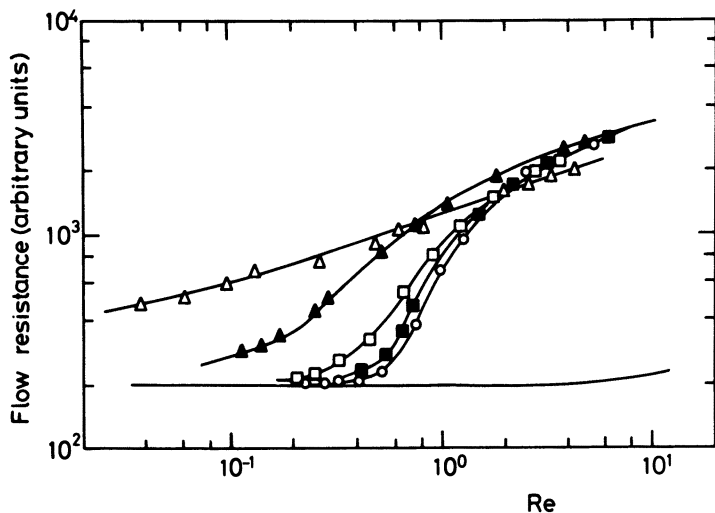
Figure 18. Influence of the ionic strength I_s of the solvent (NaCl addition) on the flow resistance factor for solutions of HPAA (30.5% hydrolysis, $\overline{M}_v$ 8.7 × 10^6). NaCl M: △, 0.00; ▲, 0.05; □, 0.20; ■, 0.5; and ○, 2.00. (After ref. 51.)
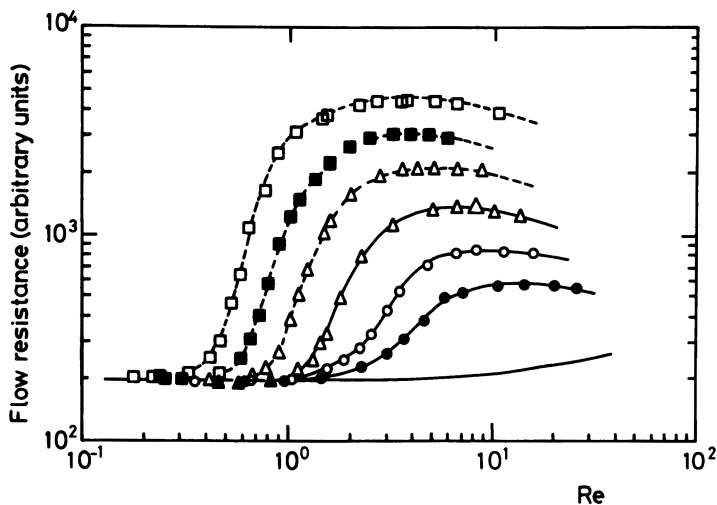
Figure 19. Flow resistance vs. Reynolds number (Re) as a function of polymer concentration (ppm) for solutions of PAA in 0.5 M NaCl ($\overline{M}_w$ 18 × 10^6): □, 100; ■, 50; △, 25; ▲, 12; ○, 6; and ●, 3. The solid line without points refers to the behavior of a Newtonian fluid. (After ref. 21.)

$C^*[\eta] = 0.07$ as the boundary between the dilute and semidilute regions (25, 49).

During flow in the dilatant region, Haas and co-workers observed accompanying degradation of the molecules and associated reduction in the degree of viscosity enhancement (Figure 20). Typically they found that such degradation is not restricted to the high molecular weight components but occurs across a broad range of molecular weights for which the extension condition is satisfied.

More recently some of the extensional flow dilatant effect has been associated with aggregation and entanglements in the solution (50, 51).

In this section we discuss the application of our elongational flow techniques to polymer solutions (i.e., high molecular weight hydrolyzed polyacrylamides in brine) widely used in pore and capillary flow experiments. By observing the flow-induced birefringence, we can determine whether dramatic increases in flow resistance (monitored simultaneously) are due to the stretching out of isolated molecules or of overlapping chains. Even though we are confined to our specific technique for creating model elongational flow fields, our conclusions are pertinent to inhomogeneous flow fields with persistently extensional components in general.

Two partially hydrolyzed polyacrylamide samples were used. The first one, manufactured by Aldrich, has a broad molecular weight distribution and $\overline{M}_w > 5 \times 10^6$. The second one, manufactured by BDH, is also supposed to have $\overline{M}_w > 5 \times 10^6$. The degree of hydrolysis of both samples was
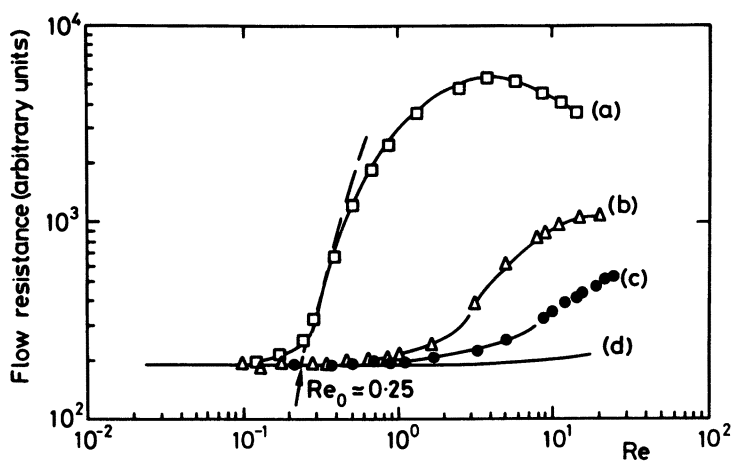
Figure 20. Flow resistance vs. Reynolds number (Re) for a PAA copolymer of ultrahigh molecular weight ($\overline{M}_w$ 27 × 10⁶) in 0.5 M NaCl: a, first run; b, second run after forcing the solution through the porous medium at Re = 15; c, third run after forcing the solution through at Re = 20; d, Newtonian fluid. The onset Reynolds number where the non-Newtonian effect sets in (Re₀) is indicated for curve a. (After ref. 22.)

estimated by IR and found to be ~7% for the Aldrich and ~16% for the BDH. Both $\overline{M}_w$ values are as quoted by the manufacturers.

The initial solvent used was freshly distilled and additionally deionized water. HPAA is known to be difficult to solubilize (*11, 52*). Solutions were, therefore, prepared with very slow stirring, allowing 48 h to ensure complete dissolution of the HPAA.

The Behavior of HPAA as a Function of Ionic Environment.
The first set of experiments examined the behavior of the HPAA polymers in the high ionic strength limit. We used throughout 0.5 M NaCl solutions. Our experience showed that higher ionic strengths had no further effect (discussed later), a result in agreement with previous works using similar polymers.

As the strain rate is increased in a semidilute solution, the first observation is of a narrow localized line of highly stretched molecules. This line is visible both by birefringence and scattered light observations. Figure 21a shows an example of the birefringence line at $\dot{\epsilon}_c$. At higher strain rates the line, observed by both birefringence and light scattering, progressively broadens and develops into a pipe at $\dot{\epsilon}_p$ (Figure 21b).

At even higher strain rates (beyond $\dot{\epsilon}_p$), the pipe structure breaks down, and the flow becomes unstable as visualized by light scattered by tracer particles. This instability signals the onset of the flare behavior. The associated delocalization of birefringence (as in Figure 6b) can be observed, but the signal is now very weak because of the low polarizability of HPAA. This sequence of events for the collapsed HPAA molecule resembles closely the behavior of other highly flexible molecules such as PEO and a-PS.

All these phenomena depend upon concentration and strain rate. Figure 22 shows a "phase-diagram" illustrating the observed behavior. At all concentrations and low strain rates the molecules exist in a coil-like state. At higher strain rates (above $\dot{\epsilon}_c$), the molecule undergoes a coil–stretch transition. $\dot{\epsilon}_c$ is a slow function of concentration, reflecting the slightly increased viscosity of the solution. For concentration greater than 0.05% at higher strain rates ($\dot{\epsilon}_p$), the pipe appears, followed at strain rates greater than $\dot{\epsilon}_n$ by flare behavior. $\dot{\epsilon}_p$ and $\dot{\epsilon}_n$ are both strong functions of concentration, rapidly increasing to the maximum attainable strain rates as the concentration is reduced toward C^+_n.

Figure 23 shows the pressure drop across the jets (ΔP_2) as a function of strain rate for the Aldrich HPAA (0.5 M NaCl) for a range of concentrations. At each concentration, when the strain rate exceeds $\dot{\epsilon}_n$ (i.e., the system flares), there is a corresponding enormous increase in flow-resistance compared with deionized water (open circles) and to polymer solution below C^+_n (curve f).

The HPAA molecule can be considered as a polyelectrolyte. As already discussed, in the presence of excess counterions, the polyelectrolyte behavior
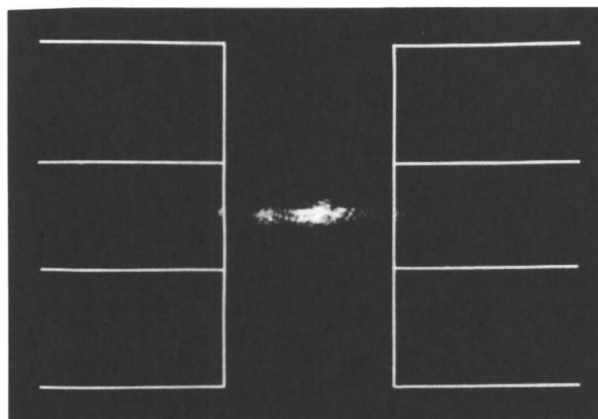
(a)
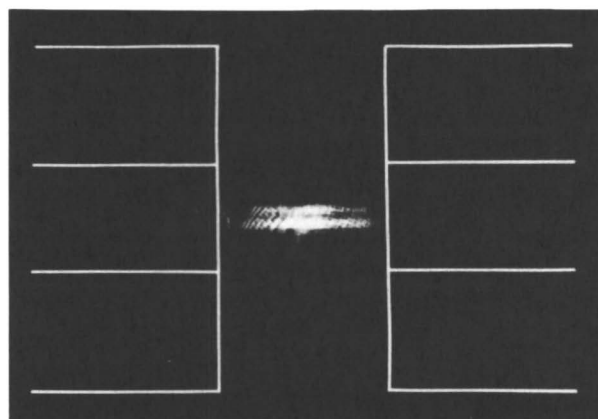
(b)

Figure 21. a, A birefringent line between the jets for a 0.15% Aldrich HPAA–deionized water solution, $\dot{\epsilon} = 1000\ s^{-1}$ ($\dot{\epsilon} \geq \dot{\epsilon}_p$). b, A birefringent line between the jets for a 0.15% Aldrich HPAA–deionized water solution, $\dot{\epsilon} = 450\ s^{-1}$ ($\dot{\epsilon} \geq \dot{\epsilon}_c$).

is masked, and the molecule behaves as a flexible coil, the conformation of which depends on solvent quality, and the extensional flow behavior can be explained by comparison with nonionic flexible molecules. In deionized water the coil is expected to be highly expanded (20), and this expansion dramatically affects its extensional flow behavior.

The behavior of HPAA in deionized water is indeed strikingly different. Figure 24 presents the flow resistance data as a function of strain rate and ionic strength for the BDH polymer. In deionized water (curve b), the flow
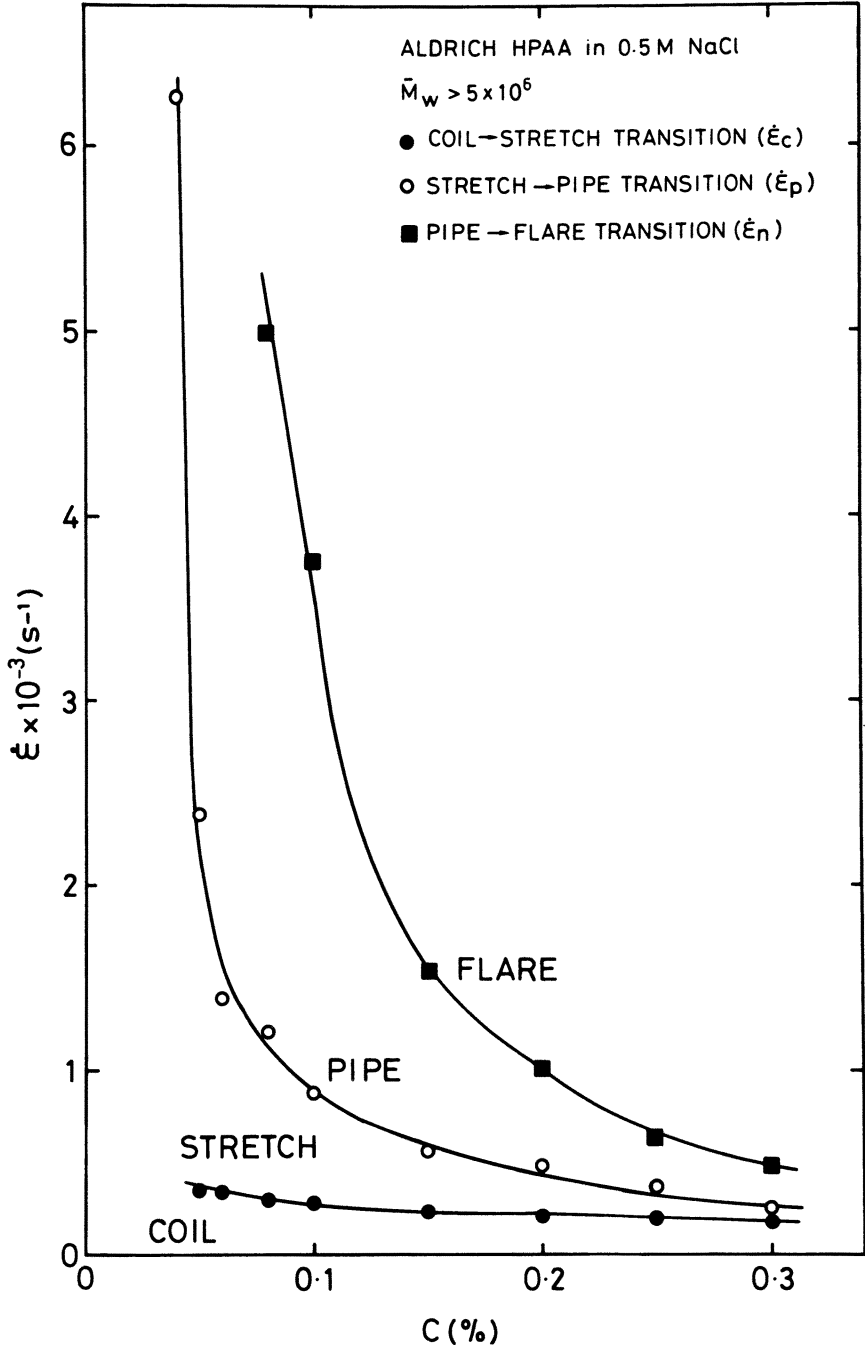
Figure 22. A "phase diagram" of the development of connectivity as a function of strain rate and concentration (Aldrich HPAA in 0.5 M NaCl solutions).
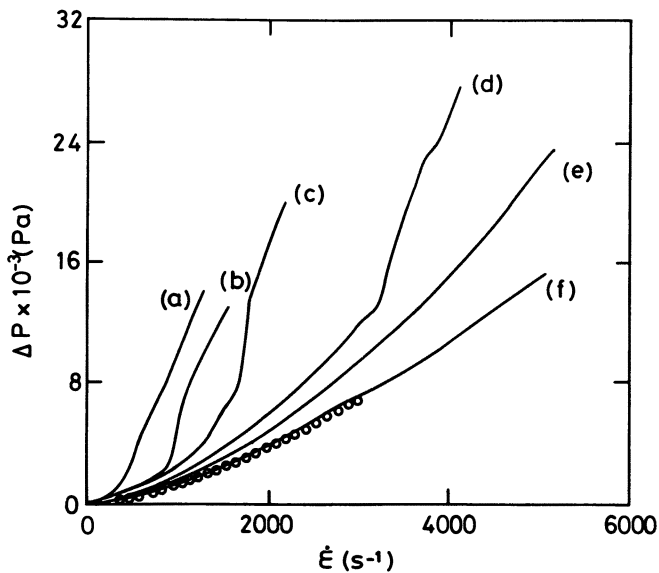
Figure 23. Pressure drops across the jets vs. $\dot{\epsilon}$ for the Aldrich HPAA in 0.5 M NaCl solutions at a, 0.3%; b, 0.2%; c, 0.15%; d, 0.1%; e, 0.06%; and f, 0.01%. Open circles are for deionized water.
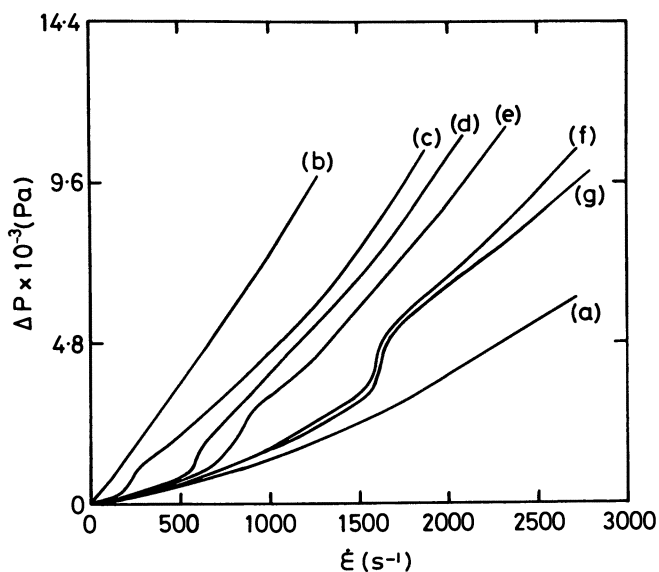
Figure 24. Pressure drop across the jets vs. $\dot{\epsilon}$ for a, deionized water and b–g, a 0.005% BDH HPAA in NaCl solution of molarity b, 0; c, 0.05; d, 0.1; e, 0.15; f, 0.3; and g, 0.5.

resistance of the polymer solution is much higher than deionized water alone (curve a) from the lowest strain rates (i.e., there is no apparent criticality in the onset of flow resistance). Also, the flow is always unstable; a laminar flow field as in Figure 1b is never observed even at the lowest strain rates. Reruns of curve b exhibit progressive reduction in pressure drop, indicative of degradation. All these observations suggest that this solution is always in the flare state; indeed, in HPAA concentration above 400 ppm, this behavior could be visually identified as flare from birefringence observations.

In the presence of salt, the flow resistance enhancement occurs only above a critical strain rate that progressively increases with the salt concentration. Beyond 0.3 M, no further changes were observed (Figure 24, curves c–g).

The effective elongational viscosity η_e' is depicted in Figure 25. The horizontal line for the water corresponds to a constant Newtonian type behavior. The solution in deionized water (open circles) shows a greatly increased low strain rate elongational viscosity gradually increasing with strain rate, corresponding to flare type behavior from the lowest strain rates. For the 0.5 M solution (filled circles) the low strain rate viscosity is indistinguishable from water. Beyond 500 s^{-1}, however, it becomes strongly non-Newtonian, rising through a maximum then progressively increasing toward the value of the solution in deionized water.

The peak in η_e' is known from birefringence, flow-field, and light-scattering observations to correspond to the highest $\dot{\epsilon}$ for which a stagnation
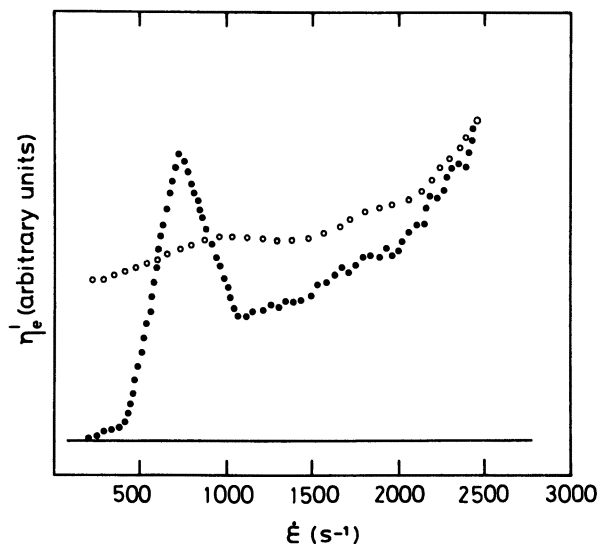
Figure 25. η_e' vs. $\dot{\epsilon}$ for ○, 0.01% BDH HPAA–deionized water solution; ●, 0.01% BDH HPAA in 0.5 M NaCl solution; and —, deionized water.

point type flow is maintained. At higher strain rates the solution flares, and the effective elongational viscosity drops. This fall in η_e' is due to the loss of the stagnation point, which means that the solution no longer needs to achieve extremely high strains during the opposed jet flow. A peak in the effective viscosity (the gradient of flow resistance versus strain rate) is also implicit in earlier data (Figures 18–20). This peak is not the expectation for a coil–stretch transition in a truly dilute solution.

The behavior of the HPAA molecule is sensitive not only to the presence of salt but also to the solution pH. As prepared in deionized water, all the solutions are slightly acid (pH 6). The addition of 0.1% by volume glacial acetic acid reduces the pH to 3.5. The effect of this pH reduction on the measured flow resistance is very similar to the effect of excess salt.

Figure 26 shows the BDH polymer in deionized water (curve b) and with the addition of 0.1% glacial acetic acid (curve c). This polymer, however, will flare in the acid environment beyond 400 s^{-1}, as it did in the excess salt environment. Curves c–f of Figure 26 illustrate successive runs of the same polymer solution. The progressive shift of $\dot{\epsilon}_n$ to higher values and the progressive reduction in the effectiveness of flow resistance are indicative of degradation. This degradation occurs only while the solution is flowing in the flare state ($\dot{\epsilon} > \dot{\epsilon}_n$), a behavior that is essentially the same as previously reported for PEO (in the section on the evolution of network).
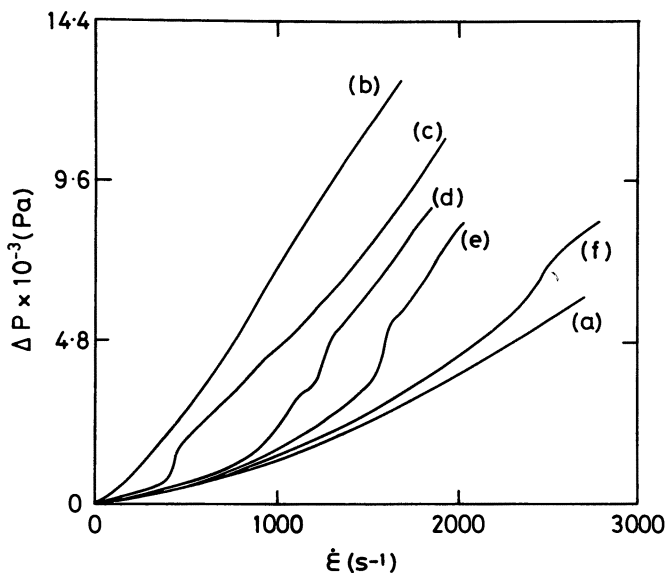
Figure 26. Pressure drops across the jets vs. $\dot{\epsilon}$ for a, deionized water; b, 0.02% BDH HPAA–deionized water solution; c, as b after addition of 0.1% glacial acetic acid; d, as c after two runs; e, as c after four runs; f, as c after six runs.

HPAA in Pore Flow. The preceding findings lead us to reinterpret results from porous media and capillary entrance flow. Strong non-Newtonian effects have previously been attributed to the increase in extensional viscosity associated with the coil–stretch transition, occurring when the strain rate exceeds the reciprocal of the lowest order conformational relaxation time (47–49).

This approach presents two problems. First, these polymers are invariably highly polydisperse, and polydispersity would result in a wide range of relaxation times ($\tau \propto M^{1.5}$). Further, the effective pore radius distribution is large (49). Together these effects should produce a rather gradual onset of increased flow resistance when $\dot{\epsilon}$ increases beyond $\dot{\epsilon}_c$, but a gradual onset is not the case. The observed onset of flow resistance enhancement is very sudden (*see* Figures 18–20).

Second, the strain required to stretch out a high molecular weight polymer into its nonlinear region is typically 200 (6). In capillary entrance experiments, however, the fluid strain is often quite small (≤ 25) (24). This small fluid strain does not apparently prevent the observation of the phenomenon of flow-resistance enhancement. The primary effect observed corresponds to the transient network flare behavior, and the evidence for this conclusion is as follows.

The visually observed coil–stretch transition does not correspond to pronounced viscosity effects such as seen in refs. 4–6 and 47–49). Such effects are seen in our experiments, but are always associated with the flare.

The degradation that is always observed in the flare state (but not in the stretch state) parallels that of Figure 20, and has been reported to occur in all cases where flow resistance is encountered (26). Further, degradation is not restricted to the largest molecules, as would be the expectations for stretched molecules in isolation at $\dot{\epsilon} \geq \dot{\epsilon}_c$ (13), but occurs in all molecular weight ranges.

The flow resistance, as measured in our experiments, may increase apparently indefinitely beyond $\dot{\epsilon}_n$ (*see* Figures 23 and 24). This result is in contrast to the effects seen in pore-flow experiments (typically Figure 19) where the flow resistance levels off, and may even reduce at high strain rates. This continuing rise is associated with new, previously unstretched molecules entering the flow field, which are then broken for the first time by flow.

The dependence of our flow-resistance anomalies for HPAA upon salt concentration (Figure 24), is strikingly similar to the salt dependence of pore-flow viscosity enhancement (Figure 18). The critical onset strain rate from our experiments varies in the same way as the critical onset Reynolds number in pore flow. In both experiments no further dependence on salt concentration is observed beyond 0.5 M. Further, in pure water, both experiments show non-Newtonian behavior (in our case identifiable as flare) even at the lowest flow rates.

Monodisperse Polymer Behavior

All the previous systems were polydisperse in nature, so that the coil–stretch transition was broad (because the relaxation time depends upon molecular weight). Also, only a part of the molecular weight distribution (the longest molecules) becomes stretched by the flow. It therefore proved impossible to determine the dependence of the coil–stretch or interaction behavior upon molecular weight. For these reasons, we examine the behavior of a model system, monodisperse atactic polystyrene (a-PS) in the θ solvent decahydronaphthalene. We will explore separately, both by assessment of molecular strain and macrorheology, the onset of interaction behavior, particularly as a function of molecular weight, and the associated flow-induced degradation.

To determine an overlap concentration, we examined the viscometric behavior of solutions of a-PS in decahydronaphthalene as a function of $\dot{\epsilon}$ and concentration. Figure 27 shows results for a 4×10^6 $\overline{M}_w$ sample. Curve b shows a typical dilute behavior (as in Figure 5) where the extension of isolated molecules determines the higher η_e' compared with the solvent (curve a). As the concentration is increased, the dilatant non-Newtonian behavior is progressively developed and shifted to lower strain rates. Simple visual inspection shows a sudden marked change in dilatancy, both in character and degree for concentrations greater than 0.25% (curve c).

Nevertheless, a method to quantify this non-Newtonian effect was needed. The method we have adopted is as follows. The solvent contributions
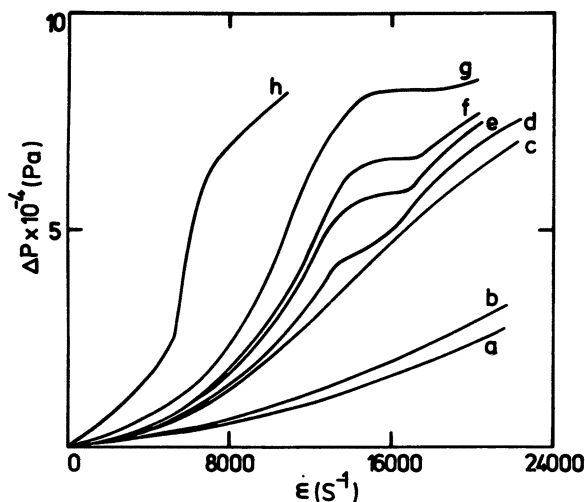
Figure 27. Pressure drop across the jets vs. strain rate for a, decahydronaphthalene; and solutions of a-PS in decahydronaphthalene at the following concentrations: b, 0.04%; c, 0.25%; d, 0.30%; e, 0.35%; f, 0.40%; g, 0.50%; and h, 1.00%.

(curve a) are subtracted from all the polymer curves to highlight the polymer contribution only. Subsequently, the curves are differentiated to obtain η_e' as in Figure 28. Only the first part of each curve is shown (including the maximum). As observed in flow visualization experiments, only the initial rise in in η_e' up to the maximum corresponds to well-behaved stagnation point flow. Therefore, the maximum value of the η_e' curve was used to characterize the progressive development of dilatancy with concentration. This peak value was always reproducible and corresponds to a well-defined flow field, with Reynolds number always lower than 1000.

Figure 29 shows how the $\eta_{e\,max}'$ increases linearly with concentration. By extrapolating to zero, a value can readily be calculated below which this excess dilatancy is not observed. This critical extrapolated value of concentration is C^+. Below C^+ the behavior is essentially that of a dilute solution, but above C^+ the value of η_e' cannot be accounted for on the basis of extension of isolated molecules.

In the section on the evolution of network, we described the visual development of strain patterns in the flow of interacting PEO solutions (Figure 10) leading to fully developed flow instability (flare). Similar effects can be found in well-characterized monodisperse a-PS, as shown in Figure 30, for a $7.7 \times 10^6\,\overline{M}_w$ a-PS dissolved in decahydronaphthalene (0.35%) and its corresponding ΔP vs. $\dot{\epsilon}$ trace (Figure 27). Complex dilatant effects can be observed (curve b) when compared with pure solvent (curve a) and with dilute solutions (Figure 5).
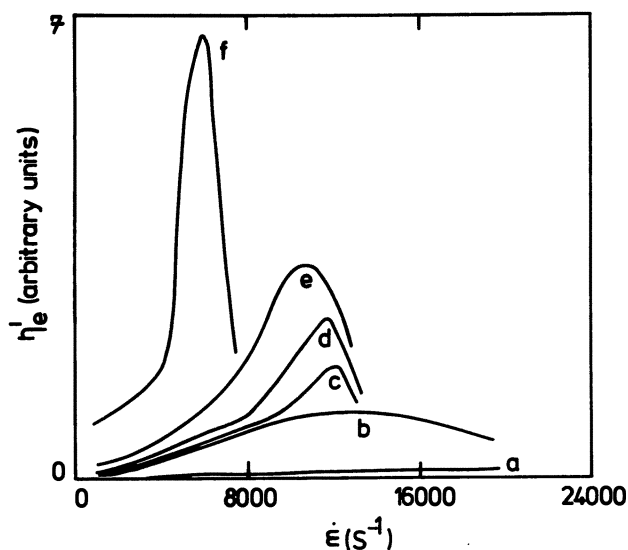
Figure 28. Effective elongational viscosity vs. $\dot{\epsilon}$ for solutions of a-PS in deca-hydronaphthalene at the following concentrations: a, 0.04%; b, 0.25%; c, 0.30%; d, 0.35%; e, 0.50%; and f, 1.00%.
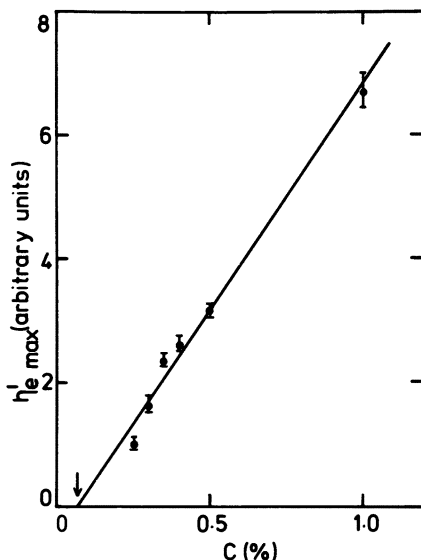
Figure 29. Maximum value of effective elongational viscosity vs. solution concentration. The extrapolated value of $C^+ \sim 0.064\%$ is indicated by an arrow (a-PS–decahydronaphthalene, $\overline{M}_w$ 4×10^6).

Greater rheological effects will be a consequence of greater molecular effects. Such molecular effects are directly mapped by the observation of strain patterns. The monodisperse a-PS in semidilute solution apparently is more difficult to extend than similar long-chain flexible, but polydisperse, polymers like PEO and HPAA also in semidilute solution. Thus, the monodisperse material shows large viscometric effects well below the flare condition where long-range mechanical connectivity is to be expected (with a concomitant delocalization of the birefringence and an unstable velocity profile). A comparison of semidilute solutions of a-PS with those of PEO and HPAA cannot be easily established in terms of polydispersity index only. Other important factors must be considered: solvent quality, chain length, chemical structure, etc. Nevertheless, polymers as disparate as PEO and HPAA behaved so similarly that it is attractive to generalize the behavior of polydisperse systems. This monodisperse system apparently does not fall into line with such generalizations, and the dispersivity of a system is an important factor in determining its behavior. A crucial test of the validity of our interpretation in terms of a transient network is to examine how the value of C^+ changes with molecular weight.

Repeating the procedure of Figures 27–29 for another five fractions (described in Table I), qualitatively the same behavior was observed, and this observation enabled the molecular weight dependence of C^+ to be found. Figure 31 shows a plot of log C^+ vs. log $\overline{M}_w$, which yields a straight

(a)   (b)

(c)   (d)

(e)   (f)

(g)   (h)
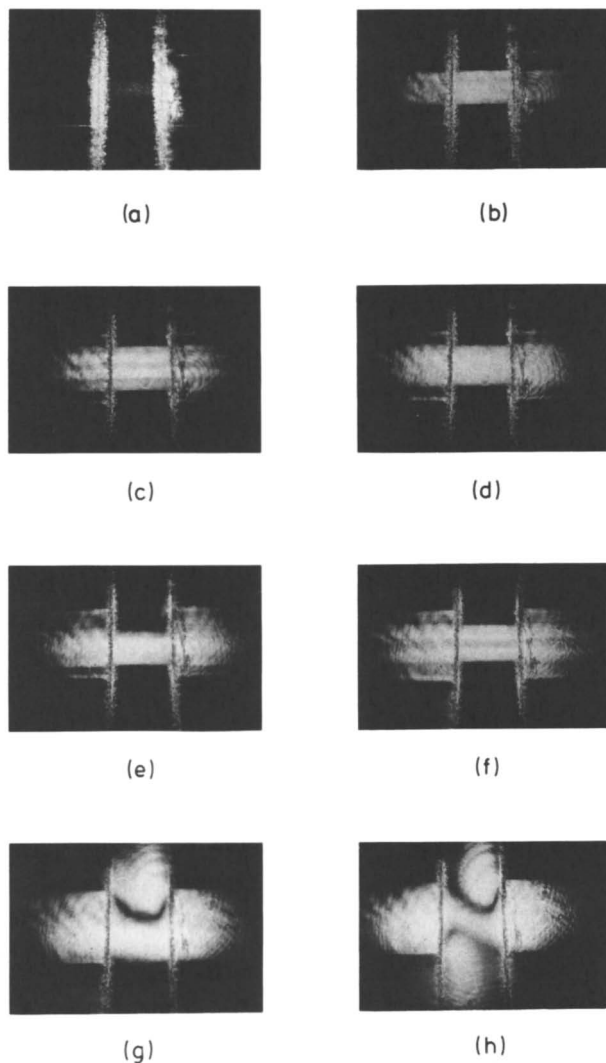
Figure 30. Stages of development of connectivity as the strain rate is increased. The strain rate values (s^{-1}) for this 0.35% solution of a-PS in decahydronaphthalene ($\overline{M}_w$ 7.7 × 10^6) are a, 750; b, 3,000; c, 3,800; d, 4,500; e, 5,500; f, 9,000; g, 10,000; and h, 11,000.

line so that $C^+ \propto M^a$, a being -0.55 ± 0.1. This result is in line with expectations of $a = -0.5$ for a pairwise interaction of coils in a θ solvent.

Our results support our previous contention that the non-Newtonian phenomena are genuinely due to intermolecular interactions.

Table I. Value of $\overline{M}_w$ and Polydispersity of a-PS Samples

$\overline{M} \times 10^{-6}$	$\overline{M}_w/\overline{M}_n$
2.75	1.06
4.00	1.04
4.40	1.06
7.70	1.2
8.00	1.10
12.25	1.30
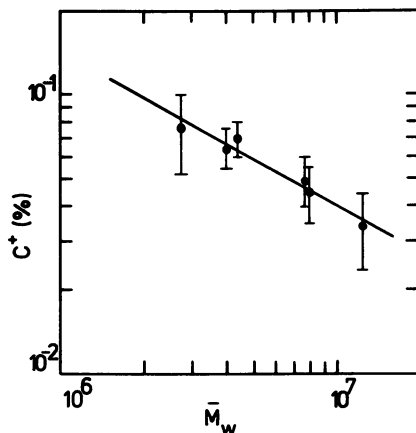
Figure 31. log C^+ vs. log $\overline{M}_w$ for a-PS–decahydronaphthalene, slope = -0.55 ± 0.1.

Degradation of Interacting Molecules

The scission of isolated molecules in extensional flow fields has been the subject of a number of investigations (*11–15, 53*). The scission occurs very precisely at the center of the polymer chain and at strain rates that broadly correspond to expectations for extended bead-rod models and covalent C–C bonds.

Marked differences were anticipated in the degradation behavior of stretched overlapping molecules. These differences were qualitatively verified for polydisperse PEO and HPAA, where scission rates in unstable flow greatly exceeded corresponding scission rates in dilute solution (*32, 33*). In this section we examine the degradation behavior of closely monodisperse a-PS semidilute solutions. At this stage of the study we are relying on the onset and extent of irreversibility in I and ΔP vs. $\dot\epsilon$ behavior as indicators of chain scission. A preliminary attempt was made to study, under controlled conditions, the degradation behavior of a semidilute solution of a-PS (0.35%, $\overline{M}_w$ 7.7 × 10^6); the results are shown in Figure 32 and Table II. The procedure involved running the solution at a constant value of $\dot\epsilon$ (five times)
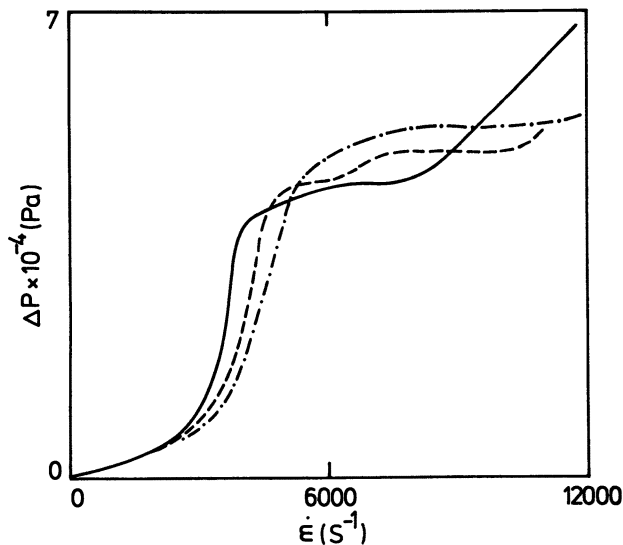
*Figure 32. Pressure drop across the jets vs. ε̇ for a 0.35% a-PS–decahydro-naphthalene solution (M̄*ᵥᵥ* 7.7 × 10⁶). The solid line corresponds to the fresh solution, and the other two lines show degradation stages (see Table II).*

Table II. Degradation Conditions Applied to a 0.35% a-PS–Decahydronaphthalene Solution, $\overline{M}_w$ 7.7 × 10⁶

ε̇ During Degradation (s^{-1})	Shift Factor (arbitrary units)	Symbol Used in Figure 32
0	0	—
1,500	0	none
3,000	0	none
3,800	1	none
3,900	2.5	none
4,100	4.0	none
4,500	5.5	- -
5,000	6.5	none
6,500	7.5	none
9,000	9.0	none
16,000	10.0	-.-.

and then repeating the ΔP vs. ε̇ curve to check for degradation. The sequence of experiments performed in the original solutions (solid line) are presented in Table II, where next to the value of the constant strain rate used is a shift factor that indicates how much the ΔP vs. ε̇ curve deviates from the original data, and therefore qualitatively gives an estimate of the degree of degradation. The same solution was used throughout the 50 runs involved in the experiment.

Table II shows that the degradation started only after running the so-

lution at 3800 s^{-1}, that is, after the breakdown of the flow field (Figure 30). Although this degradation was occurring below the flare condition, the shift in the curve was very small, so small that the degraded curve is not shown in Figure 32 in order to preserve clarity. Only two stages in the degradation process are shown, after degrading runs at 4500 and 16,000 s^{-1} (where a full flare was developed). The onset of degradation is sudden (at 3800 s^{-1}), but the rate of degradation does not appear to increase much for high values of strain rate. In terms of absolute rate of degradation, however, compared with PEO and HPAA (e.g., Figure 17 in ref. 28 and Figure 19 in ref. 29), the a-PS solutions were more resistant to flow-induced degradation.

This difference in degradation behavior can also be attributed to the difference in the process of development of the transient network. As shown in Figure 30 in the case of monodisperse a-PS, the initially deformable and localized network strengthens with increasing $\dot{\epsilon}$ in such a way that it induces a breakdown of the flow field instead of itself being broken by the stagnation point flow. Again, as discussed in the section on the evolution of network, the polydispersity may play a vital role in the transient network behavior. For PEO or HPAA, the longest molecules of the distribution of molecular weight play a dominant role in the formation of a transient network. For monodisperse a-PS, the majority of the molecules can participate in the formation of interactions: the much greater strength of the resulting network is attributed to this participation. This distinction between mono- and poly-dispersity is fundamental. The behavior of a polydisperse sample as regards elongational flow-induced network formation and consequent chain breakage does not appear to be a simple additive function of its monodisperse constituents.

Conclusions

We have illustrated the many ways in which elongational flow behavior can provide novel information about the behavior of macromolecules. Special emphasis has been given to rheological changes associated with extensional flow fields.

As anticipated by a number of theories, the elongational viscosity increases significantly when the isolated molecule undergoes a coil–stretch transition in dilute solution.

As concentration is increased, the elongational flow behavior reveals the important role of molecular interactions, which in strong flow fields can occur at much lower concentrations than generally realized. These interactions are interpreted as the development of transient networks; such networks often are responsible for extreme dilatant behavior in extensional flow. Many anomalous non-Newtonian effects reported previously in flows that contain appreciable elongational components parallel these phenomena, particularly pore flow, and are themselves due to the existence of transient networks.

Elongational viscometry provides a method for assessing the overlap concentration, which is proportional to $M^{-0.55}$, in agreement with our hypothesis that the non-Newtonian effects detected are due to polymer interactions.

Degradation during flow of entangled monodisperse solutions is quite different in character and degree from degradation of either isolated or entangled polydisperse molecules. Polydispersity may play an important role in the development of transient networks and their subsequent extensibility.

Acknowledgments

References

1. Odell, J. A.; Keller, A.; Miles, M. J. *Polymer* **1985**, *26*, 1219.
2. Chow, A.; Keller, A.; Müller, A. J.; Odell, J. A. *Macromolecules* **1988**, *1*.
3. Pope, D. P.; Keller, A. *Colloid Polym. Sci.* **1978**, *256*, 751.
4. Farrell, C. J.; Keller, A.; Miles, M. J.; Pope, D. P. *Polymer* **1980**, *21*, 129.
5. Keller, A.; Odell, J. A. *Colloid Polym. Sci.* **1985**, *263*, 181.
6. Odell, J. A.; *Polymer Flow Interactions*; American Institute of Physics, La Jolla Institute: La Jolla, CA, 1985, p 33.
7. Peterlin, A. *J. Polym. Sci. B* **1966**, *4*, 287.
8. De Gennes, P. G. *J. Chem. Phys.* **1974**, *60*, 5030.
9. Brestkin, Yu V.; Saddikov, I. S.; Agranova, S. A.; Baranov, V. G.; Frenkel, S. *Polym. Bull.* **1986**, *15*, 147.
10. Atkins, E. D. T.; Attwool, P. T.; Miles, M. J.; to be published.
11. Müller, A. J.; Odell, J. A.; Keller, A. *Polym. Commun.*, accepted, 1989.
12. Odell, J. A.; Keller, A.; Miles, M. J. *Polym. Commun.* **1983**, *24*, 7.
13. Odell, J. A.; Keller, A. *J. Polym. Sci., Polym. Phys. Ed.* **1986**, *24*, 1889.
14. Odell, J. A.; Keller, A.; Rabin, Y. *J. Chem. Phys.* **1988**, *88*, 4022.
15. Nguyen, T. Q.; Kausch, H. H. *J. Non-Newtonian Fluid Mech.* **1988**, *30*, 125.
16. Rabin, Y. *J. Chem. Phys.* **1987**, *86*, 5215.
17. Ryskin, G. *J. Fluid Mech.* **1987**, *178*, 423.
18. Odell, J. A.; Atkins, E. D. T.; Keller, A. *J. Polym. Sci., Polym. Lett. Ed.* **1983**, *21*, 289.
19. Odell, J. A.; Keller, A.; Atkins, E. D. T. *Macromolecules* **1985**, *18*, 1443.
20. Miles, M. J.; Tanaka, K.; Keller, A. *Polymer* **1983**, *24*, 1081.
21. Bird, R. B.; Hassager, O.; Armstrong, R. C.; Curtiss, C. F. *Dynamics of Polymeric Liquids*; Wiley: New York, 1977, Vol. 2.
22. Ferry, J. D. *Viscoelastic Properties of Polymers*; Wiley: New York, 1980, 3rd ed.
23. MacWilliams, D. C.; Rogers, J. H.; West, T. J. In *Polymer Science and Technology*; Bikales, N. B., Ed.; Plenum: New York, 1973, Vol. 2, p 105.
24. Chauveteau, G.; Moan, M.; Magueru, A. *J. Non-Newtonian Fluid Mech.* **1984**, *16*, 315.
25. Durst, F.; Haas, R.; Kaczmar, B. U.; *J. Appl. Polym. Sci.* **1981**, *26*, 3125.
26. Haas, R.; Kulicke, W. M. In *Proc. IUTAM Symposium: The Influence of Polymer*

Additives on Velocity and Temperature Fields; Gampert, B., Ed.; Springer: Berlin, p 119.

27. Hinch, E. J. *Phys. Fluids* 1977, *20*, 522.
28. Henyey, F. S.; Rabin, Y. *J. Chem. Phys.* 1985, *82*, 4362.
29. Warner, H. R., Jr. *Ind. Eng. Chem. Fundam.* 1972, *11*, 379.
30. Kramers, H. A. *Physica* 1944, *11*, 1.
31. Curtiss, C. F.; Byrd, R. B.; Hassager, O. *Adv. Chem. Phys.* 1976, *35*, 31.
32. Keller, A.; Müller, A. J.; Odell, J. A. *Prog. Colloid Polym. Sci.* 1987, *75*, 179.
33. Odell, J. A.; Müller, A. J.; Keller, A. *Polymer* 1988, *29*.
34. Mackley, M. R.; Keller, A. *Philos. Trans. R. Soc. London, Ser. A* 1975, *278*, 29.
35. Martin, J. E. *Macromolecules* 1984, *17*, 1279.
36. Leger, L.; Hervet, H.; Rondolez, F. *Macromolecules* 1981, *14*, 1732.
37. Cotton, J. P.; Nierlich, M.; Bove, R.; Daoud, M.; Farnoux, B.; Janninck, G.; Dupplesix, R.; Picot, C. J. *J. Chem. Phys.* 1976, *65*, 1101.
38. Flory, P. J. *Principles of Polymer Chemistry*; Cornell University: Ithaca, NY, 1966, 5th ed.
39. Tan, H.; Moet, A.; Hiltner, A.; Baer, E. *Macromolecules* 1983, *16*, 28.
40. Odell, J. A.; to be published.
41. Farinato, R. S., Abstract and Lecture, Bristol Conference, "Flexibility of Macromolecules in Solution," Institute of Physics, London, 1986.
42. Gardner, K.; Pike, E. R.; Miles, M. J.; Keller, A.; Tanaka, K. *Polymer* 1982, *23*, 1432.
43. Lyazid, A.; Scrivener, O.; Teitgen, R. In *Rheology*; Asterita, G.; Marrucci, G.; Nicolais, L., Eds., Plenum: New York, 1980; Vol. 2, p 141.
44. *Proc. IUTAM Symposium: The Influence of Polymer Additives on Velocity and Temperature Fields*; Gampert, B., Ed.; Springer: Berlin.
45. Lumley, J. L. *Ann. Rev. Fluid Mech.* 1969, *1*, 367–384.
46. Odell, J. A.; Tucker, I. M.; Ferry, M.; Müller, A. J., to be published.
47. Ouibrahim, A.; Fruman, D. H. *J. Non-Newtonian Fluid Mech.* 1980, *7*, 315.
48. Moan, M.; Chauveteau, G.; Choniem, S. *J. Non-Newtonian Fluid Mech.* 1979, *5*, 463.
49. Kulicke, W. M.; Haas, R. *Ind. Eng. Chem. Fundam.* 1984, *23*, 308; Haas, R.; Kulicke, W. M. *Ind. Eng. Chem. Fundam.* 1984, *23*, 316.
50. James, D. F.; McLaren, D. R. *J. Fluid Mech.* 1975, *70*, 733.
51. Christiansen, R. L.; Bird, R. B. *J. Non-Newtonian Fluid Mech.* 1978, *3*, 161.
52. Fuller, G. G.; Cathey, C. A.; Hubbard, B.; Zebrowski, B. E. *J. Rheology* 1987, *31*, 235.
53. Merrill, E. W.; Horn, A. F. *Polym. Commun.* 1984, *25*, 144.

Importance of Elongational Flows in the Performance of Water-Borne Formulations

Raymond H. Fernando, David J. Lundberg, and J. Edward Glass

Department of Polymers and Coatings, North Dakota State University, Fargo, ND 58105

Applications in which dynamic uniaxial elongational viscosities (DUEVs) have been important to the performance of water-borne formulations are discussed. The achievement of high viscosities at low shear rates with minimum mechanical degradation of the water-soluble polymer and with minimum viscoelastic effects in applications that involved converging flows are discussed. These two factors serve as driving forces for the acceptance of hydrophobically modified water-soluble polymers. Complexities arising from the combined contribution of shear and elongational deformations in applications and in their measurement are discussed in the final section.

DRAG-REDUCTION PHENOMENA WERE ACTIVELY INVESTIGATED in the 1960s to determine their relationship with the elongational behavior of fluids. Some doubt remains (1) as to the role of elongational viscosity in drag-reduction phenomena, but the early interest resulted in a variety of experimental techniques (2) for estimating the dynamic uniaxial elongational viscosity (DUEV) of synthetic water-soluble polymers. Earlier studies (2–5) provided the framework for delineating the importance of elongational viscosities in the performance of many formulations. These areas will be highlighted in this chapter along with the reasons why hydrophobically modified water-soluble polymers provide greater latitudes to formulators in many applications.

Most applications using dispersed systems (e.g., coatings, cosmetics, petroleum, and textiles) require high viscosities at low deformation rates to inhibit settling of the disperse phases and moderate-to-low viscosity at high rates to minimize the energy required during application. These properties can be attained by using high molecular weight polymeric thickeners. The use of these thickeners, however, imparts viscoelastic properties to the dispersions that detract from optimum performance during application. In formulations to be used over multiple stress cycles, the degradation of high molecular weight polymers results in a marked decrease in the low-shear-rate viscosities. Attempts can be made to overcome both of these limitations of high molecular weight polymers by using lower molecular weight, hydrophobically modified, water-soluble polymers. These associative polymers offer specific advantages in different applications, but greater mechanical stability and lower viscoelasticity in solutions with high viscosities at low shear rates (LSVs) comparable to higher molecular weight polymers are desired in all areas.

Mechanical Stability of Polymers

The instability of high molecular weight synthetic polymers was one of the considerations in pioneering the synthesis of the hydrophobically modified styrene–maleic acid copolymers (3). "An improved polymer system [that] would not degrade mechanically and [that] would retain [its] viscosity in the presence of electrolytes and heat was required" (4).

The mechanical stability of polymers was related to the polymer's conformation in some of the earlier drag-reduction studies. Above a critical stress, degradation was faster the more contracted and entangled the polymer's conformation (5–7). In petroleum applications the mechanical instability of synthetic relative to carbohydrate polymers was well-recognized. The relative stability problems (possibly related to DUEVs (8)) encountered in the use of high molecular weight hydrolyzed poly(acrylamide) (HPAM) led to the development of an inverse-emulsion polymerization technique (9). (Current research directions using this technique are discussed in Chapter 9.)

The solution conformation of a macromolecule under deformation, and therefore its stability, is not always predictable, particularly for carbohydrate polymers. This aspect of carbohydrate polymer stability has been investigated and related to the DUEVs of the aqueous solutions (10). Increasing entanglements at higher concentrations and higher shear deformations can also result in mechanical degradation (11).

Converging Flows

Extensional deformations are imposed on fluids when they undergo converging flows (e.g., roll, spray, and penetration of porous media), and the

elongational response of the fluid will play an important part in its behavior. Examples that shall be discussed include the roll application of trade-sale latex paints and water-reducible industrial coatings. Petroleum applications involving enhanced oil recovery and primary recovery areas such as drilling fluids are also considered. In spray applications, elongational viscosities are related to mechanical stability (as delineated in some of the studies just mentioned), to combustion efficiencies of coal–water slurries, and to sprayability in interior can coatings.

Roll Coating Applications. An example of a classical approach to high viscosities at low shear rates (LSVs) in disperse systems is illustrated (Figure 1) in the shear-thinning behavior of a vinyl–acrylic latex thickened with (hydroxyethyl)cellulose (HEC) of various molecular weights and with a poly(oxyethylene) of high molecular weight. The viscosity–shear rate profiles of the variable molecular weight HECs follow the melt viscosity trends observed by several investigators. Significant dissipation of the coating as spatter (Figure 2) is realized (12) when titanium dioxide and other ingredients commonly used in coatings formulations are added to this latex dispersion, and the higher molecular weight water-soluble polymers are used as thickeners. This phenomenon in a variety of commercial and experimental coatings did not correlate with any shear deformation response (e.g., shear
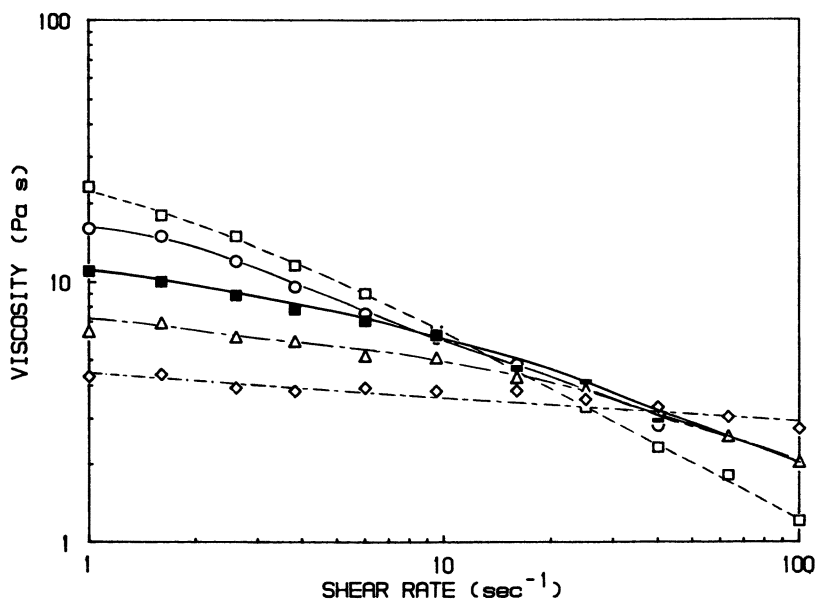
Figure 1. Vinyl acetate–acrylic latex variable aqueous thickener solutions. Key:
□, *MW HEC 800,000;* ○, *MW HEC 650,000;* △, *MW HEC 300,000;* ◇, *MW HEC 70,000;* ■, *MW POE 800,000.*
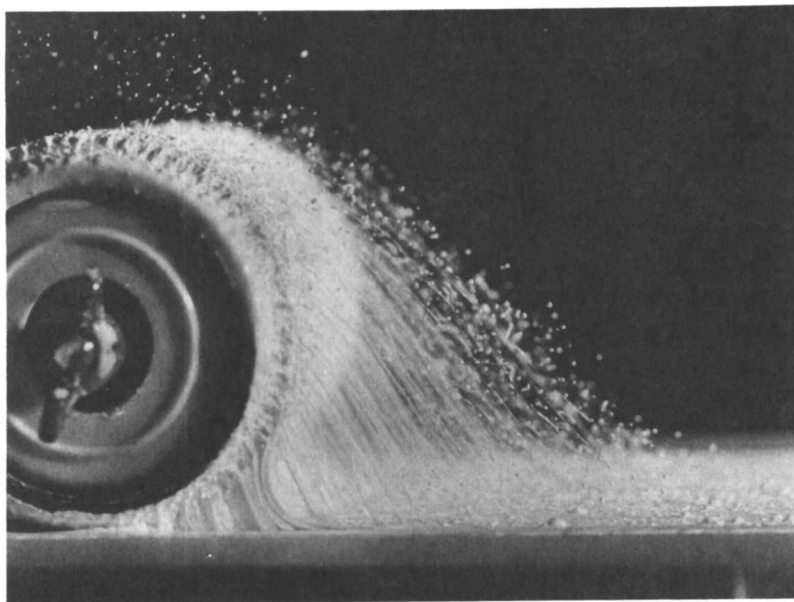
Figure 2. Spatter generation via fiber dissipation. Horizontal rollout: 37 ft/s.

thinning, thixotropy, storage or complex modulus, and first normal stress difference (13)). Cinematographic studies revealed that the flows were extensional in nature. When parallel components are used (e.g., an HEC steric-stabilized latex) and the molecular weight of a nonassociating thickener such as HEC is varied, the spatter behavior and extensional viscosity have been approximated by first normal stress difference (N_1) by using the Maxwell–Oldroyd equation (14).

Recent improvements in the sensitivity (15) of the vacuum-suction fiber-drawing technique for elongational viscosity measurements have permitted the evaluation of cellulose-thickened coatings with a small-particle latex (16). The data (Table I) indicate that the DUEV involves contributions not only from the thickener but also from the components of the formulation. On the basis of earlier observations (17), this contribution was assumed to arise from high-aspect ratio flocculents formed by the latex and pigment in extension.

Trade-sale coatings are applied at low peripheral velocities. Most industrial coatings (for paper, metal, or other substrates) are applied at high roll velocities (e.g., 300 vs. 2 ft/s). Lower viscosity, water-reducible coil coatings applied at greater roll velocities can exhibit finer fiber dissipations, and result in "misting". Such coatings applied to metal substrates (file cabinets, etc.) that were used in this study were provided by a commercial manufacturer. One coating exhibited little tendency to mist ("good"); the other exhibited a greater tendency to mist ("fair"). The rib sizes of these

Table I. Dynamic Uniaxial Extensional Viscosities and Shear Viscosities of Aqueous HEC Solutions and HEC-Thickened Trade-Sale Paints

Solution	$\overline{M}_v$ of HEC ($\times 10^5$)	Thickener Concentration (wt %)	Shear Viscosity (Pa · s)	DUEV (Pa · s)
Trade-sale paints				
80KU	7.0	0.72	0.29	1.10
105KU		1.14	0.52	5.35
Aqueous solution	9.5	1.00	0.71	1.22

NOTES: M_v is viscosity-average molecular weight. Deformation rate is 100 s^{-1}. The percent pigment to disperse component volume concentration is 35; the volume fraction of dispersed components is 32; the latex median particle size is 117 nm; the concentration of HEC is based on the aqueous phase.
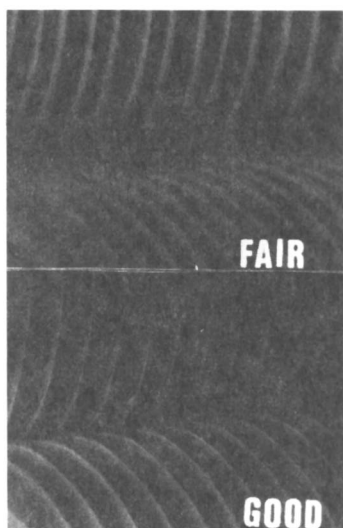
Figure 3. Comparison of ribbing in industrial coatings. "Good" paint (little misting), DUEV 0.1 Pa · s. "Fair" paint (adequate misting), DUEV 0.58 Pa · s.

unpigmented formulations are illustrated in Figure 3. The formulations with the greater DUEV exhibited a larger rib size in our studies and the greatest misting in industrial applications (*16*).

High molecular weight thickeners are not employed in water-reducible coatings. The trade-sale coating formulations studies discussed contained cellulose ethers as thickeners. Hydrophobic (e.g., $C_{16}H_{33}$-unit) modification of HEC will effect the higher LSVs realized with higher molecular weight HEC but with lower solution viscoelasticity. Our extensional viscosity studies of hydrophobically modified water-soluble polymers are now in a preliminary stage; lower N_1 values, which parallel, in homologous component formulations, lower spatter observations (*18*) in a comparative study (discussed in Chapter 18), were obtained with the hydrophobically modified HEC. Additional benefits associated with the use of associative thickeners in coatings when other structural features are present are discussed in Chapter 26.

Petroleum Applications. The relative drilling rates of clay, modified clay, and polymer-only thickened fluids were cited (*19*) and related (*20*) to their viscoelastic behavior through N_1 measurements. At that stage of our studies, there was insufficient sensitivity in the DUEV measurement procedure to quantify differences in elongational viscosities. In applications involving mobility control for improved recovery from "depleted" reservoirs (*21, 22*), there were differing opinions regarding the role of DUEVs in flow-through porous media. In studies that involved continuous converging flow sequences, Chauveteau (*22*) concluded that the relaxation time of the deformed polymer was increased, and therefore, the coil–stretch transition, which led to increased resistance factors (pressure differential measurements taken during core testing) occurred at a much lower deformation rate in continuously converging flows pattern (*see* Figures 14 and 15 in ref. 22).

Recently (*23*), comparison of elongational viscosity of an HPAM solution before and after passing through a glass bead pack at a high strain rate revealed an elongational viscosity drop from 13,300 to 339 cP, although the maximum resistance factor of the sheared HPAM decreased only 33% relative to the original solution. These studies were interpreted in light of other investigations (*24*) that concluded, for cones and wedges, that converging flow of a viscoelastic fluid with a high extensional viscosity–shear viscosity ratio could be approximately described as a core of fluid in a pure extensional flow that is lubricated by a thin layer of shear flow at the confining walls of the convergence. If a similar fluid flow distribution occurs in converging pore throats, the weak elongational viscosity dependence of flow resistance observed might be explained. The shear rate in a thin shear layer would be very high, although high extensional flows occur in the core at relatively low strain rates. In this case, the pressure drop would be dominated by shear flow even though the overall flow pattern is dictated by the high extensional viscosity–shear viscosity ratio (*23*).

Previous studies (*25*) revealed ways in which blending water-soluble polymers of different segmental rigidities can effect fluids that vary in DUEV characteristics while maintaining equivalent solution viscosities over a broad shear-rate range (Figure 4). Use of these polymer blend fluids permitted delineation of the role of elongational viscosities in the roll application of coating formulations. Similar blends were used to assess the role of DUEVs in mobility control (Figure 5). A proper analysis of the data would necessitate corrections for adsorption and degradation of the polymers in the core (*26*).

The following statement is made in the concluding sections of Chapter 26: "despite our lack of understanding of associative thickeners in coatings technology, these products have gained commercial acceptance." A classic parallel in the use of polymers in mobility control buffer applications exists. Xanthan gum was used successfully in pilot tests of the low-permeability (<40 mDaries) formation, Big Muddy Field, near Casper, WY (*27*). Just before production-scale flooding of this reservoir, the price of xanthan gum
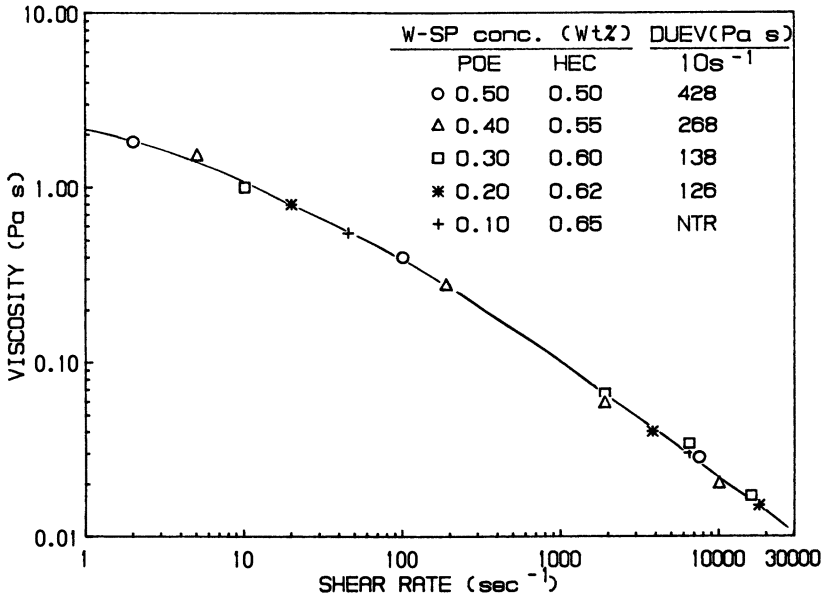
Figure 4. Shear viscosity profiles of variable-concentration (ppm) POE–HEC aqueous blends.
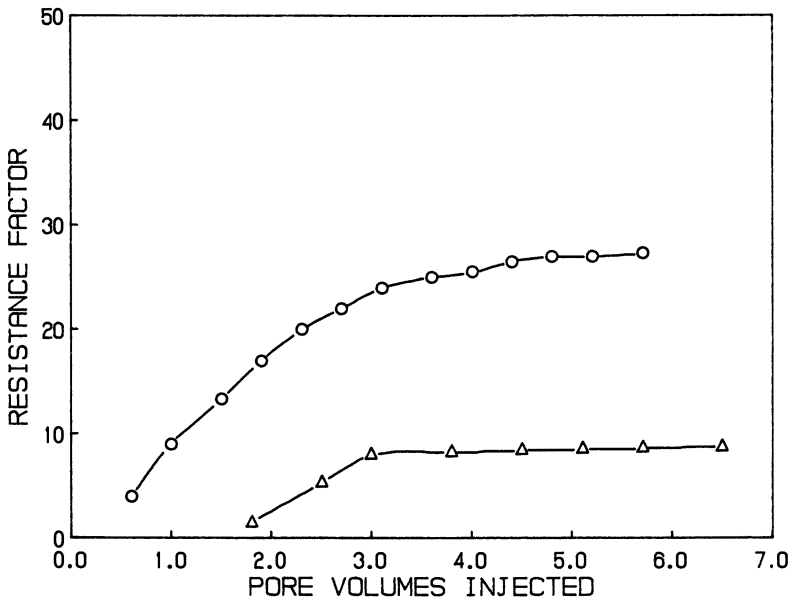
Figure 5. Dependence of resistance factor on number of pore volumes injected in 160-mD Berea core. Key: ○, 1000–4200-ppm POE–HEC blend; △, 500–3000-ppm POE–HEC blend.

increased. This increase led to a management decision to use HPAM. In-
jectivity problems were encountered in the initial phase of the full-scale
endeavor with a competitive HPAM, presumably because of this polymer's
elongational behavior (related to HPAM size and the relative pore-size dis-
tribution of the reservoir). Mechanical degradation of the synthetic polymer
before injection resolved the injectivity problem, and the ensuing flood,
albeit at a low frontal velocity, proceeded without other significant problems.

Spray Applications.   In sprays, atomization of the fluid is generally
the desired goal. The critical breakup length of the filament was described
over a decade ago by equation 1 in terms of a dimensionless breakup length
(28), $L/2a$, for HPAM-thickened fluids.

$$L/2a = C[\sqrt{We} + 3We/Re] \tag{1}$$

where a is the diameter of the fiber and C is the capillary number, and

$$We \text{ (Weber number)} = 2\rho aV^2/\sigma \tag{2}$$

$$Re \text{ (Reynolds number)} = 2\rho Va/\eta \tag{3}$$

ρ is density, V is the exit velocity, σ is surface tension, and η is viscosity.
In coatings formulations, density is determined by the amount of titanium
dioxide used. The surface tension is constant because an excess of formulation
surfactant is used, at least in water-borne latex coatings. This assumption
may not be valid over very short time periods because of surfactant diffusion
to the new surface. With this assumption, the remaining parameter that can
be controlled by variation in formulation components is the viscosity. When
ρ and σ are held constant, variations in spatter do not relate to the formu-
lation's shear viscosity. This observation led to examination of elongational
viscosities. An inverse relationship between the elongational viscosity of a
viscoelastic fluid and its mistability in spray application would be expected.

Coal–Water Fuels.   The following was extracted from a publication (29)
of a joint study arising from dialogue at the 1984 Philadelphia symposium
on water-soluble polymers.

> Stabilizers, dispersants, and particle size distributions can have
> tremendous impacts on the elongational rheology of coal–water
> fuels while minimally impacting the shear rheology. In particular,
> stabilizer structure and aspect ratios of the particles present in
> the slurry may exert profound influences on the atomization of

CWF [coal–water fuels] undetectable by shear rheological meas-
urements.... The rheology of slurries having unimodal particle
size distribution, similar coal loadings but different polymeric
stabilizers were investigated. The rheologies of the fuels at 1000
to 10,000 s⁻¹ were similar. Using the data at shear rates of 10–
100 s⁻¹, better atomization performance for slurry 1 would be
expected. Slurry 1 has a higher resistance to extensional defor-
mation than slurry 2 completely reversing the results found under
shear [Figure 6]. The slurry with the higher extensional viscosity
sprays poorly when compared to the slurry with a lower exten-
sional viscosity, despite having similar shear viscosities.

Water-Reducible Coatings.   Water-reducible coatings (*30*) are the pri-
mary materials used to coat the interiors of metal beverage containers. Their
application requires the formation of thin films produced by the atomization
of the coating to very fine droplets. The DUEV of the interior can coatings
could not be measured as received; however, correlation of the coating's
misting tendency with the reciprocal of the fluid's DUEVs was observed
when coatings of variable misting tendencies were blended with low con-
centrations (<100 ppm) of high molecular weight poly(oxyethylene) (POE).
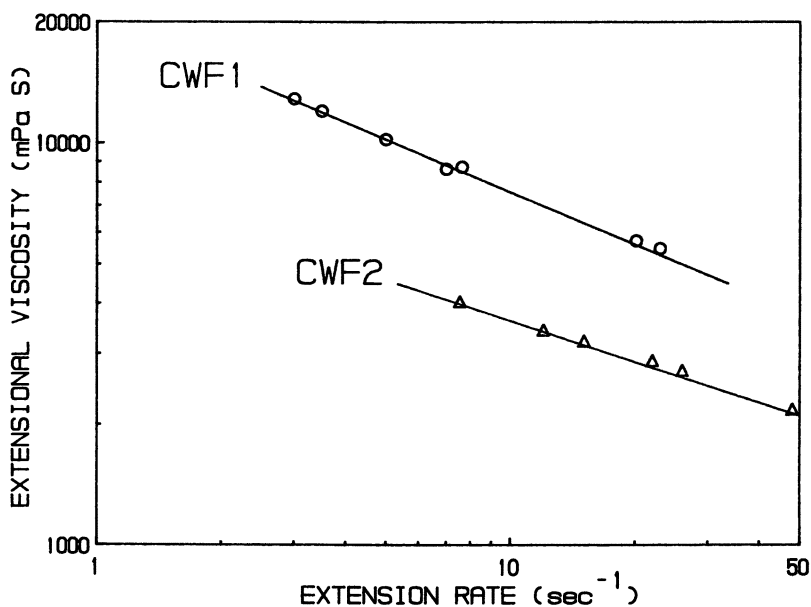
Figure 6. *Dynamic uniaxial extensional viscosities of coal–water fuels for-
mulated with different stabilizers.*

The inverse relationship of the fluid's sprayability and DUEV is evident when the fluids are thickened with water-soluble polymers of variable segmental and conformational flexibilities (31). POE, a segmentally and conformationally flexible polymer in aqueous solutions, contributes relatively little to the shear viscosity relative to comparable molecular weight fermentation carbohydrate polymers (32) such as xanthan gum or scleroglucan (SGPS). The reverse is true (25) with respect to their contribution to the elongational viscosity of aqueous solutions. SGPS solutions with high shear viscosities and high storage modulus but low DUEV values readily mist on exit from a spray gun. POE solutions, with notable DUEVs even at low concentrations (1000 ppm), string rather than mist on exit from the spray nozzle.

These polymers also exhibit the same behavior in roll application, but misting is observed only with the higher elongational viscosity fluid because the fluid with the lower elongational behavior does not support fiber growth that results in misting. These observations are consistent with the use of the traditional method of measuring dynamic surface tensions, when such forces are absent, to assess the fluid's elongational viscosity (33).

Interfacial Elongational (Dilational) Viscosities

The viscosity emphasized in this chapter, called elongational or extensional viscosity, was originally designated (34) tensile viscosity. When this bulk-phase parameter is near the interface, its two-dimensional equivalent is called the surface dilational viscosity. The importance of this parameter in the foaming of coatings, which arises from differences in surfactant structures, has been discussed (35). In cosmetic applications, foam and gel structures are important and probably reflect the reason the hydrophobically modified acrylic acid polymers were emphasized in the last section of Chapter 7.

(Hydroxyethyl)cellulose is used in blends with xanthan gum as it serves to flocculate the drilled solids so that they are released at the surface. Those experienced in this technology are aware of the difficulty in controlling the foaming of such blends. Foaming is normally seen with cellulose ethers of high molecular weight. The more hydrophobic (methoxyl)cellulose forms gelatinous surface structures and will provide infinite droplet stability to oil-in-water dispersions (36). Hydrophobic modification of HEC and its derivatives would, therefore, be expected to yield solutions that would readily foam. This property has been recognized and used in cosmetic applications.

HEC has found limited use as a thickener for cosmetic formulations. Modification of this polymer with small amounts of tetramethylamine functionality expanded its end use by providing substantivity to hair and inhibiting surfactant penetration of human skin (37). Hydrophobic modification of quaternary HEC increases the polymer's surface activity (38) as reflected in its foam stability (Figure 7).

The precise mechanism for the increase in foam stability is unknown.
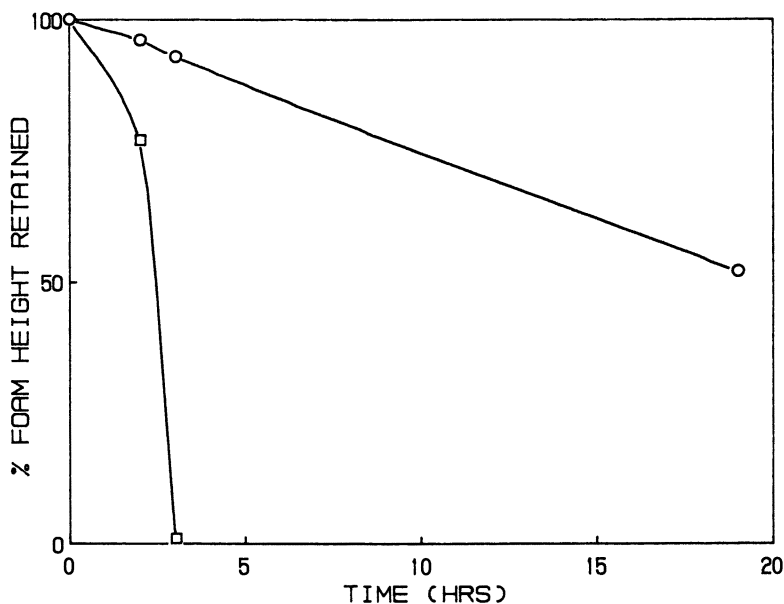
Figure 7. Foam study done by conventional cylinder shake test. Key: □, 0.1 wt % quaternary derivative of HEC; ○, 0.1 wt % hydrophobically modified, quaternary derivative of HEC.

For example, fluorescence measurements, as noted in several chapters in this text, reflect a difference in phase transformation relative to micelle formation (i.e., aggregation in polymer solutions takes place over a wide range of concentrations). Furthermore, foam stability is increased in the presence of surfactant if the surfactant is of opposite charge to the quaternary group in the derivatized HEC. Interactions with ethoxylated surfactants are relatively weak. Although a strong interaction with sodium dodecyl sulfate occurs with both the quaternary HEC and the hydrophobically modified derivative, the interactions are evident with the hydrophobically modified polymer at lower concentration. The viscosity of the solutions in the lamellae region is postulated to be considerably higher than that observed in conventional surfactant lamellae; the adsorbed polymer hydrophobes may form hemimicelle-type structures at the water–air interface. The resultant viscous surface and subsurface regions are apparently responsible for the low drainage and the consistent long-term stability of the foams generated by the hydrophobically modified, quaternary amine-modified HEC (39).

Complexities in Analysis

A variety of procedures evolved in the early 1960s to measure DUEVs. The procedures reported in the more recent literature are the use of vacuum-suction filament-draw apparatus (15, 16) (from which most of the data dis-
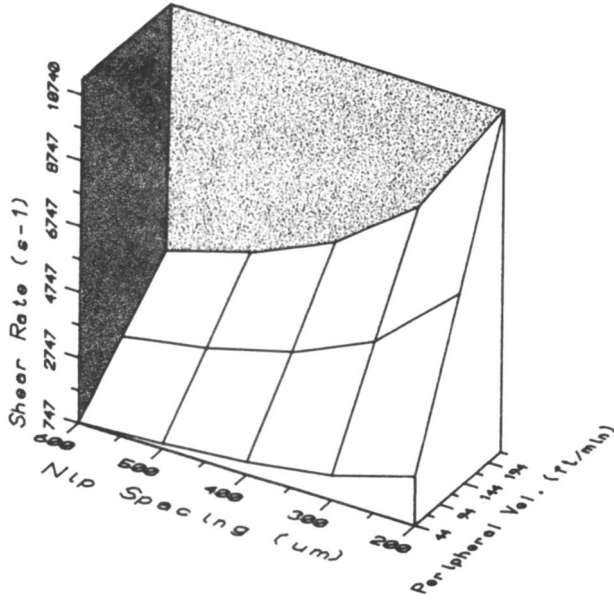
Figure 8. Dependence of shear rate on nip spacing and roll peripheral velocity.
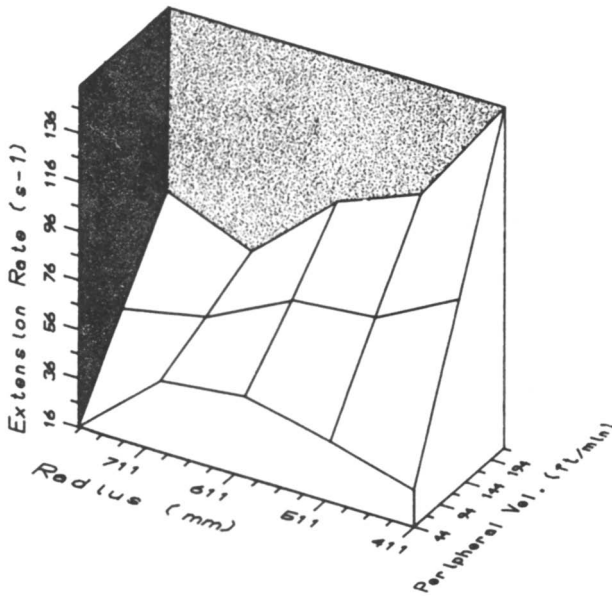
Figure 9. Dependence of extension rate on roll radius and roll peripheral velocity.

cussed in this chapter have been taken) and modification of the stagnation flow device (*40*) described in the preceding chapter.

For evaluation of DUEVs, with less shear viscosity contribution to the total response, the modified stagnation technique is the procedure of preference. For practical applications the vacuum-suction filament-draw technique is probably the more valuable because the deformation rates in many applications are not solely extensional in nature. The comments regarding the velocity gradients in the tubeless siphon (*41*) are appropriate to the fiber-suction approach: "flow in a tubeless siphon approximates extensional flow in a sense that the largest components of the velocity gradient tensors are diagonal ones."

The nature of the shear viscosifying component and possibly the magnitude of the shear viscosity can contribute to the magnitude of the DUEVs (*42*). This information will relate to many applications in which extrusion rates are not totally extensional in nature (e.g., automotive sealants and mobility control studies (*23, 26*) in which the permeability of the formation is a critical factor). For roll-applied films, the magnitude of these different deformation rates (*16*) are significantly different (Figures 8 and 9) and their relative contribution to a formulation's performance may be complex.

Summary

Extensional deformations are imposed on fluids when they undergo converging flows. The elongational response of the fluid will play an important part in its behavior. Examples in the areas of the roll application of trade-sale latex paints and water-reducible industrial coatings, petroleum applications involving enhanced oil recovery and drilling fluids, the spray application of coal–water slurries and of interior can coatings were discussed in the context of elongational viscosity contributions. These relationships have the potential to provide insights in other applications in which shear viscosity considerations alone have not been adequate in resolving formulation performances. Hydrophobically modified, water-soluble polymers have many applications because of their lower viscoelastic properties.

Acknowledgment

References

1. Society of Rheology winter meeting, 1987, Santa Monica, CA, private communications.
2. Walters, K. *Rheometry*; Wiley: New York, 1975; Chapter 7.

3. Evani, S.; Lalk, R. H. U.S. Patent 3 779 970, 1973.
4. Evani, S. R.; Rose, G. D. *Proceedings of the ACS Division of Polymeric Materials: Science and Engineering* **1987,** *57,* 510–515.
5. Zakin, J. L.; Hunston, D. L. *J. Appl. Polym. Sci.* **1978,** *22,* 1763–1766.
6. Merril, E. W.; Leopairat, P. *Polym. Eng. Sci.* **1980,** *20*(7), 505.
7. Miles, M. J.; Tanaka, K.; Keller, A. *Polymer* **1983,** *24,* 1801.
8. Maerker, J. M. *Soc. Pet. Eng. J.* **1975,** 311–322 August; *Trans. Am. Inst. Min., Metall. Pet. Eng.,* 259.
9. Vanderhoff, J. W.; Bradford, E. B.; Tarkowski, H. L.; Shaffer, J. B.; Wiley, R. M. In *Polymerization and Polycondensation Processes*; Platzer, N. A. J., Ed.; Advances in Chemistry 34; American Chemical Society: Washington, DC, 1962; pp 32–51.
10. Soules, D. A.; Glass, J. E. *The Role of Polymers in Enhanced Oil Recovery*; Stahl, G. A.; Schulz, D. N., Eds.; Plenum: New York, 1988; pp 253–260.
11. Nguyen, T. Q., Henning, H. H. *Chimia* **1986,** *40*(4), 129.
12. Glass, J. E. *J. Coat. Technol.* **1978,** *50*(641), 56.
13. Glass, J. E. *J. Coat. Technol.* **1978,** *50*(640), 53, 61; *50*(641), 72.
14. Massouda, D. F. *J. Coat. Technol.* **1987,** *57*(722), 27.
15. Khagram, M.; Gupta, R. K.; Sridhar, T. *J. Rheol. (N.Y.)* **1985,** *29*(2), 191.
16. Soules, D. A.; Fernando, R. H.; Glass, J. E. *J. Rheol. (N.Y.)* **1988,** *32,* 181.
17. Weinberger, C. B.; Goddard, J. D. *Int. J. Multiphase Flow* **1974,** *1,* 465.
18. Shaw, K. G.; Liepold, D. P. *J. Coat. Technol.* **1985,** *57*(727), 63.
19. Estes, J. C. In *Water-Soluble Polymers: Beauty with Performance*; Advances in Chemistry 213; Glass, J. E., Ed.; American Chemical Society: Washington, DC, 1986; Chapter 10.
20. Heinle, S.; Shaw, S.; Glass, J. E. In *Water-Soluble Polymers: Beauty with Performance*; Advances in Chemistry 213; Glass, J. E., Ed.; American Chemical Society: Washington, DC, 1986; Chapter 11.
21. Argabright, P. A.; Rhudy, J. S. Trujillo, E. M. In *Water-Soluble Polymers: Beauty with Performance*; Advances in Chemistry 213; Glass, J. E., Ed.; American Chemical Society: Washington, DC, 1986; Chapter 15.
22. Chauveteau, G. In *Water-Soluble Polymers: Beauty with Performance*; Advances in Chemistry 213; Glass, J. E., Ed.; American Chemical Society: Washington, DC, 1986; Chapter 14.
23. Manke, C. W.; Southwick, J. G. *Proceedings of the ACS Division of Polymeric Materials: Science and Engineering* **1987,** *57,* 123.
24. Hull, A. M.; Pearson, J. R. A. *J. Non-Newtonian Fluid Mech.* **1984,** *14,* 219.
25. Fernando, R. H.; Glass, J. E. *J. Rheol. (N.Y.)* **1988,** *32,* 199.
26. Fernando, R. H.; Glass J. E.; Burnett, D. A. Society of Petroleum Engineers International Symposium on Oilfield and Geothermal Chemistry, SPE Publication No. 13584, Phoenix, AZ, April 9–11.
27. "Big Muddy Field Low-Tension Flood Demonstration Project", U.S. Department of Energy Publication SF/01424–39, 1981, and subsequent publications.
28. Gordon, M.; Yerushalmi, J.; Shinnar, R. *Trans. Soc. Rheol. (N.Y.)* **1973,** *17,* 303.
29. Rakitsky, W. G.; Knell, E. W.; Murphy, T. J. *Proc. 11th Int. Conf. Slurry Technol.* **1986,** 137.
30. Wu, J. T. K.; Eley, R. R. In *Water-Soluble Polymers: Beauty with Performance*; Advances in Chemistry 213; Glass, J. E., Ed.; American Chemical Society: Washington, DC, 1986; Chapter 16.
31. Soules, D. A., Ph.D. thesis, North Dakota State University, in preparation.
32. Glass, J. E., Proceedings of the Society of Rheology winter meeting, 1987, Santa Monica, CA, Chapter 1.

33. Schummer, P.; Tebel, K. H. *J. Non-Newtonian Fluid Mech.* **1983**, *12*, 331.
34. Trouton, F. T. *Proc. R. Soc. London, A* **1906**, *77*, 426.
35. Eley, R. R.; Zander, R. A.; Koehler, M. E. In *Water-Soluble Polymers: Beauty with Performance*; Advances in Chemistry 213; Glass, J. E., Ed.; American Chemical Society: Washington, DC, 1986; Chapter 16.
36. Glass, J. E.; Lundberg, R. D.; Bailey, F. E., Jr. *J. Colloid Interface Sci.* **1970**, *33*(4), 491.
37. Goddard, E. D. *Kem.-Kemi* **1985**, *12*, 375.
38. Padmanabhan, K. P. A.; Leung, P. S.; Goddard, E. D. *Proceedings of the ACS Division of Polymeric Materials: Science and Engineering* **1987**, *57*, 507.
39. Goddard, E. D.; Braun, D. B. *Cosmet. Toiletries* **1985**, *100*(7), 41.
40. Fuller, G. G.; Cathey, C. A.; Hubbard, B.; Zebrowski, B. E. *J. Rheol. (N.Y.)* **1987**, *31*(3), 235.
41. Astarita, G.; Nicodemo, L. *Chem. Eng. J. (Loughborough, Engl.)* **1970**, *1*, 57.
42. Lundberg, D. J.; Soules, D. A.; Dinga, G. P.; Glass, J. E. *Proceedings of the ACS Division of Polymeric Materials: Science and Engineering* **1988**, *58*.

13

Macromolecular Complex Formation and Polymer Adsorption on Colloidal Particles in Aqueous Solution

David J. Hemker, Kookheon Char, Hideko T. Oyama, Alice P. Gast, and Curtis W. Frank[1]

Department of Chemical Engineering, Stanford University, Stanford, CA 94305–5025

Excimer fluorescence from pyrene groups labeled at the ends of poly(ethylene glycol) chains was used to monitor the configurational behavior of the probe chain during formation of macromolecular complexes with poly(methacrylic acid) or poly(acrylic acid) and during adsorption on colloidal silica or polystyrene colloidal particles in water. The excimer to monomer intensity ratio was separated into intramolecular and intermolecular contributions to follow the decrease in intramolecular cyclization probability during complex formation. Hydrophobic attractive interactions between the pyrene groups are suggested to occur for the free probe chain in water as well as with the compact poly(methacrylic acid) and the colloidal polystyrene particles. Excitation spectra provide significant qualitative information about the local environment of the pyrene rings.

T HE CONFIGURATIONAL PROPERTIES OF WATER-SOLUBLE POLYMERS and their interactions with other polymers and with colloidal particles are relevant to understanding the intermolecular interactions in associative thickeners and steric stabilization of colloidal particles. We used fluorescence spectroscopy to study both the dynamic and the static equilibrium properties

---

[1]Address correspondence to this author.

of polymer chains that participate in the polymer–polymer and polymer–colloid interactions of interest. Fluorescence methods have been increasingly used in recent years to elucidate problems in polymer physics, and a number of excellent monographs (1, 2) and symposium proceedings (3–5) are available. In general, the advantages of a fluorescence method are its high sensitivity to a small number of fluorescent groups and the detail it can provide on local molecular structure.

Three classes of polymers are amenable to study by fluorescence techniques. The first class of materials is that consisting of extrinsic fluorescent molecules incorporated into the polymer solution. This class has applications in the study of solubilization of small molecules in block copolymer micelle cores (6) but is not of interest for configurational studies such as the present work.

The second class contains a fluorescent chromophore, also referred to as a fluorophore, on every repeat unit, either pendent to the chain or in the backbone. Examples of compounds having chromophores pendent to the chain are polystyrene and poly(2-vinylnaphthalene), both of which have been extensively studied as components of polymer blends (7–13). Compounds having chromophores in the backbone are represented by an aromatic polyamide, polyester (14), or polyurethane (15).

The third class consists of an inherently nonfluorescent polymer chemically modified to include a small number of fluorescent species. This modification could involve preparation of a copolymer having a low percentage of aryl-containing groups, such as the methyl methacrylate–2-vinylnaphthalene copolymer (16–19). Other possibilities are the random attachment of fluorophores to polystyrene through chloromethylation followed by esterification (20) or the transesterification reaction of an aryl alcohol with poly(methyl methacrylate) (21). Still another example, and the one used in the present study, is the terminal modification of the chain ends to incorporate just two chromophores. This modification may be accomplished through termination of an anionic polymerization [e.g., reaction of bromobutylpyrene with the dianion of polystyrene (22) or by esterification of the hydroxy terminal groups of poly(ethylene glycol) (23)].

The specific fluorescent probe technique used in the present research is excimer formation between pyrene groups terminally attached to both ends of poly(ethylene glycol) (PEG) chains. Excimer formation in such a labeled polymer may result from both intramolecular and intermolecular interactions. A large body of literature over the past decade deals with intramolecular cyclization as detected by fluorescence techniques. This work has come largely from three groups. Cuniberti and Perico (24, 25) were the first to explore the possibility that excimer fluorescence could be used as a probe of end-to-end cyclization dynamics. Later, Horie and co-workers (26, 27) used triplet annihilation as a probe of cyclization in long chains. By

far the most work, however, has come from Winnik and his collaborators (28, 29).

The essential feature of the intramolecular cyclization of short polymer chains containing terminal pyrene groups is that the process is diffusion controlled at room temperature. As such, the cyclization process is expected to obey an Einstein relation with both the rate constant for cyclization and the ratio of excimer to monomer emission intensities (I_D/I_M) proportional to the reciprocal of the solvent viscosity. The more interesting aspect of this diffusion-controlled process is that the two pyrene (Py) groups possess an inherent correlation because of their attachment to the polymer chain. As a consequence, much effort has been directed toward the study of the effect of molecular weight of the tagged polymer on the cyclization probability (30, 31).

The question of whether the labeled probe chain is benign in the sense of not affecting the phenomenon under study is not settled, however. We have previously examined the end-to-end cyclization of Py–PEG–Py in a series of solvents and have determined that the rate constant for cyclization is apparently much higher in aqueous solution than in organic solvents (32). We attributed this result to a hydrophobic attraction between the pyrene groups (32, 33). Although this issue must be considered when using the end-tagged chains as probes of polymer interactions in solution, one can just as easily exploit the problem to one's advantage. Specifically, we refer to the broad interest in associative thickeners. The labeled polymer provides an excellent prototype for a double-headed amphiphilic molecule. Thus, photophysical measurements on our probe chain may provide the most direct possible measure of the associative effects in aqueous solution; this subject, however, is beyond the scope of this study.

With the increased level of understanding of the cyclization dynamics as monitored by intramolecular excimer fluorescence, it is now possible to extend this probe to the study of systems more complex than dilute solutions. One such situation involves the structure and dynamics of macromolecular complexes formed between polymeric proton donors and acceptors in aqueous solution. For example, there has been widespread interest in the complexes formed between poly(ethylene glycol) and poly(acrylic acid) or poly(methacrylic acid) in aqueous solution (34, 35). A second, complicated morphological problem is to describe the configurational behavior of polymer chains adsorbed on colloidal particles. This research has relevance to the understanding of steric stabilization. One system of particular interest is the interaction of poly(ethylene glycol) and colloidal silica (36–40).

Both the macromolecular complexes and the adsorption on colloidal particles may be examined through study of the configurational properties of the terminally labeled Py–PEG–Py probe chain. One feature of interest is the degree to which the mobility of the labeled chain is reduced when it

interacts with another polymer or with a solid surface. A second aspect is the extent of local chain aggregation that is exhibited by the labeled chain. In our experimental design, we considered the labeled chain to participate in either the complexation or the adsorption, and we used the photophysical behavior to infer some aspect of the chain structure or dynamics.

The goal of this chapter is to explore the analogy between macromolecular complex formation of the labeled probe chain and a polymeric proton donor, such as poly(acrylic acid) (PAA) or poly(methacrylic acid) (PMAA), and the adsorption of the probe chain on colloidal particles such as silica or polystyrene. The basis for a possible analogy between these two situations arises from the nature of the local interactions. Macromolecular complex formation arises from specific interactions such as hydrogen bonding; likewise, we expect that similar specific interactions exist between the PEG and the silica or polystyrene substrate. In essence, we consider the macromolecular complex to represent an interaction with a molecular substrate, whereas the colloidal problem involves a solid substrate.

To explore this analogy, we will review previous work on the influence of stoichiometry as well as present new results on the effect of neutralization on macromolecular complex formation. In addition, we will review very recent results for adsorption on colloidal silica and present preliminary results for the adsorption on colloidal polystyrene. The excimer to monomer emission intensity ratio, the excitation spectra, and the lifetimes of the excimer and monomer are the observable experimental parameters.

Experimental Details

The pyrene-terminated poly(ethylene glycol) probe molecules (Py–PEG–Py) of weight-average molecular weights 4800 and 9200, based upon the PEG starting material, have been described previously (32). New samples of molecular weights 4250 and 8650 were labeled by the same procedure as the original materials. The poly(acrylic acid) (PAA) sample of molecular weight 890,000 and poly(methacrylic acid) (PMAA) sample of molecular weight 9200 have also been described (41). Two types of colloidal particles were used. The first was the silica Ludox AM (Du Pont) with an average particle diameter of 15 ± 2 nm as determined by dynamic light scattering. The second was polystyrene particles, synthesized at Stanford, with an average particle diameter of 130 ± 5 nm.

Photostationary fluorescence and excitation spectra were obtained on a spectrofluorometer (SPEX Fluorolog 212). Transient data were obtained on a Photochemical Research Associates model 3000 nanosecond fluorometer.

Results

Macromolecular Complex Formation.   The ultimate objective of the studies on complex formation between polymers in aqueous solution is to understand how the PEG chains interact with either the PMAA or PAA chains on the molecular level. For example, we would like to know whether

the interaction is precisely a one-to-one correlation of repeat units, as in a ladderlike structure, or whether there are many loose loops and dangling chain ends of the PEG in combination with concerted sequences of complementary segment pairs. Moreover, we would like to know whether the configurational structure of the PMAA or PAA is modified by the PEG upon complex formation.

Excimer to Monomer Intensity Ratio. Our approach toward the determination of this information is to focus on the configurational behavior of the pyrene-terminated PEG. Two sets of experiments were performed to separate the intramolecular behavior of the isolated Py–PEG–Py chains from the intermolecular interactions that occur between labeled PEG chains. First, we performed photostationary fluorescence measurements of I_D/I_M for fully labeled PEG as a function of the molar ratio of the poly(carboxylic acid) to that of the PEG. These results will contain both intermolecular and intramolecular contributions to the excimer fluorescence. Next, we performed analogous measurements with the same total amount of PEG but with only 1% having pyrene labels. The selection of the relative amount of the tagged polymer is somewhat arbitrary, but it appears to be sufficiently low to provide a reasonable approximation to the behavior of the isolated, labeled PEG chain. These fluorescence results are then subtracted from those for the fully tagged system, leaving just the intermolecular contribution.

It is worth specifying the experimental protocol in some detail, because the question of whether or not the complexation is an equilibrium phenomenon has not yet been clearly established. In our experiments, the PEG is first dissolved in water, with total concentration of labeled and unlabeled material generally being 1×10^{-3} M. A concentrated solution of the poly(carboxylic acid), generally 1×10^{-1} M, is then added to the first solution, and the fluorescence properties are measured. We have not observed any time-dependent phenomena that might suggest that the initial complexes exchange to the extent that would cause the configuration of the labeled PEG to change. We cannot rule out this possibility, however, considering that we have been limited to room-temperature experiments because the ester linkage attaching the pyrene group to the PEG chain is hydrolytically unstable, particularly under basic conditions. This problem should be resolved when labeled compounds with ether linkages are prepared; this work is in progress.

Typical fluorescence results for the intramolecular component of the labeled PEG are shown in Figure 1 for Py–PEG–Py of weight-average molecular weights 4800 and 9200. Most of the raw data for I_D/I_M have been taken from previous work (32, 41) but have been normalized to the values of I_D/I_M observed in aqueous solution before the addition of any poly(carboxylic acid). The values of these free-solution data points differ by
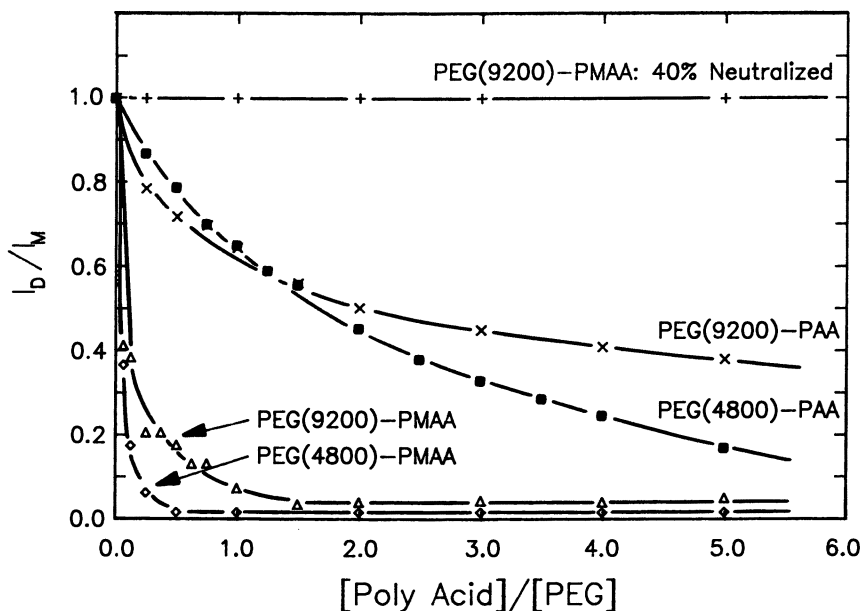
Figure 1. Intramolecular excimer to monomer emission intensity ratio as a function of the molar ratio of poly(carboxylic acid) to PEG for Py–PEG–Py of weight-average molecular weights 4800 and 9200. All data are normalized by the I_D/I_M value for a 1% pyrene-tagged PEG solution with no polyacid added.

an order of magnitude; the cyclization probability is much higher for the low molecular weight PEG. Our initial experiments (32, 41) were separate studies of complexes of Py–PEG–Py with PMAA of viscosity-average molecular weight 9500 and PAA with viscosity-average molecular weight 890,000. We expected that the ideal complexation would be complete at the stoichiometric ratio, if all of the interaction sites were equally accessible and participated in the complex.

There is some question as to the significance of comparing poly-(carboxylic acids) whose molecular weights differ by about 3 orders of magnitude. Although we do not yet understand the details of the molecular weight dependence of the poly(carboxylic acid) on I_D/I_M, we have observed qualitatively similar results for complexes of either Py–PEG–Py(4800) or Py–PEG–Py(9200) with PAA(1850) and PAA(890,000) (32). Likewise, we have seen similar behavior for complexes of both labeled PEG samples with PMAA(1530) and PMAA(9500) (41). We believe that a more significant difference is the configurational behavior of the poly(carboxylic acids). We expect that the PMAA exists in a compact coiled structure at low pH because of the strong hydrophobic attractions arising from the α-methyl group. In contrast, we expect the PAA structure to be relatively open.

Several qualitative observations can be made about Figure 1. For a given PEG molecular weight, I_D/I_M for PMAA decreases much more dramatically than that for PAA. In fact, essentially all of the excimer fluorescence is quenched by the point at which the stoichiometric ratio is reached. Also, the I_D/I_M for PMAA remains lower than the I_D/I_M for PAA at high acid-to-PEG ratios. One parameter related to the rate of the decrease of the I_D/I_M data is the acid-to-PEG ratio at which I_D/I_M has decreased to half of its normalized starting value, $R_{1/2}$. $R_{1/2}$ for the PAA data is approximately 2, whereas the $R_{1/2}$ for the PMAA is less than 1/8. This fact shows that the pyrene excimer is destroyed by the addition of much less PMAA than PAA, probably because of the hydrophobic interactions between PMAA and the hydrophobic pyrene tags. The fact that the PMAA data remain lower at high acid-to-glycol ratios indicates that these interactions persist well above the stoichiometric ratio. Finally, for a given acid, I_D/I_M for the systems with a PEG molecular weight of 4800 is generally lower than that for the systems with a PEG molecular weight of 9200. This result probably indicates that when the shorter chains participate in a complex with an acid, there is less mobility of the chain ends because of shorter free chain ends.

We have also included preliminary results on the effect of neutralization of PMAA(9500) on the intramolecular contribution to the excimer fluorescence for Py–PEG–Py(9200) in Figure 1. Our objective in this experiment was to change the number of sites on the PMAA that were available for interaction with the ethylene oxide segments. We expected that interactions based upon hydrogen bonding would be reduced upon ionization of the carboxylic acid groups. A more important effect may have been the possibility of an extensive configurational change of the PMAA as the number of ionized groups increased. When 40% of the carboxyl groups were ionized by the addition of NaOH, the intramolecular cyclization probability became independent of solution composition. This behavior indicated that there was no complexation between the Py–PEG–Py and PMAA because of either the reduction in the absolute number of interaction sites or to some configurational change in the PMAA.

Figure 2 presents results for the fully labeled systems of the same composition as for Figure 1. We have selected these data instead of the derived intermolecular contribution to make a more direct comparison with the adsorption results to follow. For a given PEG molecular weight, PMAA has a higher relative I_D/I_M maximum than PAA. Also, this maximum occurs at a lower acid-to-glycol ratio for the PMAA systems. However, the I_D/I_M values are higher for the PAA systems at high acid-to-glycol ratios. For a given acid, the relative magnitudes of the maxima are approximately independent of PEG molecular weight, but the maxima occur at lower acid-to-glycol ratios for the Py–PEG–Py(4800) systems. These maxima are also sharper than their Py–PEG–Py(9200) counterparts. As was seen in Figure
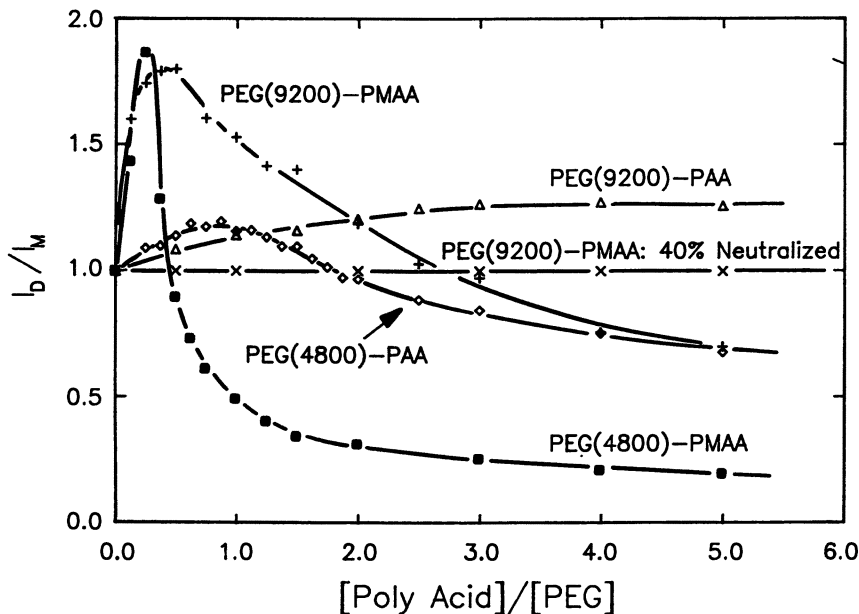
Figure 2. Total excimer to monomer emission intensity ratio as a function of the molar ratio of poly(carboxylic acid) to PEG for labeled systems of the same composition as in Figure 1. All data are normalized by the I_D/I_M value for a 100% pyrene-tagged PEG solution with no polyacid added.

1, I_D/I_M for Py–PEG–Py(4800) is lower than for Py–PEG–Py(9200) at high acid-to-glycol ratios.

The high overshoot for the PMAA may indicate an initially high degree of hydrophobic clustering of pyrene molecules when a small amount of hydrophobic PMAA is added. As more PMAA is added, these pyrene clusters are broken up by the greater number of hydrophobic PMAA molecules. Thus, in the PMAA systems, the initial aggregation of pyrene molecules is broken up by two forces. One force is the dilution effect of adding more PMAA chains, which results in complexes with fewer PEG chains per PMAA chain. As a result, local pyrene concentration decreases. A second driving force is the hydrophobic interaction between pyrene and PMAA. In the PAA systems, only the dilution effect is present; for this reason, the maxima are sharper at lower acid-to-glycol ratios for the PMAA systems. At high acid-to-glycol ratios, the PAA systems show a higher relative I_D/I_M because the pyrene molecules, not hindered by an additional hydrophobic attraction to the acid, have more freedom to diffuse. When 40% of the carboxyl groups are ionized, no complexation occurs (Figure 2). Because all of the PEG chains are end-labeled with pyrene, this result is better evidence of no complexation than the similar result shown in Figure 1, in which only 1% of the PEG chains were tagged.

Excitation Spectra. We have made qualitative use of both the monomer and excimer excitation spectra to study the constrained states imposed by the complex formation. An excitation spectrum is obtained by monitoring the emission at a particular wavelength while scanning the excitation wavelength; it allows separate interrogation of the aromatic rings that are isolated and those that are in excimer-forming sites. The first way in which this was done was to compare the excimer and monomer excitation spectra for Py–PEG–Py(4800) in water (*32*). We observed a red shift of the excimer relative to the monomer excitation spectrum of approximately 2 nm that indicated the presence of ground-state interactions between some of the pyrene chromophores that were in excimer-forming-site (EFS) geometries. This observation is qualitatively consistent with the enhancement in I_D/I_M over the end-to-end cyclization value expected for nonaqueous solvents. Addition of methanol caused the monomer and excimer excitation spectra to be superimposable (*33*). A corresponding decrease in I_D/I_M was also observed, which demonstrated that the methanol broke up the initial aggregates of pyrene groups, thus eliminating the source of the ground-state interaction.

The second way we used excitation spectra was to follow the changes in excitation maxima as a function of the molar ratio of the poly(carboxylic acid) to the PEG (*41*). We observed that the initial red shift of the excimer excitation spectrum relative to the monomer for Py–PEG–Py(4800) remained approximately constant as the PAA(890,000) content was increased. There was, however, an enhancement in the relative shift of the excimer for PMAA(9500) up to the stoichiometric equivalence of PMAA to PEG. Thereafter, the shift between excimer and monomer remained constant. One form of comparison of these results is shown in Figure 3, where we present the monomer excitation spectra for Py–PEG–Py(4800) free in aqueous solution and complexed with PMAA(9200) at [PMAA] to [PEG] ratio of 5:1.

Finally, we obtained monomer excitation spectra for 1% and 100% Py–PEG–Py(9200) as a function of [PMAA(9500)]/[PEG] for both 0% and 30% neutralized PMAA. These results are shown in Figure 4. The 1% and 100% labeled results at 0% neutralization are given in Figures 4a and 4b, respectively. No change in monomer excitation spectra occurred for the intramolecular data of Figure 4a, but a significant red shift occurred for the 100% labeled sample of Figure 4b. This observation indicates the presence of ground-state interactions in the fully tagged systems. These interactions disappeared for the 30% neutralized results shown in Figures 4c and 4d.

Adsorption onto Colloidal Particles.

In addition to our studies of complexation with polymeric carboxylic acids, we have also investigated adsorption of the same end-tagged PEG on colloidal surfaces. Just as the hydrophobic or hydrophilic character of the acid can be changed, in colloidal
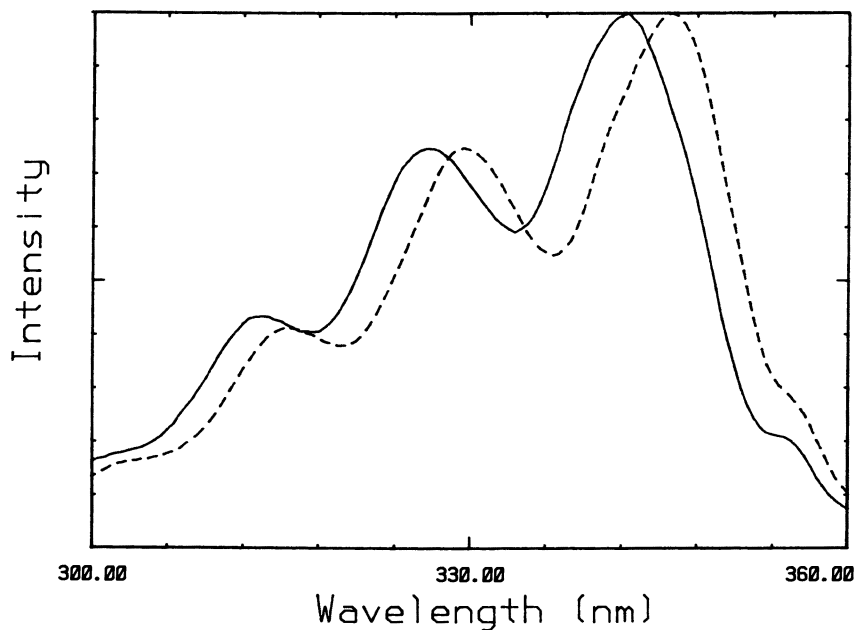
Figure 3. Monomer excitation spectrum monitored at 376 nm for 100% tagged
PEG(4800) (——) and PMAA/100% tagged PEG(4800) in a 5:1 ratio (- - -).

surface adsorption we also have the ability to adjust the surface chemistry
and to probe its effect on the adsorbed chain configurations. Thus far, we
have studied two colloidal species: colloidal silica particles with surface silanol
functionality and colloidal polystyrene that is believed to have sulfonate
groups surrounded by hydrophobic patches. Future efforts will include mod-
ifications to these surfaces by silanization of the silica particles to produce
more hydrophobic siloxane and hydrocarbon surfaces and by changes to the
charge density on the polystyrene particles. A review of some results for
adsorption of these species onto silica (42) and a presentation of new infor-
mation regarding the adsorption onto colloidal polystyrene follow.

Excimer to Monomer Intensity Ratio.   In our previous work (42), we
studied I_D/I_M as a probe of changing polymer configuration upon displace-
ment from silica with untagged chains. We first adsorbed tagged chains of
molecular weights 4250 and 8650 onto colloidal silica. There were no tagged
chains in the supernate; thus we could study their displacement upon ad-
dition of untagged polymers. Upon adsorption, I_D/I_M dropped for both spe-
cies to values of 20 to 40% of the free-solution value. For the adsorption of
Py–PEG–Py(8650) at a concentration corresponding to one chain per par-
ticle, we found an overshoot in I_D/I_M relative to that of the bulk solution as
we increased the PEG(22,000) displacer concentration. We attributed this
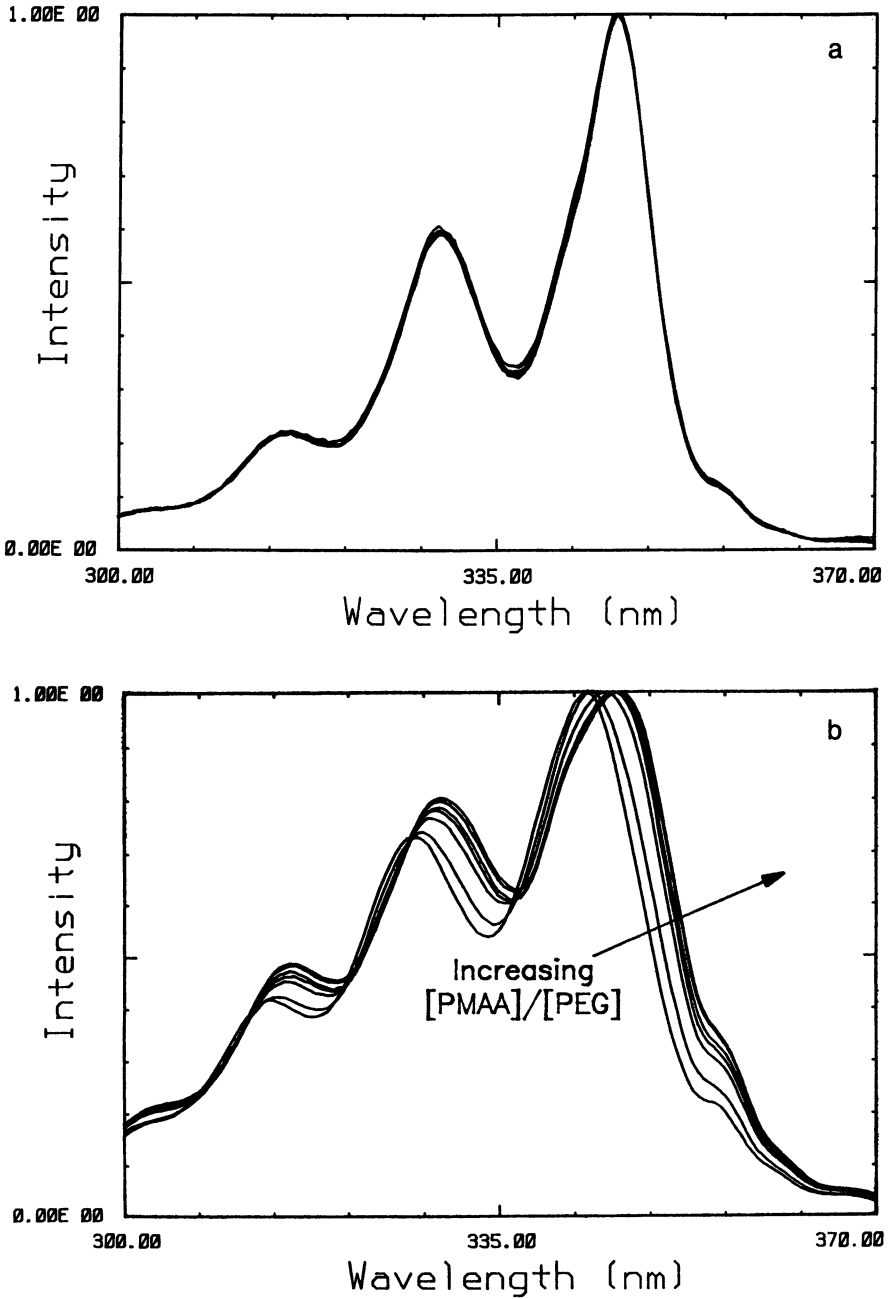
Figure 4. Monomer excitation spectra monitored at 376 nm at PMAA(9500): PEG(9200) ratios of 1:8, 1:4, 1:2, 3:4, 1, 2, and 4. a, 1% tagged PEG, 0% neutralization. b, 100% tagged PEG, 0% neutralization. Continued on next page.
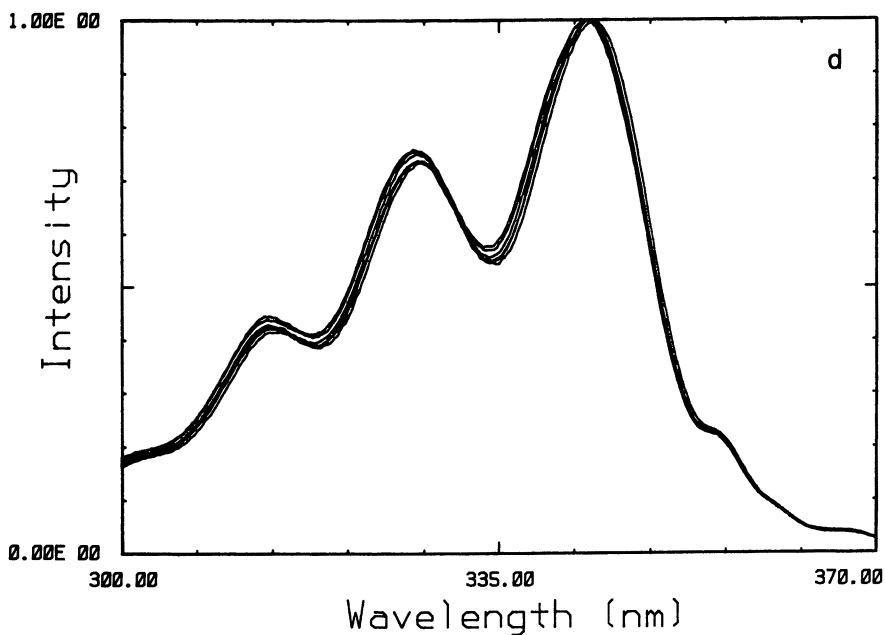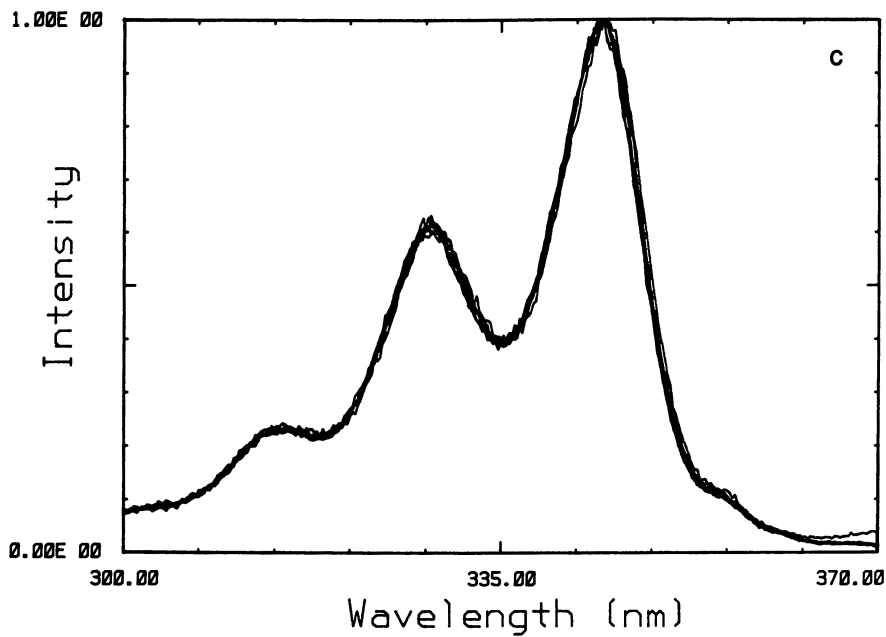
Figure 4.—Continued. c, 1% tagged, 30% neutralization. d, 100% tagged PEG, 30% neutralization. All spectra are normalized with respect to the excitation maximum.

overshoot to rearrangement of the Py–PEG–Py(8650) before displacement, a conclusion supported by analysis of the supernatant pyrene concentration. In this work, we also investigated the effect of a variety of displacing polymer molecular weights and found that larger chains are more effective displacers than smaller ones. In this chapter, we focus our attention on the situation where we have adsorbed only tagged chains onto silica and look at the effect of adsorption on the excimer signal. In all these experiments, the dilute polymer solution was mixed with the colloidal suspension overnight before measuring the fluorescence.

In Figure 5, I_D/I_M relative to the I_D/I_M for free solution is plotted against the number of particles per chain (a variable analogous to the molar ratios
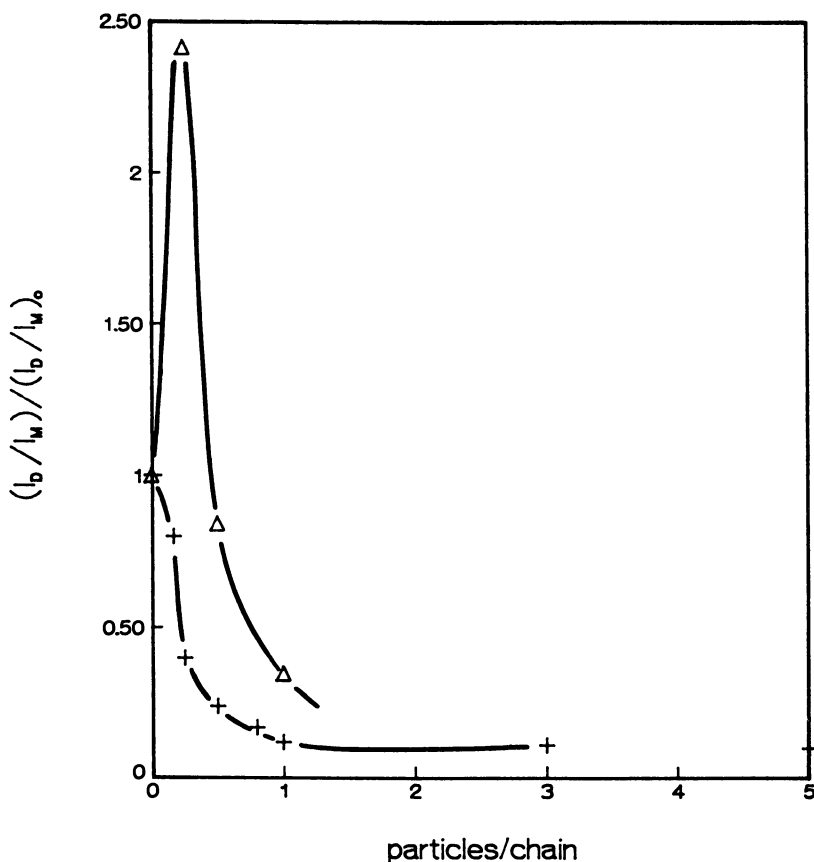
Figure 5. Excimer to monomer intensity ratio relative to that in free solution for Py–PEG–Py(4250) (+) and Py–PEG–Py(8650) (Δ) as a function of the number of colloidal silica particles available per chain on average. All initial solutions were in the dilute (intramolecular) regime before the addition of particles.

used in the complexation results). The behaviors of a Py–PEG–Py solution with approximately 100 units, Py–PEG–Py(4250), and one having approximately 200 units, Py–PEG–Py(8650), were very different. Addition of particles to the solution containing smaller chains caused the excimer fluorescence to drop monotonically, whereas the larger chains went through a maximum in relative excimer intensity at a concentration where there were several chains per particle. The smaller chains were apparently so restricted by adsorption onto colloidal silica that the possibility of two pyrenes forming an excimer dropped rapidly. The longer chains, however, formed a high density of excimers when adsorbed at higher surface coverage, probably because of increased intermolecular excimer formation.

We envision the adsorption of Py–PEG–Py onto colloidal silica to be qualitatively similar to its complexation with polar polymer molecules. Upon adsorption, the labeled PEG takes on a flattened configuration; the length of the pyrene-terminated tails depends on both the surface concentration and the molecular weight (43, 44). Longer chains retain longer tails, hence a greater ability to form excimers. These results were similar to our observations for the complexation case. Poly(ethylene glycol) adsorbs to silica, probably through hydrogen bonding between the backbone and the Si–OH moieties. Variation of the surface chemistry by silanization or alternate synthetic techniques will allow altering the polymer–surface interaction energy. We are currently developing a field equation model to describe the positions of end tags during adsorption in order to probe the origins of the excimer intensity behavior.

Adsorption onto colloidal polystyrene results in very different behavior because of the hydrophobic nature of that surface. The addition of even a small amount of polystyrene particles to the polymer solution results in the complete disappearance of the excimer emission (Figure 6). In this case, the hydrophobic pyrene groups are strongly attracted to the polystyrene surface; thus, the formation of excimers is precluded. A similar disappearance of the excimer was observed upon complexation with PMAA, a result indicating that the hydrophobic character of that polymer may hinder the formation of excimers by adsorbing the pyrene groups into a hydrophobic pocket. This observation is further supported by the fluorescence excitation spectra, presented in the next section.

Excitation Spectra and Fluorescence Lifetimes.   In this section, we further examine adsorption onto colloidal polystyrene by investigating the excitation spectrum of the adsorbed species. In Figure 7a, we show the excitation spectra of Py–PEG–Py(4250) before and after the addition of polystyrene particles. The spectrum undergoes a substantial red shift upon adsorption; the main peak moves approximately 4 nm. A similar effect is found in the complexation with PMAA, as shown in Figure 3, where the monomer spectrum is again shifted to higher wavelengths. From these spectral shifts, we infer a spectral sensitivity to the environment. This sensitivity is illus-
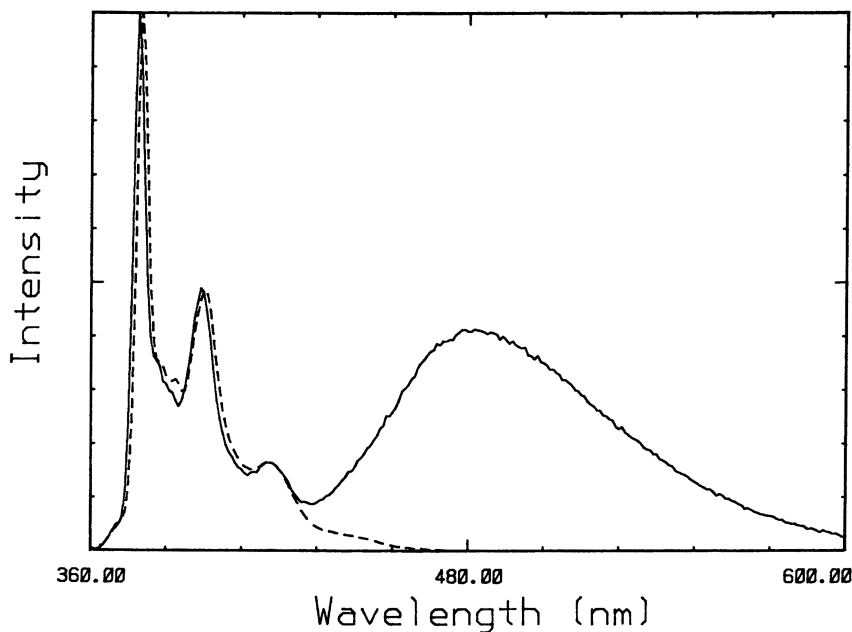
Figure 6. Fluorescence emission spectrum of a 1 × 10⁻⁶ M solution of Py–PEG–Py(4250) before (——) and after (- - -) the addition of 0.1 wt % colloidal polystyrene particles.

trated in Figure 7b, in which we compare the dissolution of Py–PEG–Py(4250) in water with that in toluene. Indeed, the hydrophobic environment accounts for a red shift of approximately 2 nm, whereas the larger shift upon complexation with PMAA or adsorption onto colloidal silica must be associated with additional changes in the pyrene upon confinement in these situations.

Upon adsorption onto colloidal silica, the monomer excitation spectrum remained essentially unchanged from that of the solution. In this system, the excimer persisted, allowing study of its excitation spectrum. In this experiment, a substantial shift in the excimer excitation spectrum occurs, indicating that, although excimer-forming sites remain, they exist in a strained state. This observation is further supported by the time dependence of the excimer fluorescence decay. Whereas chains remain adsorbed on the colloidal silica surface, the excimers formed are substantially shorter lived than those in free solution.

This correlation is illustrated in Table I, which shows the fluorescence lifetime and frequency shift for the excimer excitation spectrum relative to that of the free solution. The first six values correspond to different polymer solution concentrations ranging from [Py–PEG–Py(8650)] = 1 × 10⁻⁶ to 4 × 10⁻⁶ M with added untagged PEG(22,000) of 0 and 1 × 10⁻⁶ M. In this regime, the tagged chains remain on the silica particle surfaces. All these
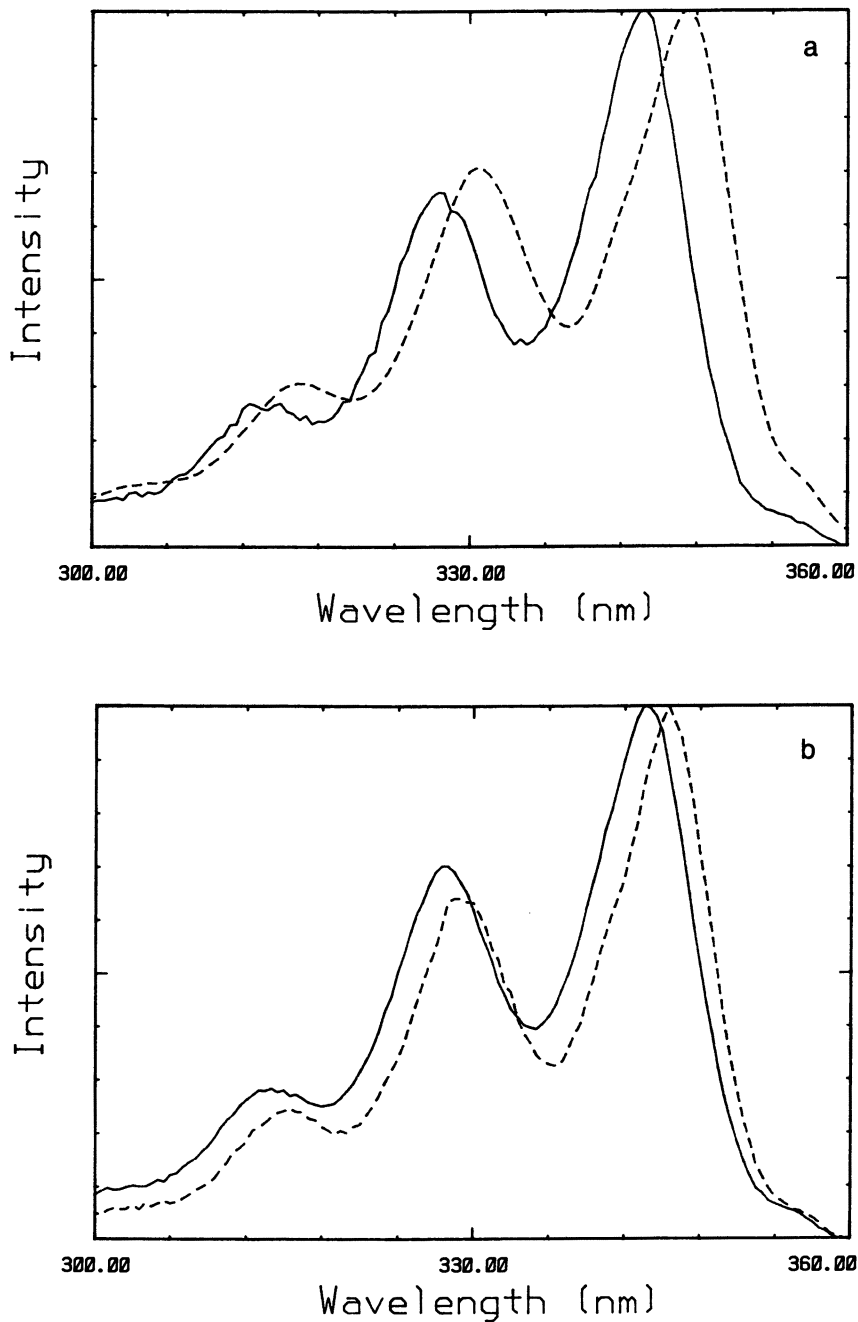
Figure 7. Monomer excitation spectrum for a 1 × 10⁻⁶ M solution of Py–PEG–Py(4250) a, before (——) and after (- - -) the addition of 0.1 wt % polystyrene particles; and b, in water (——) and in toluene (- - -).

Table I. Fluorescence Lifetimes and Frequency Shifts

Polymer	$(\tau_B - \tau)/\tau_B$	$(\nu_B - \nu)\ cm^{-1}$
Py–PEG–Py(8650)/PEG(22,000)		
$1 \times 10^{-6}/0$	0.29	56
$1 \times 10^{-6}/1 \times 10^{-6}$	0.25	86
$2 \times 10^{-6}/0$	0.28	55
$2 \times 10^{-6}/0.7 \times 10^{-6}$	0.26	77
$4 \times 10^{-6}/0$	0.30	99
$4 \times 10^{-6}/0.5 \times 10^{-6}$	0.29	99
$1 \times 10^{-6}/8 \times 10^{-6}$	−0.19	−6
$2 \times 10^{-6}/8 \times 10^{-6}$	−0.02	0
$4 \times 10^{-6}/8 \times 10^{-6}$	−0.13	0
PAA/Py–PEG–Py(4800) molar ratio		
1	0	84
2	−0.02	125

NOTES: τ is the fluorescence lifetime of Py–PEG–Py in the presence of colloidal particles and (possibly) displaced chains; τ_B is the fluorescence lifetime of Py–PEG–Py in water; ν is the excimer fluorescence excitation spectrum band position of Py–PEG–Py in the presence of colloidal particles and (possibly) displaced chains; and ν_B is the excimer fluorescence excitation spectrum band position of Py–PEG–Py in water.

samples had excimer lifetimes approximately 30% shorter than the polymer in bulk solution. Likewise, these samples exhibited a frequency shift in the excimer excitation spectrum corresponding to some strain in the excimer complex. By contrast, the next three entries in Table I correspond to solutions where 70% of the tagged chains had desorbed from the surface; in these cases, the excimer lifetime and excitation spectrum are relatively unchanged from the original bulk solution. Thus, we found a trend showing a frequency shift coupled to a decrease in lifetime and indicating a strained excimer-forming site, somehow perturbed by the chain adsorption onto the colloidal surface.

In the analogous complex-formation study with polar PAA, the excimer excitation frequency was substantially shifted upon complexation; it was not, however, accompanied by the decrease in excimer lifetime found in the adsorption work. Two representative results are included in Table I corresponding to [PAA]/[Py–PEG–Py(4800)] molar ratios of 1 and 2. This difference indicates that perhaps the excimer is not as strained or destabilized by complexation as it is by adsorption onto solid particles. Therefore, the complexation may result in enough environmental change to shift the excimer excitation spectrum, but the excimers are not strained by complexation nearly as much as by adsorption onto a solid surface.

Discussion

The thrust of the research just described has been to understand the molecular-level interactions that take place between poly(ethylene glycol) and a variety of polymeric or colloidal substrates in aqueous solution. Use of the

fluorophore end-labeled probe to study these interactions is a novel concept and, as such, must be examined closely to ensure that its power as well as its limitations are understood.

The experimental quantity easiest to observe in a photophysical experiment such as the ones described herein is I_D/I_M, the ratio of excimer to monomer emission intensities. Interpretation of the results is not completely straightforward, however. Winnik (28) has shown that I_D/I_M for the end-labeled polymers in dilute solution is proportional to the rate constant for cyclization; as such, it may be interpreted in terms of the influence of molecular weight and solvent quality on the configurational statistics of the chain.

The situation is considerably more complicated for the macromolecular complexes and adsorption studies. For example, the intramolecular contribution to I_D/I_M decreased when low molecular weight Py–PEG–Py chains were either complexed with PAA (890,000), as shown in Figure 1, or adsorbed on colloidal Ludox AM silica particles, as shown in Figure 4. The straightforward explanation of these particular observations is that the probe chain mobility was reduced as a result of interactions of the ethylene oxide backbone units with either the carboxylic acid moieties of the PAA or with the surface silanol groups of the silica particle. Although this hypothesis seems quite reasonable, it is then perplexing, on the basis of only the I_D/I_M data, to understand why the decrease in cyclization rate is so much more dramatic when the Py–PEG–Py interacts with the PMAA or the colloidal polystyrene particle. Moreover, differences in the behavior of the low and high molecular weight Py–PEG–Py samples persist after the results are normalized to the initial solution values before complexation or adsorption.

Part of the difficulty in interpretation may arise from the fact that intermolecular interactions between Py–PEG–Py will also contribute to the observed I_D/I_M. This point was explicitly examined in the initial work on the macromolecular complexation (32, 41). In this work, it was assumed that the intermolecular contribution was simply that resulting when the intramolecular portion was subtracted from the I_D/I_M value of the fully labeled PEG sample, but as Figure 2 shows, normalization to the initial solution value of I_D/I_M before addition of the poly(carboxylic acid) did not provide much simplification. With reference to the data for the Py–PEG–Py(9200) mixed with the 40% neutralized PMAA(9500) for which no complexation occurs, we see that there are dramatic overshoots at low poly(carboxylic acid) content and plateau values at high acid content that lie either above or below the neutralized data.

It may be possible to explain the decreases in the normalized I_D/I_M values for the fully labeled PEG (Figure 2) below the initial solution value through consideration of the influence of the complexation on the hydrophobic attraction between the pyrene groups. We previously observed (32) that the short-chain Py–PEG–Py molecules exhibit an apparent cyclization

rate that is about 7 times higher in water than in an organic solvent of the same viscosity. This difference was attributed to the formation of aggregates of pyrene groups that allowed the reduction of the amount of ordered water molecules that result when a hydrophobic group is surrounded by a solvent shell of water molecules. When a poly(carboxylic acid) chain is added to the solution containing the aggregated Py–PEG–Py, it is expected that these clusters would be broken up if the interactions between the PEG backbone units with the poly(carboxylic acid) were strong enough. Figure 2 suggests that the PMAA(9500) is completely effective in breaking up the initial aggregate of the Py–PEG–Py(4800) because the plateau value is approximately one-fifth of the initial. The PAA(890,000) is not as efficient, however. Although the trend was the same for the Py–PEG–Py(9200) sample, the final plateau values bracket that observed for the neutralized PMAA.

Interpretation of the initial overshoot in Figure 2, solely on the basis of the emission spectra, is much more difficult. One reason might be that contributions to the I_D/I_M ratio come from two general processes. The first encompasses all physical phenomena associated with the diffusion of fluorophores close enough to form a suitable excimer forming site (EFS). This portion of the overall photophysical process will depend upon the molecular weight of the polymer, the thermodynamic quality of the solvent, the temperature, and the concentration. These variables are important when one is attempting to use the end-labeled polymers as probes of chain configuration and morphology.

The second contribution to the emission spectra comes from factors that influence the stability of the EFS once it is formed, specifically, local interactions of the immediate solvent shell with the paired chromophores in an EFS. For large fused-ring systems such as pyrene, many possible types of overlap of the rings could permit excimer formation. This expectation is supported by the very large binding energy of the pyrene excimer relative to other aromatic rings (45). Although the binding energy is commonly assumed to be independent of the solvent (45), we have found that excimer formation in poly(1-vinylnaphthalene) depends upon solvent shape and size for a homologous series of alkylbenzenes (46). If a similar situation applies for the pyrene excimer, the changing environment of the Py–PEG–Py in the PMAA and PAA complexes and adsorbed on the silica or polystyrene particles probably would be reflected in the I_D/I_M value.

It should be possible, in principle, to separate the two contributions to I_D/I_M by control of the temperature. Extensive experiments with solutions of aromatic chromophores unbound to polymer chains have shown that at sufficiently low temperatures, excimer formation will be diffusion controlled. At sufficiently high temperatures, the Birks dynamic equilibrium regime will be reached, and the binding energy of the system will be the important parameter. This treatment of the photophysics appears to work quite well for the free chromophores in solution and even for the end-labeled chains

in dilute solution, but it may break down for the special situation of the constrained geometry in the macromolecular complex or in the colloidal adsorption cases. This problem occurs because both situations can cause the pyrene rings to be juxtaposed in sufficiently strained geometry that ground-state interactions can occur. It is not possible to detect this effect solely from measurement of I_D/I_M, but it can be monitored with the excitation spectra.

A major lesson that we have learned in this work is that the excitation spectra provide very localized information about the environment of the isolated or paired pyrene chromophores. We do not yet have a detailed understanding of the quantitative significance of the magnitude of the shifts in excitation spectra or of the changes in bandwidths; however, the monomer excitation spectra demonstrate that the placement of the isolated ring in an hydrophobic environment leads to a red shift. This conclusion was true for complexation with PMAA, adsorption on polystyrene particles, or dissolution in toluene solution. Shifts in the excimer-excitation spectra show clearly that the excimer-forming site is somehow different when the Py–PEG–Py is involved in a macromolecular complex or adsorbed on silica than free in solution. Finally, the shorter lived excimer lifetimes observed for adsorption on silica compared to no change in lifetime during complexation with PAA show that adsorption on colloidal particles strains the excimer complex more than does the interaction with the poly(carboxylic acid).

Acknowledgment

References

1. Guillet, J. *Polymer Photophysics and Photochemistry*; Cambridge University Press: Cambridge, 1985.
2. *Polymer Photophysics*; Phillips, D., Ed.; Chapman and Hall: London, 1985.
3. *Luminescence from Biological and Synthetic Macromolecules—Eighth Katzir Conference*; Morawetz, H.; Steinberg, I. Z., Eds.; New York Academy of Sciences: New York, 1981; Vol. 366.
4. *Photophysical and Photochemical Tools in Polymer Science*; Winnik, M. A., Ed.; NATO ASI Series C: Mathematical and Physical Sciences; Reidel: Dordrecht, 1986; Vol. 182.
5. *Photophysics of Polymers*; Hoyle, C. E.; Torkelson, J. M., Eds.; ACS Symposium Series 358; American Chemical Society: Washington, DC, 1987.
6. Tang, W. T. Ph. D. Thesis, Stanford University, 1987.
7. Gashgari, M. A.; Frank, C. W. *Macromolecules* 1981, *14*, 1558–1567.
8. Gelles, R.; Frank, C. W. *Macromolecules* 1982, *15*, 741–747.

9. Gelles, R.; Frank, C. W. *Macromolecules* **1982**, *15*, 747–752.
10. Gelles, R.; Frank, C. W. *Macromolecules* **1983**, *16*, 1448–1456.
11. Semerak, S. N.; Frank, C. W. *Macromolecules* **1984**, *17*, 1148–1157.
12. Semerak, S. N.; Frank, C. W. In *Polymer Blends and Composites in Multiphase Systems*; Han, C. D., Ed.; Advances in Chemistry 206; American Chemical Society: Washington, DC, 1984; pp 77–100.
13. Frank, C. W.; Zin, W. C. In *Photophysics of Polymers*; Hoyle, C. E.; Torkelson, J. M., Eds.; ACS Symposium Series 358; American Chemical Society: Washington, DC, 1987; pp 18–36.
14. Hemker, D. J.; Frank, C. W.; Thomas, J. W. *Polymer* **1988**, *29*, 437–447.
15. Hoyle, C. E.; Kim, K. J. In *Photophysics of Polymers*; Hoyle, C. E.; Torkelson, J. M., Eds.; ACS Symposium Series 358; American Chemical Society: Washington, DC, 1987; pp 201–218.
16. Ediger, M. D.; Fayer, M. D. *J. Phys. Chem.* **1984**, *88*, 6108–6116.
17. Ediger, M. D.; Domingue, R. P.; Peterson, K. A.; Fayer, M. D. *Macromolecules* **1985**, *18*, 1182–1190.
18. Peterson, K. A.; Fayer, M. D. *J. Chem. Phys.* **1986**, *85*, 4702–4711.
19. Peterson, K. A.; Zimmt, M. B.; Linse, S.; Domingue, R. P.; Fayer, M. D. *Macromolecules* **1987**, *20*, 168–175.
20. Tang, W. T.; Hadziioannou, G.; Smith, B. A.; Frank, C. W. *Polymer* **1988**, *29*, 1313–1317.
21. Jeng, Y. H.; Shi, M. L.; Frank, C. W., submitted to *Macromolecules*.
22. Tang, W. T.; Hadziioannou, G.; Smith, B. A.; Frank, C. W. *Polymer* **1988**, *29*, 1718–1723.
23. Oyama, H. T.; Tang, W. T.; Frank, C. W. In *Photophysics of Polymers*; Hoyle, C. E.; Torkelson, J. M., Eds.; ACS Symposium Series 358; American Chemical Society: Washington, DC, 1987; pp 422–433.
24. Perico, A.; Cuniberti, C. *J. Polym. Sci., Polym. Phys. Ed.* **1977**, *15*, 1435.
25. Cuniberti, C.; Perico, A. *Prog. Polym. Sci.* **1984**, *10*, 271.
26. Ushiki, H.; Horie, K.; Okamoto, A.; Mita, I. *Polym. J.* **1981**, *13*, 191.
27. Horie, K.; Schnabel, W.; Mita, I.; Ushiki, H. *Macromolecules* **1981**, *14*, 1422.
28. Winnik, M. A. *Acc. Chem. Res.* **1985**, *18*, 73–79.
29. Winnik, M. A. In *Photophysical and Photochemical Tools in Polymer Science*; Winnik, M. A., Ed.; NATO ASI Series C: Mathematical and Physical Sciences; Reidel: Dordrecht, 1986; pp 293–324, Vol. 182.
30. Winnik, M. A.; Redpath, A. E. C.; Paton, K.; Danhelka, J. *Polymer* **1984**, *25*, 91–99.
31. Redpath, A. E. C.; Winnik, M. A. *Ann. N. Y. Acad. Sci.* **1981**, *366*, 75–92.
32. Oyama, H. T.; Tang, W. T.; Frank, C. W. *Macromolecules* **1987**, *20*, 474–480.
33. Char, K.; Frank, C. W.; Gast, A. P.; Tang, W. T. *Macromolecules* **1987**, *20*, 1833–1838.
34. Bekturov, E. A.; Bimendina, L. A. *Adv. Polym. Sci.* **1981**, *41*, 99.
35. Tsuchida, E.; Abe, K. *Adv. Polym. Sci.* **1982**, *45*, 1.
36. Howard, G. J.; McConnell, P. *J. Phys. Chem.* **1967**, *71*, 2974–2980.
37. Killmann, E. *Polymer* **1976**, *17*, 864–868.
38. Rubio, J.; Kitchener, J. A. *J. Colloid Interface Sci.* **1976**, *57*, 132–142.
39. Jopplen, G. R. *J. Phys. Chem.* **1978**, *82*, 2210–2215.
40. Hommel, H.; Legrand, A. P.; Tougne, P.; Balard, H.; Papirer, E. *Macromolecules* **1984**, *17*, 1578–1581.
41. Oyama, H. T.; Tang, W. T.; Frank, C. W. *Macromolecules* **1987**, *20*, 1839–1847.
42. Char, K.; Gast, A. P.; Frank, C. W. *Langmuir* **1988**, *4*, 989–998.
43. Scheutjens, J. M. H. M.; Fleer, G. J. *J. Phys. Chem.* **1980**, *84*, 178–190.

44. Scheutjens, J. M. H. M.; Fleer, G. J.; Cohen Stuart, M. A. *Colloids Surf.* **1986**, *21*, 285–306.
45. Birks, J. B. *Photophysics of Aromatic Molecules*; Wiley–Interscience: New York, 1970.
46. Frank, C. W., unpublished results.

Determination of the Unperturbed Dimensions of Polymers of (+)-Catechin and (−)-Epicatechin

The Role of Fluorescence

Wayne L. Mattice

Institute of Polymer Science, The University of Akron, Akron, OH 44325

Polymers of (+)-catechin and (−)-epicatechin have an intrinsic fluorescence because chromophores are an integral part of each monomer unit. The time-resolved emission from well-characterized dimers can be used to determine the relative populations of two rotational isomers at the interflavan bond between monomer units. When combined with the solid-state conformations, molecular mechanics calculations, and rotational isomeric state analysis, the interpretation of the time-resolved fluorescence leads to the unperturbed dimensions of the polymers. Significant population of both rotational isomers causes the chains to have unperturbed dimensions comparable with those in atactic polystyrene molecules of the same molecular weight.

POLYMERS OF (+)-CATECHIN AND (−)-EPICATECHIN are known as polymeric procyanidins or condensed tannins (*1–3*). The monomer units are depicted in structure 1. Polymers with monomer units connected by carbon–carbon bonds from C-4 to either C-6 or C-8 are widespread in the plant kingdom. An example of polymers with C-4 to C-8 bonds is depicted in structure 2. Monomers and smaller oligomers are soluble in water, but solubility decreases at the higher degrees of polymerization. The polymeric procyanidins form complexes with a wide range of water-soluble polymers; formation of complexes with poly(amino acids) provides the molecular basis for their

1. Covalent structure of (+)-catechin. Hydrogen atoms bonded to carbon atoms are omitted. The numbering system for the carbon atoms in the heterocyclic ring system is shown. The covalent structures of (+)-catechin and (–)-epicatechin differ in their stereochemistry at C-3.
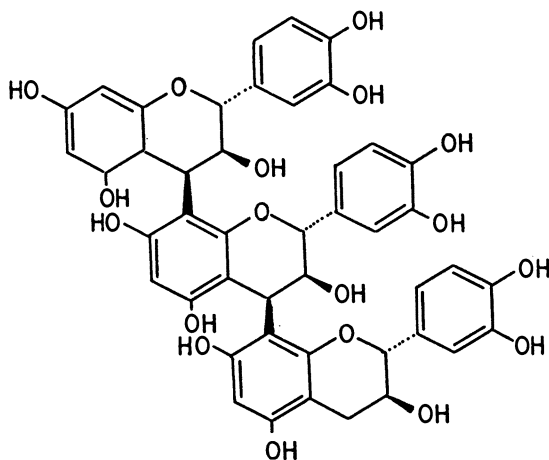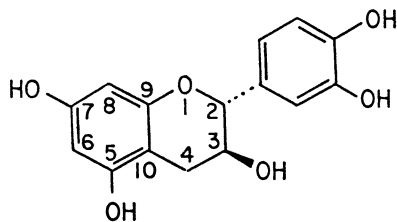
2. A short homopolymer of (+)-catechin with 4β→8 interflavan bonds. Heavy lines denote the main chain considered in the evaluation of $<r^2>_0$ (see definition on p 291). Hydrogen atoms bonded to carbon atoms are omitted.

biophysical role as agents that protect a plant from predation (4–7). Complex formation also occurs with commercially important water-soluble polymers such as poly(vinylpyrrolidone).

Determination of the unperturbed dimensions of the polymeric procyanidins presents special challenges. Well-characterized samples of high molecular weight are not readily available, and the solubility characteristics of the high polymers are incompatible with the application of the classical techniques for the measurement of the dimensions of a macromolecule. An alternative route to the unperturbed dimensions exploits structural determinations in the solid state (8, 9), spectroscopic studies of well-characterized oligomers in dilute solution (10, 11), molecular mechanics (MM2 software) (12) calculations (13, 14), and rotational isomeric state analysis (15–17) to provide a realistic description of the dimensions of the high polymers. A vital piece of information comes from the time-resolved fluorescence of the monomers and oligomers of well-defined covalent structure. The fluorescence measurements also show promise for the characterization of the com-

plexes formed by polymeric procyanidins and other water-soluble polymers. The status of this effort is described in this chapter.

Structures in the Solid State

Two independent determinations of the structure of (–)-epicatechin in the crystalline state have been performed (8, 18). The reports describe the same basic structure, but that of Fronczek et al. (8) provides higher resolution. The heterocyclic ring is approximately a half-chair with C-2 26.3 pm above and C-3 49.5 pm below the mean plane of the fused ring system (8). The dihydroxyphenyl substituent at C-2 adopts a pseudoequatorial position. Thus far, (+)-catechin has resisted crystallization into a form amenable to a structure determination. Molecular mechanics calculations that reproduce the observed structure of (–)-epicatechin predict that the heterocyclic ring in (+)-catechin has a similar conformation (9).

Crystal structures have been reported for several derivatives of (+)-catechin and (–)-epicatechin (9, 19–22). The heterocyclic rings adopt a different conformation in some of these derivatives. The most dramatic instance is seen in penta-O-acetyl-(+)-catechin, in which the heterocyclic ring is puckered so that the dihydroxyphenyl substituent at C-2 adopts a pseudoaxial axial position (20). The derivative that has the greatest relevance for the polymers is depicted in structure 3, as reported by Porter et al. (9). The bond from C-4 to the phloroglucinol substituent is similar to the bond from C-4 to the next monomer unit in a C-4–C-6- or C-4–C-8-linked polymer. The bulky phloroglucinol substituent at C-4 causes the heterocyclic ring to adopt a conformation different from that seen in free (–)-epicatechin (8). Molecular mechanics (MM2) predicts a conformation for the heterocyclic ring that is in excellent agreement with the structure determined in the crystal (9). The ability of molecular mechanics to describe correctly the heterocyclic ring conformations in underivatized (–)-epicatechin and also in
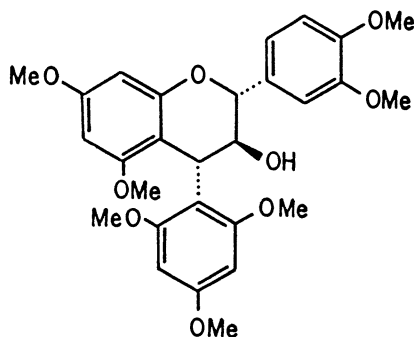
3. Covalent structure of (2R,3S,4R)-3',4',5,7-tetramethoxy-4(2,4,6-trimethoxyphenyl)flavan-3-ol. Hydrogen atoms bonded to carbon atoms are omitted.

the derivative depicted in structure 3 justifies use of this force field for the prediction of the conformations adopted in dimers.

Theoretical Conformational Analysis of Dimers

Molecular mechanics has been used to optimize the conformations of 32 dimers (13, 14). The 32 dimers arose from the exhaustion of all possible combinations of (+)-catechin or (–)-epicatechin for the first monomer unit, (+)-catechin or (–)-epicatechin for the second monomer unit, C-4–C-6 or C-4–C-8 linkage of the two units, α or β stereochemistry at C-4, and pseudoequatorial or pseudoaxial orientation of the dihydroxyphenyl rings at C-2 in both monomers. Dimers are of lower energy when the dihydroxyphenyl rings at C-2 adopt pseudoequatorial positions (14). The conformation of the heterocyclic ring depends on the selection of a pseudoaxial or pseudoequatorial orientation for the dihydroxyphenyl substituent at C-2. In addition, the heterocyclic rings respond to the linkage type and to the dihedral angle adopted at the interflavan bond (13, 14). The heterocyclic rings adopt a continuous range of conformations that are obtained by coordinated movement over a range of about 40 pm of C-2 and C-3 with respect to the mean plane of the fused ring system. The structures of the heterocyclic rings for the various derivatives in the crystalline state fall in the ranges defined by the molecular mechanics calculations for the 32 dimers. The dihedral angles have been tabulated for the bonds in the heterocyclic rings in the optimized structures for 32 dimers (13, 14).

Each dimer has two distinct low-energy conformations at the interflavan bond. These two rotational isomers are separated by a rotation of about 180 °C. The dihedral angles at the minima can be accurately defined because the wells are narrow. Consequently, the geometry of the rotational isomers is well-established in each dimer (13, 14). Precise specification of the relative energies at the two minima is difficult. There are simply too many interactions and too many degrees of freedom by which the dimer can achieve substantial changes in energy with very small changes in the dihedral angles in the heterocyclic rings, at the interflavan bond, and at C–O bonds to hydroxyl groups. The difference in the energies between the two minima appears to be sufficiently small so that there will be significant population of both rotational isomers at ordinary temperatures.

The unperturbed dimensions of the high polymers depend very strongly on the relative populations of the two rotational isomers at the interflavan bond. If one rotational isomer in a homopolymer were populated to the exclusion of the other, the local conformation would describe a helix and the overall shape would be that of a rod. Significant population of the second rotational isomer converts the rod to a random coil. The molecular mechanics calculations do not provide the relative energies of the two rotational isomers with the accuracy required for description of the unperturbed dimensions.

Populations Deduced from Time-Resolved Fluorescence

Absorption spectra for the un-ionized monomers in dilute solution show a single band near 280 nm. Separate contributions from the two aromatic ring systems cannot be resolved. Excitation at 280 nm produces a single emission band at 310–320 nm (*10, 11*). Attempts to resolve contributions from the individual chromophores have been unsuccessful. Neither the location of the emission band nor the quantum yield for fluorescence depends convincingly on excitation wavelength, and the time, t, dependence of the emission, $I(t)$, can be described by a single exponential decay with lifetime τ.

$$I(t) = \alpha \exp(-t/\tau) \tag{1}$$

where α is the preexponential factor.

The monomers have similar excitation spectra, emission spectra, fluorescence quantum yields, and fluorescence lifetimes (*10, 11*). Although each monomer contains two chromophores, it can be treated as a single-chromophore system. For purposes of fluorescence measurements, (+)-catechin and (–)-epicatechin are identical. The lifetimes obtained in dioxane solutions are 2 ns, as shown in Table I. In aqueous solution, both the quantum yields and lifetimes are reduced by a factor of 3, but, otherwise, the behavior is the same as in dioxane. Measurements are more conveniently performed in dioxane because the quantum yields for fluorescence are larger in this medium.

Dimers exhibit steady-state emission in the same spectral range as the monomers, but with reduced quantum yield (*10*). An important difference exists between the time-resolved emission of the monomers and various dimers. In the absence of artificial constraints on the rotation about the interflavan bond, the time dependence of the emission from a dimer cannot

Table I. Fluorescence Lifetimes and Preexponential Factors in Dioxane

Compound	τ_1 (ns)	τ_2 (ns)	$\alpha_1/(\alpha_1 + \alpha_2)$
C	2.00 ± 0.05		1
E	2.04 ± 0.05		1
E(4β→6)C	1.08 ± 0.05	1.9 ± 0.3	0.85 ± 0.08
E(4β→8)C	1.25 ± 0.08	2.0 ± 0.4	0.75 ± 0.15
Constrained	1.06 ± 0.10		1
Peracetylated	0.48 ± 0.05	1.4 ± 0.2	0.90 ± 0.05

NOTES: C, (+)-catechin; E, (–)-epicatechin; constrained, the dimer depicted in structure 4; peracetylated, the decaacetate of E(4β→6)C.
SOURCE: Ref. 10.

be described by equation 1. The time dependence is, however, well-described by a sum of two exponential decays.

$$I(t) = \alpha_1 \exp(-t/\tau_1) + \alpha_2 \exp(-t/\tau_2) \qquad (2)$$

The values of the parameters for (−)-epicatechin-(4β→6)-(+)-catechin and (−)-epicatechin-(4β→8)-(+)-catechin, are presented in the third and fourth lines in Table I. The lifetimes are shorter for the dimers than for the monomers. The two decay processes do not contribute equally to the time dependence of the emissions from the dimers. The preexponential factor is larger for the shorter lifetime. Two independent types of experiments that will be described, show that rotational isomerism at the interflavan bond is responsible for the heterogeneity of the time-dependence emission from the dimers.

The fifth line in Table I presents the decay parameters for the constrained dimer, structure 4. The bridging ring forces the population of a single rotational isomer at the interflavan bond. The time dependence of the emission for the constrained dimer is satisfactorily described by the single exponential decay (equation 1). In contrast, a satisfactory description of the emission from unconstrained dimers requires the sum of two exponential decays (equation 2).

The last line in Table I presents decay parameters for a dimer in which all 10 hydroxyl groups have been acetylated. Acetylation reduces τ_1 and τ_2, but there is not much change in α_1 and α_2. More importantly, acetylation increases the size of the energy barrier that must be surmounted when the dimer undergoes the conformational transition from one rotational isomer to the other. For this reason, the rate of intramolecular conformational change is much slower in the peracetylated dimer than in the free phenol forms; it is slow enough so that 400-MHz proton NMR can resolve distinct signals from the two rotational isomers in dioxane-d_8 solution (10). The
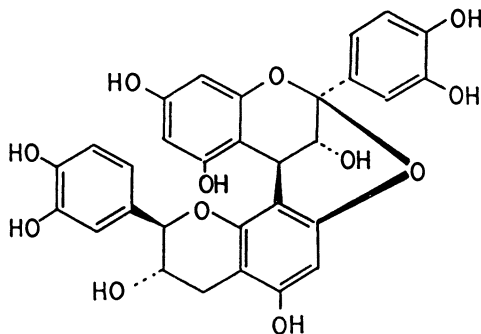
4. Covalent structure of a bridged dimer. The extra ring prohibits rotation about the interflavan bond. Hydrogen atoms bonded to carbon atoms are omitted.

resonances are easily assigned by the scheme used by Rauwald (*23*) for the same compound in nitrobenzene-d_5. Comparison of the integrated areas under the peaks assigned to the two rotational isomers in the NMR spectrum yields populations of 84:16 for the two species of the peracetylated dimer. The last line in Table I shows that a similar population (90:10) is deduced from the ratio of the preexponential factors. Removal of the acetyl groups produces a first-order NMR spectrum in dioxane-d_8, but the rotational isomers are still resolved in the fluorescence measurement because the time scale for fluorescence (nanoseconds) is much faster than the NMR time scale.

The description of the emission in the constrained dimer by equation 1, and the successful correlation of the populations deduced for the peracetylated dimer from 400-MHz proton NMR, with the preexponential factors in equation 2 show that the heterogeneity of the emission in the unconstrained dimers arises from the population of two rotational isomers at the interflavan bond. The populations of these rotational isomers in the free phenol forms can be deduced from the preexponential factors on the third and fourth lines of Table I. This assignment of the populations provides the necessary ingredient for a rotational isomeric state analysis of the unperturbed dimensions of the polymers.

Rotational Isomeric State Analysis of the Unperturbed Dimensions

The information required to construct a rotational isomeric state description of a polymer consists of the bond lengths, bond angles, dihedral angles, and weighting of the rotational isomers that arises from the presence of short-range interactions (*24*). All of this information is produced by the crystal structures, molecular mechanics calculations, and time-resolved fluorescence measurements already described. Straightforward implementation of the usual rotational isomeric state formalism yields the unperturbed dimensions of polymers in which the dihydroxyphenyl substituents at C-2 adopt pseudoequatorial positions and the interflavan bonds extend from C-2 to C-8 (*15*) or from C-2 to C-6 (*16*). The influence of the incorporation of monomer units in which the dihydroxyphenyl group at C-2 adopts a pseudoaxial position has also been evaluated (*17*). The parameter of ultimate interest is the characteristic ratio, C_x, defined here for a chain composed of x monomer units as

$$C_x = <r^2>_0 / \Sigma\, l_i^2 \qquad (3)$$

where $<r^2>_0$ denotes the mean square end-to-end distance for an ensemble unperturbed by long range interactions, and the denominator is the sum of the squares of the lengths of the bonds in the chain from one end of the atom to the other. This chain runs from the free C-8 at one end to the free C-4 at the other end, as shown in structure 2. It contains $4x - 1$ bonds. A

generator matrix, G, is formulated for each bond in the usual manner (24), and $<r^2>_0$ is calculated by (15–17)

$$<r^2>_0 = G_1 G_2 \cdots G_{4x-1} \tag{4}$$

As x becomes infinite, C_x approaches a limiting value, unless one rotational isomer is populated to the exclusion of the other. The limit is denoted simply by C. The value of C is quite sensitive to the relative population of the two rotational isomers at the interflavan bond (15–17). C is also affected by the type of interflavan linkage, either C-2→C-6 or C-4→C-8, and by the stereochemistry at C-4; however, it is rather insensitive to the substitution of (–)-epicatechin for (+)-catechin (i.e., it is insensitive to the stereochemistry at C-3). The smallest C values are obtained when there is an approximately equal population of the two rotational isomers. These minimum C values range from 3 to 14 and are smallest for polymers with 4α→6 interflavan linkages (16) and largest for polymers with 4α→8 interflavan linkages (15).

Somewhat larger values of C are obtained when the rotational isomers are populated in the manner described by the preexponential factors listed in the third and fourth lines of Table I for dimers in which there is β stereochemistry at C-4. The calculated values of C for polymers with β stereochemistry then range from 5 to slightly above 20, with the C-4→C-6-linked polymers tending to have the lower dimensions. The range of C values for the C-4→C-6-linked polymers is about 5–15 (16); for the C-4→C-8-linked polymers it is 16–23 (15). The significance of these values becomes clearer upon comparison with polystyrene. A peracetylated polymeric procyanidin and a polystyrene chain of the same molecular weight will have identical $<r^2>_0$ values if C is 27 for the procyanidin polymer (15). This value is obtained from C for atactic polystyrene (25) and incorporation of the different mass per bond in the two types of monomers. Because the calculated values of C for the β-linked polymeric procyanidins are less than 27, they are less extended than unperturbed polystyrene chains of the same molecular weight. This conclusion is compatible with the behavior of peracetylated procyanidin polymers and polystyrene in gel-permeation experiments (2). The improved molecular picture of the conformational properties of the polymeric procyanidins and the ability to study rotational isomerism by the time-resolved fluorescence of these chains may be useful in the development of an understanding of their formation of complexes with β sheets (26), poly(vinylpyrrolidone), and poly(L-proline) (11).

Acknowledgment

References

1. Haslam, E. *Phytochemistry* 1977, *16*, 1625.
2. Porter L. J. *Rev. Latinoam. Quim.* 1984, *15*(2), 43.
3. Hemingway, R. W. In *Natural Products Extraneous to the Lignocellulosic Cell Wall of Woody Plants*; Rowe, J. W., Ed.; Springer-Verlag: Berlin, in press.
4. Haslam, E. *Biochem. J.* 1974, *139*, 285.
5. Oh, H. I.; Hoff, J. E.; Armstrong, G. S.; Hoff, L. A. *J. Agric. Food Chem.* 1980, *28*, 384.
6. Hagerman, A. E.; Butler, L. G. *J. Biol. Chem.* 1981, *256*, 4494.
7. Karchesy, J. J.; Kreibich, R. E. *J. Appl. Polym. Sci.: Appl. Polym. Symp.* 1984, *40*, 79.
8. Fronczek, F. R.; Gannuch, G.; Mattice, W. L.; Tobiason, F. L.; Broeker, J. L.; Hemingway, R. W. *J. Chem. Soc., Perkin Trans. 2* 1984, 1611.
9. Porter, L. J.; Wong, R. Y.; Benson, M.; Chan, B. G.; Viswanadhan, V. N.; Gandour, R. D.; Mattice, W. L. *J. Chem. Res.* 1986, (S) 86, (M) 830.
10. Bergmann, W. R.; Barkley, M. D.; Hemingway, R. W.; Mattice, W. L. *J. Am. Chem. Soc.* 1987, *109*, 6614.
11. Bergmann, W. R.; Mattice, W. L. In *Photophysics of Polymers*; Hoyle, C. E.; Torkelson, J. M., Eds.; ACS Symposium Series 358; American Chemical Society, Washington, D.C., 1987; p 162.
12. Allinger, N. L.; Yuh, Y. H. Quantum Chemistry Program Exchange, 1980, No. 395.
13. Viswanadhan, V. N.; Mattice, W. L. *J. Comput. Chem.* 1986, *7*, 711.
14. Viswanadhan, V. N.; Mattice, W. L. *J. Chem. Soc., Perkin Trans. 2* 1987, 739.
15. Viswanadhan, V. N.; Bergmann, W. R.; Mattice, W. L. *Macromolecules* 1987, *20*, 1539.
16. Bergmann, W. R.; Viswanadhan, V. N.; Mattice, W. L. *J. Chem. Soc., Perkin Trans. 2*, 45.
17. Viswanadhan, V. N.; Mattice, W. L. *Int. J. Biol. Macromol.* 1988, *10*, 9.
18. Spek, A. L.; Kojic-Prodic, B.; Labadie, R. P. *Acta Crystallogr., Sect. C: Cryst. Struct. Commun.* 1984, *C40*, 2068.
19. Engel, E. L.; Hattingh, M.; Hundt, K. L.; Roux, D. G. *J. Chem. Soc., Chem. Commun.* 1987, 695.
20. Fronczek, F. R.; Gannuch, G.; Mattice, W. L.; Hemingway, R. W.; Chiari, G. W.; Tobiason, F. L.; Houglum, K.; Shanafelt, A. *J. Chem. Soc., Perkin Trans. 2* 1985, 1383.
21. Einstein, F. W. B.; Kiehlmann, E.; Wolowidnyk, E. K. *Can. J. Chem.* 1985, *63*, 2176.
22. Boevens, J. C. A.; Denner, L.; Kolodziej, H.; Ferreira, D.; Roux, D. G. *J. Chem. Soc., Perkin Trans. 2* 1986, 310.
23. Rauwald, H. W. *Planta Med.* 1982, *46*, 110.
24. Flory, P. J. *Macromolecules* 1974, *7*, 381.
25. Flory, P. J. *Statistical Mechanics of Chain Molecules*; Wiley: New York, 1969; p 40.
26. Tilstra, L. F.; Maeda, H.; Mattice, W. L. *J. Chem. Soc, Perkin Trans. 2* 1988, 1613.

Fourier Transform Infrared and Raman Spectroscopy of Water-Soluble Polymers

Structural Analysis and Interactions

Marek W. Urban

Department of Polymers and Coatings, North Dakota State University, Fargo, ND 58105

This chapter covers the applications of Fourier transform infrared (FTIR) and Raman spectroscopy to the characterization of water-soluble polymers. The structural analysis of poly(oxyethylene), poly(ethylene glycol), poly(methacrylic acid), and poly(acrylic acid), and the interactions of selected polymers with solvents and surfactants are presented. Structural features of these compounds in the crystalline and melt states are compared with their structural features upon dissolution in aqueous solvents. Special emphasis is given to the recent studies of the interactions between water-soluble polymers or copolymers and solvents or surfactants. New experimental approaches and the sensitivities of both FTIR and Raman spectroscopy to monitor such interactions are presented.

Т HE VIBRATIONAL SPECTRUM of any material consists of two parts: the infrared (IR) and Raman spectra. IR spectroscopy is sensitive to the changes in dipole moment that occur during the vibrations of atoms that are forming chemical bonds. Raman spectroscopy detects the polarizability tensor changes of the electron clouds that surround these atoms. These apparent differences in the physical principles of both effects have led to the development of these two distinctly different techniques. IR and Raman spectra complement each other. Because they are sensitive to the vibrations of atoms, they are called vibrational spectra.

When monochromatic radiation of frequency ν_0 irradiates a sample in a region in which it is transparent, the light is scattered from the sample. Most of this scattered light consists of radiation at the frequency of the incident light but differs in the direction of propagation. This elastic scattering process is known as *Rayleigh scattering*. A small fraction of the scattered light is composed of new modified frequencies ($\nu_0 \pm \nu_k$). The frequency change is equal to the frequencies associated with transitions between various vibrational energy levels of the molecule. Scattering of the radiation with change of frequency (inelastic scattering) is called the *Raman effect*.

At one time, the progress in the field of Raman spectroscopy of polymers was heavily dependent upon laser technology. The advent of accessible laser sources made it possible to replace the mercury-discharge lamp as an excitation source. Other developments, such as photomultipliers, computerization, or, most recently, sensitive array detectors made a tremendous impact on applications of this method in polymer analysis.

IR spectroscopy is based on the absorption of IR light as it passes through a sample. A plot of transmitted energy as a function of wavenumber is called the IR spectrum. In recent years, this old technique has diverged into two apparently different spectroscopies: dispersive and interferometric. The techniques provide the same information with different degrees of sensitivity. Because of its high-energy throughput, speed of measurement, and enhanced sensitivity, Fourier transform IR (FTIR) spectroscopy belongs to the category of interferometric methods that now dominates the field. These advantages led to the development of various sampling techniques, one of which, attenuated total reflectance (ATR) spectroscopy, plays a key role in the studies of species dissolved in aqueous solvents.

The theory of IR (or FTIR) and Raman spectroscopy has been reviewed in several monographs (*1–3*) and various general references on Raman spectroscopy (*3–6*). The objective of this review is to survey the spectroscopic results obtained for various water-soluble polymers and to evaluate recent experimental techniques. In particular, this chapter will focus on the studies of selected water-soluble polymers and copolymers and their interactions with solvents and surfactants.

Polyoxyethylene

Macromolecules exist in a variety of conformational forms that range from randomly coiled chains to more spatially ordered structures. Of particular interest are the polymers that adopt helical symmetry. Helical conformation is a result of an orderly repeated unit with internal rotational angles along the polymer backbone. In the crystalline state, polyoxyethylene exists in a helical conformation that contains seven chemical units (–CH_2CH_2–O–) and two turns in a backbone identity period of 19.3 Å (*7–9*).

Although this structure is well-established today, in the early 1970s it was widely debated until Koenig et al. (9) identified dihedral symmetry of this polymer on the basis that no Raman bands were observed at the same frequencies as the parallel IR bands. The Raman spectrum of polyoxyethylene (POE) is given in Figure 1, and Table I lists the band assignments. The band assignments were obtained on the basis of the symmetry considerations and Urey–Bradley force-field calculations.

Vibrational spectra were treated by the cyclic factor group $C(4\Pi/7)$ or $C(10\Pi/7)$ and the dihedral factor group $D(4\Pi/7)$ or $D(10\Pi/7)$, depending upon whether the helical chain possessed two twofold axes with one axis passing through the oxygen atom and the other bisecting the C–C bond. The calculations indicated that for the cyclic group analysis ($C(4\Pi/7)$ and its isomorph $C(10\Pi/7)$), the IR and Raman bands should be observed at the

**Table I. Band Assignments for the Raman Spectrum
of Solid Polyoxyethylene**

Observed (cm^{-1})	Calculated[a] (cm^{-1})	Assignment	Mode[b]
1484	1479	A_1	$\delta(CH_2)_i$
1471	1476	E_1	$\delta(CH_2)_o$
1448	1471	E_1	$\delta(CH_2)_o$
1396	1423	A_1	$w(CH_2)_i, \nu(C-C)$
1376	1353	E_1	$w(CH_2)_i, \nu(C-C)$
1286			amorphous
1283	1286	E_1	$t(CH_2)_o, t(CH_2)_i$
1237	1234	E_1	$t(CH_2)_i, t(CH_2)_o$
1234	1252	A_1	$t(CH_2)_o$
1142	1142	A_1	$\nu(CH_2)$
1125	1137	A_1	$\nu(C-C), w(CH_2)$
1073	1073	A_1	$\nu(C-O)_i, r(CH_2)$
1065	1060	E_1	$\nu(CO)_i, r(CH_2)_i$
947	941	E_1	$r(CH_2)_i, \nu(CO)_i$
936			amorphous
860	866	A_1	$r(CH_2)_i, \nu(CO)_i$
846	847	E_1	$r(CH_2)_o$
832			end-group OH
811			amorphous
583			
537	524	E_1	$\delta(OCC)_o$
364	366	E_1	$\delta(COC)_o, \delta(OCC)_i$
281	274	A_1	$\delta(COC)_i, \delta(COC)$
231	212	A_1	$\delta(OCC)_i, CO_i$
	216	E_1	$\delta(OCC)_i, CO_i$

SOURCE: Reproduced with permission from ref. 9. Copyright 1971.
[a]From ref. 35.
[b]Key: ν, stretching; δ, bending; w, wagging; t, torsional; r, rocking; o, out-of-plane; i, in-plane.
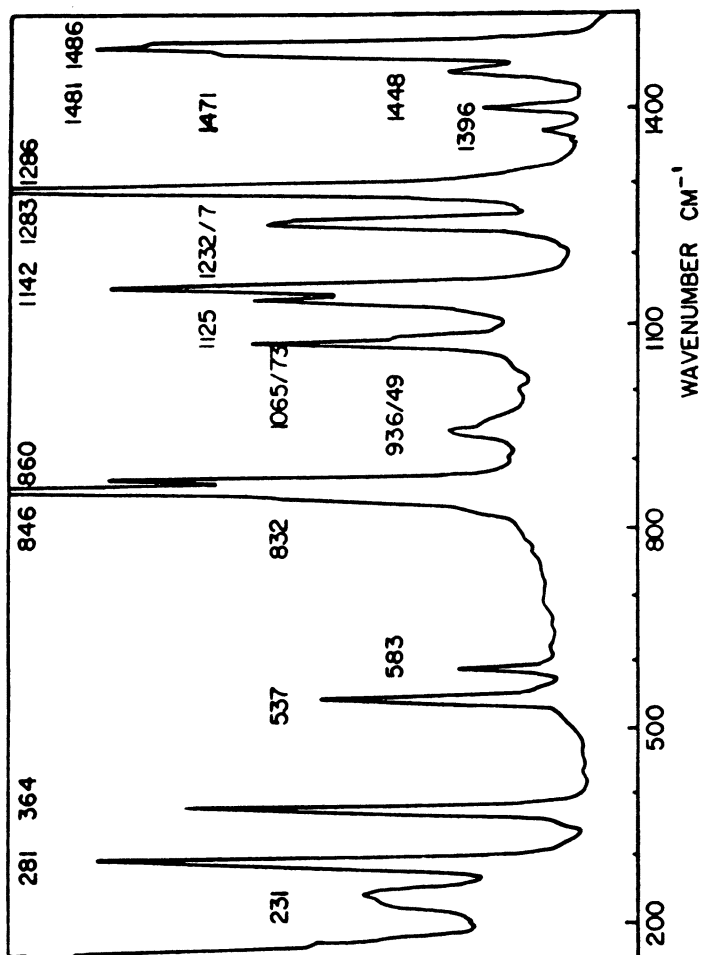
Figure 1. Raman spectrum of solid polyoxyethylene. (Reproduced with permission from ref. 9. Copyright 1971.)

same frequencies. For the dihedral group, the parallel A_2 IR modes are forbidden in Raman spectrum, and 10 A_1 modes polarized in the Raman are forbidden in IR.

The E_1 modes, perpendicularly polarized in the IR, are depolarized in the Raman spectrum. Finally, the modes with the E_2 symmetry are Raman-active and depolarized but inactive in the IR. Thus, with the use of vibrational spectroscopy and group theory, Koenig (9) deduced the helical structure of POE that consisted of a succession of *trans, gauche,* and *trans* forms around the O–C, C–C, and C–O bonds, respectively. These results were confirmed later (*10, 11*).

When a polymer is melted, the molecular conformations become disordered. As a result, the vibrational spectrum is significantly different from the spectrum of the crystalline state. Because of the presence of new conformations in the melt, many new vibrational bands appear in the spectrum, or splitting of the bands observed in crystalline phase disappears. The vibrational modes are broad because of the variety of structures in the melt. Because the structures are disordered, no specific selection rules can be applied. The Raman spectrum of molten POE is presented in Figure 2 (dashed line). The band assignments for the molten state become difficult, not only because of the broadening, but also because of the large number of local structures with small vibrational energy differences that may be present.

In the solid state, the *trans–gauche–trans* (TGT) conformation predominates where three chain bonds per repeating unit each have a *trans* (O–C), *gauche* (C–C), and *trans* (C–O) form. The possible conformations in the molten state include TGT, GGG, TTT, TTG, and GTG. The statistical weight of each conformation was estimated from the abundance ratio (G + G')/T (*12*). If the ratios of 8:2 for CH_2–CH_2 and 2:8 for CH_2–O bonds are used, the statistical weights are TGT,1; TTT, 1:4; TGG, 1:4, TTG, 1:8; GGG, 1:64; and GTG, 1:128. By using vibrational analysis of the models responsible for helical segments of each conformation, it was shown (*12*) that, although the predominant TGG isomer is present in the molten state, a number of *trans* ethylene units (TTT, TTG, GTG) are also significant.

Poly(ethylene glycol)

The structure of low molecular weight polyoxyethylene (poly(ethylene glycol) [PEG]) was investigated by many methods, including vibrational spectroscopy. Raman studies in particular contributed to the understanding of the conformational changes in this polymer upon dissolution in aqueous and organic solvents (9). These studies are of particular interest because the conformational changes upon dissolution are effected by pH, salt concentration, or ionic strength of the solution.
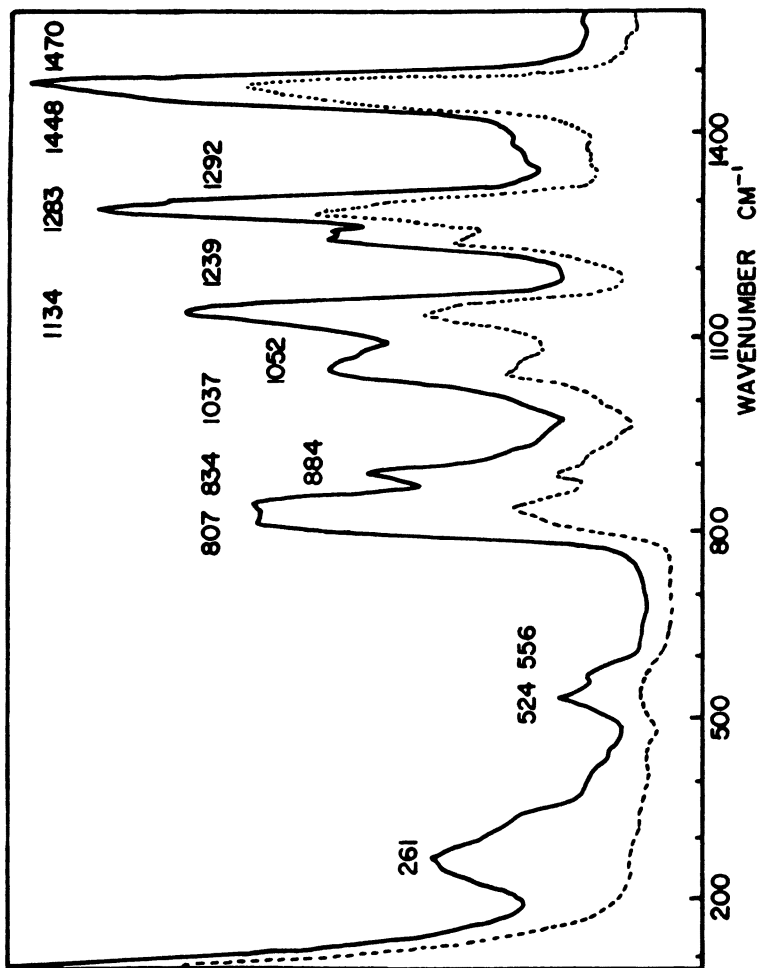
Figure 2. Raman spectra of molten polyoxyethylene (---) and crystalline polyoxyethylene (—). (Reproduced with permission from ref. 9. Copyright 1971.)

The Raman spectra of PEG in aqueous and chloroform solutions are shown in Figure 3 (9). A comparison of the spectra of aqueous solution with that of the melt (not shown) indicates that the changes on dissolution in water are significantly less drastic than observed on melting. Interestingly enough, the spectrum of PEG in chloroform is very similar to the spectrum in melt. Because of the presence of characteristic Raman bands at 884, 845, and 807 cm^{-1} in the aqueous solution, the TGT methylene structure is more prevalent than the TGG, TTG, and GGG structures. These results are in good agreement with the IR and NMR results (13).

Recently, the IR studies of PEG have indicated that the hydroxyl region of the spectrum may determine the interactions between donor and acceptor functional groups (14). Three types of H-bonded species are formed. These species, together with the characteristic frequencies of the OH stretching vibrations, are shown in Chart I. The hydrogen bonds result from the interactions between the end hydroxyl and ether groups of the PEG backbone. The strength of the hydrogen bonding is affected by three factors:

1. the short-range interactions of the immediately adjacent units of the functional groups,

2. the long-range order effect due to favorable configurations of the molecules that leads to interactions with molecular segments located away from the functional groups, but at a small distance in space, and

3. the intermolecular interactions between two chains.

The 3610-cm^{-1} band remained unchanged upon concentration and molecular weight (within the range of 300 to 6000) changes and thus was attributed to the intermolecular hydrogen-bonded hydroxyl groups, such as shown in Chart I, structure A. On the other hand, the 3510-cm^{-1} band broadens, and its maximum is shifted toward higher frequencies, both with the increase of molecular weight and concentration. This behavior was attributed to the inter- and intramolecular hydrogen bonding (*see* Chart I, structure B). The intramolecular hydrogen bonding leads to the formation of large (greater than five members) rings. The band at 3450 cm^{-1} was observed only for molecular weights less than 2000, and, on the basis of the spectra of the model compounds, it was assigned to the hydroxyl groups bonded by inter- or intramolecular hydrogen bonds, which resulted in the formation of 10-member ring structures.

Poly(acrylic acid)

Poly(acrylic acid) (PAA) has several vibrational modes in the 900–1350-cm^{-1} region whose activity depends on the tacticity of the polymer. Figure 4
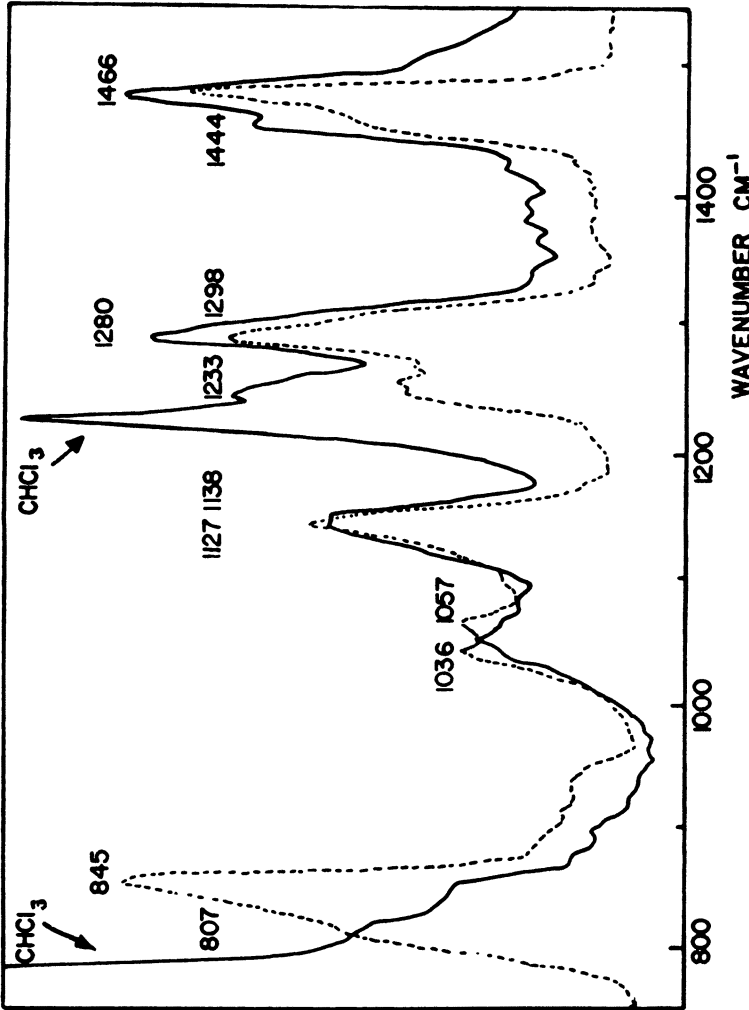
Figure 3. Raman spectra of PEG in aqueous solution (--) and chloroform (—). (Reproduced with permission from ref. 9. Copyright 1971.)

$3610 \ cm^{-1}$ $3510 \ cm^{-1}$ $3450 \ cm^{-1}$

A B C
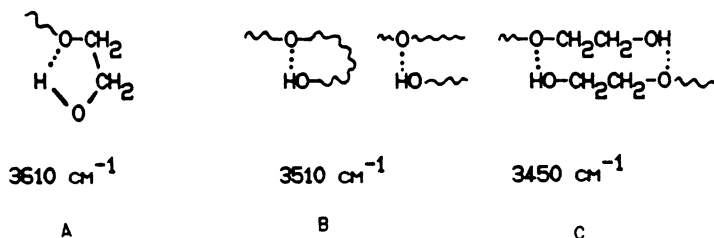
Chart 1. H-bonded species in poly(ethylene glycol) and their characteristic frequencies.

illustrates the IR spectra of three forms of poly(acrylic acid): isotactic, atactic, and syndiotactic (*15*). Several spectral features are associated with the stereoregularity of this polymer. Specifically, syndiotactic poly(acrylic acid) has strong, characteristic band at 1240 cm^{-1}, whereas the 930-cm^{-1} band is attributed to the isotactic form and splits to two bands at 1215 and 1275 cm^{-1}. Quite often, these bands are used to determine the stereoregularity of the commercial polymers. Several studies have shown that the degree of syndiotacticity is strongly dependent upon the preparation of the polymer. Apparently, the highest degree of syndiotacticity was achieved through photopolymerization of isopropyl acrylate. Although this form of the polymer is insoluble in water or dioxane for molecular weights above 10^6, it can be dissolved in a dioxane/water (80%/20%) mixture at ambient temperatures. In contrast, the atactic form of poly(acrylic acid) is soluble in all three solvents. Recent studies on thermal characteristics of the atactic poly(acrylic acid) have shown that upon heating, new bands at 1806, 1757, and 1030 cm^{-1} simultaneously appear in the IR spectra. These bands indicate a formation of anhydride from carboxylic acid (*16*).

Poly(methacrylic acid)

Because of their inability to obtain fiber patterns, X-ray studies have not provided any conclusive evidence as to the nature of the conformations of syndiotactic poly(methacrylic acid) (PMMA). IR dichroism measurements cannot be applied because the oriented films cannot be prepared; however, it was possible to obtain Raman depolarization data in aqueous solutions (*17*). Figure 5 shows Raman spectra in the solid state and in aqueous solution. Because of striking similarity of the spectra, it was concluded that the local conformations in both phases are similar. The frequency shift of two bands at 1452 and 1685 cm^{-1} was attributed to the differences in the extent of hydrogen bonding. On the basis of the IR and Raman activity of polarized and depolarized spectra, it was proposed that both solid and aqueous PMMA exist as helices that contain more than six monomer repeating units per two
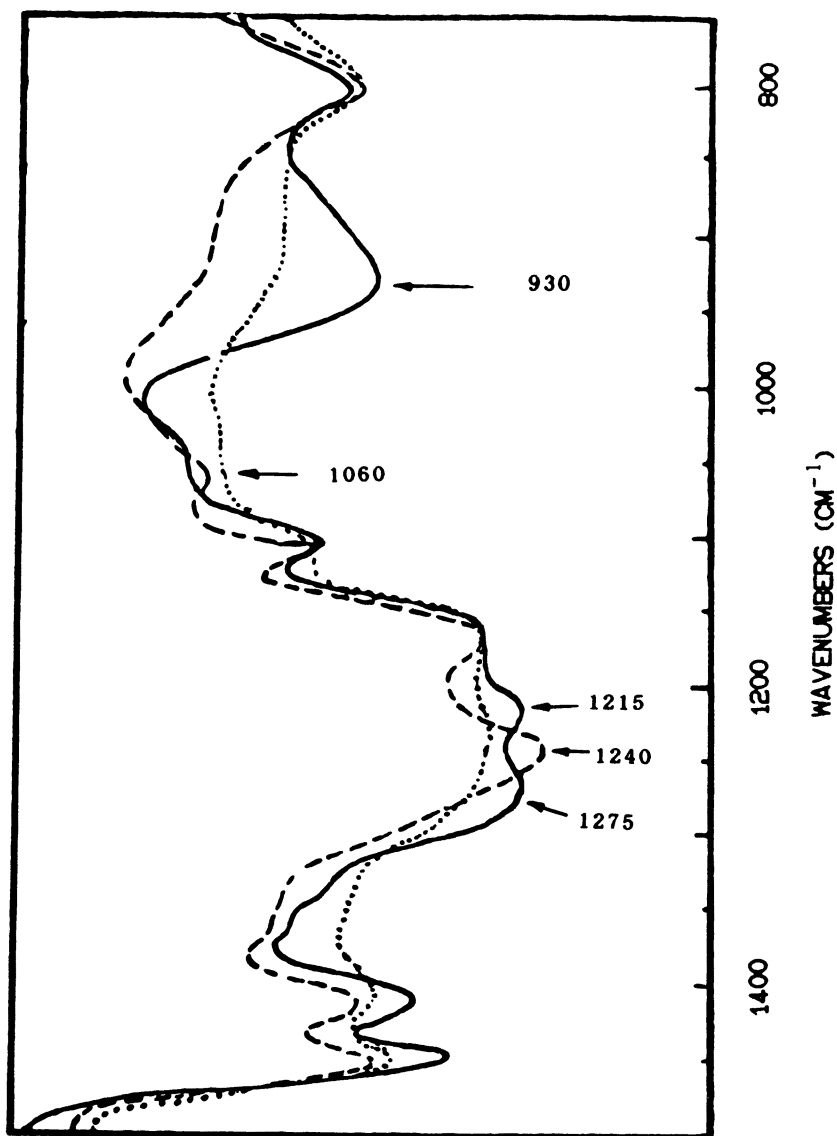
Figure 4. IR spectra of isotactic (—), syndiotactic (---), and atactic (· ·) poly(acrylic acid). (Reproduced with permission from ref. 15. Copyright 1972 Société Chimique de France.)
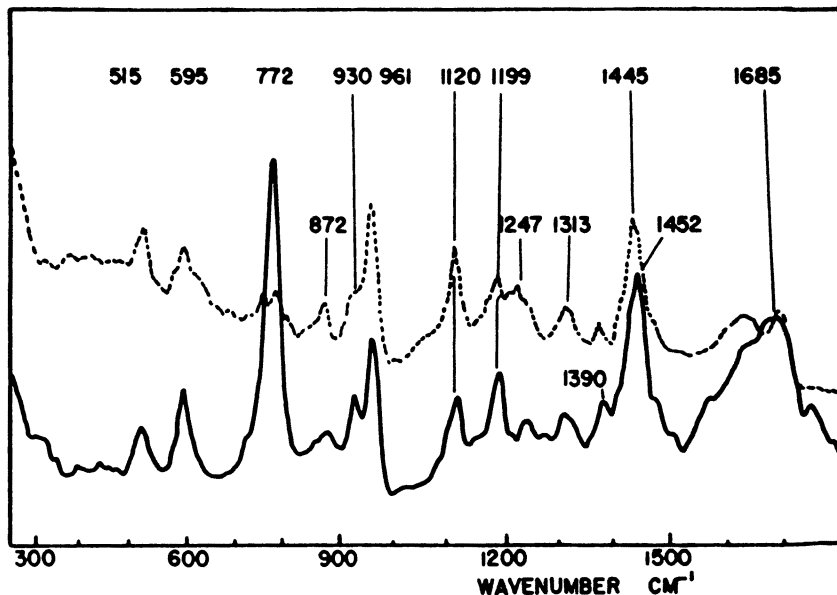
Figure 5. Raman spectrum of PMMA in the solid state (——) and aqueous solution (---). (Reproduced with permission from ref. 9. Copyright 1971.)

turns of the helix. Similarly, vibrational spectra suggested that poly(sodium methacrylate) (PNaMA) has the helix conformation. However, for PNaMA, the helix conformation is more open because the highly charged carboxylate ions repel each other and result in in slight uncoiling.

The conformational changes of PMMA in aqueous solution are influenced not only by the presence of solvent but also by the degree of neutralization of the polyelectrolyte. Apparently, the conformational transition occurs when the degree of neutralization, α, is in the range of 0.2–0.3. Initially, it was suggested that the formation of more extended forms of the PMMA chains was responsible for this process that occurs through subsequent ionization of carboxyl groups (18). The analysis of the Raman spectra with various degrees of neutralization indicated that a simple ionization process cannot explain these data (17). Specifically, the Raman band at 772 cm^{-1} due to the C–C stretching mode showed apparent broadening that suggested the presence of additional, unresolved bands. The appearance of new bands was observed upon increased neutralization. These observations indicated that a multiplicity of structures exist, not just simple ionized (COO$^-$) and un-ionized (COOH) forms of carboxyl groups. If both structures were present, two bands due to ionized and un-ionized groups would be observed. Thus, the transformation is not a simple process but rather progressive randomization of structures.

Polymer–Solvent, Polymer–Surfactant, and Solvent–Surfactant Interactions

IR spectroscopy has not generally been used to study water-soluble polymers because the presence of strongly absorbing water bands obscured the already-complex spectral information. However, with the advent of FTIR, modern sampling accessories, and computerized data processing procedures, the spectrum of the polymer and its interactions with a solvent can be determined. One of the sampling methods recently designed to study aqueous systems is the attenuated total reflectance (ATR) technique. Figure 6 depicts the ATR attachment. A combination of mirrors brings the energy of the spectrometer beam into focus on the surface of the ATR crystal at an average angle of 45°. The light propagates through the crystal and exits through the other end where it is redirected by another set of mirrors towards the IR detector. The sample of the polymer dissolved in aqueous medium is placed in a boat surrounding the crystal. Such configuration diminishes the strong water bands.

Recently, we used this attachment to determine the environment of a styrene/acrylic acid (S/AA) random copolymer (MW 3000; 59 mol % styrene, 41 mol % acrylic acid) dissolved in basic water solution (19, 20). By using the data processing techniques and high sensitivity of the ATR cell, we found that the aqueous solutions of LiOH, NaOH, or NH_4OH ionize the acrylic acid segments of the copolymer. Figure 7 shows FTIR subtraction spectra in which two bands at 1547 and 1405 cm^{-1} due to the symmetric and asymmetric stretching vibrations of the COO^- groups are detected. These spectra are significantly different from those of the bulk samples that exhibit a strong carbonyl band at 1733 cm^{-1}. The changes are caused by ionization of the acrylic segments to form of the COO^- groups that are coordinated through positive counterions to the solvent molecules.

Spectroscopic studies of aqueous solutions are of particular interest if they provide information about the microenvironment of the copolymer. In the case of S/AA copolymer, the water band at about 3420 cm^{-1} cannot be subtracted completely. This behavior indicates that some solvent molecules
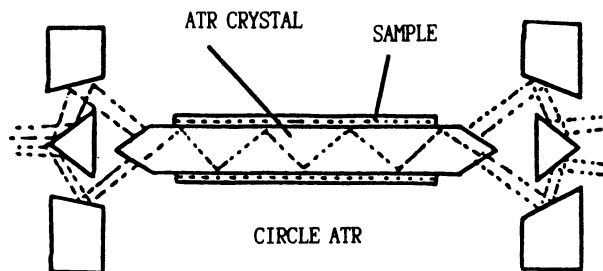
Figure 6. Attenuated total reflectance (ATR) cell.
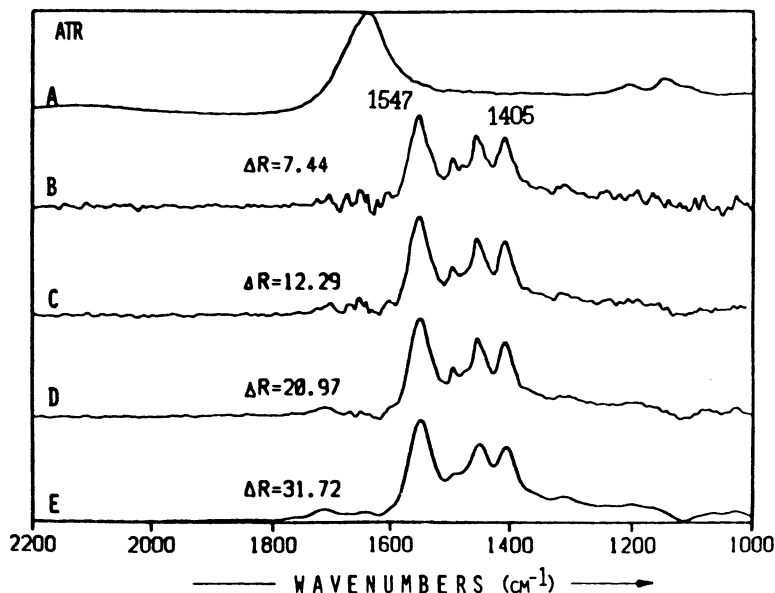
Figure 7. ATR FTIR spectra of the styrene/acrylic acid copolymer in the 2200–1000-cm⁻¹ region. A is the aqueous solvent spectrum. B through E are the difference spectra of various concentrations of styrene/acrylic acid minus solvent. (Reproduced with permission from ref. 19. Copyright 1987 Applied Spectroscopy.)

are coordinated to the copolymer, and thus give rise to a new vibrational state of water. Because carboxylic acid groups are in the ionic form, the subtraction method provides some evidence of the environment of the acrylic acid groups and their interaction with the solvent. Because the presence of counterions in the aqueous solution leads to ionization of the acrylic acid segments of the copolymer, the spectral changes in the water absorption region are of particular interest.

There are few numerical methods that enhance the spectral information and may provide additional information about the environment of the polymer. These methods are Lorentzian curve fitting and factor analysis. By using these two independent methods, we found (20) that two types of water molecules are present in the aqueous S/AA copolymer: water acting as a solvent and water molecules associated with carboxylic groups through positively charged cations. As a result, only acrylic segments are "exposed" to the solvent environment and protect styrene units from water. Thus, in the presence of a highly polar or ionic solvent, the S/AA copolymer forms aggregates such that the styrene segments are surrounded by acrylate groups. This conformation is shown schematically in Figure 8A.

The presence of immiscible aqueous and hydrocarbon phases in the S/AA solution was also investigated (19). On the basis of spectral analysis of
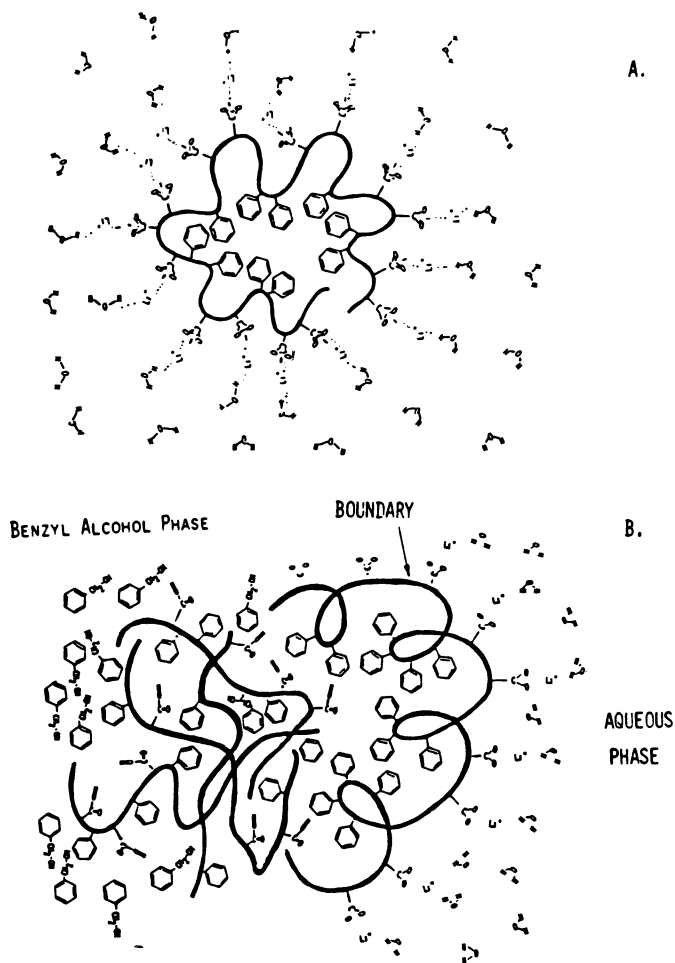
Figure 8. A shows the ionization of acrylic segments of styrene/acrylic acid and the chain conformation in aqueous solution. B shows the presence of water and benzyl alcohol and the formation of the phase boundary.

the COO^- and $C{=}O$ bands due to acrylic segments of S/AA copolymer, we believe that as the counterions penetrate the phase boundary between two phases, ionization of the $C{=}O$ groups in the organic phase occurs. Such a mechanism is possible if the S/AA copolymer forms a coil such that the acrylic segments are preferentially in the aqueous phase and the styrene segments are in the organic phase. This conformation is shown schematically in Figure 8B.

The presence of copolymer and surfactant together alters the rheological properties of solutions, adsorption on solid particles, solubility, and stability of colloidal dispersions. The solution properties are mainly influenced by

the hydrophobic and electrostatic interactions between copolymer, surfactant, and solvent. Spectroscopic FTIR studies of S/AA copolymer in the presence of sodium dodecyl sulfate (SDS) (20) showed that the asymmetric C–H stretching band at 2929 cm^{-1} is very sensitive to a formation of new micelle structures. This behavior is indicated by a shift to lower frequency. Apparently, SDS micelles interact with the carboxylic groups of the S/AA copolymer and give rise to the splitting of COO$^-$ symmetric and asymmetric vibrations shown in Figure 9. Such spectral features suggested that the SDS micelles were trapped between COO$^-$ groups and formed structures such as that depicted in Figure 10A. The nonpolar CH$_3$ groups occupy the interior of the micelle, whereas polar SO$_3^-$ exterior groups interact with negatively charged COO$^-$ groups through counterions such as Li$^+$ or Na$^+$ and give rise to a splitting of the 1547-cm^{-1} band. Thus, the formation of the micelles may lead to stronger interactions between counterions and COO$^-$ groups which, in turn, destroy a local symmetry of the COO$^-$ species.

Although the considerations just mentioned suggest the existence of the structures such as that depicted in Figure 10A, interactions between these structures and the solvent molecules are not obvious. Although at present there is no experimental evidence for the existence of interactions between aggregates, the presence of outer styrene units may lead to the formation of clusters, such as those depicted in Figure 10B. Otherwise, the styrene molecules would be "exposed" to aqueous medium. More research on a molecular level is needed to gain further insights into the aggregate formation and their interactions.
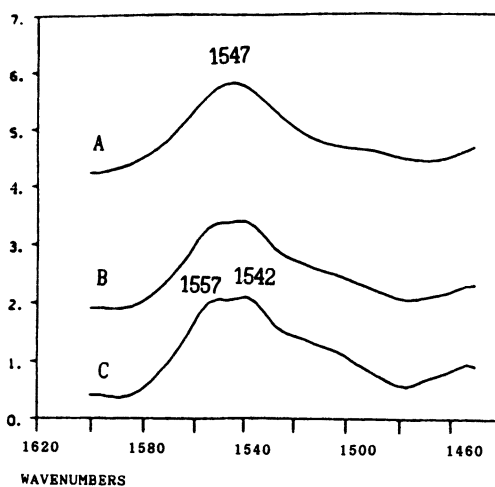
Figure 9. ATR FTIR spectra of styrene/acrylic acid copolymer in the C–O stretching region in the presence of SDS surfactant. SDS concentrations: A, 0.005 M; B, 0.01 M; C, 0.025 M. (Reproduced with permission from ref. 20. Copyright 1987 Applied Spectroscopy.)

A

AQUEOUS PHASE

B
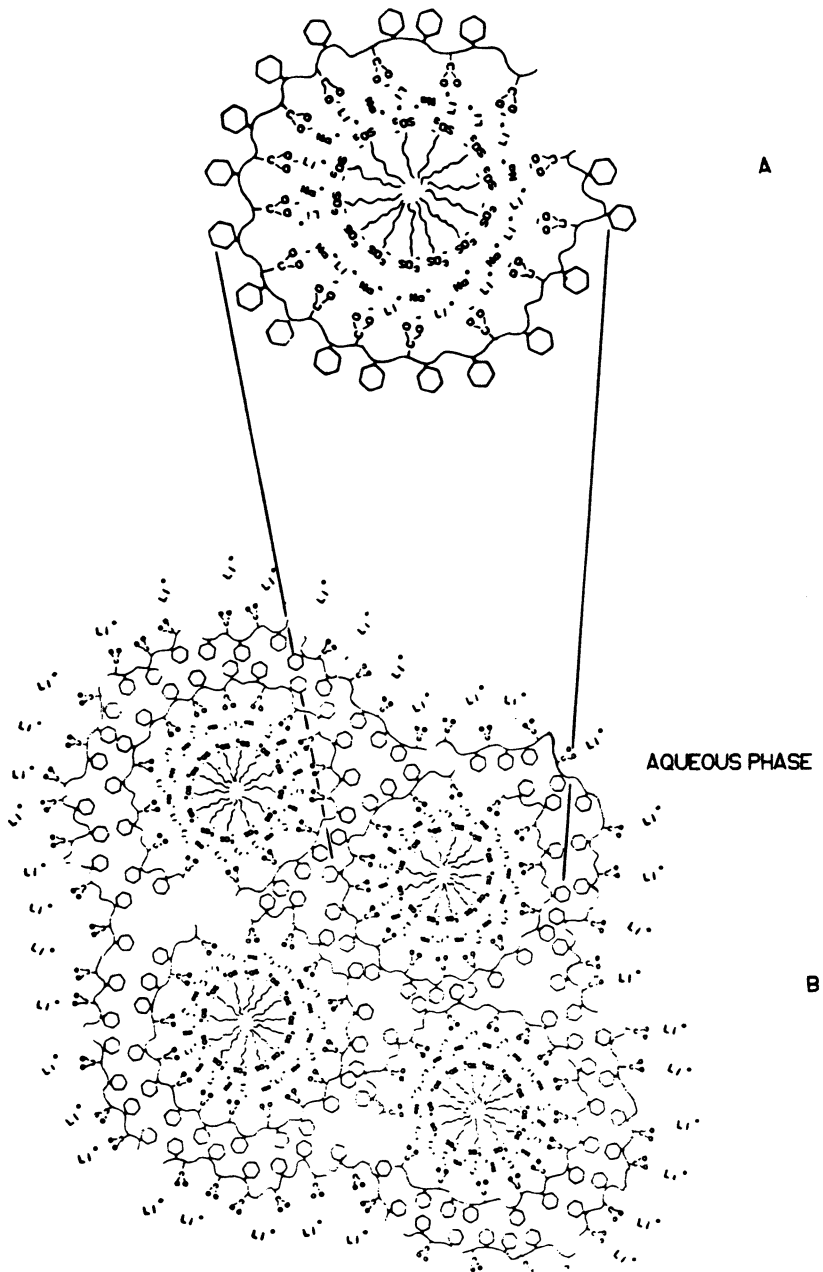
Figure 10. A shows interactions of styrene/acrylic acid copolymer with SDS surfactant. B is a model of cluster formations.

    The sensitivity of vibrational spectroscopy allows interactions of poly-electrolytes and surfactants to be monitored in aqueous and nonaqueous solutions. The solubilization and conformational properties of a comb-shaped copolymer of 1-octadecane-*co*-maleic anhydride in aqueous solution in the presence and absence of SDS depend on the degree of ionization of the copolymer (*21*). The C–H stretching region of the Raman spectrum is sensitive to such interactions. Figure 11 illustrates how the C–H stretching band shifts as a function of solvent (in this case water and heptane).

    The presence of micelles in aqueous surfactant solution influences the solubilization effect of nonpolar substances in water. Recent FTIR studies (*22*) have shown that the presence of both phenyl acetate and benzyl acetate in the aqueous sodium decanoate ($C_9H_{18}COO^-Na^+$) micelle solution affects the environment of the nonpolar phases. The spectral changes in the C=O and C–O regions of acetates, such as band splitting, shift to lower vibrational energy, and band broadening suggests that acetates are solubilized into the surface polar layer of micelles and are affected by hydrogen bonding with the aqueous phase. When the concentration of acetates reaches saturation, aggregates are formed on the surfaces of micelles and may diffuse into the core of the micelle. A polar environment around the solubilized acetates may also induce conformational changes in the micelle.

    An ATR cell (shown in Figure 6) was also used to monitor interactions of nonionic surfactants with a solid hydrocarbon phase (eicosane) (*23*). The circular crystal was coated with a thin layer of eicosane, and flowing surfactant
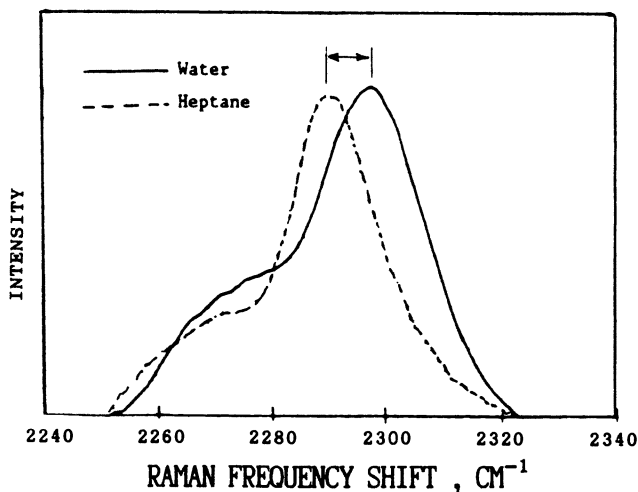
Figure 11. The C–H stretching region of Raman spectrum in aqueous and organic solvents. (Reproduced from ref. 21. Copyright 1986 American Chemical Society.)

solution was passed through the cell. The time-resolved FTIR spectra were recorded as the hydrocarbon phase was washed out from the surface of the crystal by the detergent action of the surfactant solution. By monitoring the band intensities of both eicosane and surfactants (Neodel 25-3, Shell Chemical Company and Triton, Rohm and Haas Company), Scheuing (23) found that significant adsorption of the surfactants on the layer of the hydrocarbon phase occurs. The more hydrophilic ethoxylated alcohol (Neodel 25-3) causes more rapid removal of eicosane from the surface of the ATR crystal.

The solubility of hydrocarbons in water is greatly enhanced by the presence of surfactants. Similarly, the addition of hydrocarbons to aqueous surfactant solution induces change in the physical properties of the surfactant (24, 25). Thus, the quantitative analysis of the partitioning of hydrocarbons between micelle interior and aqueous phase has been a subject of numerous studies. Among the many techniques used to determine the partitioning, only fluorescence (26), FT-pulsed-gradient spin echo NMR (27), and recently, Raman spectroscopy (28) have demonstrated sufficient sensitivity.

Determination of partitioning with the Raman technique is based on the observation that some chemical bonds display a shift in vibrational frequency when parameters of the solvent environment change. Larsson and Rand (29) were the first to observe that the C–H stretching band in the hydrocarbon solvent shifts by 7 cm^{-1} when a solute is dissolved in water. This observation was confirmed by the other workers (30, 31) who detected similar frequency shifts as a function of the solvent environment in the surfactant solutions. The Raman studies (28) of SDS aqueous solutions containing deuterated benzyl alcohol have shown that the estimated fractions of SDS in the hydrocarbon phase are in good agreement with the NMR results (27).

Summary

Applications of vibrational spectroscopy to the studies of water-soluble polymers fall into two categories: structural characterization and the analysis of interactions of various molecular segments with solvents or other phases. Structural characterization was pioneered in the early 1970s with major contributions from Koenig's group, but the analysis of interactions is in its infancy, possibly because the presence of strongly absorbing water often obscures the spectral features from the solute. These features were particularly obscured in IR spectroscopy; however, with improved sensitivity, enhanced selectivity, and modern sampling techniques, IR spectroscopy opens new vistas in the analysis of local molecular structures of water-soluble polymers and their interactions with solvents, surfactants and the environment. Because water does not strongly demonstrate the Raman effect, and therefore does not obscure the spectra of polymer dissolved in aqueous solutions, Raman spectroscopy has not been extensively used in the studies of solute–solvent interactions.

More research is needed with both spectroscopic tools, especially with the recent advances in the field of Fourier transform Raman spectroscopy and the tremendously improved sensitivity and stability of the IR interferometers. In addition, the availability of new algorithms such as the ratio method (32), factor analysis (20, 33), and recently developed nonlinear techniques (34), coupled with an easy access to fast computers, will advance spectral analysis tremendously and make it more precise and reliable.

References

1. Griffiths, P. R. *Chemical Fourier Transform Infrared Spectroscopy*; Wiley: New York, 1975.
2. Ferarro, J. R.; Basile, L. J. *Fourier Transform Infrared Spectroscopy*, Vols. 1 and 2; Academic: New York, 1978.
3. Painter, P. C.; Coleman, M. M.; Koenig, J. L. *The Theory of Vibrational Spectroscopy and Its Application to Polymeric Materials*; Wiley: New York, 1982.
4. Gilson, T. R.; Hendra, P. J. *Laser Raman Spectroscopy*; Wiley: New York, 1970.
5. Koningstein, J. A. *Introduction to the Theory of the Raman Effect*; Reidel: Dordrecht, 1972.
6. Tobin, M. C. *Laser Raman Spectroscopy*; Wiley: New York, 1972.
7. Matsui, Y.; Kubota, T.; Tadokoro, H.; Yoshikara, Y. *J. Polym. Sci.* 1965, A3, 2275.
8. Schaufele, R. F. *J. Opt. Soc. Am.* 1967, 57, 105.
9. Koenig, J. L. *Appl. Spectrosc. Rev.* 1971, 4(2), 233.
10. Takahashi, Y.; Tadokoro, H. *Macromolecules* 1973, 6, 672.
11. Takahashi, Y.; Tadokoro, H.; Hirano, T.; Sato, A.; Tsurua, T. *J. Polym. Sci., Polym. Phys. Ed.* 1975, 13, 285.
12. Tobin, M. J. *J. Chem. Phys.* 1969, 50, 4551.
13. Liu, J.; Parsons, J. L. *Macromolecules* 1969, 2, 529.
14. Philippova, O. E.; Kuchanov, S. I.; Topchieva, I. N.; Kabanov, V. A. *Macromolecules* 1985, 18, 1628.
15. Monjol, P.; Champetier, G. *Bull. Soc. Chim. Fr.* 1972, 4, 1302.
16. Maurer, J. J.; Eustance, D. J.; Ratcliffe, C. T. *Macromolecules* 1987, 20, 196.
17. Koenig, J. L.; Angood, A. C.; Semen, J.; Lando, J. B. *J. Am. Chem. Soc.* 1969, 91, 7250.
18. Liquori, A. M.; Barone, G.; Crescenzi, V.; Quadrifoglio, F.; Vitagliano, V. *J. Macromol. Chem.* 1966, 1, 291.
19. Urban, M. W.; Koenig, J. L.; Shih, L. B.; Allaway, J. *Appl. Spectrosc.* 1987, 41(4), 590.
20. Urban, M. W.; Koenig, J. L. *Appl. Spectrosc.* 1987, 41(6), 1028.
21. Shih, L. B.; Lucas, M. H.; Warner, R. J. *Polym. Prepr. (Am. Chem. Soc., Div. Polym. Chem.)* 1986, 27(2), 288.
22. Shinjiro, S.; Matsui, T.; Tanaka, S. *Appl. Spectrosc.* 1987, 41(8), 1438.
23. Scheuing, D. R. *Appl. Spectrosc.* 1987, 41(8), 1343.
24. McBain, M. E. L.; Hutchinson, E. *Solubilization and Related Phenomena*; Academic: New York, 1955.
25. Elworthy, P. H.; Florence, A. T.; McFarlane, C. B. *Solubilization by Surface Active Agents and Its Application in Chemistry and the Biological Sciences*; Chapman & Hall: London, 1968.
26. Abuiu, E. B.; Lissi, E. A. *J. Colloid Interface Sci.* 1983, 95, 198.
27. Stilbs, P. *J. Colloid Interface Sci.* 1982, 87, 385.

28. Shih, L. B.; Williams, R. W. *J. Phys. Chem.* **1986**.
29. Larsson, U.; Rand, R. P. *Biochim. Biphys. Acta* **1973**, *326*, 245.
30. Amorim da Sosto, A. M.; Geraldes, C. F. G. C.; Teixera-Dias, J. J. C. *J. Colloid Interface Sci.* **1982**, *86*, 254.
31. Brooker, M. H.; Jobe, D. J.; Reinsborough, V. C. *J. Chem. Soc., Faraday Trans. 2* **1984**, *80*, 73.
32. Hierschfeld, T. B. *Anal. Chem.* **1981**, *53*, 2232.
33. Antoon, M. K.; D'Esposito, L.; Koenig, J. L. *Appl. Spectrosc.* **1979**, *33*, 349.
34. Liu, J.; Koenig, J. L. *Anal. Chem.* **1987**, *59*, 2609.
35. Matusura, H.; Miyazawa, T. *Bull. Chem. Soc. Jpn.* **1968**, *41*, 1798.

Hydrophobic Polyelectrolytes

Ulrich P. Strauss

Department of Chemistry, Rutgers, The State University of New Jersey, New Brunswick, NJ 08903

The incorporation of hydrophobic side chains into a polyelectrolyte can produce profound changes in the physical chemical behavior of the parent macromolecule. The hydrophobic attractions of the side chains can cause contractions in the molecular dimensions and aggregate formation. The presence of intramolecular micelles allows the solubilization of compounds with normally low water solubility. The solubilized compounds can have sizable effects on both intra- and intermolecular interactions. Selected studies carried out to determine the effects of hydrophobic group content and size, electrical charge, ionic strength, solubilization, and temperature on intramolecular micelle formation and intermolecular aggregation are reviewed. This chapter also discusses the solubilization of fluorescent probes, which has recently been found especially useful for following conformational transitions and for determining the size of the micelles.

OUR RESEARCH ON HYDROPHOBIC POLYELECTROLYTES arose from the notion that, because soap molecules form micelles spontaneously in aqueous solution, micelle formation could be expedited by chemically attaching surfactant molecules to polymers. Our first such "polysoap" was prepared by the partial quaternization of poly(2-vinylpyridine) with *n*-dodecyl bromide (1). Viscosity measurements indicated that this polysoap exhibited abnormally compact molecular dimensions in aqueous solutions, a result suggesting intramolecular micelle formation. This idea was confirmed by the fact that the polysoap solubilized normally water-insoluble hydrocarbons. The amount solubilized was greater than that solubilized by an equal amount of chemically related simple soap. In contrast to the monosoap, no critical

micelle concentration was necessary before solubilization occurred with the polysoap. The solubilization was proportional to the polysoap concentration, a finding confirming that the micelles were intramacromolecular (1). The early studies (2–5) showed that the solubilized hydrocarbons had pronounced effects on the viscosity of the polysoap solutions, and that these effects were both qualitatively and quantitatively different depending on whether the hydrocarbon was aliphatic or aromatic.

Effect of Hydrophobicity on Polysoap Behavior

To study the effects of varying the number of soap molecules attached to a polymer chain while holding the total linear charge density constant, derivatives of poly(4-vinylpyridine) were prepared by quaternizing to various extents with n-dodecyl bromide and completing the process with ethyl bromide. In this way, close to 100% substitution was attained (6, 7). The variety of viscosity behavior of the derivatives, dissolved in dilute aqueous electrolyte, is illustrated in Figure 1 (7). A logarithmic scale was used to fit the reduced viscosity curves on the same graph.

The curves fell into two distinct groups. The top two curves characterize an all ethyl bromide derivative (PEB) and a derivative with 6.7 mol % of the pyridine groups substituted with n-dodecyl bromide and most of the remainder substituted with ethyl bromide (6.7% polysoap). These curves indicate highly extended molecular dimensions typical of normal polyelectrolyte behavior. Of the two derivatives, the 6.7% polysoap has a lower intrinsic viscosity but a larger increase of the reduced viscosity with concentration; this result shows the intra- and intermolecular effects, respectively, of the hydrophobic attractions between the dodecyl groups.

The bottom three curves, corresponding to 13.6%, 28.5%, and 37.9% polysoaps, show intrinsic viscosities about 2 orders of magnitude smaller than those of the top two curves and indicate compact conformation brought about by intramolecular micelle formation. The sharp change in intrinsic viscosity from the top to the bottom group suggests the existence of a critical dodecyl group content necessary for micelle formation, which might be considered the intramolecular equivalent of the critical micelle concentration of nonpolymeric surfactant (7). The steeper slope of the 37.9% polysoap curve compared to those of the 13.6% and 28.5% polysoap curves indicates intermolecular aggregation brought about by hydrophobic interactions.

The behavior of polysoaps is also strongly influenced by their concentration, the ionic strength, and temperature. A typical example is presented in Figure 2, which shows the effect of added potassium bromide on the reduced viscosity of the 37.9% polysoap at two polysoap concentrations and two temperatures. The primary effect of the increase in ionic strength is a suppression of the electrostatic repulsions between the ionic groups. The decreased repulsions result in an intramolecular contraction (a well-known
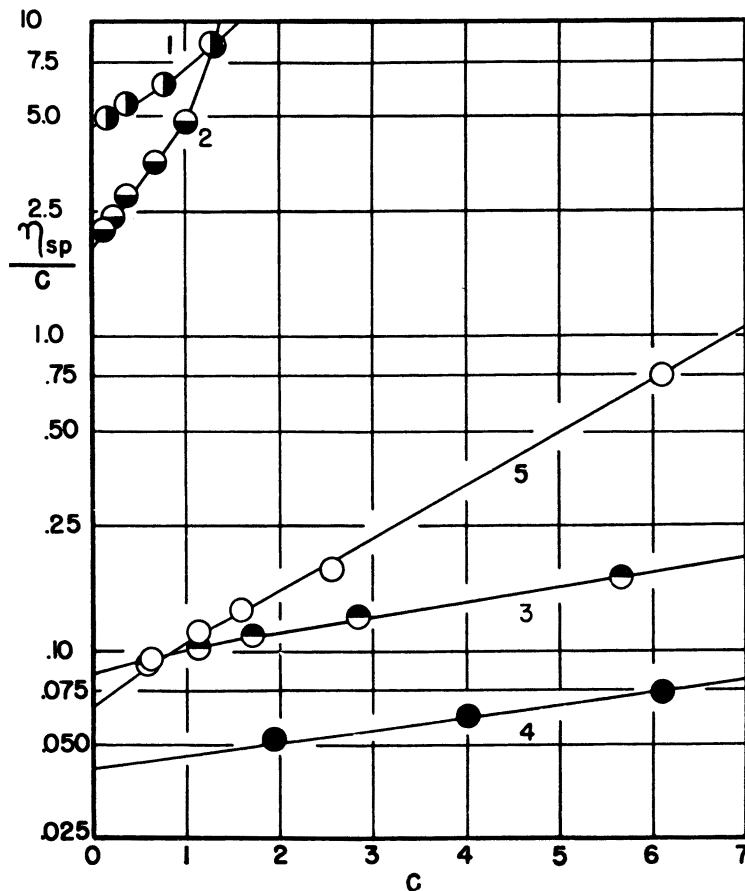
Figure 1. Effect of dodecyl group content on reduced viscosity of poly(4-vinylpyridine) derivatives in 0.0226 M KBr at 25 °C. Key: 1, PEB; 2, 6.7% polysoap; 3, 13.6% polysoap; 4, 28.5% polysoap; 5, 37.9% polysoap. (Reproduced from ref. 7. Copyright 1956 American Chemical Society.)

polyelectrolyte effect manifesting itself in the initial negative slopes of the curves), and in an intermolecular aggregation evident from the positive slopes at higher ionic strengths. The intermolecular aggregation is clearly much more pronounced in the 6% than in the 1% polysoap solution. The effects of a temperature increase from 25 to 45 °C are most significant where the intermolecular interactions are greatest, a finding indicating that the aggregates are destabilized by heat. The 6% solution at 25 °C turned into a clear thixotropic jelly when the potassium bromide molality exceeded 0.035.

Similar homogeneous gels could also be obtained with many other polysoap systems. The aggregation and disaggregation processes of the 37.9% polysoap were slow enough at 25 °C to be observed by appropriate viscosity
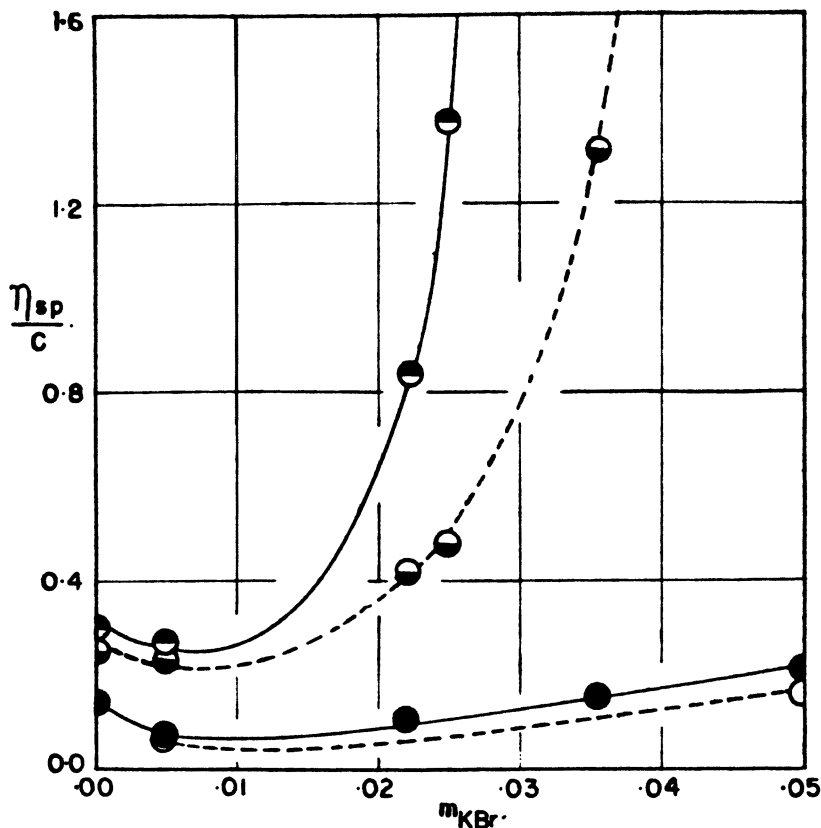
Figure 2. Effect of KBr on reduced viscosity of 37.9% polysoap. Key: ●, ○,
1.00% polysoap solution at 25 and 45 °C, respectively; ◐, ◑, *6.00% polysoap
solution at 25 and 45 °C, respectively. (Reproduced from ref. 7. Copyright
1956 American Chemical Society.)*

experiments, but too fast at 45 °C; therefore, the aggregates are stabilized
by a substantial activation energy (7). Polysoaps with more than 40 mol %
of the pyridine groups substituted with dodecyl bromide were not water-
soluble at room temperature (8). These results and their interpretations were
later confirmed by light-scattering experiments (9) and by studies on similar
polyvinylpyridine derivatives (10, 11).

Solubilization Effects

Organic molecules with limited water solubility were solubilized by those
polysoaps for which viscosity studies indicated micellar behavior (6). The
solubilization had varied effects on the viscosity of the polysoap solutions,
depending on the nature of the solubilized compound and the concentration

of the polysoaps (2–6). Aliphatic solubilized compounds depressed the viscosity under all conditions, whereas aromatic compounds depressed the viscosity at low polysoap concentrations but produced increasingly prominent viscosity maxima as the polysoap concentration was raised. Still more complex and pronounced viscosity effects were observed with amphiphilic compounds, such as long-chain aliphatic alcohols and nitroaromatic compounds, for which viscosity minima were observed at all polysoap concentrations. Maxima similar to those induced by aromatic hydrocarbons were found at high polysoap concentrations.

With the help of supplementary light-scattering and electrical conductance studies, the following method of accounting for these viscosity effects emerged (12, 13): Aliphatic hydrocarbons are solubilized in the hydrocarbon core of the micelle where they cause a small contraction in the molecular dimensions of the polysoap molecules. Aromatic and amphiphilic molecules are solubilized by bridging the hydrocarbon and polar domains of the micelles. As a result, the polar regions are significantly contracted. Hydrophobic groups are then exposed to the aqueous environment and, in turn, cause aggregate formation. The molecular weight of the aggregates increases until the solubilization limit is reached. The viscosity maxima occur because the aggregation proceeds from asymmetric to globular complexes.

Conformational Transitions

In addition to the polyvinylpyridine derivatives, the alternating copolymers of maleic acid and alkyl vinyl ethers have provided useful information about the behavior of hydrophobic polyelectrolytes. For these polyacids, hydrophobicity can be controlled by the alkyl group size, and the charge density can be varied by pH (14, 15). With the alkyl group containing up to three carbon atoms, the macromolecules behave as typical polyacids (16), whereas when the alkyl group contains 12 or more carbon atoms, the macromolecules behave like typical polysoaps (17). The copolymers whose alkyl group size falls between these extremes have compact conformations (typical of polysoaps) at low pH where their charge density is small and random coil conformations at high pH where their charge density is large (14, 15).

This effect is illustrated most strikingly with the fluorescence behavior of a chemically attached dansyl probe (18). The emission of this probe near 500 nm is large in nonpolar and small in polar media. In Figure 3, the fluorescence intensity at 520 nm of a dansylated butyl copolymer is given as a function of α, the degree of deprotonation (defined so as to equal 2 at complete deprotonation) (18). At low α, the fluorescence intensity is large, a result that indicates that the probe molecules are surrounded by nonpolar groups. This conformation would be expected from compact micellar regions consisting of the nonpolar butyl groups. As the ionic charge on the polyacid is increased, the fluorescence intensity drops sharply, a result that indicates

a transition from the compact micellar conformation to a random coil state in which the butyl groups are separated from one another and the probe is surrounded by a polar aqueous environment. The figure also shows that added electrolyte stabilizes the compact structure. The initial fluorescence intensity is increased, and the conformational transition is shifted to higher values of α. The stabilization is presumably due to a reduction in repulsion between the ionized groups of the polyacid.

Changes in the polymer concentration had no significant effect on the fluorescence behavior; therefore, the transition was an intramolecular rather than an intermolecular phenomenon. In contrast to the butyl copolymer, the dansylated methyl copolymer, whose fluorescence is also shown in Figure 3, undergoes no transition; its fluorescence is essentially constant over the whole ionization range. The low value is characteristic of the aqueous environment that the probe experiences in the random coil conformation.

Micelle Size

The conformational transition of the butyl copolymer, as well as those of the pentyl, hexyl, and octyl copolymers, has also been observed by viscosity (15), by potentiometric titration (14, 15, 19), and by calorimetric studies (16,
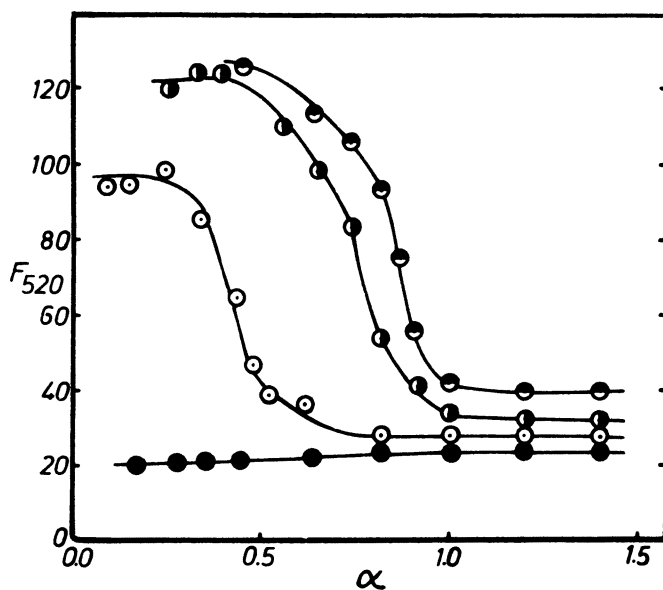
Figure 3. Dependence of F_{520}, the fluorescence emitted at 520 nm by dansylated copolymers, on the degree of deprotonation, α. Key: ⊙, ◑, ◓, butyl copolymer in water, 0.2 M NaCl, and 0.5 M NaCl, respectively; ●, methyl copolymer in water. (Adapted from ref. 18. Copyright 1975 American Chemical Society.)

20, 21). Analysis of the potentiometric titration data suggested that the transition could be described in terms of a cooperative break-up of uniformly sized small micelles formed from adjacent chain elements. A method was developed for estimating the size of these micelles from potentiometric titration data. By this method, the micelle for the butyl copolymer was found to comprise close to 20 repeat units (*22, 23*); however, this method was not easy to apply to the copolymers with larger hydrocarbon groups because the conformational transition was not sharp enough.

A method based on fluorescence quenching that did not depend on the nature of the transition was used to determine the micelle size of the hexyl copolymer (*24*). The basic idea underlying this method is that, in a solution containing luminescent probe and quencher molecules, both solubilized in an excess of micelles, the quenching will be inversely related to the number of micelles, because the more micelles there are, the smaller is the chance of both a probe and a quencher molecule inhabiting the same micelle (*25–27*). The hexyl copolymer used in our study had a degree of polymerization of 1700. The fluorescent probe was tris(2,2'-bipyridine)ruthenium(II) ion [$Ru(bpy)_3^{2+}$], the quencher was 9-methylanthracene (9-MeA), and the solvent was an aqueous 0.1 M LiCl solution. The fluorescence experiments were supplemented with solubilization experiments; from these, the distribution of the 9-MeA between the polymer molecules and the solvent molecules, as well as the extent to which the polymer was in micellar form, could be simultaneously determined. The results indicated that the micelles inside the domain of a macromolecule encompassed approximately 24 repeat units, and that this micelle size was independent of the polymer concentration, of the probe concentration, and the extent to which the polymer was micellized.

Conclusion

The research reviewed here demonstrates that polyelectrolytes experience a variety of profound alterations in their physicochemical behavior with the controlled introduction of hydrophobicity into their chemical structure. The wide range of untried structural variations that can be envisioned ensures continuing exploration in this fertile area of research and gives promise of further attractive applications.

References

1. Strauss, U. P.; Jackson, E. G. *J. Polym. Sci.* **1951**, *6*, 649.
2. Strauss, U. P.; Jackson, E. G. *J. Polym. Sci.* **1951**, *7*, 473.
3. Layton, L. H.; Jackson, E. G.; Strauss, U. P. *J. Polym. Sci.* **1952**, *9*, 295.
4. Strauss, U. P.; Layton, L. H. *J. Phys. Chem.* **1953**, *57*, 352.
5. Layton, L. H.; Strauss, U. P. *J. Colloid Sci.* **1954**, *9*, 149.

6. Strauss, U. P.; Gershfeld, N. L. *J. Phys. Chem.* **1954,** *58,* 747.
7. Strauss, U. P.; Gershfeld, N. L.; Crook, E. H. *J. Phys. Chem.* **1956,** *60,* 577.
8. Strauss, U. P.; Assony, S. J.; Jackson, E. G.; Layton, J. H. *J. Polym. Sci.* **1952,** *9,* 509.
9. Strauss, U. P.; Williams, B. L. *J. Phys. Chem.* **1961,** *65,* 1390.
10. Woerman, D.; Wall, F. T. *J. Phys. Chem.* **1960,** *64,* 581.
11. Inoue, H. *Kolloid Z.* **1964,** *195,* 102.
12. Strauss, U. P.; Slowata, S. S. *J. Phys. Chem.* **1957,** *61,* 411.
13. Richlin, J. Ph.D. Thesis, Rutgers University, 1964.
14. Dubin, P.; Strauss, U. P. *J. Phys. Chem.* **1967,** *71,* 2757.
15. Dubin, P. L.; Strauss, U. P. *J. Phys. Chem.* **1970,** *74,* 2842.
16. Martin, P. J.; Strauss, U. P. *Biophys. Chem.* **1980,** *11,* 397.
17. Itko, K.; Ono, H.; Yamashita, Y. *J. Colloid Sci.* **1964,** *19,* 28.
18. Strauss, U. P.; Vesnaver, G. *J. Phys. Chem.* **1975,** *79,* 2426.
19. Strauss, U. P.; Schlesinger, M. S. *J. Phys. Chem.* **1978,** *82,* 571.
20. Delben, F.; Crescenci, V. *J. Solution Chem.* **1978,** *7,* 597.
21. Martin, P. J.; Morss, L. R.; Strauss, U. P. *J. Phys. Chem.* **1980,** *84,* 577.
22. Strauss, U. P.; Barbieri, B. *Macromolecules* **1982,** *15,* 1347.
23. Barbieri, B. W.; Strauss, U. P. *J. Phys. Chem.* **1985,** *18,* 411.
24. Hsu, J. L.; Strauss, U. P. *J. Phys. Chem.* **1987,** *91,* 6238.
25. Turro, N. J.; Yekta, A. *J. Am. Chem. Soc.* **1978,** *100,* 5951.
26. Chu, D. Y.; Thomas, J. K. *J. Am. Chem. Soc.* **1986,** *108,* 6270.
27. Chu, D.Y.; Thomas, J. K. *Macromolecules* **1987,** *20,* 2133.

Photophysical Studies of Hydrophobically Modified Polyelectrolytes

Deh-Ying Chu and J. K. Thomas

Department of Chemistry, University of Notre Dame, Notre Dame, IN 46556

Studies in aqueous solutions of PA-18K$_2$ (a potassium salt of the co-polymer of maleic anhydride and 1-octadecene) and poly(methacrylic acid) (PMA) were carried out via steady-state and time-resolved fluorescence-probe techniques and energy-transfer of cationic dyes (i.e., from rhodamine 6G to rhodamine B). Pyrene and some of its derivatives can be readily solubilized in PA-18K$_2$ over the entire pH range, but in PMA solubilization occurs only at low pH range. The formation of a ground complex of polymer–donor–acceptor favors an intra-molecular energy-transfer process and a short-range nonradiative mechanism. The relative efficiency of energy transfer is larger in PA-18K$_2$ than that in PMA at pH 4–5, and much larger than that in water. Polymeric micelles of PA-18K$_2$ hinder reactions of guest molecules to a greater extent than simple micellar systems.

SYNTHETIC WEAK POLYELECTROLYTES provide hydrophobic microdomains in the low pH range. Typical examples are poly(methacrylic acid) (PMA) (*1–3*), copolymers of maleic anhydride and *n*-alkylvinyl ethers (*n* = 4–9) (*4, 5*), and copolymers of maleic anhydride and styrene or methylstyrene (*6*). The compact polymer coils are formed only in acidic solution, but the compact conformation is converted into the extended rod or coil form at high pH because of repulsion of ionized carboxyl groups. At low pH, many hydrophobic molecules can be hosted by the polymer coils, a condition that disappears at high pH. However, a hydrophobic environment is required

close to neutral pH for any practical use of the polymer as a host material for hydrophobic molecules.

Photophysical studies on a conformational transition of PMA induced by cationic surfactants have been reported (7). The stretched PMA chain at pH 8 collapses on addition of cationic surfactants; that is, the hydrophobic interactions between the cationic surfactants that are bonded to the PMA chain lead to refolding of the polymer chain, and thus provide a hydrophobic site for fluorescence probes at pH 8. The cationic polyelectrolyte poly(4-vinylpyridine) quaternized with n-dodecyl bromide (8–10) or hexadecyl bromide (11) are also examples of hydrophobically modified polyelectrolytes.

Polyelectrolytes modified via covalent bonding with long hydrocarbon chains are expected to behave as hypercoils over the entire pH range. The hydrophobic interaction between the paraffinic side chains in these systems leads to stabilization of compact structures even at high pH. Such polymers have been called "polysoaps" or intramolecular micelle-forming polymers.

PA-18K$_2$, which is a potassium salt of an alternating copolymer of maleic anhydride and 1-octadecene, is a polysoap and can be used in the neutral pH range much as a conventional micelle. In this chapter, we summarize photophysical and photochemical studies in aqueous solutions of PA-18K$_2$, especially energy transfer of cationic dyes. These studies via steady-state and time-dependent techniques provide direct evidence for the existence of hydrophobic microdomains in aqueous solutions of PA-18K$_2$ (12). Studies in PA-18K$_2$ are compared to studies in aqueous solutions of PMA in order to ascertain the effect of long hydrocarbon side chains on the formation of intramolecular micelles, and the effect of conformational transitions (13–15) on electronic energy-transfer processes. To study the effect of the polymer main chain on quenching kinetics and exciplex formation processes, a comparison of the polymeric micelle with normal simple micellar systems is also presented.

Experimental Details

Cationic Dyes. The cationic dyes rhodamine 6G, R6G (the donor, D) and rhodamine B, RB (the acceptor, A) were used in studies of electronic energy-transfer processes as received. Stock solutions of dyes were 2×10^{-4} M. Figure 1 shows the emission spectrum of R6G and the absorption spectrum of RB in aqueous solutions of PA-18K$_2$. The dashed spectrum shows the emission of pure RB in PA-18K$_2$, excited at 550 nm. The sample solutions of R6G and RB mixtures were excited at 480 nm, where only the donor R6G absorbs the light. Because of overlap of the emission of RB and R6G, the absolute energy-transfer efficiency was difficult to measure. The energy-transfer processes were then monitored by the relative fluorescence intensity ratio I_{RB}/I_{R6G}; the larger value of I_{RB}/I_{R6G} indicates a relatively higher energy-transfer efficiency. I_{RB}/I_{R6G} is I_{570}/I_{550} in water and I_{580}/I_{550} in polymer, according to the emission spectrum of single dye in these systems. The energy transfer is very efficient even in water at dye concentrations above 1×10^{-5} M. To show clearly the effect
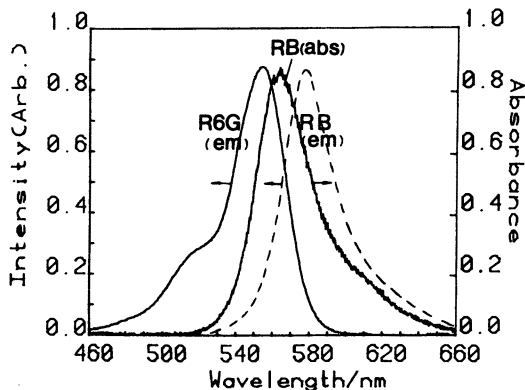
Figure 1. The emission spectrum of rhodamine 6G excited at 480 nm and the absorption spectrum of rhodamine B in aqueous solutions of PA-18K$_2$ (0.01 g/L). The dashed line is the emission spectrum of rhodamine B excited at 550 nm.

of polymer on energy-transfer processes, mixtures of 4×10^{-6} M R6G and 2×10^{-7} to 4×10^{-6} M RB were used.

Fluorescent Probes and Quenchers.   Pyrene, 1-pyrenebutyltrimethylammonium bromide (C_4PN^+), 1-pyreneundecyltrimethylammonium iodide ($C_{11}PN^+$), 1-pyrenebutanoic acid (PyC_3COOH), 1-pyrenedecanoic acid (PyC_9COOH), and 2-methylanthracene were employed as fluorescent probes.

Sodium iodide, thallium(I) sulfate, nitromethane (CH_3NO_2), dimethylaniline (DMA), and 1-dodecylpyridinium chloride (DPC) were used as quenchers.

Surfactants.   Sodium dodecyl sulfate (SDS) was chosen as a simple micellar system for comparison at room temperature, and sodium cetyl sulfate (SCS), because of its low solubility in water at room temperature, was used at 40 °C. The concentration of surfactants was 5×10^{-2} M SDS and 2×10^{-3} M SCS.

Polymer Materials.   PA-18K$_2$ was prepared by hydrolysis of PA-18 (a 1:1 alternating copolymer of maleic anhydride and 1-octadecene, Chevron/Gulf Co.) as described previously (*12*). The IR spectra in Figure 2 show that hydrolysis of the starting material was complete; the stretching bands of $C=O$ (1780 and 1850 cm^{-1}) completely shifted to lower frequencies (1400 and 1580 cm^{-1}) because of the release of anhydride ring strain and the conversion of carbonyl groups to carboxyl groups. The molecular weights of the PA-18K$_2$ sample were measured by HPLC in their acid form in tetrahydrofuran and calibrated with standard samples of polystyrene. The molecular weight of PA-18K$_2$ was 1.0×10^4. A PA-18K$_2$ sample (SP^2 Scientific Polymer Products Inc.) of molecular weight 7×10^3 was used for studying the effects of molecular weight on the aggregation number of monomer units in PA-18K$_2$. The concentrated PA-18K$_2$ stock solution (20 g/L) was prepared by heating the mixture above 70 °C.

Poly(methacrylic acid) (Polyscience Inc.) was purified by repeated solution in water followed by freeze-drying. The molecular weight of PMA was determined by
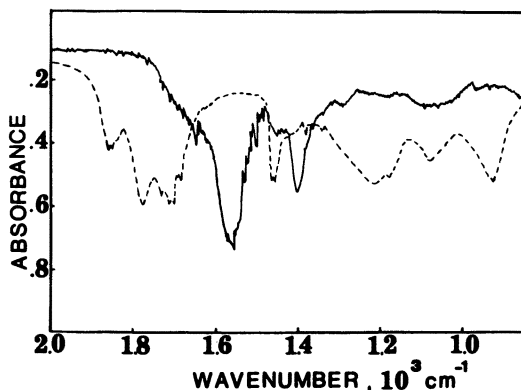
Figure 2. Infrared absorption spectra (1000–2000 cm⁻¹) of PA-18K₂ (—) and PA-18 (- - -) in KBr pellets.

standard viscosity techniques to be 1.1×10^4; the concentration of the stock solution of PMA was 10 g/L. The pH of polymer samples was adjusted with concentrated HCl or NaOH (in PMA) or KOH (in PA-18K₂) solution. The concentration of polymer samples was 1 g/L in these studies, except for the energy-transfer section (0.01– 1 g/L).

Measurements. Steady-state absorption and emission spectra were recorded on a Perkin-Elmer 552 UV–visible and an MPF-44B fluorescence spectrophotometer, respectively. Fluorescence decay rate constants, k_o, and quenching rate constants, k_q, were measured with a PRA LN-100 nitrogen laser system with fast spectroscopic detection (16, 17). Measurement of the degree of polarization (18–20) and transient absorption via laser photolysis were described in previous studies (21).

The binding sites for cationic dyes in one polymer chain are estimated as the product of ionization degree times carboxyl units in one polymer chain; for example, the number of binding sites in PMA at pH 4–5 is approximately 20 (20% × 100), and is 45 (90% × 25 × 2) in PA-18K₂ at pH 8. The number of binding sites is greater than the average molecular number of cationic dyes per polymer chain.

Results and Discussion

Pyrene and Its Derivatives in PA-18K₂ and PMA. The ratio of the pyrene fluorescence intensities of peak 3 (λ 384 nm) to peak 1 (λ 373 nm) has been shown to monitor the environment of excited pyrene. Higher values of I_3/I_1 indicate a more hydrophobic environment for pyrene (22).

In aqueous solutions of PA-18K₂ the ratio I_3/I_1 is almost constant at 1.09–1.04 over the entire pH range. These data contrast with those observed in aqueous solutions of PMA where the ratio I_3/I_1 sharply decreases from 0.88 to 0.55 at pH > 4. The data indicate that PMA acts as a host for pyrene only in the low pH range. However, PA-18K₂ provides hydrophobic micro-domains and acts as a host over the entire pH range. Increasing pH increases the ionization of the polymers, and increased ionization leads to a repulsive

interaction of negatively charged carboxyl COO^- groups and tends to expand the polymer. In the PA-18K$_2$ system, a strong hydrophobic interaction among the long hydrocarbon side chains stabilizes the compact conformations even at high pH.

The fluorescence decay rate constants, k_o, of several fluorescent probes in various systems (Table I) provide further evidence for hydrophobic microdomains in PA-18K$_2$ aqueous solutions. All the decays are single exponential decays except for $C_{11}PN^+$ in aqueous solutions of PMA at pH 8. All the k_o values in PA-18K$_2$ aqueous solutions at pH 4, 8, and 10 are similar to those found in hexanol and much smaller than those in water and aqueous solutions of PMA at pH 8. In summary, PA-18K$_2$ readily solubilizes pyrene and some positively and negatively charged derivatives of pyrene, especially long-chain derivatives.

Fluorescence spectra of a long-chain cationic derivative of pyrene, $C_{11}PN^+$, in aqueous solutions of PMA and PA-18K$_2$ are shown in Figure 3. A large amount of pyrene excimer is formed at a very low concentration (2×10^{-6} M) of $C_{11}PN^+$ in aqueous solutions of PMA at pH 8 (dashed line). The excimer formation leads to double exponential decay (Table II). This result can be explained if the long hydrocarbon chains of the $C_{11}PN^+$ cause a local clustering of the probes on the negatively charged extended PMA

Table I. Decay Rate Constants of Fluorescence of Several Fluorescent Probes

	PA–18K$_2$ (1 g/L)					PMA (1 g/L)	
Probe	pH 4	pH 8	pH 10	Hexanol	Water	pH 3	pH 8
PyC$_3$COOH	0.42	0.74	0.79	0.45	0.80	0.42	0.82
PyC$_9$COOH	0.45	0.46	0.49	0.43	0.87	0.48	0.90
Pyrene	0.25	0.25	0.24	0.25	0.49	0.24	0.48
C$_4$PN$^+$	0.56	0.44	0.44	0.44	0.70	0.41	0.75
C$_{11}$PN$^+$	0.47	0.47	0.48	0.53	0.78	0.50	—[a]

NOTE: All values are for k_o, 10^7 s^{-1}.
[a]$k_1 = 10.0$, $k_2 = 0.7$, and $\alpha = 0.4$; double-exponential decay (6).
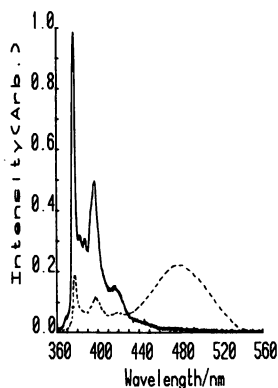
Figure 3. Fluorescence spectra of 2×10^{-6} M $C_{11}PN^+$ in aqueous solutions of PA-18K$_2$ (—) and in PMA (- - -) at pH 8, 1 g/L.

Table II. Quenching Rate Constants of Pyrene Fluorescence in Various Systems

Quenchers	PA–18K$_2$ (pH 8)	SDS	Heptane	Water
None	2.5×10^6 s^{-1}	2.9×10^6 s^{-1}	2.2×10^6 s^{-1}	4.8×10^6 s^{-1}
Tl$^+$	7.6×10^{10}	2.6×10^{10}		6.2×10^9
O$_2$	3.2×10^9	9.2×10^9	5.5×10^{10}	9.8×10^9
CH$_3$NO$_2$	1.2×10^8	3.0×10^9	1.7×10^9	9.5×10^9
I$^-$	$<10^6$	2.6×10^6		1.3×10^9

NOTES: All results are for k_q, M^{-1} s^{-1}. [pyrene] $= 2 \times 10^{-6}$ M.

chain and thus enhance static excimer formation. The time-dependent emission data show an immediate formation of the $C_{11}PN^+$ excimer in aqueous PMA solutions at pH 8, corresponding to the previous discussion. However, in an aqueous solution of PA-18K$_2$ (pH 8), the fluorescence spectrum of $C_{11}PN^+$ exhibits a typical and enhanced monomer spectrum of pyrene derivative with fine structure.

These data indicate that the environment of $C_{11}PN^+$ in PMA and in PA-18K$_2$, both at pH 8, where both polyelectrolytes are almost fully ionized, is quite different. $C_{11}PN^+$ experiences a water phase in PMA, and the interaction between $C_{11}PN^+$ and PMA is electrostatic in nature. In PA-18K$_2$ solution, $C_{11}PN^+$ was solubilized in polymer hydrophobic microdomains because of a hydrophobic interaction between the long hydrocarbon chains and because of electrostatic bonding.

Energy Transfer from R6G to RB in PA-18K$_2$ and PMA.

A substantial overlap between the emission spectrum of R6G and the absorption spectrum of RB (Figure 1) predicts an efficient electronic energy transfer from the excited R6G to the ground state of RB (23–25). When aqueous solutions of 4×10^{-6} M R6G and 4×10^{-6} M RB were excited at 480 nm, a broadened emission spectrum was observed in the absence of PA-18K$_2$ (shown in Figure 4, curve a) because of some degree of energy transfer leading to overlap emission of R6G and RB, where the ratio I_{RB}/I_{R6G} is close to 1. However, in the presence of PA-18K$_2$ (0.01 g/L), a typical RB emission spectrum appears around 580 nm, and the relative energy-transfer efficiency I_{RB}/I_{R6G} is equal to 9.5 (Figure 4, curve b). Binding of cationic dyes to the negatively charged polymer compact microdomains leads to high efficiency of energy transfer between R6G and RB because of the close proximity of D–A pairs.

Figure 5 shows the effect of pH on the relative efficiency of energy transfer. The ratio I_{RB}/I_{R6G} is almost constant and remains 9.5 at pH ≥ 5. However, a sharp decrease in the ratio I_{RB}/I_{R6G} is observed at pH ≤ 4, and the spectra exhibit two peaks (550 and 580 nm) at pH 3. The decreased ratio I_{RB}/I_{R6G} is explained by the low ionization of polyelectrolyte PA-18K$_2$ at pH ≤ 4, leading to less electrostatic binding between cationic dyes and polymer;
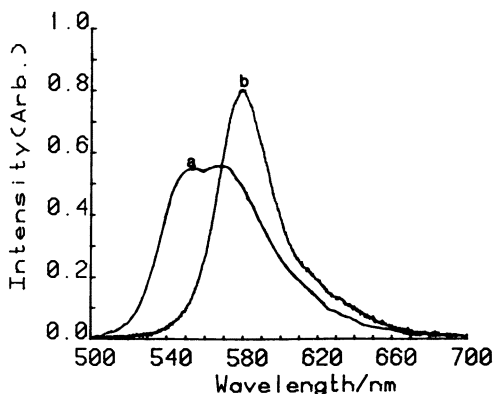
Figure 4. Fluorescence spectra of aqueous solutions of 4 × 10⁻⁶ M R6G and 4 × 10⁻⁶ M RB in the absence (a) and presence (b) of PA-18K₂ (0.01 g/L).
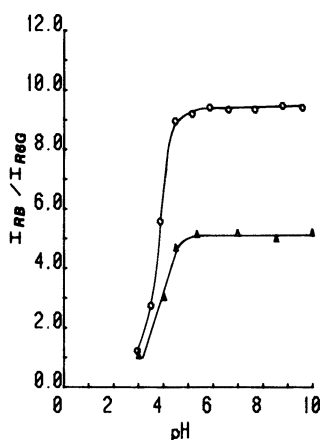
Figure 5. The relative fluorescence intensity ratio I_{RB}/I_{R6G} as a function of pH in aqueous solutions of PA-18K₂. The concentrations of PA-18K₂ are 0.01 (○) and 1 g/L (▲).

cationic dyes are partially ejected from the polymer to the aqueous phase. Increasing the concentration of PA-18K₂ to 1 g/L reduces the energy efficiency because of the increasing number of cationic dye binding sites and the separation of D–A pairs of cationic dye.

Fluorescence studies (14, 15) using pyrene, pyrene derivatives, and cationic probes in poly(methacrylic acid) have shown that a conformational transition from a closed compact coil to extended form induced by pH is a progressive process over several pH units (pH 4–6). The emission spectrum of 4 × 10⁻⁶ M R6G and 4 × 10⁻⁶ M RB excited at 480 nm in water is not dependent on pH. However, in aqueous solutions of PMA, the spectra are significantly dependent on pH (shown in Figure 6). At pH 4–5, the spectra are similar to the typical emission of RB; at pH 2–3 and 6–7, the spectra in PMA display stronger emission at 550 nm; and at pH 8, the spectra are identical to those in water.
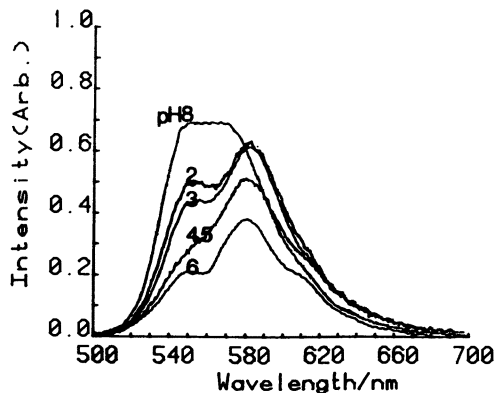
Figure 6. Fluorescence spectra of aqueous solutions of 4 × 10⁻⁶ M R6G and 4 × 10⁻⁶ M RB in aqueous solutions of PMA at pH 2, 3, 4.5, 6, and 8.

The data indicate that the interaction between cationic dyes and the polymer PMA chain is similar to the interaction of Auramine O with PMA (*15*). This interaction is stronger at pH 4–5 than at other pH levels. Increasing electrostatic binding of cationic dyes in aqueous solutions of PMA at pH $\geq$ 6 does not lead to a higher efficiency of energy transfer, but partially ionized PMA (pH 4–5) causes a higher efficiency of energy transfer. The ratio I_{RB}/I_{R6G} in aqueous solutions of PMA as a function of pH is shown in Figure 7. The ratio I_{RB}/I_{R6G} exhibits a significant enhancement on increasing the pH from 2 to 4.5 and a marked decrease at pH values beyond 5. The relative ratio reaches a maximum around pH 4.5. The maximum ratio in aqueous solutions of PMA (0.01 g/L) is twice as great as that in water.

A simple explanation of these data is as follows. Anionic sites are formed on PMA as the compact PMA coil opens with increasing pH; cationic dyes are bound to these sites. On binding, the cationic dyes tend to organize the
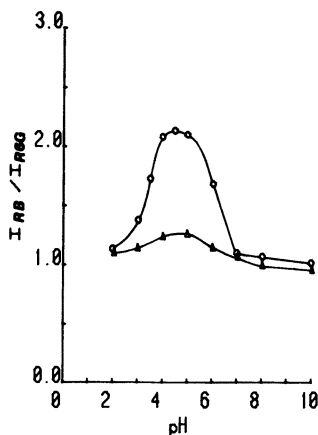
Figure 7. The relative fluorescence intensity ratio I_{RB}/I_{R6G} *as a function of pH in aqueous solutions of PMA. The concentrations of PMA are 0.01 (○) and 1 g/L (▲).*

polymer chain around the probe molecules, and this organization thus decreases the separation of D–A pairs and increase the efficiency of energy transfer. At pH $\geq$ 6, although the polymer is largely ionized but in an extended form, it has little effect on organizing the cationic dyes in close proximity, in contrast to PA-18K$_2$ at this pH. At pH 2 no electrostatic binding of dye and polymer exists, but RB or R6G molecules may be partially solubilized in the compact polymer coil, so that the ratio is slightly higher than in water.

These data are in agreement with previous studies with Auramine O and Ru(bpy)$_3{}^{2+}$ and indicate again that the conformational transition of PMA induced by pH is a progressive continuous process over several pH units, and, beginning at pH 4–5, that the compact polymer coil is partially swollen. This particular pH region allows cationic species to bind into the swollen polymer coils of PMA. A decreased effect of PMA at pH 4–5 on energy transfer is also observed on increasing the PMA concentration, and the decrease is similar to that in PA-18K$_2$. The energy-transfer ratio is fourfold smaller in PMA (pH 4–5) than in PA-18K$_2$. Perhaps the hydrophobic interaction between the long hydrocarbon side chains in PA-18K$_2$ makes this polymer more rigid and leads to a much closer pairing of the reactants and to a higher energy-transfer efficiency than in a swollen PMA coil at pH 4–5.

Figure 8 shows the absorption spectra of 4×10^{-6} M R6G and 4×10^{-6} M RB in aqueous solutions of PA-18K$_2$ (0.01 g/L), in PMA (0.01 g/L, pH 4.5), and in water. In water the spectrum consists of two absorbing bands because of the absorbance of the mixture of R6G and RB. However, for PA-18K$_2$, only one band was observed. Possibly a ground complex PA-18K$_2$–R6G–RB was formed because of the binding of R6G and RB to the
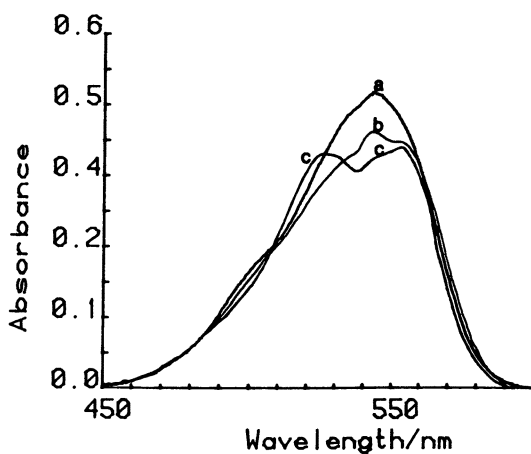
Figure 8. UV–visible absorption spectra of mixtures of 4×10^{-6} M R6G and 4×10^{-6} M RB in aqueous solutions of PA-18K$_2$ (0.01 g/L) (a), PMA (0.01 g/L) (b), and water (c). Polymer concentrations are 0.01 g/L.

carboxyl groups next to each other on the PA-18K$_2$. At pH 4.5–10, the absorbance of the band increases, but the shape of the spectrum is not changed, a result indicating that formation of the ground complex is complete in PA-18K$_2$ above pH 4. Data in PMA at pH 4–5 are similar to PA-18K$_2$ at pH 3. The spectrum consists of one peak (ground complex) with two shoulders (absorbing bands of R6G and RB). This finding indicates that the ground complex is only partially formed because of the fewer binding sites in the polymer PMA coil. At pH > 7, the spectrum in PMA is similar to that in water, a result indicating that no complex is formed under these conditions.

The first-order fluorescence decay curves of 4×10^{-6} M R6G, ln I vs. t (fluorescence intensity versus time), in various systems, are plotted in Figure 9. Figure 9a is the decay in the absence of acceptor RB. The lifetime is identical in water and in aqueous solutions of PA-18K$_2$ and PMA (both 0.01 g/L), equal to 4.5 ns. However, in the presence of 4×10^{-6} M RB the situation is changed: the lifetime reduces to 3.6 ns in PMA solution at pH 4.5 (curve c), and to 3.0 ns in PA-18K$_2$ solutions at pH 8 (curve d), with almost no change in water (curve b).

Figure 10 shows the steady-state experimental data as a relationship between the fluorescence intensity ratio I_{RB}/I_{R6G} and the concentration of acceptor RB. On increasing the concentration of RB, the ratio I_{RB}/I_{R6G} increases; that is, quenching of excited R6G via energy-transfer processes increases. The effect of the concentration of acceptor RB on the increase of the ratio I_{RB}/I_{R6G} is on the order of PA-18K$_2$ > PMA (pH 4–5) > water. In water this effect is small but still significant. The fluorescence spectrum gradually broadens, and at [RB] of 4×10^{-6} M, I_{RB}/I_{R6G} is 1.8 times larger than at an [RB] of 2×10^{-7} M. This result contrasts with the unchanged lifetime of excited donor R6G. Therefore, the radiative mechanism probably is mainly operative in the energy transfer between cationic dyes R6G and
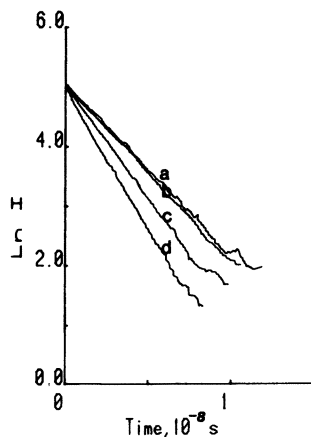
Figure 9. Plots of ln I of 4 × 10⁻⁶ M R6G fluorescence vs. time in the absence of 4 × 10⁻⁶ M RB (a), in the presence of 4 × 10⁻⁶ M RB in water (b), in aqueous solutions of PMA at pH 4.5 (c), and in aqueous solutions of PA-18K₂ (d). Polymer concentrations are 0.01 g/L.
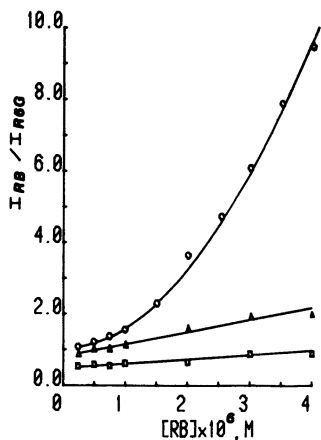
Figure 10. Relationship between the ratio I_{RB}/I_{R6G} and the concentrations of RB in aqueous solutions of PA-18K$_2$ (○), in aqueous solutions of PMA (▲), and in water (□). Polymer concentrations are 0.01 g/L.

RB in water. This process may be represented by equation 1.

$$D^* + A \xrightarrow{\lambda_D} D + h\nu_D + A \to D + A^* \to D + A + h\nu_A \qquad (1)$$
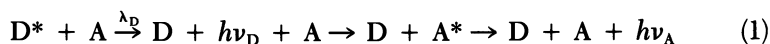
where λ_D is the absorbing band of donor, and $h\nu_D$ and $h\nu_A$ are the fluorescence of D and A, respectively. No direct interaction occurs between the donor (D) and the acceptor (A) molecules, and the donor decay time is not affected by the process or by the concentration of acceptor molecules. Thus, as the concentration of the acceptor is increased, the fluorescence yield of the donor decreases, but the fluorescence decay time of the donor remains unaffected. For PA-18K$_2$ and PMA, both fluorescence lifetime and fluorescence yield of R6G are reduced on increasing the concentration of the acceptor RB. Most likely, mainly nonradiative transitions are involved in energy-transfer processes in these polymer systems. This situation can be envisaged if in PA-18K$_2$ (pH 8) and in PMA (pH 4–5), cationic D and A molecules are electrostatically bound in close proximity in a polymer at distances at which nonradiative short-range transfer is the dominant route for energy transfer. It is unlikely that direct encounters between electrostatic bound D–A molecules, leading to intermolecular energy transfer, occur in the rigid polymer hydrophobic microdomains. In other words, an intramolecular energy-transfer process (*26*) occurs, such as

$$D-A \xrightarrow{\lambda_D} D^*-A \xrightarrow{k_{ET}} D-A^* \to D-A + h\nu_A \qquad (2)$$
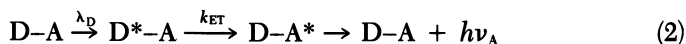
where k_{ET} is the rate constant for energy transfer. The completion of the ground complex of polymer D–A favors the short-range energy-transfer mechanism rather than the long-range mechanism. A nonlinear and rapid increase in I_{RB}/I_{R6G} is observed at higher concentrations of RB in aqueous solutions of PA-18K$_2$ (where [RB]/[R6G] is closer to 1) which can be ex-

plained by an increase in the ground complex formed in the PA-18K$_2$ system at higher concentrations of RB. This concentration effect is larger than in PMA because of efficient formation of ground complex (Figure 8, curve a) and because of the unique nearest-neighbor binding of D–A pairs in PA-18K$_2$.

PA-18K$_2$ and Simple Micellar Systems.   The data just presented show that PA-18K$_2$ in aqueous solution forms compact hydrophobic micro-domains over the entire pH range. To compare this system with simple micellar systems, PA-18K$_2$ samples were adjusted to pH 8, where the car-boxyl groups are almost fully ionized, and where PA-18K$_2$ is structurally analogous to simple micelles. An ordinary micelle is a dynamic structure that exists in equilibrium with its monomer, where monomer units are both leaving and entering the micelle. On the other hand, aqueous solutions of the polymeric intramolecular micelles do not possess free monomer units, and monomer units are bound together covalently via a polymer main chain. Differences in behavior in the two systems are thus expected.

Pyrene fluorescence decay curves show that the lifetime of the excited singlet pyrene in PA-18K$_2$ (400 ns) is much longer than in water (208 ns) and also longer than in SDS (315 ns). The fluorescence spectroscopic data show that the ratio I_3/I_1 of pyrene fluorescence in PA-18K$_2$ (1.08) is much larger than in water (0.55) and even larger than in SDS (0.82). However, the I_3/I_1 (0.95) and lifetime ($\sim$ 300 ns) of pyrene fluorescence in PA-18K$_2$ at 40 °C are similar to those observed in SCS micellar aqueous solutions, where the hydrocarbon chain length is identical to the side chains of PA-18K$_2$. These data indicate that guest molecules in PA-18K$_2$ experience a larger hydrophobicity than in SDS micelles, but one that is similar to that in SCS micelles.

Previous studies (27) showed that the quenching of pyrene fluorescence by DMA is via an exciplex process. The transient absorption spectra of pyrene and DMA have been measured (12) by laser flash photolysis. The relative ratio of the quantum yield of excited triplet pyrene, ϕ_T to the quantum yield of anion pyrene ϕ_- is estimated as 3.3 in PA-18K$_2$, and 1.3 in SDS micellar system. Mataga and coworkers (28, 29) indicated that the yields of pyrene anion are related to the dielectric constants of the solvent. In polar solvents the ionic photodissociation process, k_{ip}, is dominant among the decay process of exciplex (P*---D)$_s$ and the relative ratio of ϕ_T to ϕ_- is low. On the contrary, in nonpolar solvents k_{ip} is greatly depressed and the intersystem crossing process gives the exciplex, which then dissociates to P_T*, and a higher yield of ϕ_T relative to ϕ_- is obtained. The higher ratio of ϕ_T to ϕ_- observed in PA-18K$_2$ again indicates that the environment of the pyrene–DMA pair in PA-18K$_2$ is less polar than that in SDS.

The time-dependent data shown in Figure 11 indicate that the py-rene–DMA exciplex in SDS micellar solution is formed rapidly in several
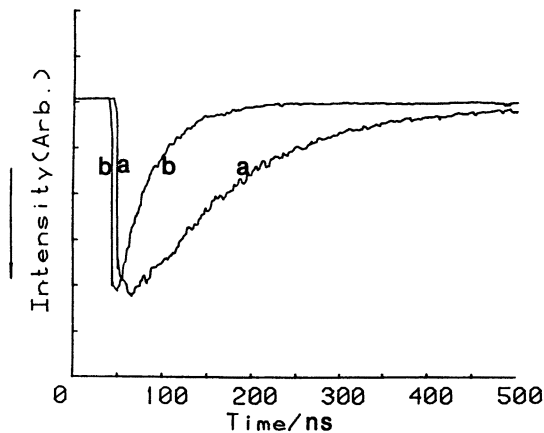
Figure 11. Time-dependent profiles of exciplex fluorescence pyrene–DMA observed at 470 nm in a, PA-18K₂; and b, in SDS. [pyrene] = 6 × 10⁻⁵ M, [DMA] = 3 mM. (Reproduced from reference 12. Copyright 1987 American Chemical Society).

nanoseconds, and then decays with a lifetime of 43 ns. However, the intensity of the exciplex in PA-18K$_2$ grows to a maximum over 40 ns, followed by a decay over 121 ns. This behavior mirrors that observed in hexane (130 ns). A slower formation of exciplex can be attributed to the restriction of movement of pyrene and DMA molecules by the PA-18K$_2$, and the longer lifetime of the exciplex originates from the nonpolar environment of the guest molecules in PA-18K$_2$.

Further evidence to support this conclusion is provided by the measurement of the degree of polarization of 2-methylanthracene. The data show that 2-methylanthracene in PA-18K$_2$ at pH 8 ($\sim$ 0.14) is much larger than that in SDS ($\sim$ 0.01), but slightly less than that observed in PMA at pH 2 ($\sim$ 0.17). This result illustrates that 2-methylanthracene in PA-18K$_2$ micelles experiences a much more rigid environment than in SDS, but somewhat less than that in PMA compact coil at pH 2.

The bimolecular quenching rate constants, k_q, of pyrene fluorescence in various systems are presented in Table II. The values of k_q with the quenchers such as oxygen, nitromethane, and sodium iodide in PA-18K$_2$ polymer–micellar solutions are much smaller than in water or in homogeneous nonpolar solvents (viz. heptane) and even smaller than in SDS micellar solutions. The data suggest that the penetration of the selected quenchers to the pyrene hosted in the polymer micelle is inhibited by the main chain of the host polymer micelle. This restrictive effect is larger than in simple micellar systems, and it results from the more rigid environment of pyrene in polymer micellar systems.

Furthermore, the k_q with iodide ion in the SDS and PA-18K$_2$ micellar systems is over 10^3-fold smaller than in water because of the electrostatic repulsive interaction between the negatively charged micellar surface and the negatively charged quencher molecules. The negatively charged surfaces of polymer micelles or of simple micelles cause cations such as thallium ions to bind to these surfaces, and the k_q values in micelles are 10 times larger than in water. The percentage of binding of thallium ions to micelles was obtained (13) by measuring the quenching rate constants of sodium 1-pyrenesulfonate (PySO$_3$Na) by thallium sulfate in water and in micellar solution. Binding of Tl$^+$ in PA-18K$_2$ ($\sim 80\%$) was more efficient than in SDS ($\sim 20\%$), and the result is more efficient quenching of pyrene fluorescence in PA-18K$_2$ than in SDS.

The Poisson kinetic quenching rate constants of C$_4$PN$^+$ by DPC, k_q, in SDS micelle is twice as fast as that in PA-18K$_2$, a result indicating again the greater restriction to movement in the polymer micelle (12).

Aggregation Number of Monomer Units in PA-18K$_2$ Micelle.
Poisson quenching kinetics, which are successful in measuring mean aggregation numbers in simple micellar systems (30–35), can also be used to investigate polymer intramolecular micelles. Quenching of 1-pyrenebutyltrimethylammonium bromide fluorescence by 1-dodecylpyridinium chloride (DPC) in aqueous solutions of PA-18K$_2$ was carried out via steady-state studies and pulsed-laser studies. Experimental data confirm the Poisson distribution of DPC molecules among the polymer micelles. Figure 12 shows that a plot of I_0/I vs. [DPC] is not linear, but the plot of ln (I_0/I) vs. [DPC] is linear and fits the Poisson quenching kinetics:

$$\ln (I_0/I) = \frac{[DPC]}{[\text{micelle}]} \qquad (3)$$
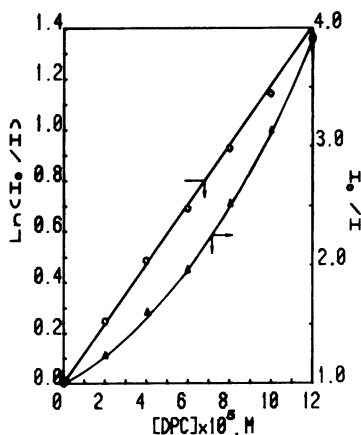
Figure 12. Quenching of C$_4$PN$^+$ fluorescence by DPC in aqueous solution of PA-18K$_2$. I_0 and I are the relative intensities of pyrene fluorescence in the absence and presence of DPC, respectively. The slope of the plot of ln [(I$_0$)/I] vs. [DPC] = 1.1 × 10^4, [PA-18K$_2$] = 1 g/L. Key: ○, plot of ln (I$_0$/I) vs. [DPC]; ▲, plot of I$_0$/I vs. [DPC].

The slope of the plot of ln (I_0/I) vs. [DPC] is 1/[micelle], and the concentration of monomer units $[PA\text{-}18K_2]_M$ is known. The mean aggregation number, $\overline{N}$, can be calculated by

$$\overline{N} = \frac{[PA-18K_2]_M - CMC}{[\text{micelle}]} \tag{4}$$

where the CMC for the polymeric micelle is taken as zero, as $PA\text{-}18K_2$ does not possess free monomer units. Similar experiments were done at different polymer concentrations. The average aggregation number of monomer units in $PA\text{-}18K_2$ of molecular weight 1×10^4 was obtained as 24 ±2. The average aggregation number in $PA\text{-}18K_2$ of molecular weight 7×10^3 was 17 ± 2. The polymeric micelle weight, $\overline{W}_{\text{micelle}}$, was calculated via equation 5 where M_m is the molecular weight of monomer. ($M_m = 428$ for $PA\text{-}18K_2$.)

$$\overline{W}_{\text{micelle}} = \overline{N}M_m \tag{5}$$

The polymer micelle weight calculated from Poisson quenching kinetics corresponds to that measured by gel permeation chromatography. This finding indicates that one $PA\text{-}18K_2$ polymer molecule of low molecular weight (order $\sim 10^4$) forms one polymeric micelle. Because of the degradation during the hydrolysis of PA-18, we have been unable to obtain a higher molecular weight sample.

Conclusion

Photostudies with pyrene and pyrene derivatives show that compact hydrophobic coil conformations are formed in $PA\text{-}18K_2$ over the entire pH range, quite unlike PMA, which forms compact coils only in the low pH range. A marked proximity effect leading to a high efficiency of electronic energy transfer of cationic dyes R6G and RB was observed in aqueous solutions of $PA\text{-}18K_2$. Experimental data indicate that a nonradiative short-range energy-transfer mechanism dominates in this process, which is also called intramolecular energy transfer. Meanwhile, in water a radiative mechanism is suggested. The relative efficiency and mechanism of this energy transfer in aqueous solution of PMA is dependent on pH, and the efficiency reaches a maximum around pH 4.5.

Studies on the effect of the conformational transition of PMA on R6G–RB energy transfer provide further information on the intermediate states that lie between compact coil and extended polymer chain. These studies confirm that the conformational transition of PMA induced by pH is a progressive process over several pH units, and that the polymer is partly swollen coil at pH 4–5.

The polymer micelle $PA\text{-}18K_2$ provides an interesting extension of nor-

mal micelles, with regard to both solubilizing power and the effects of polymer chain on photoreactions induced in the system. The guest molecules in polymer micelles experience a much more rigid and less polar environment than in SDS micelles. The polymer main chain places a steric restrictive effect, an electrostatic effect, or both effects on the movement of guest reactants. These studies also show that the interior of a PA-18K$_2$ polymer micelle is more hydrophobic than SDS, but is similar to that in SCS.

Acknowledgments

References

1. Geacintov, N. E.; Prusic, T.; Khosrofian, J. *J. Am. Chem. Soc.* **1976**, *98*, 6444 and references therein.
2. Barone, G.; Crescenzi, V.; Quadrifoglio, F. *J. Phys. Chem.* **1967**, *71*, 2341.
3. Chen, T.; Thomas, J. K. *J. Polym. Sci., Polym. Chem. Ed.* **1979**, *17*, 1103.
4. Strauss, U. P. In *Microdomains in Polymer Solutions*; Dubin, P., Ed.; Plenum: New York, 1985; pp 1–12.
5. Hsu, J.-L.; Strauss, U. P. *J. Phys. Chem.* **1987**, *91*, 6238.
6. Sugai, S.; Nitta, K.; Ohno, N. In *Microdomains in Polymer Solutions*; Dubin, P., Ed.; Plenum: New York, 1985; pp 13–32.
7. Chu, D. Y.; Thomas, J. K. *J. Am. Chem. Soc.* **1986**, *108*, 6270.
8. Strauss, U. P.; Gersheld, N. L. *J. Phys. Chem.* **1954**, *58*, 747.
9. Strauss, U. P.; Gersheld, N. L.; Crook, E. H. *J. Phys. Chem.* **1956**, *60*, 577.
10. Strauss, U. P.; Gersheld, N. L.; Crook, E. H. *Polym. Prepr. (Am. Chem. Soc., Div. Polym. Chem.)* **1986**, *27*(1), 425.
11. Nakahira, T.; Grätzel, M. *Makromol. Chem. Rapid Commun.* **1985**, *6*, 341.
12. Chu, D. Y.; Thomas, J. K. *Macromolecules* **1987**, *20*, 2133.
13. Chu, D. Y.; Thomas, J. K. *Macromolecules* **1984**, *17*, 2142.
14. Chu, D. Y.; Thomas, J. K. *J. Phys. Chem.* **1985**, *89*, 4065.
15. Chu, D. Y.; Thomas, J. K. In *Photophysics of Polymers*; Hoyle, C. E.; Torkelson, J. M., Eds.; ACS Symposium Series 358; American Chemical Society: Washington, DC, 1987; pp 434–451.
16. Hashimoto, S.; Thomas, J. K. *J. Am. Chem. Soc.* **1985**, *107*, 4655.
17. Hashimoto, S.; Thomas, J. K. *J. Phys. Chem.* **1985**, *89*, 2771.
18. Azumi, T.; McGlynn, S. P. *J. Chem. Phys.* **1962**, *37*, 2413.
19. Shinitzky, M.; Dianoux, A. C.; Gitler, C.; Weber, G. *Biochemistry* **1971**, *10*, 2106.
20. Grätzel, M.; Thomas, J. K. *J. Am. Chem. Soc.* **1973**, *95*, 6885.
21. Thomas, J. K. *The Chemistry of Excitation at Interfaces*; ACS Monograph 181; American Chemical Society: Washington, DC, 1984.
22. Kalyanasundaram, K.; Thomas, J. K. *J. Am. Chem. Soc.* **1977**, *99*, 2039.
23. Förster, T. *Discuss. Faraday Soc.* **1959**, *27*, 7.
24. Birks, J. B. *Photophysics of Aromatic Molecules*; Wiley: New York, 1970; Chapter 11.

25. Berlman, I. B. *Energy Transfer Parameters of Aromatic Compounds*; Academic: New York, 1973.
26. Speiser, S. *J. Photochem.* **1983,** *22,* 195.
27. Birks, J. B. *Photophysics of Aromatic Molecules*; Wiley: New York, 1970; p 479.
28. Mataga, N.; Okada, T.; Yamamoto, N. *Bull. Chem. Soc. Jpn.* **1966,** *39,* 2562.
29. Mataga, N.; Okada, T.; Yamamoto, N. *Chem. Phys. Lett.* **1967,** *1,* 119.
30. Turro, N. J.; Yakta, L. A. *J. Am. Chem. Soc.* **1978,** *100,* 5951.
31. Thomas, J. K. *The Chemistry of Excitation at Interfaces*; ACS Monograph 181; American Chemical Society: Washington, DC, 1984; p 172.
32. Fendler, J. H. *Membrane Mimetic Chemistry*; Wiley: New York, 1983.
33. Tachiya, M. *Chem. Phys. Lett.* **1975,** *33,* 289.
34. Tachiya, M. *J. Chem. Phys.* **1982,** *76,* 340.
35. Atik, S. S.; Singer, L. A. *Chem. Phys. Lett.* **1978,** *59,* 519.

Synthesis and Solution Properties of Hydrophobically Modified (Hydroxyethyl)cellulose

Arjun C. Sau[1] and Leo M. Landoll[2]

[1]Aqualon Company, Research and Development Center, Little Falls Centre One, 2711 Centerville Road, P.O. Box 15417, Wilmington, DE 19850–5417
[2]Hercules, Inc., Research Center, Wilmington, DE 19894

Hydrophobically modified water-soluble polymers (HMWSPs) exhibit enhanced solution viscosity and unique rheological properties. These properties can be explained in terms of intermolecular associations via hydrophobes. This chapter describes the synthesis and solution properties of HMWSPs. Particularly discussed are the solution properties of hydrophobically modified (hydroxyethyl)cellulose (HMHEC) in aqueous and surfactant systems. HMHECs interact with surfactants and thus modify solution viscosities. The structure and the concentration of the surfactant dictate the solution behavior of HMHEC. The unique solution properties of HMHEC can be exploited to meet industrial demands for specific formulations or applications.

WATER-SOLUBLE POLYMERS (WSPs) are an important class of industrial polymers. They have many applications in solution and in the solid state. In solution, they are widely used as thickeners to control the rheology of various water-based formulations, such as latex paints, drilling muds, foods, cosmetics, and building materials. Chemically modified natural polysaccharides such as starch, cellulose, and guar are a large class of commercial water-soluble polymers. The appropriate chemical modification of these polysaccharides can lead to the modified solution properties needed for specific applications.

In many applications and formulations, WSPs with surface-active properties are desirable. These properties are imparted to a polymer by chemical modification of the hydrophilic WSP with appropriate hydrophobic substituents. Examples of commercially available surface-active WSPs based on cellulose include its methyl, hydroxypropyl, and methylhydroxypropyl derivatives.

Recently, a new class of surface-active synthetic WSPs called "synthetic associative thickeners" was introduced to the latex coatings industry. These compounds have generated interest because of their unique rheological characteristics in aqueous systems (1). These synthetic macromolecules are composed of hydrophilic and hydrophobic components.

A few years ago, Landoll (2–4) reported that grafting a small amount of long-chain alkyl hydrophobes onto a nonionic water-soluble polymer leads to associative thickening behavior (i.e., enhanced viscosity, surface activity, and unusual rheological properties). This chapter deals with the general methods of preparation and solution properties of hydrophobically modified nonionic WSPs. Particularly described are the solution properties of hydrophobically modified (hydroxyethyl)cellulose (HMHEC) in aqueous and surfactant systems.

Experimental Details

The HMHECs discussed in this chapter were prepared according to Landoll's method (2) (i.e., by the reaction of HEC with the appropriate 1,2-epoxyalkane or the alkyl halide ($\geq C_8$) in an alkaline slurry process).

The hydrophobe content of the HMHEC was determined by exhaustive cleavage of the polymer with 57% aqueous hydroiodic acid for 2 h at 185–195 °C followed by analysis of the iodoalkane formed by gas chromatography on a column packed with 10% OV-17 (phenylmethylsilicone) on 80–110-mesh Chromosorb W-HP (diatomaceous earth, Alltech Associates) in a Perkin-Elmer 3920B gas chromatograph. All samples were run in triplicate.

Aqueous viscosity was measured at room temperature with a Brookfield and Ubbelohde viscometer. Intrinsic viscosities were measured by a five-point dilution method; no shear-rate corrections were made for the data. Interfacial tension was measured with a DuNouy ring tensiometer against toluene at various polymer concentrations. The formulations used to evaluate the HMHECs for latex paints have been described elsewhere (5).

Results and Discussion

Methods of Preparation of Hydrophobically Modified WSPs (HMWSPs). *Incorporation of Hydrophobes into WSPs.* Water-soluble cellulose derivatives ((hydroxyethyl)cellulose, (hydroxypropyl)cellulose, methylcellulose, etc.) or synthetic polymers containing hydroxyl groups (e.g., poly(vinyl alcohol)) can be reacted with a long-chain alkyl halide (2), acyl halide (2), acid anhydride (6), isocyanate (2), or epoxide (2, 3) under appropriate conditions to form an HMWSP. These reactions are shown in Scheme I. These postmodifications can be done in solution or in hetero-

i) $\quad R\!\!-\!\!OH + X\!\!\sim\!\! \xrightarrow{\ NaOH\ } R\!\!-\!\!O$

ii) $\quad R\!\!-\!\!OH + X\!\!-\!\!\overset{\displaystyle O}{\overset{\|}{C}}\!\!\sim\!\! \xrightarrow{\ NaOH\ } R\!\!-\!\!O\!\!-\!\!\overset{\displaystyle O}{\overset{\|}{C}}\!\!\sim$

iii) $\quad R\!\!-\!\!OH +$ (anhydride) $\longrightarrow R\!\!-\!\!O\!\!-\!\!\overset{O}{\overset{\|}{C}}\!\!-\!\!C\!\!-\!\!C\!\!-\!\!\overset{O}{\overset{\|}{C}}\!\!-\!\!OH$

iv) $\quad R\!\!-\!\!OH + O\!\!=\!\!C\!\!=\!\!N\!\!\sim\!\! \longrightarrow R\!\!-\!\!O\!\!-\!\!\overset{\displaystyle O}{\overset{\|}{C}}\!\!-\!\!NH\!\!\sim$

v) $\quad R\!\!-\!\!OH +$ (epoxide) $\longrightarrow R\!\!-\!\!O\!\!-\!\!CH_2\!\!-\!\!\underset{\underset{\displaystyle OH}{|}}{CH}\!\!\sim$

R: polymeric backbone containing hydroxyl group
$\sim$: alkyl hydrophobe
X: halogen atom
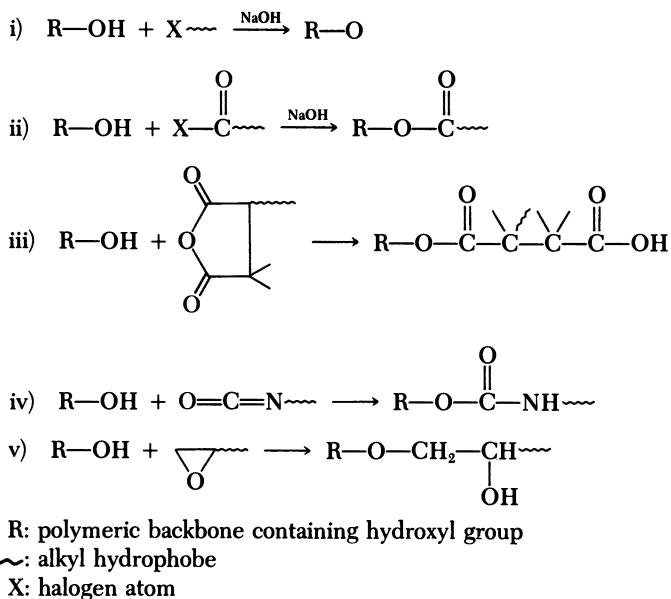
Scheme I

geneous slurry processes. However, on an industrial scale, slurry processes are preferred because of viscosity build-up during modification in solution.

Copolymerization. Synthetic HMWSPs can be prepared according to this approach by the copolymerization of a vinyl or epoxide monomer (*4*) with a small amount of a specific hydrophobic monomer that is copolymerizable with the primary monomer as shown in Scheme II. The hydrophobe content of the polymers can be tailored by controlling the amount of the hydrophobic comonomer used in the polymerization process. The nature of the group (i.e., ether, ester, carbamate, etc.) connecting the "long-chain

i) $\ CH_2\!\!=\!\!\underset{\underset{\displaystyle OAC}{|}}{CH} + CH_2\!\!=\!\!\underset{\underset{\displaystyle O\sim}{|}}{CH} \xrightarrow{\ polymerization\ }$

$\xrightarrow{\ H_2O\ } \left[\!\!-\!\!(CH_2\!\!-\!\!\underset{\underset{\displaystyle OH}{|}}{CH})_m\!\!-\!\!(CH_2\!\!-\!\!\underset{\underset{\displaystyle O\sim}{|}}{CH})_n\!\!-\!\!\right]$

ii) $\ CH_2\!\!-\!\!CH_2$ (epoxide) $+ CH_2\!\!-\!\!CH\!\!\sim$ (epoxide) $\xrightarrow{\ polymerization\ }$

$\left[\!\!-\!\!(CH_2\!\!-\!\!CH_2\!\!-\!\!O)_m\!\!-\!\!(CH_2\!\!-\!\!\underset{\underset{\displaystyle \sim}{|}}{CH}\!\!-\!\!O)_n\!\!-\!\!\right]$
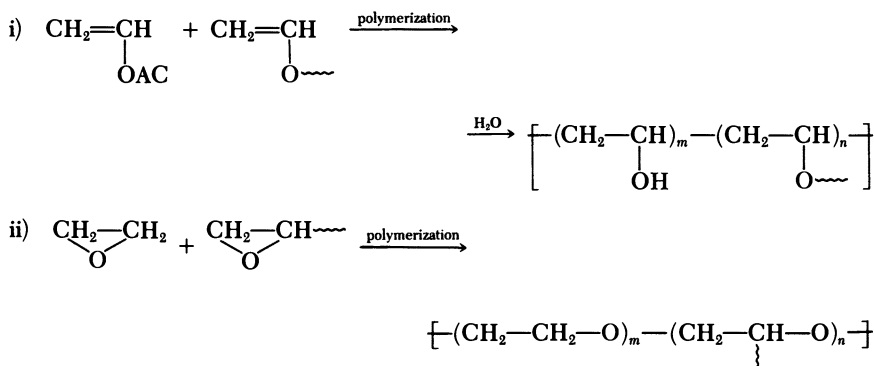
Scheme II

alkyl group" to the WSP backbone has no noticeable effect on the solution properties of the resulting HMWSP.

Thickening Mechanism of HMWSPs. HMWSPs exhibit enhanced solution viscosity as compared to their unmodified counterparts. Figure 1 compares the Brookfield viscosity of a C_{16} hydrophobically modified HEC (C_{16}HMHEC) with that of a similar molecular weight HEC. The enhanced solution viscosity of HMWSPs is the result of intermolecular associations via the hydrophobic groups (Figure 2). These hydrophobic associations can be viewed as pseudo-cross-links. A three-dimensional network results because of the tendency of the hydrophobes to cluster and thereby minimize the disruption of water structure. This network leads to an apparent increase in the hydrodynamic volume, which is reflected in enhanced solution viscosities.

Effect of Hydrophobe Level on Solution Behavior of HMHEC

The general solution viscosity behavior of a C_{12}HMHEC is shown in Figure 3. This behavior is common to all nonionic HMHECs that contain hydrophobes of different chain lengths (C_8–C_{24}). The peak viscosity and solubility of a given type of HMHEC depend on the amount and chain length of the hydrophobe (3). At a given hydrophobe level, the longer the chain length, the higher the viscosity. Also, the peak viscosity at a given hydrophobe level
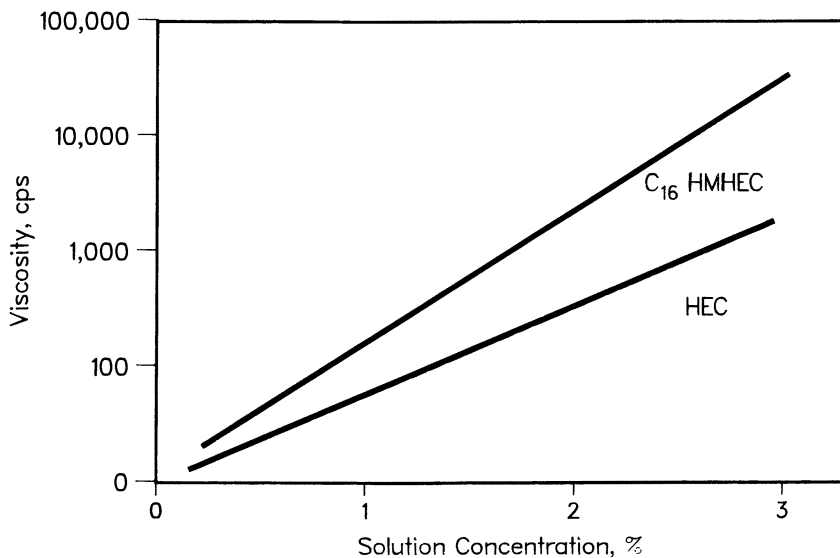
Figure 1. Brookfield viscosity (at 30 rpm) vs. concentration of C$_{16}$HMHEC and HEC of equivalent molecular weight.

Polymer Backbone

Hydrophobe
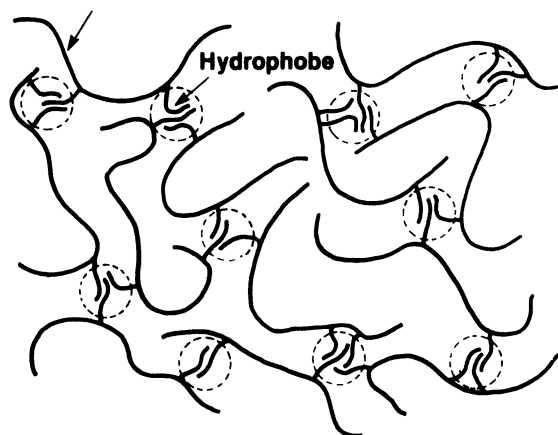
Figure 2. Structure of HMHEC in solution.
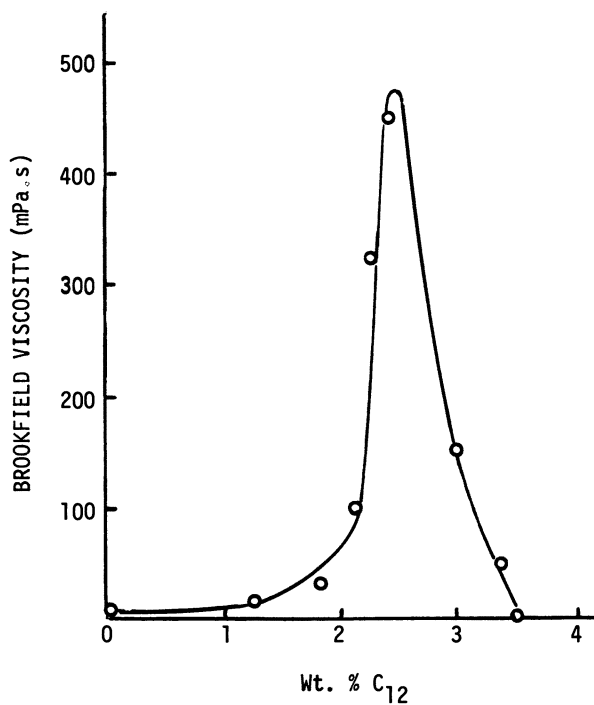
Figure 3. Brookfield viscosity of a C_{12}HMHEC as a function of polymer concentration. (Reproduced with permission from ref. 10. Copyright 1987 TAPPI Press.)

is much higher when the alkyl chain is longer. These relationships are shown in Figure 4, which compares the aqueous viscosities of HMHECs that contain C_8, C_{12}, and C_{16} hydrophobes.

As the hydrophobe content of the HMHEC increases, the viscosity first increases, reaches a maximum, and then decreases rapidly. The viscosity finally approaches that of the solvent as the polymer becomes insoluble. A minimum hydrophobe level (discussed in detail later) is necessary to achieve an observable increase in viscosity as compared to that of the unmodified HEC. Above this threshold, viscosity increases rapidly with increase in the hydrophobe content. After reaching the peak viscosity at an appropriate hydrophobe level, the viscosity decreases upon further increase in hydrophobe level. This decrease is not caused by a diminution in the degree of hydrophobic association, but by the incomplete solubility of the sample. That is, a given HMHEC sample has a distribution of polymer chains with different hydrophobe levels. The proportion of insoluble species increases as the overall hydrophobe content of the sample increases. The hydrophobe
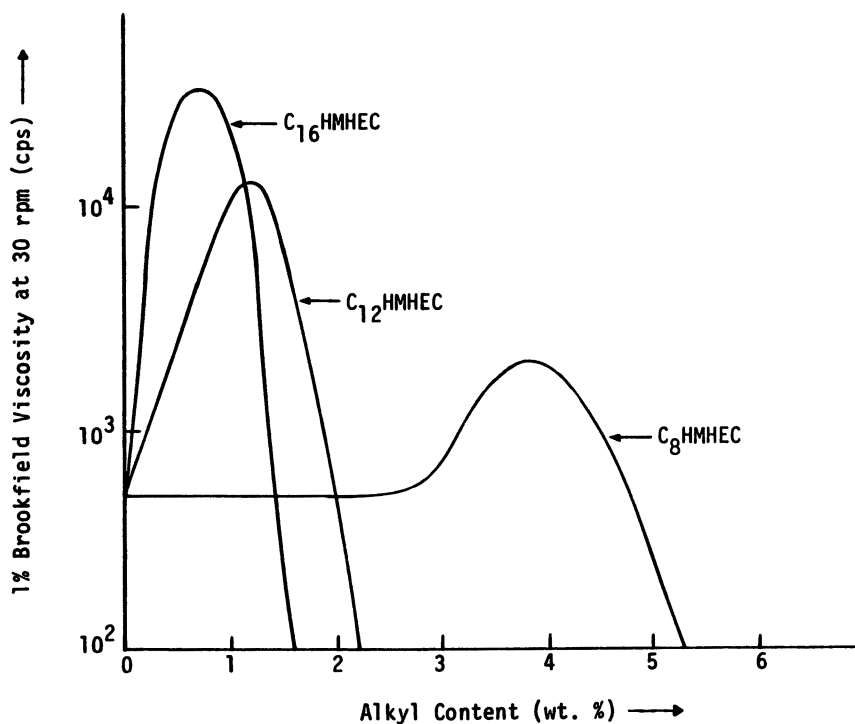
Figure 4. Brookfield viscosity (at 30 rpm) of HMHEC solution vs. alkyl group content of hydrophobe. (Reproduced with permission from ref. 3. Copyright 1982 Wiley).

substitution level, when analytically measured, reflects the average degree of substitution for all HMHEC species.

Correlation of Hydrocarbon Chain Length and Level with Solution Properties

Landoll (3) proposed a scheme to quantify structural effects of hydrophobes on solution properties. Two particular hydrophobic modification levels, designated H_o and H_I, were used. H_o is the hydrophobe level of HMHEC at which solution viscosity begins to increase markedly; H_I is the level at which the HMHEC becomes water-insoluble. On the basis of experimental data, it has been found that H_I is logarithmically related to the alkyl hydrophobe chain length. If H_I is defined in terms of hydrophobes per chain, then the polymer backbone molecular weight does not significantly influence H_I, and a general curve, as shown in Figure 5, is obtained.
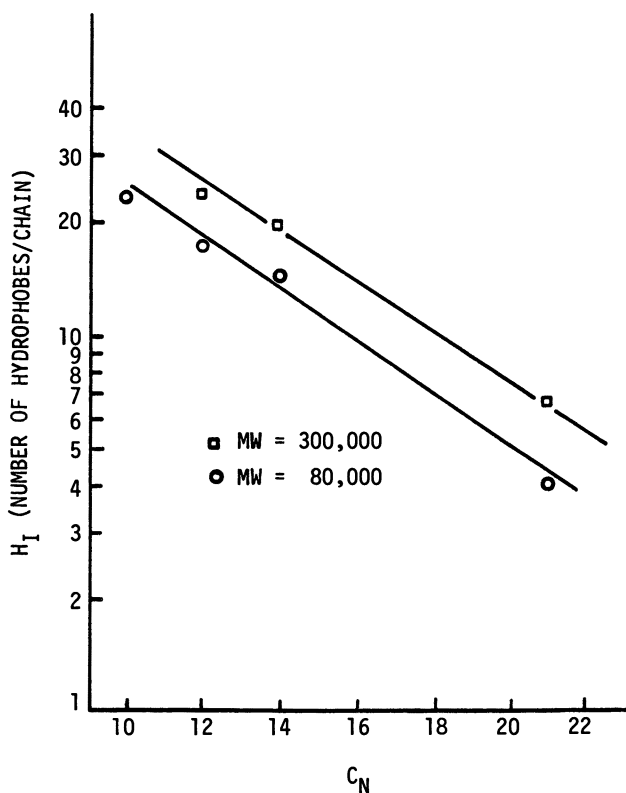
Figure 5. log H_I vs. C_N for HMHEC.

In Figure 5, the number of hydrophobes necessary to render the HMHEC insoluble is between 1 and 40 depending on the carbon chain length (C_{25} to C_{10}). This number is in sharp contrast with an earlier report (7) that hydrophobically modified polyelectrolytes with 100 or more C_{12} hydrophobes are water-soluble. These polyelectrolytes were made by the reaction of *n*-dodecyl bromide with poly(4-vinylpyridines) with varying amounts of *n*-bromododecane and bromoethane. Because of their enhanced hydrophilicity, polyelectrolyte backbones can effectively drag more hydrophobes into solution. Strauss and Gershfeld (8) have reported the intrinsic behavior of these systems. Figure 6 shows Strauss and Gershfeld's results for polysoaps, which are polymers to whose chain structure soap molecules are chemically attached. Their data suggest a contraction of the flexible polymer coil (Figure 6) in solution. As a result, these polyelectrolytes have reduced hydrodynamic volumes and do not exhibit enhanced viscosity.
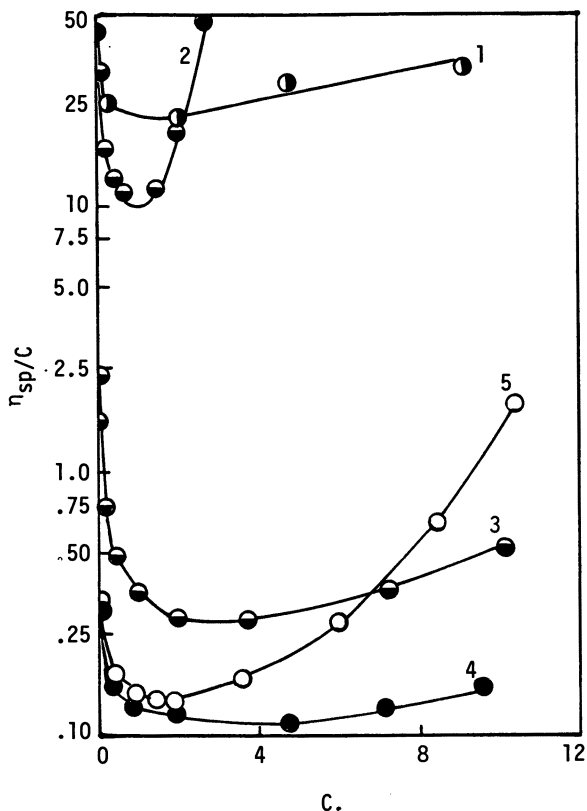
Figure 6. Effect of C_{12} content on reduced viscosity of polyelectrolytes. Key: 1, poly(vinyl-N-ethylpyridinium bromide); 2, 6.75% polysoap; 3, 13.6% polysoap; 4, 28.5% polysoap; 5, 37.9% polysoap. (Reproduced from ref. 8. Copyright 1954 American Chemical Society.)

This solution behavior might be explained in light of intramolecular hydrophobic association of molecules. The abundance of hydrophobes on the polyelectrolyte's backbone favors intramolecular hydrophobic association. The nonionic cellulose ethers containing fewer hydrophobes, on the other hand, do not have this choice and tend to undergo strong intermolecular hydrophobic association. This association results in the formation of large aggregates that are manifested by higher viscosity.

The argument just made hinges on the concept that aggregates of hydrophobes behave very much like surfactant micelles, in that they effectively form only above a certain critical concentration, H_o, which can be estimated by measuring several other solution properties, such as intrinsic viscosity and interfacial surface tension. The results of these measurements are shown in Figures 7 and 8. If these phenomena are used to find H_o as a function of hydrophobe chain length (C_N is the number of carbons in the hydrophobe), the result is the logarithmic relationship shown in Figure 9.

The observed linear relationship

$$\log H_o = -0.078C_N - 0.53 \tag{1}$$

is quite similar to that normally found for the critical micelle concentration (CMC) of nonionic surfactants (9)

$$\log (\text{CMC}) = -kC_N + X \tag{2}$$
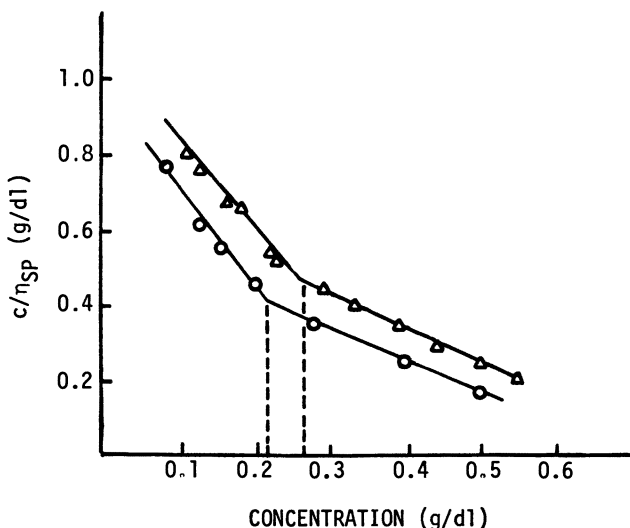
Figure 7. Plot of inverse intrinsic viscosity (c/η_{sp}) vs. c for two C_{20}–C_{24} HMHECs (MW 80,000) that contain 0.7 (○) and 0.65 (△) wt % hydrophobe. (Reproduced with permission from ref. 3. Copyright 1982 Wiley.)
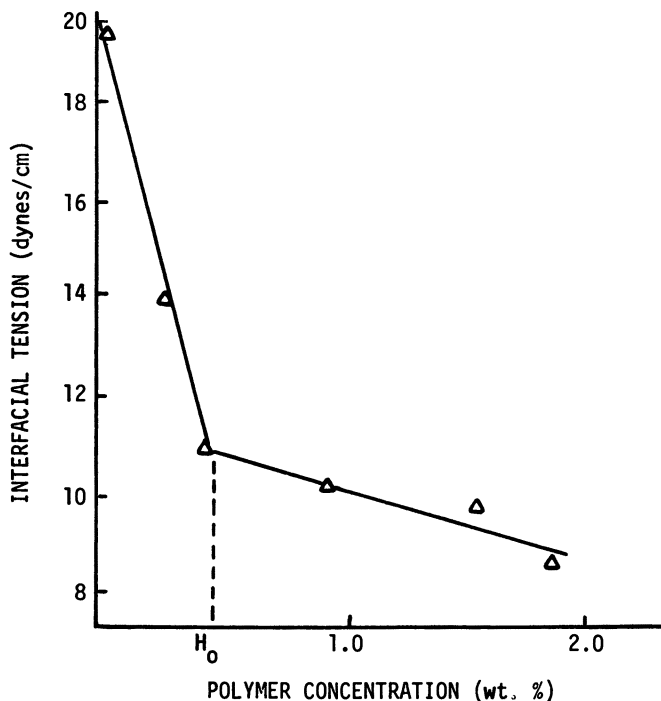
Figure 8. Water–toluene interfacial tension vs. C_{14}HMHEC concentration.
(Reproduced with permission from ref. 3. Copyright 1982 Wiley.)

In fact, the value of H_o (ca. 10^{-3} g/dL) is exactly that found for a wide range of nonionic surfactants (9). Thus, the same thermodynamic forces that cause micellization of surfactants or phase separation of hydrophobic solvents appear to govern the solution properties of HMHECs (9).

Dilute Solution Properties of HMHEC

Figure 10 shows a plot of intrinsic viscosity versus hydrophobe level for two HMHEC samples that have different hydrophobes. As the hydrophobe content at fixed molecular weight increases, the intrinsic viscosity decreases. This behavior is even more striking for C_{16}HMHEC. In dilute solutions, the HMHEC molecules are separate and untangled, and no intermolecular association occurs. However, to minimize the disruption of water structure, hydrophobes on the same chain tend to cluster. This clustering results in a much reduced hydrodynamic volume, and a lower viscosity is observed. Therefore, the dilute solution properties of HMHEC are consistent with intramolecular hydrophobic association (10). Because of intramolecular association and incomplete solubility, the intrinsic viscosity of HMHEC cannot be appropriately correlated with its molecular weight. Hence, to obtain meaningful intrinsic viscosity data, intramolecular association must be com-
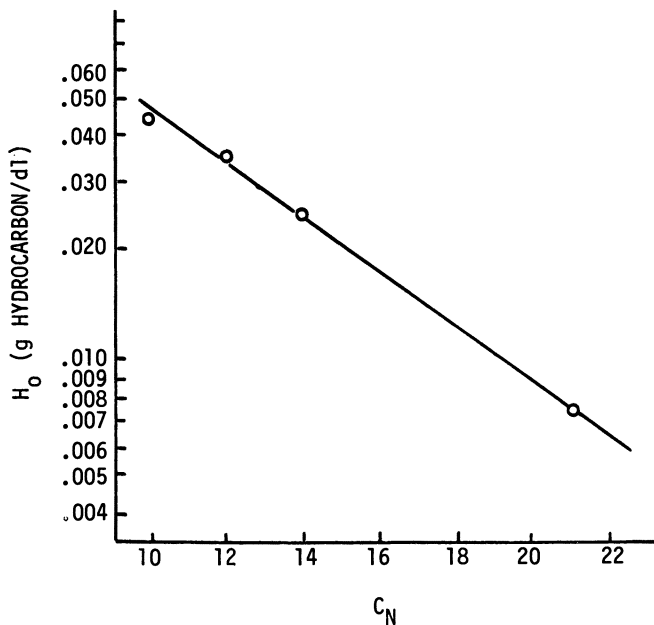
Figure 9. log H_o vs. alkyl modifier length (C_N) for various HMHECs. (Reproduced with permission from ref. 3. Copyright 1982 Wiley.)
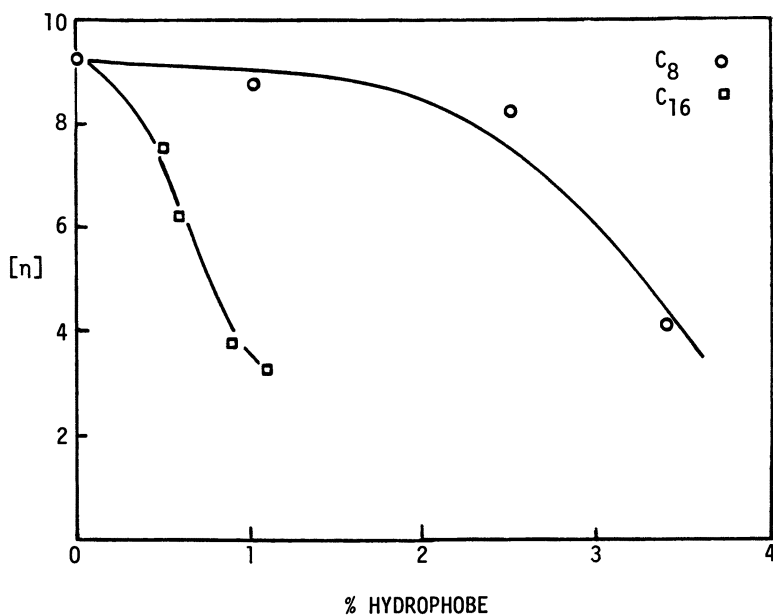
Figure 10. Aqueous intrinsic viscosity of C_8HMHEC (○) and C_{16}HMHEC (□) vs. their hydrophobe contents. (Reproduced with permission from ref. 10. Copyright 1987 TAPPI Press.)

pletely disrupted. Gelman and Barth (*11*) found that this disruption can be done by a number of solvents that contain methanol or surfactants, and they reported the Mark–Houwink constants for HMHEC in 0.1% sodium oleate solution.

Rheological Properties of HMHEC Solutions

Solutions of HMHEC with specific ranges of hydrophobic modification exhibit non-Newtonian behavior at low shear rates. This behavior is interesting in that solutions of HEC under similar conditions are Newtonian. Because the enhanced viscosity arises from the intermolecular association of polymers, the application of shear results in a disruption of the aggregates, and viscosity drops quickly. Figure 11 compares the viscosity profiles of HMHEC and HEC of equivalent molecular weight under different shear rates.

Because of their tendency to aggregate, HMHEC solutions exhibit increased elasticity or higher normal forces (Figure 12). A high molecular weight HEC is included for comparison. As can be seen from Figure 12, an HMHEC with molecular weight equivalent to that of HEC exhibits higher normal forces at 0.8% than the low-viscosity HEC does at 4.4% concentration. However, under shearing conditions, the association is completely disrupted and elasticity is destroyed.

This unique behavior of an HMHEC can be exploited in applied-flow systems, such as latex paints. High molecular weight HECs tend to retain their elasticity even at high shear because of the entropic recoiling forces
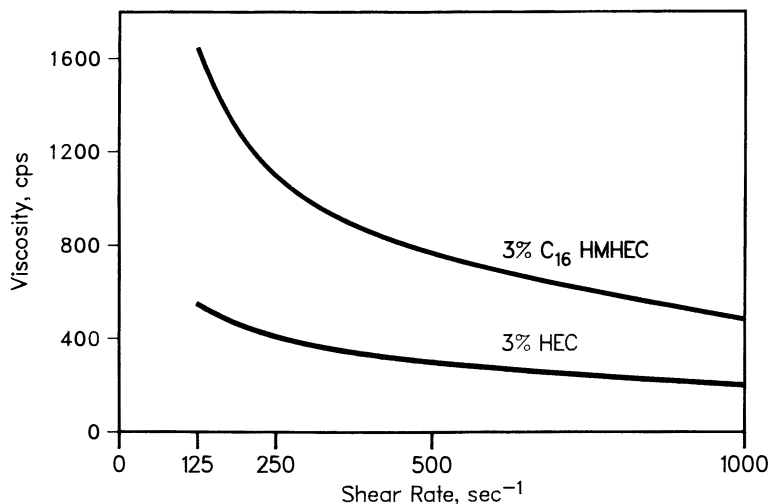
Figure 11. Apparent viscosity vs. shear rate for HEC and C$_{16}$HMHEC of equivalent molecular weight.
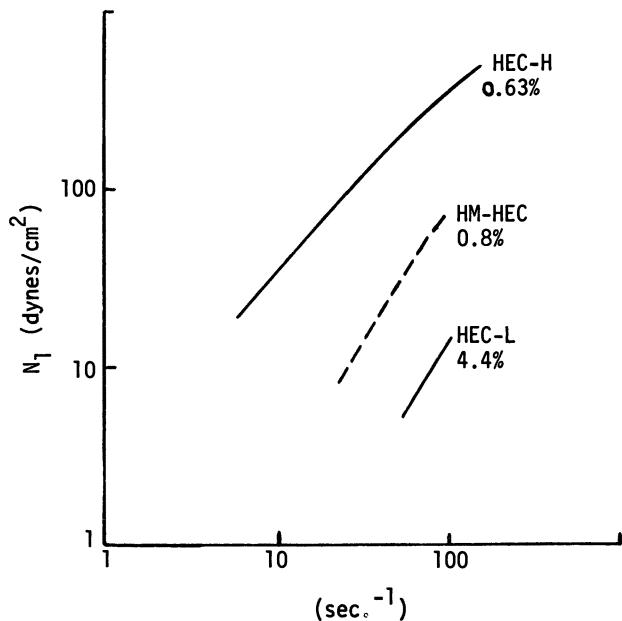
Figure 12. First normal force difference vs. shear rate for an HMHEC and
an HEC of equivalent molecular weight and an HEC of high molecular weight
(HEC-H). The percentages indicate the respective polymer concentration.

that result in paint spattering (12). By contrast, latex paints thickened with
low molecular weight HMHEC exhibit excellent spatter resistance (5).

Interaction of HMHEC with Surfactants

HMHECs can be viewed as polymeric surfactants. They tend to interact
with low molecular weight surfactants and thus modify solution viscosity.
The viscosity changes, however, depend on the nature (nonionic or ionic)
and concentration of the surfactant. The molecular behavior of HMHEC in
the presence of various types of surfactants has been described by Gelman
(10) and Steiner (13).

Nonionic Surfactants. Gelman (10) studied the effect of a nonionic
surfactant (Triton X-100, an ethoxylated octylphenol surfactant containing
67.5 wt % ethylene oxide) on the viscosity of two C_{16}HMHECs. The results
are shown in Figure 13. The Brookfield viscosity of these polymers along
with that of the unmodified HEC is included for comparison. In the presence
of 0.5% surfactant, there was a dramatic drop in viscosity. In fact, at this
surfactant level, the HMHEC viscosity profile was very similar to that of
the control HEC. The following explanation has been offered to account for
these findings.

Because of their chemical similarity, the polymer-bound hydrophobes have a tendency to interact with the hydrophobic part of the surfactant molecule. If the surfactant concentration in the system is high enough, micelles are formed. If there are enough micelles in the system, then all the hydrophobes will get bound to micelles (Figure 14). As a result, there will be no intermolecular hydrophobic association (Figure 2) and no viscosity
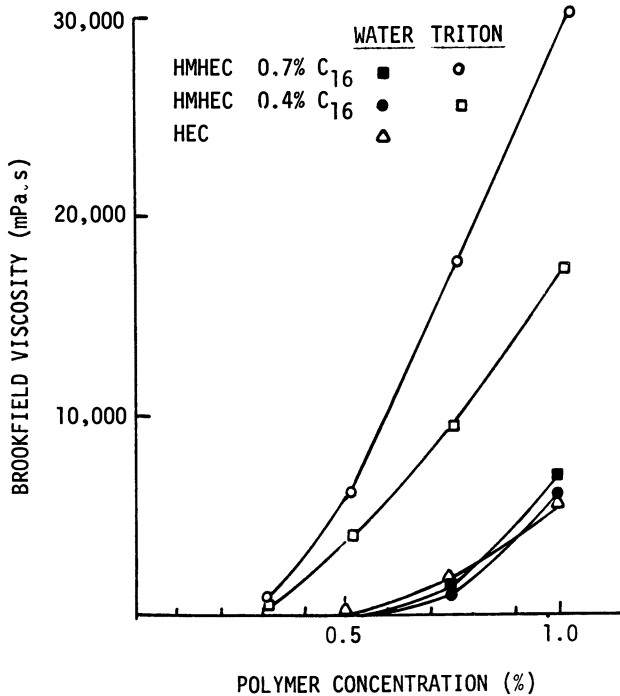
Figure 13. Brookfield viscosity as a function of HMHEC concentration with and without a surfactant. (Reproduced with permission from ref. 10. Copyright 1987 TAPPI Press.)

Figure 14. Schematic of the interactions between HMHEC surfactant molecules above the critical micelle concentration. (Reproduced with permission from ref. 10. Copyright 1987 TAPPI Press.)
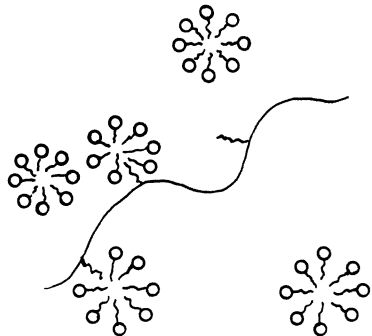
enhancement. In fact, this was the situation in the experiments in which the concentration of surfactant used was such that there were more micelles than the number of hydrophobes.

Ionic Surfactants.   The change in HMHEC viscosity with the change in surfactant concentration is interesting (*10*). The chemical nature of the surfactant is an important factor in dictating its effect on the association of the polymer. Figure 15 shows the effect of sodium oleate concentration on the viscosity of two HMHEC samples. At very low surfactant concentrations (0.01–0.1 wt %), the viscosity first increases, reaches a maximum, and then drops sharply to the original value. The magnitude of the peak viscosity varies with the sample's hydrophobe content. However, the peak viscosity occurs at a particular sodium oleate concentration, regardless of the sample's hydrophobe content. For C_{16}HMHEC samples, the peak viscosity occurred at a surfactant concentration of about 0.05% (w/v).

These results imply that the dramatic changes observed in viscosity were not due to specific interactions between polymer and surfactant, but were related to the concentration at which micelles form. We suggest that at a surfactant concentration just below the critical micelle concentration, poly-
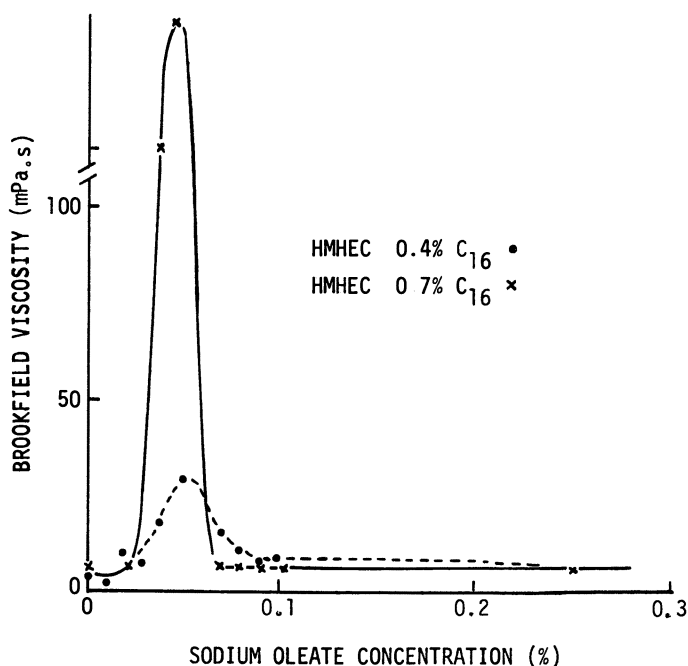
Figure 15. Brookfield viscosities of HMHECs as a function of sodium oleate concentration. (Reproduced with permission from ref. 10. Copyright 1987 TAPPI Press.)

mer-bound hydrophobes are present in sufficient quantity to permit micelle formation. If more than one hydrophobe from different polymer chains is incorporated into these micelles, the polymer chains are effectively cross-linked (Figure 16) and occasion a large viscosity enhancement. As the surfactant concentration is increased, the number of micelles per polymer-bound hydrophobe increases, and the micelles can no longer act as cross-linkers. Consequently, the viscosity decreases.

As mentioned earlier, the magnitude of the peak viscosity increases with the increase in the polymer concentration in the presence of oleate (Figure 17). At low polymer concentrations (<0.06% (w/v)), no viscosity change is noted over wide range of surfactant concentrations. If the viscosity increase is associated with polymer bridging of micelles, there is likely too little polymer to effectively build a "micellar network". A small increase in viscosity is discernible at polymer concentrations from 0.08 to 0.095% (w/v). The peak viscosity occurs at an oleate concentration of 0.04% (w/v), the critical

(Fewer Micelles)

(Excess of Micelles)
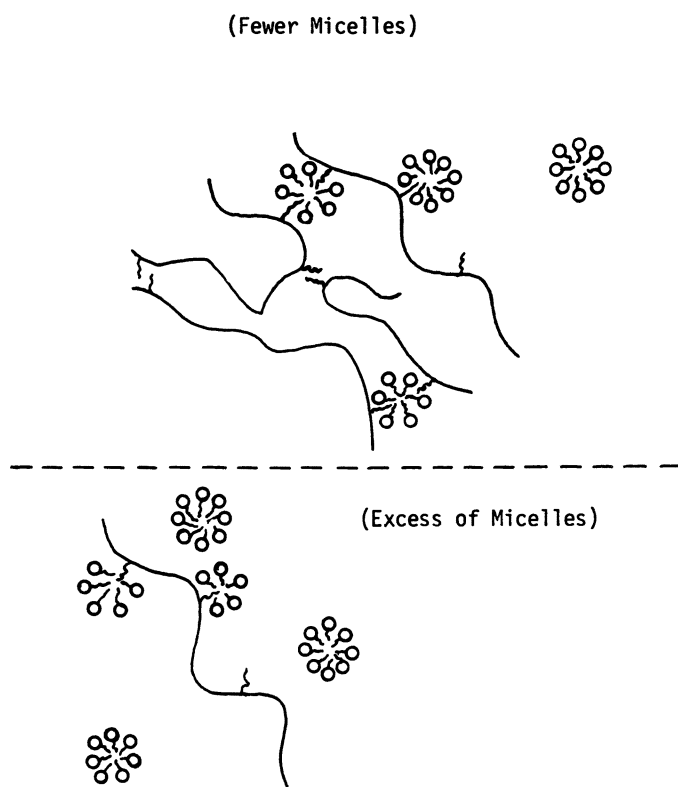
Figure 16. Schematic of the molecular interactions between HMHEC and surfactant molecules below the critical micelle concentration. (Reproduced with permission from ref. 10. Copyright 1987 TAPPI Press.)
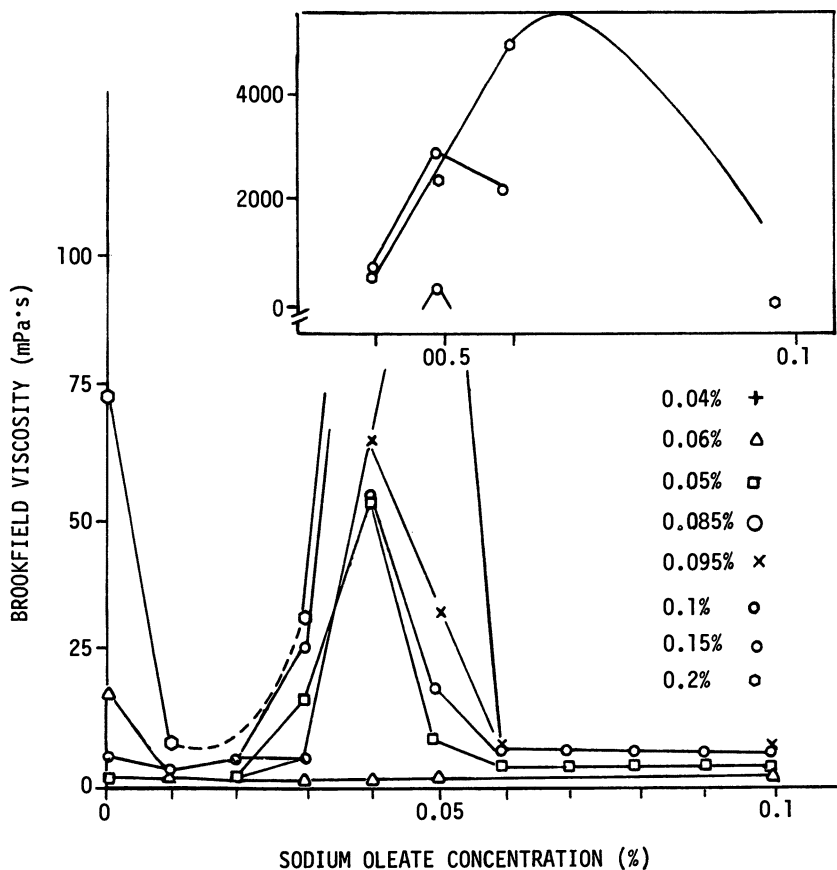
Figure 17. Effect of HMHEC concentration on the peak viscosity as a function of sodium oleate concentration. (Reproduced with permission from ref. 10. Copyright 1987 TAPPI Press.)

micelle concentration of sodium oleate. When the polymer concentration increases, then a slight shift in the maximum to higher sodium oleate levels is observed. The shift in the surfactant concentration at which the maximum occurs is probably related to polymer–micelle interactions. As the polymer becomes associated with the surfactant, there is likely to be some spreading of ionic groups that would reduce charge repulsions and alter micellar size, aggregation number, and critical micelle concentration.

Amphoteric Surfactants. Steiner (*13*) reported the nature of the interactions between a water-insoluble HMHEC and a commercial amphoteric surfactant (Miranol HS, a sulfonated amphoteric imidazoline derivative) at various pH levels. She found that the HMHEC was solubilized in the presence of a large excess (between 10 and 20%) of the surfactant. (More

highly substituted HMHECs, which are water-insoluble, are also solubilized by surfactants (*14*), presumably because of the breaking up of intermolecular associations and increased chain hydrophilicity caused by the ionic head groups of surfactants associated with the polymer chain). Steiner also noted a linear decrease in viscosity with time after a finite hydration time, although no molecular weight loss of the polymer occurred. Interestingly, at 10% surfactant concentration, the viscosity loss was at a maximum around pH 6 (the isoelectric point of the surfactant), whereas at pH above or below 6, the viscosity loss was significantly smaller (Figure 18).

The solubilization of the HMHEC in the surfactant was attributed to the interactions between surfactant micelles and polymer-bound hydrophobes. The effect of pH on polymer–surfactant solution viscosity was explained in terms of charge effects at the surface of the surfactant micelles. Steiner (*13*) proposed that at pH levels above or below the isoelectric point, the surfactant has a net charge on the head groups that causes repulsion within a single micelle. This repulsion leads to a relatively open micelle–aqueous phase interface through which polymer-bound hydrophobes can enter and experience stable polymer–surfactant interactions. These interactions anchor the polymer chains in an extended configuration.

At the isoelectric point, the micelles are neutral and bear both positively and negatively charged species on the head groups. As a result, the head groups experience Coulombic attraction that leads to the formation of a
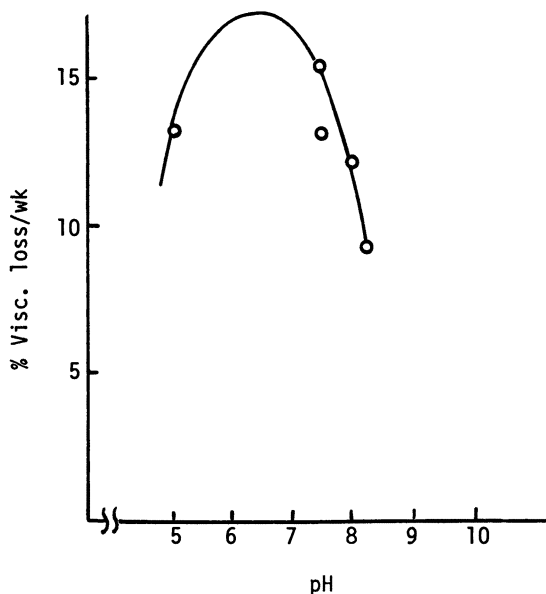
Figure 18. Effect of pH on HMHEC viscosity stability in 10% Miranol HS surfactant.

densely packed micelle–aqueous phase. This phase hinders the entry of polymer-bound hydrophobes such that the unsolubilized hydrophobes tend to interact in the aqueous phase. Initially, these aqueous-phase hydrophobic interactions lead to the formation of clusters that involve hydrophobes from several polymer molecules. This clustering results in an entangled polymer network and a high viscosity. However, on standing and at elevated temperatures, these intermolecular hydrophobic interactions are disrupted, presumably because of thermal motion of the polymer chains, and the viscosity decreases. This mechanism is supported by dynamic rheological analysis of the polymer–surfactant system.

An alternative mechanism might involve changes in micellar aggregation size and number at the isoelectric point caused by the adsorption of polymer at the micellar surface. With time, polymer micellar bridges could diminish as a result of stronger adsorption of polymers on the neutral (isoelectric point) surface and lead to lowering of the viscosity. Considerably more work is needed to understand these time–pH-dependent viscosity changes in amphoteric systems.

The effect of different counterions on the viscosity stability of HMHEC–surfactant at pH 7 was also studied at 10% and 20% surfactant concentrations (Tables I and II). The most stable solutions were formed in the presence of fumaric and mellitic (benzenehexacarboxylic) acid. By contrast, citric and maleic acid occasioned relatively higher viscosity loss. These results indicate that the viscosity stability of a polymer–surfactant solution is dependent on the counterion configuration. It appears that flexible and difunctional anions, such as citrate, and *cis*-difunctional anions such as maleate ions can potentially bridge two surfactant head groups on a single

Table I. Effect of Counterions on Heat Stability of 1% C_{16}HMHEC in 10% Miranol HS at pH 7

Acid	Initial Viscosity (cPs)	Slope (cPs/week)	Viscosity Stability (% loss/week)
Maleic	1050	−170	16
Citric ($N = 2$)	990 ± 8%	−160 ± 4%	16 ± 0.6
Fumaric	810	−110	14
Mellitic ($N = 2$)	1280 ± 5%	−150 ± 1%	12 ± 0.5

Table II. Effect of Counterions on Heat Stability of 1% C_{16}HMHEC in 20% Miranol HS at pH 7

Acid	Initial Viscosity (cPs)	Slope (cPs/week)	Viscosity Stability (% loss/week)
Citric ($N = 2$)	990 ± 4%	−80 ± 33%	8 ± 2
HCl–Na citrate	1100	−110	10
Mellitic	990	−60	6
Fumaric	1060	−20	2

micelle and cause reduction of the total micelle surface area. Because of this association, polymer hydrophobes cannot penetrate and experience stabilizing interactions. Hence, hydrophobes are forced to remain in the aqueous phase.

On the other hand, the *trans* configuration of fumarate ions and rigidity of benzenetetracarboxylate ions do not allow them to interact simultaneously with two surfactant head groups on a single micelle. In the presence of these ions, polymer-bound hydrophobes penetrate more readily into the micelles. In addition, these counterions can potentially bridge two or more micelles, and further stabilize the solution.

Applications of HMWSPs

HMHEC polymers are improved rheological modifiers for latex paints. They retain the benefits of traditional cellulosic ethers (compatibility with a wide range of coatings ingredients, storage stability, better sag resistance, etc.) but overcome many deficiencies of synthetic associative thickeners (sensitivity to latex systems and pH of paint formulations, poor sag resistance, etc.). The combined advantages offered by HMHEC are best suited for interior and exterior flat paints (5).

Hydrophobically modified nonionic cellulose ethers or poly(ethylene oxide) (HMPEO) act as unique stabilizers in suspension polymerization of vinyl and acrylic monomers (15). The use of HMHEC as a stabilizer in emulsion polymerization of vinyl and allylic monomers has also recently been reported (16).

HMHECs greatly reduce liquid–liquid interfacial tensions even at very low polymer concentrations and are reported to be extremely effective emulsifiers for organic liquids in water (17). The HMHEC monolayer at such an interface was found to strongly retard the rate of transport of small molecules across the interface (18). As described earlier, water-insoluble HMHECs containing a high hydrophobe level can be dissolved with a large excess of surfactants (13, 14). The use of HMHECs as effective emulsifiers in cosmetic lotions and as thickeners in systems containing high concentrations of surfactants, such as shampoos (14), is suggested. HMHECs may also be used as thickeners in enhanced oil recovery (19) and as rheology-control additives in cementing operations during oil-well drilling.

HMPEOs are soluble in concentrated mineral acids and exhibit superior resistance to thermal degradation in solution (4). Because these copolymers are of low molecular weight, they are less shear-sensitive than high molecular weight commercial poly(ethylene oxide), which can lose 90–95% of its solution viscosity when subjected to high shears at room temperature for 5 min. By contrast, HMPEOs lose no more than 30% of their viscosity in water or acid solution. These unique properties of HMPEOs make them ideal candidates for applications in petroleum recovery via acid fracturing.

Conclusions

Incorporation of long-chain hydrocarbon hydrophobes into a cellulose ether backbone leads to an interesting new class of polymeric surfactants. Their enhanced solution viscosity can be explained in terms of intermolecular associations via the hydrophobe moieties. Entropic forces cause the polymer hydrophobes to cluster to minimize the disruption of water structure. The same thermodynamic principles that are used to explain the micellization of surfactants can be applied to explain the solution behavior of HMHEC. HMHECs interact with surfactants that modify their solution viscosities. The chemical nature and the concentration of the surfactant dictate its effect on HMHEC solution behavior. The unique rheological ·properties of HMHEC can be exploited to meet industrial demands for specific formulations and applications.

Acknowledgments

References

1. *Symposium Proceedings: The Influence of Associative Thickeners and Rheology on Coatings Performance*; Des Plaines, IL, 1982; available from Glass, J. E., organizer; North Dakota State University, Fargo, ND, 1983.
2. Landoll, L. M. U.S. Patent 4 228 277, 1980.
3. Landoll, L. M. *J. Polym. Sci., Polym. Chem. Ed.* 1982, 20, 443–455.
4. Landoll, L. M. U.S. Patent 4 304 092, 1981.
5. Shaw, K. G.; Leipold, D. P. *J. Coatings Technol.* 1985, 57(727), 63–72.
6. Peuscher, M.; Engelskirchen, K.; Gruenberger, E.; Ger. Offen. DE 3,620,991, 1988; *Chem. Abstr.* 1988, 108, 223327m.
7. Strauss, U. P.; Assony, S. J.; Jackson, E. G.; Layton, L. H. *J. Polym. Sci.* 1952, 9, 509–518.
8. Strauss, U. P.; Gershfeld, N. L. *J. Phys. Chem.* 1954, 58, 747–753.
9. Carless, J. E.; Challis, R. A.; Mulley, B. A. *J. Colloid Sci.* 1964, 19, 201–212.
10. Gelman, R. A. International Dissolving Pulp Conference, TAPPI, February 1987, pp 159–165.
11. Gelman, R. A.; Barth, H. G. In *Water-Soluble Polymers*; Glass, J. E., Ed.; Advances in Chemistry Series 213; American Chemical Society: Washington, DC, 1986; pp 101–110.

12. Glass, J. E. *J. Coatings Technol.* **1978**, *50*(640), 61–68.
13. Steiner, C. A. *Polym. Prepr. (Am. Chem. Soc., Div. Polym. Chem.)* **1985**, *26*(1), 224–225.
14. Landoll, L. M. U.S. Patent 4 243 802, 1981.
15. Landoll, L. M. U.S. Patent 4 352 916, 1982.
16. Craig, D. H. U.S. Patent 4 684 704, 1987.
17. Liang, S.-J.; Fitch, R. M. In *Polymer Adsorption and Dispersion Stability*; Goddard, E. D.; Vincent, B., Eds.; ACS Symposium Series 240; American Chemical Society: Washington, DC, 1984; pp 185–202.
18. Liang, S.-J.; Fitch, R. M. *J. Colloid Interface Sci.* **1982**, *90*, 51.
19. Landoll, L. M. U.S. Patent 4 529 523, 1985.

19

The Rheological Properties of a Hydrophobically Modified Cellulose

J. W. Goodwin[1], R. W. Hughes[1], C. K. Lam[1], J. A. Miles[2], and B. C. H. Warren[2]

[1]Department of Physical Chemistry, University of Bristol, Cantock's Close, Bristol BS8 1TS, England
[2]Chemical Defence Establishment, Porton Down, Wiltshire, England

Dilute solution behavior of a water-soluble cellulose derivative that had been modified by grafting approximately three hexadecyl hydrocarbon chains per cellulose molecule onto the backbone was studied by capillary viscometry and refractometry. Both techniques indicated that aggregation occurred at concentrations over 0.075 g dL^{-1}. At concentrations over 0.1 g dL^{-1}, phase separation was observed. The number-average weight of the hydrophobically modified cellulose was 1×10^5 daltons. The viscoelastic properties were investigated at concentrations up to 2 g dL^{-1}. Shear stress–shear rate measurements were performed, and power-law behavior was observed. Forced-oscillation measurements were carried out over a frequency range of 0.001–20 Hz, and shear-wave rigidity measurements were carried out at 200 Hz to give the wave-rigidity modulus.

THE USE OF HYDROPHOBIC INTERACTIONS to produce associative thickeners has increased markedly over the past 10 years in such diverse areas as surface coatings and enhanced oil recovery. The desired thickening properties are produced by relatively low molecular weight polymers that are reversibly cross-linked by pendant hydrophobic moieties to give a three-dimensional network. To maintain solubility, the number of hydrophobes per soluble molecule is low, and the chain length is typical of that used in surfactants (i.e., C_8–C_{16}). In solution, the hydrophobes appear to associate in an analogous fashion to micellization, in that, in the absence of surfactants,

a critical concentration appears to be required. Added surfactants can aid the association at low concentrations by contributing to the molecular aggregates, whereas at concentrations in excess of their critical micelle concentration, surfactants may prevent association by forming micelles around the pendant groups.

This chapter is concerned with just one of this class of thickeners, namely a hydrophobically modified (hydroxyethyl)cellulose (HMHEC), Hercules WSP D-47. Gelman and Barth (1) reported on the viscosity of such HMHECs. This sample contained up to four hexadecyl chains grafted to the cellulose backbone. The preparative route was that described by Landoll (2). The dilute solution properties were characterized by capillary viscometry, whereas the more concentrated solutions were characterized by continuous-shear viscometry, forced oscillation measurements, and shear-wave propagation. In addition, the adsorption onto polymer latex particles was investigated.

Experimental Details

Materials. The HMHEC was used as supplied. All the water was double-distilled. The NaCl was BDH (British Drug Houses) Analar grade. The polymer was dissolved in water containing 5×10^{-3} mol L^{-1} NaCl; the solutions were stored at 4 °C for at least 48 h before use to ensure dissolution.

The polystyrene latex was prepared by the emulsion polymerization of styrene (3) by using Alcopol OS (Allied Colloids plc) as the emulsifier and potassium persulfate as the initiator. After preparation, the latex was extensively dialyzed against distilled water to remove emulsifiers. The particle size was determined from electron microscopy and the latex was found to be monodisperse with a number-average diameter of 140 mm and a coefficient of variation of less than 2%.

Capillary Viscometry. The viscosity of dilute solutions of the polymer was determined with a Canon–Fenske capillary viscometer set in a thermostat bath at 25 ± 0.05 °C. A stock solution of 0.15 g dL^{-1} was prepared in distilled water, stored at 4 °C for 2 days, and then filtered through a No. 1 sinter glass funnel to remove fibers and detritus from the preparation of the cellulose ether. Nine other solutions were prepared from this stock by dilution with filtered distilled water. All these solutions were then stored at 4 °C for a further 24 h to ensure that all the solutions had the same temperature history, as this factor has been shown to be important in producing reproducible solutions of cellulose ethers (4, 5). The concentration range prepared was 0.015–0.15 g dL^{-1}, and the flow times ranged from 294 to 1609 s.

Adsorption Isotherm. A stock latex suspension was prepared at a volume fraction, ϕ, of 0.005 in 5×10^{-4} mol L^{-1} NaCl solution. Four grams of this latex was used in each case. Increasing quantities of a 1% HMHEC stock solution in NaCl were added, and the systems were made up to 11 g with NaCl solution. The suspensions were mixed by slowly turning them end-over-end for 4 days at 25 °C to allow adsorption equilibrium to be attained. Centrifugation at 15,000 rpm was used

to separate the particles from the continuous phase, which was then analyzed for polymer in solution. The assay was carried out by using a Hilger–Watts interferometer, and by comparing the refractive indexes of the supernatant solutions with a calibration graph covering the range 0–0.25% polymer.

Shear Wave Propagation.   A pulse shearometer (Rank Bros.) was used to measure the propagation velocity of a shear wave through the weak gels formed by the solutions of HMHEC in dilute NaCl. The polymer concentration range studied was 0.5–2.0%. With this apparatus, the frequency of the shear wave is approximately 1200 rad s^{-1}, and the strain is $<10^{-4}$. At this strain, most systems behave in a linear viscoelastic fashion, and the wave-rigidity modulus, $\tilde{G}$ is

$$\tilde{G} = \rho_s v^2 \tag{1}$$

where v is the measured wave velocity and ρ_s is the density of the solution. When the wave attenuation is small (i.e, when the storage modulus is much greater than the loss modulus),

$$\tilde{G} \approx G(\infty) \tag{2}$$

$G(\infty)$ is the high-frequency limit of the storage modulus and is a useful probe of the structure in the gel (6).

Rotational Rheometry.   Two instruments were used for these measurements. An Instron model 3250 rheometer was used for measuring rotational viscometry and forced oscillation as a function of frequency with strains in the region of 0.5. A Bohlin VOR rheometer was used for dynamic measurements at smaller strains (i.e., ≈0.1).

The Bohlin VOR was also used for stress relaxation experiments. Experiments were carried out over a frequency range from 0.01 to 60 rad s^{-1}. Strain sweeps were carried out on both instruments at 6 rad s^{-1}, and the viscoelastic response was linear over a range of strain of 0.25–0.65 on the Instron instrument, whereas the Bohlin VOR also showed a linear response over the range used (i.e., 0.05–0.20).

Results and Discussion

Capillary Viscometry.   The viscosity data are plotted in Figure 1 as the reduced viscosity (η_{red}) as a function of concentration. The curve shows two linear plots that intersect at a polymer concentration, c, of 0.075 g dL^{-1}. If the Huggins equation (5)

$$\eta_{red} = [\eta] + k'[\eta]^2 c \tag{3}$$

is applied to the lowest concentration data, an intrinsic viscosity, $[\eta]$, of 4.7

dL g^{-1} is obtained with a Huggins coefficient, k', of 2.25. These values are close to those obtained by Gelman and Barth (1) for a similar HMHEC, with 0.9% by weight of hexadecyl chains, dissolved in water.

If the Mark–Houwink equation (5) is used with $[\eta] = 4.7$ dL g^{-1}, constant $K_1 = 4.7 \times 10^{-4}$, and power law index $a = 0.8$ (4) in

$$[\eta] = K_1 M_n{}^a \tag{4}$$

where M_n is the number-average mol wt, then $M_n = 1 \times 10^5$, which is similar to the values quoted by Gelman and Barth (1) for the molecular weight of their HMHEC. However, those authors also pointed out that the high value of the Huggins coefficient indicated that molecular aggregation occurred in water. We agree with this interpretation but wish to make an additional distinction. At low concentrations (i.e., at $c < 0.075$ g dL^{-1}), a limited aggregation of the polymer molecules leads to effectively higher molecular weight units. At $c > 0.075$ g dL^{-1}, a much more extensive aggregation leads to a three-dimensional network or gelation of the polymer solution. This behavior is analogous to the micellization of short-chain surfactants and can be referred to as the *critical aggregation concentration*
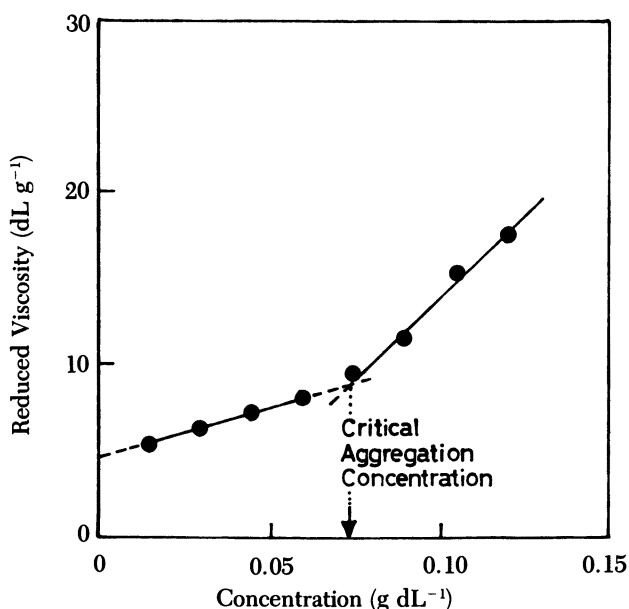
Figure 1. Reduced viscosity as a function of concentration for HMHEC polymer D-47.

(CAC) for the associative thickener. Although it is tempting to call this the "critical gelation concentration", this name would be misleading as systems a little above this concentration were observed to phase-separate into a lower gel phase and an upper lower viscosity phase if left to stand for a time in excess of 2 weeks. The increased slope of the η_{red} vs. c plot for $c > 0.075$ g dL^{-1} is a clear indication of very extensive aggregation.

Adsorption Studies.   The calibration curve for the Hilger and Watts interferometer is shown in Figure 2. Again, two straight-line portions were observed. In this case, the break occurred at the slightly higher concentration of 0.10 g dL^{-1}.

Figure 3 shows the adsorption isotherm for the HMHEC D-47 onto a cleaned polystyrene latex with a particle diameter of 140 nm. The curve shows a relatively slow approach to a plateau. At concentrations in excess of 0.08 g dL^{-1}, a step occurs in the isotherm. The area occupied per molecule on the plateau before the step was 26.1 nm^2 mol^{-1}, whereas after the step, the area was reduced to 17.1 nm^2 mol^{-1}, although a true plateau was not reached even at equilibrium concentrations as high as 0.18 g dL^{-1}. The data in Figures 2 and 3 confirm the polymer aggregation process at $c > 0.075$ g
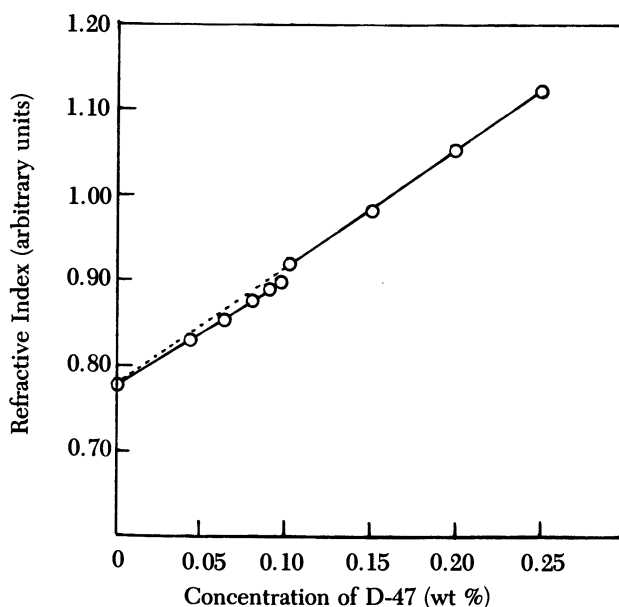
Figure 2. *Interferometer calibration curve with refractive index in arbitrary units.*
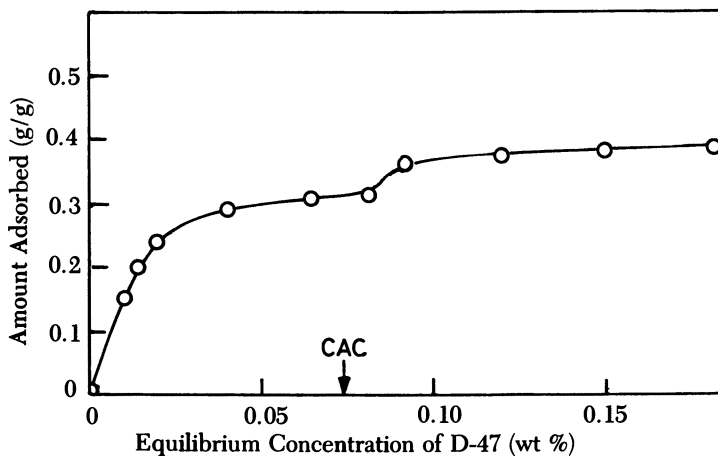
Figure 3. Adsorption isotherm for HMHEC on cleaned polystyrene latex of particle diameter 140 nm.

dL^{-1} with steps in the plots at concentrations just above this value. The adsorption density is 4 to 5 times that found for an ethyl HEC (EHEC) of similar molecular weight (6). This much higher value of adsorption on the low-concentration side of the step indicates that some molecular aggregation may be occurring in addition to an increase in adsorption due to the pendant alkyl chains. Because the extensive aggregation occurring at $c > 0.075$ g dL^{-1} results in only a 25% increase in adsorption, the preaggregation process probably does not account for more than this. The tentative conclusion is that the pendant alkyl chains cause a marked enhancement of adsorption of the polymer by direct interaction with the surface.

Wave Propagation Experiments.   These experiments were carried out at much higher polymer concentrations, the range covered from 0.5 to 2.0 g dL^{-1}. A monotonic increase in the wave-rigidity modulus was observed throughout this range, and the experimental data are shown in Figure 4. The size of the experimental points indicates the uncertainty in each measurement. The values are similar to those observed for EHEC (6).

At these polymer concentrations, the solutions form continuous viscoelastic gels with moduli in the region 0.02–0.3 kPa. Such swollen networks can be treated as heavily swollen elastomers (6) by applying the theory of rubber elasticity (5, 7–9) to them. For a continuous network that is subjected to a small strain and at a frequency that is sufficiently high for there to be no stress relaxation, the wave rigidity modulus can be equated to the high-frequency limit of the storage modulus. The rigidity is then proportional to the cross-link density.

$$G\ (\infty)\ =\ 2ANkT \tag{5}$$
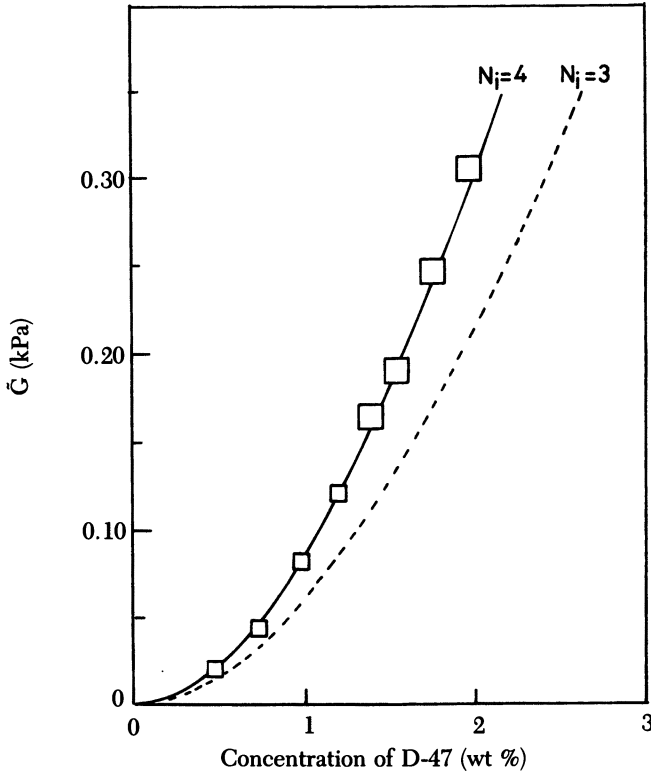
Figure 4. Wave-rigidity modulus as a function of concentration. The points are experimental data, and the solid line is calculated for $N_i = 4$ with the broken line for $N_i = 3$.

where kT is the thermal energy (the Boltzmann constant and the absolute temperature), N is the number of cross-links in unit volume of gel, and the front factor A ($\frac{1}{2} < A < 1$) increases with cross-link functionality (8, 9). The number of cross-links per cubic centimeter is directly related to the number of cross-linking sites on each chain, N_i, and the polymer concentration

$$\frac{N}{c} = \frac{(N_i - 2)N_a c}{200 M_n} = Bc \qquad (6)$$

where N_a is Avogadro's number. The cross-link density will be increased by entangling chains, and, in the concentration regime used here, the cross-link density will vary as c^2 (10). However, some neighboring sites can be lost by the formation of closed loops, and this closed-loop formation depends on the stiffness of the chain and on c (11). The resulting equation is (6)

$$G(\infty) = 2AkTBc\{(1 + Rc/BkT) - (1 + f)\} \qquad (7)$$

where A = 1 for a multifunctional network junction; the constant R = 250 (6); and f is a function of molecular weight of the skeletal bond (69 for HEC), the bond length (0.187 nm), and the characteristic ratio. $C(\infty)$ = 6.38 (12). As f is a function of polymer concentration, the range of values used was $0.79 > f > 0.486$.

The curves plotted in Figure 4 are from equation 1 with N_i = 3 and 4. The curve for four cross-linking sites per mole is in very good agreement with the chemical estimate of the number of pendant hydrophobes.

Rheological Characterization

Shear Rate Dependence.   Experiments were performed on the Instron rheometer and covered the shear-rate range 10^{-2} to 10^3 s^{-1}. Data for a 0.75-g dL^{-1} solution of polymer D-47 in 5 × 10^{-3} mol dm^{-3} NaCl are shown in Figure 5. A low-shear limiting Newtonian viscosity, $\eta(0)$, was observed. At high shear rates, the usual power-law behavior of polymers was observed with a power-law index of –0.86. This value is close to that predicted theoretically and observed for concentrated polymer solutions and undiluted polymers (13) and indicates an extensive network.

Forced-Oscillation Experiments.   The dynamic moduli were measured as a function of frequency. At high strains (ca. 0.6), the Instron rheometer was used, whereas at lower strains (typically 0.16), the Bohlin VOR rheometer was used because of its greater sensitivity. Figure 6 shows the results obtained for the storage (G') and loss (G'') moduli for a 0.5-g dL^{-1}
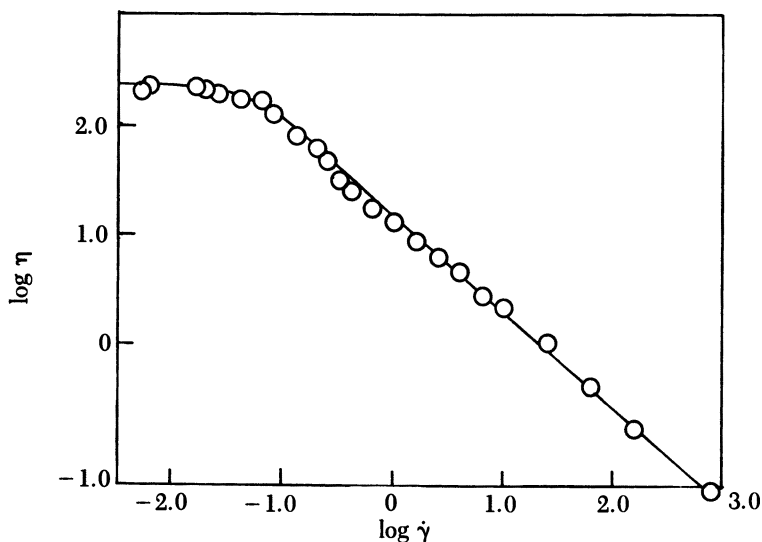
Figure 5. Viscosity as a function of shear rate for a 0.75% solution of polymer D-47 in 5 × 10^{-3} mol dm^{-3} NaCl.
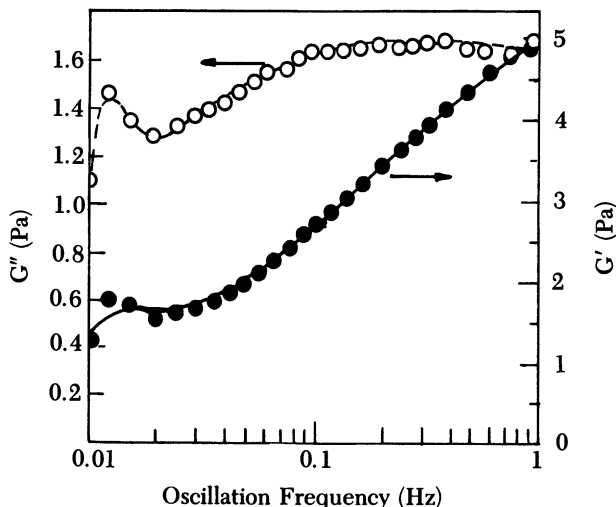
Figure 6. Dynamic moduli as a function of frequency for a 0.5% solution of D-47 in NaCl at 62.5% strain.

solution of polymer at 62.5% strain. There is a step in the G' curve and a secondary peak in the loss curve at 0.015 Hz. Initially, we thought that this behavior might indicate the presence of two distinct relaxation processes, but the width of the secondary peak is too narrow to be fitted by a process with a single relaxation time. (A process with a single relaxation time will respond to a forced oscillation over at least a decade in frequency.) This sharp peak was not observed at lower strains, as illustrated in Figure 7, where the same solution was measured at 20% strain. We concluded that the secondary peak could be an indication of the onset of nonlinear behavior at these high strains. This possibility will be investigated more fully in the future, as the systems were still linear at 1 Hz as shown in Figure 8. The curves in Figure 7 are generally similar to those in Figure 6, but the moduli are approximately 40% lower—a further indication of the strain sensitivity.

The curves in Figure 7 indicate a relatively narrow relaxation behavior for a polymer solution (as do the curves in Figure 6), with $G' = G''$ close to the maximum value of G''. At 2 Hz, G' has already reached 25% of the value of the modulus measured at 200 Hz by wave propagation. The concentration dependence of G' is shown in Figure 9, where the range 0.5–2.0% is shown. The moduli increased rapidly with concentration, but there was no tendency for G' to reach a limiting value over the frequency range available, even at the highest concentration used, although at 2%, G' had reached greater than 60% of the modulus measured at 200 Hz.

Figure 10 shows curves for G'' vs. frequency and concentration. In all cases, there is a clear inflection at 1–2 rad s^{-1} followed by an increase at higher frequencies. Instrument resonance did not produce large errors at over 10 Hz with the measuring system chosen. The temporal position of the step is not dependent on polymer concentration but only on the magnitude
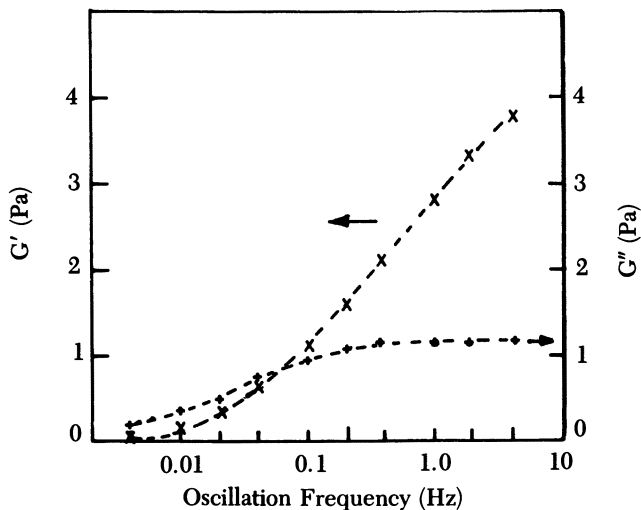
Figure 7. Dynamic moduli for a 0.5% solution of D-47 in NaCl at a strain of 20%.
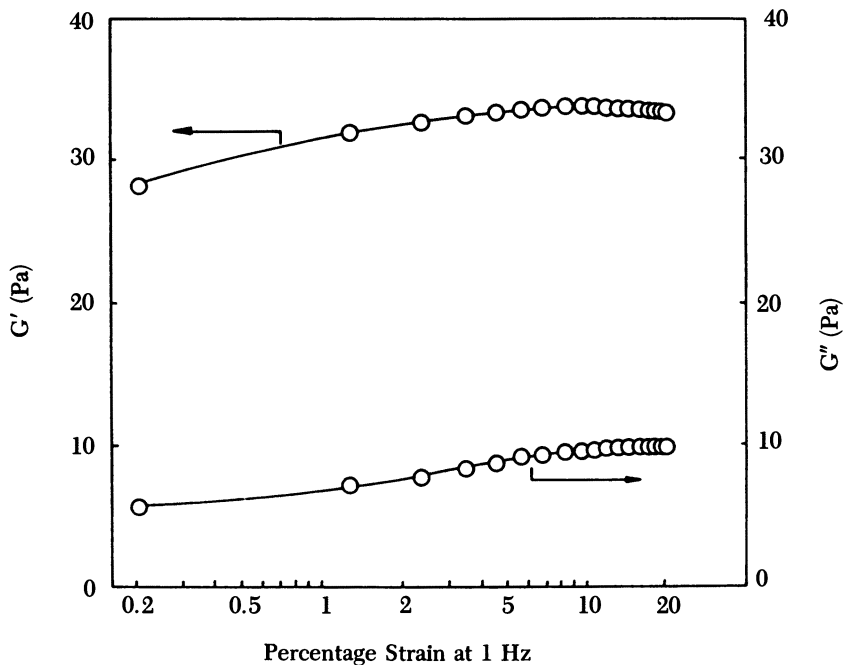
Figure 8. The strain dependence of the dynamic moduli of a 1.0% solution of D-47 in NaCl at 1 Hz.
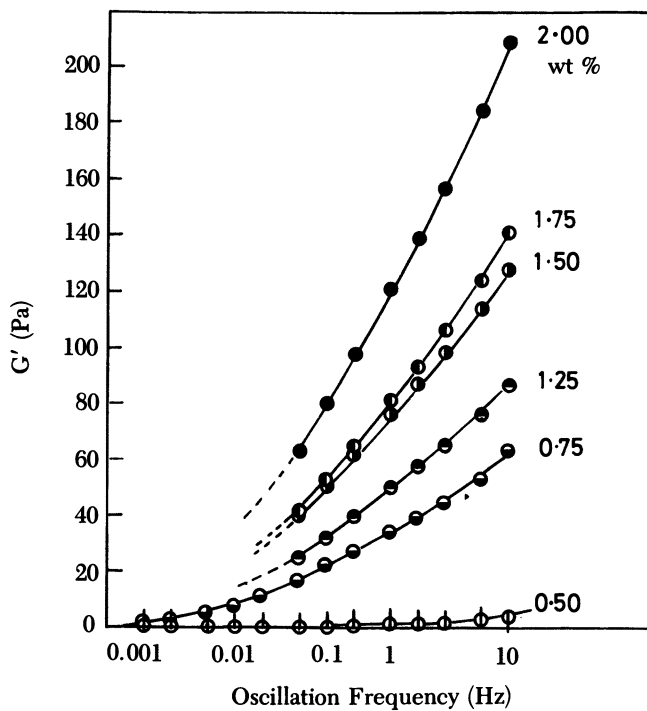
Figure 9. The concentration dependence of the storage modulus of solutions of D-47 in NaCl at 16% strain.

of the modulus. It is, therefore, tempting to associate this behavior with a relaxation process that is not very dependent on the center-of-mass diffusion of the polymer chain. The dissociation of the aggregated hydrophobes would be such a process.

Stress Relaxation.   Figure 11 shows the relaxation spectra obtained from the stress relaxation measurements carried out on the Bohlin VOR rheometer. The same concentration of polymer was studied as in the forced-oscillation experiments. A peak associated with the instrument compliance occurs at 15 ms in each case. The general trend is for the spectra to increase and broaden with increasing polymer content, as expected for a polymer gel. However, again, there is a shoulder on the spectra that moves very little with polymer content and occurs at about 1 s. This feature is in good agreement with the oscillatory measurements and confirms the presence of a narrow relaxation process that is insensitive to polymer content. As the concentration increased, progressively more stress remained stored at long times, as would be expected for a polymer gel of increasing concentration (i.e., there is either an increasing broad underlying relaxation process so that $\eta(0)$ increases strongly, or there is an increasing residual modulus, $G(0)$, so that an increasing yield stress value would be observed).
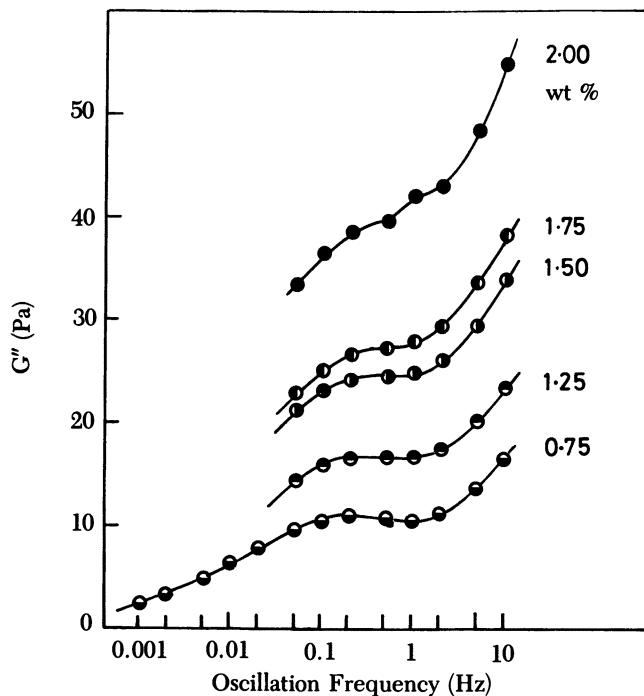
Figure 10. *The concentration dependence of the loss modulus of solutions of D-47 in NaCl at 16% strain.*

Summary

The HMHECs used in these experiments provided good examples of an associative thickener, in that clear evidence of a critical aggregation concentration was seen from the dilute-solution behavior. Although some limited molecular aggregation may occur below this concentration, once this concentration is achieved, a three-dimensional network starts to form. This network formation leads to a significant enhancement of adsorption onto polymer latex particles from which the surfactant has been removed. The adsorption density is high for a cellulosic polymer of the equivalent molecular weight.

Wave propagation experiments were performed on solutions at concentrations sufficiently high to form weak gels. The results could be fitted with the theory of elasticity of swollen elastomers by using the same density of cross-linking sites per chain as pendant hexadecyl groups grafted to the molecular backbone. This density of four per chain was much lower than the 22 per chain required to give a similar rigidity modulus for an EHEC system of similar molecular weight (6).

Forced-oscillation experiments indicated the presence of a relatively sharp relaxation process that appeared to show little dependence on polymer
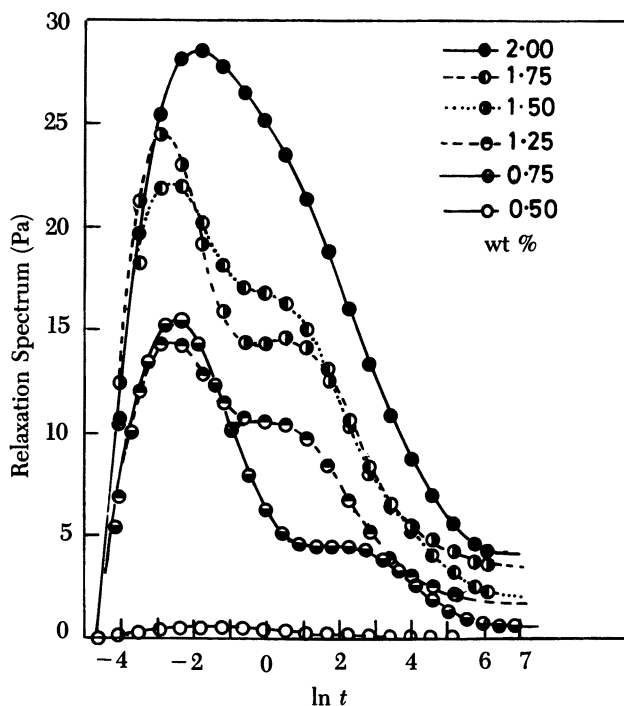
Figure 11. The relaxation spectra for various concentrations of HMHEC D-47 in NaCl solutions from a strain of 16%.

content over the concentration range studied. This observation was confirmed by stress relaxation measurements on the same solutions. This relaxation process was tentatively assigned to the disaggregation of the grafted hydrophobes. An additional increasing and broadening response occurred with increasing polymer content, but it was not investigated.

Symbols

a	power law index in Mark–Houwink equation
A	constant related to the functionality of a cross-link (6)
c	polymer concentration (g dL^{-1})
$C(\infty)$	characteristic ratio
f	concentration-dependent function due to the probability of a polymer chain forming loops (6)
G'	storage modulus
G''	loss modulus
$G(\infty)$	high-frequency limit of the storage modulus
$G(0)$	low-frequency limit of the storage modulus (static modulus)
$\tilde{G}$	wave-rigidity modulus
k	Boltzmann constant

k'	Huggins coefficient
K	temperature in Kelvins
K_1	constant in the Mark–Houwink equation
M_n	number-average molecular weight
N	number of cross-linking sites per unit volume
N_a	Avogadro's number
N_i	number of cross-linking sites on each chain
R	constant related to entanglements (6)
v	wave velocity
$[\eta]$	intrinsic viscosity
η_{red}	reduced viscosity
$\eta(0)$	low-shear-rate viscosity
ρ_s	*density of the solution*
ϕ	*volume fraction*

Acknowledgment

References

1. Gelman, R. A.; Barth, H. G. In *Water-Soluble Polymers: Beauty with Perform-ance*; Glass, J. E., Ed.; Advances in Chemistry 213, 1986; pp 101–110.
2. Landoll, L. M. J. *J. Polym. Sci., Polym. Chem. Ed.* **1982**, *20*, 443.
3. Vanderhoff, J. W. *Science and Technology of Polymer Colloids*; Poehlein, G. W.; Ottewill, R. H.; Goodwin, J. W., Eds.; NATO ASI Series E, Martinius Nijhoff: Boston, MA, 1983; Vol. 1.
4. Manley, R. St. J. *Ark. Kemi* **1956**, *9*, 44.
5. Flory, P. J. *Principles of Polymer Chemistry*; Cornell University: Ithaca, 1953.
6. Goodwin, J. W.; Khidher, A. M. *Colloid and Interface Science—Hydrosols and Rheology Hydrosols and Rheology*; Kerker, M., Ed.; Academic: New York, 1976.
7. James, H. M.; Guth, E. *J. Chem. Phys.* **1947**, *15*, 669.
8. Graessley, W. W. *Macromolecules* **1975**, *8*, 186.
9. Graessley, W. W. *Macromolecules* **1975**, *8*, 865.
10. Allen, G.; Holmes, P. A.; Walsh, D. J. *Faraday Discuss. Chem Soc.* **1974**, *57*, 19.
11. Walsh, D. J.; Allen, G.; Ballard, G. *Polymer* **1974**, *15*, 366.
12. Flory, P. J. *Statistical Mechanics of Chain Molecules*; Interscience: New York, 1969.
13. Ferry, J. D. *Viscoelastic Properties of Polymers*, 3rd ed.; Wiley: New York, 1980.

Polymerization of Hydrophobically Modified Polyacrylamide

Effects of Surfactants and Comonomers

William J. Peer

The Dow Chemical Company, Midland, MI 48667

This chapter reports on a model system that appears to indicate the relative effects of monomer type and concentration and of surfactant type and concentration on the copolymer structure of micellar solution polymerized hydrophobe association polymers. Typical such polymers are copolymers of <1 mol % lauryl methacrylate (LMA) with acrylamide and a mixed surfactant consisting of sodium dodecyl sulfate and dodecyl penta(oxyethylene glycol) monoether. Direct measurement of polymer structure is difficult because of the low (<1 mol %) amount of hydrophobic monomer in the copolymer. Results from the model system seem to show that LMA behaves as a cosurfactant in the monomer–surfactant prepolymerization solution. Increasing the acrylamide concentration in the prepolymerization solution appears to increase the LMA sequence length in the copolymer. Varying the alkyl chains on the anionic surfactant from decyl to octadecyl does not appear to affect LMA sequence length in the copolymer. Moving the anionic head group of the anionic surfactant further from the micelle core by inserting oxyethylene groups does not seem to change the sequence length of the LMA blocks in the copolymer. This result also implies that the aggregation number of the mixed micelles is constant for that change in the anionic surfactant.

FOR AQUEOUS POLYMERS, HYDROPHOBIC INTERACTIONS can be important determinants of molecular conformation and intermolecular association. For

example, hydrophobic regions of proteins are key factors in determining protein conformation and enzymatic activity (1). Similarly, synthetic water-soluble polymers with hydrophobic regions can associate because of hydrophobic interactions and thereby produce greater viscosity than for the polymer without the hydrophobic regions (2–24).

Hydrophobic regions can be one or two small, well-defined blocks of pendant hydrophobic moieties in an otherwise water-soluble polymer (2–4). An example is a water-soluble sulfonated BAB triblock copolymer where B is hydrophobic t-butylstyrene and A is vinyltoluene (2). However, hydrophobic regions can also be less well-defined as well as more numerous in a polymer molecule than is the case for a triblock copolymer (5–22). For example, pendant alkyl esters appear to have been randomly incorporated in styrene–maleic anhydride (5) and vinyl benzyl ether–styrene–maleic anhydride (6–11) copolymers. Also, alkyl polyoxyethylene acrylate monomers can be copolymerized with acrylamide to yield copolymers with pendant hydrophobic chains (12–15). More recently it was found (16–22) that small amounts of water-insoluble monomers that are solubilized by surfactants into aqueous solutions of a hydrophilic monomer produce copolymers with pendant hydrophobic chains, but the size, number, and nature of the hydrophobic regions has not been determined.

There are two types of micellar solution polymerized polymers. One type employs a surfactant during copolymerization of the two monomers, but the surfactant is removed before using the polymer for rheology control applications (16–19). In the second type, the surfactants necessary for copolymerizing water-soluble and water-insoluble monomers remain with the polymer during use (20–22). Furthermore, a nonionic surfactant is used, and it responds to changes in temperature or electrolyte concentration such that unique rheology is obtained (20–24). One such copolymer is composed of acrylamide (AAm) and less than 1 mol % lauryl methacrylate (LMA). A mixed surfactant is used for the polymerization of this copolymer; the surfactants are generally sodium dodecyl sulfate (SDS) and dodecyl penta-(oxyethylene glycol) monoether ($C_{12}EO_5$). This type of polymer, designated a micellar hydrophobe association polymer (MHAP), is the concern of this work.

Polymer–surfactant interactions are the basis for the rheological behavior of MHAPs. Other surfactant–polymer systems have previously been investigated. One example is the interaction of surfactants with polymers such as poly(ethylene oxide), which results in greater solution viscosities than with the polymer alone (e.g., ref. 25 and references therein). The interaction of surfactants or latexes with hydrophobically modified water-soluble polymers has also been shown to produce unique rheology (2, 5, 26, 27). In these systems, the latex particles or the surfactant micelles serve as reversible cross-link points with a hydrophobic region of a polymer molecule in dynamic association with a latex particle or surfactant micelle (27).

Proposed Mechanism of MHAP

Figure 1 illustrates the polymerization process believed to occur for MHAP. LMA is insoluble in water (to the extent that it is not detectable by gas chromatography); therefore, the fact that LMA is soluble in the surfactant solution suggests residence in the micelles. Likewise, the Vazo 52 (2,2'-azobis(2,4-dimethylpentanenitrile)) initiator (designated I• in the figure) is practically insoluble in water (90 ppm solubility at 25 °C, ref. 28) but soluble in heptane (6 wt % at 25 °C, ref. 28), and this condition suggests that virtually all the initiator molecules are also contained in the micelles. Thus, a reasonable assumption is that the micelle-resident monomers will polymerize with themselves before polymerizing with any aqueous-phase monomer. The use of an oil-soluble initiator rather than a water-soluble one is significant and differentiates this system from typical emulsion polymerization that uses a water-soluble initiator.

Some time after the LMA in a particular micelle is polymerized, the poly(lauryl methacrylate) (PLMA) radical can break through the micellar head-group region and begin adding the hydrophilic monomer to the PLMA
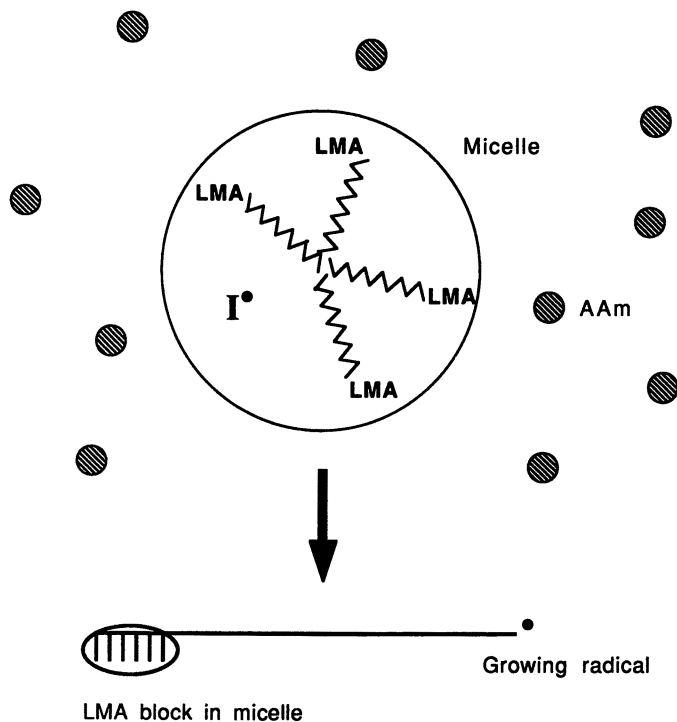
Figure 1. Schematic representation of the micellar solution polymerization process.

block radical. The bottom of Figure 1 illustrates the concept of a propagating radical soon after leaving the micellar environment. The hydrophobic block with its surfactant sheath is at the left of the diagram and the radical on the hydrophilic monomer is on the right. Eventually, the propagating hydrophilic radical will enter the micellar head-group region of an uninitiated micelle and initiate a block polymerization of the solubilized LMA. Hence, polymerization in a micelle may be initiated either by the oil-soluble initiator or by the aqueous-phase polymer radical.

The viscosity of the copolymer–surfactant solution depends upon the nature and extent of association of the hydrophobic blocks (27). Figure 2 illustrates the possibilities. If no surfactant is present (top of Figure 2), the hydrophobic blocks can associate intermolecularly, intramolecularly, or a combination of both. If the system is swamped with surfactant (middle of Figure 2), each hydrophobic block is completely solvated by surfactant so that there is no cross-linking. As heat, electrolyte, or other additives affect the number and aggregation number of micelles, various amounts of intermolecular or intramolecular cross-linking are produced (bottom of Figure
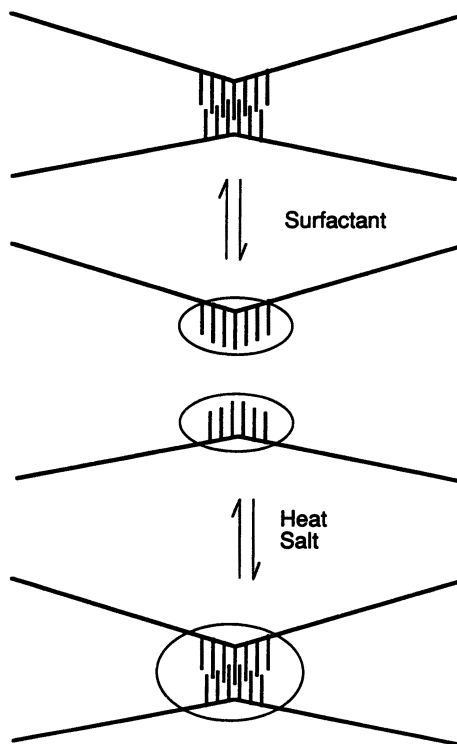
Figure 2. Schematic representation of the effect of surfactant, heat, and electrolyte on polymer cross-linking by a hydrophobic mechanism.

2). The balance of the many possible interactions in these MHAP produces unique rheological behavior (20–24, 27). Thus, the surfactant in the MHAP is an integral component of the polymer–surfactant system, serving a dual function of aiding the formation of the polymer architecture during polymerization as well as being reversible cross-link points in solution.

The following discussion illustrates the prepolymerization solution composition of a MHAP and the hypothetical results this composition could have on polymer architecture. Typical concentrations are 0.035 M SDS, 0.049 M $C_{12}EO_5$, 0.011 M LMA, 67 ppm by wt Vazo 52 initiator, and 1.4 M AAm. Solely for purpose of illustration, assume 25 LMA molecules in a micelle. (This number is reasonable within a factor of 2 or 3.) Assume that the SDS critical micelle concentration (CMC) for the mixed micelle is approximately that of $C_{12}EO_5$ (reasonable from the results of refs. 29 and 30) and assume that all of the Vazo 52 molecules are in the micelle. It is then calculated that the micelle consists of the 25 LMA molecules, 80 SDS molecules, 112 $C_{12}EO_5$ molecules, and 0.6 initiator molecules. Assuming complete polymerization, a 5×10^6 molecular weight (MW) molecule would then consist of 22 blocks of 25 LMA monomers each and 3100 AAm monomers between each block of LMA.

MHAPs have a number of advantages. Properly formulated, such polymers can produce a constant or even an increasing viscosity as temperature or electrolyte concentration increases. The polymer solutions are more shear-thinning than equivalent polymers without the hydrophobic regions. They can also be very thixotropic (gel-forming or structure-building). Because of the dynamic equilibrium between the micelle molecules and the hydrophobic regions of the polymer, cross-links can re-form after being broken by shear. Therefore, MHAP solutions of the same viscosity as normal polyacrylamide (PAAm) solutions are more stable to mechanical degradation by shear. Finally, a lower concentration of MHAP can be used to obtain the same viscosity as a higher concentration of the same MW polymer without the hydrophobic regions.

The reversible hydrophobic cross-links are the key to the rheology of these systems. The factors that determine the cross-links' contribution to the rheology are as follows:

1. the number of hydrophobic regions in the polymer

2. the number of micelles in solution

3. the strength of the micelle–hydrophobic region interaction (which depends on the sequence length of the hydrophobic region, energy of incorporation of the hydrophobic region into the micelles, etc.)

4. the functionality (the number of polymer branches at a cross-link point) of the micellar cross-link

The presence of a nonionic surfactant can change the micellar aggregation number, the CMC, and the number of micelles upon change in temperature or electrolyte concentration. These changes would then change the number and functionality of the cross-links.

Of these factors, the work presented in this chapter focuses on determining the relative sequence lengths of the hydrophobic regions in MHAP. For a given total concentration of hydrophobic monomer, longer sequence lengths result in fewer hydrophobic regions (an inverse relationship), so that the relative number of hydrophobic regions in the copolymer is also indirectly addressed. Determining relative sequence lengths is accomplished by using a model system that is similar to the monomer–surfactant solution during polymerization.

Description of the Model System

The structure of the hydrophobically modified polymer is set by the number of micelles and the number of hydrophobic monomers present during polymerization. Determination of the structure of the polymer is a problem because of the extremely small concentration of the hydrophobic monomers in the polymer (< 1 mol %). Normal analytical techniques such as NMR are not sufficiently sensitive to determine the number or the sequence length of the hydrophobic regions in such polymers.

Thus, we developed a model system wherein acrylamide (AAm) monomer, in effect a diluent of the hydrophobic monomer, is removed and replaced by propanamide (the saturated analog of acrylamide) and a chain-transfer agent (CTA) to mimic the effects of AAm during polymerization. The hydrophobic monomer and the surfactant system are the same as already described. The model system is thus similar to an emulsion polymerization except that an oil-soluble initiator is used. After polymerization of the LMA, analysis of the resulting PLMA is straightforward. The PLMA can be separated from the aqueous polymerization mixture and transferred to a tetrahydrofuran (THF) solution by solid-phase extraction. Size exclusion chromatography (SEC) gives the relative molecular weights of these polymers, which are believed to give the relative sequence length (number of LMA monomers) of the hydrophobic region in a similarly prepared hydrophobically modified polymer. This model system does not yield absolute numbers for the sequence length of the hydrophobic region; rather, it yields information regarding the relative effects of surfactant type, surfactant concentration, monomer, and polymerization conditions on the hydrophobic regions.

Experimental Details

Propanamide (97%) and sodium dodecyl sulfate (98%) were used as received from Aldrich. The lauryl methacrylate was the commercial material from Rohm and Haas

(typically 62% dodecyl methacrylate and 25% tetradecyl methacrylate). The sodium alkyl sulfates were a Polystep series by Stepan. The sodium lauryl polyoxyethylene sulfates were a Sipon series by Alcolac; the sodium lauryl polyoxyethylene sulfonates were the Avanel series by PPG.

The dodecyl penta(oxyethylene glycol) monoether was synthesized from Aldrich dodecyl alcohol (98%) by adding 5 mol of ethylene oxide per mol of alcohol; this reaction produces the typical distribution in degree of ethoxylation. The synthesis of nonylphenyl methacrylate was by a straightforward reaction of methacryloyl chloride (Aldrich) and nonylphenol (Kodak). Proton NMR spectroscopy just before use indicated 77% double bonds; the rest were alkyl hydrogens, presumably because of polymerization.

For the model system polymerizations, solutions containing the surfactants, LMA, initiator, and other additives as necessary were prepared in 4-oz narrow-mouth bottles, placed in a Branson B-52 ultrasonic bath for more than 10 min with nitrogen flow into the top of the bottle, capped with Polyseal tops, and tumbled in a water bath overnight at 60 °C. The ultrasonic bath was used both to aid in degassing the sample and to ensure complete equilibrium in the surfactant solutions.

The order of component addition is important. The mixing of concentrated anionic and nonionic surfactants must be avoided because it produces gels that dissolve very slowly. Typically, a master batch of nonionic surfactant, initiator, and LMA was prepared for use with all the solutions of a series of experiments. This approach ensures that the small concentration components are all at the same concentration. To a portion of this well-mixed master batch was added more nonionic surfactant if necessary, propanamide (if used), water to about 80 g, anionic surfactant, mercaptoethanol, and water to 100 g, with stirring as appropriate.

The relative PLMA MW was determined by using nonaqueous SEC with THF as solvent and an HP1037A refractive index detector from Hewlett-Packard. A solid-phase extraction cartridge (Waters Sep-Pak) was used to take the PLMA and surfactants from the water phase to THF and to adjust the concentration for SEC. Sodium sulfate was used to dry the THF extract before injection into the SEC columns. For some samples there was too much surfactant present, and it overloaded the cartridge; in such cases ion-exchange beads were used to reduce the concentration of the ionic surfactants in the aqueous phase before extraction. The advantage of this extraction procedure is its simplicity. The overall separation scheme is shown in Scheme I.

Sample
↓
(Ion exchange if too much surfactant)
↓
1-mL sample through pre-wet Sep-Pak cartridge
↓
3 mL of THF
↓
Dry with Na_2SO_4
↓
SEC based on polystyrene standards
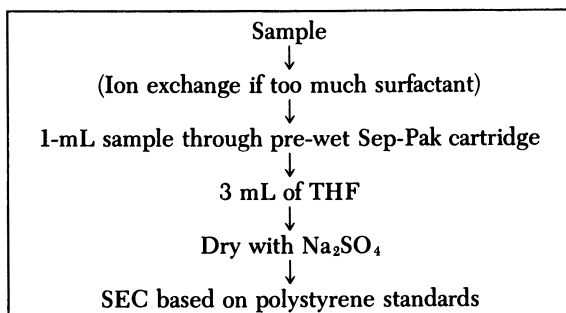
Scheme I.

To verify this method, two blanks were run. The first consisted of a blank "polymerization" with no LMA but all of the other components present. The solution

was extracted by this method; the SEC chromatogram had a flat baseline in the region before the $C_{12}EO_5$ peaks where PLMA normally occurs. The second blank consisted of extracting deionized water. One cartridge from each new Sep-Pak box was tested by this procedure and always gave a straight SEC baseline. This result demonstrates that the cartridges do not contain anything that can be extracted by THF. Finally, further verification of this method was obtained from a comparison of SEC results of PLMA extracted with methylene chloride and PLMA extracted using this solid-phase procedure. No differences in the SEC peak positions were observed.

The molecular weights reported in this chapter are based on a comparison of the polymer peak positions with the peak positions of polystyrene standards and are thus not actual PLMA molecular weights. Therefore, the degree of polymerization of PLMA cannot be determined; only relative differences in the degree of polymerization are found.

Results

Validation of the Model System. Several experiments were performed to validate the model system. Simply substituting propanamide for AAm in a polymerization recipe might seem to be sufficient to mimic the effect of AAm on the micelle. Without a CTA, however, the PLMA MW is found to be >100,000 (the exclusion volume of the columns used). This high MW is thought to be due to intermicellar transfer of the PLMA radical. Small additions of water-soluble mercaptoethanol dramatically decrease the measured MW (Figure 3). Presumably, the PLMA radical is terminated before intermicellar transfer can occur. An excess of mercaptoethanol, however, can change both the micelle's CMC and aggregation number. These changes would change the number of LMA molecules in a micelle. Furthermore, excess mercaptoethanol could potentially terminate the growing micelle-resident radical in the micelle head-group region before all of the
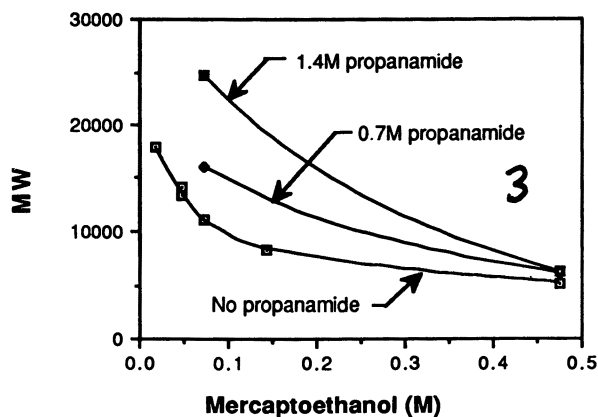
Figure 3. PLMA MW as a function of mercaptoethanol concentration. Polymerization conditions: 0.014 M LMA, 0.035 M SDS, 0.049 M $C_{12}EO_5$.

LMA in the micelle is reacted. Further investigation would be required to determine the cause of the continuing small decrease of PLMA MW with added mercaptoethanol shown in Figure 3.

Other CTAs and inhibitors also tried (about 0.05 M) were anionic mercaptoacetate and mercaptosuccinate and cationic isopropylamine, 1-dimethylamino-2-propanol, cysteamine hydrochloride, and copper sulfate. The pH was adjusted as necessary to yield the desired ions. None of the ionic CTAs reduced the measured PLMA MW, although mercaptoacetic acid at a pH of 2.2 (mixed anionic and neutral species) reduced the molecular weight almost to that obtained with mercaptoethanol. The ionic CTAs may increase the micelle aggregation number (electrolyte effect). Cu(II) precipitated surfactant, but the other solutions were clear.

One possible explanation for these results is that the charges on ionic CTA molecules keep them sufficiently far from the charged micellar head-group region so that intermicellar radical transfer is permitted, whereas the uncharged mercaptoethanol may even be in the head-group region. The CTA concentrations (roughly a factor of 5 greater than the monomer concentration) are all far beyond what even a weak CTA is normally effective at; yet, in this case they are ineffective. For AAm polymerization, isopropylamine is a good CTA or inhibitor; small amounts of $CuSO_4$ are used as an inhibitor for aqueous AAm. Thus, the water-soluble CTAs used are expected to chain transfer or kill any aqueous-phase radicals if they can get to the live radicals. In any case, the nonionic mercaptoethanol is the optimal CTA to use to prevent intermicellar radical transfer.

These results demonstrate that with this model system it is not possible to determine the precise number of LMA monomers in a micelle or in a hydrophobic region of the polymer molecule; rather, by choosing an appropriate level of mercaptoethanol and keeping it constant throughout all experiments, the change in the average PLMA MW as polymerization conditions are changed is determined. For this work, 0.072 M mercaptoethanol was always used. Because the model system yields relative results, a series of experiments were often run without propanamide to reduce the experimental complexity.

Independent data are desirable to validate the model system as representative of MHAP polymerization. One such attempt used SDS as the sole surfactant. The known aggregation number and CMC of SDS would allow calculation of LMA MW and hence provide independent verification. However, addition of LMA (as well as other hydrophobic monomers) to clear SDS solutions in sufficient quantities to be detectable with this technique always resulted in turbid solutions; that is, the micelle structure was changed by the solubilizate. Another potential method for validating the model system is through light-scattering experiments. Such studies would be difficult to interpret. Light-scattering experiments require that concentration be varied in order to extrapolate to zero concentration. Because there are two surfac-

tants and a solubilizate, the correct change in concentrations necessary for the extrapolation to infinite dilution is not obvious; in fact, the micellar structure probably changes as concentration is varied in such systems.

The effect of initiator concentration in the model system is shown in Table I. Amounts of Vazo 52 from 67 to 335 ppm by wt produce practically an invariant PLMA MW, although there might be a slight maximum at 134 ppm (1 sigma error is ~300). This result is contrary to the usual case where an increase in initiator concentration causes a decrease in MW. This relative insensitivity to initiator concentration is consistent with the micellar solution polymerization model already described because molecules in a micelle are in their own microenvironment. A concentration of 200 ppm of initiator is always used for polymerization in the model system because this concentration usually gives at least one initiator molecule per micelle. These results prove that initiator concentration is not a factor in these experiments.

Effect of Hydrophilic Monomer (Acrylamide).   Figure 3 and Table I also demonstrate the effect of propanamide concentration. In this surfactant system, addition of propanamide increases the MW of the PLMA. One possible explanation is that the CMC is raised (urea added to dilute nonionic surfactant solutions increases the CMC, ref. 31) so that the number of micelles is reduced. Another possible explanation is that the aggregation number is increased by the propanamide. Perhaps both occur. Nevertheless, this result implies that for MHAP, addition of AAm increases the LMA sequence length in the AAm–LMA copolymer and therefore decreases the number of hydrophobic blocks. Thus, AAm concentration in the prepolymerization solution will affect the polymer performance; the higher the AAm concentration, the poorer the rheology because of fewer hydrophobic blocks. Also, the sequence length of the hydrophobic blocks may change as the polymerization proceeds; this change would make analysis of the synthesized copolymer even more difficult. Model system experiments with varying amounts of PAAm added are one method of confirming this possibility.

Effect of Hydrophobic Monomer Concentration.   Results of the effect of LMA concentration in the prepolymerization solution are given in

Table I. Effect of Initiator Concentration on PLMA MW

Initiator (ppm)	No Propanamide	1.4 M Propanamide
67	8,700	11,860
134	9,310	12,990
200	8,950	12,200
335	[8,600]	10,780

NOTE: Polymerization conditions: 0.035 M SDS, 0.049 M $C_{12}EO_5$, 0.011 M LMA, 0.072 M mercaptoethanol. Square brackets indicate that MW has larger error than normal.

Figure 4. At constant surfactant concentration, a linear relationship should be found between the MW of PLMA and LMA concentration in the pre-polymerization solution with an intercept of zero if there is no micellar rearrangement. At low LMA concentrations, a linear relationship does occur (Figure 4). At concentrations greater than about 0.005 M, however, the actual MW is lower than that from the extrapolated line. Generally, as a nonpolar solubilizate is added to a surfactant mixture, the surfactant re-arranges to increase the aggregation number of a micelle and therefore decrease the number of micelles (32). If that type of rearrangement occurred in this system, the PLMA MW would be larger than without the rearrange-ment. Clearly this situation is not the case. Instead, the MW is lower than if no rearrangement had occurred, a result implying that a greater number of smaller micelles are formed as LMA is added to the surfactant system. Thus, LMA behaves as a cosurfactant in the system rather than as an oil. This behavior is generally desirable because it maximizes the number of hydrophobic regions in the polymer and therefore maximizes the potential number of cross-link points for the copolymer.

This analysis assumes that the added LMA does not significantly change the mixed micelle CMC. In previous measurements of nonionic–anionic mixed micelle CMC, the CMC for a 60:40 mixture is nearly that of the nonionic surfactant (29, 30). Therefore, the surfactant concentration in these solutions is probably more than 100 times greater than the CMC (the CMC of $C_{12}EO_5$ is 5.9×10^{-5} M at 25 °C, ref. 33). Assuming for the sake of argument that the surfactant concentration is only 10 times the CMC, then a decrease of the CMC to zero would increase the number of micelles only by 10%, not nearly enough to account for the deviation in PLMA MW in
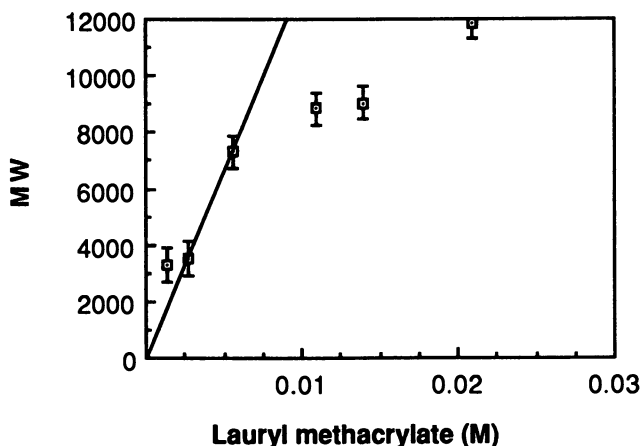
Figure 4. Effect of LMA concentration on PLMA MW. Polymerization conditions: 0.035 M SDS, 0.049 M $C_{12}EO_5$, 0.072 M mercaptoethanol, no propanamide.

Figure 4. Therefore, the LMA reduces the aggregation number of the mixed micelle.

Nonylphenyl methacrylate was synthesized as a UV-absorbing monomer to confirm the effect of this type of hydrophobic monomer on the surfactant solution. Results are shown in Figure 5 (the monomer concentration has been adjusted on the basis of the number of double bonds obtained from the NMR results; *see* the Experimental Details section). Although the points are in an almost straight line, the intercept of a least-squares line through all of the points would be about 5000; however, the intercept must be zero. Therefore, there must be an initial linear relationship that includes the origin. At higher nonylphenyl methacrylate concentrations, the MW is lower than extrapolated from the initial line. Thus, this hydrophobic monomer also acts as a cosurfactant.

Effect of the Alkyl Chain Length of the Anionic Surfactant. Table II displays the PLMA MW in the model system as a function of the alkyl chain length of the anionic surfactant, all other concentrations remaining constant. When the prepolymerization solution contains only $C_{12}EO_5$, the solution is opaque and the PLMA MW is large; this result implies the existence of large micelles. Addition of sodium 2-ethylhexyl sulfate to the $C_{12}EO_5$–LMA prepolymerization solution at the concentration used for SDS (0.035 M) dramatically increases the MW. This result is presumably due to an electrolyte effect that increases nonionic surfactant aggregation numbers (*31*), because the sodium 2-ethylhexyl sulfate concentration is far below the surfactant's CMC. However, doubling the sodium 2-ethylhexyl sulfate con-
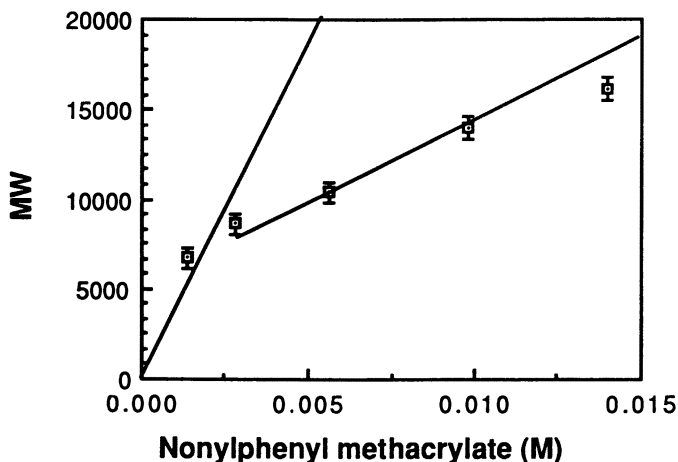
Figure 5. Effect of nonylphenyl methacrylate concentration on poly-(nonylphenyl methacrylate) MW. Polymerization conditions: 0.035 M SDS, 0.049 M $C_{12}EO_5$, 0.072 M mercaptoethanol, no propanamide.

Table II. Effect of Alkyl Chain Length of Anionic
Surfactant on PLMA MW

Length	Concentration (M)	MW	CMC[a] (M)
No anionic		20,760[b]	
C_6C_2	0.035	>100,000	0.13
C_6C_2	0.069	19,500	
C_{10}	0.035	12,300	0.034
C_{12}	0.035	12,300	0.008
C_{16-18}	0.035	12,200	6.2×10^{-4}
			1.7×10^{-4}

NOTE: Polymerization conditions: 0.011 M LMA, 0.049 M $C_{12}EO_5$,
0.072 M mercaptoethanol, 1.4 M propanamide.
[a]CMC of the anionic surfactant at 25 °C (33).
[b]Solution is 0.010 M lauryl methacrylate.

centration lowers the PLMA MW, presumably because the anionic surfactant molecules are beginning to incorporate into the $C_{12}EO_5$ micelles, and in so doing make the micelles smaller.

On the other hand, sodium decyl sulfate, sodium dodecyl sulfate, and a sodium hexadecyl–octadecyl sulfate mixture result in equal PLMA MW for equal surfactant concentrations. These anionic surfactant concentrations are at or above their CMCs. That there is little or no influence on the aggregation number of the mixed micelles as the anionic surfactant tail varies from decyl to octadecyl is an indication of the importance of steric and electrostatic effects in the head-group region in these mixed micelles, at least for the 60:40 nonionic–anionic composition investigated here (34, 35).

Effect of Ethoxylated Anionic Surfactants.

Model system results for a series of sodium lauryl polyoxyethylene sulfates and sulfonates are presented in Table III. Surprisingly, the PLMA MW does not vary with the degree of ethoxylation! However, the sulfonate results have larger MWs than the sulfate results.

Discussion

The results of the model system are consistent with the theory that a MHAP is a block copolymer. A consistent PLMA MW of 8500–20,000 (MW referenced to polystyrene) in the model system as surfactants and monomers are changed is one point of support. Further support is that the PLMA MW is independent of initiator concentration (Table I), as would be expected if polymerization occurs only within one micelle and the polymerization of the LMA in a micelle is complete once initiated. The leveling off of PLMA MW at concentrations greater than about 0.15 M mercaptoethanol (Figure 3) is also consistent with this theory. Thus, changes in PLMA MW in this work

Table III. Effect of Degree of Ethoxylation in Sodium
Lauryl Polyoxyethylene Sulfates and Sulfonates
on PLMA MW

Moles EO[a]	MW	CMC[b] (M)
Sulfates		
0	10,000	7.6×10^{-3}
1	10,500	4.9×10^{-3}
2	10,200	3.05×10^{-3}
4	10,100	1.2×10^{-3}
7	10,400	
Sulfonates		
3	11,400	
7	12,300	
9	11,400	
15	11,500	

NOTE: Polymerization conditions: 0.014 M LMA, 0.035 M sodium lauryl polyoxyethylene sulfate, 0.049 M $C_{12}EO_5$, 0.072 M mercaptoethanol, no propanamide.
[a]Ethylene oxide.
[b]CMC of the anionic surfactant at 50 °C (33).

are identified as changes in the hydrophobic sequence length in the MHAP copolymer.

Assuming that the model system is a valid model for a MHAP prepolymerization solution, these results for the model system can be applied to the MHAP. The model system results suggest that the micelle solution copolymerization process can be a means of producing multiblock copolymers in which hydrophobic and hydrophilic blocks alternate. At constant monomer concentration, the number of blocks in the copolymer molecule is inversely related to the number of monomers in the block. Thus, factors that increase the sequence length of a block decrease the number of blocks. The monomer concentrations and the polymer MW are also factors governing the sequence length and number of blocks in the copolymer. Polymerization conditions (e.g., surfactant type and concentration) can be used to control the block size to some extent.

In the model system, mercaptoethanol is required to prevent production of very high MW PLMA—a MW higher than can be reasonably assumed to occur during copolymerization with AAm. If the model of micellar polymerization of LMA into AAm discussed in the beginning of this chapter is correct, this need for a CTA can be explained as follows. From the point of view of LMA polymerization, AAm acts to end the propagation of the PLMA radical in one micelle and, after radical propagation in the aqueous phase (during which time AAm is added) to initiate polymerization of the LMA in another micelle. If it is desired to keep the LMA from different micelles as separate polymer molecules, then a CTA is necessary terminate the PLMA radical in each micelle. Without such termination the PLMA radical appears to transfer between micelles.

The model system appears to be useful for determining how polymerization variables (monomer concentration, surfactant type and concentration) affect the hydrophobic block sequence length and therefore the number of hydrophobic blocks in MHAP. Increasing AAm concentration caused an increase in hydrophobic sequence length. On the other hand, the hydrophobic monomer, LMA, acts as a cosurfactant for the system used in this work. This action results in the block sequence length remaining almost constant in a critical LMA concentration range during which the number of blocks in the copolymer increases.

The effect of anionic surfactant on the LMA sequence length in this system was one important area investigated. For the sodium alkyl sulfates at concentrations above their CMCs and for an alkyl chain length of 10 to 18 carbon atoms, the addition of these surfactants to a solution of LMA solubilized by a nonionic surfactant causes a decrease in the LMA sequence length compared to the use of only the nonionic surfactant. This result means that the number of micelles is increased and their aggregation numbers are decreased by the addition of these anionic surfactants. For the conditions investigated, alkyl chain lengths of 10 to 18 carbon atoms have no effect on those parameters. When sodium 2-ethylhexyl sulfate is used at the same concentration as the other surfactants (a concentration below its CMC), it increases the LMA sequence length, presumably by an electrolyte effect. At a higher concentration near its CMC, it performs similarly to the other surfactants, causing a decrease in the LMA sequence length.

Adding oxyethylene monomers between the sulfate head group and the alkyl tail of the sodium lauryl sulfate results in no change in the block size of the PLMA for a degree of ethoxylation up to 7. Thus, the mixed micelle aggregation number for the system, which includes LMA, does not change. Similar invariant results were obtained for the sodium lauryl polyoxyethylene sulfonates. The insertion of polyoxyethylene places the charged head groups further from the micelle interior and closer to the ends of the $C_{12}EO_5$ molecules. This positioning is expected to change the micelle surface charge density because the head-group charges would be further apart. Also, the steric factor for the head group changes. Yet, the results for PLMA MW strongly suggest that the aggregation number does not change in these 60:40 nonionic–anionic mixed micelles.

These results are contrary to expectations. For example, Nagarajan (*34*) finds that three factors determine aggregation number in mixed micelles: micelle core-water interfacial energy, steric repulsion, and electrostatic repulsion (which is based on surface charge density in the model). A reduction in surface charge density is expected to result in larger micelles. Yet, the experimental results of this work are that the change in surface charge density that is expected to occur as polyoxyethylene is inserted between the anionic head group and the alkyl chain does not produce a change in aggregation number.

On the other hand, the fact that the aggregation numbers for the sulfate

and sulfonate mixed micelles were slightly different suggests that the charge density of the anionic head groups themselves has some effect. This result is in accord with a difference previously found for sodium dodecyl sulfate and sulfonate interaction parameters with nonionic molecules in mixed micelles (36).

Obviously many variables were not investigated, such as the effect of the type of nonionic surfactant, broader ranges of surfactant concentration, and broader ranges of monomer concentration. However, the results of this work are sufficient to demonstrate that the block copolymer architecture can be modified in MHAP by modifying the anionic surfactant concentration and type. These results have supported but not proved the block copolymer theory for this type of polymer–surfactant system. This model system is also a simple means of studying some aspects of mixed surfactant systems, an area of much current interest (e.g., ref. 37).

Acknowledgments

References

1. Tanford, C. *J. Am. Chem. Soc.* **1962**, *84*, 4260.
2. Rose, G. D.; Dennis, K. S.; Evani, S. U.S. Patent 4 505 827, 1985.
3. Valint, P. L., Jr.; Bock, J. U.S. Patent 4 492 785, 1985.
4. Valint, P. L., Jr.; Bock, J. *Polym. Mater. Sci. Eng.* **1986**, *55*, 361.
5. Evani, S.; Lalk, R. H. U.S. Patent 3 779 970, 1973.
6. Evani, S.; Corson, F. P. U.S. Patent 3 963 684, 1976.
7. Evani, S.; Corson, F. P. U.S. Patent 4 029 872, 1977.
8. Evani, S.; Corson, F. P. U.S. Patent 4 029 873, 1977.
9. Evani, S.; Corson, F. P. U.S. Patent 4 029 874, 1977.
10. Evani, S.; Corson, F. P. U.S. Patent 4 008 202, 1977.
11. Evani, S.; Corson, F. P. U.S. Patent 4 105 649, 1978.
12. Schulz, D. N.; Maurer, J. J.; Bock, J. U.S. Patent 4 463 151, 1984.
13. Schulz, D. N.; Maurer, J. J.; Bock, J. U.S. Patent 4 463 152, 1984.
14. Maurer, J. J.; Schulz, D. N.; Bock, J. U.S. Patent 4 579 926, 1986.
15. Schulz, D. N.; Maurer, J. J.; Bock, J.; Kowalik, R. M. Eur. Patent Application EP 116 779 A1, 1984.
16. Bock, J.; Siano, D. B.; Kowalik, R. M.; Turner, S. R. Eur. Patent Application EP 115 213 A2, 1984.
17. Turner, S. R.; Siano, D. B.; Bock, J. U.S. Patent 4 520 182, 1985.
18. Turner, S. R.; Siano, D. B.; Bock, J. U.S. Patent 4 521 580, 1985.
19. Turner, S. R.; Siano, D. B.; Bock, J. U.S. Patent 4 528 348, 1985.
20. Evani, S. U.S. Patent 4 432 881, 1984.
21. Evani, S. Eur. Patent Application EP 057 875 A2, 1982.
22. Constien, V. G.; King, M. T. U.S. Patent 4 541 935, 1985.
23. Constien, V. G. *Polym. Prepr. (Am. Chem. Soc., Div. Polym. Chem.)* **1986**, *27*(1), 243.

24. King, M. T.; Constien, V. G. *Polym. Mater. Sci. Eng.* **1985**, *52*, 414.
25. Prud'homme, R. K.; Uhl, J. T. *SPEJ, Soc. Pet. Eng. J.* **1984**, *24*, 431.
26. Thibeault, J. C.; Sperry, P. R.; Schaller, E. J. In *Water-Soluble Polymers*; Glass J. E., Ed.; Advances in Chemistry Series 213; American Chemical Society: Washington, DC, 1986; pp 375–389.
27. Evani, S.; Rose, G. D. *Polym. Mater. Sci. Eng.* **1987**, *57*, 477.
28. *Vazo Polymerization Initiators* E. I. du Pont de Nemours & Company publication E–50140, Wilmington, DE.
29. Schick, M. J.; Manning, D. J. *J. Am. Oil Chem. Soc.* **1966**, *43*, 133.
30. Nishikido, N. *J. Colloid Interface Sci.* **1977**, *60*, 242.
31. Becher, P. In *Nonionic Surfactants*; Schick, M. J., Ed.; Marcel Dekker: New York, 1967; p 478.
32. Shinoda, K.; Nakagawa, T.; Tamamushi, B.-I.; Isemura, T. *Colloidal Surfactants: Some Physicochemical Properties*; Academic: New York, 1963; pp 97–178.
33. *Polymer Handbook*, 2nd ed.; Brandrup, J.; Immergut, E. H., Eds.; Wiley: New York, 1975.
34. Nagarajan, R. *Langmuir* **1985**, *1*, 331.
35. Scamehorn, J. F. In *Phenomena in Mixed Surfactant Systems*; Scamehorn, J. F., Ed.; ACS Symposium Series 311; American Chemical Society: Washington, DC, 1986; pp 1–27.
36. Rosen, M. J. In *Phenomena in Mixed Surfactant Systems*; Scamehorn, J. F., Ed.; ACS Symposium Series 311; American Chemical Society: Washington, DC, 1986; pp 144–162.
37. *Phenomena in Mixed Surfactant Systems*; Scamehorn, J. F., Ed.; ACS Symposium Series 311; American Chemical Society: Washington, DC, 1986.

21

Synthesis and Characterization of Hydrophobically Associating Polymers

P. L. Valint, Jr.[1], Jan Bock, and D. N. Schulz[2]

Exxon Research and Engineering Company, Clinton Township, Route 22 East, Annandale, NJ 08801

Novel polymerization techniques were used to synthesize new macromolecules that consisted of a water-soluble backbone with small amounts of hydrophobic functionality. Micellar polymerization is based on the capability of surfactant micelles to solubilize hydrophobic molecules into an aqueous medium; it was used to copolymerize acrylamide and hydrophobically substituted acrylamide monomers. A critical aspect of these polymerizations was the incorporation of the hydrophobic monomer into the water-soluble polymers. A method that used the UV chromophore of newly synthesized N-aryl substituted acrylamides was developed to quantify incorporation at the low levels of hydrophobe normally used (about 1 mol %). The synthesis of the substituted acrylamides, the UV technique, and results obtained with it are discussed.

Hydrophobically associating water-soluble polymers have been investigated in alternative approaches to aqueous viscosification by ultrahigh molecular weight and chain expansion in polymers (1–12). Above the overlap concentration, (i.e., the semidilute concentration regime) these polymers associate intermolecularly in solution to build hydrodynamic size via the introduction of a small number of hydrophobic groups along the backbone

[1]Current address: Bausch & Lomb, 1400 North Goodman Street, Rochester, NY 14692
[2]Current address: Exxon Chemical Company, Linden, NJ 07036

of a water-soluble polymer. This association results in enhanced viscosification and altered response of other solution rheological properties (*13, 14*).

Because the level of hydrophobic monomer in the feed is usually low (<1 mol %), no analysis has been successful in measuring hydrophobe incorporation into the polymer. To date, hydrophobe incorporation has been inferred on the basis of a comparison of hydrophobe-containing polymer solution properties to those of corresponding polymers with no hydrophobe. The subject of this chapter is to present recent results obtained with a technique developed to quantitatively determine the incorporation of hydrophobic monomer into a water-soluble polymer.

Experimental Details

Reagents. Acrylamide (Aldrich Chemical Company) was recrystallized from acetone twice before use. Electrophoresis grade sodium dodecyl sulfate (SDS) (Polysciences, Inc.) was used without further purification. Distilled water was purified additionally by treatment with a water purification system (Milli-Q, Millipore) to give water with a resistivity of greater than 18 MΩ-cm.

N-4-Alkylphenylamides. The preparation of the various N-alkylacrylamides and model propionamides used in this study is exemplified by the following procedure for N-4-ethylphenylacrylamide.

Freshly distilled 4-ethylaniline (20.0 g [0.16 mol]), and 300 mL of ether were added to a 1-L flask and cooled to −10 °C. Triethylamine (18.3 g [0.18 mol]) dissolved in 100 mL of ether was added and was followed by the slow addition of of acryloyl chloride (16.3 g [0.18 mol]) dissolved in 100 mL of ether. The mixture was allowed to warm to room temperature. After 18 h, 250 mL of 10% HCl was added. The two-phase solution was separated, and the ether layer was washed with 500 mL each of 10% $NaHCO_3$ and saturated NaCl. The ether solution was dried and evaporated under vacuum. The residue was recrystallized twice from a hexane/acetone solution to give 15.9 g (57%) of desired product with a melting point of 108 °C. Infrared and NMR spectra of this product and all other analogs were consistent with the structures of the desired compounds. The analytical data for the compounds prepared are given in Table I.

1-Amido-1-phenylalkanes. The preparation of the various 1-acrylamido-1-phenylalkanes and model propionamido analogs used in this study is exemplified by the following procedure for 1-acrylamido-1-phenylhexane.

Acrylonitrile (28.1 g [0.53 mol]) was cooled to −10 °C, and concentrated sulfuric acid (10.5 mL) was added at a rate to maintain the temperature at −10 °C. After stirring for 0.5 h, 25.0 g (0.14 mol) of 1-hydroxy-1-phenylhexane was added dropwise at −10 °C. The mixture was allowed to warm to room temperature. After 18 h, the

Table I. Analytical Data for Hydrophobic Acrylamides and Model Propionamides

Compound	mp (°C)	Yield (%)	% Carbon		% Hydrogen		% Nitrogen	
			Calculated	Found	Calculated	Found	Calculated	Found
Acrylamides								
N-Ethylphenyl	108	57	75.40	75.46	7.48	7.14	7.99	7.93
N-Butylphenyl	100	54	76.82	76.68	8.42	8.21	6.89	6.84
1-Phenylhexane	88	75	77.86	78.15	9.17	8.94	6.06	5.90
1-Phenyloctane	61	72	78.70	78.80	9.73	9.45	5.40	5.54
1-Phenylnonane	70	80	79.05	79.11	9.97	9.83	5.12	5.10
Propionamides								
N-Ethylphenyl	91	89	74.55	74.74	8.52	8.48	7.90	7.90
N-Butylphenyl	95	68	76.04	76.35	9.35	9.23	6.82	6.96
1-Phenylhexane	75	88	77.19	77.45	9.95	10.03	6.00	5.86
1-Phenyloctane	50	74	78.09	78.20	10.43	10.35	5.36	5.25
1-Phenylnonane	52	70	78.47	78.53	10.63	10.68	5.09	4.79

reaction mixture was poured into ice water and extracted with ether. The ether layer was washed with 10% NaHCO₃ and saturated NaCl solution. The ether solution was dried and evaporated under vacuum. The residue was recrystallized twice from a hexane/acetone solution to give 25.1 g (77%) of desired product with a melting point of 88 °C. Infrared and NMR spectra of this product and all other analogs were consistent with the structures of the desired compounds. The analytical data for the compounds prepared are given in Table I.

Polymerization of Hydrophobically Associating Polymers.   The following procedure for the preparation of 0.75 mol % N-4-butylphenylacrylamide–acrylamide polymer is typical of all the polymers discussed in this report.

A solution of 21 g of SDS in 700 mL of deoxygenated water was prepared. N-4-Butylphenylacrylamide (0.444 g) was dissolved in this solution followed by 20.6 g of acrylamide. The resulting solution was carefully transferred to a 1-L Morton-style resin kettle fitted with a chilled water condenser, thermometer, inert gas sparger, and mechanical stirrer. The temperature was adjusted to 50 °C and polymerization was initiated by the addition of 1.47 mg of $K_2S_2O_8$. After stirring for 1.5 h at 50 ± 2 °C, a 100-mL portion of the viscous solution was poured slowly into 3 L of methanol. The precipitated polymer was then masticated in with methanol in a blender (Waring), filtered, and dried under vacuum at 30 °C. The yield of polymer was 0.86 g (28.7%). After 16 h, the solution was diluted with 600 mL of distilled water and a 200-mL aliquot was removed. The polymer was isolated to yield 2.94 g (98.0%).

NaOH (0.4 equiv) was added to the remainder of the polymer solution, and the resulting solution was stirred for 2 h at 50 °C. The solution was then poured slowly into 3 L of methanol, and the precipitated polymer was then masticated with methanol and acetone in a blender, filtered, and dried under vacuum at 30 °C. The yield of hydrolyzed polymer was 12.85 g (85.5%).

The mole and weight fractions of sodium acrylate in the hydrolyzed polymers were determined from sodium elemental analysis and calculated according to equations 1 and 2, respectively.

$$m_{AA} = \frac{x_{Na}[(MW_H - MW_{AM})m_H + MW_{AM}]}{AW_{Na} + x_{Na}(MW_{AM} - MW_{AA})} \tag{1}$$

$$x_{AA} = \frac{m_{AA}/MW_{AA}}{m_{AA}/MW_{AA} + m_H/MW_H + m_{AM}/MW_{AM}} \tag{2}$$

The terms are defined in the list of abbreviations.

For studies of hydrophobe incorporation as a function of conversion of monomer to polymer, aliquots were removed from the reaction polymerization mixture at various times, weighed, and slowly poured into methanol that contained 1000 ppm of hydroquinone. The precipitated polymer was isolated as described and then weighed to determine percent conversion.

UV Spectral Analysis.   Aqueous solutions of the model compounds were prepared at a broad range of concentrations to determine the linearity of absorbance response to concentration. The UV absorption spectra were obtained in the range

of 200 to 300 nm with a spectrophotometer (Lambda 5, Perkin-Elmer). Similarly, the polymers were measured in the same solvent as that for the model compound that represented the hydrophobe of the polymer. Solutions containing polymers with 1-acrylamido-1-phenylalkane hydrophobes were measured with 10-cm-path length cells, whereas all other spectra were obtained with 1-cm cells. The UV absorption of the nonhydrophobic portion of the polymer was removed from the spectra by using a polymer that was similar to the analyte polymer but did not contain hydrophobe as the reference. The calculations used to convert the measured absorbances into hydrophobe incorporation are discussed in the next section.

Results and Discussion

Hydrophobically associating polymers consist primarily of water-soluble monomer units with a small number of water-insoluble monomer units. Synthesis of high-molecular-weight random copolymers of acrylamide and alkylacrylamides required a novel aqueous surfactant micellar solution polymerization (2–4) because of the mutual immiscibility of the water-soluble and hydrophobic monomers. The use of surfactant micelles enabled solubilization of the hydrophobic monomer (alkylacrylamide [R]) into the aqueous phase containing the water-soluble monomer (acrylamide [AM]). The resulting RAM polymer after isolation provided homogeneous aqueous solutions.

   The evidence for the formation of such a polymer consisted almost exclusively of the comparison of its aqueous solution properties to a corresponding analog devoid of hydrophobic monomer. In this manner, qualitative and relative information was obtained concerning the effects of various synthesis parameters on hydrophobe incorporation. However, the detailed data required to understand hydrophobe incorporation and its relation to the microstructure and composition of the polymers, the keys to controlling solution properties, have been lacking. Analytical techniques such as NMR and IR spectroscopy, GC–pyrolysis, and the use of a ^{14}C-labeled monomer have been evaluated. To date, all of these techniques have proven unsatisfactory for providing quantitative information on hydrophobe incorporation. Some techniques are still being pursued (e.g., NMR and isotopic labeling) for hydrophobe incorporation and other determinations. Progress in these areas will be the subject of future reports.

   Determination of Hydrophobe Incorporation.   A quantitative UV spectrophotometric technique was developed for the determination of the incorporation of hydrophobic monomer into a water-soluble polymer. The technique was based on UV spectroscopic detection of hydrophobic monomers containing phenyl groups. The placement of the phenyl groups into

the monomer molecules was varied to provide different chromophoric functionality and UV absorptivities. When using this technique to infer the incorporation of N-alkylacrylamide, it was assumed that the phenyl group caused no significant effect.

This procedure was designed to provide a measure of the absorptivity of the hydrophobic monomer through the use of a model. The use of a monomeric model compound to represent equivalent chromophores attached to polymer molecules was recently reported for polystyrene (15, 16). UV methods were also used in the determination of copolymer composition and reactivity ratios for isocyanate-containing acrylate polymers (17).

The UV-active monomers chosen as hydrophobes in this study are shown in Chart I. The saturated analogs to the acrylamides, 1 and 2, were the propionamides, 3 and 4, respectively. These analogs were the corresponding model compounds that represented the chromophoric functionality of the hydrophobe when incorporated into a polymer backbone. The polymer systems chosen for this initial attempt to quantify hydrophobe incorporation were copolymers of the hydrophobes and acrylamide (RAM) and their partially hydrolyzed analogs (HRAM), which are terpolymers of hydrophobe, acrylamide, and acrylate.

The various model compounds synthesized in our laboratory are listed in Table II. The absorptivity of each model was calculated using Beer's law and a linear regression through the origin. These data are also presented in Table II along with the correlation coefficient (r^2) for the regressions. As can be seen from these data, the absorptivities of the N-alkylphenylpropionamides (3) were almost 2 orders of magnitude higher than the 1-propionamido-1-phenylalkanes (4). Because of lower sensitivity, 1-acrylamido-1-phenylalkanes were not used to determine hydrophobe incorporation.

The RAM polymers were synthesized with the micellar polymerization technique, in which the hydrophobic monomer was solubilized into the aqueous medium with a surfactant SDS. The polymerizations were initiated with potassium persulfate at 50 °C. In some cases, a sample of the reaction

Table II. Model Propionamides and Their Absorptivities

Propionamide[a]	Alkyl Group	Solvent	Absorptivity ($Lg^{-1}cm^{-1}$)	r^2
3	C_2H_5	2% ethanol	71.3	0.9996
3	$n\text{-}C_4H_9$	2% ethanol	65.0	0.9983
3	$n\text{-}C_4H_9$	3% SDS[b]	69.3	0.9999
4	$n\text{-}C_5H_{11}$	50% ethanol	0.815	0.9992
4	$n\text{-}C_7H_{15}$	50% ethanol	1.14	0.9999
4	$n\text{-}C_8H_{17}$	50% ethanol	0.906	0.9999

[a]See Chart I.
[b]Sodium dodecyl sulfate.

Hydrophobic Monomers

n = 1, 3   n = 3, 5, 6

Model Compounds

n = 1, 3   n = 3, 5, 6
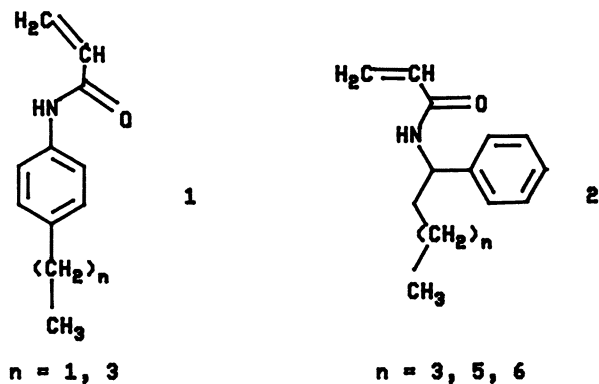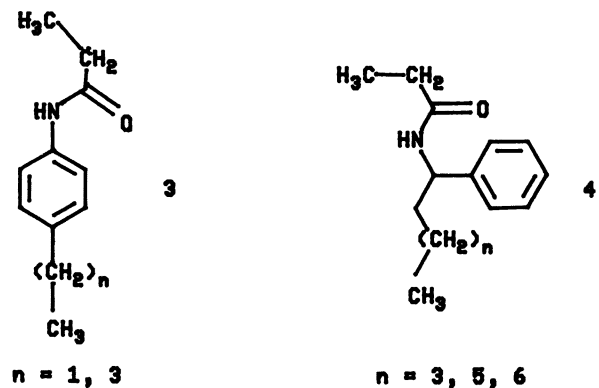
Chart I. UV-active hydrophobic monomers and their models.

solution was withdrawn after 90 min and the polymer was isolated. A portion of the complete polymerization product was reacted with NaOH to partially hydrolyze some of the acrylamide units to sodium acrylate and to provide a more water-soluble polymer system, an HRAM. Ethanolic solvents and 3% SDS were chosen because they dissolved both the polymers and their corresponding model propionamides.

The isolated polymer samples were dissolved in the solvent systems that corresponded to the model hydrophobe, and their UV spectra were obtained. The first polymers examined were the ethylphenylacrylamide RAM (C_2RAM) and HRAM (C_2HRAM) and the butylphenylacrylamide HRAM (C_4HRAM). The butylphenyl-containing RAM polymer was not soluble in 2% ethanol as were the other systems. The spectra of the RAM and HRAM polymers were obtained vs. reference solutions that contained appropriate concentrations of the corresponding non-hydrophobe-containing acrylamide and hydrolyzed acrylamide polymers, respectively. The resulting spectra were essentially identical to those of the model propionamides (Figure 1).

The incorporation of hydrophobic monomer into the polymers was determined by a comparison of the absorptivity of the hydrophobe unit in the polymer to the corresponding model. With the assumption that the absorptivity of the hydrophobe in the polymer is the same as that of the model, the ratio of polymer absorptivity to model gives the weight fraction of hydrophobe (x_H) in the polymer (equation 3). Converting x_H to mole fraction and dividing by the feed content in mole percent of hydrophobic monomer (M_f) results in the hydrophobe incorporation. The expressions for incorporation into RAM and HRAM polymers are given by equations 4 and 5, respectively.

$$x_H = a_P/a_M \tag{3}$$

$$H_{inc}(\%) = \frac{x_H/MW_H}{[x_H/MW_H + (1 - x_H)/MW_{AM}]M_f} \times 100 \tag{4}$$

MW_H is the hydrophobic unit molecular weight and MW_{AM} is the acrylamide molecular weight.

$$H_{inc}(\%) =$$

$$\frac{x_H/MW_H}{[x_H/MW_H + x_{AA}/MW_{AA} + (1 - x_H - x_{AA})/MW_{AM}]M_f} \times 100 \tag{5}$$

x_{AA} is the weight fraction of sodium acrylate units and MW_{AA} is the molecular weight of sodium acrylate.
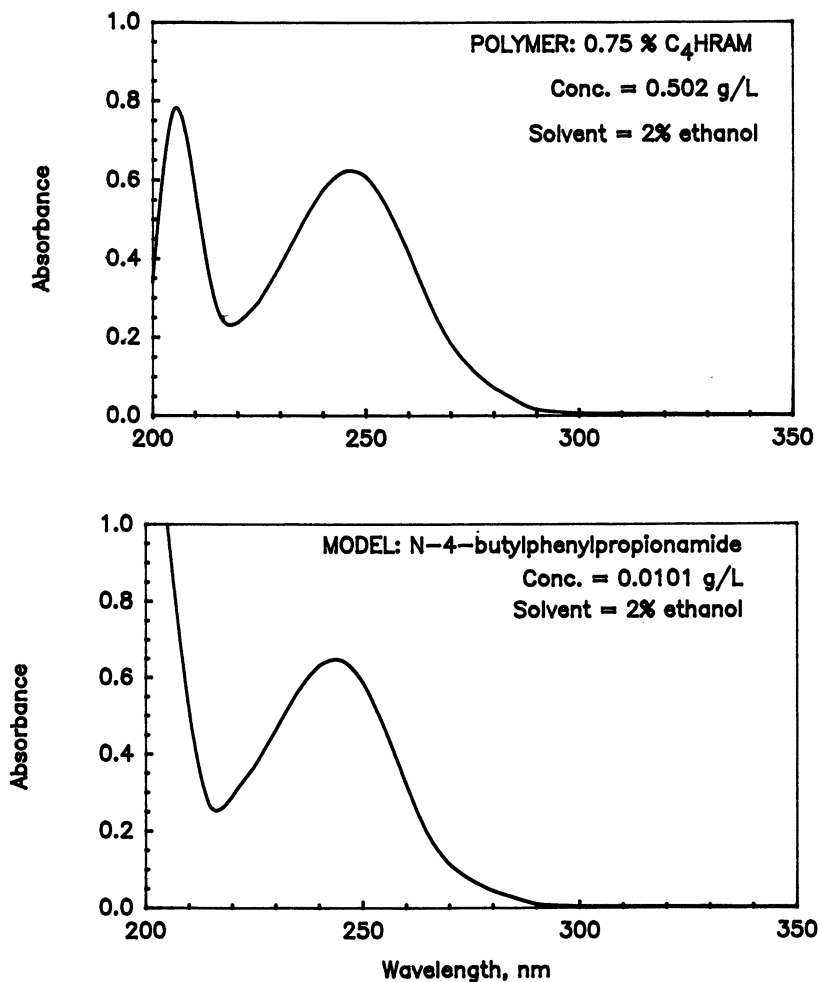
Figure 1. UV spectra of C₄HRAM polymer and model compound, N-4-butyl-phenylpropionamide.

To ensure a linear response of absorbance to concentration, the absorbance was measured at a number of polymer concentrations. The absorptivities were determined by linear regression with the origin as the intercept. The absorptivities of the polymers are given in Table III with their correlation coefficients for the regression. The correlation coefficients in Table III are consistent with a linear response of absorbance to polymer concentration. This method provided the confidence to use the calculated absorptivities to determine the incorporation of hydrophobe into these polymers.

Hydrophobe Incorporation.   With *N*-4-ethylphenylacrylamide as the hydrophobic monomer, it was possible to determine incorporation into

both the unhydrolyzed polymer (C_2RAM) and the hydrolyzed analog (C_2HRAM) in 2% ethanol. From the data in Table III, it can be seen that the hydrophobe was effectively incorporated into the polymer (87%) and was completely stable to the hydrolysis conditions.

C_4RAM at all concentrations of N-butylphenylacrylamide hydrophobe was not soluble in ethanolic solvent; therefore, only the hydrolyzed polymers (C_4HRAM) were evaluated in 2% ethanol. As shown by the data in Table III, all of the hydrolyzed polymer systems of C_4HRAM and one polymer (1-C_6HRAM) that contained 1-acrylamido-1-phenylhexane were determined to have >90% hydrophobe incorporation.

The data just described were obtained on high-conversion polymer samples, which represent a composite of all polymer molecules produced from the beginning to the end of the polymerization. No information was obtained to discern the extent of compositional heterogeneity with regard to hydrophobe content. If incorporation is heterogeneous, polymer samples at various levels of conversion must be examined to gain an understanding of polymer composition. Our initial efforts to gain such information included sampling during polymerizations of N-4-butylphenylacrylamide and acrylamide at 1.5 h after initiation and comparing with the polymer obtained at complete reaction.

The data presented in Table IV show that the polymer that formed at the early stages of the polymerization (i.e., about 30% conversion) had a much higher hydrophobe content than polymer produced toward the end

Table III. Hydrophobe-Containing Polymer Absorptivities

Hydrophobe	Absorptivity ($Lg^{-1}cm^{-1}$)	r^2	Incorporation (%)
N-4-Alkylphenylacrylamide			
0.75% C_2RAM	1.14	0.9859	87
0.75% C_2HRAM	1.08	0.9998	87
0.75% C_4HRAM	1.23	0.9998	93
1.0% C_4HRAM	1.63	0.9999	95
1.25% C_4HRAM	1.98	0.9996	91
1-Acrylamido-1-phenylalkane			
1.0% 1-C_6HRAM	0.0237	0.9845	97

Table IV. Hydrophobe Incorporation as a Function of Monomer Conversion

C_4RAM (%)	Conversion (%)	Absorptivity ($Lg^{-1}cm^{-1}$)	r^2	Incorporation (%)
0.75	28.7	1.93	0.9920	134
0.75	98.0	1.35	0.9840	91
1.0	34.7	2.80	0.9933	144
1.0	98.0	1.79	0.9903	91
1.25	31.7	3.29	0.9515	136
1.25	103	2.37	0.9948	96.9

of the reaction. Therefore, the resultant total polymer sample was heterogeneous with regard to hydrophobic monomer content. On the basis of the solution properties of similar polymers, compositional heterogeneity was suspected; however, it was felt that the heterogeneity resulted from low initial hydrophobe incorporation followed by high incorporation toward the end of the polymerization.

Originally, the hydrophobic monomer was thought to be relatively inaccessible, solubilized within the micelle. Apparently, the double bond of the hydrophobe is readily available to attack by the propagating radical moiety. More detailed study is required to fully understand incorporation during micellar polymerization.

Summary

A critical aspect of the micellar polymerization of hydrophobically substituted acrylamides and water-soluble monomers is the incorporation of the hydrophobic monomer into the resultant water-soluble polymers. Because of the low levels of hydrophobic monomer (<1 mol %), previous analyses were unsuccessful in measuring hydrophobe incorporation into the polymer. By using the UV chromophore of newly synthesized *N*-aryl-substituted acrylamides, a method was developed to quantify incorporation at the low levels of hydrophobe normally used. In all the cases examined, the hydrophobic monomer was incorporated at close to feed levels with complete conversion to polymer. Incorporation varied as a function of conversion; therefore, the resultant polymers were compositionally heterogeneous. Research is continuing to gain a better understanding of hydrophobe incorporation.

Abbreviations

a_M	absorptivity of hydrophobe model
a_P	absorptivity of polymer
AW_{Na}	atomic weight of sodium
H_{inc}	percent hydrophobe incorporation
m_{AA}	mole fraction of sodium acrylate monomer unit in hydrolyzed polymer
m_H	mole fraction of hydrophobic group
M_f	hydrophobic monomer feed concentration in mol %
MW_{AA}	molecular weight of sodium acrylate monomer
MW_{AM}	molecular weight of acrylamide monomer
MW_H	molecular weight of hydrophobic group
x_{AA}	weight fraction of sodium acrylate monomer
x_H	weight fraction of hydrophobic group
x_{Na}	weight fraction of sodium in hydrolyzed polymer

Acknowledgments

References

1. Valint, P. L., Jr.; Bock, J. U.S. Patent 4 492 785, 1985.
2. Turner, S. R.; Siano, D. B.; Bock, J. U.S. Patent 4 528 348, 1985.
3. Turner, S. R.; Siano, D. B.; Bock, J. U.S. Patent 4 520 182, 1985.
4. Turner, S. R.; Siano, D. B.; Bock, J. U.S. Patent 4 521 580, 1985.
5. 5. Schulz, D. N.; Maurer, J. J.; Bock, J. U.S. Patent 4 463 152, 1984.
6. Landoll, L. M. *J. Polym. Sci., Polym. Chem. Ed.* **1982**, *20*, 443.
7. Evani, S. U.S. Patent 4 432 881, 1984.
8. Emmons, W. D. U.S. Patent 4 079 028, 1978.
9. Emmons, W. D.; Stevens, T. E. U.S. Patent 4 155 892, 1979.
10. Hoy, K. L.; Hoy, R. C. U.S. Patent 4 426 485, 1984.
11. Dehm, D. C.; Hoy, K. L.; Hoy, R. C. U.S. Patent 4 496 708, 1985.
12. Landoll, L. M. U.S. Patent 4 304 902, 1981.
13. Valint, P. L., Jr.; Bock, J. *Polym. Mater. Sci. Eng. Prepr.* **1986**, *55*, 361.
14. Bock, J.; Valint, P. L., Jr. *Polym. Mater. Sci. Eng. Prepr.* **1986**, *55*, 355.
15. Garcia-Rubio, L. H.; Ro, N.; Patel, R. *Macromolecules* **1984**, *17*, 1998.
16. Garcia-Rubio, L. H.; Ro, N. *Can. J. Chem.* **1985**, *63*, 253.
17. Brown, R. G.; Glass, J. E. J. *Polym. Mater. Sci. Eng. Prepr.* **1986**, *54*, 690.

Structure and Properties of Hydrophobically Associating Polymers

Jan Bock, D. B. Siano, P. L. Valint, Jr.[1], and S. J. Pace

Exxon Research and Engineering Company, Clinton Township, Route 22 East, Annandale, NJ 08801

Hydrophobically associating polymers are synthetically derived water-soluble polymers containing a small number of oil-soluble or hydrophobic groups. In aqueous solution, hydrophobic associations can dominate polymer conformation and, in turn, solution rheological properties. We have studied a series of copolymers of acrylamide and N-substituted alkylacrylamides and terpolymers that contain anionically charged carboxyl groups to define the relationships between polymer structure and solution properties. Intrinsic viscosity and Huggins interaction coefficients provided information on the conformation and intramolecular aggregation behavior of these polymers in dilute solution. Viscoelastic properties above the polymer overlap concentration provided a measure of intermolecular interactions. These rheological properties were studied as functions of polymer composition, molecular weight, and solvent quality to observe the structure–property relationships in hydrophobically associating polymers.

T HE RHEOLOGICAL PROPERTIES OF WATER-BASED FLUIDS can be controlled with hydrophobically associating polymers. *Hydrophobically associating polymers* are synthetically derived, water-soluble polymers that contain a small number of oil-soluble or hydrophobic groups. When these polymers are dissolved in aqueous solution, the hydrophobic groups aggregate to minimize their exposure to water, in a fashion analogous to that of surfactants

[1]Current address: Bausch & Lomb, 1400 North Goodman Street, Rochester, NY 14692

above the critical micelle concentration. The influence of this association on the rheological properties of water-based fluids is studied in this chapter.

The nature of hydrophobic interactions and their effects on the structure and properties of water have been extensively studied, particularly for small molecules (*1–3*). In contrast, the introduction of hydrophobic associations into synthetic water-soluble polymers to control solution rheology has received rather limited and recent study (*4–7*). To better understand the relationships between polymer structure and solution properties, we have synthesized and characterized a series of copolymers of acrylamide and *N*-substituted alkylacrylamides and terpolymers containing anionically charged carboxyl groups. Solution properties of these systems have been obtained in both the dilute and semidilute concentration regime, to probe the influence of intra- and intermolecular interactions. In addition, the influence of the shear field and solvent quality on the associations was studied.

Experimental Details

Polymer Synthesis.   Copolymers of alkylacrylamide (R) and acrylamide (AM), which we called RAM, were prepared with a micellar polymerization technique (*4*). A micellar surfactant solution was used to disperse the hydrophobic alkylacrylamide monomer into an aqueous phase that contained acrylamide. The monomers were polymerized with a standard free-radical initiator (e.g., potassium persulfate) or a redox initiator to yield the desired random copolymer. Varied temperature and initiator concentrations were used to provide polymers of different molecular weights. Polymerizations were taken to essentially complete conversion. Compositions, in terms of hydrophobe level reported in this chapter, were based on amounts charged to the reactor. Further details on the synthesis and structure of these RAM polymers

$n = 3 - 11$ $R = i\text{-}C_3H_7 - n\text{-}C_8H_{17}$ $m + n = 5, 6, 9$ $R = C_2H_5, C_4H_9$
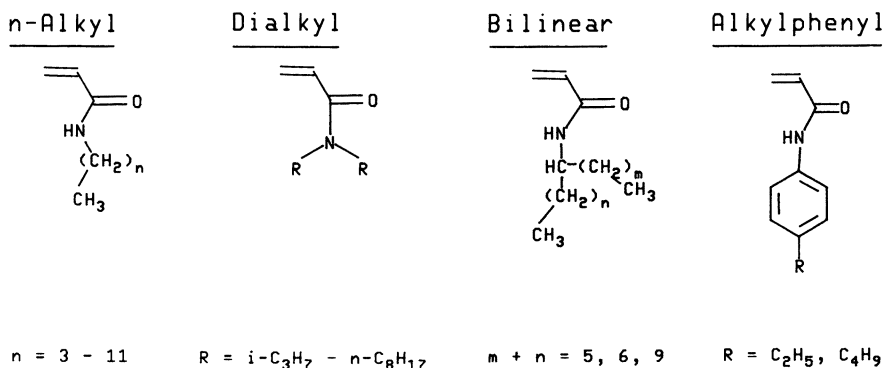
Chart I. Hydrophobe monomer structures.

can be found elsewhere (5). A series of different hydrophobic monomers (*see* Chart I) were synthesized to explore the effect of monomer structure on solution properties.

To impart ionic charge onto the polymer molecule, a controlled level of hydrolysis (*H*) was achieved under base (sodium hydroxide)-catalyzed conditions at elevated temperature (e.g., 50 BC). The amount of base, temperature, and reaction time were used to regulate the level of carboxyl groups in the resulting terpolymers, which we called HRAM.

Characterization.   Polymer composition was determined by a variety of classical analytical techniques that included elemental analysis and NMR. The carboxyl content of the polymers was determined by potentiometric titration following conversion to the acid form with an ion-exchange column. Analysis of the sodium content in the polymers gave carboxyl values within a few percent of those found by the titration technique. The number of hydrophobic groups in the polymers in this study was too low to allow quantification by conventional analytical techniques. The levels cited in this chapter refer to amounts added to the reactor and complete incorporation into the polymer was assumed. A recent study (8) using a UV spectroscopic technique on model hydrophobic monomers indicated that this was a fairly good assumption.

The molecular weights of many of the polymers used in this study were determined by either a classical laser light-scattering (LLS) technique or by a sedimentation–LLS technique (8, 9) that also provided information about the molecular weight distribution. A multiangle LLS apparatus (Dawn model B, Wyatt Technology) was used to determine the scattered light intensity at 15 angles simultaneously. Molecular weights were determined by performing a Zimm analysis of the data with the software supplied by the manufacturer.

Solution Rheology.   Polymers were hydrated in distilled, filtered water and were agitated gently until dissolution was complete. To prepare polymer solutions containing salt, concentrated sodium chloride solutions were added to polymer previously dissolved in distilled water. An alternative procedure was used to evaluate the effect of salinity on solution rheology. Solid sodium chloride was slowly added to various concentrations of polymer in solution. To ensure complete dissolution, the solutions were allowed to equilibrate for approximately 24 h before viscometric measurements were obtained. Turbidity measurements were made with a turbidimeter (Hach) on 1500-ppm solutions in 3% NaCl and 0.3% $CaCl_2$ brine, which we called 3.3% brine.

Low-shear-rate solution viscosity was measured on a Couette-type rheometer (Contraves LS 30) with a No. 1 bob and cup. The viscosity–shear rate profile was determined from 10^{-2} to 10^2 s^{-1} at 25 BC. The system was allowed to reach steady state at each shear rate before the measured viscosity was recorded.

Dilute solution viscosities used for determining the intrinsic viscosity of the polymer systems in 2.0 wt % NaCl were obtained in a capillary viscometer (Ubbelohde) by using standard methods (10, 11). Some of the measurements were obtained from an automatic capillary viscometer (Schott AVS/G). A conventional Huggins relationship (11) in which reduced viscosity is a linear function of polymer concentration was used to fit the data. A regression analysis was used to yield the intrinsic viscosity (the intercept) and the Huggins interaction coefficient, K_h, (the slope divided by the square of the intrinsic viscosity).

It was assumed that the solutions were Newtonian at the shear rates in the capillary. This assumption was assessed with Couette viscometer measurements of these dilute solutions over a range of shear rates and was reasonable. Deviations were found for solutions at the higher concentrations, as indicated by negative departure from linearity of the reduced-viscosity–concentration plots; these values were not used for intrinsic viscosity and Huggins constant determination.

Another issue was the applicability of this approach to characterize the dilute-solution properties of associating polymers. Reduced viscosity is a linear function of the polymer concentration at low concentrations for the systems in this study, so the use of a Huggins-type relationship is justified.

Results and Discussion

Dilute Solution Properties.   The rheology of dilute polymer solutions has been used extensively to gain insight into the structure and conformation of polymers in solution (11). The intrinsic viscosity provides a measure of the molecular weight of a polymer through a relationship such as the Mark–Houwink–Sakurada equation. Earlier studies of polyacrylamide (PAM) systems and details of the complexity of the characterization of high-molecular-weight water-soluble systems can be found in references 9, 13, and 14.

To explore the influence of hydrophobe structure and content, a reference PAM was prepared that had a weight-average molecular weight of 3×10^6 g/mol and an intrinsic viscosity of 7.3 dL/g (Table I). These values agreed with the Mark–Houwink parameters found for PAMs synthesized by other techniques (13). With data obtained from a large variety of PAM samples studied in water at 25 °C, Kulicke et al. (13) proposed the following relationship:

$$[\eta] = 1.0 \times 10^{-4} \times MW\ 0.755 \tag{1}$$

where $[\eta]$ is the intrinsic viscosity in dL/g and MW is the viscosity average molecular weight.

The molecular weight and intrinsic viscosity for our PAM sample was also consistent with the other Mark–Houwink relationships for PAM in water containing various levels of salt (13). Thus, the presence of salt in the water did not appear to affect the measured intrinsic viscosity or molecular weight (determined by light scattering) of PAM polymers. This observation is reasonable because, in solution, PAM behaves as an uncharged random-coil polymer.

Table I. Polymer Systems and Solution Properties

Polymer Class	Hydrophobe Type	Hydrophobe Level (mol %)	Charge (mol %)	MW[a] (× 10⁶)	Intrinsic Viscosity[b] (dL/g)	K_h^c
PAM			0.4	2.9[d]	7.3	0.4
HPAM			24	0.49	2.4	0.32
HPAM			20	3.0	9.9	0.45
HPAM			18	5.8	12.3	0.46
RAM	n-C₈	1.0	0.3	3.0[d]	3.4	2.5
HRAM	n-C₈	1.0	18		2.0	0.92
HRAM	n-C₈	1.0	18	3.2[d]	7.6	1.10
HRAM	n-C₈	1.0	18		8.4	1.94
HRAM	n-C₈	1.25	15	2.9[d]	5.4	1.80

[a]Laser light scattering (LLS).
[b]2% NaCl.
[c]K_h is the Huggins interaction coefficient.
[d]Sedimentation–LLS.

A reference partially hydrolyzed polyacrylamide (HPAM) was prepared by controlled hydrolysis of the PAM polymer just described. The HPAM had essentially the same molecular weight (3.0 vs. 2.9 × 10⁶ g/mol) as the precursor PAM; this finding indicated that no breakdown or cross-linking occurred during the hydrolysis reaction. A higher intrinsic viscosity was obtained for the HPAM polymer relative to the precursor PAM (9.9 vs. 7.3 dL/g). This result agreed with other studies of anionically charged polyacrylamides (15). In addition, two other HPAMs of different molecular weights were prepared and characterized as shown in Table I.

The introduction of hydrophobic groups into a water-soluble polymer complicates the dilute-solution viscometrics. As shown in Table I and Figure 1, the intrinsic viscosities of both the RAM and HRAM polymers tended to decrease, and the Huggins constants increased as the amount of hydrophobe on the polymer increased. The effect was more pronounced beyond a certain level of hydrophobe that seemed to depend on the amount of charge in the polymer. As shown in Figure 1, HRAM polymers containing approximately 18 mol % carboxyl groups required a higher hydrophobe content to exhibit changes in dilute solution properties relative to uncharged RAM polymers. One explanation of this behavior that is consistent with these observations is that for polymers containing random hydrophobic functionality in the dilute concentration regime, intramolecular associations cause a contraction of the coil in solution and result in a decrease in intrinsic viscosity. The increase in the Huggins constant indicates a decrease in solvent quality with increasing hydrophobe content. Thus, a Huggins constant greater than the usual 0.3–0.8 for conventional polymers (16, 17), appears to be a good indicator of hydrophobic associations. These observations are consistent with
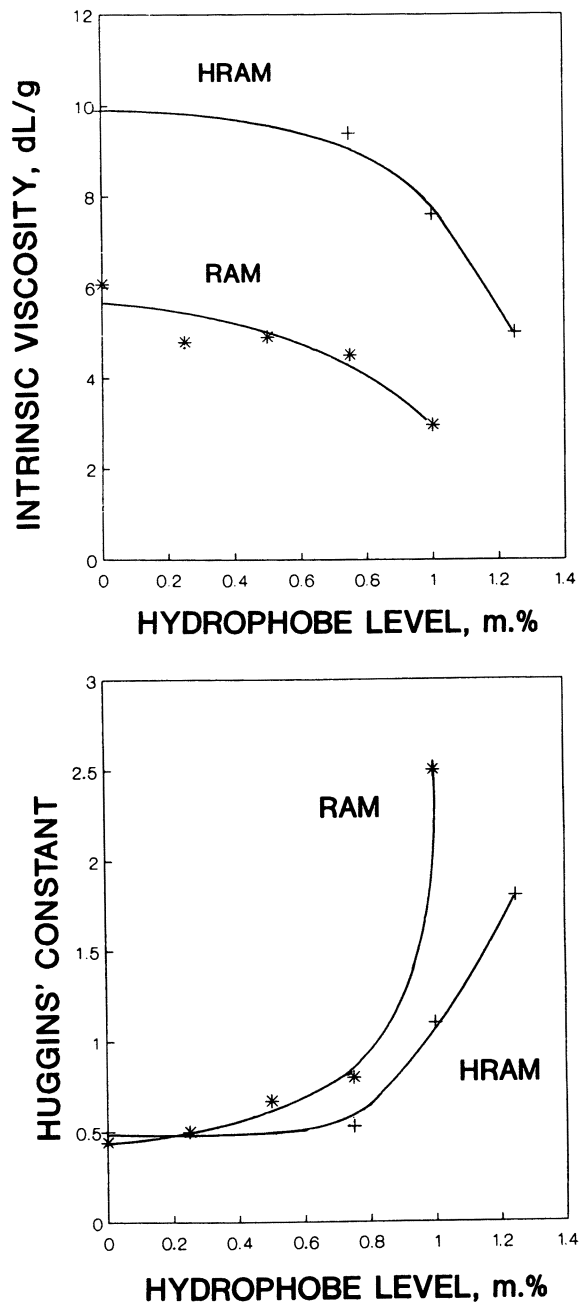
Figure 1. Dilute solution viscometrics in 2.0 wt % NaCl. Hydrophobe monomer is N-n-octylacrylamide. Hydrolysis level of HRAM polymers is 18 mol %.

the dilute-solution behavior of ionomers (hydrocarbon-soluble polymers containing a small number of ionic groups) in a hydrocarbon solvent (*18*).

The presence of charge in the form of anionic acrylate functionality on the polymer had an opposite effect to that of hydrophobic functionality. Increasing the amount of sodium acrylate groups on the polymer increased the intrinsic viscosity and reduced the Huggins constant for a given hydrophobe level. The acrylate functionality seemed to improve the solvent quality and opened the polymer coil in dilute solution. The solubility characteristics and associative properties of these polymers can be modulated because charged groups and hydrophobic groups have opposite effects.

Another way to modulate the properties of water-soluble polymers is to change the solvent quality by adding salt. As shown in Figure 2, the intrinsic viscosity decreased and the Huggins constant increased with increasing ionic strength or salt level for a series of HRAM polymers with about 18 mol % sodium acrylate and varying *N-n*-octylacrylamide content. As the hydrophobe content increased, the influence of salinity in the water became stronger, and there appeared to be a critical hydrophobe level required to cause a change in intrinsic viscosity and Huggins constant. As before, the Huggins constant appeared to be a sensitive indicator of the presence of hydrophobe on the polymer. If the Huggins constant is an indication of associative effects, then these interactions are present even in dilute solution where nonassociating polymer molecules are believed to be isolated and acting independently. The addition of salt to the solution enhanced the associations, which may have been predominantly intramolecular, in this concentration regime. A study of the structure and conformation of these hydrophobe-containing molecules in dilute solution could be performed with a scattering probe and would be useful in interpreting the macroscopic rheological information.

Semidilute Viscometrics.

Solution viscometrics at concentrations above the overlap concentration (C^*) indicated dramatic effects caused by the associative nature of the hydrophobic groups in the polymer. As shown by the reduced viscosity–concentration profiles of Figure 3, the introduction of only 1.0 mol % *N-n*-octylacrylamide to polyacrylamide can increase the viscosification efficiency dramatically. Increasing the hydrophobe level to 1.25 mol % further increased solution viscosity. At 2000 ppm, the presence of the hydrophobe caused a greater that 10-fold increase in viscosity. This result was in contrast to the behavior of these polymers in dilute solution (*see* the box in Figure 3). The presence of hydrophobic functionality on the polymer resulted in a decrease in the reduced viscosity at concentrations below C^*. In dilute solution, intramolecular hydrophobic associations decreased the hydrodynamic radii of the polymer coils and thus reduced the
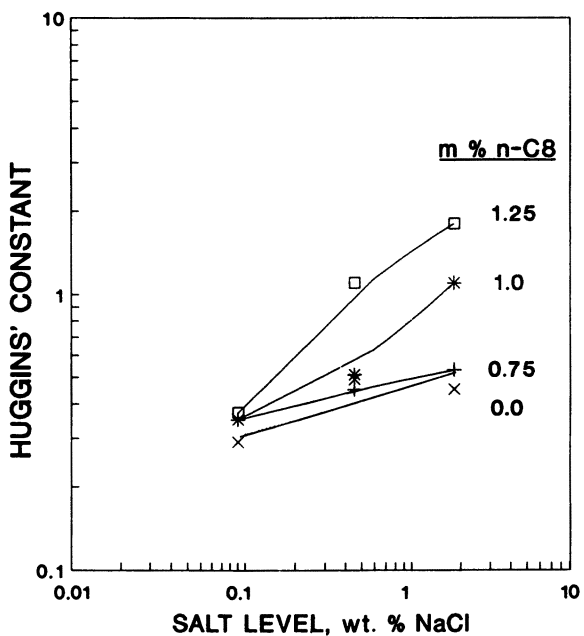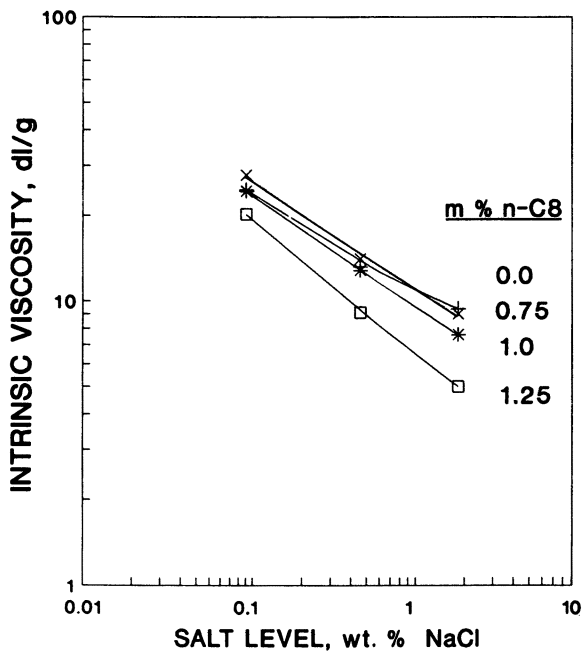
Figure 2. Dilute solution viscometrics. Hydrophobe monomer is N-n-octyl-acrylamide. Hydrolysis level is 18 mol %.
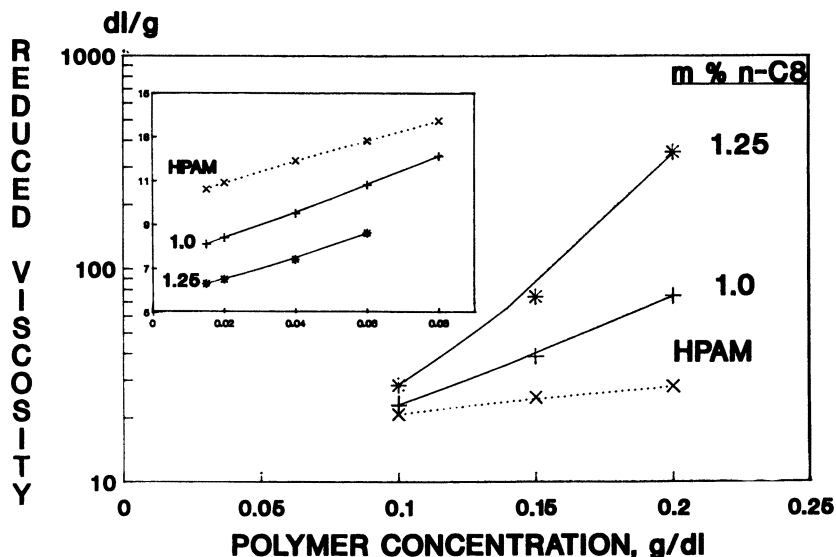
Figure 3. Solution viscometrics. Solvent is 2.0 wt % NaCl, hydrophobe monomer is N-n-octylacrylamide. Hydrolysis level is 18 mol %.

viscosity. Above C^*, intermolecular associations increased the resistance to flow or solution viscosity. This behavior indicates an increase in the hydrodynamic radii of the coils caused by intermolecular associations.

Generally, hydrodynamic radii of polymer coils in solution have been controlled by controlling polymer molecular weight. To study this parameter, different molecular weight HRAM polymers containing 1.0 mol % *N-n*-octylacrylamide and 18 mol % sodium acrylate were prepared. Viscosity at 1.3 s^{-1} shear rate was determined as a function of polymer concentration on solutions of these polymers in 2% NaCl. As shown in Figure 4, polymers with higher intrinsic viscosities, which corresponded to higher molecular weight, exhibited higher solution viscosity at a given polymer concentration.

Although hydrophobic associations contributed to the viscosification efficiency, the molecular weight of the polymer was an important structural parameter for solution viscosity control. Quantification of these relationships would be useful in polymer design. One approach would involve testing the validity of conventional scaling laws (*19*) to describe the dependence of the zero-shear viscosity of hydrophobically associating polymers on concentration and molecular weight, but data covering a broader range of these variables would be needed.

A further complication to understanding the rheology of hydrophobically associating polymers is their unique response to shear rate and solvent quality (e.g., salt content). As shown in Figures 5 and 6, the viscosity can be independent (Newtonian), decrease (pseudoplastic), or even increase (dilatant)
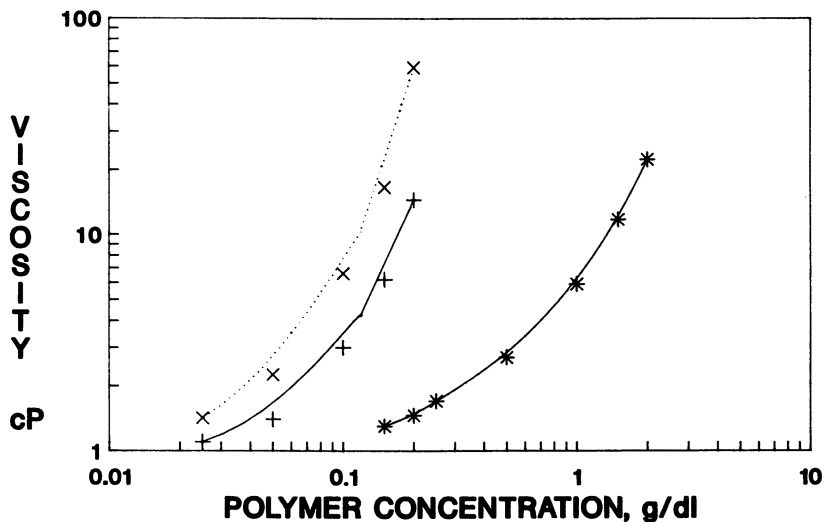
Figure 4. Effect of molecular weight on the concentration dependence of viscosity at 1.3 s⁻¹. Solvent is 2.0 wt % NaCl. Hydrophobe monomer is 1.0 mol % N-n-octylacrylamide. Hydrolysis level is 18 mol %. Intrinsic viscosity (dL/g): *, 2.0; v, 7.6; x, 8.4.
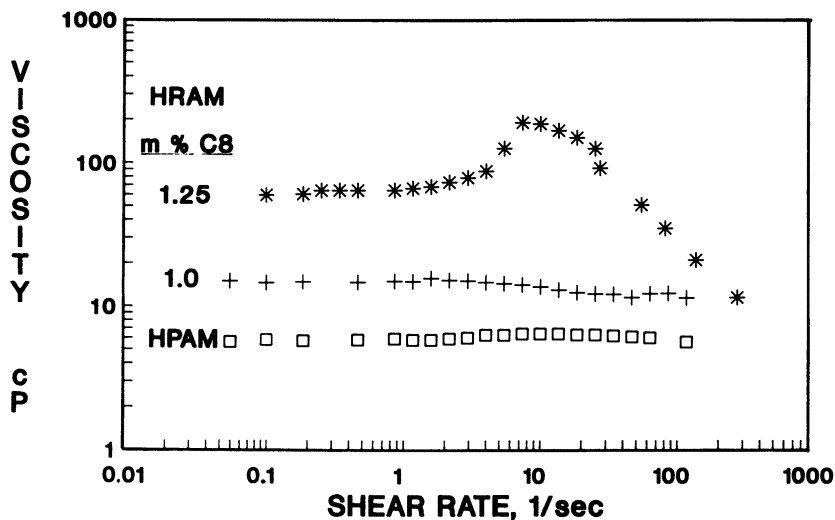
Figure 5. Effect of hydrophobe level on the shear rate dependence of viscosity. Solvent is 2.0 wt % NaCl. Hydrophobe monomer is N-n-octylacrylamide. Hydrolysis level is 18 mol %. Polymer concentration is 2000 ppm.
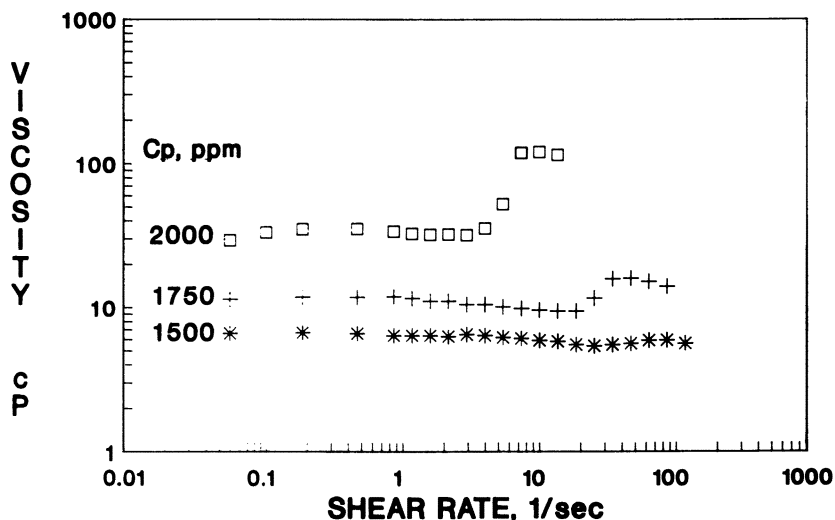
Figure 6. Effect of polymer concentration on the shear rate dependence of viscosity. Solvent is 3.3 % brine. Hydrophobe monomer is 1.24 mol % N-n-octylacrylamide, hydrolysis level is 18 mol %.

with shear rate depending on the level and type of hydrophobe, polymer concentration, solvent quality, and shear rate. As the hydrophobe level and polymer concentration increase beyond a critical value, a shear rate region in which viscosity increases with shear is observed. Below and above this shear rate region, the viscosity behaves quite normally, with shear, and the time required to reach a steady state or equilibrium is relatively short. However, within the boundaries of the shear regime for shear thickening, polymer relaxation times increase significantly. An explanation of the molecular behavior of the system for shear thickening involves a change in the relative amount of intra- and intermolecular associations with shear. As the polymer chains are extended under a shear field, the number of intermolecular associations increase, which results in enhanced viscosity. This theory has been used to explain the shear-thickening behavior of ionically associating polymers in hydrocarbon solvents (20).

The response of solution viscosity to the ionic strength or salt content of the solvent (e.g., water) also depends on polymer concentration and hydrophobe level (Figure 7). At concentrations above the overlap concentration, hydrophobically associating polymers appear to be less sensitive to salinity than nonassociating polymers of comparable molecular weights and ionic charges. Increasing the salt concentration appeared to enhance the hydrophobe associations and thus reduce the effect of polymer chain collapse caused by shielding of the ionic charge on the polymer. Further study is needed to quantify the effects of ionic strength on both the nature of hydrophobe aggregation behavior and chain expansion due to the ionic groups.
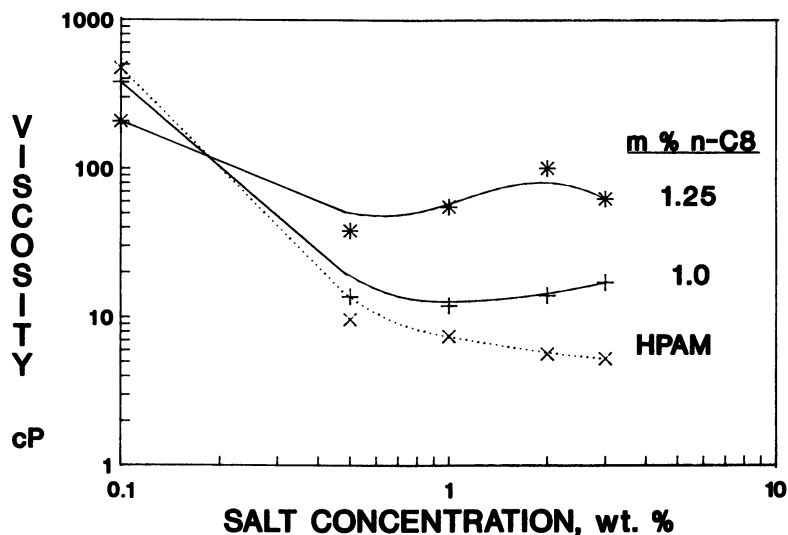
Figure 7. *Effect of salt on viscosity at 1.3 s⁻¹, 2000 ppm of polymer, 18 mol % charge.*

This study was performed on hydrophobically associating polymers that contained the *N-n*-octylacrylamide functionality. Other hydrophobe structures that have been studied are shown in Chart I. The length of the hydrophobe group, the nature of hydrophobe branching, and the presence of a phenyl group can have a significant effect on polymer properties. Figure 8 shows the effect of hydrophobe structure on solution viscosity as a function of hydrophobe content in the polymer. Increasing hydrophobe chain length and total hydrocarbon in the hydrophobic group resulted in an increase in solution viscosity at high hydrophobe content. In addition, the presence of a phenyl group in the hydrophobe significantly increased solution viscosity.

Conclusions

Hydrophobic associations can dominate polymer conformation in solution and solution rheological properties. Intrinsic viscosity and Huggins interaction coefficients provided information on the conformation and intramolecular aggregation behavior of these polymers in dilute solution. The presence of hydrophobic associations caused a decrease in the intrinsic viscosity and an increase in the Huggins constant. These effects could be counterbalanced by increasing the ionic charge on the polymer through hydrolysis or by copolymerization with sodium acrylate.

Viscoelastic properties of hydrophobically associating polymers were significantly affected above the overlap concentration. Increased hydrophobe
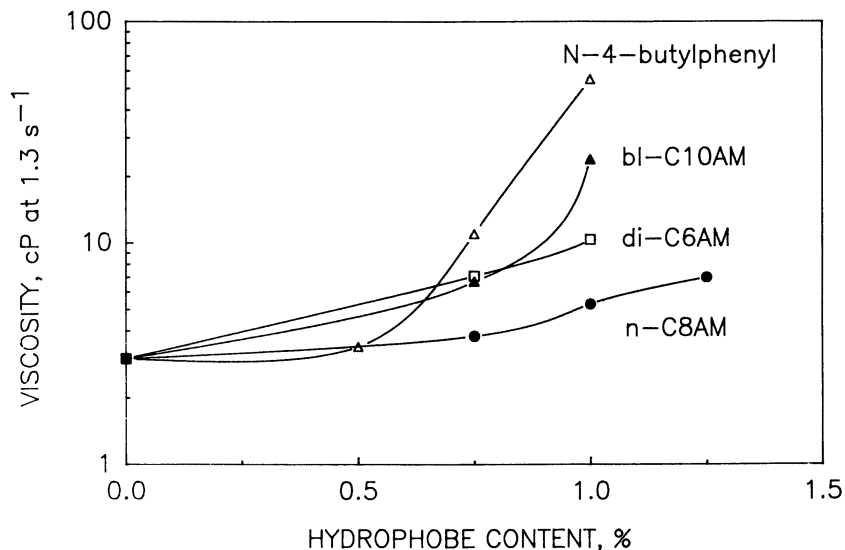
Figure 8. Dependence of solution viscosity on hydrophobe level for different hydrophobe structures.

content and chain length resulted in enhanced viscosification and increased dependence of polymer concentration on viscosity. Two unique aspects of the rheology of hydrophobically associating polymers were observed: shear thickening and reduced salt sensitivity. These phenomena are believed to be caused by the relative amounts of intra- and intermolecular associations of the polymer in solution. Polymer structural parameters, such as composition and molecular weight, strongly influenced the nature of the associations and, in turn, the solution's rheological properties. In addition, the solvent quality (e.g, salinity) and shear field also affected the associations and properties. Further work will be needed to develop quantitative scaling relationships and better definition of the conformation of these polymers in solution.

Acknowledgments

We thank S. R. Turner, J. Wagonsommer, and J. Ogletree for ably synthesizing the polymers and E. Habeeb for careful characterization of the rheological properties.

References

1. Franks, F. *Water: A Comprehensive Treatise*, Vol. 4; Franks, F., Ed.; Plenum: New York, 1975.

2. Ben-Naim, A. *Hydrophobic Interactions*; Plenum: New York, 1980.
3. Tanford, C. *The Hydrophobic Effect: Formation of Micelles and Biological Membranes*; Wiley Interscience: New York, 1973.
4. Bock, J.; Siano, D. B.; Schulz, D. N.; Turner, S. R.; Valint, P. L.; Pace, S. J. *Polym. Mater. Sci. Eng.* **1986,** 55, 355.
5. Turner, S. R.; Siano, D. B.; Bock, J. U.S. Patents 4 528 348, 4 520 182, and 4 521 580, 1985.
6. Schulz, D. N.; Maurer, J. J.; Bock, J. U.S. Patents 4 463 151 and 4 463 152, 1984.
7. Valint, P. L.; Bock, J. *Polym. Mater. Sci. Eng.* **1986,** 55, 361; U.S. Patents 4 492 785 and 4 548 735, 1985; *Macromolecules* **1988,** 21, 175.
8. Valint, P. L.; Bock, J.; Schulz, D. N. *Polym. Mater. Sci. Eng.* **1987,** 57, 482.
9. Holzwarth, G. M.; Soni, L.; Schulz, D. N.; Bock, J. Presented at the 192nd National Meeting of the American Chemical Society, Anaheim, CA, September 7–12, 1986; paper PMSE 106.
10. Whorlow, R. H. *Rheological Techniques*; Halsted: New York, 1980.
11. Van Wazer, J. R.; Lyons, J. W.; Kim, K. Y.; Colwell, R. E. *Viscosity and Flow Measurement*; Wiley Interscience: New York, 1963.
12. Flory, P. J. *Principles of Polymer Chemistry*; Cornell University Press: Ithaca, 1953; p 635.
13. Kulicke, W. M.; Kniewske, R.; Klein, J. *Prog. Polym. Sci.* **1982,** 8, 373–468.
14. Klein, J.; Conrad, K. D. *Makromol. Chem.* **1980,** 181, 227–240.
15. Kulicke, W. M.; Horl, H. H. *Coll. Polym. Sci.* **1985,** 263, 530–540.
16. Molyneux, P. *Water-Soluble Synthetic Polymers: Properties and Behavior*; CRC Press: Boca Raton, 1985; Vols. I and II.
17. *Polymer Handbook*; Brandrup, J.; Immergut, E. H., Eds.; Wiley Interscience: New York, 1975; pp iv–19.
18. Lundberg, R. D.; Phillips, R. R. *J. Polym. Sci., Polym. Phys. Ed.* **1982,** 20, 1143.
19. DeGennes, P.-G. *Scaling Concepts in Polymer Physics*; Cornell University Press: Ithaca, 1979.
20. Witten, T. A.; Cohen, M. H. *Macromolecules* **1985,** 18, 1915.

Fluorescence and Light Scattering from Water-Soluble Hydrophobically Associating Polymers

D. B. Siano[1], Jan Bock[2], P. Myer[1], and P. L. Valint, Jr.[2,3]

[1]Exxon Chemical Company, Linden, NJ 07036
[2]Exxon Research and Engineering Company, Clinton Township, Route 22 East, Annandale, NJ 08801

Light scattering and fluorescence of dye bound to water-soluble hydrophobically associating polymers of acrylamide and alkylacrylamide were used to elucidate the properties of the polymers in dilute aqueous solutions where they show enhanced viscosification efficiency. The shift of the emission wavelength of fluorescence of the ammonium salt of 8-anilino-1-naphthalenesulfonic acid and its polarization as a function of polymer concentration showed unequivocally the presence of regions of lowered polarity and increased microviscosity in the copolymers, and appeared to give evidence of intrapolymer hydrophobic regions at polymer concentrations well below the threshold overlap concentration. The light-scattering data were compared to a simple singlet–doublet association model to give an estimate for the association constant as a function of the amount of incorporated hydrophobe.

HYDROPHOBICALLY ASSOCIATING WATER-SOLUBLE COPOLYMERS of acrylamide and an alkylacrylamide, such as octyl- or dodecylacrylamide, need contain only a small mole fraction of the alkylacrylamide in order for their properties to be dramatically altered from the properties of the homopolymer (*1*). For example, the inclusion of only 1 mol % of octylacrylamide in a

[3]Current address: Bausch & Lomb, 1400 North Goodman Street, Rochester, NY 14692

copolymer with acrylamide can lead to a substantial increase in the dilute solution viscosity (2). The increase in viscosity in hydrophobically associating polymers is large enough to be of some technological interest in such applications as enhanced oil recovery and paint formulations, and has been explored by a number of investigators recently (3–7). The increase in viscosity is presumed to occur because of the increased effective hydrodynamic volume of the polymer chains, which is a result of the interchain associations that may occur even at relatively low polymer concentrations. This assumption is inferred from the increased values of the Huggins coefficient that are measured—values as high as 2 or 3 may be observed (8).

A more complete understanding of the nature of the associations, however, by means other than simple viscosity measurements is of interest. Because of the low concentration of the associating groups, few techniques are available to provide more direct information. The quantities of most interest for modeling the phenomenon, naturally, are such things as the aggregation number; critical micelle concentration for the associating groups; and the association constants as functions of copolymer composition, temperature, and polymer concentration. This chapter will describe two methods, light scattering and fluorescence of bound dye, that were carried out in an attempt to arrive at a more complete picture of the behavior of these interesting and potentially technologically important molecules.

Experimental Details

The copolymers of acrylamide and alkylacrylamide were prepared according to a micellar process in which sodium dodecyl sulfate was used to solubilize the water-insoluble monomer to enable copolymerization with the water-soluble monomer to occur (1). The mixture before the polymerization was clear and free of any emulsion particles or undispersed monomer. Potassium persulfate was used to initiate polymerization, which was taken to complete conversion at 50 °C for 24 h. The polymers were purified from the surfactant by acetone precipitation–redissolution and then dried in a vacuum oven at 25 °C. The amount of hydrophobe actually incorporated was taken to be equal to that used in the polymerization.

Steady-state fluorescence measurements were made on a Perkin-Elmer model 650-40 fluorimeter with a polarization attachment. The dye used was the ammonium salt of 8-anilino-1-naphthalenesulfonic acid (ANS) from Aldrich. The polymer stock solutions were prepared at a concentration of 5000 ppm in 2 wt % NaCl (results were substantially unchanged in the absence of salt) about 1 week before measurements were made. A concentrated solution of ANS was added to the stock polymer solution to give an ANS concentration of 10^{-5} M and a polymer concentration of 4550 ppm. Serial dilutions of this solution were made by the successive additions of 2 wt % NaCl and 10^{-5} M ANS or of 2 wt % NaCl according to whether the ANS concentration or the ANS–polymer ratio was to be held fixed. The solutions thermostatted at 25 °C were excited at 377 nm with a slit width of 5 nm, and measurements were integrated for 10 s to increase the signal-to-noise ratio. The polarization and intensities were corrected for the background measured on corresponding solutions of polymer in the absence of dye. A minimum of three measurements were taken, and the results were averaged.

Light-scattering measurements were carried out with a Brice-Phoenix duophotometer with a cylindrical cell having flat entrance and exit windows, thermostatted at 25 °C. The stock solutions were prepared at 2000 ppm in 2 wt % NaCl and clarified by centrifugation at 6000 rpm for 2 h. The solutions were transferred into the light-scattering cell by pipette. The solutions were checked for fluorescence and changes in concentration, but no significant changes were found. Because only unhydrolyzed, nonionic polymers were measured (less than about 0.2 % hydrolysis was measured), the polymer solutions were not dialyzed against the solvent. The wavelength of light used was 436 nm, and it was unpolarized. Alignment of the cell was carefully checked by measurements of dilute solutions of Ludox colloidal silica (Du Pont), and the light-scattering volume was determined by measurement of intensity of fluorescence from dilute fluorescein solutions (9).

Measurements of the specific refractive index increment (dn/dc) were made with a differential refractometer (C. N. Wood Manufacturing Company, model RF-600). The values found were uncorrelated with the amount of hydrophobe in the polymer, and the average found of 0.166 ± 0.01 mL/g was used in the analysis of the light-scattering data.

Results and Discussion

Fluorescence. ANS is an amphoteric molecule that binds selectively at the boundary between aqueous and hydrophobic regions (10). When binding occurs, the fluorescence spectrum changes dramatically from that exhibited by the dye in an aqueous environment. When excited at 377 nm, the single broad band that has an emission peak at 520 nm in water (or 2% NaCl) can shift to a wavelength as low as 462 nm when the dye is in a hydrophobic region. Simultaneously, the intensity of the fluorescence may increase as much as 2 orders of magnitude. These two quantities are measures of the dielectric constant or polarity of the dye environment.

The local viscosity of the dye-binding region may also be roughly measured (11, 12) by determining the polarization (P) of fluorescence of the dye. In water or 2 % NaCl this polarization has a value of about 0.12, and it has a maximum value in a very viscous or rigid environment of about 0.45. Because ANS is a small molecule, in dilute or semidilute polymer solutions in which no binding occurs, P is found to be independent of the macroscopically measured viscosity. A value of P markedly greater than 0.12, a wavelength shift, or both implies that a significant fraction of the dye has bound to the polymer.

One experiment using this technique is illustrated in Figure 1. This figure shows a comparison of the results using ANS at a constant concentration of 10^{-5} M as the polymer concentration varied from 0.5 wt % down to 0.01 wt %. Two polymers were used: a homopolymer of acrylamide and a copolymer of acrylamide with dodecylacrylamide having a mole ratio of 99:1. The interpretation of the results for the homopolymer case is straightforward: the shift in wavelength of the excitation peak from the 520 nm found for the dye is negligible over the entire concentration range of the polymer. Likewise, the polarization of the ANS did not differ from that obtained in
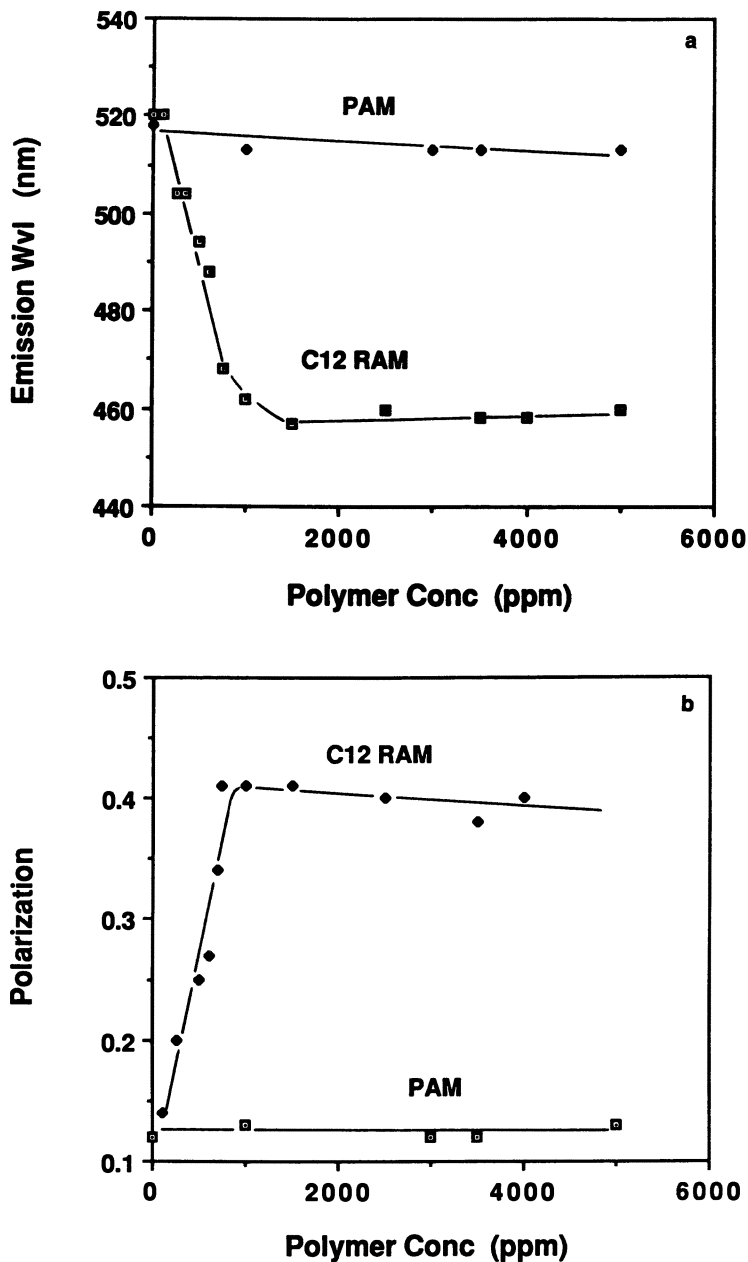
Figure 1. a, The emission wavelength for the fluorescence of 10^{-5} M ANS in solutions of varying concentration of polyacrylamide (PAM) and a polyacrylamide copolymerized with 1 mol % dodecylacrylamide (C12RAM). b, The polarization of fluorescence of 10^{-5} M ANS from the same solutions of PAM and the hydrophobic copolymer with dodecylacrylamide.

the absence of polymer. Both of these results are consistent with the hypothesis that the dye does not bind to the homopolymer and is therefore presumptive evidence that no hydrophobic region or binding site for the dye exists on the polymer.

The large, constant blue shift of about 50 nm found for the dye in the presence of the hydrophobic polymer, on the other hand, shows that above a polymer concentration of about 1000 ppm, virtually all of the dye must be bound to a region having a low dielectric constant. At the same time, the very high polarization, near its theoretical maximum, implies that the dye must be in a very viscous or rigid environment. The fall-off in the polarization occurred at about the same concentration where the break in the emission wavelength was observed. As the hydrophobic polymer concentration decreased below about 1000 ppm, the properties of the fluorescence of the dye changed monotonously toward those observed for the dye in 2 wt % NaCl. Superficially, the changes in the fluorescence of the dye appear to be similar to that expected for the "micellization" of the hydrophobic groups. This monotonous change is most likely due to the increased proportion of unbound dye, but may be also confounded with changes in the properties of the presumed hydrophobic aggregates as well. Separating these two effects may be done to some extent by diluting the polymer and the dye together from a high starting concentration down to a concentration at which the fluorescence signal becomes too small to measure reliably.

An illustrative experiment of this sort is shown in Figure 2, wherein the starting polymer concentration is 4500 ppm, the ANS starting concentration was 10^{-5} M, and the dilution toward the solvent axis kept the ratio of the polymer to ANS concentration constant. Here a copolymer of acrylamide and octylacrylamide at a mole ratio of 98.75:1.25 that was hydrolyzed by base to 20% sodium acrylate was used. The results show that the emission wavelength at the highest concentration was not blue-shifted as much as in the preceding example, nor was the polarization nearly as high as the maximum attainable. Thus the aggregates in this polymer appear to have a higher polarity than in the preceding case, and their microviscosity is also less. No significant "break" was seen in either the wavelength of the emission peak or in the polarization. However, because of the smaller magnitude of the total change in these properties, the standard error of the measurements may be too high to provide a reliable indication of a break.

One other insight that these data may provide is that the wavelength of the emission maximum never attains the value that the dye would have had if it all had been solubilized in an aqueous environment. Therefore, even at the lowest polymer concentration, 100 ppm, some aggregates, presumably intramolecular (because this concentration is well below the threshold overlap concentration for this polymer), must be present.

Fluorescence measurements at a fixed concentration of copolymer (with 1 mol % of octylacrylamide) and fixed concentration of ANS as a function of
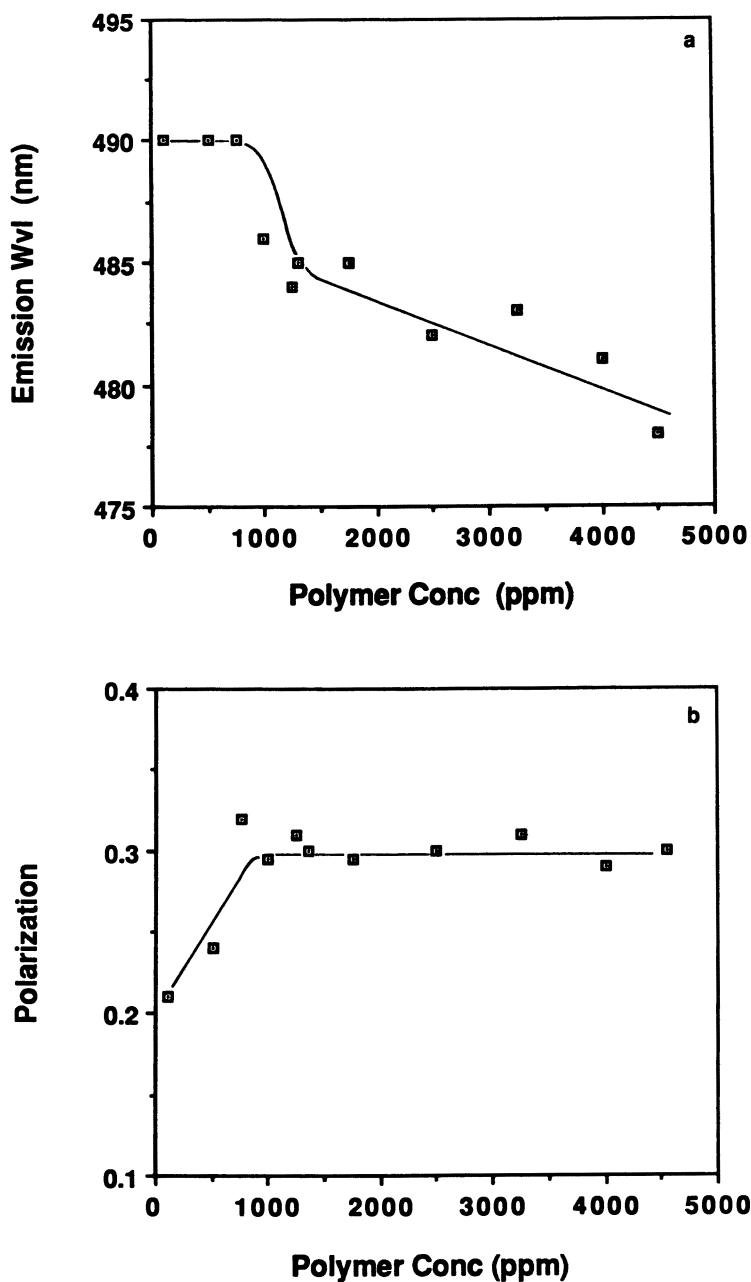
Figure 2. a, The emission wavelength for solutions with constant ANS–
copolymer concentrations. The copolymer has a mole ratio of acrylamide–
octylacrylamide of 98.75:1.25 and has been partially hydrolyzed to 20% sodium
acrylate. b, The polarization for the same solutions.

temperature are shown in Figures 3a and 3b. The results on similar solutions of homopolyacrylamide are shown for comparison. The emission wavelength shifted toward the red, and the fluorescence intensity decreased as the temperature increased for the copolymer, but no change was observed for the homopolymer. These results appear to indicate that the hydrophobic regions become less polar, there are fewer of them at higher temperatures, or both of these conditions. The effect is quite dramatic and easily measured, and it most likely indicates a decrease in the equilibrium constant for the association at higher temperatures. This decrease is in line with the increased solubility of the hydrophobic moiety with temperature. At 25 °C the measured solubility of octylacrylamide is 30 ppm, and at 50 °C it is 50 ppm.
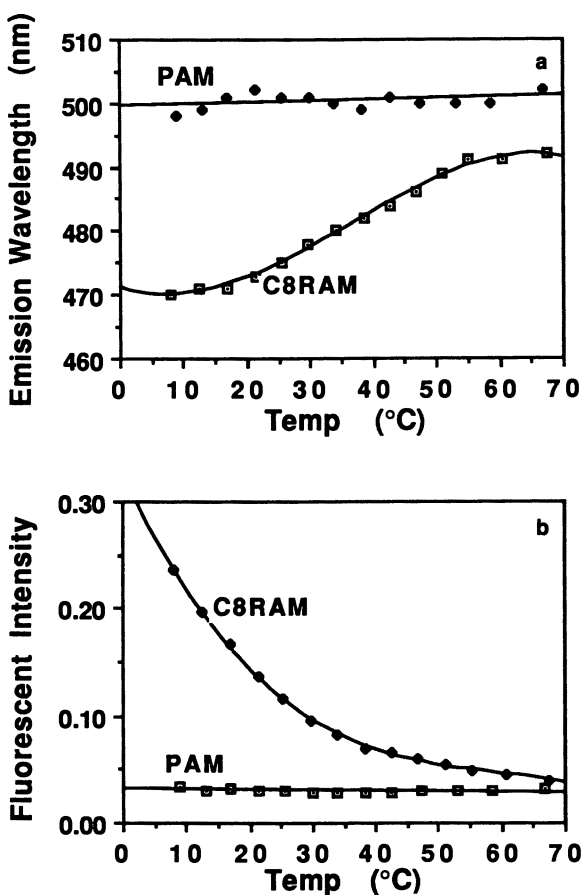
Figure 3. a, The emission wavelength from a 3000-ppm solution of PAM and from a 3000-ppm solution of a copolymer having a mole ratio of acryl-amide–octylacrylamide (C8RAM) of 99:1 as a function of temperature. b, The polarization as a function of temperature. Both solutions contained 10^{-5} M ANS.

Although these observations of the fluorescence of bound ANS provide some qualitative clues on the behavior of the associating groups, the picture is still quite incomplete. In particular, these observations provide no estimate of the magnitude of the association constant nor of the size of the presumed aggregates.

Light Scattering.   To provide more information on the properties of the aggregates, a series of light-scattering experiments was performed on a similarly prepared set of polymers in which the mole fraction of octylacrylamide in the synthesis varied between 0 and 1.0 mol %. Measurements were made in a concentration range from 2000 ppm to about 300 ppm, where the light scattered at a scattering angle of 90° was about 10 times that of the solvent. Debye plots of the results, extrapolated to a scattering angle of 0°, are shown in Figure 4. When no octylacrylamide was incorporated, the fitted line was straight, giving a second virial coefficient of 27 mL g^{-2} mol and a molecular weight of 3.6×10^6 g/mol. With increasing amounts of incorporated hydrophobe, the data clearly require a quadratic term in concentration to give a satisfactory fit. The curvature is undoubtedly a manifestation of the associations that occurred.

The molecular weight and radius of gyration for the polymers as a function of the amount of incorporated hydrophobe are shown in Figures 5 and 6. These values were obtained by fitting the Zimm plot data with an expression that is linear in $\sin^2 \theta/2$ and quadratic in polymer concentration. The weight-average molecular weight apparently increased with the amount of incorporated hydrophobe by a factor of 3 or so. This result may be interpreted as being due to the difficulty of taking reliable data at a low enough concentration to provide a reliable estimate of the single-chain, unassociated
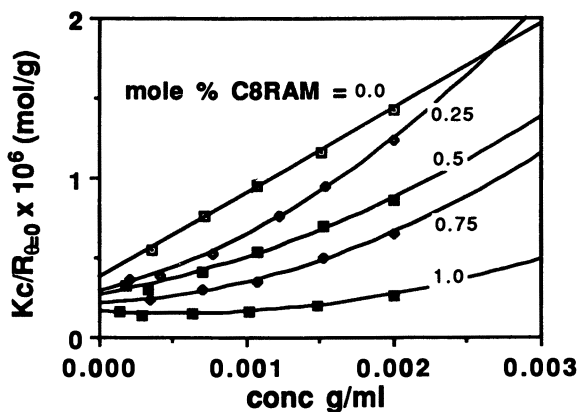
Figure 4. The Debye plots for the scattering power, extrapolated to zero scattering angle, of solutions of copolymers of acrylamide and varying amounts of incorporated octylacrylamide as a function of polymer concentration.
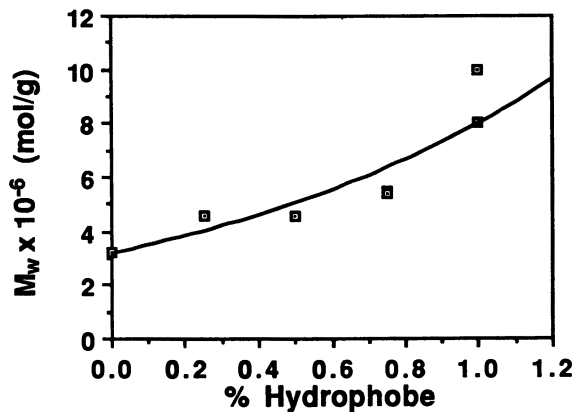
Figure 5. *The weight-average molecular weight obtained by light scattering for copolymers with varying amounts of incorporated hydrophobe.*
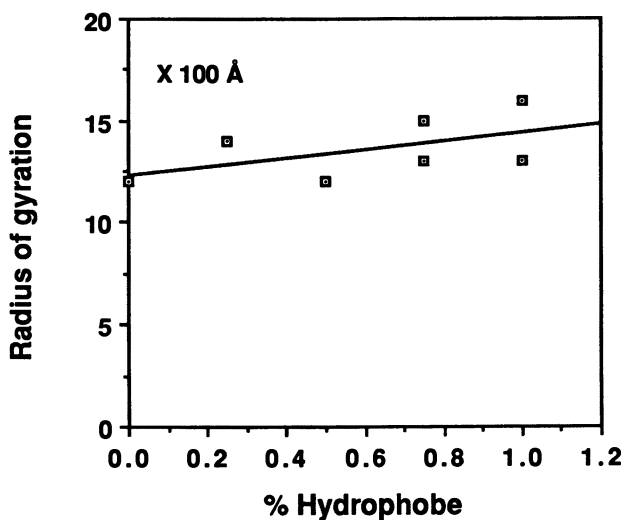
Figure 6. *The radius of gyration of the copolymers as a function of the amount of incorporated octylacrylamide.*

molecular weight. The single-chain, unassociated molecular weight would be expected to be independent of the amount of incorporated hydrophobe. The radius of gyration obtained, on the other hand, was found to be nearly independent of the amount of incorporated hydrophobe. This result means that even at 1 mol % of hydrophobe, the polymer chains were not appreciably smaller than that found for the homopolymer of acrylamide. That is, no "chain collapse" regime was seen in the composition range studied.

These observations may be compared to the behavior expected on the

basis of a simple singlet-dimer association model, which at sufficiently low concentration should be at least approximately true. This process of closed association has an association constant of $K = c_D/c_S^2$, where c_D is the concentration of doublets and c_S is the concentration of singlets in grams per milliliter. This relationship may be shown to lead to an expression for the light scattering to first order in total polymer concentration, c:

$$kcM_S/R_{\theta=0} \approx 1 + (2A_SM_S - K)c \qquad (1)$$

where the subscript S denotes the singlet species, A is the second virial coefficient, M is the weight-average molecular weight, k is an optical constant, and $R_{\theta=0}$ is the Rayleigh ratio extrapolated to a scattering angle of $0°$. The coefficient of c is seen to be linear in the singlet-dimer association constant, and larger K gives a lower slope. This result is in qualitative agreement with Figure 4. If the copolymers form a homologous series, all with the same molecular weight, M_S, and second virial coefficient, A_S, of singlet molecules, equal to the values obtained for the similarly synthesized homopolymer, then the association constant could be obtained from the linear term in the fit of the Debye plots. A plot of the coefficient of c obtained by fitting the light-scattering data with a second-order polynomial in c against the amount of incorporated hydrophobe is shown in Figure 7. This plot shows that K is monotonic (approximately linear) with the amount of incorporated hydrophobe. For the nominal case of a copolymer containing 0.75 mol % octylacrylamide, the association constant found was about 1200 mL/g. This figure is a rough estimate, at best, but appears to be reasonable. However, this simple model does not explain the apparent increase in the observed molecular weight, and therefore the simple dimer association
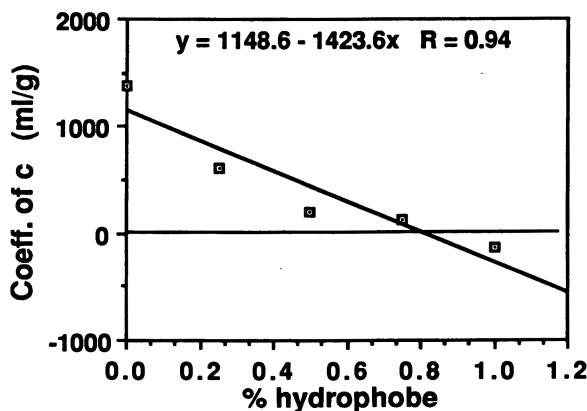
Figure 7. The coefficient of the concentration in the least-squares fit of the data of Figure 4 as a function of the amount of incorporated hydrophobe.

model is clearly inadequate to explain all of the features of the light-scattering data.

Conclusions

The light-scattering and fluorescence data on a presumably homologous series of hydrophobically associating polymers are not fully explained on the basis of a simple dimer association model in which the association between single chains (having a molecular weight independent of the amount of incorporated hydrophobe) is governed by a single association constant. The decrease in the apparent second virial coefficient with increasing amounts of hydrophobe was expected, but the small change in the radius of gyration, coupled with the increase in the molecular weight, is not simply explained on the basis of this model. Therefore, although the existence of hydrophobic aggregates was unequivocally demonstrated by the properties of bound fluorescent dye, and some qualitative features of the aggregation behavior could be deduced, a complete picture of the associations did not emerge from this study and remains as something of a challenge.

References

1. Turner, S. R.; Siano, D. B.; Bock, J. U. S. Patent 4 528 348, 1985.
2. Bock, J.; Siano, D. B.; Schulz, D.; Turner, S. R.; Valint, P. L., Jr.; Pace, S. *Polym. Mater. Sci. Eng.* **1986**, *55*, 355.
3. Landoll, L. M. *J. Polym. Sci., Polym. Chem. Ed.* **1982**, *20*, 443.
4. Evani, S.; Rose, G. D. *Polym. Mater. Sci. Eng.* **1987**, *57*, 477.
5. Siano, D. B.; Bock, J.; Myer, P.; Valint, P. L., Jr. *Polym. Mater. Sci. Eng.* **1987**, *57*, 609.
6. Glass, J. E. *Polym. Mater. Sci. Eng.* **1987**, *57*, 618.
7. McCormick, C. L.; Hoyle, C. E.; Clark, M. D. *Polym. Mater. Sci. Eng.* **1987**, *57*, 643.
8. Bock, J.; Siano, D. B.; Valint, P. L., Jr.; Pace, S. J. *Polym. Mater. Sci. Eng.* **1987**, *57*, 487.
9. Utiyama, H. In *Light Scattering from Polymer Solutions*; Huglin, M. B., Ed.; Academic: New York, 1972; Chapter 4.
10. Stryer, L. *J. Mol. Biol.* **1965**, *13*, 482.
11. Cantor, C. R.; Schimmel, P. R. *Biophysical Chemistry, Part II, Techniques for the Study of Biological Structure and Function*; W. H. Freeman and Co.: San Francisco, 1980; Chapter 8–2.
12. Weber, G. *Adv. Protein Chem.* **1953**, *8*, 415.

24

Synthetically Structured Water-Soluble Copolymers

Associations by Hydrophobic or Ionic Mechanisms

Charles L. McCormick and C. Brent Johnson

Department of Polymer Science, University of Southern Mississippi, Hattiesburg, MS 39406–0076

Copolymers with sites for association in aqueous solutions were prepared by copolymerizing acrylamide with N-alkylacrylamides or with the ampholytic monomer pairs sodium 2-acrylamido-2-methylpropanesulfonate (NaAMPS) and 2-acrylamido-2-methylpropanedimethylammonium chloride (AMPDAC). The copolymers were characterized by elemental analysis, ^{13}C NMR and Fourier transform infrared spectroscopy, and low-angle laser and quasielastic light-scattering measurements. Rheological properties were studied as a function of microstructure, molecular weight, polymer concentration, electrolyte concentration, and shear rate. On the basis of those results, a conceptual model that is based on microheterogeneous domain formation in aqueous solutions is proposed.

DEVELOPMENT OF WATER-SOLUBLE ASSOCIATIVE POLYMERS has been the focus of studies in industrial and academic laboratories during the past decade. The dependence of solution viscosity on shear rate, electrolyte concentration, and copolymer composition renders these systems useful in current or developing technologies. Uses include mobility control agents for enhanced oil recovery; drilling fluids; channel blockers; drag reduction polymers; formulation thickeners for coatings, cosmetics, or other personal care items; superabsorbents; bioactive-agent release systems; phase-transfer catalyst carriers; and flocculants.

Traditional viscosifiers rely on chain extension and physical entangle-
ment of solvated chains for development of solution properties. In dilute
solution, extension of individual chains is reflected by the hydrodynamic
volume (HDV) or the total volume encompassed by the chain and its asso-
ciated solvent. Fundamentally, HDV is controlled by the number of seg-
ments along the chain; their lengths, valence, and rotational bond angles;
and solvent, ionic, and segmental interactions. In more concentrated solu-
tions (semidilute) the HDVs of separate polymer chains interact at a con-
centration often referred to as C^*. Above C^*, chain entanglements occur,
and higher apparent viscosities result. For simple polymer systems capable
of undergoing physical entanglement, apparent viscosity (η) is proportional
to both molecular weight (m^a) and concentration (c^b).

$$\eta \propto m^a c^b \tag{1}$$

Typical behavior of a physically associating homopolymer of given molecular
weight is illustrated in Figure 1. The value of b in equation 1 changes
dramatically above and below C^*.

Although not within the scope of this chapter, the theoretical description
of simple polymers in dilute, semidilute, and concentrated solutions dis-
cussed by Flory, DeGennes, Doi, Edwards, and others is of great value to
the synthetic chemist when tailoring more complicated water-soluble poly-
mers. The parameters just discussed as well as associations of a chemical
nature must be considered. These chain–chain enthalpic and entropic in-
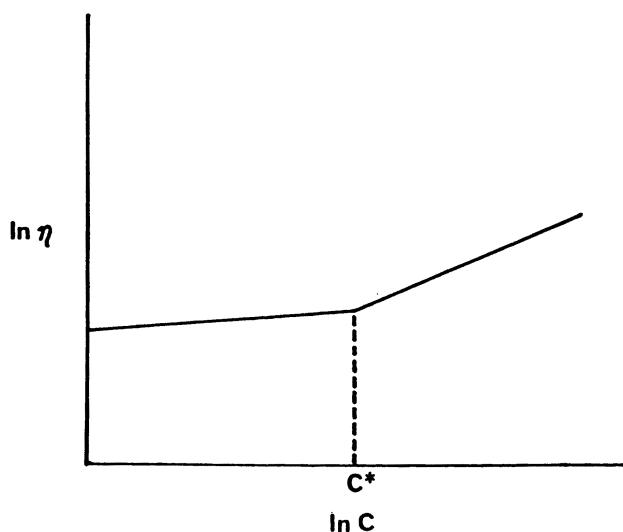
Figure 1. Relationship between apparent viscosity (η) and concentration for
a conventional polymer in solution.

teractions, illustrated in Figure 2, are developed with microheterogeneous copolymers in solution. Statistical treatments fail to describe the behavior of these systems, yet the interactions result in profound property changes of potential commercial importance.

Extensive studies in our laboratories over the past few years have focused on synthesis of molecules that in aqueous electrolyte solutions can maintain or increase viscosity (*1–23*). In this chapter, we focus on our recent efforts at tailoring macromolecules that rely on intermolecular hydrophobic or ionic interactions of certain chain segments and strong hydration of others for solution viscosification (*1*). Although such associations have long been noted for biopolymers and more recently for synthetic thickeners (*24–29*), the relationships between molecular structure and rheological behavior are poorly understood. The major objective of our continuing work is to develop such relationships by studying carefully prepared and characterized copolymers with the use of techniques including classical and dynamic light scattering; ^{13}C NMR, Fourier transform infrared (FTIR), and steady-state spectroscopy; lifetime measurements of fluorescence probes; and solution rheometry.

Experimental Details

Polymer Synthesis. *Synthesis of* N-*Alkylacrylamide Copolymers.* Hydrophobic comonomers were synthesized in the following manner. *N-n*-Octyl-, *N-n*-decyl-, and *N-n*-dodecylacrylamides were synthesized by the reaction of acryloyl chloride (0.55 M) with the corresponding alkylamine (0.55 M) in tetrahydrofuran (THF) at 10 °C with triethylamine (0.60 M) present as the acid receptor. Following filtration of triethylamine hydrochloride and evaporation of THF, the crude product was twice recrystallized in acetone at −25 °C. The products were characterized by elemental analysis, melting point, FTIR and ^{13}C NMR spectroscopy, and gas chromatography.

The *N*-alkylacrylamides were copolymerized with acrylamide via micellar co-
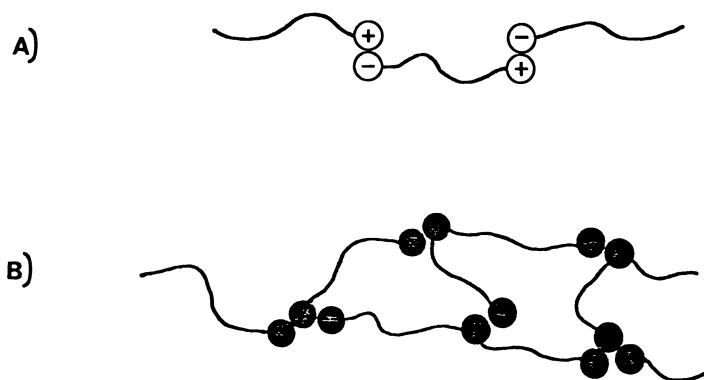
Figure 2. *Conceptual representation of intramolecular entropically driven hydrophobic associations (A) and enthalpic ionic interactions (B) in solution.*

polymerization with sodium dodecyl sulfate as the surfactant and potassium persulfate as the free-radical initiator. Monomer feed mole ratios were varied from 0.25:99.75 to 0.75:99.25 of N-alkylacrylamide–acrylamide. Following reaction, the polymers were purified by precipitation in acetone, dialysis, and lyophilization. Elemental analysis confirmed the absence of surfactant in the copolymers.

Synthesis of Polyampholytes. Low to moderate charge density terpolymers of acrylamide (AM) with 2-acrylamido-2-methylpropanedimethylammonium chloride (AMPDAC) and sodium 2-acrylamido-2-methylpropanesulfonate (NaAMPS) were prepared. The synthesis was conducted in water with potassium persulfate as the free-radical initiator. A typical synthesis involved the dissolution of a specified quantity of the monomers in separate solutions, followed by the addition of an equimolar quantity of inorganic components, NaOH for NaAMPS and HCl for AMPDAC. The monomers were then mixed to form a single solution. Following adjustment of the pH to 6, the reaction mixture was purged with nitrogen for 15 min, then initiated with a specified quantity of potassium persulfate. Following the collection of reaction aliquots at low and high conversion, the samples were purified by three cycles of precipitation in acetone and redissolution in water. Finally, the samples were lyophilized to remove nonsolvent acetone and water. Terpolymer compositions were determined by using elemental analysis for carbon, nitrogen, and sulfur.

Polymer Characterization. *Viscosity.* Solution viscosities of the NaAMPS copolymers were determined with a Cannon-Ubbelohde four-bulb shear dilution viscometer (size 100). Solution viscosities of the associative polymers were determined with a Contraves low-shear rotational rheometer at a shear rate of 1.28 s^{-1}. All viscosity studies were conducted in the absence of surfactant at temperatures in the range of 25–45 °C and [NaCl] ranging from 0 to 0.684 M.

Light Scattering. Low-angle laser light-scattering measurements, used in determining weight-average molecular weights and second virial coefficients, were performed with a Chromatix KMX-6 photometer. Refractive index increments were determined with a Chromatix KMX-16 laser differential refractometer. All light-scattering measurements were conducted at 25 °C in 1 M NaCl aqueous solutions at pH 6.

^{13}C NMR Spectroscopy. ^{13}C NMR spectra were obtained at 22.5 MHz on a JEOL FX-90Q spectrometer with a 5000-Hz window. Approximately 30,000 transients were accumulated for each sample consisting of 0.1–0.2 g of copolymer in 2 mL of D_2O in 10-mm tubes.

Fluorescence. Pyrene (Aldrich Chemical Company) was recrystallized five times in methanol prior to use. All polymers were initially dissolved in deionized water. The pyrene–polymer samples were prepared in the following manner. A 10^{-4} M solution of pyrene in methanol was first prepared. From this solution, 10 mL was then pipetted into a scintillation bottle. The bottle was slowly heated to allow the methanol to evaporate. Then 10 mL of the polymer solution was placed in the bottle containing the pyrene residue. This mixture was heated at 40 °C for 6 h and then centrifuged for 1 day.

Steady-state fluorescence spectra were recorded ($\lambda_{ex} = 347$ nm) on a Perkin-Elmer model 650-10S fluorescence spectrometer. The absorbance of pyrene (10^{-7} M) in each solution was between 0.01 and 0.05 at the excitation wavelength. Fluorescence quantum yields were obtained by comparison with a quinine bisulfate

standard. Fluorescence lifetimes were measured on a Photochemical Research Associates single-photon counting fluorescence decay apparatus. The excitation and emission wavelengths used in the fluorescence lifetime studies were 347 and 380 nm, respectively.

Elemental Analysis.   Elemental analyses to determine the carbon, hydrogen, and nitrogen content of each copolymer were conducted by M-H-W Laboratories of Phoenix, AZ.

Results and Discussion

Hydrophobically Associating Copolymers.   Hydrophobically modified cellulose derivatives (28) and N-alkylacrylamido copolymers (24, 25, 27) were among the first nonionic associative thickeners reported in the patent literature. The concentration of hydrophobic units allowed for dissolution in aqueous solution is usually less than 1–2 mol %. Like conventional polymers, apparent viscosity is proportional to molecular weight and concentration. However, with associative copolymers, a very dramatic increase in apparent viscosity occurs at a critical concentration, C^*, which clearly is related to a phenomenon other than simple entanglement. Viscosity dependence on hydrophobe concentration, size, and distribution suggests microheterogeneous phase formation. Surfactants enhance viscosity behavior in some instances (24), yet clearly reduce viscosity in others (1).

To elucidate the mechanism of chain association, we prepared three series of N-alkylacrylamide–acrylamide copolymers containing up to 0.75 mol % of C_8, C_{10}, and C_{12} N-alkylacrylamide monomers. The copolymerizations were conducted with potassium persulfate as the initiator in an aqueous medium containing a high concentration of sodium dodecyl sulfate surfactant (28). The reaction parameters and solubility of the resulting copolymers are given in Table I. Table I indicates solubility in water of all

Table I. Reaction Parameters and Solubility Properties
for N-Alkylacrylamide–Acrylamide Copolymers

Sample Name	Monomer Feed Ratio	Water Solubility	Percent Conversion
C_8–0.25	99.75:0.25	soluble	33.5
C_8–0.50	99.50:0.50	soluble	35.5
C_8–0.75	99.25:0.75	soluble	36.1
C_{10}–0.25	99.75:0.25	soluble	33.7
C_{10}–0.50	99.50:0.50	soluble	35.6
C_{10}–0.75	99.25:0.75	soluble	36.5
C_{12}–0.25	99.75:0.25	soluble	28.6
C_{12}–0.50	99.50:0.50	insoluble	31.4
C_{12}–0.75	99.25:0.75	insoluble	31.3

CONDITIONS: Total monomer concentration = 0.44 M; sodium dodecyl sulfate concentration = 0.12 M; $[K_2S_2O_8]$ = 7.86 × 10^{-5} M; T = 50 °C.

copolymers through C_{12}–0.25. Copolymers with 0.50 and 0.75 mol % of the dodecylacrylamide comonomer in the feed were insoluble.

The rates of solubilization, however, and the apparent homogeneity of the solutions deserve comment. First, the extent of incorporation of the N-alkylacrylamide in the copolymer is not determinable from elemental analysis or NMR measurements because of the low concentration in the feed initially. Second, solubilization of purified, freeze-dried samples is often difficult because of inter- and intramolecular associations. Finally, even under dilute conditions, a time dependence on dissolution is observed with some solutions, which require weeks to reach constant values of apparent viscosity. Optical cloudiness with "stringy" texture is often observed with the longer alkyl chains at higher concentration.

For comparative purposes, the homopolyacrylamide prepared under conditions identical with those in Table I had a viscosity-average molecular weight of 1.2×10^6 (1). Most likely, the "nonassociated" forms of the C_8 through C_{12} polymers have similar values. Although light-scattering techniques are utilized routinely in our laboratory, the associative nature of these polymers and regional dn/dc differences for these microheterogeneous systems preclude meaningful characterization of molecular weight in this manner.

Effects of Copolymer Composition.   Figure 3 illustrates the effect of changes in C_8 hydrophobe composition on the apparent viscosity versus
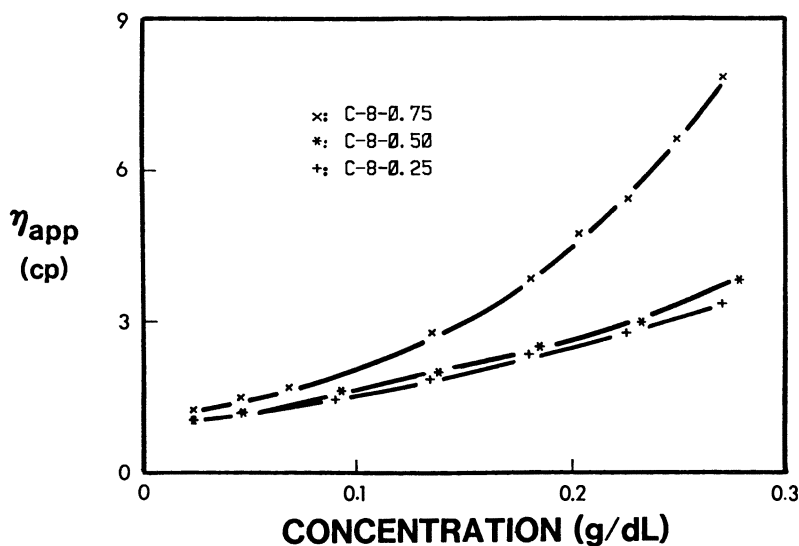
Figure 3. Effect of copolymer concentration on the apparent viscosity of copolymers of acrylamide with octylacrylamide in 0.342 M NaCl at 25 °C and a shear rate of 1.28 s^{-1}.

copolymer concentration curve. Viscosities were measured at a shear rate of 1.28 s^{-1} at 25 °C in 0.342 M NaCl. Only in the C_8–0.75 copolymer are associations sufficient in aqueous solution to observe marked viscosity enhancement. The C_{10} copolymers (Figure 4) with 0.75 and 0.50 mol % of the decylacrylamide in the feed demonstrate dramatic increases in viscosity near a concentration of 0.15 g/dL. The 0.75-mol % copolymer possesses a steeper slope beyond C^*. The C_{10}–0.25 copolymer shows almost identical behavior to the homopolyacrylamide sample.

Analysis of the apparent viscosity data reveals that the C_8–0.75 and C_{10}–0.50 copolymers have very similar concentration dependencies. The only soluble copolymer of the C_{12} series, C_{12}–0.25, has a slightly lower value of C^* and a steeper slope beyond C^* than the C_{10}–0.50 copolymer.

Effects of Added Electrolyte.   Figure 5 illustrates the effect of ionic strength on apparent viscosity of C_{10}–0.50 at a shear rate of 1.28 s^{-1} and a copolymer concentration of 0.25 g/dL. The apparent viscosity increases dramatically with added NaCl and less so with $CaCl_2$; polyacrylamide is unaffected.

Effect of Surfactant.   Added nonionic or anionic surfactant dramatically decreases apparent viscosity at concentrations above C^*, as illustrated in Figure 6 for C_{10}–0.50.
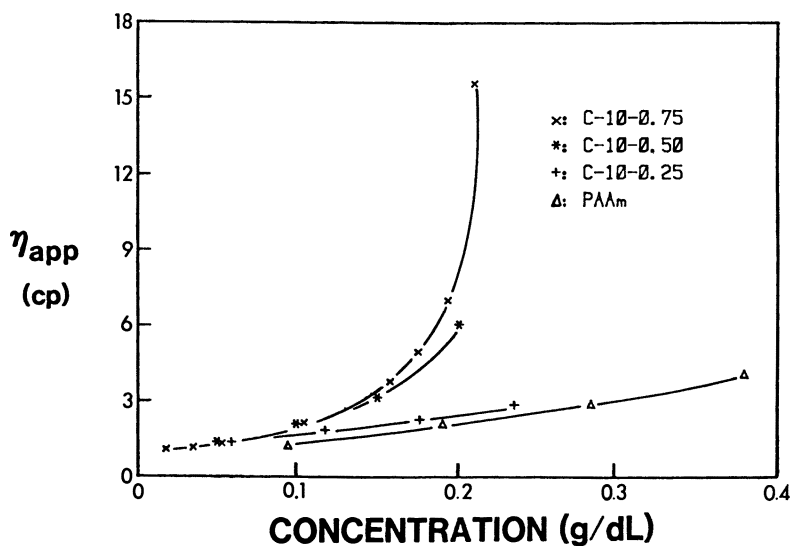
Figure 4. Effect of copolymer concentration on the apparent viscosity of copolymers of acrylamide with decylacrylamide in 0.342 M NaCl at 25 °C and a shear rate of 1.28 s^{-1}.
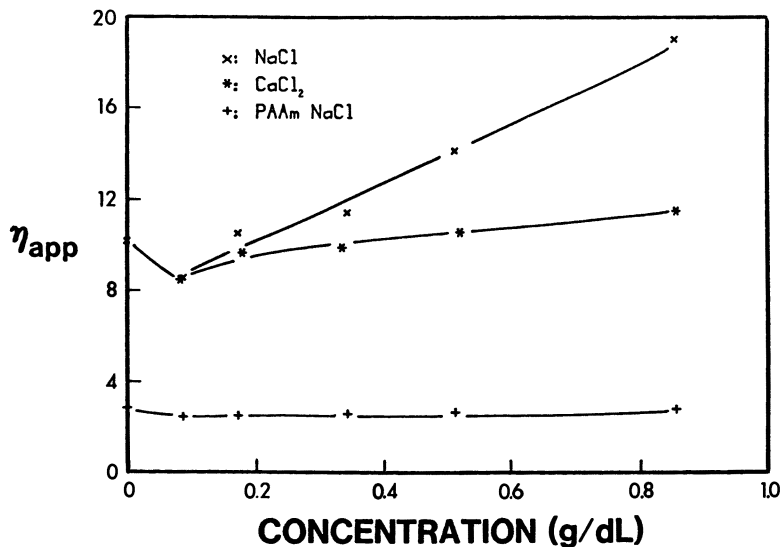
Figure 5. Effect of ionic strength of NaCl and CaCl₂ solutions on the apparent viscosity of a copolymer of acrylamide with 0.50 mol % decylacrylamide at 25 °C, a shear rate of 1.28 s⁻¹, and a copolymer concentration of 0.25 g/dL.
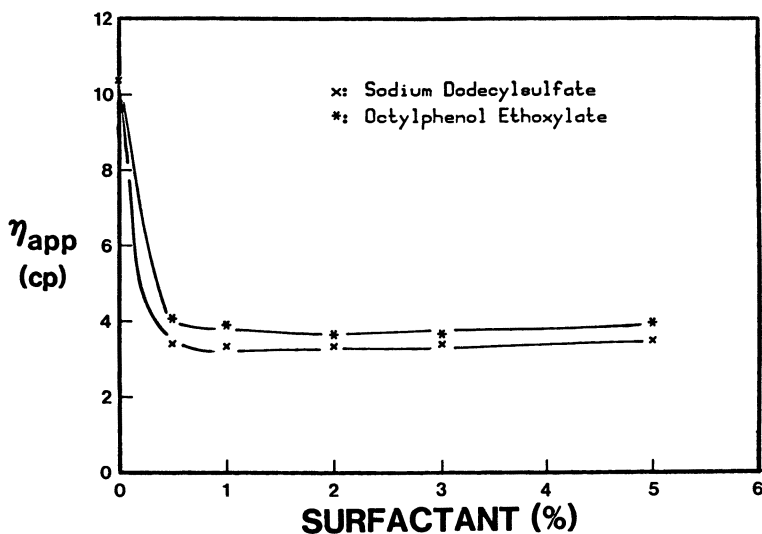
Figure 6. Effect of surfactant concentration on the apparent viscosity of a copolymer of acrylamide with 0.50 mol % decylacrylamide at 25 °C, a shear rate of 1.28 s⁻¹, and a copolymer concentration of 0.25 g/dL.

Effect of Molecular Weight. In Figure 7 reduced viscosity is plotted as a function of concentration for C_{10}–0.50 copolymer of varying molecular weights. The copolymers were prepared by micellar copolymerization by varying the initiator concentration and reaction temperature. The degree of viscosity increase at a given concentration increases with molecular weight.

Effect of Shear Rate. The effect of changing shear rate on the apparent viscosity of C_{10}–0.75 at three concentrations is shown in Figure 8. In a shear-rate cycling experiment, the shear rate was increased from 1.28 to 94.5 s^{-1} and then decreased. At concentrations above C^*, the apparent viscosity at each value of shear rate was higher on the decreasing portion of the cycle. Furthermore, the final viscosity value measured at 1.28 s^{-1} was unchanged after 2 weeks. The C_{10}–0.5 copolymer showed similar but less dramatic shear history behavior. Interestingly, apparent viscosity for both samples increased further but to a smaller extent during the second cycle (Figure 9).

Conceptual Model. The behavior of the hydrophobically modified acrylamide copolymers of this work has led us to propose the model illustrated in Figure 10. The hydrophobic groups on the N-alkylacrylamide–acrylamide copolymers exhibit concentration-dependent association. In region 1, low hydrophobe concentration on the copolymer, low copolymer concentration, or both conditions are insufficient to bring about significant association. In region 2, hydrophobic association increases, but associations
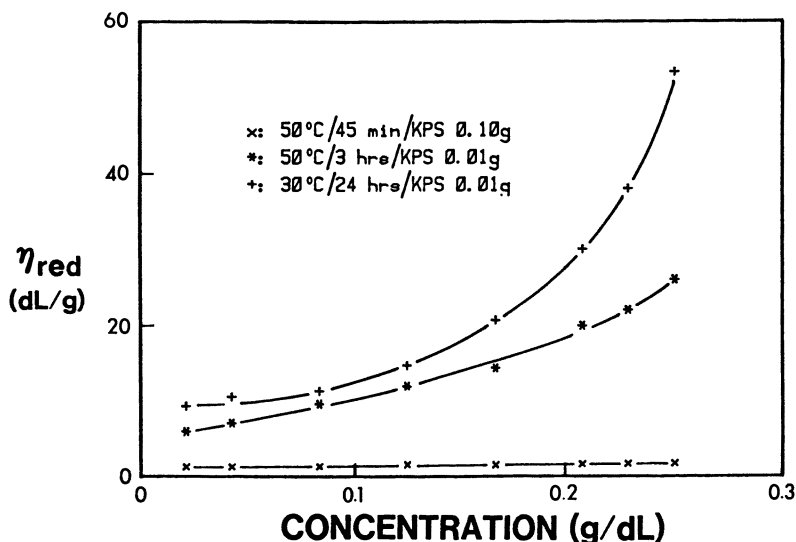
Figure 7. *Effect of copolymer concentration on the reduced viscosity of copolymers of acrylamide with 0.50 mol % decylacrylamide of varying molecular weights in 0.342 M NaCl at 25 °C and a shear rate of 1.28 s⁻¹.*
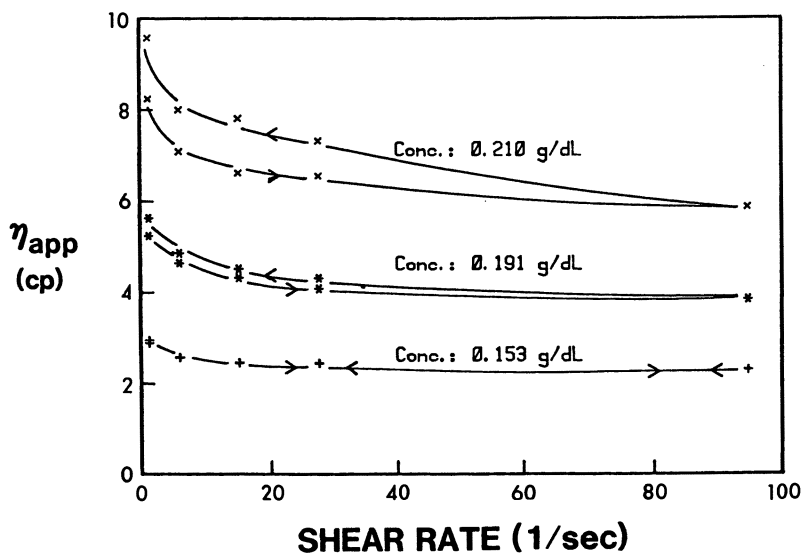
Figure 8. *Effect of one cycle of shear rate on the apparent viscosity of a copolymer of acrylamide with 0.75 mol % decylacrylamide in 0.342 M NaCl at 25 °C and copolymer concentration ranging from 0.153 to 0.210 g/dL.*
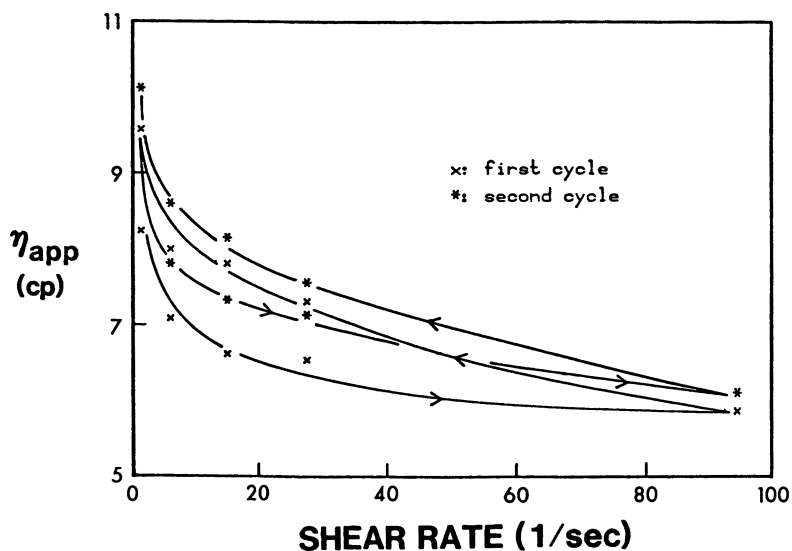
Figure 9. *Effect of two cycles of shear rate on the apparent viscosity of a copolymer of acrylamide with 0.75 mol % decylacrylamide in 0.342 M NaCl at 25 °C and a copolymer concentration of 0.210 g/dL.*
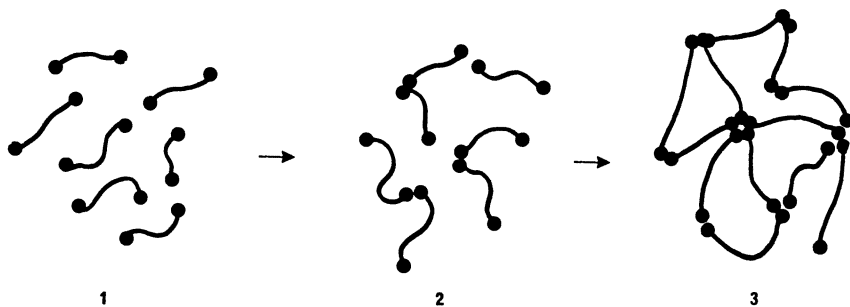
Figure 10. Schematic representation of hydrophobic associations in aqueous solution.

are not sufficient to cause appreciable viscosity enhancement. In region 3, ordered associations or domains result in microphase networking and large increases in apparent viscosity.

The onset of domain networking on a macroscopic scale depends on the parameters of hydrophobe length, distribution, and concentration as well as copolymer molecular weight. Clearly C^* or apparent chain overlap occurs earlier with increases in hydrophobe concentration and size and with increased molecular weight of the copolymer. For the C_{10} and C_{12} copolymers of nearly 1 million molecular weight, hydrophobe concentration of >1 mol % in the feed results in insolubility, possibly because of too many associations for hydration. Addition of electrolytes, particularly NaCl, seems to organize domains at concentrations above C^*, and the result is higher apparent viscosity. Increasing temperature has a similar but less dramatic effect. Shear-rate cycling experiments indicate that ordering or perfection of domains may be responsible for enhanced viscosity. Addition of surfactants above C^* disrupts associations or domains and leads to reduced apparent viscosities.

Recently we conducted preliminary experiments with an externally added pyrene fluorescent probe. At low concentrations (0.02 g/dL) of C_{10}–0.75 or C_{12}–0.25 (region 1) the fluorescence lifetime of pyrene is the same as that observed in water (~230 ns). However above 0.05 g/dL of C_{10}–0.75, a long-lived component of the fluorescence lifetime of 350 ns is observed, and this finding indicates some probe incorporation into organized hydrophobic regions. Shorter-lived components are also observed, and therefore quantitative interpretation is impossible. Similar results are seen from steady-state measurements of the 1–3 ratios of the pyrene monomer fluorescence. Clearly a portion of the pyrene is incorporated into micellelike hydrophobic regions. Because the concentration (0.02 g/dL) at which lifetime enhancement is first observed is well below that for the viscosity enhancement (0.15 g/dL for C_{10}–0.50), we suggest an ordering that progresses with concentration to eventual networking, as depicted in Figure 10. The

pyrene probe is unable to clearly discriminate between ordering of the type shown in region 2 or region 3.

Although this conceptual model is consistent with solution behavior of these N-alkylacrylamide copolymers, many questions remain unanswered. Are the hydrophobic comonomers incorporated in a blocky or random manner during polymerization? How large are the domains or micellelike associations? Are they reversible upon dilution? Can such copolymers be tailored in a manner to be easily solubilized and to possess reproducible rheological characteristics? These and other questions are currently being investigated by a number of industrial and academic research groups. Our research group is currently working on covalently incorporated fluorescence probes as reporters of local ordering.

Polyampholytes. Ampholytic copolymers (*1*, *30–35*) exhibit interesting viscosity behavior in electrolyte solutions that is quite opposite to the behavior of conventional polyelectrolytes. Recently we prepared high charge density copolymers from the matched, nonhydrolyzable comonomer pairs sodium 2-acrylamide-2-methylpropanesulfonate (NaAMPS) and 2-acrylamide-2-methylpropanedimethylammonium chloride (AMPDAC) (*1*, *33*) (*see* structures).

$$CH_2{=}CH$$
$$|$$
$$C{=}O$$
$$|$$
$$NH$$
$$|$$
$$CH_3{-}C{-}CH_3$$
$$|$$
$$CH_2$$
$$|$$
$$SO_3Na$$

NaAMPS

$$CH_2{=}CH$$
$$|$$
$$C{=}O$$
$$|$$
$$NH$$
$$|$$
$$CH_3{-}C{-}CH_3$$
$$|$$
$$CH_2$$
$$|$$
$$H{-}\overset{+}{N}(CH_3)_2\overset{-}{Cl}$$
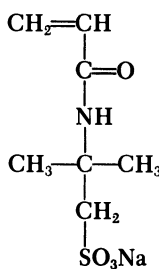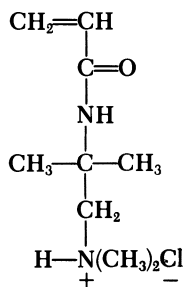
AMPDAC

The copolymers containing equimolar concentrations of the two monomers exhibited a threefold increase in intrinsic viscosity when the solvent was changed from deionized water to aqueous 0.514 M NaCl. Under dilute solution conditions, intramolecular interactions predominate; attractive macroions collapse the chain; this collapse results in low hydrodynamic volume. The attractive forces are disrupted by the addition of NaCl; solvation and chain expansion result.

The sensitivity of stoichiometrically balanced polyampholytes to addition of simple electrolytes is also a function of chain stiffness, counterion binding, and side-chain length. In semidilute solutions, physical entanglements,

charge interactions of both inter- and intramolecular nature, and solvation effects dictate rheological behavior.

Effects of Composition. Reactivity ratio studies of the NaAMPS–AMPDAC pair showed high alternation as expected for ion-paired systems (*1, 33*). The acrylamide functionality of both monomers would also be expected to terpolymerize well with acrylamide. Therefore, the series of terpolymers shown in Table II was prepared. Molecular weights, second virial coefficients, and intrinsic viscosities at 25 °C in 1.0 M NaCl solutions are given in Table III. The numbers following the ADASAM acronym represent

Table II. Reaction Parameters and Compositions of NaAMPS–AMPDAC–AM Terpolymers

Sample Name	Feed Composition, AMPDAC–NaAMPS–AM	Terpolymer Composition[a], AMPDAC–NaAMPS–AM
ADASAM 0.5–0.5	0.5:0.5:99.0	1.03:1.49:97.49
ADASAM 2.5–2.5L[b]	2.5:2.5:95.0	5.20:3.36:91.44
ADASAM 2.5–2.5	2.5:2.5:95.0	5.39:3.44:91.16
ADASAM 5–5L	5:5:90	8.59:5.84:85.57
ADASAM 5–5	5:5:90	8.24:6.21:85.55
ADASAM 10–10L	10:10:80	11.14:12.56:76.30
ADASAM 10–10	10:10:80	10.69:12.57:76.74
ADASAM 15–15L	15:15:70	20.08:15.95:63.98
ADASAM 15–15	15:15:70	19.51:15.54:64.95
ADASAM 5–10L	5:10:85	8.21:10.70:81.09
ADASAM 5–10	5:10:85	8.31:10.22:81.47
ADASAM 10–5L	10:5:85	13.31:8.20:78.49
ADASAM 10–5	10:5:85	12.56:7.23:80.21

CONDITIONS: pH = 6.0; T = 30 °C; total monomer concentration = 0.45 M; [$K_2S_2O_8$] = 4.5 × 10⁻⁴ M.
[a]Determined via elemental analysis for carbon, nitrogen, and sulfur.
[b]L denotes low conversion.

Table III. Low-Angle Light-Scattering and Intrinsic Viscosity Data for NaAMPS–AMPDAC–AM Terpolymers

Sample Name	$\overline{M}_w$ x 10⁻⁶ (mol⁻¹)	A_2 x 10⁴ (mL mol g⁻²)	$\overline{DP}_w$ (x 10⁻⁴)	[h][a] (dL g⁻¹)
ADASAM 0.5–0.5	1.03	—	13.8	1.79
ADASAM 2.5–2.5	7.40	2.93	88.3	14.7
ADASAM 5–5	8.77	9.27	95.1	17.5
ADASAM 10–10	7.57	2.87	71.8	14.1
ADASAM 15–15	12.0	2.78	98.3	8.31
ADASAM 5–10	10.5	2.43	107	15.6
ADASAM 10–5	3.75	—	37.7	7.19

CONDITIONS: pH = 7.0; T = 25 °C; [NaCl] = 1.0 M.
NOTE: $\overline{M}_w$ is weight-average molecular weight; η is intrinsic viscosity; A_2 is the second virial coefficient; and $\overline{DP}_w$ is the degree of polymerization.
[a]via Contraves low-shear LS-30 rotational rheometer.

the mole composition of the AMPDAC and NaAMPS in the terpolymer. Despite alternation in copolymers of AMPDAC–NaAMPS, actual compositions of terpolymers do not precisely reflect feed ratios.

Terpolymer solution behavior is dependent on compositional microstructure, polymer concentration, ionic strength, pH, temperature, and shear history. The viscosities of these low charge density terpolymers would be expected to be insensitive to changes in ionic strength below the critical overlap concentration, C^*; above C^* intermolecular attractive forces might be expected to cause enhanced viscosities similar to those of hydrophobically associating copolymers.

Effects of Concentration. In Figure 11 apparent viscosity is plotted as a function of concentration for each of the terpolymers at low shear in water. For those terpolymers with relatively high molar concentrations of monomer pairs in the feed, significant enhancement in viscosity is observed beyond C^*. For polymers with less than 5 mol % of each comonomer, little viscosity enhancement is observed over the entire concentration range as compared to homopolyacrylamide of similar molecular weight.

A similar study was conducted in aqueous 0.514 M NaCl solutions. Interestingly, the terpolymers with moderate amounts of each monomer in the feed (approximately 5%) showed enhanced viscosities over smaller or larger monomer pair compositions at high terpolymer concentrations. Ap-
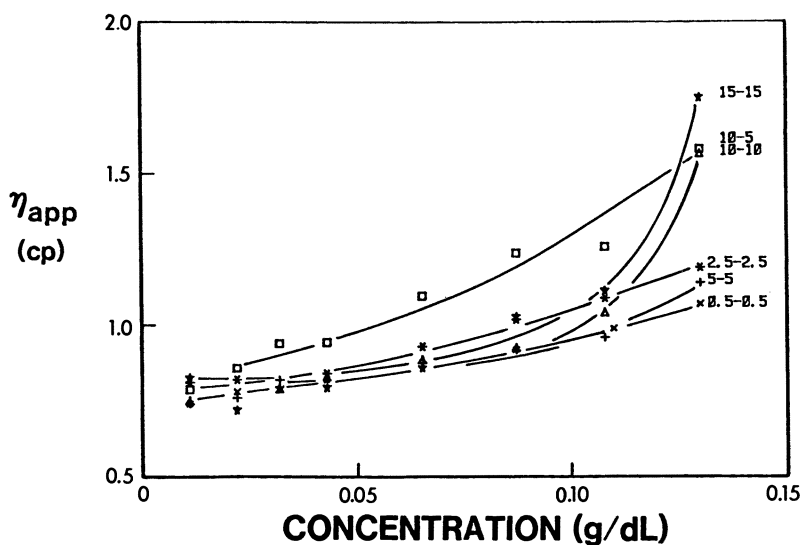
Figure 11. Effect of polymer concentration on the apparent viscosity of the ADASAM series of terpolymers in pure water at a temperature of 30 °C, a shear rate of 1.75 s⁻¹, and a pH of 7.

parently an appropriate balance of chain solvation and intermolecular inter-
action is reached for the 5–5 and 5–10 samples.

The area below C^* in Figure 12 is consistent with the low concentration
data in Table IV. Diffusional light-scattering data in dilute 1.0 M NaCl so-
lutions indicate Stokes diameters of 2680 and 4240 Å, respectively. Actual
AMPDAC–NaAMPS ratios are 8.2:6.1 and 8.3:10.2, respectively, in the
terpolymers. As the concentration of the 5–10 and 10–10 samples increases,
crossover is observed beyond C^*. These data suggest that a terpolymer with
7–8 mol.% of each comonomer might have the optimal characteristics for
viscosification throughout the concentration range.

Effects of Ionic Strength. Figure 13 illustrates the effect of NaCl con-
centration on intrinsic viscosity for each terpolymer. Of course, this exper-
iment should demonstrate only the effects of added electrolyte on individual
chain contraction or expansion. The chains with sufficient monomer pairs
exhibit increases in viscosity as expected with addition of NaCl. The best
chain expansion is seen for the 5–5 sample, which is rapidly solvated with
increasing ionic strength. The 5–10 sample shows some typical poly-
electrolyte behavior because it has an excess of macroanions at pH 7.

The ADASAM 5–5 sample was studied in pure water and in NaCl
solutions, as shown in Figure 14. As expected, the reduced viscosities in-
creased dramatically with concentration, especially in higher salt concen-
trations. Similar behavior was observed for the 10–10 sample.
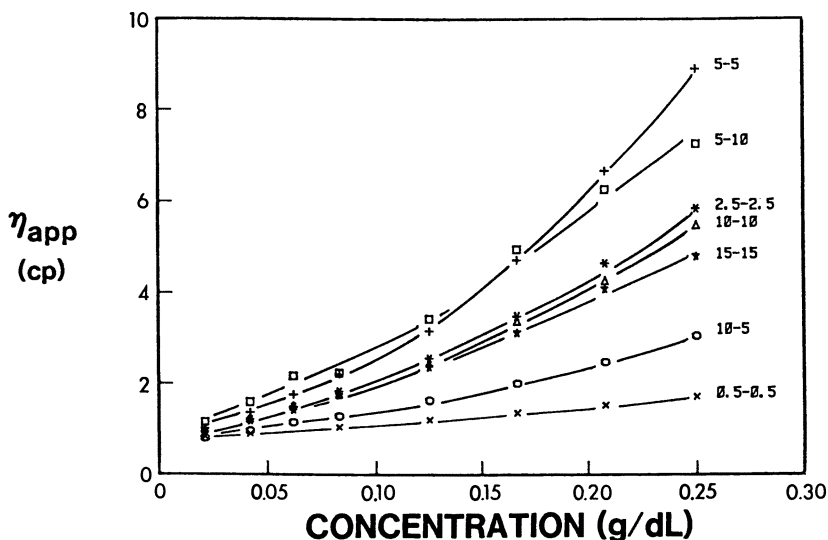
*Figure 12. Effect of polymer concentration on the apparent viscosity of the
ADASAM series of terpolymers in 0.514 M NaCl at a temperature of 30 °C,
a shear rate of 1.75 s⁻¹, and a pH of 7.*

Table IV. Quasi-Elastic Light-Scattering and Intrinsic
Viscosity Data for NaAMPS–AMPDAC–AM
Terpolymers

Sample Name	$\overline{DP}_w$ x 10^{-4}	$[h]^a$ $(dL\ g^{-1})$	D_o x 10^8 $(cm^2\ s^{-1})$	d_o $(\mathring{A})$
ADASAM 0.5–0.5	1.38	1.79	1.82	2560
ADASAM 2.5–2.5	8.83	14.6	1.67	2790
ADASAM 5–5	9.51	17.5	1.74	2680
ADASAM 10–10	7.18	14.1	1.52	3070
ADASAM 15–15	9.83	8.31	1.57	2970
ADASAM 5–10	10.7	15.55	1.10	4240
ADASAM 10–5	3.77	7.19	1.76	2650

CONDITIONS: pH = 7.0; T = 25 °C; [NaCl] = 1.0 M.
NOTE: $\overline{DP}_w$ is the degree of polymerization; η is intrinsic viscosity; D_o is the diffusional coefficient; and d_o is the hydrodynamic diameter.
[a]via Contraves low-shear LS-30 rotational rheometer.
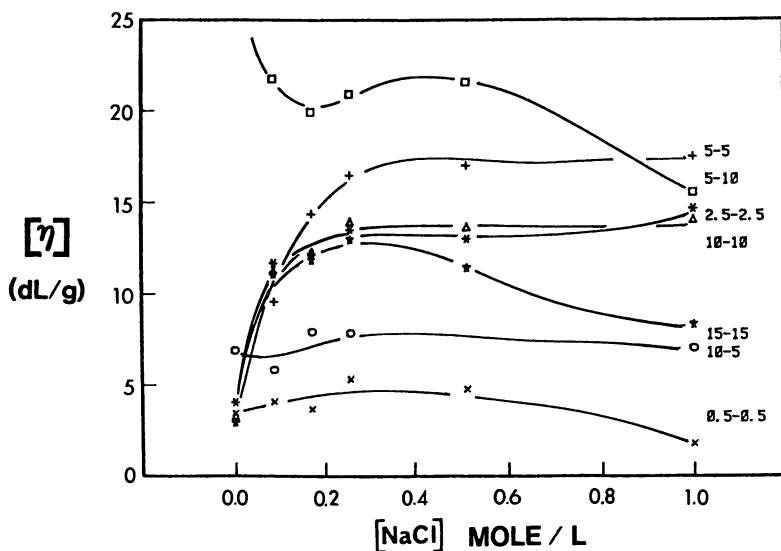
Figure 13. Effect of NaCl concentration on the intrinsic viscosity of the ADASAM series at a shear rate of 1.75 s^{-1}, a temperature of 30 °C, and a pH of 7.

Effects of Shear Rate and Temperature. In nearly all instances, the polyampholytes showed only slight pseudoplastic or Newtonian behavior in deionized water and salt solutions in the dilute regime. In semidilute solutions near C^*, some shear thinning was observed by using Contraves rheometry; however, the behavior was not pronounced. Only the imbalanced terpolymer systems, which are in essence polyelectrolytes, exhibited pseu-
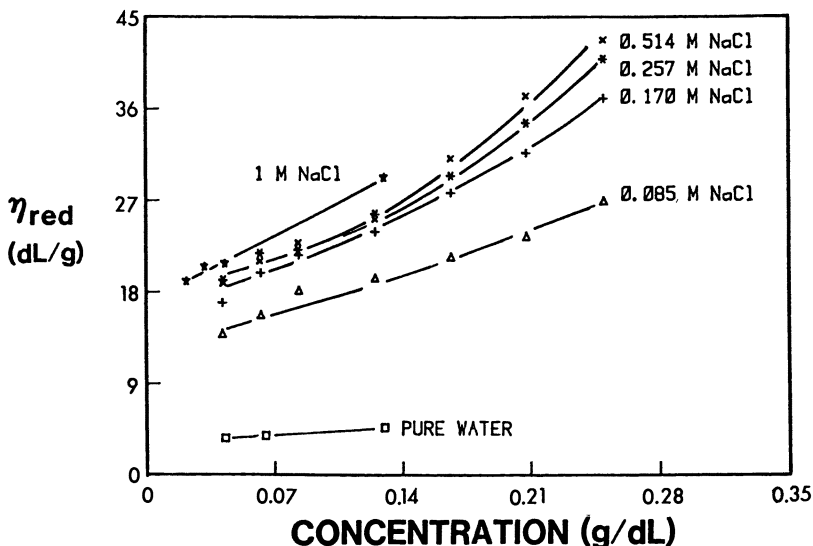
Figure 14. Effect of polymer concentration on the reduced viscosity of ADASAM 5–5 in pure water and NaCl solutions ranging from 0.085 to 1 M at a shear rate of 1.75 s⁻¹, a temperature of 30 °C, and a pH of 7.

doplastic behavior in dilute solution in the absence of added electrolyte. Additionally, in the dilute regime, reduced viscosities were nearly invariant to increasing temperature over the range of 30 to 60 °C.

Conclusions

Domain associations in hydrophobically modified copolymers and associations of macroions in aqueous solution can lead to remarkable solution properties in properly tailored systems. An example of each type and selected observations of experimental findings were presented herein. The challenge now for the scientific community is to thoroughly understand the balance of structural forces responsible for macroscopic behavior so that systems may be properly tailored for specific commercial application.

Acknowledgments

References

1. Johnson, C. B. Ph.D. Dissertation, University of Southern Mississippi, 1987.
2. McCormick, C. L.; Chen, G. S. *J. Polym. Sci., Chem.* 1982, *20*, 817.

3. McCormick, C. L.; Chen, G. S.; Hutchinson, B. H., Jr. *J. Appl. Polym. Sci.* **1982**, *27*, 3103.
4. Neidlinger, H. H.; Chen, G. S.; McCormick, C. L. *J. Appl. Polym. Sci.* **1984**, *29*, 713.
5. McCormick, C. L.; Park, L. S. *J. Polymer Sci., Chem.* **1984**, *22*, 49.
6. McCormick, C. L.; Chen, G. S. *J. Polymer Sci., Chem.* **1984**, *22*, 3633.
7. McCormick, C. L.; Chen, G. S. *J. Polym. Sci., Chem.* **1984**, *22*, 3649.
8. McCormick, C. L.; Park, L. S. *J. Appl. Polym. Sci.* **1985**, *30*, 45.
9. McCormick, C. L.; Blackmon, K. P. *J. Polym. Sci. Chem.* **1986**, *24*, 2635.
10. McCormick, C. L.; Blackmon, K. P.; Elliott, D. L. *J. Polym. Sci., Chem.* **1986**, *24*, 2619.
11. McCormick, C. L.; Elliott, D. L. *Macromolecules* **1986**, *19*, 542.
12. Hutchinson, B. H., Jr.; McCormick, C. L. *Polymer* **1986**, *27*(4), 623.
13. McCormick, C. L.; Hutchinson, B. H., Jr.; Morgan, S. E. *Makromol. Chem.* **1987**, *188*, 357–370.
14. McCormick, C. L.; Blackmon, K. P. *Macromolecules* **1986**, *19*, 1512.
15. McCormick, C. L.; Elliott, D. L. Blackmon, K. P. *Macromolecules* **1986**, *19*, 1516.
16. McCormick, C. L.; Blackmon, K. P. *J. Macromol. Sci., Chem.* **1986**, *A25*(12), 1451.
17. McCormick, C. L.; Blackmon, K. P.; Elliott, D. L. *J. Macromol. Sci., Chem.* **1986**, *A23*(12), 1469.
18. McCormick, C. L.; Blackmon, K. P. *Polymer* **1986**, *27*, 1971–1975.
19. McCormick, C. L.; Blackmon, K. P.; Elliott, D. L. *Polymer* **1986**, *27*, 1976–1980.
20. McCormick, C. L.; Blackmon, K. P. D. *Angew. Makro. Chem.* **1986**, *144*, 73.
21. McCormick, C. L.; Blackmon, K. P.; Elliott, D. L. D. *Angew. Makro. Chem.* **1986**, *144*, 87.
22. McCormick, C. L.; Elliott, D. L. *J. Polym. Sci. Chem. Polym. Chem.* **1986**, *A25*, 1329–1337.
23. McCormick, C. L.; Blackmon, K. P. U.S. Patent 4 584 358, 1986.
24. Turner, S. R.; Siano, D. B.; Bock, J. U.S. Patent 4 520 182, 1985.
25. Evani, S. U.S. Patent 4 432 881, 1984.
26. Hoy, K. L.; Hoy, R. C. U.S. Patent 4 426 485, 1984.
27. Emmons, W. D.; Stevens, T. E. U.S. Patent 4 395 524, 1983.
28. Landoll, L. M. U.S. Patent 4 288 277, 1980.
29. Pfeiffer, D. G.; Lundberg, R. D. *Polymer* **1985**, *26*, 1058.
30. Salamone, J. C.; Tsai, C. C.; Olson, A. P.; Watterson, A. C. In *Ions in Polymers*; Eisenberg, A., Ed.; Advances in Chemistry 187: American Chemical Society; Washington, DC, 1980; pp 337–346.
31. Salamone, J. C. et al. *J. Macromol. Sci., Chem.* **1985**, *A22*(5–7), 653.
32. Salamone, J. C.; Tsai, C. C.; Watterson, A. C. *J. Macromol. Sci., Chem.* **1979**, *A13*, 665.
33. McCormick, C. L.; Johnson, C. B. *Macromolecules* **1988**, *21*, 694.
34. McCormick, C. L.; Johnson, C. B. *Macromolecules* **1988**, *21*, 686.
35. McCormick, C. L.; Johnson, C. B. In *Water-Soluble Polymers for Petroleum Recovery*; Stahl, G. A.; Schulz, D. N., Eds.; Plenum: New York, 1988; pp 161–180.

Alkali-Swellable and Alkali-Soluble Thickener Technology

A Review

Gregory D. Shay

DeSoto, Inc., Administrative and Research Center, 1700 South Mount Prospect Road, Des Plaines, IL 60017

Carboxyl-containing copolymers that are prepared by the addition polymerization of ethylenically unsaturated monomers and that swell or solubilize to thicken aqueous media on neutralization are commonly referred to as alkali-swellable or alkali-soluble thickeners (ASTs collectively). These thickeners are broadly classified as either conventional (presumably nonassociative) or associative, depending on their chemical architecture and dominant mechanism of thickening. ASTs prepared by emulsion polymerization and supplied in latex form have received the greatest commercial acceptance. These polymers consist of conventional alkali-swellable or -soluble emulsions (ASE) and those that are classified associative by hydrophobe modification (hydrophobically modified alkali-swellable or -soluble emulsions, HASE). This review examines various aspects of AST technology, including chemical composition, thickening mechanisms, methods of polymerization, and factors affecting the swelling and dissolution behavior of these polymers.

ALKALI-SWELLABLE AND ALKALI-SOLUBLE THICKENERS (ASTs), as defined herein, are carboxyl functional copolymers produced by the free-radical polymerization of ethylenically unsaturated monomers. The copolymers are substantially insoluble in water at low pH, but exhibit thickening on swelling or dissolution in aqueous media at higher degrees of ionization. In their ionic form (partially or fully neutralized), ASTs generally belong to the broad

classes of aqueous polymers known as WSPs (water-swellable or water-soluble polymers) and HWSPs (hydrophobically modified, water-swellable or water-soluble polymers). The acronyms WSP and HWSP are used hereafter to be consistent with other popular acronyms.

ASTs have the distinction, however, of being anionic (carboxyl functional) and normally water insoluble on preparation and prior to final end-use application (i.e., prior to neutralization). This distinction has permitted a variety of synthetic techniques for their preparation, including solution polymerization in organic solvent, precipitation polymerization in organic diluent, aqueous suspension polymerization, or, more commonly and most advantageously, aqueous emulsion polymerization. Because of their performance characteristics and convenient handling (particularly the emulsions), ASTs find wide industrial application in latex paints, carpet backing, adhesives, paper coatings, print pastes, agrochemical products, personal care products, household and industrial cleaners, and in oil field drilling–recovery operations.

Classification by Chemical Composition

ASTs are generally classified structurally as either "conventional" (those lacking associative functionality) or "associative", and the structural distinction usually is supported by the contrast in the rheological properties observed. A wide variety of ethylenically unsaturated monomers have been copolymerized to prepare conventional and associative ASTs. The only substantial limitation for both types of thickeners is that at least one of the monomer components be carboxyl functional and be present in sufficient concentration to render the polymer water swellable or water soluble on partial or complete neutralization with an appropriate base.

Among the carboxylic acid and anhydride functional monomers that have been employed in the synthesis of these thickener polymers are acrylic acid, methacrylic acid, itaconic acid, citraconic acid, maleic acid, fumaric acid, crotonic acid, maleic anhydride, and citraconic anhydride. The copolymers containing maleic and citraconic anhydride monomers are either hydrolyzed or partially esterified to obtain the required carboxyl functionality. Among these carboxylic monomers, maleic anhydride and particularly methacrylic acid are most frequently favored. Carboxylic homopolymers, where they can be formed, might be considered the simplest examples of ASTs were it not for the fact that they are not copolymers as defined, and some are water soluble in their un-ionized states. Examples of carboxylic homopolymers are the un-ionized free-radical-polymerized atactic forms of polyacrylic acid (1) and polymethacrylic acid (2), which are both readily soluble in water.

Most conventional ASTs are copolymers consisting of just two monomers, and these thickeners are presumed to lack associative properties except for a few possible exceptions, which will be discussed later. For water in-

solubility at low pH, conventional ASTs must contain one or more hydrophobic comonomers in addition to the more hydrophilic carboxyl-containing acid monomers previously mentioned. The hydrophobic monomers must also be present in appropriate concentration to provide proper hydrophilic–hydrophobic balance to render the copolymer water insoluble prior to neutralization, but allow swelling or solubility in aqueous media at some higher pH. The carboxylic and hydrophobic monomers are mutually dependent in that respect. Typical hydrophobic monomers that have been used in the preparation of conventional ASTs are the alkyl acrylates, alkyl methacrylates, styrene, vinyl acetate, ethylene, butadiene, and acrylonitrile. Ethyl acrylate is most frequently cited.

More recently, conventional ASTs have been modified with monomers (macromonomers) containing ethoxylation and terminal hydrophobe functionality to produce associative ASTs. There is overwhelming agreement that these and the more common nonionic associative polymers (e.g., HEUR, or hydrophobically modified, ethoxylated urethane) represent a significant advance in thickener technology by conferring higher degrees of thickening or unique rheology to aqueous solutions and aqueous media containing dispersed-phase components. The advantages and disadvantages of associative thickeners in general (3) and their influence on coating performance have been assessed (4–8).

From a theoretical point of view, any WSP potentially can be suitably modified to construct an associative thickener. Associative ASTs, however, are usually terpolymers consisting of a carboxylic monomer, a hydrophobic monomer, and a third monomer that is associative. These thickeners are prepared by using many of the same polymerization procedures used for conventional ASTs, and many of the same carboxylic acid monomers and hydrophobic monomers are employed. The presence of carboxylic or anhydride monomer is, of course, mandatory, but the hydrophobic monomer can be omitted if the associative monomer is able to impart the proper hydrophilic–hydrophobic balance for the necessary pH-dependent solubility. In Figure 1, the schematic structure of an associative AST is contrasted with that of a conventional AST. Also depicted are other associative moieties, including a nonionic surfactant, an ethoxylated anionic surfactant, and a typical nonionic associative thickener structure. The structural features common to the anionic species and those common to the associative species become obvious.

The associative monomers used to prepare associative ASTs most frequently contain a long-chain hydrophilic segment terminated with a hydrophobic group. The hydrophilic segment usually consists of polyethoxylation or poly(ethoxylation–propoxylation) situated between the ethylenic unsaturation at one end of the molecule and the terminal hydrophobe at the other end. In one common mode of synthesis, the associative macromonomers are conveniently prepared by coupling the hydroxyl end group of a conventional

Nonionic Surfactant

Nonionic Associative Thickener

Anionic Surfactant

Conventional AST

Associative AST

Where: Terminal Hydrophobe

Hydrophobic Linking Group

Carboxylic Monomer Or Group

Hydrophobic Monomer
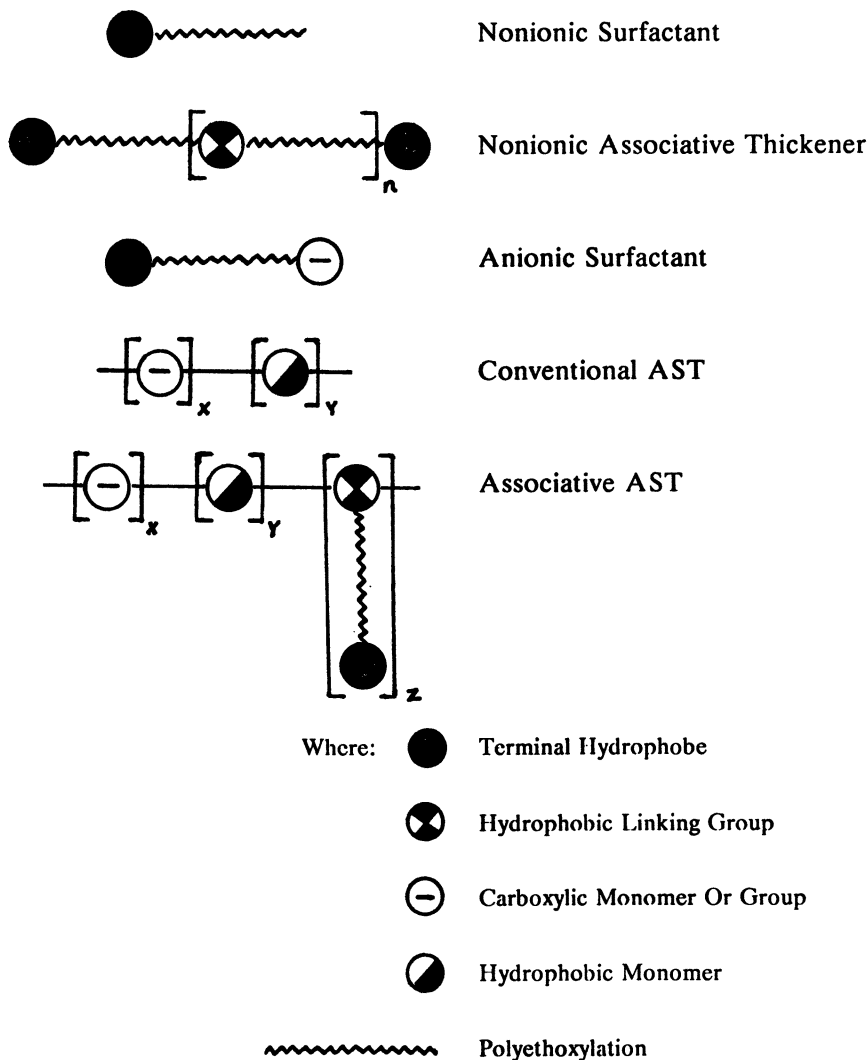
Polyethoxylation

Figure 1. Schematic representations of a nonionic surfactant (e.g., 30 mol of ethoxylate of lauryl alcohol), a nonionic associative thickener (e.g., HEUR) where n is typically 1–10 units, a hypothetical anionic surfactant with ethoxylation and carboxyl end group, a conventional AST (e.g., ASE or ASNE), and an associative AST (e.g., HASE or HASNE) where x, y, and z are normally of random distribution, and molecular weight is from 50,000 to 1,000,000 or more.

nonionic surfactant with a monomer containing polymerizable ethylenic unsaturation. Variability within the macromonomer structure is obtained by altering the type of terminal hydrophobe, type of ethylenic unsaturation, ratio and degree of poly(ethoxylation–propoxylation), and component-linking functionalities.

As an option in both associative and conventional ASTs, some minor amounts of other water-soluble or water-insoluble monomers may be included, as well as minor amounts of polyethylenically unsaturated monomers, to provide a low degree of cross-linking. The nuances of classification by chemical architecture are elaborated on further in this chapter under the section entitled "AST Thickening Mechanisms", subsection "Associative or Nonassociative?"

Classification by Polymerization Process

As mentioned previously, both aqueous and nonaqueous processes have been employed in the preparation of conventional and associative ASTs. In addition to classification by structure, a distinction between processes is also made in the literature.

The AST process receiving the greatest industrial and academic attention by far has been that of emulsion polymerization, and because of the relative importance of the emulsion thickeners, these polymers will be the object of considerable discussion in this review. When conventional ASTs are specifically prepared by this process, alkali-swellable or alkali-soluble emulsions (ASE) are obtained. For conventional ASTs produced by processes other than emulsion polymerization (nonemulsion), the acronym ASNE has been adopted herein. The associative ASTs have analogous designations. HASE is the common acronym for hydrophobically modified, alkali-swellable or alkali-soluble emulsion, and HASNE is the adopted acronym for the associative nonemulsion thickeners. The family of AST polymers reflecting this classification scheme is shown in Figure 2.
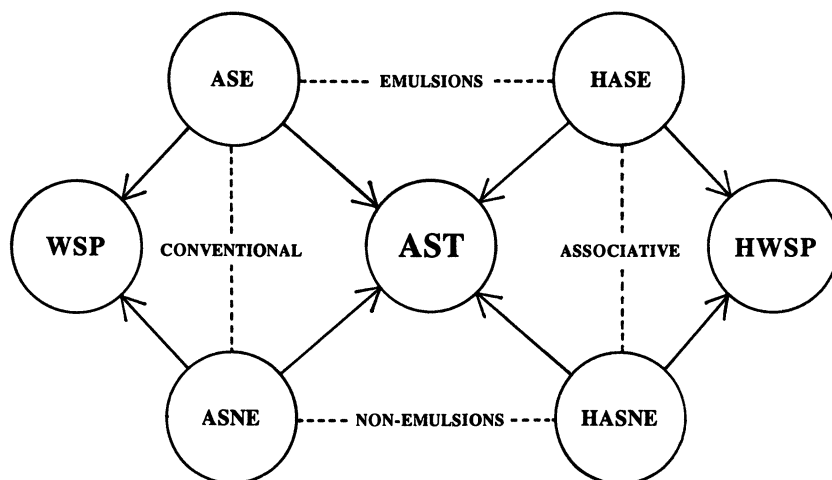
Figure 2. Classification scheme for the family of alkali-swellable and alkali-soluble thickeners (AST). All acronyms are defined in the text and in the list of Symbols and Abbreviations.

The AST emulsion polymers (ASE and HASE) typically are prepared with 10–80% carboxylic acid monomer, water-soluble persulfate initiators, and a preference for anionic surfactant stabilizers. In early accounts, Fordyce et al. (9, 10) highlighted some of the advantages of ASE thickeners over the usual acrylic water-soluble salts that are prepared as aqueous solutions or powders. Among the advantages claimed were in situ thickening, production at relatively high solids, low emulsion viscosity, ease of dilution, solubilization with a variety of bases, and high thickening efficiency resulting from inherently high molecular weight. In contrast, polymers made in aqueous solution required low solids production for high molecular weight. This reduced yield adversely affected manufacturing and shipping costs. The acrylic water-soluble salts that are dry powders were developed to overcome this limitation, but these polymers were usually hygroscopic, dusty, and relatively slow to dissolve. Although not mentioned, the large amount of water needed for dilution of the higher molecular weight aqueous solution and powdered thickeners limits use in many applications because not enough water is available for formulating other components. A more comprehensive treatment of the compositions, polymerization processes, and performance features of industrially developed ASE and HASE thickeners is presented later in this review under the section entitled "A Survey of the Patent Literature".

Rogers-Moses and Schaller (11) and Shay and Rich (12) discussed the advantages of the HASE thickeners in pigmented coatings. Included were the advantages of emulsion thickeners in general as previously discussed, plus those unique to the presence of the associative components (i.e., improvements in thickening efficiencies, flow and leveling, brush-drag, spatter resistance, and gloss development). Improved aqueous solution viscosities are also occasionally observed with the HASE thickeners, and the Newtonian or less pseudoplastic rheology imparted by these thickeners is useful in other coatings and noncoatings applications.

Carboxylic Acid Distribution Within ASE and HASE Latices

In the nonaqueous polymerization processes that are conducted in organic solvent or diluent, many of the carboxyl-containing monomers cited have successfully been used in the preparation of ASNE and HASNE ASTs. Reactivity ratios, rates of reaction, monomer–polymer solubilities, economics, and degree of polymerization were among the criteria considered in monomer selection. However, in the important aqueous processes of suspension and particularly emulsion polymerization, the water solubility and hydrophilicity of the carboxylic monomer was found to be of considerable importance. Fordyce and Ham (13) observed that a significant portion of itaconic acid polymerized in the aqueous phase when emulsion polymerization was carried out with styrene. Fordyce et al. (9, 10) reported that

attempts to replace methacrylic acid with acrylic acid or itaconic acid were unsuccessful because of poor emulsion stability. Guziak and Maclay (*14*) found that acrylic acid (more water soluble and more hydrophilic than methacrylic acid) diffused with difficulty into the polymer particles and formed more water-phase polymer, while methacrylic acid diffused easily and copolymerized well. Greene (*15*) also reported a large proportion of acrylic acid in the aqueous phase of carboxylated styrene–butadiene latices, and the amount of acid located there increased substantially with increasing degrees of neutralization during polymerization.

Using primarily potentiometric and conductometric titration, several investigators also reported variations in the distribution of the carboxylic acid monomer within the AST emulsion particles. Guziak and Maclay (*14*) showed that carboxylic acid monomers tended to concentrate near the particle surface of the styrene–acrylic and styrene–butadiene latices studied. Acrylic acid had a greater tendency for surface concentration than did methacrylic acid. Treatment of the latices containing greater than about 20% carboxylic acid monomer with inorganic base produced clear aqueous solutions that were extremely viscous. In an electrophoretic study, Matsumoto and Shimada (*16*) also found a preferential concentration of acrylic acid near the surface of latices. In contrast, methacrylic acid diffused readily into the particles, where it copolymerized favorably with methyl methacrylate.

Muroi (*17*) obtained similar results on examining the swelling–dissolution behavior and acid distribution of high carboxyl-containing latex emulsions as a function of pH for copolymers of ethyl acrylate with acrylic and methacrylic acids. The acid distribution within the ASE particles was determined by conductometric and potentiometric titration, and end points were obtained that accounted for all of the acid incorporated into the polymerization recipes. The conductometric titration was particularly useful in that three equivalence points were observed: the first for strong acid initiator species, the second for particle surface plus aqueous-phase carboxyl groups, and a third for particle core carboxyl groups. By concurrently following the optical density of the diluted emulsions as a function of pH, morphological changes in the emulsion particles were observed with supporting observations by electron microscopic examination. As the pH was raised, the surface layers of the latex particles began to dissolve, and the cores began to swell near the second conductometric equivalence point. Cores deficient in carboxyl only swelled and would not dissolve even at high pH, and the extraction of films containing these polymers cross-linked with melamine resin produced polymer containing no carboxyl functionality (*18, 19*). These findings suggested that most of the carboxyl groups were indeed near the particle surface.

Using an improved conductometric titration procedure, Nishida et al. (*20, 21*) and Loncar et al. (*22*) quantitatively investigated the alkali-swelling behavior of highly carboxylated MMA–MAA copolymers. The ratio of surface

to core carboxyls in the particles tended to increase with increasing concentration of acid for batch latices, but the acid was more evenly distributed throughout the particles in similar latices made by semicontinuous emulsion polymerization. The effect observed for the batch latices was believed to be due to conformational changes in the copolymer chains to maximize the number of carboxyl groups at the surface.

Although carboxylic acid monomer concentrations were too low to form alkali-responsive thickeners in many instances, several other studies generally confirmed prior observations of acid concentration at the latex particle surface. Greene (15) used neutron activation analyses and turbidimetric titration, separately, to determine total acid and surface acid. Approximately three times as many carboxyl groups were found at the surface of styrene–butadiene latices as were in the particle cores, regardless of the initial amount of acid present (1–5%) during polymerization. In the preparation of soap-free carboxylated polystyrene latices, Sakota and Okaya (23) concluded that the observed localization of acid on the particle surface was governed by the electrostatic repulsion between the carboxyl groups. The concentration of carboxyl groups at the particle surface was also dependent on the degree of neutralization during polymerization, but the surface area occupied by individual carboxyl groups remained almost constant with pH. Using the conductometric back titration method of Hen (24), Vijayendran (25) determined the acid distribution of polystyrene latices containing low levels of various carboxylic acid monomers. He showed that the partition coefficients of the acids between styrene and water (methacrylic acid > acrylic acid > itaconic acid) were in the inverse order of observed particle surface concentration. Also observed was a decrease in surface-bound acid with increasing particle diameter. In other low-acid-containing latices, Bassett and Hoy (26) and Egusa and Makuuchi (27) independently determined that most of the measured acrylic acid carboxyl groups incorporated were near the surface of the acrylic latices prepared.

AST Thickening Mechanisms

Conventional Linear ASTs. The increase in viscosity that occurs on neutralization of certain types of carboxylated copolymers in aqueous media is a well-known phenomenon, and the earliest theoretical descriptions of the process are still substantially accepted (28–30). In the generalized case for linear polymers forming true solutions, as pH is raised and carboxyl groups are neutralized, the polymer molecules become hydrated, and their molecular coils expand because of electrostatic repulsion of the carboxyl-anion charge centers. This coil expansion results in dissolution and an increase the polymer's hydrodynamic dimensions, which in turn increases intermolecular entanglement and resistance to flow. The increase in solution viscosity that occurs in this process is referred to as "hydrodynamic thickening".

The thickening mechanisms of linear carboxyl-containing emulsion polymers have been studied in considerable detail. The polymer molecules of AST emulsions are initially in a coiled configuration within individual latex particles of submicrometer size, and the viscosity of the diluted latex emulsion is similar to that of water prior to neutralization. On the addition of base, the carboxyl groups are ionized, and hydrophilic polymer is formed within the particles. Depending on various factors, which will be elaborated on later in this chapter under the section entitled "Factors Affecting the Swelling Dissolution Behavior of Conventional ASTs", the particles may only swell or dissolve completely, or the surface polymer may dissolve and leave swollen cores.

Verbrugge (31) concluded that a single mechanism explains the thickening process during neutralization of all (conventional) acid-containing latices: varying degrees of particle swelling followed by dissolution of the more hydrophilic copolymers. The particles commonly exhibit a highly swollen state with maximum viscosity at some lower degree of neutralization. At some higher pH, the polymers are solubilized if they are sufficiently hydrophilic, and the viscosity drops. However, the solution viscosity at the higher pH is still much greater than that of the unneutralized latex. Muroi (17) reported coagulation on reacidification of what appeared to be solubilized ASE polymer, a result suggesting that the particles had been mostly dissolved and could not be reconstituted to their original particulate form. Destabilization of swollen latex particles on reacidification due to surfactant depletion or increased salt concentration may have been an alternate explanation.

Cross-Linked Conventional ASTs. The incorporation of small amounts of polyethylenically unsaturated monomers to enhance the swelling of ASTs has been variously reported and apparently is a fairly common practice. This option is frequently cited in the patent literature, and in a few instances, it is a necessary condition for optimum thickening. The polyfunctional monomers are included in the thickener recipes to lightly cross-link the latex particles. When diluted and swollen with alkali, clear microgel solutions are formed that are often indistinguishable to the naked eye from ASTs forming true solutions. The swellable emulsions are said to be substantially more efficient thickeners for both water and dispersed-phase aqueous systems, but efficiency is very dependent on the level of cross-linker (10). Cross-linker levels of less than about 1% are normally employed, and some optimum level generally exists for maximum thickening efficiency. Amounts too low produce excessive solubility and insufficient swelling, and higher levels produce polymer so tightly cross-linked that the microgel particles cannot swell appreciably or may not swell at all.

Verbrugge (31) separately prepared ASEs containing hydrophilic cross-linking and non-cross-linking monomers. The cross-linked polymers had alkaline viscosities much higher than any of the non-cross-linked polymers prepared as controls. The general thickening mechanism that he proposed

for linear and cross-linked ASEs was further supported by microscopic examination of the particles as a function of pH (32). Depending on composition and molecular weight, some polymers went directly into the aqueous phase without swelling to form true solutions. Some showed surface polymer dissolution with swelling of the polymer cores, and others only showed swelling.

Fordyce et al. (10) considered the thickening mechanism of the cross-linked microgel particles to be quite different from that of linear polymers, which are truly solubilized in water. Chain entanglement of individual molecules in solution is the primary mechanism of thickening for the solublized linear polymers, but the mechanism proposed for microgel particles was thought to be a consequence of the swollen state occupying a much larger volume of the solution. In theory and actual practice, swelling diameters several hundred times the original particle dimensions can be obtained, and in the limiting case, the swollen particles can occupy the entire volume of solution. This proposed mechanism of thickening suggests that the viscosity of the microgel solution should be less sensitive to temperature, and lower sensitivity was indeed found to be the case (10).

Conventional ASTs in Dispersed-Phase Systems.

Much of the industrial and academic development of ASTs has been directed to use in thickening compounded and uncompounded latices (e.g., latex paints, carpet backing latex). Fordyce et al. (9, 10) and Brown and Garrett (33) postulated that the primary thickening action of what we now categorize as "conventional" AST polymers in dispersed-phase latex systems was due to adsorption of individual polyelectrolyte thickener molecules on the latex particle surfaces. This interparticle adsorption or "molecular bridging" was proposed to build structure into the latex system, resulting in viscosity enhancement. Their data supported this conclusion by showing that the aqueous solution viscosities of these thickeners were magnitudes lower at equal thickener concentration than those obtained in the presence of latex emulsions. Although crowding may have been a factor to some degree, the addition of certain surfactants markedly reduced the viscosity of the thickened latices. This effect was attributed to preferential absorption of the surfactant and displacement of the thickener from the latex particle surface.

Associative ASTs.

Nonionic and anionic associative thickeners are presently considered state of the art in many important industrial applications. The anionic associative thickeners are a subclass of hydrophobically modified, water-soluble polymers (HWSPs), and are predominantly represented by hydrophobically modified ASTs (HASEs and HASNEs), the chemical architectures of which were previously described. Because these polymers are very similar to conventional ASTs in molecular weight and carboxyl content, thickening is by a dual mechanism: hydrodynamically (a function of molecular weight, anionic content, cross-link density, and other

factors), and associatively (because of hydrophobic interactions). Because the hydrodynamic component of thickening is present for both conventional and associative ASTs, it is the associative mechanism that is responsible for the enhanced thickening and unique rheology frequently observed in aqueous solutions and dispersed-phase aqueous systems containing these thickeners.

The associative mechanism of thickening has been variously described, but is generally thought to result from nonspecific hydrophobic association of water-insoluble groups in water-soluble polymers (*34, 35*). For associative ASTs, the terminal hydrophobes of the ethoxylated side chains are considered to be the primary interactive components. These hydrophobes can interact with each other via intermolecular association, and can also interact with hydrophobic particle surfaces when present. The specific interaction with dispersed-phase components such as latex particles has been shown to be one of surface adsorption (*36*). In essence, the associative component of thickening in dispersed-phase systems also has dual character resulting from the building of structure within the aqueous phase and interaction with particle surfaces.

The intermolecular association of the terminal hydrophobes of associative ASTs in aqueous solution is analogous to the association of surfactant hydrophobes to form micelles. But, unlike conventional surfactants that have hydrophilic–hydrophobic (head–tail) polarity, the associative ASTs, if relatively uniform in composition, would be expected to have an overall hydrophilic–hydrophobic symmetry, resulting in a tendency to micellize in continuous associative networks. However, because of the functional similarities to surfactants, these polymers are sometimes referred to as "polymeric surfactants" or "polysoaps". Chu and Thomas (*37*) reported that under appropriate conditions, polyelectrolytes with hydrophobic side chains form microdomains in solution, exhibiting behavior reminiscent of polar surfactant micelles. Using a spectroscopic adaptation of the iodine solubilization method of Ross and Olivier (*38*), Brown and Glass (*39*) determined the critical micelle (association) concentrations of model associative star polymers to study their structure–property relationships. They determined that more hydrophobic polymers associate at lower concentration than do homologous polymers of lower hydrophobicity. Unlike the sharp CMC (critical micelle concentration) end points observed for surfactants, however, those of polymeric micelles tend to be more broad and not as well defined. Diblock copolymers that form polymeric micelles structurally similar to the star polymers were also studied (*40*). A model proposed by de Gennes (*41*) is the basis of current thermodynamic theories of polymeric micelle formation. Chung and Rehfeldt (*42*) provided a general overview of analytical techniques for the characterization polymeric surfactants.

Structurally, the backbone of an associative AST copolymer is predominantly hydrophilic because it contains sufficient carboxyl anion to render it water soluble at elevated pH. The ethoxylated side chains attached to the

backbone are also hydrophilic, and thus, the interior portion of the molecule would be expected to be highly hydrated. The terminal hydrophobes at the ends of the ethoxylate side chains hypothetically would be repelled from this environment and at the same time attracted to other terminal hydrophobes or hydrophobic surfaces if present. Like surfactants, the driving force for association is a result of the entropy gained by loss of water structuring around the hydrophobes and a minimization of the water-hydrophobe contacts (43).

Associative or Nonassociative?   On the basis of the evidence presented in the literature, little doubt remains about the associative nature of ASTs containing hydrophobically terminated ethoxylate macromonomers. Although the term "associative" was not used at the time, the bridging mechanism proposed by Fordyce et al. (9, 10) in the late 1950s for what we now consider to be conventional AST polymers (EA–MMA–MAA) in dispersed-phase aqueous media actually represented an associative component of thickening. The association exhibited, however, was likely to have been of relatively low order of magnitude, and due only to adsorption of the thickener molecules onto the dispersion particle surfaces. Little aqueous-phase intermolecular association would have been expected for these polymers other than the usual chain entanglements, which occur for both associative and nonassociative ASTs. Possible exceptions to this expectation might be heterogeneous AST block copolymers or AST polymers lacking ethoxylated segments but containing particularly long-chain hydrophobic monomers (e.g., dodecyl methacrylate, octadecyl acrylamide). For octadecyl acrylamide, these monomers may be of sufficient length to extend beyond the carboxyl environment, and thereby increase the possibility for intermolecular hydrophobic association. This situation would be in contrast to the more commonly used short-chain hydrophobic monomers like ethyl acrylate, which are are more hydrophilic and probably too short for significant associative interaction.

Hydrophobic microdomain structures (polymeric micelles) exist even in the low pH range for copolymers of maleic anhydride and alkyl vinyl ethers, but only compact coils exist at very low pH (44). Although the molecular weight of the polymer was quite low relative to most ASTs, Chu and Thomas (37) also reported hydrophobic microdomain structure (one polymer molecule per micelle) for the potassium salt of alternating copolymers of maleic anhydride and 1-octadecene. McCormick and Middleton (45) examined the associative properties of carboxyl-containing acrylamide-co-N-n-decylacrylamide copolymers prepared by a micellar polymerization technique. Although these polymers, strictly speaking, are not ASTs because of the high level of water-soluble acrylamide present, they bear a strong resemblance structurally. Unique solution properties and enhanced viscosity resulting from interchain association of the n-decylacrylamide hydrophobes were re-

ported with and without carboxyl present. A quantitative spectroscopic technique was developed by Valint et al. (46) to determine the incorporation of phenyl-containing hydrophobe monomers into similar carboxy functional anionic and nonionic acrylamide copolymers.

In the particular instances just discussed, and in the patent literature to be cited later, the classification of an AST as either conventional or associative may not be immediately obvious without physical characterization. All ASTs in fact may exhibit some level of association, and any distinction may, therefore, be only one of degree. For purposes of classification within this chapter, however, a chemical distinction has been made: only ASTs containing hydrophobically terminated ethoxylate macromonomers are classified as associative. An indication of the true mechanisms operating for other chemical architectures might be ascertained by comparing solution to dispersed-phase viscosities, or by observing the effects of surfactant addition on viscosity and polymer desorption from hydrophobic surfaces. The chemical description and use of some individual AST emulsions described in the literature suggest potential for multiple thickening mechanisms: particle swelling due to cross-linking or cores deficient in carboxyl groups, chain extension and chain entanglements of dissolved polymer, intermolecular association of hydrophobes, and association–adsorption of hydrophobes with dispersed-phase particle surfaces when present.

Factors Affecting the Swelling Dissolution Behavior of Conventional ASTs

Many studies were conducted by various investigators to determine the effects of polymerization and other parameters on the thickening, swelling, and dissolution behavior of conventional ASTs. A listing of factors known to to have an effect in conventional AST emulsion thickeners (ASE) is given in List 1, and details concerning some of these are provided in the following discussion.

Factors Affecting Solubility. Using optical density as a measure of solution clarity, Muroi (17, 19, 47) examined some of the chemical and physical factors that affect the degree of solubility for conventional ASTs prepared by emulsion polymerization. The solubility was shown to depend on the type of carboxylic acid used, the amount of carboxyl present, the hydrophilicity of the hydrophobic comonomers, the degree of polymerization, polymer chain configuration, and the dissolution temperature. For the carboxylic monomers studied (acrylic and methacrylic acids), the pH at which optical density started to decrease (beginning of dissolution) shifted to the acid side with increasing carboxyl concentration, and methacrylic acid (MAA) units dissolved more sharply at higher pH than did those with acrylic acid (AA). The relative hydrophilic character of the hydrophobic comonomers

List 1. Factors Known To Affect the Thickening, Swelling, or Dissolution Behavior of Conventional AST Emulsion Polymers (ASE Thickeners)

Type of carboxylic monomer
Level of carboxylic monomer
Hydrophilicity of the hydrophobic comonomer
Glass transition temperature of the hydrophobic comonomer
Polymer chain configuration
Degree of polymerization
Degree of cross-linking
Degree of neutralization
Swelling and dissolution temperature
Monomer polarity
Monomer sequence distribution
Polymerization procedure
Emulsion particle size

NOTE: The factors listed here for conventional AST emulsions are also generally applicable to the associative AST emulsions.

was predicted from the cohesive energy density (CED) values of the respective homopolymers. On the basis of these values, an increase in hydrophilicity of the comonomer generally resulted in an increase in alkali solubility. When the ethyl acrylate (EA)–MMA ratios of carboxylated terpolymers were varied, percent solubility increased rapidly with increasing levels of EA for both series. Because the CED values for both hydrophobic monomers were similar, Muroi suggested that lower copolymer glass transition temperature (T_g) results in higher alkali solubility. Styrene exhibited the lowest solubility of all, and when substituted for MMA, which has the same homopolymer T_g, little or no thickening was observed. Verbrugge (32) and Muroi (47) both reported increased solubility with decreasing molecular weight. Muroi attributed this observation to increased particle swelling and Verbrugge to decreased chain entanglement.

Factors Affecting Thickening Efficiency. Fordyce et al. (9, 10) reported significant viscosity increases for methyl methacrylate (MMA)–EA–MAA terpolymer emulsions on addition of base. Using light scattering, Wesslau (48) found a direct relationship between the degree of thickening of a latex and the volume change of the particles on addition of ammonia for low-acid-containing copolymers. For higher degrees of carboxylation, however, clear solutions are frequently obtained for many AST systems, which may be true solutions in the limiting case, swollen particles, or a combination of both. This result makes their microscopic characterization difficult. Optical density measurements are also subject to interpretation because they are greatly influenced by small amounts of impurities or polymer inhomogeneity. Because of these difficulties, Verbrugge (31) examined the magnitude and character of thickening as a function of pH for acid-containing emulsion copolymers by means of viscometry at constant shear

rate. In preliminary experiments, he reported that the viscosities of freshly neutralized AST latex samples decrease with time at all pH values. Equilibration was mostly complete after 1 day, and completely stable viscosities were obtained after 2 days.

Variables that affect thickening were studied by using the equilibrium viscosity measurements obtained versus pH for several series of MAA-containing copolymers. The most important variables determined for maximum thickening were the level of methacrylic acid (high concentration best), the polymer T_g (low T_g best), and the hydrophilicity of the comonomers (more hydrophilic best). Carboxylic copolymers containing styrene (very hydrophobic, high T_g monomer) did not even swell, and at the other extreme, ethyl acrylate copolymers dissolved completely. Decreased particle swelling with decreased molecular weight was also observed by viscosity measurements and microscopic examination for both hard and soft monomers. The type of base used for neutralization had no observable effect on the magnitude of swelling and dissolution, but the slight viscosity reduction occurring above 100% neutralization for NaOH-neutralized latices compared with ammonia was attributed to an ionic effect.

Loncar et al. (22) examined the alkali swellability of carboxylated copolymer emulsions varying in the type of hydrophobic comonomer and the homopolymer T_g of the comonomer. At higher levels of carboxylic acid, copolymers with MMA showed good swelling behavior, but those containing styrene (more hydrophobic) showed little or no swelling, as indicated by much smaller changes in particle size and viscosity. The high percentage of unneutralized carboxyl groups in the styrene-containing copolymers was also consistent with this finding. Cross-linking further suppressed swelling of the styrene-containing copolymers, and only a small percentage of the carboxyl groups could be neutralized. These observations suggested that the combination of limited chain mobility (high T_g) and high hydrophobicity prevented penetration of the hydroxyl ions and resulted in a nonswelling polymer. However, low T_g copolymers with a more water-insoluble comonomer (2-ethylhexyl acrylate, EHA) than styrene (0.01% versus 0.03%) produced similar nonswelling behavior. The EHA copolymer had a much larger fraction of acid in the particle surface layers than did the styrene copolymer. The investigators suggested that the much higher mobility of the soft EHA copolymer chains facilitated their rearrangement and allowed the carboxyl groups to migrate to the surface. An important resulting conclusion of this work was that even low T_g monomer, if sufficiently hydrophobic, can exhibit little or no particle swelling in ASTs.

Effect of Degree of Ionization. In an idealized AST neutralization, as the degree of ionization approaches 100%, solution viscosity reaches a maximum value because of maximums in electrostatic repulsion and hydrodynamic chain volume. However, Yudelson and Mack (30) reported that

many carboxyl-containing copolymers show peculiar viscosity maxima in a relatively narrow pH range at degrees of ionization considerably less than 100%. The viscosities at the maxima were so high as to suggest gelation in spite of the fact that the intrinsic (very dilute solution) viscosities were substantially less than those at 100% neutralization. The addition of alcohols, salts, and surfactants reduced the viscosity of these low ionization maxima. The salt effect suggested that electrostatic repulsive effects in addition to hydrogen bonding were operating in the gelation region, and that at the viscosity maxima, forces of attraction (hydrogen bonding), and forces of repulsion (coulombic repulsion of carboxylate ions) were equal. The predominant force of attraction was attributed to carboxyl–ester interaction for the acrylate copolymers studied. Longer chain hydrophobic monomers such as butyl acrylate produced no gelation tendencies, and the investigators believed that the formation of the carboxylate–ester bonds is obstructed in these copolymers.

In the equilibrium viscosity studies conducted by Verbrugge (31), all the data (viscosity versus level of ionization) obtained fit one of three general curve shapes: (1) no viscosity increase or a slight increase to some plateau value, (2) a significant increase in viscosity to a plateau value that remains constant or decreases slightly, or (3) a sharp maximum (possibly at a degree of ionization less than 100%) followed by a lower plateau value. The third curve shape is similar to that observed by Yudelson and Mack (30). According to Verbrugge (32), the final state (swollen or dissolved) of the neutralized latices can be revealed by examining the shapes of the neutralization curves.

Later, Nishida and co-workers (20, 21) also reported observing viscosity maxima at ionization levels less than 100%. Hydrogen bonding was presumed to be an important factor. They hypothesized that swelling should be quite high at the viscosity maxima to allow the particles to strongly interact with each other. Under these conditions, the unneutralized carboxyl groups could more easily form intermolecular and intramolecular hydrogen bonds with other carboxyl and ester groups, and this bond formation would lead to further viscosity enhancement. At higher levels of neutralization, the remaining carboxyl groups would predictably be ionized, and the result would be a loss of carboxyl hydrogen bonding and consequential reduction in viscosity.

Stackman and Hurley (49) used turbidimetric measurements and dissolution experiments to characterize the aqueous solubility characteristics of various acrylate–acrylic acid copolymers prepared by solution polymerization in methanol. When phase diagrams of percent neutralization versus percent acrylic acid were generated, the phase boundaries for solubility fell on nearly the same line. This result allowed approximation of the neutralization requirement for other acrylate ester–AA copolymers.

Effects of Polymerization Procedure.   Polymerization procedures have been studied in considerable detail to determine effects on the particle

morphology and thickening behavior of carboxylated latex systems. Sakota and Okaya (50) demonstrated that the distribution of carboxyl groups within styrene–isoprene latices can be controlled by altering the method of introduction of the carboxylic monomer. Bassett and Hoy (26) and Hoy (51) examined the expansion characteristics and effects of reaction pathway on carboxylic emulsion polymers of relatively low acid content. As reported previously, they concluded that most of the carboxyl groups were concentrated near the surface region of the particles. What was surprising, however, was that this concentration occurred whether the acid was added near the beginning or the end of the polymerization. Because no buffer or neutralizing agent was used, the propagating species was presumed to be the un-ionized acid.

At higher pH, however, the acid was increasingly partitioned to the aqueous phase. Sedimentation was used to determine particle surface layer expansion as a function of pH. Maximum expansion was found near the point of complete neutralization, and the highest level of expansion occurred when the acid was added late in the polymerization and was least when fed uniformly throughout the polymerization. The swelling variations observed were apparently related to acid sequence distribution and chain entanglement. The trend for maximum expansion with respect to the carboxylic acid incorporated was acrylic > methacrylic >> itaconic. No particle swelling was observed for PS or PMMA latices containing similar amounts of carboxyl functionality. In fact, some contraction was observed. The investigators concluded that the polymer backbone was too stiff to allow expansion, and thus prevented the carboxyl groups from migrating to the surface.

In another set of carboxylated emulsions prepared with similar T_g, styrene–ethyl acrylate (S–EA) copolymers showed no expansion, but MMA–EA copolymers did. This finding strongly suggested that monomer polarity is also an important factor. The more polar MMA copolymer apparently was able to interact with the highly polar aqueous phase and was thereby plasticized.

Egusa and Makuuchi (27) examined the acid distribution of carboxylated latices prepared by radiation-initiated versus chemically initiated emulsion polymerization. As determined by conductometric titration, the radiation-initiated polymers contained considerably lower levels of "free" (aqueous phase) acid and somewhat higher levels of "buried" (subsurface or particle core) acid. Again, most of the acid was located at the particle surface, but the amount present was similar for both processes. Nishida and co-workers (20, 21) quantitatively examined the effects of polymerization procedure (batch versus semicontinuous emulsion polymerization) on the thickening behavior of methacrylic acid containing ASTs cleaned by serum replacement. Molecular weight was found to be independent of MAA content and polymerization process; however, the molecular weight distribution was somewhat broader for the batch process. The semicontinuous latices showed several orders of magnitude increase in solution viscosity on neutralization,

but the batch latices even at the highest MAA content remained milky in appearance and exhibited little viscosity increase. The viscosity of the semicontinuous latices also showed a stronger dependence on shear rate, a result suggesting extensive structure formation in the dispersion due to strong interaction between the dispersed material.

Using turbidity (optical density) measurements of dilute ammonia solutions and NMR for monomer sequence distribution, Morgan and co-workers (52, 53) studied emulsion polymerization process variables to improve on the copolymer homogeneity of relatively low molecular weight styrene–acrylic acid copolymers. In spite of very favorable reactivity ratios, they reported that emulsion copolymers of S–AA in general are quite heterogeneous, containing relatively long sequences of water-insoluble polystyrene. Of the variables studied, the most important for improved heterogeneity (solution clarity) was a slower monomer addition rate, making the system more monomer starved, and thereby improving copolymerization.

Factors Affecting the Swelling Dissolution Behavior of Associative ASTs

Because the hydrodynamic thickening mechanism of conventional ASTs (ASE and ASNE) is also present in the associative ASTs (HASE and HASNE), common factors affecting the thickening behavior of both types of thickeners would be expected, and are indeed observed. In a previously unpublished study (DeSoto, Inc. internal report), Brizgys and Shay examined the effect of the nonassociative hydrophobic comonomer on the thickening behavior of urethane-functional HASE thickeners prepared under identical conditions of semicontinuous emulsion polymerization. The results (Table I) obtained with respect to T_g and water solubility of the hydrophobic comonomer were generally similar to those observed for conventional ASTs by others cited earlier in this chapter.

Factors that affect the associative properties of the HASE thickeners have also been studied, and a summary of those having an effect on the thickening or rheology of these thickeners in aqueous and dispersed-phase systems is given in List 2. In a review of commercialized and proposed associative thickener technologies, Evani and Rose (54) discussed the chemical parameters affecting the viscosity behavior of styrene–maleic anhydride copolymers that were condensed with nonionic surfactants to form HASE thickeners. They reported increased thickening efficiency with increasing molecular weight, increasing chain length of the terminal hydrophobe, increasing degree of ethoxylation in the esterification surfactant, and increasing degree of anhydride esterification. These thickeners, which are frequently referred to as SMAT (styrene maleic anhydride thickeners) marked the commercial introduction of HASE thickeners to the coatings industry. However,

Table I. Effect of Hydrophobic Comonomer on Aqueous Solution Properties
of Associative AST Terpolymer Emulsions

Hydrophobic Monomer in AST Terpolymer[a]			1% Aqueous Solution of AST[b]	
Type	Homopolymer T_g (°C)	Water Solubility (% at 25 °C)	Viscosity[c] (cP)	Clarity[d] (relative)
2-Ethylhexyl acrylate	−86	0.01	76	clear
Butyl acrylate	−54	0.20	13,400	clear
Ethyl acrylate	−22	1.50	33,200	clear
Methyl acrylate	8	5.00	43,400	clear
Methyl methacrylate	105	1.50	216	opaque
Styrene	100	0.03	680	very hazy

[a]The terpolymers had the following constant composition by weight: 30% hydrophobic monomer, 35% methacrylic acid, 35% associative monomer. The associative monomer is a 50 mol ethoxylated dinonylphenol adduct of α,α'-dimethyl-*m*-isopropenylbenzyl isocyanate. The procedures for the associative monomer and AST syntheses are those described in ref. 10. All raw material lots and reaction conditions were identical.
[b]Solutions were neutralized to pH 9.0 with ammonia.
[c]Viscosities were determined on a model RVTD Brookfield viscometer at 10 rpm.
[d]Clarities were relative in a one-pint jar.

List 2. Factors Known To Affect the Thickening Efficiency or Rheology
of Associative AST Emulsions (HASE Thickeners)

Type of terminal hydrophobe*
Length of terminal hydrophobe*
Degree of ethoxylation*
Type of linking functionality*
Type of polymerizable unsaturation*
Level of associative monomer
Presence of water-soluble solvents, salts, and surfactants
Presence of dispersed hydrophobic particles

*In the associative macromonomer.

the SMAT thickener was withdrawn from the market because of poor hydrolytic stability (*54*), and because of a tendency for "lifting" or "picking" of newly applied coatings containing this thickener over certain substrates (*3*). To improve hydrolytic stability, the ester groups were later replaced with benzyl ether linkages.

The effects of monomer ratio, associative monomer terminal hydrophobe, and degree of associative monomer ethoxylation on aqueous and dispersed-phase thickening were examined with urethane functional HASE thickeners (*12*). The effect of monomer ratio was complex, but higher levels of associative monomer generally increased aqueous thickening efficiency and improved the leveling and gloss development of pigmented coatings. The very hydrophobic dinonyl hydrophobe was most effective in producing high aqueous solution viscosity, although the solutions were generally more pseudoplastic. In pigmented coatings, ethoxylate side chains of intermediate length produced the best balance of leveling, brush drag, and thickening

efficiency. However, because of the complexity of interactions within associative thickener environment, some of the effects observed most likely are system dependent, and care must be exercised in applying generalizations to other associative ASTs.

Thiebeault and co-workers (34, 36) examined the flocculation and rheological characteristics of mixtures of binder latices with water-soluble polymeric thickeners. Included in the study was a HASE thickener with a molecular weight of approximately 400,000. Measurements of thickener adsorption on the binder latex particles were carried out by centrifugation of equilibrated thickener–latex mixtures. Evidence for associative thickening was obtained from the strong adsorption and lack of flocculation observed for the HASE thickener relative to the HEC thickener tested. Adsorption of this AST and other associative thickeners increased with decreasing particle diameter. Although a nonassociative ASE thickener was not included in the study, the investigators concluded that the dominant mode of interaction of nonassociative thickeners with latex particles is "volume restriction" or "depletion" flocculation (i.e., the water-soluble polymer and latex are mutually incompatible and this incompatibility results in phase separation).

On closer examination, a flocculation level was observed for the HASE thickener, but it was significantly below the level of use for paint thickening. Because of the similarities to surfactant molecules, complete desorption of the thickener was effected by addition of a sufficient level of surfactant, and the amount required increased with decreasing particle size of the binder latex. Water-soluble cosolvents were also effective in causing desorption, although larger amounts were necessary than with the surfactants. Another important observation was that the associative thickeners were markedly more Newtonian. This observation suggested that desorption and readsorption of the thickener are continually taking place under shear. The judicious addition of surfactants and cosolvents (below that necessary for flocculation) to optimize rheological properties was also discussed.

In related studies, Schaller and co-workers (35, 55) examined the effects of surfactants and cosolvents in further comparisons between nonionic associative and AST associative thickeners. At low shear rates, the low molecular weight nonionic associative thickeners lost viscosity rapidly on desorption with surfactant, and the much higher molecular weight AST thickener did not. The proposed reason for this result was that the hydrodynamic mechanism is still operational for the AST. Again, adsorption was found to increase with decreasing particle size for both thickener types, and a fit of the data to a Langmuir-type isotherm was adequate to support the hypothesis of adsorption dependence on total particle surface area. This hypothesis was said to be consistent with a model depicting hydrophobic sections of a mostly hydrophilic thickener attaching themselves to hydrophobic latex binder sites. Because latices vary greatly in their particle size

distributions and in the hydrophobicity of their particle surfaces, the choice of latex binder had a major effect on interactions with the anionic and nonionic associative thickeners examined. The type and particle size of pigments and extenders was said to be not usually important because these particles are mostly hydrophilic. Solvents that are water miscible can change the solubility parameter of the aqueous continuous phase, and these different solubility parameters altered the associative interactions. In contrast, water-insoluble coalescing agents showed little effect.

Film Formation Properties of Conventional and Associative ASTs

The hot water solubility of dried thickener films of highly carboxylated butadiene copolymer latices was examined by Verkholantsev et al. (*56*) as a function of the degree of ammonia neutralization (0–200%) and drying temperature (20 and 100 °C). The greatest water sensitivity (highest extractables) of the dried films was observed at the 50% neutralization level on Soxhlet extraction. The low extractables at 0% were attributable to the natural hydrophobicity of the copolymer, and those at 100% were apparently due to stronger film formation. This condition was believed to be the result of conformational changes in the polymer chains as a consequence of more complete dissolution during neutralization. Lower extractables of the films dried at 100 °C were partially attributed to autoxidation of the butadiene segments.

Muroi (*17*) found carboxylated ethyl acrylate emulsions to be highly swollen at high pH. He suggested that this highly swollen state may explain the empirical observations of others (*57*) that copolymerization of unsaturated acid improves film formation in spite of an elevation in the glass transition temperature. LeSota et al. (*58*) reported improvements in the exterior durability of house paints containing HASE thickeners when zinc oxide or other zinc-containing compounds were present. Early blistering was eliminated by the relatively low level addition of these compounds, which apparently combine with ammonia to form zinc complexes ionically cross-linking the thickener carboxyl groups and other carboxyl-containing components in the coating. In another investigation (*12*), the minimum film-forming temperatures (MFTs) of similar (same EA–MAA ratio) ASTs with and without a urethane functional associative monomer present were determined to study contribution to film formation. A significantly lower MFT was observed for the HASE thickener, an observation suggesting that the associative monomer was relatively "soft". The improved film formation characteristics of this monomer may also explain the improved scrub resistance obtained.

A Survey of the Patent Literature

As a result of a robust industrial interest in AST technology, many patents were sought and granted over the past 3 decades, half of which are of recent issue (*59–106*). However, the fundamental polymer chemistry on which these patents are based appears in the literature at a much earlier date. Hubbuch (*107*) describes an invention applied for in 1938 that has utility in coating compositions, textiles, and tanning agents. Although thickeners apparently were not contemplated, the products of this invention were water-soluble salts of interpolymers consisting of 30–98% by weight of monomeric methacrylic acid and from 2% to 70% of another polymerizable compound, (e.g., methyl methacrylate and propyl methacrylate). The anionic copolymers were prepared by free-radical initiation in an organic solvent. In another U.S. application 2 years later, Trommsdorff et. al. (*108*), disclosed the preparation of methacrylic acid copolymers and their use as thickeners. These polymers were said to be initially insoluble in water, but swelled and dissolved readily in aqueous alkali solution to form polymeric salts.

To provide a more comprehensive treatment of the patent literature, Tables II–VI were compiled. The patents cited in these tables are primarily compositional, and for historical perspective, they are listed in chronological order by date of issue. "Use only" patents are not included, but selected examples of these will be highlighted later. Because the U.S. patents predominate, these are listed first unless there is no U.S. equivalent to a relevant foreign issue. Also, to avoid redundancy, patents that are U.S. divisions of earlier U.S. issues (these would be nearly identical in content and claims), and any frequently cited foreign equivalents of U.S. issues are listed beside their counterparts in an adjacent column in Table II along with their issue dates.

The polymer compositions claimed (usually Claim 1) and preferred (in the body of the patent or optionally in the patent examples) are detailed in Tables IV and V. Included in these tables are the carboxylic acid monomers (A) and the hydrophobic comonomers (B) of conventional ASTs and a third associative comonomer (C) if present. As mentioned earlier, the classification of the thickeners as either conventional or associative here is a structural one based on the presence or absence of ethoxylate side-chain structures containing terminal hydrophobes. The associative mechanism of thickening is very likely to be present for those polymers classified as such. However, this mechanism may also be present, although probably to a lesser degree, for some of the polymers categorized as conventional by the defined classification system. The possibility of an associative mechanism in the conventional polymers would be more likely where longer chain hydrophobic monomers are present, as previously discussed. The "Coupling Agent" in Table V is the ethylenically unsaturated component of the associative mon-

omer to which an ethoxylated terminal hydrophobe has been adducted. The claimed and preferred coupling agents, ethylene oxide chain lengths, and terminal hydrophobes of the associative monomers are compared in this table.

Although not detailed in the tables, many of the patents optionally claim small amounts of cross-linking monomer, and in the case of associative ASTs, some propylene oxide in the ethylene oxide side chains is frequently allowed. Any additional monomers beyond these that are optional or a requirement of the patents are detailed in the text of Table VI.

On examination, the conventional AST polymers of the patent literature differ primarily in the type of hydrophobic monomer employed and in the method of polymerization. The carboxylic acid monomers (MAA is used predominantly) are normally incorporated by copolymerization with the hydrophobic and associative monomers. However, in one of the citations (66), the carboxylic monomer is generated in situ by the partial hydrolysis of poly(methyl acrylate). Although they are not classified as associative, some of the conventional AST patents employ hydrophobic monomers with long-chain hydrocarbon groups (73, 74, 80, 90, 95). As mentioned earlier, these may be of sufficient length to provide some associative thickening, which may account for the claims of improved leveling and rheology in the last two citations. Another patent (94) classified as conventional is actually quite unconventional. The emulsion polymer in this patent is prepared by using core-shell methodology. Most of the carboxylic acid incorporated in the composition is located in the core, and when encapsulated with a soft shell, a base-swellable thickener (ASE or HASE) is obtained. When the core is preneutralized with a volatile base and higher T_g monomers are used to make a hard shell, polymeric microvoids are produced. Another curious conventional thickener patent of recent issue employs an antioxidant monomer as the hydrophobic monomer (104) to minimize the effects of oxidation in coatings.

On further examination, over half of the AST patents listed were classified as associative in this review. Although most of these occur in more recent years, the earliest found (59) happens to be the first entry in the tables. In this and four other former issues (62, 64, 69, 70) that differ in the type of hydrophobic monomer employed, a maleic-anhydride-containing prepolymer is prepared and subsequently post-esterified with a nonionic surfactant. In essence, the associative side chains are grafted onto the polymer backbone. In nearly all of the other associative patents, the associative monomers are synthesized first and then copolymerized with the carboxylic acid and hydrophobic monomers. Many similarities also exist between the various associative AST patents. In refs. 62, 64, 69, and 70, the hydrophobic monomer was an obvious variable. In some others, differentiation is a manifestation of the type of coupling agent used,

Table II. Issue, Assignee, and

Patent Ref. No.	Patent Number	Divisions (D) & Equivalents (E)		Issue Dates
59	US 2,921,930	–	–	60/ –
60	GB 870,994	US-E	NONE	61/ –
61	US 3,035,004	–	–	62/ –
62	US 3,301,829	..	–	67/ –
63	GB 1,057,723	US-E	NONE	67/ –
64	US 3,306,863	–	–	67/ –
65	US 3,499,876	–	–	70/ –
66	US 3,501,445	–	–	70/ –
67	US 3,652,497	US-D	3,708,445	72/73
68	US 3,657,175	GB-E	1,276,271	72/72
69	US 3,660,339	–	–	72/ –
70	US 3,779,970	–	–	73/ –
71	US 3,794,608	–	–	74/ –
72	US 3,894,980	–	–	75/ –
73	US 3,915,921	–	–	75/ –
74	US 3,940,351	–	–	76/ –
75	US 4,008,202	–	–	77/ –
76	US 4,085,167	US-D	4,167,502	78/79
77	US 4,110,291	US-D	4,346,190	78/82
78	US 4,128,520	US-D	4,321,181	78/82
79	US 4,138,380	–	–	79/ –
80	US 4,138,381	–	–	79/ –
81	EP 3,235	US-E	NONE	79/ –
82	EP 13,836	US-E	AP 101,615	80/79
83	US 4,226,754	GB-E	2,025,434	80/83
84	US 4,230,844	–	–	80/ –
85	US 4,268,641	–	–	81/ –
86	US 4,338,239	–	–	82/ –
87	US 4,384,096	EP-E	11,806	83/80
88	US 4,410,673	–	–	83/ –
89	US 4,421,902	–	–	83/ –
90	US 4,423,199	EP-E	107,403	83/84
91	US 4,429,097	–	–	84/ –
92	GB 2,127,836	US-E	NONE	84/ –
93	US 4,464,524	–	–	84/ –
94	US 4,468,498	EP-E	73,529	84/83
95	US 4,509,949	–	–	85/ –
96	US 4,514,552	–	–	85/ –
97	US 4,525,581	DE-E	3,302,496	85/84
98	JP 60,235,815	US-E	NONE	85/ –
99	US 4,569,965	EP-E	121,230	86/84
100	US 4,600,761	–	–	86/ –
101	EP 190,892	US-E	NONE	86/ –
102	US 4,616,074	–	–	86/ –
103	US 4,663,385	EP-E	109,820	87/84
104	US 4,666,974	–	–	87/ –
105	US 4,764,554	EP-E	248,612	88/87
106	US 4,801,671	–	–	89/–

which determines the linkage between the ethylenically unsaturated portion of the molecule and the hydrophobically terminated ethoxylate side chain.

Examples of various coupling agents in order of appearance are maleic anhydride (59), alkyl vinyl ether (65), acrylic or methacrylic acid (67), vinyl

Inventors in AST Patent References

```
Assignee                        Inventors
---------------------------     -----------------

Koppers Co.                     Suhrie
Rhom & Haas Co.                 -
Rohm & Haas Co.                 Glavis
General Aniline & Film Corp.    Woodward & Grifo
Styrene Co-Polymers Ltd.        Piggot & Smith
Geigy Chemical Corp.            Leitner
GAF Corp.                       Field & Williams
Celanese Corp.                  Faust & Summit
General Latex & Chem. Corp.     Junas & LaTorre
Standard Brands Inds. Inc.      Zimmerman
Nalco Chemical Co.              Schuh
Dow Chemical Co.                Evani & Lalk
Dow Chemical Co.                Evani et al.
Rohm & Haas Co.                 Detommaso
B.F. Goodrich Co.               Schlatzer
B.F. Goodrich Co.               Schlatzer
Dow Chemical Co.                Evani & Corson
Rohm & Haas Co.                 Lewis & Miller
GAF Corp.                       Barabas et al.
GAF Corp.                       Barabas et al.
GAF Corp.                       Barabas & Klein
E.I. DuPont & Co.               D.Chang et al.
BASF Aktiengesellschaft         Becker et al.
Rohm & Haas Co.                 C.Chang & Stevens
NL Industries Inc.              Yun & Whitton
E.I. DuPont & Co.               D.Chang et al.
Union Carbide Corp.             Koenig & Bryant
Celenese Corp.                  Dammann
Dow Chemical Co.                Sonnabend
S.C. Johnson & Son Inc.         Schultz & Wilson
Rohm & Haas Co.                 C.Chang & Stevens
Rohm & Haas Co.                 C.Chang & Stevens
Rohm & Haas Co.                 C.Chang & Stevens
Uniroyal Inc.                   Peascoe
Sherwin-Williams Co.            Karickhoff
Rohm & Haas Co.                 Kowalski et al.
B.F. Goodrich Co.               Huang & Schlatzer
DeSoto Inc.                     Shay et al.
BASF Aktiengesellschaft         Denzinger et al.
Sansui K. K.                    Skakai
Hoeckst Aktiengesellschaft      Engel et al.
Alco Chemical Corp.             Ruffner
Rohm & Haas Co.                 C.Chang
Alco Chemical Corp.             Ruffner
Rohm & Haas Co.                 C.Chang & Stevens
Dow Chemical Co.                Keskey & Willency
Crown Decorative Products       Tonge
DeSoto Inc.                     Shay et al.
```

benzyl chloride (*71*), allyl glycidyl ether (*86*), acrylic acid oligomer (*89*), acrylamide (*90*), ethyl acrylate oligomer (*91*), isocyanate functional monomer (*96*), chloroethyl vinyl ether (*98*), crotonic acid (*99*), and itaconic acid (*102*). For other patents, differentiation may be by the method of polymerization, type of terminal hydrophobe, or some other factor or combination of factors,

Table III. Classification, Preferred Process,

Patent Ref. No.	Thickener Classification	Preferred Process	
		Polymerization	Medium
59	HASNE	Solution	Organic
60	ASE	Emulsion	Aqueous
61	ASNE	Dispersion	Aqueous
62	HASNE	Dispersion	Aqueous
63	ASE	Emulsion	Aqueous
64	HASNE	Prepolymer	Aqueous
65	HASNE	Solution	Organic
66	ASE	Emulsion	Aqueous
67	HASNE	Solution	Aqueous
68	HASE	Emulsion	Aqueous
69	HASNE	Solution	Organic
70	HASNE	Solution	Organic
71	HASNE	Solution	Organic
72	HASE	Emulsion	Aqueous
73	ASNE	Precipitation	Organic
74	ASNE	Precipitation	Halocarbon
75	HASNE	Solution	Organic
76	ASNE	Solution	Organic
77	ASE	Emulsion	Aqueous
78	ASE	Emulsion	Aqueous
79	ASE	Emulsion	Aqueous
80	HASNE	Solution	Glycol/Water
81	HASNE	Solution	IPOH/Water
82	HASE	Emulsion	Aqueous
83	ASE	Emulsion	Aqueous
84	HASNE	Solution	Glycol/Water
85	HASNE	Precipitation	Organic
86	HASNE	Solution	Organic
87	HASE	Emulsion	Aqueous
88	ASNE	Suspension	Aqueous
89	HASE	Emulsion	Aqueous
90	ASE	Emulsion	Aqueous
91	HASE	Emulsion	Aqueous
92	HASE	Emulsion	Aqueous
93	HASE	Emulsion	Aqueous
94	ASE	Emulsion	Aqueous
95	ASNE	Precipitation	Organic
96	HASE	Emulsion	Aqueous
97	ASNE	Precipitation	Organic
98	HASE	Emulsion	Aqueous
99	HASE	Emulsion	Aqueous
100	HASE	Emulsion	Aqueous
101	HASE	Emulsion	Aqueous
102	HASE	Emulsion	Aqueous
103	HASE	Emulsion	Aqueous
104	ASE	Emulsion	Aqueous
105	HASE	Emulsion	Aqueous
106	HASE	Emulsion	Aqueous

and analogous comparisons can be made. Like the conventional ASTs, the type of carboxylic acid monomer is rarely a factor in differentiation, because the claims for it are usually nonspecific. In practice, maleic anhydride, acrylic acid, and particularly methacrylic acid are preferred in nearly all of the formulations.

and Improvement Claims in AST Patents

```
Primary Improvements Claimed
------------------------------------

Efficiency
Efficiency
Efficiency
Processing
Water Resistance
Efficiency
Salt Tolerance
Efficiency
Leveling
Efficiency
Leveling
Leveling
Stability, Leveling
Hand, Water Resistance
Salt Tolerance
Salt Tolerance
Storage Stability
Efficiency
Efficiency, Stability
Efficiency
Redox Process
Leveling, Sag Resistance
Efficiency
Process
Several compared with HEC
Rheology in Paint
Efficiency, Salt Tolerance
Efficiency
Stability, Leveling
Processing
Efficiency, Leveling, Salt Tolerance
Efficiency, Salt Tolerance
Efficiency, Leveling, Salt Tolerance
Brush Drag, Leveling
Brush Drag
Leveling
Rheology, Less Stringy
Rheology, Stability
Efficiency
Rheology, Gloss, Water Resistance
Efficiency, Rheology
Efficiency, Stability
Efficiency, Rheology
No Specific Claims
Stability, Salt Tolerance
Oxidation Stabilizer
Color Float, Rheology
Reactor Plating, Emulsion Stability
```

Although many similarities exist, some of the associative formulations contain features that are particularly unique. Four issues (*67, 75, 84, 85*) disclose copolymer compositions that consist of only the carboxylic acid and associative monomers; such compositions indicate that sufficient hydrophilic–hydrophobic balance is obtained without the addition of a hydropho-

Table IV. Carboxylic and

| Patent Ref. No. | A. Carboxylic Monomer | | | |
| | Monomer Type | | Monomer Amount | |
	Claim 1	Pref	Claim 1	Pref
59	Dibasic	MAh	45-50 M	50 M
60	MAA	Same	25-70	25-50
61	MAA	Same	35-56	Same
62	+	MAh	+	50 M
63	+	MAA	+	7.5-30
64	MAh	Same	50 M	Same
65	MAh	Same	50 M	Same
66	-	-	-	-
67	C2-C6	M(AA)	70-95	Same
68	MAA	Same	20-55	40-55
69	MAh	Same	50 M	Same
70	Anhydride	MAh	30-50 M	Same
71	Hydrophilic	MAh	25-99 M	40-80 M
72	M(AA)	Same	15-40	20-35
73	+	AA	50-95	60-95
74	+	AA	50-95	Same
75	+	MAh	Balance	97-99 M
76	+	AA	>= 30	>= 97
77	MAA,EAA	MAA	30-75	50-65
78	+	MAA	30-85	50-70
79	MAA,EAA	Same	30-75	50-65
80	+	MAA	10-98	30-88
81	C3-C5	M(AA)	2-80	10-70
82	M(AA)	Same	20-70	30-45
83	MAA	Same	15-35	30
84	M(AA)	Same	30-65	Same
85	+	AA	90-99 M	96-99 M
86	M(AA)	AA	> 60	Same
87	+	M(AA)	15-60	35-55
88	+	AA	+	33
89	Several	MAA	>= 10	30-45
90	Several	MAA	>= 10	30-45
91	Several	MAA	>= 10	30-45
92	+	MAA	30-70	36-54
93	+	MAA	30-60	Same
94	+ (Core)	Several	> 5	10-70
95	M(AA)	Same	95.9-98.8	96-97.9
96	+	MAA	20-70	Same
97	+	M(AA)	70-99.9	76-99.7
98	M(AA)	MAA	15-60	38
99	+	M(AA)	1-45	8-40
100	+	M(AA)	5-70	35-45
101	+	MAA	+	30-50
102	+	M(AA)	5-70	35-45
103	Several	MAA	10-70	30-45
104	+	M(AA)	>= 20	25-60
105	M(AA)	MAA	25-45	30-40
106	+	+	15-50	20-45

Hydrophobic Monomers in AST Patents

B. Hydrophobic Monomer

Monomer Type		Monomer Amount	
Claim 1	Pref	Claim 1	Pref
S	Same	50 M	Same
AA*C1-C4	EA	> 10	Same
AA*C1-C8	AA*C1-C3	44-65	Same
VE	MVE	+	50 M
+	EA+MMA	+	20-65
Ethylene	Same	50 M	Same
VE*C1-C5	MVE	38-99 M	Same
AA*C1-C4	MA	100	Same
-	-	-	-
S/Bd	Same	>= 35	35-77
VA	Same	50 M	Same
Aromatic	S	50-67 M	Same
Many	S	Balance	Same
AA*C2-C8	BA	10-65	Same
AA*C10-C30	DDMA	5-50	4-40
M(AA)*C10-30	M(AA)*C10-22	5-50	Same
-	-	-	-
-	-	-	-
MA	Same	25-70	35-50
M(AA)*C1-C8	MA,EA	5-50	20-30
MA	Same	25-70	30-50
M(AA)*C1-C30	ODMA	1-50	2-30
Many	-	< 50	None
M(AA)*C1-C4	EA	> 30	40-60
MAA*C1-C20	MMA	5-70	30
-	-	-	-
-	-	-	-
+	+	0-20	0
+	EA	15-80	20-60
+	S	+	67
+	EA	Balance	40-60
+	EA	>= 30	40-60
+	EA	Balance	40-60
+	BA	20-50	24-36
S + EA	Same	18-70	Same
+	BA	< 40	Same
M(AA)*C10-30	M(AA)*C12-22	1-3.5	Same
+	EA	20-80	Same
+	+	0-20	Balance
M(AA) Esters	EA	10-82	50
M(AA)*C1-18	M(AA)*C1-2	30-85	50-75
+	Several	10-90	50-60
C2-C12	EA	+	30-60
+	Several	10-90	50-60
+	EA	> 25	40-60
Antioxidant	Same	0.1-50	15-20
M(AA) Esters	EA	25-65	40-60
+	EA	+	> 20

Table V. Associative

Patent Ref. No.	C. Associative Monomer			
	Coupling Agent		EO Chain Length	
	Claim 1	Pref	Claim 1	Pref
59	+	MAh	+	+
60	−	−	−	−
61	−	−	−	−
62	+	MAh	+	4−20
63	−	−	−	−
64	MAh	Same	3−40	+
65	Alkyl VE	Same	1−100	+
66	−	−	−	−
67	+	AA	20−100	40−100
68	Anhydride	MAh	6−150	15−13
69	MAh	Same	10−1200	45−136
70	MAh	Same	HLB >=12	40
71	VBCl	Same	10−100	20−40
72	AA	Same	1−2	2
73	−	−	−	−
74	−	−	−	−
75	VBCl	VBCl	10−100	20−40
76	−	−	−	−
77	−	−	−	−
78	−	−	−	−
79	−	−	−	−
80	M(AA)	AA	5−80	37
81	M(AA)	Same	2−100	25−90
82	M(AA)	Same	> 1	40−60
83	−	−	−	−
84	M(AA)	AA	10−50	37
85	M(AA)	AA	5−40	> 9
86	AGE	Same	1−40	Same
87	M(AA)	Same	6−100	10−40
88	−	−	−	−
89	AA Oligomer	Same	2−60	Same
90	AM	Same	0	Same
91	EA Oligomer	Same	2−60+	10−60
92	Dibasic	MAh	10−70	Same
93	Anhydride	MAh	6−150	29
94	−	−	−	−
95	−	−	−	−
96	Isocyanate	m−TMI	+	10−60
97	−	−	−	−
98	Alkyl VE	ClEVE	5−80	+
99	CrA	Same	2−100	20−50
100	Isocyanate	IEM,TMI	1−150	Same
101	+	MMA	+	10−30
102	IA	Same	1−150	Same
103	IA	Same	0−60+	>= 10
104	−	−	−	−
105	MAh	Same	> 10	20
106	+	TMI	+	+

Monomers in AST Patents

Terminal Hydrophobe		Monomer Amount	
Claim 1	Pref	Claim 1	Pref
C12-C18	Same	1-5	5
–	–	–	–
–	–	–	–
+	+	<= 5 M	Same
–	–	–	–
+	Octylphenol	=> 50 M	Same
C12-C24	Alkylaryl	1-12 M	Same
–	–	–	–
Alkylaryl	Same	5-30	<= 15
C10-C22	C8-C16	3-35	+
–	None	+	0.001-0.1 M
+	Alkylaryl	3-15	Same
C1-C22	+	0.25-13 M	0.5-10 M
C1-C2	C1	20-60	Same
–	–	–	–
–	–	–	–
+	C10-C22	0.2-15 M	1-3 M
–	–	–	–
–	–	–	–
–	–	–	–
–	–	–	–
C1-C20	Nonylphenol	1-85	10-40
C1-C20	Same	20-98	20-80
C8-C30	C12-C18	0.5-25	1-15
–	–	–	–
Alkylaryl	Nonylphenol	35-70	Same
C4-C30	C15-C30	1-10 M	1-4 M
C1-C20	Same	0.2-20	Same
C8-C22	Same	1-30	Same
–	–	–	–
C8-C30	Same	0.5-25	1-15
C8-C30	C10-C18	0.5-25	1-15
C1-C30	C12-18 Alkyl	0.5-30	1-15
Alkylaryl	Nonylphenol	5-45	10-40
C1-C30	Nonylphenol	10-25	Same
–	–	–	–
–	–	–	–
+	+	0.5-60	Same
–	–	–	–
C8-C40	Nonylphenol	3-30	12
C2-C30	C18 Alkyl	0.5-30	Same
Sorbitan FE	Same	1-25	7-10
+	Octadecyl	+	5-20
+	+	1-25	7-10
C1-C30	C12-C18	0.5-30	1-15
–	–	–	–
C12-C25 Alkyl	Cetyl/Oleyl	1-40	3-12
+	+	> 5	> 20

Table VI. Other Comments or Requirements in AST Patents

Patent Ref. No.	Comment or Requirement
59	S/MAh copolymers are post-esterified with an alkyl surfactant in solvent.
60	The copolymers may contain 0-40 % of other neutral monomers, preferrably MMA.
61	Aqueous dispersion polymers are made, normally without an emulsifier.
62	MVE/MAh prepolymers are post-esterified with a surfactant in water above the CMC.
63	Curable thickeners are claimed which contain 5-35 % of an alkyl methylol acrylamide.
64	Ethylene/MAh prepolymers are post-esterified with a surfactant in water.
65	The polymers are made in solvent, washed, and then hydrolyzed.
66	Poly(MA) is 70-90% hydrolyzed and lightly crosslinked with allyl acrylate.
67	The copolymers contain carboxyl monomers and associative monomers only.
68	The copolymers must contain S or Bd. A dialkylaryl PEO half ester of MAh is preferred.
69	MAh/VA copolymers are post-esterified with PEO without a terminal hydrophobe.
70	A S/MAh copolymer is post-esterified with a nonionic surfactant in solvent.
71	The hydrophilic monomer can be carboxyl functional or nonionic.
72	The EO containing monomer has a short EO chain and a small hydrophobe.
73	The long chain hydrophobic monomer in this polymer possibly is associative.
74	This is a continuation of U.S. 3,915,921, but made in chlorofluoroethane.
75	A minimum amount of carboxyl, sulfate, or hydroxyl monomer is used for solubility.
76	The acid monomer is polymerized with an allyl M(AA) oligomer to form a solid thickener.
77	The thickeners are for acrylic latex. A polym. emulsifier is not mandatory.
78	The polymers also contains 0.5-20% AM or S for thickening S/Bd latex.
79	All of the monomer is present on initiation. A sulfosuccinate stabilizer is used.

80   The polymers are made in EG, PG or preferably in PG/water.
81   Sulfonate or amine functional monomers are alternates for carboxylic acids.
82   The presence of surfactant may improve thickener efficiency.
83   This latex paint thickener also contains 5-80% of a vinyl ester, preferably VA (40%).
84   The polymerization is conducted in EG or PG, optionally with water.
85   The solid thickener also works well in water/hydrocarbon emulsion print pastes.
86   AGE monomer is adducted with surfactants, fatty acids, or short chain alcohols.
87   This thickener is particularly useful in paint.
88   A low MW suspension polymer is made with cosolvent partitioning but no thickener claims.
89   The associative monomer is prepared from crude acryloxypropionic acid oligomers.
90   The associative monomer is a long chain N-alkylacrylamide without ethoxylation.
91   Crude EA oligomer is used which contains polyfunctional hydrophobe-ethoxylate units.
92   The associative monomer is preferrably an MAh ethoxylate half ester.
93   The associative monomer is a mixed ester with a C2-C10 diol.
94   The thickener is an encapsulated alkali-swellable polymer (EASP) dispersion.
95   The long chain hydrophobic monomer in this polymer possibly is associative.
96   The polymers contain relatively high levels of urethane-functional associative monomer.
97   0.1-10% of a difunctional monomer is present. The solid polymer is heated.
98   The associative monomer is prepared from 2-chloroethyl vinyl ether.
99   The associative monomer is a crotonate ester, and 0-40% of a 4th monomer may be used.
100   The hydrophobe of the associative monomer is a sorbitan fatty ester or an amine.
101   3-20% of a polymerization additive with a specific solubility parameter range is used.
102   The associative monomer is the monoester of itaconic acid (methylene succinic acid).
103   The associative monomer is the diester of itaconic acid.
104   The hydrophobic monomer is a dialkylphenol containing antioxidant compound.
105   The polymer also contains < 10% of a hydrophilic monomer (e.g. EO/PO Methacrylate).
106   The polymer also contains 0.1-0.6% unsaturated aromatic sulfonic acid for stabilization.

bic monomer. In a more recent issue (101), thickening efficiency is enhanced by employing an organic additive during emulsion polymerization that is within a specific solubility parameter range to more effectively incorporate the monomers.

Two patents of recent issue not listed in the tables are those of Emmons (109) and Siano (110). The thickeners of these patents are worthy of mention here because they are prepared by addition polymerization, optionally contain some carboxyl functionality, and are very likely to be associative. Although some carboxylic acid monomer is optionally allowed in these patents, the AST classification generally does not apply because of the high levels of hydrophilic nonionic monomer (acrylamide) present, which results in the copolymers being water soluble at low pH. Emmons describes anionic or nonionic copolymers of greater than 50% acrylamide, up to 50% of a long-chain alkyl or ethoxylated alkyl acrylamide, and optionally up to 50% of some other monomer. Siano discloses copolymers of acrylamide and 0.0–0.4 mol % of a long-chain alkyl acrylamide, which are subsequently hydrolyzed to give a terpolymer containing a rather low level of carboxyl functionality (0.1–0.3 mol %).

The gradual transition from polymers made by solution (in water or organic solvent) or precipitation polymerization (in aqueous or organic diluent) to those made by emulsion polymerization is clearly evident. The comparative advantages of the emulsion polymers as outlined previously apparently encouraged a distinct preference for latices.

Some patents or applications employ prior art AST compositions to obtain "use" features providing enhanced performance or utility. Synergistic thickening is observed, for example, when associative ASTs are combined with various other components, for example, with surfactants (82), with water-swellable clay minerals (111), or with nonionic associative thickeners (112, 113). Witiak and Dupré (114) disclose utility of AST latices in acidic media. This utility is accomplished by neutralization to a pH above 6.5 followed by reduction to some lower pH in the presence of surfactant. In spite of the low pH, the surfactant prevented coagulation on reacidification.

Symbols and Abbreviations

AA	Acrylic acid
AGE	Allyl glycidyl ether
AM	Acrylamide
ASE	Alkali-swellable or alkali-soluble emulsion
ASNE	Alkali-swellable or alkali-soluble nonemulsion
AST	Alkali-swellable or alkali-soluble thickener
BA	Butyl acrylate
Bd	Butadiene
C	Carbon

ClEVE	Chloroethyl vinyl ether
CrA	Crotonic acid
DDMA	Dodecyl methacrylate
EA	Ethyl acrylate
EAA	Ethacrylic acid
EG	Ethylene glycol
EHA	2-Ethylhexyl acrylate
EO	Ethylene oxide
FE	Fatty ester
HASE	Hydrophobically modified alkali-swellable or alkali-soluble emulsion
HASNE	Hydrophobically modified alkali-swellable or alkali-soluble nonemulsion
HEC	Hydroxyethylcellulose
HEUR	Hydrophobically modified ethoxylated urethane
HWSP	Hydrophobically modified water-swellable or alkali-soluble polymer
IA	Itaconic acid
MA	Methyl acrylate
MAA	Methacrylic acid
MAh	Maleic anhydride
MMA	Methyl methacrylate
MVE	Methyl vinyl ether
ODMA	Octadecyl methacrylate
PG	Propylene glycol
PO	Propylene oxide
S	Styrene
SMAT	Styrene–maleic anhydride thickener
VA	Vinyl acetate
VBCl	Vinylbenzyl chloride
VE	Vinyl ether
WSP	Water-soluble polymer

References

1. *Chemistry and Technology of Water Soluble Polymers*; Finch, C. A., Ed.; Plenum: New York, 1983.
2. *Water-Soluble Synthetic Polymers: Properties and Behavior*; Molyneux, P., Ed.; CRC: Boca Raton, FL, 1985; Vol. I; pp 76–103.
3. Schwab, F. G. In *Water-Soluble Polymers: Beauty with Performance*; Glass, J. E., Ed.; Advances in Chemistry Series 213; American Chemical Society: Washington, DC, 1986; pp 375–389.
4. Hall, J. E. et al. *J. Coat. Technol.* **1986**, *58*(738), 65–73.
5. *The Influence of Associative Thickeners and Rheology on Coatings Performance*; Glass, J. E., Ed.; North Dakota State University: Fargo, ND, 1983.

6. Glass, J. E.; Fernando, R. H.; England-Jongewaard, S. K.; Brown, R. G. *J. Oil Coulour Chem. Assoc.* **1984**, *67*, 256–261.
7. Fernando, R. H.; Glass, J. E. *J. Oil Coulour Chem. Assoc.* **1984**, *67*, 279–283.
8. Glancy, C. W.; Basset, D. R. *Proc. ACS Div. Polym. Mater. Sci. Eng.* **1984**, *51*, 348–352.
9. Fordyce, D. B.; Dupré, D.; Toy, W. *Ind. Eng. Chem.* **1959**, *51*, 115.
10. Fordyce, D. B.; Dupré, D.; Toy, W. *Off. Dig. Fed. Soc. Paint Technol.* **1959**, *31*, 284–302.
11. Rogers-Moses; P. J.; Schaller, E. J. *Am. Paint Coat. J.* **1984**, 54–58.
12. Shay, G. D.; Rich, A. F. *J. Coat. Technol.* **1986**, *58*(732), 43–53.
13. Fordyce, R. G.; Ham, G. E. *J. Am. Chem. Soc.* **1947**, *69*, 695–696.
14. Guziak, I. F.; Maclay, W. N. *J. Appl. Polym. Sci.* **1963**, *7*, 2249–2253.
15. Greene, B. W. *J. Colloid Interface Sci.* **1973**, *43*(2), 449–461.
16. Matsumoto, T.; Shimada, M. *Kobunshi Kagaku* **1965**, *22*, 172.
17. Muroi, S. *J. Appl. Polym. Sci.* **1966**, *10*, 713–729.
18. Muroi, S. *Kogyo Kagaku Zasshi* **1966**, *69*, 1539.
19. Muroi, S.; Hosoi, K.; Ishikawa, T. *J. Appl. Polym. Sci.* **1967**, *11*, 1963–1978.
20. Nishida, S. Ph.D. Thesis, Lehigh University, 1980.
21. Nishida, S.; El-Aasser, M. S.; Klein, A.; Vanderhoff, J. W. In *Emulsion Polymerization*; ACS Symposium Series 165; American Chemical Society: Washington, DC, 1981; pp 291–314.
22. Loncar, F. V.; El-Aasser, M. S.; Vanderhoff, J. W. *Polym. Mater. Sci. Eng.* **1985**, *52*, 299–303.
23. Sakota, K.; Okaya, T. *J. Appl. Polym. Sci.* **1976**, *20*, 1745–1752.
24. Hen, J. *J. Colloid Interface Sci.* **1974**, *49*, 425.
25. Vijayendran, B. R. *J. Appl. Polym. Sci.* **1979**, *23*, 893–901.
26. Bassett, D. R.; Hoy, K. L. In *Polymer Colloids*; Fitch, R. M., Ed.; Plenum: New York, 1980; Vol. II, pp 1–25.
27. Egusa, S.; Makuuchi, K. *J. Colloid Interface Sci.* **1981**, *79*, 350–364.
28. Hermans, J. J; Overbeek, J. Th. G. *Bull. Soc. Chim. Belg.* **1948**, *57*, 154.
29. Kuhn, W.; Kunzie, O.; Katchelsky, A. *Helv. Chim. Acta* **1948**, *31*, 1944.
30. Yudelson, J. S.; Mack, R. E. *J. Polym. Sci., Part A* **1964**, *2*, 4683–4695.
31. Verbrugge, C. J. *J. Appl. Polym. Sci.* **1970**, *14*, 897–909.
32. Verbrugge, C. J. *J. Appl. Polym. Sci.* **1970**, *14*, 911–928.
33. Brown, G. L.; Garrett, B. S. presented at the 153rd Meeting, ACS, San Francisco, CA, 1968.
34. Sperry, P. R.; Thiebeault, J. C.; Kostansek, E. C. *Proceedings of the 11th International Conference on Organic Coatings Science and Technology*, Advances in Organic Coatings Science and Technology Series; Patsis, A. V., Ed., 1985; Vol. 9, pp 1–11.
35. Schaller, E. J. *Surf. Coat. Aust.* **1985**, *22*(10), 6–13.
36. Thiebeault, J. C.; Sperry, P. R.; Schaller, E. J. *Proc. ACS Div. Polym. Mater. Sci. Eng.* **1984**, *51*, 353–358.
37. Chu, D.; Thomas, J. K. *Proc. ACS Div. Polym. Mater. Sci. Eng. Mtg.* Fall 1987, *57*, 704–707.
38. Ross, S.; Olivier, J. P. *J. Phys. Chem.* **1959**, *63*, 1671.
39. Brown, R. G.; Glass, J. E. *Proc. ACS Div. Polym. Mater. Sci. Eng. Mtg.* Fall 1987, *57*, 709–713.
40. Halerpin, A. *Macromolecules* **1987**, *20*, 2943–2946.
41. de Gennes, P.-G. In *Solid State Physics*; Liebert, L., Ed.; Academic: New York, 1978; Suppl. 14.
42. Chung, F. H.; Rehfeldt, T. K. *Proc. ACS Div. Polym. Mater. Sci. Eng.* **1984**, *51*, 353–358.

43. Tanford, C. In *The Hydrophobic Effect*, 2nd ed.; Wiley: New York, 1980.
44. Strauss, U. P. In *Microdomains in Polymer Solutions*; Dublin, P., Ed.; Plenum: New York, 1985; pp 1–2.
45. McCormick, C. L.; Middleton, J. C. *Proc. ACS Div. Polym. Mater. Sci. Eng. Mtg.* Fall 1987, *57*, 700–703.
46. Valint, P. L., Jr.; Bock, J.; Schulz, D. N. *Proc. ACS Div. Polym. Mater. Sci. Eng. Mtg.* Fall 1987, *57*, 482–486.
47. Muroi, S. *Kogyo Kagaku Zasshi* 1966, *69*, 1551.
48. Wesslau, H. *Makromol. Chem.* 1963, *69*, 220.
49. Stackman, R. W.; Hurley, S. M. *Proc. ACS Div. Polym. Mater. Sci. Eng. Mtg.* Fall 1987, *57*, 830–834.
50. Sokota, K.; Okaya, T. *J. Appl. Polym. Sci.* 1976, *20*, 2583–2587.
51. Hoy, K. L. *J. Coat. Technol.* 1979, *51*(651), 27–41.
52. Morgan, L. W.; Jensen, D. P. *Makromol. Chem.* 1985, *Suppl. 10–11*, 59–67.
53. Morgan, L. M.; Jensen, D. F.; Weiss, C. S. *Proc. ACS Div. Polym. Mater. Sci. Eng. Mtg.* Fall 1987, *57*, 689–693.
54. Evani, S.; Rose, G. D. *Proc. ACS Div. Polym. Mater. Sci. Eng. Mtg.* Fall 1987, *57*, 477–481.
55. Thiebeault, J. C.; Sperry, P. R.; Schaller, E. J. In *Water-Soluble Polymers: Beauty with Performance*; Glass, J. E., Ed.; Advances in Chemistry Series 213; American Chemical Society: Washington, DC, 1986; pp 375–389.
56. Verkholantsev, V. V. et al. *Lakokrasochnye Materialy I Ikh Primenenie* 1968, *4*, 16–18.
57. Illers, K. H. *Kolloid-Z., Z. Polymere* 1963, *190*, 16.
58. LeSota, S.; Lewandowski, E. W.; Schaller, E. J. *Proc. ACS Div. Polym. Mater. Sci. Eng. Mtg.* Fall 1987, *57*, 627–631.
59. Suhrie, E. C. U.S. Patent 2 921 930, 1960.
60. Br. Patent 870 994, 1961.
61. Glavis, F. J. U.S. Patent 3 035 004, 1962.
62. Woodward, F. E.; Grifo, R. A. U.S. Patent 3 301 829, 1967.
63. Piggott, K. E.; Smith, W. B. Br. Patent 1 057 723, 1967.
64. Leitner, G. J. U.S. Patent 3 306 863, 1967.
65. Field, N. D.; Williams, E. P. U.S. Patent 3 499 876, 1970.
66. Faust, E. E.; Wilbur, A. G. U.S. Patent 3 501 445, 1970.
67. Junas, T. B.; La Torre, A. U.S. Patent 3 652 497, 1972.
68. Zimmerman, C. A. U.S. Patent 3 657 175, 1972.
69. Schuh, T. R. U.S. Patent 3 660 339, 1972.
70. Evani, S.; Lalk, R. H. U.S. Patent 3 779 970, 1973.
71. Evani, S.; Lalk, R. H.; Fiero, T. H. U.S. Patent 3 794 608, 1974.
72. De Tommaso, G. L. U.S. Patent 3 894 980, 1975.
73. Schlatzer, R. K. Jr. U.S. Patent 3 915 921, 1975.
74. Schlatzer, R. K. Jr. U.S. Patent 3 940 351, 1976.
75. Evani, S.; Corson, F. P. U.S. Patent 4 008 202, 1977.
76. Lewis, S. N.; Miller, J. J. U.S. Patent 4 085 167, 1978.
77. Barabas, E. S.; Klein, A.; Alwani, D. W. U.S. Patent 4 110 291, 1978.
78. Barabas, E. S.; Klein, A.; Alwani, D. W. U.S. Patent 4 128 520, 1978.
79. Barabas, E. S.; Klein, A. U.S. Patent 4 138 380, 1979.
80. Chang, D. C.; Fryd, M.; Krueger, A. R. U.S. Patent 4 138 381, 1979.
81. Becker, E.; Geelhaar, H. J.; Ley, G.; Schlotterbeck, D. Eur. Patent 3235, 1979.
82. Chang, C. J.; Stevens, T. E. Eur. Patent 13836, 1980.
83. Yun, H. B.; Whitton, A. J. U.S. Patent 4 226 754, 1980.
84. Chang, D. C.; Fryd, M.; Krueger, A. R. U.S. Patent 4 230 844, 1980.

85. Koenig, H. S.; Bryant, G. M. U.S. Patent 4 268 641, 1981.
86. Dammann, L. G. U.S. Patent 4 338 239, 1982.
87. Sonnabend, L. F. U.S. Patent 4 384 096, 1983.
88. Schulz, G. O.; Wilson, D. M. U.S. Patent 4 410 673, 1983.
89. Chang, C. J.; Stevens, T. E. U.S. Patent 4 421 902, 1983.
90. Chang, C. J.; Stevens, T. E. U.S. Patent 4 423 199, 1983.
91. Chang, C. J.; Stevens, T. E. U.S. Patent 4 429 097, 1984.
92. Peascoe, W. J. Br. Patent 2 127 836, 1984.
93. Karickhoff, M. U.S. Patent 4 464 524, 1984.
94. Kowalski, A.; Vogel, M.; Blankenship, R. M. U.S. Patent 4 468 498, 1984.
95. Huang, C.; Schlatzer, R. K. U.S. Patent 4 509 949, 1985.
96. Shay, G. D.; Eldridge, E.; Kail, E. U.S. Patent 4 514 552, 1985.
97. Denzinger, W.; Hartmann, H.; Faulhaber, G.; Raubenheimer, H. J. U.S. Patent 4 525 581, 1985.
98. Sakai, M. Jpn. Patent 60 235 815, 1985.
99. Engel, D.; Rinno, H.; Zimmershied, K. U.S. Patent 4 569 965, 1986.
100. Ruffner, C. G.; Wilkerson, J. M. U.S. Patent 4 600 761, 1986.
101. Chang, C. J. Eur. Patent 190 892, 1986.
102. Ruffner, C. G. U.S. Patent 4 616 074, 1986.
103. Chang, C. J.; Stevens, T. E. U.S. Patent 4 663 385, 1987.
104. Keskey, W. H.; Willency, R.A. U.S. Patent 4 666 974, 1987.
105. Tonge, C. J. U.S. Patent 4 764 554, 1988.
106. Shay, G. D.; Kravtiz, F. K.; Brizgys, P. V.; Kersten, M. A. U.S. Patent 4 801 671, 1989.
107. Hubbuch, L. P. U.S. Patent 2 244 703, 1941.
108. Trommsdorff, E.; Gerhard, A. U.S. Patent 2 326 078, 1943.
109. Emmons, W. D. U.S. Patent 4 395 524, 1983.
110. Siano, D. B. U.S. Patent 4 673 716, 1987.
111. Dupré, J. U.S. Patent 4 351 754, 1982.
112. Blake, D. M. Jr. U.S. Patent 4 507 426, 1985.
113. Rich, A. F.; Benes, P. C.; Adams, L. E. U.S. Application 914 988, 1986.
114. Witiak, D.; Dupré, J. U.S. Patent 4 529 773, 1985.

Hydrophobically Modified Ethoxylated Urethane Architecture

Importance for Aqueous- and Dispersed-Phase Properties

A. Karunasena, Richard G. Brown, and J. Edward Glass

Polymers and Coatings Department, North Dakota State University, Fargo, ND 58105

Hydrophobically modified ethoxylated urethanes (HEURs) offer a wide latitude in the architectural design of hydrophobically modified polymers. This chapter presents approaches to the synthesis of HEUR polymers with different molecular architectures, their geometrical influences on solution and dispersion properties, and viable mechanisms by which this class of associative thickener effects desirable coatings rheology and applied film properties. The viscosity behavior of associative thickeners alone, with surfactant, and in 0.32 volume fraction latex and pigmented-latex dispersions is examined. Viscosities at high shear rates are determined by the concentration of hydrophobes and the architecture of the HEUR thickener; both reflect the importance of hydrophobe contact residence times on the fluid's response at high deformation rates. At low shear rates, polymer hydrophobe participation in formulation surfactant micelles effects viscosity at thickener concentrations significantly below those required in solutions devoid of formulation surfactant. This induced participation of most HEUR polymers complemented by an ion–dipole interaction between the cations of latex oligomeric surface acids and the oxygen atoms of the associative thickener provides efficiencies equivalent to cellulose-ether-thickened dispersions. Disruption of the micellar associations due to high free-surfactant concentrations provides the improved low-shear-rate rheology observed for latices with small particle sizes.

THE RELATIVE COST OF MANUFACTURING hydrophobically modified, water-soluble polymers is the primary determinant in their market acceptance. The lowest-cost associative thickeners used in coating formulations are hydrophobically modified, alkali-swellable emulsions (HASE). The extensive history leading to the development of this technology is reviewed in the preceding chapter; their utilization and limitations are discussed in Chapters 27 and 28.

Hydrophobically modified, ethoxylated urethanes (HEURs) are the thickeners of choice in exterior coatings and in corrosion-resistant, high-gloss industrial latex finishes. This chapter presents an overview of our research efforts and discusses approaches to the synthesis of HEUR polymers with different molecular architectures, geometrical influences on solution properties, and viable mechanisms by which this class of associative thickener effects desirable coatings rheology and applied film properties.

The ability of associative thickeners to effect higher, high-shear-rate (10^4 s^{-1}) viscosities, to obtain both greater applied film thicknesses and improved flow at low deformation rates, and to effect independent low-shear-rate viscosities by influencing the yield stress behavior of coatings was presented in a previous discussion (1). The attainment of higher gloss and other application properties also was discussed previously (2). To achieve many of the properties noted in high quality coatings, the dispersed phases should remain as independent entities. Most nonadsorptive, water-soluble polymers added for rheology control cause flocculation at a critical concentration. This effect as a function of thickener molecular weight and latex median particle size is illustrated (3–5) in Figure 1. This study delineated the importance of volume restriction or depletion (6) flocculation in nonpigmented latex dispersions. In view of the long history in developing this mechanism, it is addressed in the concluding section of this chapter.

Structural Features Important in Coating Formulations

Water-soluble polymers will lower the surface tension of water generally in proportion to the polymer's hydrophobic content. The ability to lower the surface tension of water to that of a typical surfactant, above its critical micelle concentration (e.g., ca. 32 mN/m) has been used as a general criterion in defining certain water-soluble polymers as "polymeric surfactants" (7). If such criteria were important, methylhydroxypropylcellulose or vinyl acetate–vinyl alcohol copolymers would in large measure produce the unique coatings rheology observed with associative thickeners (1), but they do not (8). In vinyl acetate–vinyl alcohol copolymers, obtained via hydrolysis of poly(vinyl acetate), the primary influence of residual acetate placement is to inhibit intra- and intermolecular hydrogen bonding, and thereby inhibit supermolecular order (9) and promote solubility.
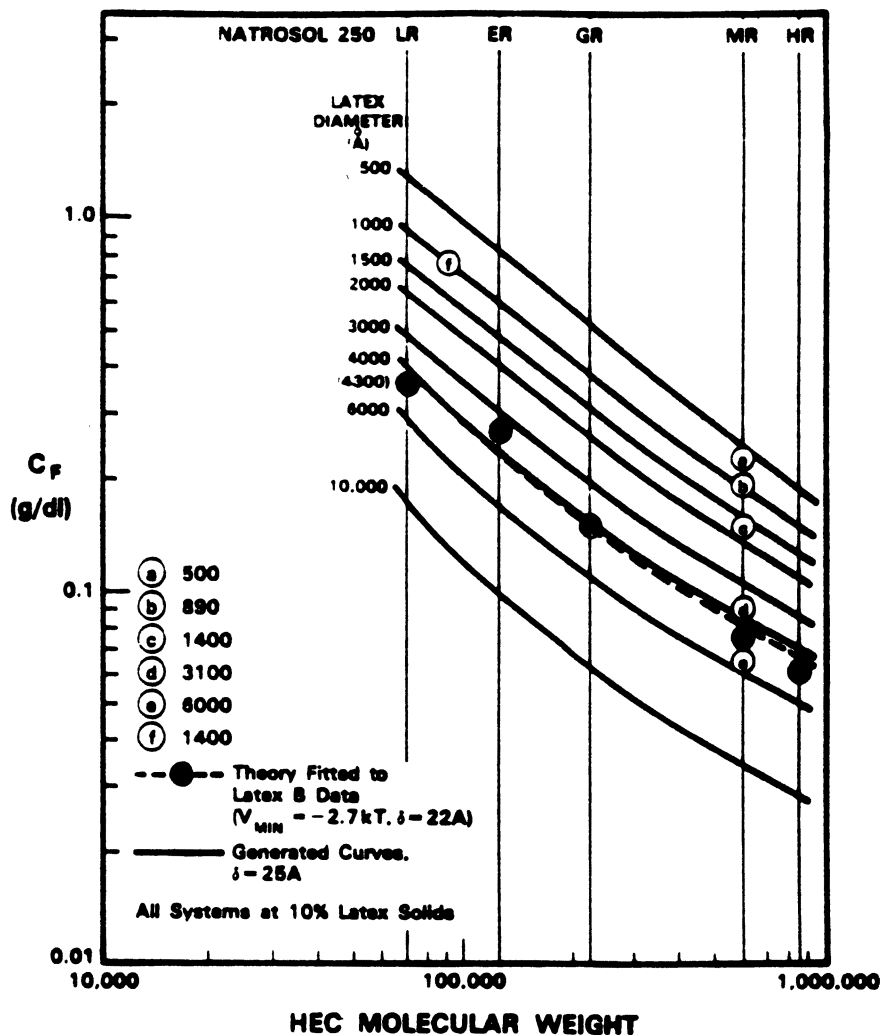
Figure 1. Critical (hydroxyethyl)cellulose concentration for latex particles floc-
culation. Dependence of both polymer molecular weight and latex median
particle size on thickener concentration is illustrated. (Reproduced with per-
mission from reference 5. Copyright 1984 Academic Press.)

The polymeric surfactants of longest standing are oxyethylene–
oxypropylene block and random copolymers (*10*). Such copolymers are not
efficient thickeners and do not effect coatings with unique rheological or
applied film properties (*8*), even though such copolymers are capable of
significantly lowering the surface tension of water. The interfacial activity
between the polymer and substrate is generally related to a specific inter-
action, which often (*11*) does not relate to the ability of the macromolecule

to lower the surface tension of water. Oxyethylene–oxypropylene copolymers form hydrophobic domains (12, 13), a more astute name that differentiates the associations formed by surface-active water-soluble polymers from the micelle behavior of surfactants. Hydrophobic domains in themselves are not sufficient to effect the improved rheology and film properties observed when the thickener is a water-soluble polymer containing hydrophobe moieties chemically similar to classical surfactant hydrophobes (e.g., alkane units containing more than eight carbons or nonylphenol groups [14]).

If unique coating properties are to be realized cost-effectively, classical surfactant hydrophobes must be chemically attached to the thickener or to a central unit (1). Higher quality exterior coatings are alkaline (pH 9). Acrylate and maleic esters and polymers containing urethane linkages in which the isocyanate units are contiguous to an aromatic ring (e.g., toluene diisocyanate) are not hydrolytically stable in alkaline dispersions. If the hydrophobe units are attached to one of these three groups, hydrolysis at ambient temperatures will occur in exterior coating formulations within 2 days, with loss in the coating's viscosity.

In addition to hydrolytic stability, other structural features appear to be required. Effective associative thickeners contain oxyethylene units, preferably with 40 or more units between the surfactant hydrophobe and the interconnecting linkage or polymer backbone. For an associative thickener to function efficiently, other formulation variables also must be within certain limits. For example, the formulation surfactant should not have an extremely low critical micelle concentration (1). The component most frequently varied that has a pronounced influence is the latex. The median particle size, particle size distribution, and the stabilizing moieties on the surface of the latex can have a dramatic influence on coating rheology, particularly when associative thickeners are in the formulation. With commercial associative thickeners of the past 4 years, higher viscosities at high shear rates are observed in formulations containing latices with particles smaller than 300 nm in diameter (15).

The types of surface moieties stabilizing the latex also are important. The binders used in waterborne coatings are not the hard-sphere, model polymer colloids used in adsorption studies. They are soft (low glass transition temperature), deformable moieties that are stabilized by grafted polymer fragments [e.g., (hydroxyethyl)cellulose (16) or poly(vinyl alcohol)] or by terpolymerized acid monomers extended from the surface of the colloid (17). Such stabilizers produce a far less hydrophobic surface than is generally depicted in colloid texts. This situation is particularly true if the composition of the latex is predominately methacrylate or vinyl acetate, as they are in most U.S. commercial products.

Synthesis of Variable Molecular Geometries

HEUR polymers offer the greatest variation in architectural design of any hydrophobically modified polymer discussed in this text. This latitude in

structural design and the cost-effectiveness imposed by different processes associated with the different synthetic routes determine the boundary of associative thickener influences on coatings rheology.

Four types of molecular geometry are discussed in this section:

1. linear dihydrophobe polyethylene glycols of different molecular weights [NPIP(EtO)$_{595}$IPNP] and [C$_{12}$H$_{25}$(EtO)$_{100}$-TMXDI(EtO)$_{100}$C$_{12}$H$_{25}$], where NP is nonylphenol, IP is isophorone diisocyanate, and TMXDI is *m*-tetramethylxylene diisocyanate;

2. trihydrophobe ethoxylated isocyanurate (e.g., the trimer of isophorone diisocyanate [(NP(EtO)$_{100}$IPDI)$_3$]), where IPDI is the isocyanurate of isophorone diisocyanate;

3. comb polymers with random hydrophobe placement; and

4. comb polymers with block hydrophobe placement.

The linear dihydrophobe represents the simplest geometrical design (Scheme I) and probably represents past European HEUR commercial products (*1*) (SCT or BR-100, LR-8500, and L-75). This approach for the production of high molecular weights has two limitations. Significant transfer reactions in the propagation sequence limit base-catalyzed polymerization of ethylene oxide to molecular weights generally less than 20,000. To minimize transfer reactions, transition metal ligand catalysis in nonaqueous solvents is necessary. In high molecular weight polymers, the concentration of end groups (i.e., the hydroxyl functionality to be capped) is low. Statistical and viscosity effects make hydrophobe modification of higher molecular weight poly(oxyethylenes) (POEs) more difficult and therefore costly. The diblock of Scheme I was synthesized with a moderate molecular weight POE (ca. 26,000) to obtain a molecular weight equivalent to significant commercial HEURs.

HEUR patents issued to U.S. manufacturers (*18, 19*) claim three or more hydrophobes per molecule. The simplest molecule containing three hydrophobes is one based on an isocyanurate of a diisocyanate, such as the trimer of isophorone diisocyanate [(NP(EtO)$_{100}$IPDI)$_3$, Scheme II]. The molecular weights obtainable by direct derivatization of the trimer are limited by the degree of ethoxylation of the surfactant moiety. Large oxyethylene segments (>100 units) per surfactant hydrophobe can be achieved; this number is an average value with a Gaussian distribution. The molecular weights obtainable through direct derivatization of the isocyanurate with an average 100-mol ethoxylate are half those obtained through the dihydrophobe modification of a 26,000 molecular weight polyethylene glycol (*20*).

The synthesis of comb-type polymers with random hydrophobe placement, via addition of the hydrophobes to the isocyanate functions of preformed polymer, is illustrated in Scheme III. This type of polymer geometry
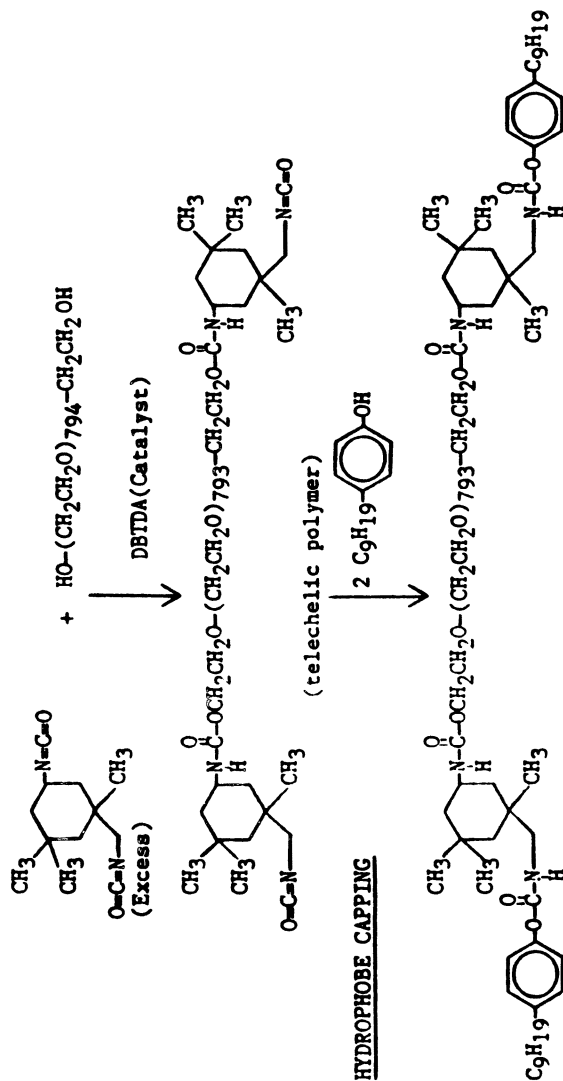
Scheme I. Reaction diagram for the synthesis of a diblock HEUR thickener.
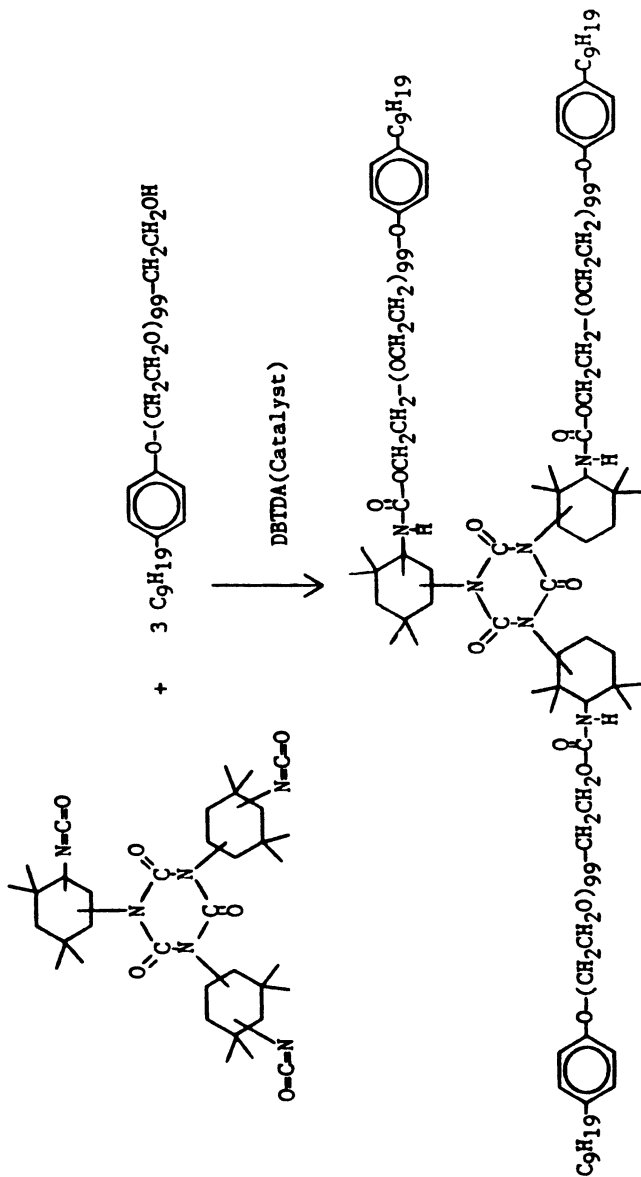
Scheme II. Reaction diagram for the synthesis of a branched (three- to four-arm star) HEUR thickener.
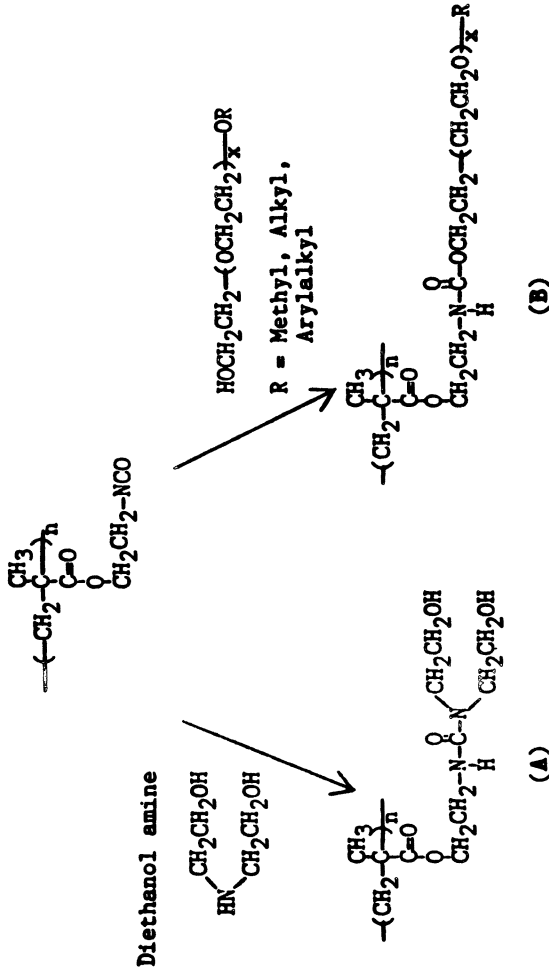
Scheme III. Reaction diagram for the synthesis of a comb-type HEUR thickener with random hydrophobe placement.

can be realized by the free-radical homo- or copolymerization of isocyanatoethyl methacrylate (IEM) or *m*-isopropenyl-α,α-dimethylbenzyl isocyanate with lower cost non-isocyanate-containing monomers. If the latter comonomer is hydrophobic, part of the isocyanate functionalities must be postreacted with components such as diethanolamine to ensure water solubility. Our studies to date have not produced an effective dispersed-phase rheology modifier (i.e., one that will effect 1.5 Pa s viscosities at moderate shear rates, 50–100 s^{-1}), by using this type of geometry (*20*); the products of Scheme III will not be discussed further. This type of geometry probably is reflected in the newer commercial products (e.g., HEUR 1514, used in coating formulations wherein blending of thickeners is employed (*see* Chapter 27).

Comb-type architecture with block placement of hydrophobes can be achieved by addition growth sequences (Scheme IV). The oxyanion of an ethoxylated surfactant is reacted via a Williamson synthesis to produce a hydrophobe with diol functionality (**4B**). These hydrophobes can be blocked
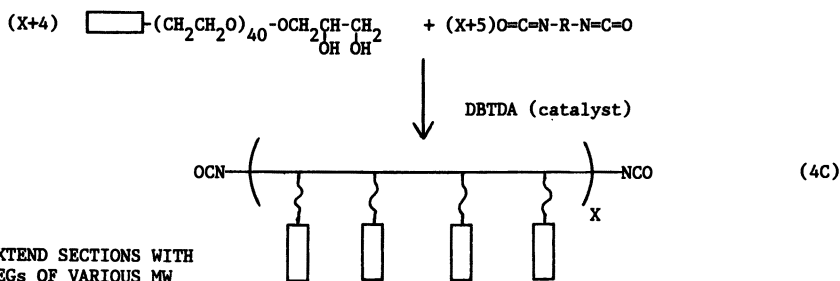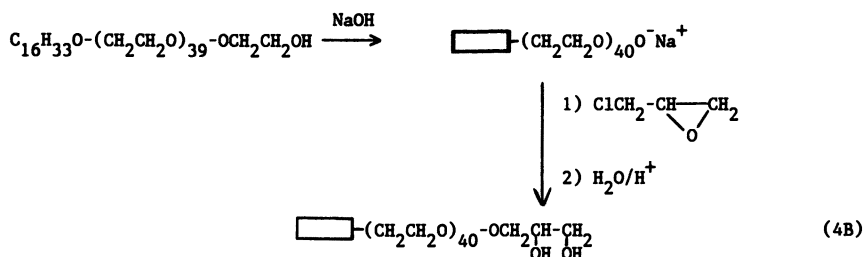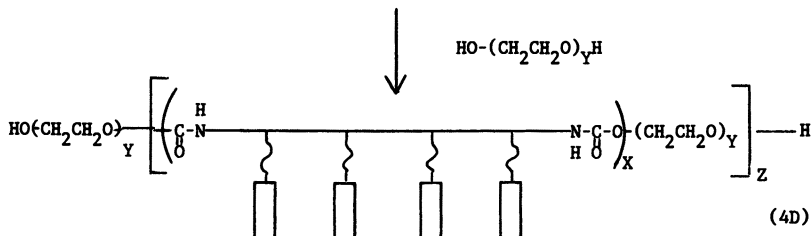
Scheme IV. Reaction diagram for the synthesis of a comb-type HEUR thickener with block hydrophobe placement.

with diisocyanates to any desired sequence (4C) length before extension of the hydrophobe blocks in the final step with a polyethylene glycol (4D) of a specific length.

Thus, the synthesis of HEUR polymers varying significantly in their hydrophobe placement geometries can be achieved. These variations in molecular architecture can effect dramatic variations in dispersion rheology and applied film properties. Differences observed with HEUR di-, tri-, and block-comb geometries will be discussed in the following sections.

Solution Properties

General Phenomena. The use of fluorescence probes to study hydrophobic domains in water-soluble polymers, presented in detail in Chapters 13 and 14, is employed in most of the chapters discussing associative thickeners in this section. The concentrations at which hydrophobic domains form with HEURs synthesized via Schemes I and II are illustrated in Figures 2 and 3, respectively. The dinonylphenol modification of the 26,000 molecular weight poly(ethylene glycol) [NPIP(EtO)$_{595}$IPNP] effects a hydrophobic domain not evident in the unmodified poly(ethylene glycol) (PEG) (Fig-
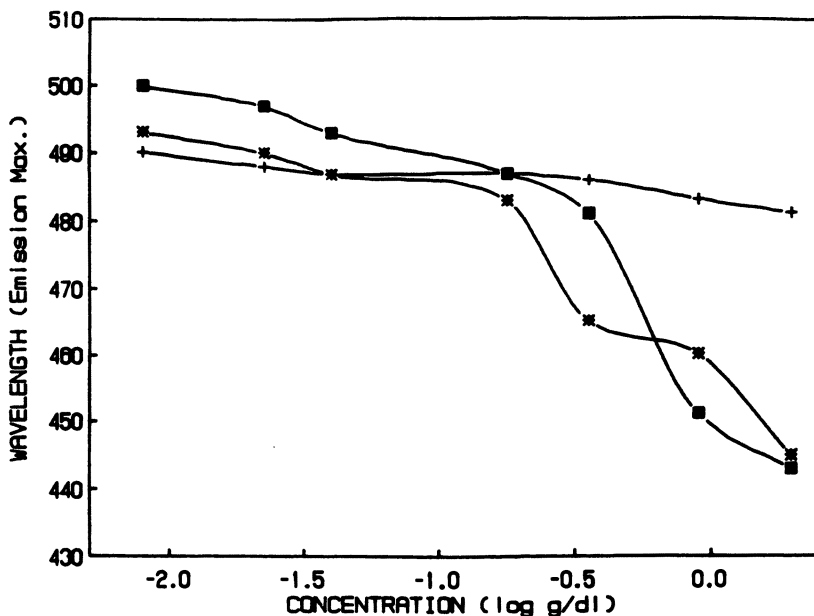
Figure 2. Fluorescence spectra of aqueous POE solutions containing 8-anilinonaphthalene-1-sulfonate (ANS, 2 × 10^{-2} M) probe. Hydrophobe-capped derivatives were synthesized according to Scheme I. Key: +, unmodified POE of 26,000 molecular weight; *, nonylphenol hydrophobe (referred to as NPIP(EtO)$_{595}$IPNP in the text); ■, C$_{14}$H$_{29}$ hydrophobe.
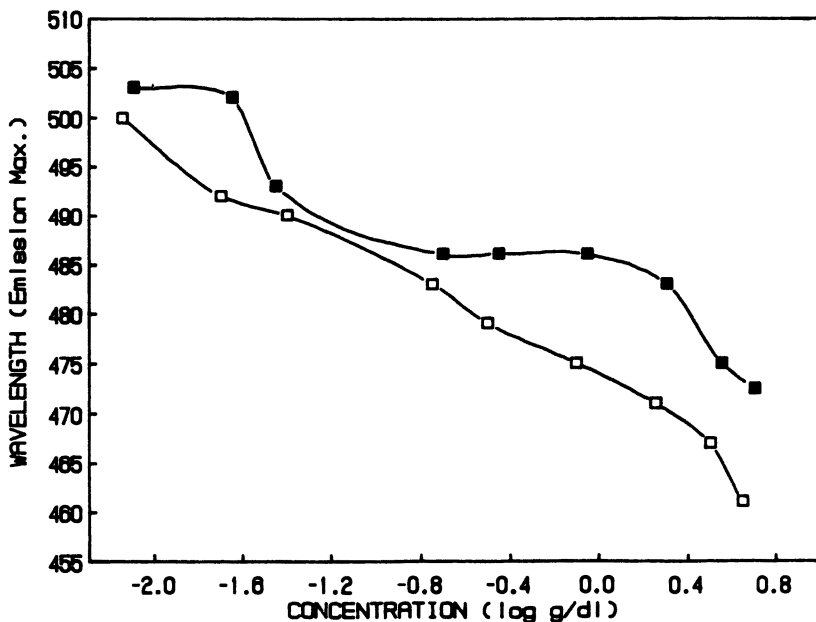
Figure 3. Fluorescence spectra of aqueous POE (average 100 mol) derivatives
of isophorone diisocyanate trimer, containing ANS (2 × 10⁻² M) probe. Hy-
drophobe-capped derivatives were synthesized according to Scheme II. Key:
■, (oxyethylene)₁₀₀ nonylphenol hydrophobe (referred to as (NP(EtO)₁₀₀IPDI)₃
in text; □, (oxyethylene)₁₀₀ with methoxyl terminal group.

ure 2). In the second class of thickener, the isophorone isocyanurate
center is hydrophobic, and a domain is formed without surfactant capping
(i.e., the end groups are methoxyl units). Nonylphenol modification
[(NP(EtO)₁₀₀IPDI)₃] appears to produce a domain at lower concentration
(Figure 3) than the methoxyl-capped polymer, but a significant difference
in the structure of the hydrophobic domains is not distinguished by the
fluorescence probe used in this study.

In the trimer series, the hydrophobic domains in the fluorescence data
reflect isocyanurate associations. The hydrophobe associations responsible
for effective thickening occur at higher concentrations. Probe studies similar
to those conducted in oxyethylene–oxypropylene block polymers (12, 13)
are warranted. The difference of importance to the rheology of dispersed
systems is likely related to the cohesiveness of the surfactant hydrophobe
interaction (21).

Conventional polymers at a given molecular weight increase in viscosity
monotonically until a critical concentration, c* (discussed in Chapter 10) is
reached. Above this concentration, the viscosity increases as a power func-
tion. The same phenomenon is observed with low molecular weight, hy-
drophobe-modified, water-soluble polymers, but the distinctive increase in

solution viscosity arises from the association of the surfactant hydrophobes in water, not from overlapping of the chains. The concentrations (c^*_h) at which a marked increase in the viscosity is observed among commercial associative thickeners are presented in Figure 4. The c^*_h values of the higher molecular weight model HEURs of Schemes I and II, synthesized in our laboratories, were 5 and 25 wt %, respectively (20).

The data in Figures 4–7 are for relatively simple systems. The associative thickener from which cosolvents and other organic additives have been removed is in water (Figure 4). In the other figures, other materials have been added: a nonionic surfactant (Figure 5), two ethoxylated anionic surfactants (Figures 6a and 6b), and a model latex containing 0.138% surfactant in the aqueous phase (Figures 7 and 8). The "free surfactant" is a residue of the latex synthesis, and in these systems the cosolvent was not removed from the commercial thickeners. Model associative thickeners of the type pre-
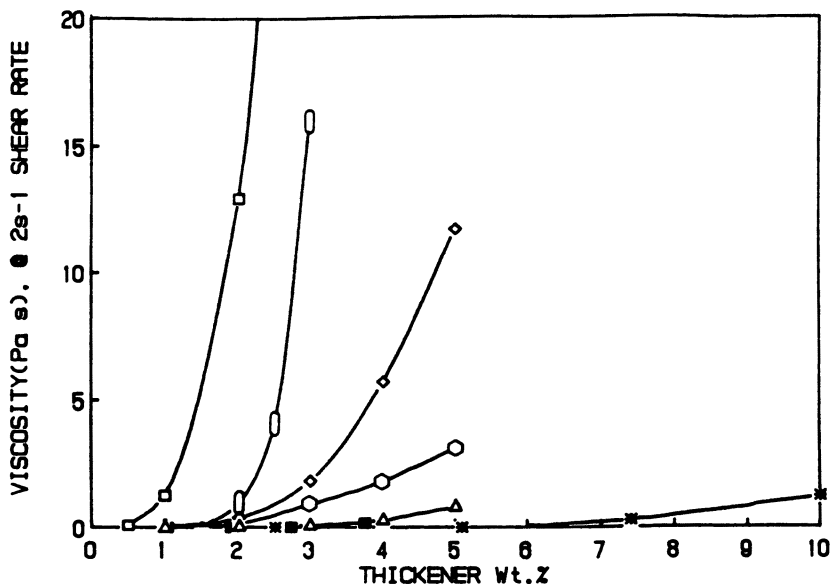
*Figure 4. Low-shear-rate (2 s⁻¹) viscosity (Pa s) dependence on thickener weight percent concentration of □, (hydroxyethyl)cellulose, M_v 700,000; ■, model HEUR-NPIP(EtO)₅₉₅IPNP, M_n 24,000; *, model HEUR-(NP(EtO)₁₀₀IPDI)₃, M_n 10,500. The remaining HEUR associative thickeners are commercial products whose molecular weights are given in ref. 1: ◖, HEUR 270; ○, HEUR 708; ◇, HEUR 200; △, HEUR 100. In the following chapter HEUR 708 will be referred to as 825 and HEUR 270 as 275. These are supplier designations of the same HEUR polymers supplied at different solids levels in aqueous solutions containing different cosolvents to lower solution viscosities. The commercial HEURs were isolated (i.e., removed from their cosolvent) and redissolved in these studies and in those described in Figures 5–8.*
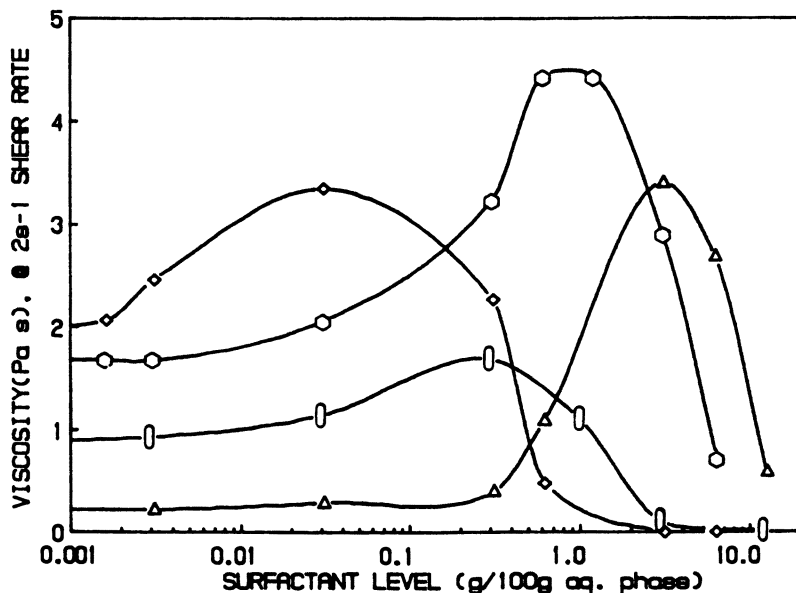
Figure 5. The effect of nonionic surfactant, Tergitol 15-S-9, on the viscosity of the associative thickener solutions. Key: △, 4% HEUR 100; ◇, 4% HEUR 200; ○, 4% HEUR 708; ◻, 2% HEUR 270.

sented in Schemes I and II were used to obtain the data illustrated in Figures 12 and 13, to delineate associative thickener characteristics important to viscosity response at low and high shear rates. The response to the addition of stabilized titanium dioxide in these simple dispersions is examined in Figures 9–11; the rheological behavior of fully formulated coatings is examined in the remaining illustrations.

Viscosity Maxima. The low-shear-rate viscosities of both commercial and model associative thickeners below their c^*_h values will increase with the addition of conventional low molecular weight surfactants or coalescing aid (*22*). With HEUR polymers, solution viscosities are observed to increase, achieve a maximum value, and then decrease with continued increase in surfactant concentration (*23*). This type of behavior is illustrated (Figure 5) for four commercial HEURs with a nonionic surfactant (typical of that used in coating formulations). A similar behavior has been observed (*24*) with a classical anionic surfactant and hydrophobically modified (hydroxy-ethyl)cellulose (HMHEC) and is reviewed in Chapter 18. Intermicellar networks, formed by the participation of one or more hydrophobes from different polymers in the micelles of conventional surfactants, were again recently suggested (*25*) to affect viscous solutions.
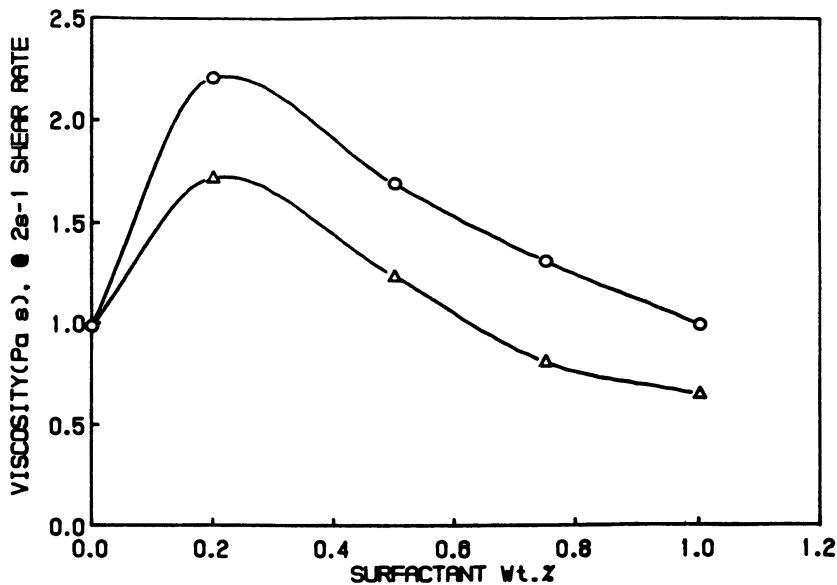
Figure 6a. The effect of anionic surfactants used in latex synthesis on the viscosity of 2% solution of HEUR 270. Key: △, ammonium salt of nonylphenol ethoxylate (average 20 oxyethylene units) sulfate; ○, ammonium salt of non-ylphenol ethoxylate (average 9 oxyethylene units) sulfate.
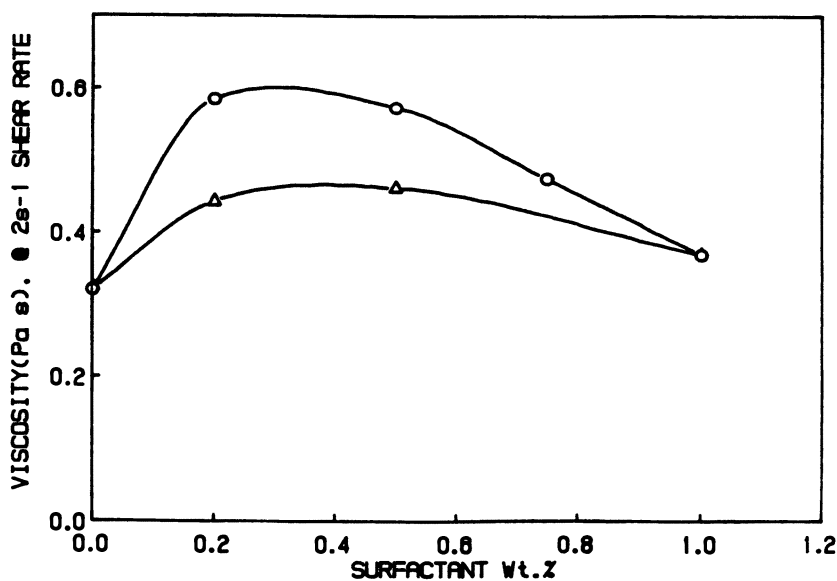
Figure 6b. The effect of anionic surfactants used in latex synthesis on the viscosity of 2% solution of HEUR 708. Surfactants used are the same as in Figure 6a.
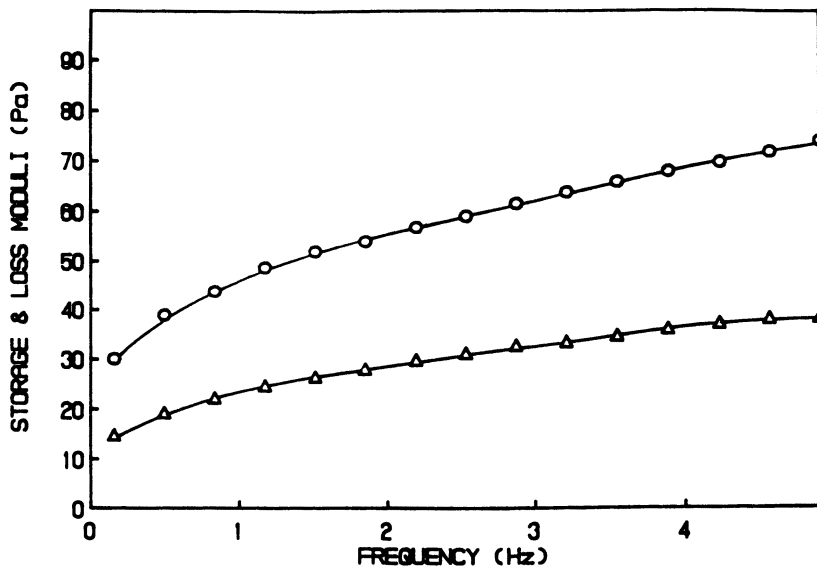
Figure 7. Storage modulus (Pa) and loss modulus (Pa) dependence on frequency (Hz) of 0.32 volume fraction dispersion of 220-nm MMA–MAA (96:04) latex, containing 0.648 × 10⁻² meq/m² surface acid at pH 9 and 0.138 wt % free surfactant in the aqueous phase. Thickener: HEUR 270, 0.5 wt % in the aqueous phase. Key: O, storage modulus; △, loss modulus.

In aqueous solutions devoid of low molecular weight surfactant, cosolvent, or coalescing aid, HEUR 270 is the most viscosifying of the associative thickeners, and it was used at half the concentration (2 vs. 4 wt %) in the nonionic formulation surfactant studies (Figure 5). The influence of surfactants (26) used in the synthesis of experimental latices on the viscosity of two commercially successful associative thickeners, HEUR 708 and HEUR 270, is illustrated in Figure 6. The viscosity maximum occurs at lower concentrations with these ethoxylated anionic surfactants; this trend is even more pronounced with the classical anionic surfactant, sodium dodecyl sulfate (23). Sodium dodecyl sulfate is seldom used in coating formulations. In a coating formulation both the synthesis and formulation surfactant are present; the latter in greater amounts. To fully understand the influence of free surfactants in coating formulations (i.e., free in the aqueous phase, to induce intermicellar viscosity enhancement of the dispersion), the behavior of associative thickeners in mixed micelles should be studied with emphasis on composition and concentration influences on micelle sizes and shapes. The magnitude of such an effort is evident in the study of simple systems (alkylacrylamide–acrylamide polymers in the absence of surfactants) described in Chapter 23. Some insight without such measurements can be gained from oscillatory measurements.
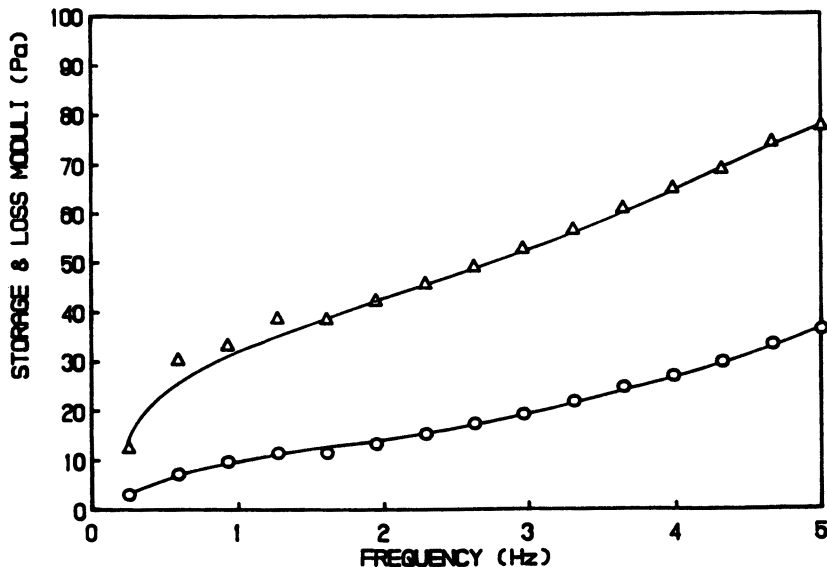
Figure 8. Storage modulus (Pa) and loss modulus (Pa) dependence on frequency (Hz) of 0.32 volume fraction dispersion of 220-nm MMA–MAA (96:04) latex, containing 0.648 × 10⁻² meq/m² surface acid at pH 9 and 0.138 wt % free surfactant in the aqueous phase. Thickener: HEUR 708, 0.75 wt % in the aqueous phase. Key: ○, storage modulus; △, loss modulus.

Geometrical Influences on Dispersed-Phase Rheology

Thickened Latex Dispersions: Viscoelastic Contributions. Elastic (G', storage modulus) and viscous (G'', loss modulus) contributions to a dispersion's viscosity (27) can be obtained from oscillatory data (the technique and terms are defined in Chapter 2). Significant differences are observed in rheological responses of commercial associative thickeners with an experimental latex (96% methyl methacrylate–4% methacrylic acid ammonium salt). The thickened dispersion contains residual surfactant in the aqueous phase from the latex's synthesis. The dispersion containing HEUR 270 exhibits a dominant G' response (Figure 7, also noted with HEUR 200 in this family of latices); the HEUR 708 dispersion exhibited a dominant G'' response (Figure 8, also observed with HEUR 100). Differences in component responses of the model HEURs also are observed with this latex: G' is dominant in NPIP(EtO)$_{595}$IPNP dispersions; G'' is dominant when the distance between the interlinking ethoxylate units is shortened to 200 mol of ethoxylate units, (i.e., the trimer (NP(EtO)$_{100}$IPDI)$_3$ and diblock C$_{12}$H$_{25}$(EtO)$_{100}$ TMXDI(EtO)$_{100}$C$_{12}$H$_{25}$).

Similar responses are observed with these associative thickeners in aqueous phases at surfactant concentrations producing viscosity maxima, but
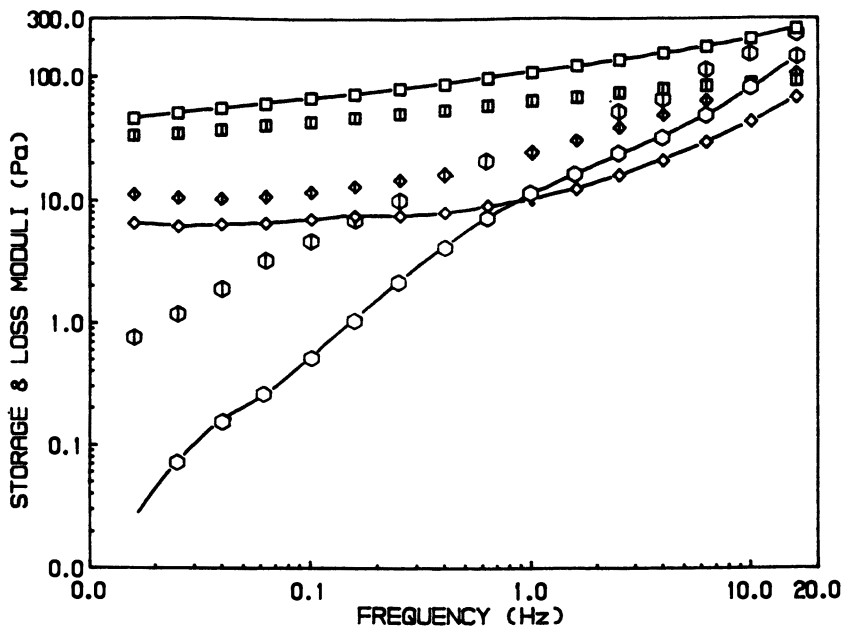
Figure 9. Storage modulus and loss modulus dependence on frequency of 0.32 volume fraction dispersion of 117-nm acrylic latex containing 0.112×10^{-2} meq/m^2 surface acid at pH 9 and 0.4% free surfactant in the aqueous phase. Key: open symbols, storage modulus; cross symbols, loss modulus. Thickeners and their concentrations in the aqueous phase: □, (hydroxyethyl)cellulose, M$_v$ 700,000, 0.65%; ○, HEUR 708, 0.67%; ◇, HEUR 200, 1.35%.

the magnitudes of the responses are significantly lower than that observed in the latex dispersions. These studies, to be described in detail in a future manuscript, provide evidence for viscosity enhancement both with and without an interlinking elastic network.

Thickened Latex–Pigment Dispersions. A "model industrial latex" containing 0.00112 meq/m^2 of methacrylic acid ammonium salt, surface moieties, and a residual nonionic surfactant in the aqueous phase was thickened with two commercial associative thickeners and HEC and evaluated with and without titanium dioxide. The latex was attractive to formulators in the 1960s, but was abandoned because of the poor rheology of small-particle latices in (hydroxyethyl)cellulose (HEC)-thickened formulations. The viscous and elastic contributions were evaluated under constant strain conditions (Rheometrics viscometer). The nonionic surfactant usually added as a wetting agent for titanium dioxide was withheld. The storage and loss moduli of the thickened latex dispersions (0.32 volume fraction) are illustrated in Figure 9. The primary response of the HEUR 708 is viscous with both the experimental and industrial latices. The dominant response of
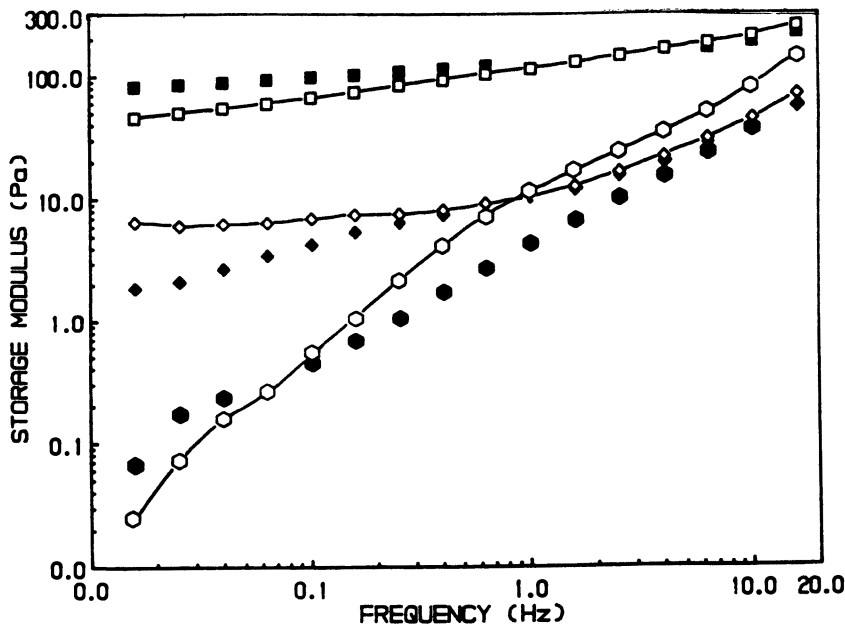
Figure 10. The influence of titanium dioxide on storage modulus (Pa) with frequency. The latex, thickeners, and their concentrations in the aqueous phase and the surfactant concentration in the aqueous phase are the same as in Figure 9. Key: open symbols, 0.32 volume fraction of latex; closed symbols, 0.32 volume fraction of latex plus pigment at a pigment to pigment plus latex volume ratio of 0.21. Titanium dioxide was stabilized with a 5000 molecular weight poly(methacrylic acid) (PMAA).

HEUR 200 dispersions, which are very sensitive (Figure 5) to low surfactant concentrations, is elastic with the experimental latex, but the loss modulus is slightly greater with the industrial latex. The results are in part related to free surfactant differences of the two latices.

Replacement of 21 vol % of the latex with pigment (TiO$_2$) does not significantly affect the relative contributions (the similarity in storage modulus is illustrated in Figure 10). A similarity and small decrease in the loss modulus of all dispersions is observed with pigment addition (Figure 11). The dominance of the elastic contribution in the HEC formulation is consistent with a previous study (27) employing this latex with the full formulation surfactant concentration (0.6 wt %) present. The decreasing storage modulus at low oscillation frequencies in the HEUR 708 formulation is consistent with a similar decrease in first normal stress difference for a parallel formulation (1) with 0.6 wt % formulation surfactant. Variations in the viscosity of pigment-only dispersions, when the structure of the dispersing aid is varied, will be reported elsewhere.
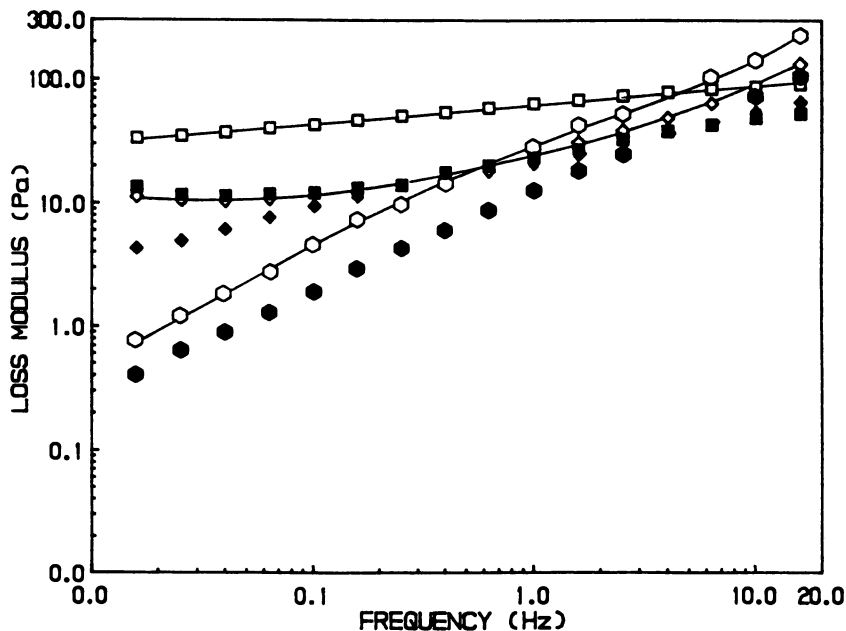
Figure 11. The influence of titanium dioxide on loss modulus (Pa) of dispersions described in Figure 10.

Mechanisms of Association. *Model HEURs: Low- and High-Shear-Rate Viscosities.* The model thickeners of Schemes I and II were used to thicken the model industrial latex just discussed. Two model diblock thickeners, of number-average molecular weight (M_n) 24,000 and 8800, were studied. The thickener of M_n 8800 can be synthesized by the reaction of *m*-tetramethylxylene diisocyanate with a 100-mol ethoxylated hydrophobe to bypass the insolubility obtained with isophorone large ($\geq C_{16}H_{33}-$) hydrophobe capping of a lower molecular weight polyethylene glycol. This low molecular weight diblock is a secondary model in that it corresponds to the hydrophobe spacing of the trimer of M_n 10,500.

The greater spacing between hydrophobes causes very high dispersion viscosities at low shear rates (Figure 12), as predicted (25) in the pyramidal network model. With increasing concentrations of thickener, the low-shear-rate viscosities (LSVs) are higher with NPIP(EtO)$_{595}$IPNP of M_n 24,000 than with a higher molecular weight (hydroxyethyl)cellulose (HEC, viscosity-average molecular weight (M_v) 700,000), but the LSVs of HEC are higher than the trimer and diblock model thickeners of lower molecular weight. The high molecular weight diblock thickener forms an elastic network; the trimer dispersions do not have a strong elastic component.

At higher deformation rates, the extensive network of the NPIP-(EtO)$_{595}$IPNP diblock is disrupted, and the viscosities are approximately the
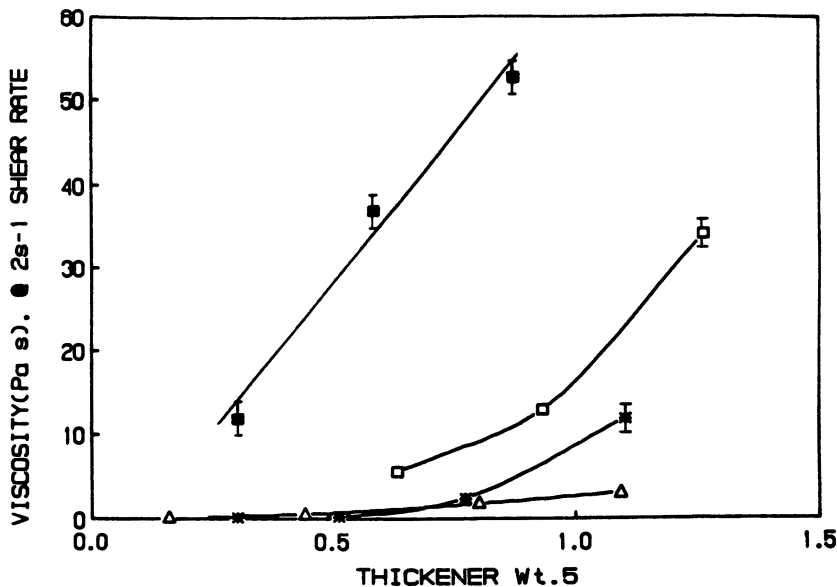
Figure 12. Low-shear-rate (2 s⁻¹) viscosity (Pa s) dependence on thickener concentration in the aqueous phase of 0.32 volume fraction dispersion of 117-nm acrylic latex containing 0.112 × 10⁻² meq/m² surface acid at pH 9 and 0.4% free surfactant in the aqueous phase. Thickeners: □, (hydroxyethyl)cellulose, M_v 700,000; ■, model HEUR-NPIP(EtO)₅₉₅IPNP, M_n 24,000; *, model HEUR-(NP(EtO)₁₀₀IPDI)₃, M_n 10,500; △, model HEUR-(C₁₂H₂₅(EtO)₁₀₀)₂TMXDI, M_n 8800.

same as those of the HEC-thickened latex. The lower molecular weight model HEUR–latex dispersions are less shear thinning and effect higher shear rate viscosities (HSVs, Figure 13). The differences, viewed from the concentration of hydrophobes (Table I) and the architecture of the HEUR thickener, reflect the influence of hydrophobe contact residence times on the fluid's response at high deformation rates. The presence of a moderate amount of free surfactant is also required (26).

The studies just discussed do not address one of the significant contributions associative thickeners make to coatings rheology: minimizing LSVs in small-particle latex formulations.

Low Shear Rates. Small-particle latices provide higher critical pigment volume concentrations and thereby greater coating formulation latitude. Their viscosities are, however, too high at low shear rates and too low at high shear rates to provide acceptable applied film properties. This phenomenon is illustrated in part in Figure 14. The latices used in this study (26) included three commercial binders (half symbols); the others were ex-
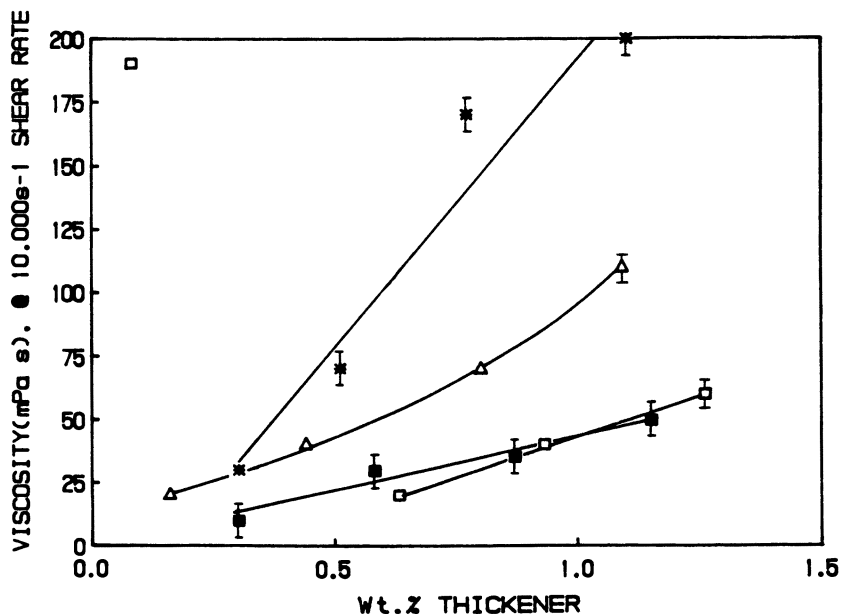
Figure 13. High-shear-rate (10,000 s⁻¹) viscosity (mPa s) dependence on the formulation described in Figure 12.

Table I. Dependence of HSV on the Concentration of Hydrophobes

Thickener	Concentrated Aqueous Phase (wt %)	Hydrophobes Concentration (mol/L × 10³)	HSV (mPa s)
(NP(EtO)₁₀₀IPDI)₃	0.30	0.62	30
	0.51	1.05	70
	0.77	1.58	170
	1.10	2.27	200
(C₁₂H₂₅(EtO)₁₀₀)₂TMXDI	0.16	0.34	20
	0.44	0.93	40
	0.80	1.68	70
	1.09	2.29	110
NPIP(EtO)₅₉₅IPNP	0.30	0.17	10
	0.58	0.32	30
	0.87	0.48	35
	1.15	0.64	50

perimental styrene (bold symbols) or methyl methacrylate compositions (i.e., either as high glass transition temperature (T_g) homopolymers or as low T_g acrylate copolymers to obtain film-forming polymer colloids). The solid symbol is a methyl acrylate (72%)–methyl methacrylate (27%) (w/w) latex. The experimental latices, prepared by the method of Donners and Peeters (28),
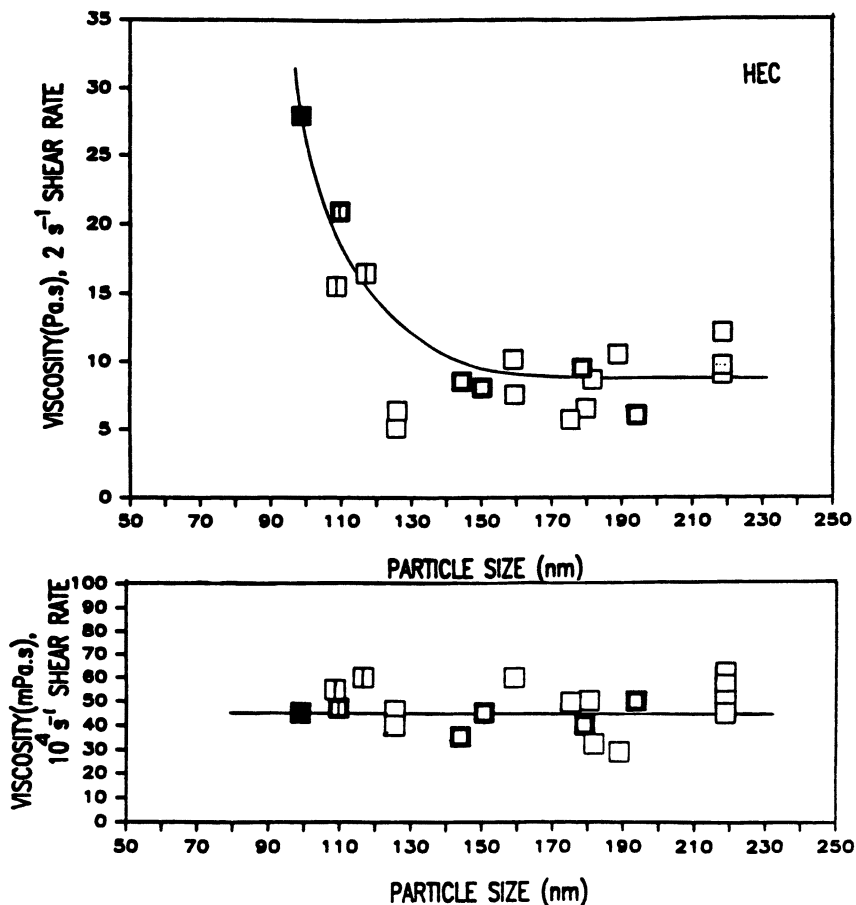
Figure 14. Low-shear-rate (2 s⁻¹) (top) and high-shear-rate (10⁴ s⁻¹) (bottom) viscosity dependence on latex median particle size of latex in 0.32 volume fraction dispersions containing TiO_2 (PMAA stabilized) at a pigment to pigment plus latex volume ratio of 0.21. The latices included three commercial binders (cross symbols); the others were experimental monodisperse latices; closed symbol is more hydrophilic (MMA–methyl acrylate–MAA 27:72:01) terpolymer latex; styrene (bold symbols), methyl methacrylate compositions (i.e., either as high T_g homopolymers or as low T_g acrylate copolymers to obtain film-forming polymer colloids). All dispersions were thickened at 1.1 wt % (hydroxyethyl)cellulose of M_v 700,000 in the aqueous phase. A nonionic $C_{15}H_{31}$-$(CH_2CH_2O)_9H$ (both hydrophobe and ethoxylate numbers are average values) was added to the formulation at 0.6 wt %, following coating formulator practices. This addition was also done in the systems reported in Figures 15–17.

were monodisperse. The dispersions contained TiO_2 stabilized with an oligomeric (5000 molecular weight) methacrylic acid (29) and an excess (0.6 wt %) of nonionic formulation surfactant. The increasing LSVs with latices below 150 nm is typical of a previous study (30). A viscosity dependence on latex particle size is not observed at high shear rates (10^4 s^{-1}), but the largest latices in this investigation are less than half the size of most of the binders examined in the previous study. Our larger latices also were not stabilized with grafted HEC fragments.

In a high-volume-fraction dispersion with electrosteric stabilization of the latex and an increasing dispersed-phase surface area, the high viscosity observed at low shear rates with decreasing latex size relates to electroviscous and hydration effects. Lower surface acid concentrations on some of the smaller latices may also result in partial flocculation of the latex and a higher effective volume fraction in the presence of coalescing aids (22, 26).

These effects in a medium thickened by a high molecular weight or pseudo high molecular weight (via hydrophobic associations) water-soluble polymer can contribute to high viscosities in small-particle latices. However, small-particle latices require a higher concentration of surfactant in their synthesis (26). For example, the "ideal industrial latex" used in much of the rheology just discussed contains a free surfactant concentration of 0.45 wt %. This amount of free surfactant, with the formulation surfactant added to a coating at 0.6 wt %, is past the concentration noted for optimum viscosity (e.g., Figure 4) with most associative thickeners. The uniqueness of associative thickeners in small-particle latex coating appears to lie in the reduced participation in formulation surfactant micelles facilitated by the excess surfactant present in most commercial small-particle latices.

Irrespective of the free surfactant's effect on the maxima in associative thickener viscosity efficiency, the sum of the maxima in the viscosity of the associative thickener and surfactant and of the latex does not equal the viscosity of the combined components in a coating. A synergistic viscosity increase from an interaction between the thickener and the latex is required to account for the total viscosity observed (26). The most popular mechanism for association is the adsorption of the thickener's hydrophobe(s) on the surface of the latex.

In concept, this mechanism could be viable because it would buffer repulsions among anionic surfactants used in the latex's synthesis. The phenomenon was originally noted in a number of studies by McBain and co-workers in the 1930s. In a coating this mechanism is unlikely for three reasons.

1. Commercial latices are sterically stabilized by grafted (hydroxyethyl)cellulose fragments (16) or electrosterically stabilized by oligomeric surface acids incorporated (17) in the latex's synthesis. These surface structures impart hydrophilicity to

the surface and would sterically inhibit interfacial participation of the associative thickener hydrophobes. Adsorption of the low molecular weight nonionic formulation surfactant on the more hydrophilic surface is more likely, because the critical micelle concentration (a primary parameter in competitive adsorptions (31) of the nonionic formulation surfactant) is lower.

2. HASE (hydrophobically modified alkali-swellable emulsion, discussed in Chapters 25 and 28) and HEUR thickeners are readily displaced from acrylic latex surfaces (32) by sodium dodecyl sulfate (SDS). A surface-active cellulose ether was also reported (33) to desorb from monodispersed poly(styrene) latices with SDS addition. In these studies, the relative critical micelle concentrations of the anionic surfactant and thickener appear to be more important than buffering of surface charges.

3. Differences in dispersion rheology associated with the surface energies (i.e., adsorption coverage) of the different latex types (e.g., vinyl acetate, 18 mN/m; methyl methacrylate, 26 mN/m; and styrene, 40 mN/m) are not realized (34).

These observations in total make it unlikely that the hydrophobes of an associative thickener interact in a coating formulation with the surface of the latex through their hydrophobic groups. The interaction must arise from a less classical mechanism. When the same latices illustrated with HEC (Figure 14) are thickened with HEUR associative thickeners, a relationship between LSVs and median particle size of the latex is not observed. The LSVs in most HEUR thickeners appear to be related to the amount of oligomeric methacrylic acid units on the latex's surface. This relationship is evident in the LSV dependence on the amount of thickener added to latices (220 nm) differing in surface acid concentrations (35) (Figures 15–17). The increase in viscosity associated with an increase in hydrodynamic volume of the latex is not dramatic in HEC dispersions (Figure 15). In these larger size latices (220 nm), depletion flocculation may promote a higher LSV with the lower surface acid latices. The LSVs of the HEUR 708 formulations are lower (Figure 16), but the low shear viscosity of the latex with the highest surface acid is significantly higher with HEUR 270 (Figure 16) than in the other thickened dispersions.

The LSV dependence on surface acid concentration observed with most associative thickeners in this pigmented 20-latex study is illustrated in Figure 17. A latex-associative thickener network model for viscosities at low shear rates is proposed in Figure 18. This model is not the poly(acrylic acid)–poly(oxyethylene) complex observed over 2 decades ago (36). The coatings discussed are alkaline (pH 9). Examination of the data presented in
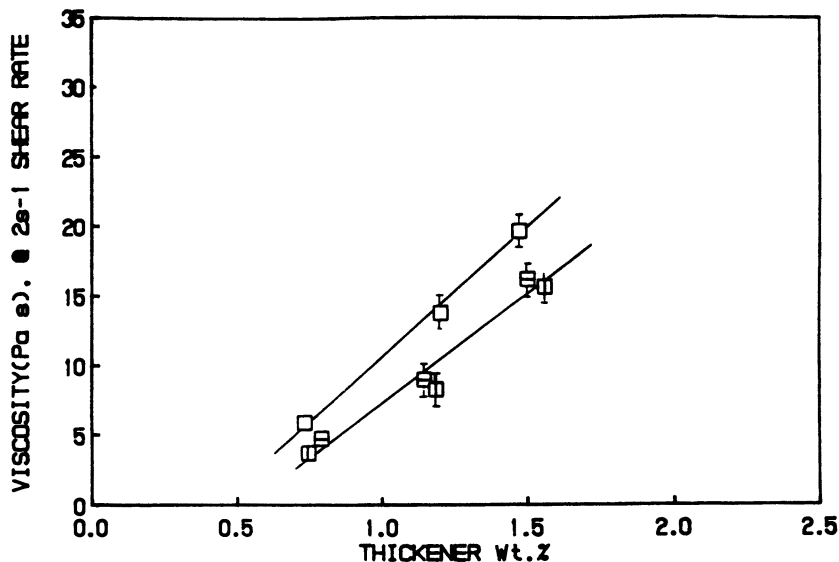
Figure 15. Low-shear-rate (2 s⁻¹) viscosity (Pa s) dependence on the concentration of thickener, HEC of M_v 700,000, in the aqueous phase of 0.32 volume fraction dispersions containing TiO₂ at a pigment to pigment plus latex volume ratio of 0.21. Key to latices: open, 220, MMA–MAA (96:04) latex containing 0.00741 meq/m² surface acid; horizontal cross, 220, MMA–MAA (97:03) latex containing 0.00222 meq/m² surface acid; and vertical cross, 220, MMA–MAA (98:02) latex containing 0.00182 meq/m² surface acid.

the original publication also provides evidence of an association between the cation of the carboxylate group and the ether linkages of the oxyethylene chain. The cation interaction is not as strong an association and is only mentioned in passing. It is not mentioned in texts that cite the publication.

Spectroscopic evidence for association through the sharing of carboxylate cations has been reported (37) (the phenomenon is discussed in Chapter 15) for surfactant–acrylic acid copolymer interactions. This dependence on surface carboxylate groups (Figure 17) is not observed in cellulose ether or in HEUR 200 formulations. This observation is made in reviewing all of the data, and probably reflects only the extreme surfactant sensitivity of HEUR 200.

Several reviewers of this chapter have stressed that the model proposed in Figure 18 is speculative. It is, in the sense that there are so many variables in a coating formulation that no mechanism will be universal (i.e., this mechanism is not being proposed for vinyl–acrylic HEC-stabilized latices). The carboxylate cation ion–dipole interaction with the oxygen atoms of the oxyethylene units is not speculative. Numerous publications other than the one ATR–FTIR (attenuated total reflectance–Fourier transform infrared)
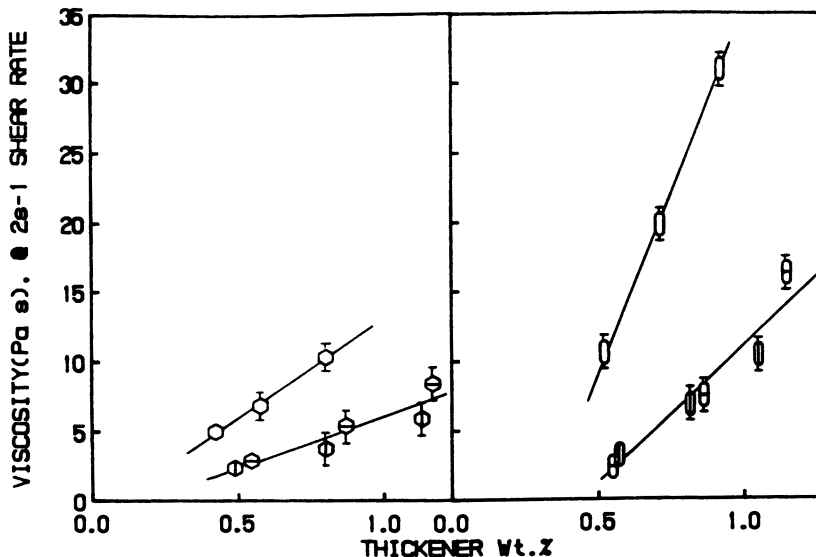
Figure 16. Low-shear-rate (2 s⁻¹) viscosity (Pa s) dependence on the concentration of the thickener in the aqueous phase of 0.32 volume fraction dispersions containing TiO₂ at a pigment to pigment plus latex volume ratio of 0.21. Thickener: O, HEUR 708; 0, HEUR 270. Latices are as described in Figure 15.

study cited will be discussed in a future publication addressing the phenomenon.

Other Phenomena

Syneresis. This chapter began with consideration of the depletion layer effect. This phenomenon can be seen in coatings that contain large latices (>300 nm) not highly stabilized by surface-attached (hydroxyethyl)cellulose fragments (16), and is in part the problem observed in the last sections of Chapter 27. The phenomenon is not necessarily restricted to HEC-thickened formulations and depletion flocculation. In our studies, syneresis is observed in thickened aqueous solutions and in dispersed systems containing the model trimer associative thickener (Scheme II); it can be overcome by addition of conventional surfactants. Syneresis in HMHEC-thickened solutions is discussed in Chapter 19 in the absence of a dispersed phase. Syneresis is discussed in the following chapter where additives that substantially enhance low shear viscosities are added to inhibit syneresis.

Water Sensitivity. Improvement in the water sensitivity and improved barrier properties of latex film has been an important goal of many coatings chemists. One of the first publications (38) on HEUR-thickened
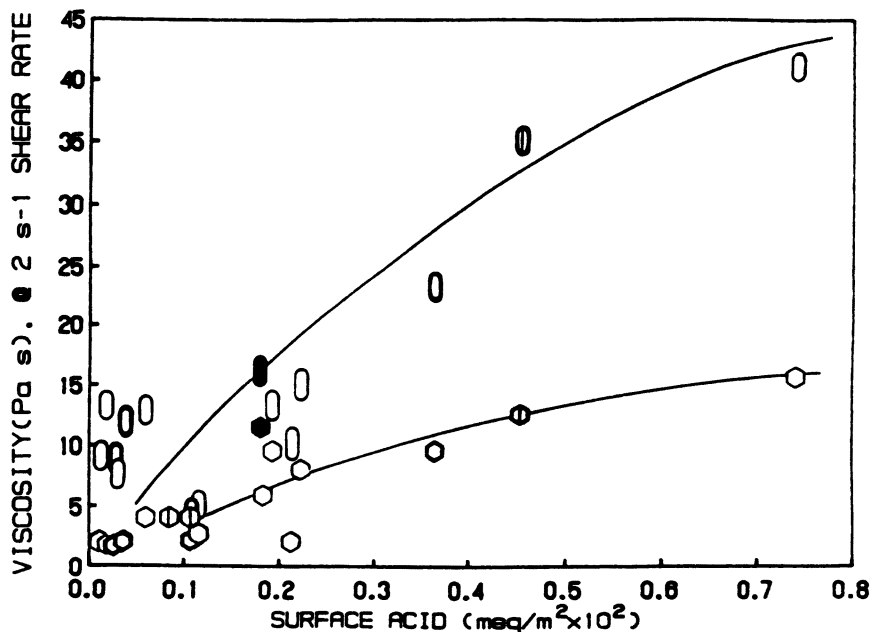
Figure 17. Low-shear-rate (2 s⁻¹) viscosity (Pa s) dependence on latex surface acid (meq/m², latices were equilibrated at pH 9 before the titration), for the latices noted in Figure 14 (in 0.32 volume fraction dispersions containing titanium dioxide at a pigment to pigment plus latex volume ratio of 0.21). All dispersions were thickened at 1.1 wt % thickeners in the aqueous phase. Thickeners: ○, HEUR 708; 〇, HEUR 270; 1.1%.

latex coatings stressed their improved water sensitivity over films obtained from cellulose-ether-thickened coatings. Differences in coatings rheology were not even mentioned in the publication. Our evaluations of formulation surfactants and HEUR-thickener influences on the water sensitivity of latex films are discussed elsewhere (*39*).

Film Gloss.   Most associative thickeners produce very shear thinning pigment slurries when the pigment stabilizer is the oligomeric methacrylic acid (*29*) discussed in this chapter. HEUR 200 is a notable exception. This exception may be due to the extreme surfactant sensitivity of HEUR 200 solutions rather than flocculation by other associative thickeners. Back-scattering studies (*40*) have indicated that associative thickeners flocculate titanium dioxide in coatings formulations. Gloss from applied films (Table II) of representative full-formulation coatings at 0.32 volume fraction and at a 35 pigment to latex plus pigment volume ratio (*41*) reflect the stabilization (i.e., Newtonian rheology) observed in HEUR 200 pigment dispersions. It is too early in our studies to delineate a mechanism for the higher film gloss noted in many formulations thickened with HEUR 200. Additional studies are needed to understand this particular phenomenon.
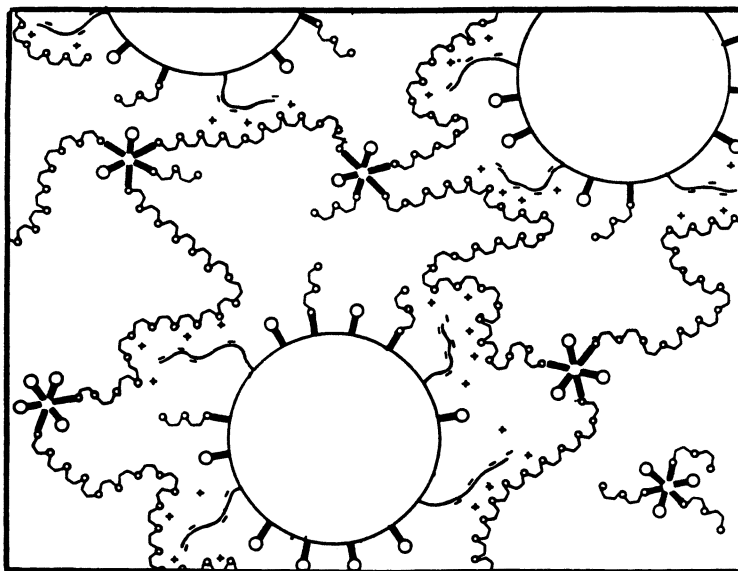
Figure 18. Mechanism for the dependence of low-shear-rate viscosity of high-volume-fraction coating formulations on free surfactants and the latex surface acid.

Table II. Comparison of Various Parameters with 60 °C Gloss Readings of 0.32 Volume Fraction, 117-nm Acrylic Latex at Two Pigment to Pigment Plus Latex Ratios (PVC)

PVC	Thickener Type	(Wt %)	Kreb Unit Viscosity, KU	Gloss	LSV (Pa s)
21	HEC	0.39	90	40	5.7
		0.52	105	31	12.3
		0.72	120	29	22.5
	HEUR–708	0.35	90	22	1.6
		0.44	105	29	2.4
		0.55	120	33	3.1
	HEUR–200	0.95	90	56	7.3
		1.22	105	64	10.3
		1.52	120	63	14.5
35	HEC	0.38	90	13	8.9
		0.48	105	13	13.4
		0.65	120	11	26.0
	HEUR–708	0.27	90	6	2.4
		0.42	105	7	3.3
		0.54	120	10	4.5
	HEUR–200	0.80	90	33	7.4
		1.08	105	34	11.2
		1.25	120	35	13.8

Conclusion

The architecture of HEUR thickeners influences pigmented, waterborne latex coatings rheology and applied film properties. High solution viscosities at low shear rates can be obtained by increasing the spacing (i.e., the number of oxyethylene units) between hydrophobes, but this increase leads to undesirable livering or gellike structure in coating formulations, and the viscosities at high shear rates are less than desired. HEURs with multiple hydrophobes and a sufficient amount of free surfactant are necessary to achieve desired higher viscosities at high shear rates. The important factor in obtaining HSVs is the resonance contact times of the associative thickeners and their participation in nonspherical micelles (26).

In HEC-thickened formulations, low-shear-rate viscosities increase with decreasing latex particle size. This effect has been a major limitation in formulating small-particle latices. The phenomenon appears to arise from electroviscous, hydration, or flocculation effects, not a depletion layer mechanism. Associative thickeners achieve efficient viscosity in coating formulations via participation in synthesis and formulation surfactant micelles to form pseudo macromolecules and via an ion–dipole interaction between the cations of surface carboxylate groups on the latex and the ether linkages of the associative thickener. Generally, an excess of synthesis surfactant is found in the production of small-particle latices. The achievement of lower viscosities in small-particle ($\sim$100 nm) latex coatings thickened with associative thickener appears to occur by extensive disruption of the polymer hydrophobe's participation in intermicellar networks.

Depletion layer effects occur in associative thickener formulations when the latex is larger in size ($\sim$500 nm) and not highly stabilized with surface (hydroxyethyl)cellulose fragments. Syneresis is also observed in simple aqueous solutions and in latex dispersions when the hydrophobicity of the associative thickener is high.

The importance of the proximity of hydrophobe placement, oxyethylene chain length, and molecular geometry has been highlighted, but their quantitative interrelationships have not been defined in a coating with a matrix of multiple interactions. Another area where a fundamental understanding is still lacking is in the relative stability of the highest energy dispersed phase, titanium dioxide, relative to the latex. Titanium dioxide can be stabilized by a variety of oligomeric acids, varying in their hydrophilicity. The influence of associative thickener structural effects on the stability of high-energy pigments and of synergies in stability with low modulus latices necessary to form the continuous film of the coating have not been determined. Despite these deficiencies in understanding, HEUR and HASE thickeners are commercial realities in the coatings area. The remaining chapters in this text present more applied formulation studies of HASE and HEUR thickeners in coatings.

Acknowledgment

References

1. Glass, J. E. *Water-Soluble Polymers: Beauty with Performance*; Glass, J. E., Ed.; Advances in Chemistry 213; American Chemical Society: Washington, DC, 1986; Chapter 21.
2. Schwab, F. G. *Water-Soluble Polymers: Beauty with Performance*; Glass, J. E., Ed.; Advances in Chemistry 213; American Chemical Society: Washington, DC, 1986; Chapter 19.
3. Sperry, P. R.; Hopfenberg, H. B.; Thomas, N. L *J. Colloid Sci.* 1981, *82*, 62.
4. Sperry, P. R. *J. Colloid Sci.* 1982, *87*, 375.
5. Sperry, P. R. *J. Colloid Sci.* 1984, *99*, 97.
6. Napper, D. N. *Polymer Stabilization and Dispersion Stability*; Academic: New York, 1983; Chapter 15.
7. Kobayashi, S.; Iijima, S.; Igarashi, T.; Saegusa, T. *Macromolecules* 1987, *8*, 1729.
8. Glass J. E. *J. Oil Colour Chem. Assoc.* 1976, *59*, 86.
9. Klenin, V. J.; Klenina, O. V.; Kolnibolotchuk, N. K.; Frenkel, S. Ya. *J. Polym. Sci., Polym. Symp.* 1973, *44*, 931.
10. Hancock, R. I. In *Surfactants*; Tadros, Th. F., Ed.; Academic: New York, 1984; Chapter 12.
11. Glass, J. E. *Water-Soluble Polymers: Beauty with Performance*; Glass, J. E., Ed.; Advances in Chemistry 213; American Chemical Society: Washington, DC, 1986; Chapter 5.
12. Turro, N. J.; Kuo, P-L. *J. Phys. Chem.* 1986, *90*, 5205.
13. Turro, N. J.; Somasundaran, R. *Colloids Surf.* 1986, *20*, 145.
14. Landoll, S. L. *J. Polym. Sci., Polym. Chem. Ed.* 1982, *20*, 443.
15. Murakami, T.; Fernando, R. H.; Glass, J. E. *Proceedings of the ACS Division of Polymeric Materials: Science and Engineering* 1985, *53*, 540.
16. Craig, D. H. *Water-Soluble Polymers: Beauty with Performance*; Glass, J. E., Ed.; Advances in Chemistry 213; American Chemical Society: Washington, DC, 1986; Chapter 18.
17. Bassett, D. R.; Hoy, K. L. *Emulsion Polymers and Emulsion Polymerization*; Bassett, D. R.; Hamielec, A. E., Eds.; ACS Symposium Series 165; American Chemical Society: Washington, DC, 1981; Chapter 23.
18. Emmons, W. D.; Stevens, T. S. U.S. Patent 4 079 028, issued to Rohm and Haas, 1978.
19. Hoy, R. C.; Hoy, K. L. U. S. Patent 4 426 485, issued to Union Carbide, 1984.
20. Brown, R. G. Ph.D. thesis, North Dakota State University, in preparation.
21. Van Oss, C. J.; Good, R. J.; Chaudhury, M. K. *Sep. Sci. Technol.* 1987, *22*(1), 1–24.
22. Karunasena, A.; Glass, J. E. *J. Coat. Technol.* in press.
23. Lundberg, D. J. Ph.D. thesis, North Dakota State University, in progress.
24. Landoll, S. L. *Proceeding Associative Thickener Symposium*, May 25, 1982, North Dakota State University Press: Fargo, ND.
25. Bieleman, J. H.; Riesthuis, F. J. J.; van der Velden, P. M. *Polym. Paint Colour J.* 1986, *176*, 450.

26. Karunasena, A.; Glass, J. E.; *Prog. Org. Coat.* in press.
27. Glass, J. E. *J. Oil Colour Chem. Assoc.* **1975**, *67*, 169.
28. Donners, W. A. B.; Peeters, L. G. *Macromol. Chem. Phys., Suppl.* **1985**, *10/11*, 297.
29. Bergh, J. S.; Lundberg, D. J.; Glass, J. E. *Prog. Org. Coat.* **1989**, *17*(2), 155.
30. Bowell, S. T. *Applied Polymer Science*; Craver, J. K.; Tess, R. W., Eds.; American Chemical Society, Washington, DC, 1975; Chapter 41.
31. Kronberg, B.; Lindström, M.; Stenius, P. *Phenomena in Mixed Surfactant Systems*; Scamehorn, J. F., Ed.; ACS Symposium Series 311; American Chemical Society: Washington, DC, 1986; Chapter 17.
32. Thibeault, J. C.; Sperry, P. R.; Schaller, E. J. *Water-Soluble Polymers: Beauty with Performance*; Glass, J. E., Ed.; Advances in Chemistry 213; American Chemical Society: Washington, DC, 1986; Chapter 20.
33. Saunders, F. L. *J. Colloid Interface Sci.* **1968**, *28*, 475.
34. Karunasena, A. Ph.D. thesis, North Dakota State University, 1989.
35. Karunasena, A.; Glass, J. E. *Proceedings of the ACS Division of Polymeric Materials: Science and Engineering* **1987**, *56*, 624–628.
36. Bailey, F. E.; Lundberg, R. D.; Callard, R. W. *J. Polym. Sci., Polym. Phys. Ed.* **1964**, 845.
37. Urban, M. W.; Koenig, J. L. *Appl. Spectrosc.* **1987**, *41*(6), 1028.
38. BASF Corporation in *Paint Colour J.* **1983**, *170*, 378.
39. Murakami, T.; Fernando, R. H.; Glass, J. E. *J. Oil Colour Chem. Assoc.* **1988**, *71*(10), 457.
40. Hall, J. E.; Hodgson, P.; Krivanek, l.; Malizia, P. *J. Coat. Technol.* **1986**, *58*(738), 65.
41. Fernando, R. H. Ph.D. thesis, North Dakota State University, 1986.

Optimizing Latex Paint Rheology with Associative Thickeners

A Practical Approach

Freidun M. Anwari and Fred G. Schwab

Coatings Research Group, Inc., 2340 Hamilton Avenue, Cleveland, OH 44114

This chapter reviews the rheological properties of one-component thickener systems and presents a practical approach to blending different thickener types to optimize the rheological profiles of latex paints. Blend ratios are used to compare thickeners of different efficiencies and rheological properties for their overall contributions to paint viscosity in different shear-rate ranges. Paint rheology was modified by changing the blend ratio to adjust high-shear (10^4 s^{-1}) viscosity, changing thickener molecular weight to fine-tune low-shear (sag and level) viscosity, and in some instances, by using a third thickener to prevent clear-liquid separation. The entire process was carried out at constant mid-shear (Stormer) viscosity.

T HE PERFORMANCE OF A LATEX COATING is evaluated with several standardized rheological tests, each of which is intended to simulate conditions in one part of the broad shear-rate range that occurs during actual use. These tests are Leneta anti-sag (1) and N.Y.P.C. (New York Production Club*) leveling (2) ratings, Stormer viscosity (3), and ICI (Imperial Chemical Industries) cone and plate (10^4 s^{-1}) viscosity (4). These tests approximately correspond to the low-, mid-, and high-shear-rate regions of a viscosity profile (5), respectively.

Although these tests give some indication of actual performance, other

*Now called New York Society for Coatings Technology.

factors are involved. ICI viscosity is used to predict properties during application; as ICI viscosity increases, brushability (6) and spreading rate (7) decrease. However, substrate texture, porosity, wettability, drying rate, and thixotropy also influence these properties. During actual application, high-shear rheology, substrate porosity, and other factors will also affect leveling and sag resistance (8) through changes in film-build. Greater substrate porosity increases viscosity through wicking, which reduces flow and leveling. Often, these interactions are not present when tests are performed that simulate actual conditions, and results may be misleading. The formulator should be aware of these interactions and ideally should attempt to change only one physical property of the coating at a time.

Paints Containing One Thickener

Cellulosic Molecular Weight. A direct relationship exists between the molecular weight (MW) of a cellulosic component and the rheological profile it imparts to a paint. Several investigators (9–11) have shown that as cellulosic molecular weight increases, Stormer thickening efficiency and roller spatter increase, and ICI viscosity decreases. This observation is valid only if paints of nearly equal Stormer viscosities are compared. Nonrheological paint properties are also affected by cellulosic molecular weight. In particular, overall enzymatic resistance or stability increases, and scrub resistance decreases as cellulosic molecular weight decreases (11).

HEUR Effective Molecular Weight. Several factors that influence the rheological behavior of hydrophobically modified ethoxylated urethane (HEUR)-type thickeners are discussed in the preceding chapter. Unlike cellulosic thickeners, which are well-characterized by the manufacturer (12–14), the specific structural features of the commercial HEUR thickeners are generally unknown to the formulator. In this chapter, HEUR thickeners will be described by their "effective" molecular weights on the basis of their efficiencies in achieving a Stormer viscosity (about a 50-s^{-1} shear rate). Although the relative ordering of HEURs may change from formulation to formulation, their effectiveness using the Stormer reference point is generally fairly constant and is designated as low (HEUR-1514), middle (HEUR-825), or high (HEUR-275) molecular weight. HEUR-825 is equivalent to HEUR-708 and HEUR-275 is equivalent to HEUR-270. These relationships were discussed in the preceding chapters. The commercial numbers given to the products in this chapter refer to variations in nonvolatile content and cosolvents. The latex used in these studies is the large-particle-size (>500 nm) vinyl acetate/butyl acrylate binder (Ucar 367) used previously in associative thickener comparisons (15). The latex is sterically stabilized by (hydroxyethyl)cellulose grafts (16).

Table I compares typical test results for low-, mid-, and high-effective molecular weight thickeners in a vinyl–acrylic latex paint. Many of the same trends are present with cellulosic and HEUR thickeners when the effective molecular weight designation for HEUR thickeners is used. As the effective molecular weight of an HEUR increases, Stormer thickening efficiency, roller spatter, and water resistance increase, whereas ICI viscosity decreases. The major difference between these two thickener types is in their low-shear behavior. As effective molecular weight increases, cellulosic paints improve in leveling and decrease in sag resistance. HEUR paints decrease in leveling and improve in sag resistance. Other property differences between these two thickener types are highlighted in Table II.

Modifying Latex Paint Rheology Through Blending

Generally, the rheological properties that are desirable in a practical paint system are somewhere between those imparted by an HEUR and a cellulosic. Flow and leveling should be sufficient without excessive sagging, and the ICI viscosity should be high enough to ensure adequate coverage during application without causing excessive brush drag. This compromise is frequently achieved by incorporating two thickeners with different rheological profiles into one formulation. In this approach, a thickener with fairly Newtonian behavior is blended with one with a very shear-thinning rheology. Typical combinations include HEUR/(hydroxyethyl)cellulose (HEC) (*see* Chapter 26), HEUR/ hydrophobically modified HEC (discussed in Chapters 18 and 19), HEUR/hydrophobically modified alkali-swellable latex, and HEUR/organoclay.

Blend Ratio. The overall thickener level can be specified as pounds per 100 gallons or, in the case of thickener solutions, as dry pounds per 100 gallons. When two or more thickeners are combined, the thickener ratio becomes very important for predicting rheological properties. Often, the thickener ratio is expressed on a dry-pound-per-dry-pound basis. A better method is to use a blend ratio (i.e., the weight ratio of base paints blended to produce a particular thickener system) in which each base paint is made at equal Stormer viscosity and contains one of the thickeners in the system. The base paints have the same ingredients except for the thickener (often, they are made from a common pigment dispersion and letdown). For example, a 60/40 HEUR/HEC-thickened paint can be made by blending 300 g of an HEUR-thickened paint with 200 g of an HEC-thickened paint, both at equal Stormer viscosity. In effect, 60% of the Stormer viscosity of the final paint blend was developed by the HEUR and 40% by the HEC. By specifying thickener combinations as blend ratios, rather than as dry-weight ratios, thickeners with different Stormer efficiencies can be compared more easily. Also, by fixing the Stormer viscosity at the desired value,

Table I. Rheological Properties of Latex Paint Thickeners in a 60% PVC–30% NVV Interior Vinyl–Acrylic Flat at 100 KU

Thickener System	Thickener Level (dry lb/100 gal)	ICI Viscosity (P)	Anti-sag[a]	Level[b]	Water Resistance[c]	Spatter Resistance[d]
Low-MW HEC	13.0	1.6	12.0	0.0	good	fair
Mid-MW HEC	7.5	1.1	9.0	4.0	very good	poor
High-MW HEC	6.5	1.0	8.0	4.0	very good	very poor
Low-MW HEUR	6.5	3.8	4.0	7.0	poor	good
Mid-MW HEUR	8.8	2.6	4.0	6.5	very poor	very good
High-MW HEUR	16.0	1.9	5.5	6.0	very poor	very good

[a]Leneta anti-sag, 12.0 = best.
[b]N.Y.P.C. leveling, 10.0 = best.
[c]Susceptibility of dry film to blistering.
[d]Spatter during roller application.

Table II. Properties of Cellulosic- and HEUR-Thickened Paints

Property	Cellulosic-Thickened	HEUR-Thickened
Flow and leveling	Poor	Good
Sag resistance	Good	Poor
Spreading rates	High	Low
Brush drag	Low	High
Roller spatter	High	Low
Resistance properties (scrub, adhesion, and ammonia sensitivity)	Good	Poor
Gloss	Low	High
Cost	Low	High
Sensitivity to other paint ingredients (e.g., colorant, surfactant, cosolvent, dispersant, latex)	Insensitive	Sensitive
Pigment settling	Little, if any	Tendency toward
Color-float problems	Few	More
Susceptibility to bacterial attack	Susceptible	Resistant

blending will affect only the low- and high-shear-rate regions of the rheological profile (*see* **Problems with Blending** for exceptions).

HEUR/HEC. HEUR/HEC is probably the most commonly used thickener combination for the reasons discussed earlier. Once the Stormer viscosity has been selected, ICI viscosity can be adjusted by changing the blend ratio. Figure 1 is a plot of ICI viscosity as a function of blend ratio for several HEUR/HEC combinations. Blends that are 0% and 100% HEUR are the HEC- and HEUR-thickened base paints, respectively. These data show that the ICI viscosity of a blend is between the ICI viscosities of the base paints used to make the blend, and that the relationship is *not* linear. For a specific ICI viscosity, decreasing the molecular weight of the HEC will shift the required blend ratio to be richer in HEC and leaner in HEUR. Increasing the effective molecular weight of the HEUR has a similar effect. Through construction of graphs of this type for a particular formulation, the correct blend ratio to achieve targeted ICI and Stormer viscosities can be predicted.

Leveling and sag resistance can be fine-tuned by deciding which HEC molecular weight to use. In blends, sagging is decreased as HEC molecular weight decreases. This behavior results from the intrinsic decrease in these properties that occurs with lower molecular weight HECs, and because lowering the HEC molecular weight will shift the blend ratio required to obtain a targeted ICI viscosity more to the HEC side. Because HECs impart less sagging than HEURs, the shift in the blend ratio will further decrease this property. This shift in the blend ratio has a much greater influence on leveling and sagging than the actual thickener molecular weight because the difference in these low-shear-rate properties is greater between the two types
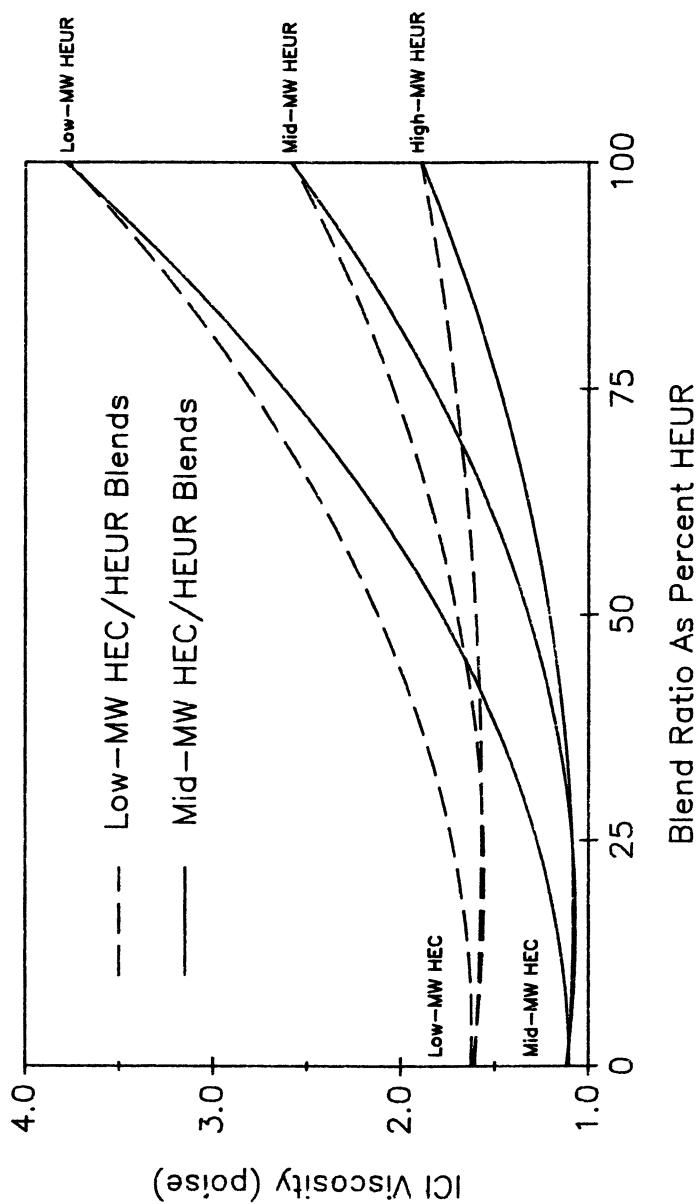
Figure 1. ICI viscosity as a function of thickener blend ratio in a 60% PVC/30% NVV vinyl–acrylic flat at 100 KU.

of thickeners than between the molecular weights of one thickener type. Therefore, decreasing the effective molecular weight of the HEUR in a blend at constant ICI will also decrease sagging and leveling even though low effective molecular weight HEURs increase these properties.

HEUR/Hydrophobically Modified HEC. Hydrophobically modified HEC (discussed in Chapters 18 and 19) can be blended with HEURs to modify paint rheology. Figure 2 is a plot of ICI viscosity as a function of blend ratio for HEUR/hydrophobically modified HEC and HEUR/mid-molecular weight HEC thickener systems having a variety of HEUR cothickeners. Because of the hydrophobic modification of the HEC (*17*), HEURs interact more with this cothickener than with unmodified HEC. With this blend combination, nearly linear dependence of ICI viscosity with blend ratio for the HEUR/hydrophobically modified HEC thickener system was observed. The 50/50 low effective molecular weight HEUR/mid-molecular weight HEC blend has an ICI viscosity 0.70 P lower than the 50/50 low effective molecular weight HEUR/hydrophobically modified HEC blend, even though the mid-molecular weight HEC-thickened base paint (0% HEUR) had an ICI viscosity only 0.15 P lower than its hydrophobically modified HEC-thickened counterpart. As a result, replacing the HEC cothickener with hydrophobically modified HEC caused a shift in the blend ratio and reduced the amount of HEUR at equal Stormer and ICI viscosities. Although hydrophobically modified HEC costs slightly more than HEC, a net reduction in cost can occur because less of the much more expensive HEUR is required. This shift in the thickener system should not substantially reduce flow and leveling or spatter resistance because hydrophobically modified HEC is often better in this respect than HEC (*see* Chapter 12).

The interaction between hydrophobically modified HEC and HEUR may be so strong that a paint with the proper degree of flow and leveling may have an excessively high ICI viscosity, particularly when a blend with low effective molecular weight HEURs. Currently, hydrophobically modified HEC is available in only one viscosity grade. Therefore, to fine-tune flow and leveling, different HEURs must be tried.

HEUR/Hydrophobically Modified Alkali-Swellable Latex. Hydrophobically modified alkali-swellable latex thickeners (Chapter 25) can also be used as cothickeners for HEURs, and, like hydrophobically modified HEC, do not suppress the ICI viscosity of HEURs. Therefore, blend ratios of HEUR/hydrophobically modified alkali-swellable latex systems will have less HEUR thickener and be less expensive than HEUR/cellulosic systems. Some hydrophobically modified alkali-swellable latexes are even more cost-efficient than cellulosic thickeners, so a further savings may be realized. Another advantage to this approach is that the HEUR/hydrophobically modified alkali-swellable latex thickener systems are not biodegradable; however,
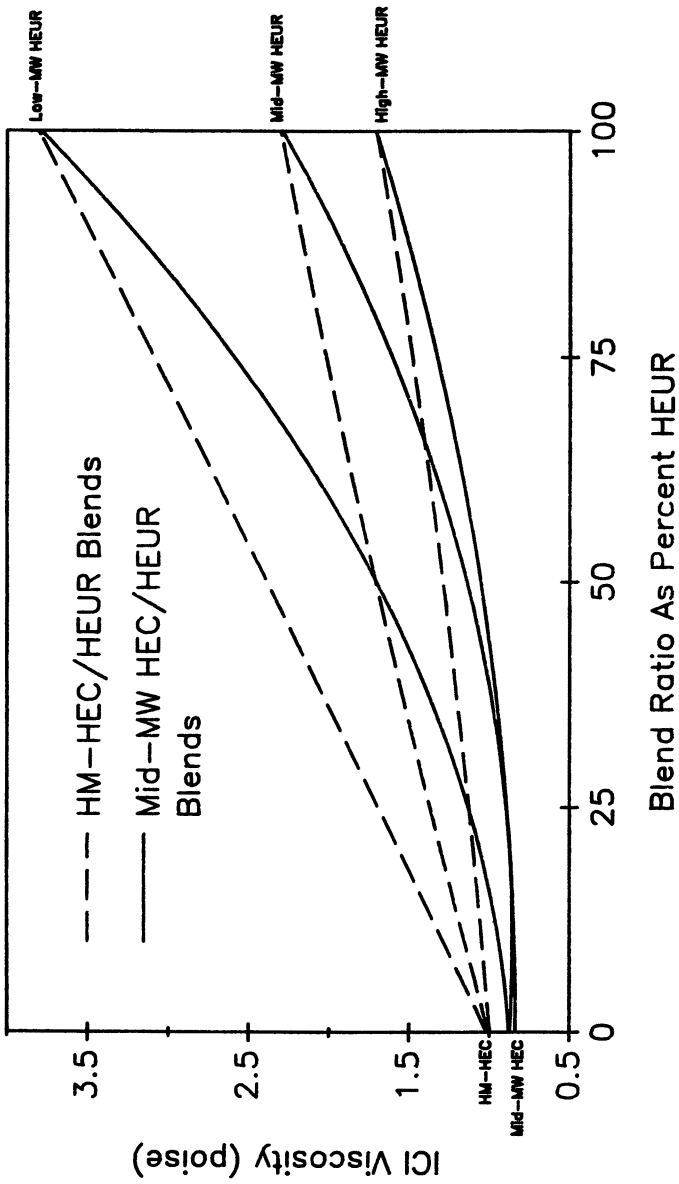
Figure 2. Comparison of mid-molecular weight HEC and hydrophobically modified HEC as cothickeners with HEUR in 60% PVC/30% NVV vinyl–acrylic flat at 90 KU.

viscosity loss may occur because of a downward drift in pH. Small amounts of 2-amino-2-methyl-1-propanol or a similar buffering agent are often used to prevent pH drift in a finished product.

The reduction of scrub resistance is the main disadvantage of HEUR/ hydrophobically modified alkali-swellable latex thickener systems (*18, 19*). Hydrophobically modified alkali-swellable latex-thickened paints often show increased water and alkali sensitivity, reduced wet and dry adhesion, and lower scrub resistance than similar cellulosic-thickened paints.

HEUR/HEUR and HEUR/HEUR/HEC.   Recently, several companies have developed two or more "effective viscosity grades" of HEUR thickener designed to be used together (*20–22*). Generally, one HEUR has a high effective molecular weight and is efficient in developing Stormer viscosity, and the other has a low effective molecular weight, which requires a greater amount of thickener to develop the same Stormer viscosity, but produces a much higher ICI viscosity. The two thickeners can be blended to cover all intermediate ICI viscosities. As seen in Figure 3, the ICI viscosity is a linear function of the blend ratio and is similar to HEUR/hydrophobically modified HEC and HEUR/hydrophobically modified alkali-swellable latex systems.

This theory of blending is significant to the formulator because it provides a system for tailoring HEURs to a particular formulation. However, several problems still exist. In many formulations, HEURs do not provide sufficient low-shear viscosity to prevent pigment settling or excessive sagging, and a third cothickener, such as a cellulosic or organoclay, may be necessary (*20*). Also, HEURs tend to be very sensitive to other paint ingredients such as surfactants, colorants, and cosolvents (*18*). In HEUR/cellulosic thickener systems, this sensitivity is reduced because less HEUR is present. Addition of a colorant at the rate of 4.0 fl oz/gal to an HEUR/HEUR system may reduce the Stormer viscosity by as much as 15 KU (Krebs unit). Although problems with these systems exist, they will probably be overcome as this technology continues to develop.

Problems with Blending.   The principle of this approach to optimizing paint rheology is that two paints with the same Stormer viscosity will produce blends with the same Stormer viscosity. In practice, this result does not always occur. For example, a 50/50 HEUR/organoclay-thickened paint made from base paints at 100 KU each may have a Stormer viscosity of only 90 KU. This result often occurs when one of the base paints is very thixotropic. Also, a paint blend may have poorer flow and leveling than either of the base paints. Poor flow indicates that some flocculation may occur during the blending process.

In some cases, it is not practical to make a one-thickener base paint. Some of the very low effective molecular weight HEURs are so inefficient
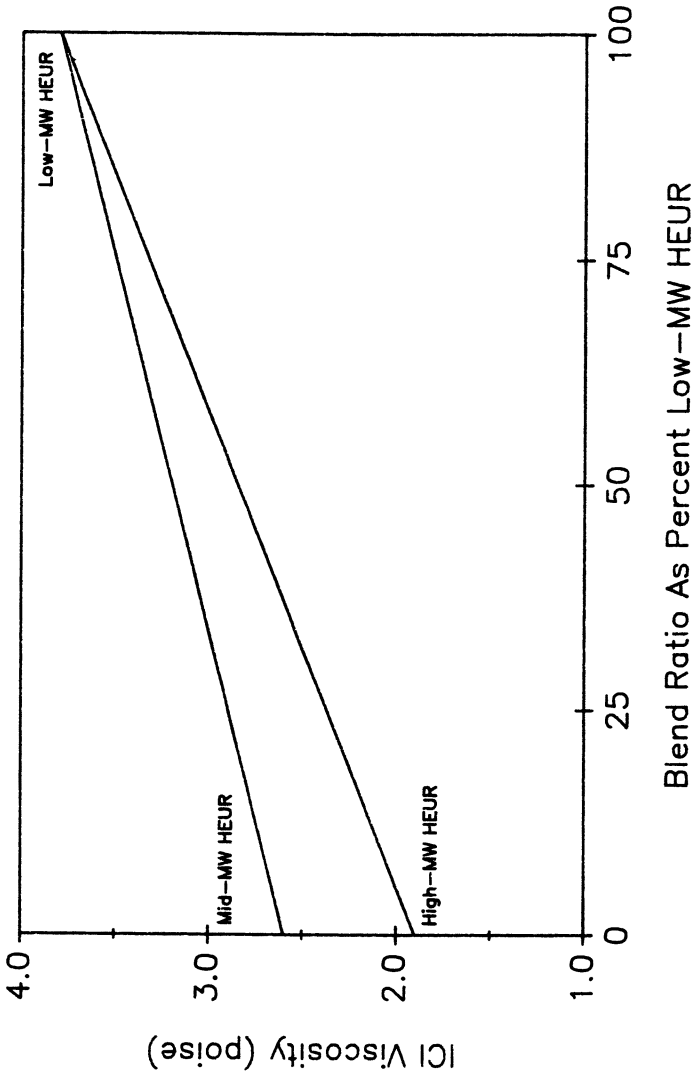
Figure 3. ICI viscosity as a function of blend ratio in 60% PVC/30% NVV vinyl–acrylic flat at 100 KU.

in developing Stormer viscosity that an unreasonably large quantity would be required to obtain the desired Stormer viscosity. Other thickeners may produce base paints that are so thixotropic that only an approximate Stormer viscosity can be determined.

Once the rheology of a paint has been optimized through blending, the final composite formulation should be remade without blending as a final check for unforeseen interactions. The order of ingredient addition is very important when using associative thickeners, and varying the order can result in large Stormer and ICI viscosity changes (*18*). Maintaining the proper order of addition is not always possible when making base paints for blending. For example, when making an unblended HEUR/cellulosic paint, the cellulosic is often added during the pigment dispersion phase and the HEUR is added afterwards. When making an HEUR base paint, the liquid in the grind phase must be reduced to achieve the proper consistency for pigment dispersion. This liquid is then added during the letdown to maintain percent nonvolatile by volume (NVV), and changes the order of addition.

Differences between the viscosity profiles of a production-made paint and the laboratory-made blend may occur. Again, the order of ingredient addition may change. Shear rate, temperature, and dispersion time often differ. Also, production-made paints are manufactured with continually changing lots of raw materials that have different properties, whereas developmental work is often carried out with only one lot. Whenever possible, laboratory conditions should simulate production conditions as closely as possible.

Other Ways To Modify Paint Rheology

NVV, Pigment Volume Content, and Latex.   Pigment volume content (PVC) and latex type and grade are important for optimizing dry film properties. Percent NVV is usually governed by the desired cost of the final product. The formulator usually does not use these variables to optimize paint rheology but should be aware of how they affect thickener efficiency.

Generally, decreasing the percent NVV will decrease the efficiency of thickeners and require more thickener to obtain a specific Stormer viscosity. Decreasing PVC at equal solids contents will increase the efficiency of HEUR thickeners because of their greater association with latex. This effect is much more pronounced in higher NVV formulations (*23, 24*). Very few, if any, HEURs work properly in low-NVV, high-PVC formulations. Increasing PVC content will increase the efficiency of hydrophobically modified HEC because HEC associates more with pigment. Also, hydrophobically modified HEC associates more strongly with calcined clay than with calcium carbonate or titanium dioxide (*17*). For HEURs, thickening efficiency is increased as latex particle size is decreased (*20, 25, 26*). Because cellulosic thickeners do

not associate with latex or pigments, PVC or latex choice does not affect cellulosic thickening efficiency significantly.

Components with More Formulating Latitude. For hydrophobically modified HEC, hydrophobically modified alkali-swellable latex, and HEURs, increasing the level or hydrophile–lipophile balance (HLB) of nonionic surfactants decreases their Stormer thickening efficiency, as does increasing the level of glycols or water-miscible coalescing aids (*19, 20, 22, 23, 27, 28*). ICI viscosity is only slightly affected by these additives. Water-insoluble solvents have little effect on these thickeners. Colorants, with their high glycol and surfactant content, often will affect the viscosity of paints with hydrophobically modified HEC, hydrophobically modified alkali-swellable latex, or HEURs in the thickener system.

The ingredients just mentioned are frequently used to modify paint rheology (*20, 22, 23*). In certain formulations, HEURs and hydrophobically modified alkali-swellable latexes have such a high degree of association that the Stormer viscosity is too high at the desired ICI viscosity. If this is the case, the level of water-soluble cosolvents or surfactants can be increased to depress the Stormer viscosity of the paint. This procedure, in effect, decreases the effective molecular weight of the thickener by decreasing the degree of association. Although this approach will work, often other paint properties are affected. Higher cosolvent levels can prolong dry time and reduce block resistance; lower levels can reduce freeze–thaw stability, cold-temperature coalescence, and open time. Surfactant type and level can affect color acceptance, defoaming, and scrub-resistance properties. Great care must be taken by the formulator to investigate all possible consequences of making these types of formula changes.

Clear-Liquid Separation

Clear-liquid separation is the appearance of a clear supernatant layer above the bulk of opaque paint after shelf-aging. This separation can occur within 1 day and be several inches thick in a 1-gal can. In tinted paints, colorant may float up into this layer and produce a very displeasing in-can appearance. Reincorporation of the supernatant layer by hand stirring or mechanical agitation usually solves the problem only temporarily because the clear-liquid layer returns after several days. HEUR/HEC- and HEUR/hydrophobically modified HEC-thickened paints are particularly prone to this separation.

Blend Ratio, HEUR Effective Molecular Weight, and HEC Molecular Weight. Table III presents data that show the effect of these variables on the clear-liquid separation that occurs in a vinyl–acrylic flat after 1 month of shelf-aging. Generally, clear-liquid separation was greatest

near a 40/60 HEUR/HEC blend ratio, fairly close to the blend that had optimum rheological properties. Although this ratio is specific to this formulation, similar results in other formulations may occur. Thickener molecular weight also had an effect on clear-liquid separation. Lower molecular weight HECs and higher effective molecular weight HEURs produced more separation.

Surfactants.   Table IV presents data that show how surfactant HLB affects clear-liquid separation in a 50/50 HEUR/HEC-thickened vinyl–acrylic flat. Generally, higher HLB surfactants decrease the amount of separation; the reduction is greater in low effective molecular weight HEUR systems. Small amounts of separation can be reduced or eliminated by adjusting the surfactant system. However, high-HLB surfactants must be used judiciously because of their adverse effect on the Stormer thickening efficiency of HEURs. Also, high surfactant levels may affect other paint properties such as color acceptance, water resistance, and scrub resistance.

Use of a Third Thickener.   The use of a third thickener is another method for eliminating clear-liquid separation. The third thickener must be very shear-thinning to build sufficient structure at rest to prevent separation, yet break down at high shear to permit proper application. It must also be very thixotropic so that the structure will not rebuild quickly and adversely affect leveling. Once paint rheology has been optimized, a base paint containing the third thickener can be blended incrementally into the formulation until clear-liquid separation is no longer present. Only low levels should be used because the optimized rheology may change. Typical thickeners for this purpose are polysaccharides, attapulgite clays, smectite clays, and hydrophobically modified alkali-swellable latexes. Because of the low blend ratios involved with these materials, the Stormer viscosity of the third thick-

Table III. Clear-Liquid Separation Occurring in a Half-Pint Can (60 mm Full) After 1-Month Shelf-Aging

Thickener System		Blend Ratio (Associative/Cellulosic)				
Associative	Cellulosic	30/70	40/60	50/50	60/40	70/30
Low-MW HEUR	Low-MW HEC	3	4	4	4	3
Low-MW HEUR	Mid-MW HEC	3	4	3	3	2
Low-MW HEUR	High-MW HEC	3	3	3	2	1
Mid-MW HEUR	Low-MW HEC	4	4	4	3	2
Mid-MW HEUR	Mid-MW HEC	3	4	2	2	1
Mid-MW HEUR	High-MW HEC	3	3	1	1	0
High-MW HEUR	Low-MW HEC	3	2	1	0	0
High-MW HEUR	Mid-MW HEC	3	1	1	0	0
High-MW HEUR	High-MW HEC	1	0	0	0	0

KEY: 0, no clear-liquid separation; 1, up to 8.3% of total depth; 2, up to 16.7% of total depth; 3, up to 25.0% of total depth; and 4, over 25.0% of total depth.

Table IV. Effect of Surfactant HLB on Clear-Liquid
Separation After 1-Month Shelf-Aging

Thickener System[a]	Nonylphenol-Based Surfactant (HLB)		
	4.0	12.9	17.1
Low-MW HEUR	3	3	3
Mid-MW HEUR	3	2	2
High-MW HEUR	3	1	0

NOTE: Surfactant level of 4.0 active lb/100 gal.
KEY: 0, no clear-liquid separation; 1, up to 8.3% of total depth; 2, up to 16.7% of total depth; 3, up to 25.0% of total depth; and 4, over 25.0% of total depth.
[a]Associative thickener blended with mid-MW HEC cellulosic thickener (50/50).

ener base paint has little effect on the Stormer viscosity of the rheologically optimized blend. The results of such a study are presented in Table V.

Summary

The basic formulating procedure to optimize latex paint rheology is as follows.

1. Base paints should be made, each with a different thickener, at the desired Stormer viscosity.

2. Two base paints should be blended, one with a high ICI viscosity and one with a low ICI viscosity, to obtain the desired ICI viscosity. During this process, the Stormer viscosity should remain constant. Typical thickener combinations used are HEUR/cellulosic, HEUR/hydrophobically modified HEC, and HEUR/hydrophobically modified alkali-swellable latex.

3. Low-shear properties can be fine-tuned in HEUR/cellulosic systems by changing thickener molecular weight in the base paints and reblending to obtain the desired ICI viscosity. Higher molecular weight thickeners may be used to improve flow and leveling; lower molecular weight thickeners are used to improve sag resistance.

4. If clear-liquid separation occurs, a third highly thixotropic, shear-thinning thickener can be incrementally blended in to determine the minimum amount required to stop the separation. Only small quantities of the third thickener should be used or the optimized paint rheology may change.

5. Paint rheology may also be changed by varying other formulation ingredients; however, possible changes in other paint properties may result.

**Table V. Effect of a Third Thickener on Clear-Liquid
Separation After 1-Month Shelf-Aging**

Third Thickener	5.0%[a]	10.0%[a]	15.0%[a]
Polysaccharide	1	1	0
Attapulgite clay	1	0	0
Smectite clay	3	2	1
HASE–615[b]	2	2	1

NOTES: Third thickener blended into a 50/50 mid-MW HEUR/
mid-MW HEC-based paint that had a clear-liquid separation rating
of 3.
KEY: 0, no clear-liquid separation; 1, up to 8.3% of total depth; 2,
up to 16.7% of total depth; 3, up to 25.0% of total depth; and 4,
over 25.0% of total depth.
[a]Level (%) of third thickener in the blend.
[b]Hydrophobically modified alkali-swellable latex thickener.

6. Remake the final formulation without blending to check for possible interactions that were not present during the blending process.

This systematic approach to rheology optimization should save the formulator considerable time in developing thickener systems for good application properties. Although this method was developed mainly for use in vinyl–acrylic formulations, it should be applicable to a wide variety of latex systems. This procedure enables the formulator to modify independently the rheological profile of latex paints in different shear-rate regions with only a minimal effect on nonrheological properties. The more commonly suggested approach of changing Stormer thickening efficiency with cosolvents or surfactants and adjusting the level of thickener to produce the desired ICI viscosity often does not accomplish this goal.

References

1. *Sag Resistance of Paints Using a Multinotch Applicator, Method A—Horizontal Stripes*; ASTM D 4400–84.
2. *Leveling Characteristics of Paints by Drawdown Method*; ASTM D 2801–69.
3. *Consistency of Paints Using the Stormer Viscometer*; ASTM D 562–81.
4. *Determination of Viscosity of Paints and Varnishes at a High Rate of Shear by the ICI Cone/Plate Viscometer*; ASTM D 4287–83.
5. Patton, T. C. *J. Paint Technol.* 1968, 40(522), 301.
6. Patton, T. C. *Off. Dig., Fed. Soc. Paint Technol.* 1964, 36(474), 745.
7. Beeferman, H. L.; Bergren, D. A. *J. Paint Technol.* 1966, 38(492), 9.
8. Smith, N. D. P.; Orchard, S. E.; Rhind-Tutt, A. J. *J. Oil Colour Chem. Assoc.* 1961, 44, 618.
9. Glass, J. E. *J. Coatings Technol.* 1978, 50(640), 61.
10. Blake, D. M. *J. Coatings Technol.* 1983, 55(701), 33.
11. Croll, S. G.; Kleinlein, R. L. In *Water-Soluble Polymers*; Glass, J. E., Ed.; Advances in Chemistry 213; American Chemical Society: Washington, DC, 1986; pp 333–350.

12. Methocel methylcellulose, product literature, Dow Chemical Company.
13. Natrosol hydroxyethylcellulose product literature, Aqualon Company.
14. Cellosize hydroxyethylcellulose product literature, Union Carbide Corporation.
15. Hall, J. E.; Hodgson, P.; Krivanek, L.; Malizia, P. *J. Coatings Technol.* **1986,** 58(738), 65.
16. Craig, D. H. In *Water-Soluble Polymers*; Glass, J. E., Ed.; Advances in Chemistry 213; American Chemical Society: Washington, DC, 1986; pp 351–367.
17. Shaw, K. G.; Leipold, D. P. *J. Coatings Technol.* **1985,** 57(727), 63.
18. Schwab, F. G. In *Water-Soluble Polymers*; Glass, J. E., Ed.; Advances in Chemistry 213; American Chemical Society: Washington, DC, 1986; pp 369–373.
19. Glancy, C. W. *J. Coatings Technol., Am. Paint & Coatings J.,* Aug 6, 1984.
20. Rheolate 255 and Rheolate 278 product literature, NL Chemicals.
21. DSX-1514, DSX-1550, and DSX-1600 product literature, Henkel.
22. Acrysol RM-825 and Acrysol RM-1020, Rohm & Haas Company.
23. Ucar thickener SCT-275 product literature, Union Carbide Corporation.
24. Fernando, R. H.; Glass, J. E. *J. Oil Colour Chem. Assoc.* **1986,** 69, 263.
25. Glancy, C. W.; Bassett, D. R. *Proceedings of the ACS Division of Polymeric Materials: Science and Engineering* **1984,** 51, 348.
26. Murakami, T.; Fernando, R. H.; Glass, J. E. *Abstracts of Papers*, 190th National Meeting of the American Chemical Society, Chicago, IL; American Chemical Society: Washington, DC 1985; PMSE 113.
27. Glass, J. E. In *Water-Soluble Polymers*; Glass, J. E., Ed.; Advances in Chemistry 213; American Chemical Society: Washington, DC, 1986; pp 391–416.
28. Thibeault, J. C.; Sperry, P. R.; Schaller, E. J. In *Water-Soluble Polymers*; Glass, J. E., Ed.; Advances in Chemistry 213; American Chemical Society: Washington, DC, 1986; pp 375–389.

Hydrophobically Modified Alkali-Soluble Emulsions as Thickeners for Exterior Latex Paints

S. LeSota, E. W. Lewandowski, and E. J. Schaller

Rohm and Haas Research Laboratories, Spring House, PA 19477

Hydrophobically modified water-soluble polymers, used by latex paint manufacturers as associative thickeners, provide significant advantages in improving film build and leveling, and decreasing spatter from roller-applied paints. Nonionic hydrophobically modified ethoxylated urethane (HEUR) thickeners provide good performance in both interior and exterior paints, but are more costly than conventional thickeners. Low-cost hydrophobically modified alkali-soluble emulsion (HASE) thickeners, although particularly well-suited for use in interior wall paints, present a risk of early blistering over chalking repaint surfaces when used in exterior house paints. Their water sensitivity is increased until the volatile base used to solubilize the thickener has left the film. Ionic cross-linking of the HASE thickeners in the paint film by incorporating soluble zinc complexes or zinc oxide into the paint formulation can significantly reduce the risk of blistering early in the life of the film.

HYDROPHOBIC ALKALI-SOLUBLE EMULSION (HASE) THICKENERS impart viscosity, flow, film build, gloss, and spatter resistance to interior latex paints (*1–3*); however, they reduce the water resistance of exterior latex paints to the extent that early blister resistance over some repaint surfaces is severely downgraded. When state-of-the-art high-adhesion latex binders are used with HASE thickeners, no blistering problem occurs over nonchalking latex or oil repaint substrates, or chalky oil substrates. However, chalking latex paints pose a severe risk of early blistering to HASE-thickened paints applied

over them. Despite this blistering problem with HASE thickeners, there is still a strong interest in using these inexpensive rheology modifiers in exterior paints. Reducing the amount of other water-sensitive paint ingredients helps, but not satisfactorily.

This chapter describes ionic cross-linking of the HASE thickener with zinc oxide or zinc ammonium complexes to improve early blister resistance. Zinc ammonium complexes have been used in ammonia-removable latex floor polishes for decades. Paint formulations containing zinc oxide have benefits but are prone to sporadic viscosity instability, which sometimes cannot be predicted by standard laboratory tests. However, many paint manufacturers have learned how to successfully stabilize these zinc oxide-containing latex paints.

Unlike conventional alkali-soluble thickeners, HASE thickeners are in the class of anionic rheology modifiers also known as associative thickeners or polymeric surfactants. These thickeners are water-soluble polymers containing hydrophobic groups capable of forming intermolecular associations and adsorbing onto the surfaces of dispersed particles; thus they provide thickening power much greater than unmodified polymers of similar molecular weight (1, 2). The more widely used nonionic, hydrophobically modified ethoxylated urethane (HEUR) associative thickeners provide good performance in both interior and exterior paints, but are more costly than conventional and HASE thickeners.

Experimental Details

A typical exterior acrylic paint formulation (see Appendix A) was thickened with a commercial HASE thickener that contained 5.23 meq/g of carboxylic acid functionality (4). This thickener was modified with 1 to 25 lb (1 lb = 0.4536 kg) of zinc oxide (French process) in the mill base in one set of paints and with post-added zinc ammonium complex such as acetate, carbonate, bicarbonate, or glycinate in another set of paints.

Two coats of these paints were applied 5 h apart over a heavily chalked latex paint on a white pine board. Because significant differences have been seen between individual chalky test substrates, common control paints containing unmodified HASE, (hydroxyethyl)cellulose (HEC), and HEUR thickeners were included in each test. Test paints were dried for 18 h at 25 BC and 50% relative humidity and then placed in a fog box for 5 h. (The fog box is a Plexiglas (poly(methyl methacrylate)) box with six spray nozzles on the inside top that continuously spray a fine mist of water over the painted panels placed about 15B off the vertical in racks about 10 in. (1 in. z 2.54 cm) below the nozzles.) We used two different fog boxes; one sprayed deionized water and one sprayed tap water.

The paints were then rated for blistering by using American Society for Testing and Materials (ASTM) pictorial blister standards (5). An ASTM blister rating of 7 was chosen as the minimum acceptable level because experience has shown that these blisters will usually shrink after drying and leave no perceptible sign that blistering had taken place. Repeated rain or fog spray showed no further blistering. Presumably, some of the water-soluble material that caused blistering had been washed out of the film.

Portions of these paints were oven aged for 10 days at 60 °C, as an indication of long-term stability. Freeze–thaw tests were also run that consisted of five cycles at −25 °C.

Results and Discussion

Zinc Oxide. We found that as little as 5 lb of zinc oxide per 100 gal (1 gal = 3.785 L) of paint was sufficient to impart acceptable early blister resistance to the paint when tested in the rain or in the tap water fog box (Table I). Higher zinc oxide levels showed no further blister-resistance improvement in this paint. Blistering in the deionized water fog box was so severe that even the HEC-thickened control had a blister rating of 4D. (The note to Table I explains the rating method used.) However, a noticeable effect occurred at zinc oxide levels of 5 lb/100 gal of paint and higher. The zinc oxide combined with the ammonia in the paint and formed a zinc ammonium complex that may ionically cross-link the carboxyl groups in the HASE thickener and other paint constituents, and thereby reduce the overall water sensitivity of the paint.

Zinc Ammonium Complexes. The zinc ammonium complexes were tested on a different chalky latex panel than the zinc oxide paints, and the entire series showed less blistering in the same deionized water fog box (Table II). The HEC-thickened control did not blister on this board. The HEUR control showed 7M blisters on this board vs. 2MD (Table I). Addition of the zinc ammonium complexes resulted in much-improved early blister resistance. Blister-resistance effectiveness differed depending on which complex was used. The four zinc ammonium complexes evaluated in the HASE-

Table I. Blister Resistance of ZnO-Modified Paints with HASE Thickener: Comparison of Three Blister Tests

Rheology Modifier or Thickener	HASE Thickener, lb/100 gal of Paint	ZnO, lb/100 gal of Paint	Zn, eq/COOH	ASTM Blister Ratings[a]		
				Deionized Water Fog Box	Tap Water Fog Box	Rain
HEC	—	0	—	4D	8M to 10	10
HEUR	—	0	—	2MD	10	7F
HASE	3.3	0	—	1D	5MD	4M
HASE	3.6	1	0.5	1D	5M	5F
HASE	2.8	5	4.0	2D	10	10
HASE	2.7	10	8.6	2MD	10	10
HASE	2.7	15	13.6	2MD	10	10
HASE	2.7	20	17.9	2D	10	10
HASE	2.7	25	22.1	2D	10	10
HASE	3.6	—[b]	0.5	1D	5M	5F

[a]ASTM ratings: 10 is best, 0 is worst; the numbers refer to blister size and the letters refer to the population density of the blisters, as illustrated in ref. 5. Abbreviations: F, few; M, medium; MD, medium to dense; and D, dense.
[b]Zinc ammonium carbonate.

Table II. Blister Resistance of HASE-Thickened Paints Modified with Zinc
Ammonium Complexes

Zn Ammonium Complex	HASE Thickener, dry lb/100 gal of Paint	COOH eq in HASE Thickener	Zn, eq	Zn, eq/COOH	Deionized Water Fog Box[a]
Glycinate	3.00	0.016	0.017	1.06	3MD
	2.94	0.015	0.023	1.53	3MD
	3.08	0.016	0.034	2.13	3M
	2.93	0.015	0.068	4.53	10
Acetate	2.94	0.015	0.017	1.13	3MD
	2.60	0.014	0.026	1.86	6MD
	2.36	0.012	0.034	2.83	10
Bicarbonate	2.79	0.016	0.017	1.06	3MD
	2.34	0.012	0.026	2.17	5MD
	2.19	0.011	0.034	3.09	10
Carbonate	2.74	0.014	0.017	1.21	2MD
	2.48	0.013	0.026	2.00	5MD
	2.33	0.012	0.035	2.92	10
None	3.30	—	—	—	1D
HEC control	—	—	—	—	10
HEUR control	—	—	—	—	7M

[a]ASTM blister ratings are described in Table I.

thickened acrylic paint in decreasing order of effectiveness in blister resistance were acetate > carbonate > bicarbonate >> glycinate >>> no complex.

The stoichiometry at effective zinc ammonium complex levels suggests that zinc reacts with more carboxyl groups in the paint (latex, dispersants, etc.) than in the HASE thickener. Even with the most efficient complex, zinc ammonium acetate, more zinc was required to obtain good blister resistance than the stoichiometric equivalent of the carboxyl groups in the HASE thickener (Table II).

Fog Boxes vs. Rain.   Like many other accelerated tests, the fog box blister-resistance test shows trends rather than an exact correlation with the results observed in actual rainfall. When deionized water is used for the spray in the fog box, the test is most stringent, and blister differences can be observed in paints that do not blister when the much less stringent tap water fog is used. The tap water test correlates more closely to what is generally seen on the test fences when paint films no more than a few days old are exposed to rain.

Early blistering due to rain depends on the rain's intensity, duration, and on how long the paints have dried before it rains. The pH of the water may also be an influential variable. The deionized water fog box had a pH of about 8 and the tap water fog box had a pH of 7, whereas the rain had a pH of about 4. The relatively more alkaline deionized water would be ex-

pected to attack the alkali solubles in the paint more than the acidic rain would.

Table II compares the zinc oxide paint results from all three sources of water. The more stringent deionized water fog box showed that even the HEC-thickened paint blisters badly, as does the HEUR paint, which shows no blistering on exterior exposures. The zinc cross-linked HASE-thickened paints blistered much more in the deionized water fog box than they did in the tap water fog box or in the rain. No significant differences were noted between 5 and 25 lb of zinc oxide per 100 gal of paint.

Paint Stability. Table III shows that paints containing the higher levels of zinc oxide had a greater viscosity drop after heat aging, and gelled after three freeze–thaw cycles. At 0.5 eq of zinc per COOH unit, both the zinc oxide and zinc ammonium carbonate paints were stable.

Table IV shows that paints containing the higher levels of zinc ammonium complexes also generally showed the greatest viscosity drop on heat aging. Table IV also shows that these paints had poorer freeze–thaw stability. Close attention to formulation techniques, such as the judicious choice of dispersants and surfactants, can minimize or eliminate this problem in zinc oxide-containing latex paints.

Conclusions

Ionic cross-linking of the water-sensitive carboxyl groups in the HASE thickeners (and probably other carboxyl groups in the paint) with either low levels of zinc oxide in the mill base or post-added zinc ammonium complexes can be effective in improving the early blister resistance of HASE-thickened latex paints over heavily chalked latex paint surfaces. Of the zinc ammonium complexes evaluated, the zinc ammonium carbonate and bicarbonate ap-

Table III. Viscosity Stability of Zinc Oxide-Modified Paints with HASE Thickener After Heat and Freeze–Thaw Testing

ZnO, lb/100 gal of Paint	Zn, eq/COOH	Equilibrated Viscosity (KU)	Viscosity Change After Heat Aging (KU)	Viscosity Change After Freeze–Thaw (KU)
0	—	96	−3	−2
1	0.5	97	−6	−5
5	4.0	113	−9	gel
10	8.6	112	−11	gel
15	13.6	105	−12	gel
20	17.9	118	−30	gel
25	22.1	112	−26	gel
—[a]	0.5	84	−4	1

[a] Zinc ammonium carbonate.

Table IV. Viscosity Stability of Zinc Ammonium Complex-Modified Paints
After Heat and Freeze–Thaw Testing

Zn Ammonium Complex	Zn, eq/COOH	Equilibrated Viscosity (KU)	Viscosity Change After Heat Aging (KU)	Viscosity Change After Freeze–Thaw (KU)
Glycinate	1.60	91	−1	9
	1.53	91	−1	7
	2.13	94	−3	12
	4.53	94	−4	41
Acetate	1.13	92	−2	gel
	1.86	90	−3	gel
	2.83	94	−12	gel
Bicarbonate	1.06	90	−3	0
	2.17	88	−6	−5
	3.09	90	−11	gel
Carbonate	1.21	89	−3	−1
	2.00	89	−5	2
	2.92	93	−10	44
None	—	96	0	10

peared to have the combined advantage of providing acceptable blister resistance and ability to maintain freeze–thaw stability in this particular paint formulation. However, the contribution of other water-sensitive species in the latex paints, varying requirements for the amount of HASE thickeners to achieve required viscosity, and sensitivity to test conditions make it important that the performance be critically assessed under actual rainfall.

Acknowledgment

Appendix A. Acrylic Exterior Paint Formulation
XW–64–7 Zn

Material	Concentration (lb/100 gal)
Water	100.0
Tamol 960 (40%)	7.1
Triton N–57	4.0
Potassium tripolyphosphate	1.5
Colloid 643 defoamer	1.0
Titanium dioxide (Ti–Pure R–902)	225.0
Zinc oxide (AZO–66LP) or zinc ammonium complex	0–25
Minex 4	148–160
Icecap K	50.0

Procedure: Mill these ingredients on a high-speed mill (Cowles dissolver) for 20 min; at lower speed, add as follows:

Material	Concentration (lb/100 gal)
Rhoplex AC–64 (60.5%)	306.0
Colloid 643 defoamer	3.0
Texanol	9.3
Super Ad-It	9.0
Methylcarbitol	59.0
Ammonia, 28%, to pH 9.5	—
HASE thickener, HEUR, or HEC and water to 90 KU	—

The formulation constants are as follows: pigment volume content, 45%; volume solids, 36%; Stormer viscosity, 90 KU; and pH, 9.5.

References

1. Schaller, E. J. *Surf. Coat. Austr.* **1985,** 22(10), 6.
2. Shay, G. D.; Rich, A. F. *J. Coat. Technol.* **1986,** 58(732), 43.
3. Hall, J. E.; Hodgson, P.; Krivanek, L.; Malizia, P. *J. Coat. Technol.* **1986,** 58(738), 65.
4. *Acrysol TT–935*; product bulletin 81A61, Rohm and Haas Company, Spring House, PA, October 1984.
5. *Pictorial Standards of Coatings Defects*; Federation of Societies for Coatings Technology: Philadelphia, PA, 1979.

Author Index

Affiliation Index

Subject Index

Blending
   of thickeners, to maintain constant
      formulation costs, 153
   problems in optimizing paint rheology,
      535
   thickeners with different rheological
      profiles, 529
Blister resistance in paints, effect of zinc
   oxide, 545
Blistering
   effect of ionic cross-linking, 547
   effect of latex binders, 543
Blocks, number related to sequence length,
   394
Bonds in gel systems, 4
Borates as cross-linker, 93
Branched HEUR thickener, synthesis, 501
Bridged dimer, covalent structure, 290
Brookfield viscosity
   dependence on shear and concentration,
      poly(acrylic acid)s, 120
   vs. alkyl group content, HMHEC, 348
   vs. concentration
      HMHEC and HEC, 346, 347
      HMHEC with and without surfactant,
         356
      neutralized type A polymer mucilages,
         126
      neutralized type B polymer mucilages,
         127
      sodium oleate, 357, 359
      unneutralized type A polymer
         mucilages, 125
   See also Viscosity
N-4-Butylphenylpropionamide, UV spectra,
   407

C

Calcium chloride, effect on degree of
   swelling, hydrogels, 24
Capillary viscometry, experimental details,
   366
Carboxylate groups, ion-binding behavior,
   156
Carboxylated copolymer emulsions, alkali
   swellability, 471
Carboxylic acid
   distribution within ASE and HASE
      latices, 462
   monomers
      in AST patents, 484
      in synthesis of thickeners, 458
(+)-Catechin
   covalent structure, 286
   fluorescence, 289
   structures in the solid state, 287
Cationic dyes
   fluorescence behavior, 326

Cationic dyes—*Continued*
   interaction with polymer PMA chain, 331
Cationic gels, preparation, 18
Cationic monomers, quaternary ammonium,
   polymerization with acrylamide,
   175–191
Cationic polymers, categories, 176
Cationic water-soluble homopolymers,
   production 175
Cellulose-thickened coatings, elongational
   viscosity measurements, 248
Cellulose-thickened paints, properties, 531
Cellulosic components, MW related to
   rheological profile, 528
Chain–chain enthalpic and entropic
   interactions, copolymers in solution,
   438
Chain-growth polymerization
   hydrophobe-modified monomers, 154
   ionogenic monomers, 156
   nonionic monomers, 155
   vinyl monomers, 155
Chain-transfer constants, various monomers,
   156
Chain association, alkylacrylamide
   copolymers, 441
Chain extension
   consequences for practical applications,
      225
   criticality in concentration, 211
   criticality in time scale, 210
   dependence on molecular weight, 197
   effect of relaxation time, 201
   effect of stiffness, 200
   principle, 194
Chain stiffness, effect on extensibility, 200
Characterization
   alkylacrylamide copolymers, 413, 440
   hydrophobically associating polymers,
      399–409
Chelates, to control reaction rate of gel
   formation, 109
Clear-liquid separation, in paint after shelf-
   aging, 538
Cloud point, definition, 137
Cluster
   copolymer–surfactant formations, 310
   definition, 5
   structural features, 5
   swelling behavior, 7
Clustering, HMHEC–surfactant, 361
Coal-water fuels, 252
Coalescence, definition, 130
Coating formulations, important structural
   features, 496
Coatings, effect of titanium dioxide on
   dissipation, 247
Coefficient of concentration, vs. amount of
   incorporated hydrophobe, 434

Energy transfer
  effect of pH, PA-18K$_2$, 331
  R6G to RB in PA-18K$_2$ and PMA, 330
Enhanced oil recovery, need for high
      viscosity, 225
Entangled systems, elongational viscosity,
      221
Entanglement density, effect of
      concentration of cross-linking agent,
      43
Entanglement formation, visual events
      related to macroscopic flow, 222
Entanglements, identifying, 207
Entropic resistance of coil, effect on
      molecule extension, 194
Enzyme-hydrolyzed curdlan, 2D NOE, 81
(-)-Epicatechin
  fluorescence, 289
  structures in the solid state, 287
Equation of motion, solvent molecules and
      polymer network, 46
Equilibrium, effect on structure of
      reversible gel, 10
Error-in-variables method, to determine
      copolymer reactivity ratio, 180
Ethoxylated anionic surfactants, effect on
      PLMA MW, 393
Ethoxylated urethanes, hydrophobically
      modified, architecture, 495–524
Ethylenically unsaturated monomers, to
      prepare conventional and associative
      ASTs, 458
Excimer formation in labeled polymer, 264
Excimer to monomer emission intensities,
      ratio, difficulty in interpreting results,
      290
Excimer to monomer intensity ratio
  adsorption of Py–PEG–Py, 272
  determination, 267
Exciplex process, quenching of pyrene
      fluorescence, 335
Excitation maxima, as function of molar ratio
      of poly(carboxylic acid) to PEG, 271
Excitation spectra
  and fluorescence lifetimes, adsorbed
      species, 276
  as function of [PMAA]/[PEG], 271
  Py–PEG–Py in water, 271
Exponential decay, equation, 289
Extending a molecule by flow, 194
Extension, chain, effect of stiffness, 200
Extension behavior, effect of concentration,
      207
Extension rate, dependence on roll radius
      and roll peripheral velocity, 256
Extensional deformations and converging
      flows, 246
Extensional flow behavior, macromolecules
      in solution, 193–243

Extensional viscosity
  PEO, as function of strain rate, 222
  polymer melts and solutions, 201
  treatments of increase, 204
Exterior coatings, high quality properties,
      498
Exterior latex paints, hydrophobically
      modified alkali-soluble emulsions as
      thickeners, 543–549
Exterior paint formulation, acrylic, 548

F

Factor analysis, to enhance spectral
      information, 307
Fast cross-linking systems, shear history and
      viscosity, 106
Film formation properties, associative and
      conventional ASTs, 477
Film gloss, associative thickeners, 521
First normal force difference vs. shear rate,
      HMHEC, 355
Flare, common features, 208
Flaring of birefringence in semidilute
      solution, 207
Flexible coils, distribution of segments, 211
Flocculation
  critical concentration, HEC, 496
  definition, 130
  mixtures of binder latices, 476
  under theta conditions, 137
Flow-induced birefringence vs. strain rate,
      atactic polystyrene, 197
Flow-induced chain scission, 199
Flow-induced degradation, a-PS, 236
Flow behavior
  polyacrylamide, effect of pH, 234
  polymer melts and solutions, 201
Flow patterns, interpretation, 218
Flow rate vs. flow resistance, 202
Flow resistance
  effect of counterions, 226
  vs. flow rate, 202
  vs. ionic strength, HPAA, 227
  vs. Reynolds number, PAA, 226–228
Fluid strain, effect on chain extension, 220
Fluorescence
  chemically attached dansyl probe, 321
  decay curves, R6G, 334
  effect of addition of particles, 276
  from water-soluble hydrophobically
      associating polymers, 425–435
  intramolecular component of labeled
      PEG, 267
  lifetimes, catechin and epicatechin, 289
  long-chain cationic pyrene derivative, 329
  methods to elucidate problems in polymer
      physics, 264
  POE solutions, 504

N

O

Viscosity—*Continued*
poly(4-vinylpyridine)s, effect of polysoap, 318
reproducibility of data, HPG–titanate gels, 104
required for applications, 246
vs. blend ratio, HEUR/HMHEC, 533
vs. coil-stretch relaxation time, a-PS, 208
vs. concentration, RAM, 417
vs. shear rate
effect of polymer concentration, 421
HMHEC, 372
neutralized type A polymer mucilages, 122
neutralized type B polymer mucilages, 124
POE–HEC blends, 251
unneutralized type A polymer mucilages, 121
unneutralized type B polymer mucilages, 123
vinyl acetate–acrylic latex, 247
vs. temperature, scleroglucan, 75
vs. thickener blend ratio, HEUR/HEC, 532
vs. thickener concentration, HEUR polymers, 506
See also Apparent viscosity, Brookfield viscosity, Elongational viscosity, Intrinsic viscosity, Inverse intrinsic viscosity, Reduced viscosity, Relative viscosity, Stormer viscosity
Visually observed events, network formation, related to macroscopic flow, 222

W

Water
as solvent, gels, 8
content and percent crystallinity, PVA hydrogels, 69
content vs. time of hydration, PVA hydrogel, 71
effect of amount of VOAc, 67
Water absorption, synthetic, semisynthetic, and biopolymer gels, 37

Water sensitivity, latex film, 520
Water solubility, effect of sulfonation of polymers, 160
Water-borne formulations, performance, importance of elongational flows, 245–258
Water-insoluble HMHEC, interactions with amphoteric surfactants, 359
Water-reducible coatings, 253
Water-soluble associative polymers, uses, 437
Water-soluble hydrophobically associating polymers, fluorescence and light scattering, 425–435
Water-soluble polymer(s)
FTIR spectroscopy, 295–313
synthesis, influence of polarity, 151–163
Water-soluble polymer gels, industrial applications, 90
Water-soluble polymeric networks, cooperative diffusion, 45–59
Water–toluene interfacial tension vs. HMHEC concentration, 352
Wave propagation experiments, HMHEC, 370
Wave-rigidity modulus vs. concentration, HMHEC, 371
Weight-average molecular weight
acrylamide copolymers, 433
See also Molecular weight
Wicking
prevented by binding of water, 130
schematic depiction, 129

Z

Zinc ammonium complexes, effect on blister resistance, paints, 545
Zinc oxide
effect on blister resistance, paints, 545
effect on exterior durability, 477
Zirconate, as cross-linker, 93, 110
Zwitterionic polymer in water, schematic model, 173
Zwitterionic sulfonate monomers, copolymerization with NVP, 170